

**CHELATION-ENFORCED METAL–ARENE INTERACTIONS:
INSIGHTS INTO SUBSTRATE BINDING AND CATALYSIS BY LATE
TRANSITION METAL COMPLEXES**

Thesis by
Sibo Lin

In Partial Fulfillment of the Requirements
for the Degree of Doctor of Philosophy

CALIFORNIA INSTITUTE OF TECHNOLOGY
Division of Chemistry and Chemical Engineering
Pasadena, California
2014
(Defended on February 24, 2014)

© 2014
Sibo Lin
All Rights Reserved

Only those who risk going too far can possibly find out how far one can go.

-T.S. Eliot

ACKNOWLEDGEMENTS

Five years ago, I was given the advice that completing graduate school is not a sprint, but a marathon. Now, 26 miles later and nearing the finish line, I better understand the analogy. And as a true marathoner performs best with an effective support team, I owe my success in graduate school to my mentors, labmates, friends, and family. Thanks to all of you.

Prof. Theo Agapie, thank you for taking me into your research group and mentoring me. Your enthusiasm for chemistry and hard work rubbed off. When inorganic chemists learn that I went to Indiana University for undergraduate studies, they usually assume that I worked for Mindiola. But just five years ago, my primary experience with chemistry experiments was *in silico*, and it was only with your help that I became a proficient experimentalist and presenter. Thanks for supporting my research efforts and taking some of my thoughts into consideration for planning research projects. I've also been able to observe firsthand the development and management of a newly founded research group, an experience that may prove invaluable in the future. Your professional support has been crucial to my scientific development. Sometimes during seminars, I am thinking about questions that you then ask to the speaker out loud, and in those moments I'm heartened that I have been trained to be a rigorous Agapie Group chemist. Although I will be an Agapie alumnus soon, I will forever feel invested in the success of your group.

Prof. John Bercaw, you are second only to Theo in influence on my development as a scientist. Thank you for letting me use your lab space before Theo's labs were complete. Your scientific advice has been very helpful numerous times. My experience of being a student and, later, head TA for Ch112 was very enlightening and my first real experience with designing and running an academic course. Also, your laid back demeanor has been a crucial counterbalance to the hustle and bustle of working in lab. I aspire to become an educator in your mold.

To the other members of my thesis committee, Dr. Jay Labinger and Profs. Bob Grubbs and Jim Heath, thank you for providing honest feedback on my scientific development. I felt that you were invested in my success, and I would have a hard time recommending a better thesis committee for any new students. Prof. Jonas Peters, thank you for moving back to Caltech. Especially during the first few years, I learned a lot from and was inspired by the research that your group was conducting. Prof. Sarah Reisman, thank you for giving me the Ch242a treatment, a full course in named reactions, Bürgi-Dunitz angles, and humility.

I started conducting labwork with Theo while he was still working at Berkeley. Thus, a lot of my early training I owe to the senior Bercaw group members (Alex Miller, Steve Baldwin, Nilay Hazari, Ned West, Ian Tonks, and Dave Weinberg) and Alexandra Velian. Thank you for introducing me to Schlenk line and glovebox techniques. You were always willing to help, even though I didn't get many results that first year. I know from some of my early mentoring experiences that I was not nearly as patient a mentor as you all were with me. Especially you, Lil' Alex. I can only imagine what you were

thinking as you, a sleep-deprived undergrad, were holding my (rubber-sheathed) hand during my first glovebox forays.

Agapie group, I have shared so many triumphs and failures with you that I feel like we're comrades-in-arms forever. Someone famous once said, "There are no atheists in gloveboxes," and I'm glad to have shared lab time with such a great group of people. Emily Tsui, thank you for being the smart one in the group to whom I could always ask chemistry questions. Steven Chao, I enjoyed founding Team Phosphine with you, and I hope you're doing well. Maddy, thank you for keeping us all safe as the Safety Officer, and for being the outgoing one who would break that awkward silence between lighting the birthday cake candles and "Happy birthday to you..." Co-hosting IOS with anyone else wouldn't have worked. Paul, I've been a huge fan of your chemistry the last couple of years, and I'm glad to have played a supporting role in some of it. To Sandy, thank you for showing me the good eats to be had in the SGV. Davide Lionetti and Jacob Kanady, thanks for initially bringing some bromance to the group, which was lacking in those early "weird vibe" years. You two were the only people I remember actively recruiting to join the group. Guy Edouard, Kyle Horak, Justin Henthorn, Josh Wiensch, and Josh Buss, you are now senior grad students, I wish you all the best in that role. Marcus Low, Jess Sampson, and HB Lee, y'all better buckle up for the next few years because the rate of chemistry in the Agapie group during your first summer is astounding. To the undergrads I interacted most with, Eva Nichols, Jade Shi, and Chung-Sun Chan, I'm pleasantly surprised that I only put one of you off of graduate research. You're a resilient bunch. And finally to the post-docs, Drs. Dave Herbert, Po-

Heng Lin, Graham de Ruiter, thanks for doing really well and inspiring me to get my Ph. D.

The resources at Caltech have been exceptional. Thank you Drs. Scott Virgil, Dave VanderVelde, Larry Henling, Mike Day, Mike Takase, Naseem Torian and Mona Shahgoli for help with advanced instruments. Larry gets extra special thanks for having a nose for free food and working late hours.

I owe my current interest in chemistry to fantastic education from my high school and undergraduate teachers and mentors: Shane Thread, Richard Lord, and Profs. Dan Mindiola, Dongwhan Lee, and Mookie Baik. And thanks, Mookie, for introducing me to academic research and supporting me over the years.

Thanks to my friends and family, who kept me sane when I wasn't in lab. In particular thanks to Lindsay Repka, Amaruka Hazari, Loi Do, and Pegah Seddiggan for playing tennis with me, even after I sprained my wrist from a bicycling accident and had to learn how to play with my left hand. Thanks to Rachel Klet, Leslie O'Leary, and Alicia Chang for getting me motivated to go cardio kickboxing. And, although I'm semi-retired these days, thanks to the Cp All-Stars basketball team (aka Buckets aka Three Turnovers per Hour): John Anderson, Henry Fong, Matt Chao, Aaron Sattler, Guy, Josh W., Josh B., Charles McCrory, Marc-Etienne Moret, and many others. We were truly awful, but we played our hearts out. The one SoCal activity I'll miss most is hiking. I went on hikes in the Sierras and San Gabriels with many of the people listed above for other reasons, but big thanks go to Emily, Josh B., and Davide for organizing our Mt. Whitney expedition! But seriously, let's never do a Whitney day hike again. Scaling the tallest peak in the lower 48 is nothing compared to the marathon we're all running.

ABSTRACT

Understanding and catalyzing chemical reactions requiring multiple electron transfers is an endeavor relevant to many outstanding challenges in the field of chemistry. To study multi-electron reactions, a terphenyl diphosphine framework was designed to support one or more metals in multiple redox states via stabilizing interactions with the central arene of the terphenyl backbone. A variety of unusual compounds and reactions and their relevance toward prominent research efforts in chemistry are the subject of this dissertation.

Chapter 2 introduces the *para*-terphenyl diphosphine framework and its coordination chemistry with group 10 transition metal centers. Both mononuclear and dinuclear compounds are characterized. In many cases, the metal center(s) are stabilized by the terphenyl central arene. These metal–arene interactions are characterized both statically, in the solid state, and fluxionally, in solution. As a proof-of-principle, a dinickel framework is shown to span multiple redox states, showing that multielectron chemistry can be supported by the coordinatively flexible terphenyl diphosphine.

Chapter 3 presents reactivity of the terphenyl diphosphine when bound to a metal center. Because of the dearomatizing effect of the metal center, the central arene of the ligand is susceptible to reactions that do not normally affect arenes. In particular, Ni-to-arene H-transfer and arene dihydrogenation reactions are presented. Additionally, evidence for reversibility of the Ni-to-arene H-transfer is discussed.

Chapter 4 expands beyond the chelated metal-arene interactions of the previous chapters. A dipalladium(I) terphenyl diphosphine framework is used to bind a variety of exogenous organic ligands including arenes, dienes, heteroarenes, thioethers, and

anionic ligands. The compounds are structurally characterized, and many ligands exhibit unprecedented binding modes across two metal centers. The relative binding affinities are evaluated spectroscopically, and equilibrium binding constants for the examined ligands are determined to span over 13 orders of magnitude. As an application of this framework, mild hydrogenation conditions of bound thiophene are presented.

Chapter 5 studies nickel-mediated C–O bond cleavage of aryl alkyl ethers, a transformation with emerging applications in fields such as lignin biofuels and organic methodology. Other group members have shown the mechanism of C–O bond cleavage of an aryl methyl ether incorporated into a *meta*-terphenyl diphosphine framework to proceed through β -H elimination of an alkoxide. First, the electronic selectivity of the model system is examined computationally and compared with catalytic systems. The lessons learned from the model system are then applied to isotopic labeling studies for catalytic aryl alkyl ether cleavage under H₂. Results from selective deuteration experiments and mass spectrometry draw a clear analogy between the mechanisms of the model and catalytic systems that does not require H₂ for C–O bond cleavage, although H₂ is proposed to play a role in catalyst activation and catalytic turnover.

Appendix A presents initial efforts toward heterodinuclear complexes as models for CO dehydrogenase and Fischer Tropsch chemistry. A catechol-incorporating terphenyl diphosphine is reported, and metal complexes thereof are discussed. Appendix B highlights some structurally characterized terphenyl diphosphine complexes that either do not thematically belong in the research chapters or proved to be difficult to reproduce. These compounds show unusual coordination modes of the terphenyl diphosphine from which other researchers may glean insights.

TABLE OF CONTENTS

Dedication	iii
Acknowledgements	iv
Abstract	ix
Table of Contents	xi
List of Figures	xiii
List of Schemes	xvi
List of Tables, Charts, and Equations	xviii
Chapter 1	1
General Introduction	
Chapter 2	6
MONO- AND DINUCLEAR GROUP 10 METAL COMPLEXES SUPPORTED BY METAL-ARENE INTERACTIONS FROM PARA-TERPHENYL DIPHOSPHINE LIGANDS	
Abstract	7
Introduction	8
Results and Discussion	9
Conclusions	35
Experimental Section	36
References	57
Chapter 3	64
INTRAMOLECULAR DEAROMATIZATION REACTIONS OF MONONICKEL TERPHENYL DIPHOSPHINE COMPOUNDS	
Abstract	65
Introduction	66
Results and Discussions	66
Conclusions	82
Experimental Section	82
References	97
Chapter 4	102
DIPALLADIUM(I) TERPHENYL DIPHOSPHINE COMPLEXES AS MODELS FOR TWO-SITE ADSORPTION AND ACTIVATION OF ORGANIC MOLECULES	
Abstract	103
Introduction	104
Results and Discussion	105
Conclusions	132
Experimental Section	133
References	156
	163

Chapter 5	
COMPUTATIONAL AND ISOTOPIC LABELING STUDIES ON NICKEL-MEDIATED HYDROGENOLYSIS OF C-O BONDS OF ARYL ALKYL ETHERS	
Abstract	164
Introduction	165
Results and Discussion	167
Conclusions	177
Experimental Section	178
References	199
Appendix A	203
TOWARD HETERODINUCLEAR ACTIVATION OF SMALL MOLECULES SUPPORTED BY A NOVEL CATECHOL-DIPHOSPHINE LIGAND	
Abstract	204
Introduction	205
Results and Discussion	207
Conclusions	221
Experimental Section	222
References	233
Appendix B	237
NOVEL COORDINATION COMPOUNDS OF PARA-TERPHENYL DIPHOSPHINES	
Abstract	238
Introduction	239
Results and Discussion	239
Conclusions	241
Experimental Section	--
References	--
Appendix C	243
Spectra	
Chapter 2	244
Chapter 3	259
Chapter 4	266
Appendix A	291

LIST OF FIGURES

Chapter 2	
Figure 2.1	13
Solid-state structures of mononuclear <i>para</i> -terphenyl diphosphine complexes	
Figure 2.2	14
Arene π -backbonding vs carbonyl/isonitrile relative binding angle	
Figure 2.3	16
VT ^1H NMR spectra and simulations for 2 and 5	
Figure 2.4	19
Cyclic voltammograms of 2 , 3 , 8 , and 9	
Figure 2.5	21
Experimental and simulated EPR spectra of 10	
Figure 2.6	22
DFT-calculated plots of spin density and SOMO of 10	
Figure 2.7	28
Solid-state structures of 12-14 , 15 , 16	
Figure 2.8	29
Comparison of Ni–Ni bond lengths between halide congener pairs	
Figure 2.9	35
Solid-state structure of 17	
Chapter 3	
Figure 3.1	68
Solid-state structures of 18 , 19 , 20 $\cdot\text{OTf}$, 20-MeCN $\cdot\text{OTf}$, 22 $\cdot\text{BArF}_{24}$	
Figure 3.2	78
COSY spectrum of 23	
Figure 3.3	78
Comparison of select ^1H NMR chemical shifts from 6 with literature compounds	
Figure 3.4	80
Stacked spectra of 23 and 23-d₄	
Figure 3.5	81
Hydrogenation of JohnPhos with Shvo's catalyst and $\text{Pd}_2(\text{dba})_3$	
Chapter 4	
Figure 4.1	108
Structures of 25 , 26 , 29-31 , 36-38	
Figure 4.2	118
Synthesis and solid-state structure of 39	
Figure 4.3	122
Structures of 42 and 43	
Figure 4.4	126
Equilibrium binding constants of various arenes and heterocycles	

Figure 4.5	127
Electrostatic potentials of unbound heterocycles	
Figure 4.6	128
Bonding interactions between diene HOMO/LUMO orbitals and Pd ₂ -based orbitals	
Figure 4.7	128
Select Pd ₂ -ligand bonding orbitals	
Figure 4.8	130
Qualitative MO bonding analysis of Pd ₂ compounds	
Figure 4.9	131
Full examples of Pd ₂ -ligand bonding orbitals	
Figure 4.10	152
Structures of 27 and 28	
Chapter 5	
Figure 5.1	168
GC-MS traces for naphthalene from reactions under D ₂	
Figure 5.2	169
GC-MS traces of synthesized partially deuterated alkoxy-naphthalenes	
Figure 5.3	170
GC-MS traces for naphthalene from reactions under H ₂	
Figure 5.4	171
GC-MS traces for hexyloxy trimethylsilyl ethers	
Figure 5.5	175
Experimentally observed rates of C-O bond cleavage	
Figure 5.6	176
Reaction energy plot for 44^R through 47^R	
Figure 5.7	177
Qualitative reaction energy diagrams for C-O bond cleavage (intra- vs intermolecular)	
Appendix A	
Figure A.1	206
Design of catechol-diphosphine to support a Ni-Fe CODH model	
Figure A.2	210
Preliminary crystal structure of 49	
Figure A.3	211
Preliminary crystal structure of 50	
Figure A.4	212
Preliminary crystal structure of 51	
Figure A.5	213
Preliminary crystal structure of 52	
Figure A.6	214
Preliminary crystal structure of unexpected trinuclear products	

Figure A.7	217
Preliminary crystal structures of 56 ^{CF₃Ph} and 57 ^{CF₃Ph}	
Figure A.8	219
Preliminary crystal structure of 61 ^{CF₃Ph}	
Figure A.9	221
Preliminary crystal structure of 64 and 65	
Appendix B	
Figure B.1	240
Preliminary crystal structures of 66 and 67	
Figure B.2	240
Preliminary crystal structures of 68 and 69	
Figure B.3	241
Preliminary crystal structures of 70	
Appendix C	

Note: Appendix C is comprised exclusively of figures displaying NMR spectra for all of the compounds in this dissertation, and it would be impractical to enumerate the figures here. They are ordered in numerical order.

LIST OF SCHEMES

Chapter 2	
Scheme 2.1	11
Synthesis of zero-valent compounds 2-5	
Scheme 2.2	11
Synthesis of Ni(0) compounds 8 and 9	
Scheme 2.3	15
Possible intermediates for central arene exchange	
Scheme 2.4	18
Phosphine dissociation-mediated ring whizzing	
Scheme 2.5	20
Chemical oxidation of 2	
Scheme 2.6	23
Protonation of 3	
Scheme 2.7	27
Synthesis of dinickel(I) halide compounds 12-15	
Scheme 2.8	27
Synthesis of biphenyldiyl complex 16	
Scheme 2.9	32
Potential exchange mechanisms that retain a Ni-Ni bond	
Scheme 2.10	34
Isotope labeling crossover experiment with 2 and 16	
Scheme 2.11	34
Mechanisms for reaction of 16 with dichloroalkanes	
Chapter 3	
Scheme 3.1	67
Synthesis and ligand disproportionation of 18	
Scheme 3.2	70
Synthesis, acetonitrile coordination, and Ni-to-Arene H-transfer	
Scheme 3.3	73
Isotope scrambling mechanisms for 20 and 18	
Scheme 3.4	77
Optimized conditions for hydrogenation of 2 by Shvo's Catalyst	
Scheme 3.5	79
Two mechanisms for hydrogenation of 2	
Chapter 4	
Scheme 4.1	106
Synthesis of dipalladium(I) compounds 25-28	
Scheme 4.2	114
Fluxional processes for heterocycle adducts	
Scheme 4.3	120
Hydrogenation and direct routes to tetrahydrothiophene adduct 40	

Scheme 4.4	121
Synthesis of allyl species 20 and heteroallyl species 21	
Chapter 5	
Scheme 5.1	166
Mechanism for Ni-mediated cleavage of model aryl alkyl ether by Kelley and Edouard	
Scheme 5.2	167
Representative catalytic hydrogenolysis of aryl alkyl ethers	
Scheme 5.3	172
Isotope scrambling into hexyloxytrimethylsilane	
Scheme 5.4	173
Mechanisms for catalytic conversion of aryl alkyl ethers to arenes	
Scheme 5.5	176
Computational models for stoichiometric C-O activation	
Appendix A	
Scheme A.1	208
Six-step synthesis of catechol diphosphine 48	
Scheme A.2	210
Well-characterized phosphine metallations of 48	
Scheme A.3	216
Protecting groups for catechol functionality	
Scheme A.4	218
Rhenium Pentacarbonyl chloride metallation	
Scheme A.5	219
Reactions of cationic rhenium tricarbonyl complexes with hydrides	
Scheme A.6	220
Deprotection and scandium attachment of 62	

LIST OF TABLES, CHARTS, AND EQUATIONS

Chapter 2	
Chart 2.1	8
Metal-Arene interaction classes	
Table 2.1	13
Central arene metrics for mononuclear complexes	
Chart 2.2	25
Dinickel complexes with bridging arenes	
Table 2.2	53
Crystal and refinement data for complexes 2-5, 8-11	
Table 2.3	54
Crystal and refinement data for complexes 12-17	
Chapter 3	
Equation 3.1	72
Chloride-induced arene-to-Ni H-transfer	
Equation 3.2	73
Isotope labeling conversion of 20-d₄ to 21-d₄	
Equation 3.3	73
Isotope labeling conversion of 18-d₄ to 19-d_x and 1-d_(4-x)	
Table 3.1	94
Crystal and refinement data for complexes 12-17	
Chapter 4	
Chart 4.1	105
Representation of dipalladium(I) compounds	
Equation 4.1	107
Exchange of central arene protons	
Equation 4.2	123
Equilibrium ligand binding experiments	
Chapter 5	
Table 5.1	174
Results of various labeling studies with triethylsilane	
Appendix A	
Chart A.1	205
Proposed active sites for Ni-Fe and Cu-Mo CODH	
Equation A.1	205
Water-gas shift reaction	
Appendix B	
Chart B.1	239
Unexpected compounds of 1 characterized by XRD	

CHAPTER 1

General Introduction

This dissertation is focused on studying metal-arene interactions and, specifically, their effects in an unusual terphenyl diphosphine environment. The study of such interactions begins with basic coordination chemistry and progresses through their transient role in catalysis on aromatic substrates. Although a few different phosphine ligands are presented in this work, they are all interrelated by forcing metal-arene interactions through rigidly oriented phosphine chelation. Although organometallic chemists have studied metal-arene interactions since the synthesis of bis(benzene)chromium in the middle of the 20th century, very few studies have been performed on chelation-enforced metal-arene interactions. With this P-arene-P framework, a variety of novel fundamental studies are presented. Thus, each research chapter of this dissertation contains a separate introduction with relevant background information and literature references; the purpose of this general introduction is to explain the author's rationale and provide a narrative for this research.

Organometallic chemistry at mononuclear transition metal sites has been well-studied, and ongoing research efforts will continue to broaden the scope of reactions that can be catalyzed at one metal center. Organometallic chemistry of multinuclear or multifunctional complexes, on the other hand, by virtue of having multiple moving parts, is less well understood. For instance, trends for rates of fundamental organometallic processes, such as ligand dissociation, oxidative addition, and reductive elimination, going down a group of the periodic table have been thoroughly studied and are now taught to undergraduate students. Yet those trends have been largely based on experimental work with mononuclear complexes. It is unclear if those trends would be predictive for multinuclear complexes. Recent research efforts toward catalysis at

heterodinuclear or bifunctional transition metal complexes have only scratched the surface of the possible permutations of nuclearity, metal, and pendant functional groups that could be explored. Thus, this research was directed toward to exploration of fundamental organometallic processes at multinuclear complexes.

Initially, a ligand was designed to study such processes using a rigid aromatic spacer between two donors, in order to bind more than one metal center. The central arene was also envisioned as a potential bridging ligand for multiple metal centers. A *para*-terphenyl diphosphine of this type was first synthesized and studied by another member of the group (Alexandra Velian).

A C–C bond forming reaction was discovered by dissolving a reactive dinickel diaryl compound in dichloromethane, resulting in activation of two C–Cl bonds and formation of two C–C bonds. This demonstration of multicentered reactivity is detailed in Chapter 2. However, one or two anionic bridging ligands, two phosphines, a Ni–Ni bond, and persistent Ni–arene interactions made for relatively unreactive compounds. Reducing the dinickel dichloride compound, to attempt to isolate a reactive dinickel(0) compound, yielded complex reaction mixtures, in some cases including mononickel products. It should be noted that a related *para*-terphenyl dicarbene ligand framework was developed by another group member and supported reduction of a dinickel dihalide precursor to a putative dinickel(0) compound (Emily Tsui). Thus, to support a dinuclear moiety in a variety of oxidation states, careful tuning of the ligand geometry and electronics may be required.

At the same time, the metal–arene interactions, which were observed crystallographically, were examined. Despite the increasing ubiquity and diversity of

multidentate ligands in transition metal compounds, there were few preexisting examples of π -bound arenes acting as a central donor in a rigid chelating ligand.

Further studies were directed toward chemistry supported by metal-arene interactions. I worked with undergraduate students Eva Nichols and Jade Shi, who were able to demonstrate chelated metal-arene interactions with a variety of mid-to-late transition metals. In a mononickel system, I was able to study H-transfer between nickel and the central arene (Chapter 3). In work with dipalladium complexes, I found the terphenyl diphosphine to act as a template for binding of an exogenous arene to form mixed dinuclear sandwich complexes (Chapter 4). My initial work demonstrating the utility of enforced metal-arene interactions in models for (otherwise) difficult to study processes led Paul Kelley and Guy Edouard to study related *meta*-terphenyl diphosphines as model substrates for C-O bond cleavage, a transformation with relevance to fine chemicals synthesis and biomass conversion. I was interested in determining if insights from Paul and Guy's model system were applicable to poorly-understood catalytic systems, and gratifyingly found evidence that that a similar mechanism is operative in both systems (Chapter 5).

In total, this dissertation shows that transient metal-arene interactions play a significant role in chemical transformations. By affixing the metal center to the arene with two pendant phosphines, a variety of unusual processes and mechanisms could be studied. Moving forward, I am interested to see if incorporation of redox-active or donor-functionalized central arenes into terphenyl-based complexes will lead to new chemistry. My initial efforts toward heterodinuclear compounds supported by a central

catecholate moiety are detailed in Appendix A, and I know younger group members including Justin Henthorn and Kyle Horak are following similar lines of research.

CHAPTER 2

MONO- AND DINUCLEAR GROUP 10 METAL COMPLEXES SUPPORTED BY METAL-ARENE INTERACTIONS FROM PARA-TERPHENYL DIPHOSPHINE LIGANDS

Published in part as:

Velian, A., Lin, S., Miller, A. J. M., Day, M. W., Agapie, T. *J. Am. Chem. Soc.*, **2010**, *132*, 6296-6297.

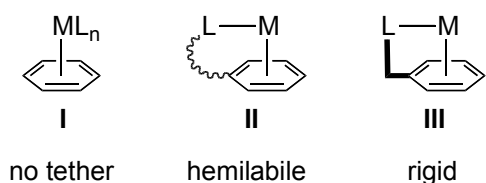
ABSTRACT

Mono- and bimetallic complexes of nickel and palladium in various oxidation states are supported by a common terphenyl diphosphine. The reported complexes show diverse metal–arene interactions in the solid state, which are fluxional in solution. The activation energy for these fluxional processes are analyzed by variable temperature NMR and found to be consistent with a ring-whizzing mechanism. In many cases, highly unusual binding motifs are enforced by the constrained geometry of the terphenyl scaffold. The complexes are analyzed by electrochemistry. While most of the complexes exhibit binding of one double-bond of the central arene per metal center, an *o,o'*-biphenyldiyl dinickel complex exhibits a $\mu\text{-}\eta^3\text{:}\eta^3$ binding mode with a highly deplanarized central ring. Reaction of this complex with CO and dichloroalkanes lead to fluorene derivatives, demonstrating the formation of carbon–carbon bonds at a bimetallic moiety and the ability of the dinucleating framework to hold two metal centers together across three or four oxidation states.

INTRODUCTION

Arenes have been used as labile π -complexed ligands in a variety of organometallic complexes. They are generally inert and their binding hapticity can vary from between η^1 to η^6 to stabilize reactive metal centers.¹ Additionally, arenes can serve as a bridging ligand for two or even three metal centers.² There are three general classes of monocyclic arene complexes determined by the topological relation of the metal-arene interaction. (Chart 2.1)

Chart 2.1. Metal-Arene Interaction Classes



In the simplest type of metal arene complex (I), the arene is not covalently tethered to another donor. The exogenous arene is held in place purely by attractive metal-arene interactions. In some cases, upon dissociation of the arene, the unmasked metal center is highly reactive.³ As arenes have been incorporated as structural elements in bulky ligands, dimeric complexes held together by a reciprocal pair of metal-arene interactions have been reported.⁴ For instance, a dimeric nickel carbene complex reduces CO_2 to CO ,³ and a dimeric nickel β -diketiminato complex reacts with N_2 .⁵

In an effort to modulate the reactivity of arene-capped metal complexes, the arene can be flexibly tethered to a more strongly binding ligand (class II). Similar to class I complexes, attractive metal-arene interactions predominate. Unique to class II complexes, however, is that following dissociation of the arene and reaction at the unveiled metal center, the arene readily recoordinates. Hemilability allows for a single ligand to have multiple coordination modes and support a wide range of redox states.⁶⁻¹¹ Thus, class II complexes has been developed as catalysts in which the arene coordination works in lockstep with a catalytic cycle⁶ or in which arene coordination (and hence catalyst behavior) can be switched by the oxidation state of a redox-active moiety attached to the arene.⁹⁻¹¹

Finally, metal arene interactions may be enforced by a rigid attachment of the arene to another donor (class III). Unlike in the previous two classes, attractive metal-arene interactions are not required in class III complexes. Even if only a weak metal-arene interaction is present, the arene must stay near the metal center and exhibit a more persistent effect on the metal center than arenes in class II complexes. Prototypical motifs employed in this class include pincer,¹²⁻¹⁴ cage,^{15,16} and macrocyclic^{17,18} complexes in which multiple donors are tethered to a central arene.

A unique motif employed in enforcing metal arene interactions is the dialkylbiarylphosphine pioneered by Buchwald for state-of-the-art cross-coupling catalysis. Although rotation about the P–biaryl bond allows for rotational isomers without close metal-arene contacts, if the P atom and biaryl have suitably large substituents, the phosphine lone pair prefers to orient over the π -system of the terminal arene.¹⁹ Thus, despite having as few as one non-arene donor, dialkylbiarylphosphines effectively enforce metal-arene proximity, and metal complexes can be classified as class III. Indeed, mononuclear Pd(0) and Pd(II) and dinuclear Pd(I) complexes have been crystallographically characterized. There is, however, a conspicuous lack of nickel congeners in the literature, given the rich chemistry generally available to these metal centers.

In order to study class III metal-arene interactions, a *p*-terphenyl diphosphine framework was envisioned as to coordinate one or two metal centers. While a mononuclear rhodium complex had been previously reported with a 2',3'5',6'-tetraphenyl variant of this scaffold,¹³ a more general synthesis and richer coordination chemistry was expected of our system.

RESULTS AND DISCUSSION

To examine a variety of metal-arene interactions, nickel and palladium compounds with *para*-terphenyl diphosphines were synthesized and characterized by single-crystal X-ray

diffraction (XRD), nuclear magnetic resonance (NMR) spectroscopy, cyclic voltammetry (CV), electron paramagnetic resonance (EPR) spectroscopy, and density functional theory (DFT) calculations. For organizational purposes, this chapter will discuss three groups of compounds: zero-valent mononuclear, oxidized mononuclear, and dinickel complexes. Nickel hydride and dipalladium complexes are only briefly mentioned in this chapter but are the focus of Chapters 3 and 4, respectively.

1. Zero-Valent Mononuclear Complexes

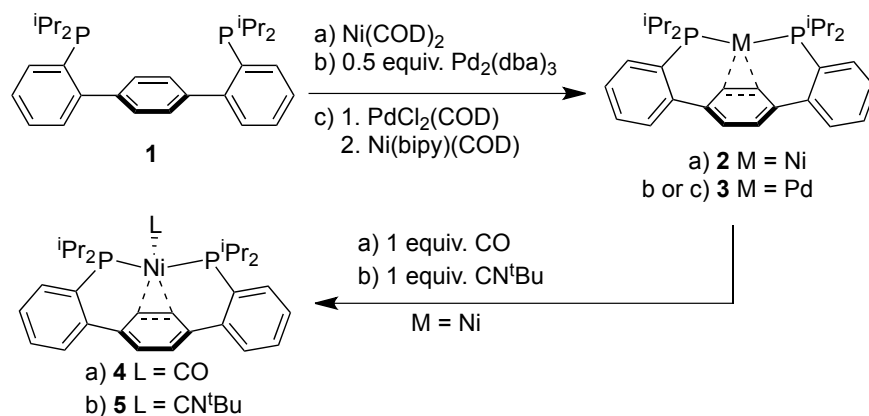
1.1. Synthesis. M(0) complexes were targeted by reaction with M(0) precursors (M = Ni, Pd; Scheme 2.1). A previously reported reaction of **1** with Ni(COD)₂ (COD = 1,5-cyclooctadiene) proceeded cleanly to form dark red Ni(0) complex **2**.²⁰ Analogous reaction of **1** with Pd₂(dba)₃ (dba = dibenzylideneacetone) yielded primarily Pd congener **3**, but dba byproducts from the reaction could not be successfully removed. Thus, *in situ* reductions of PdCl₂(COD) co-dissolved with **1** in THF (THF = tetrahydrofuran) were pursued. Although stirring with activated magnesium turnings afforded clean product, the reaction was very slow. Instead, Ni(bipy)(COD) (bipy = 2,2'-bipyridine) was found to be the most convenient reductant, with reasonable reaction times (less than 30 minutes) and facile separation of THF-insoluble byproduct Ni(bipy)Cl₂ by filtration, allowing isolation of orange Pd(0) complex **3**. Analogous reduction conditions with PtCl₂(COD) were explored, and Pt congener of **2** was identified by NMR spectroscopy and mass spectrometry (MS), but a clean product could not be isolated.

Metal-arene interactions were also interrogated by addition of an exogenous π -acidic ligand. Careful addition of 1 equiv. CO or CN^tBu to **2** yields the analogous yellow monocarbonyl complex **4** ($\nu_{\text{CO}} = 1926 \text{ cm}^{-1}$) or monoisocyanide complex **5** ($\nu_{\text{CN}} = 2026 \text{ cm}^{-1}$).

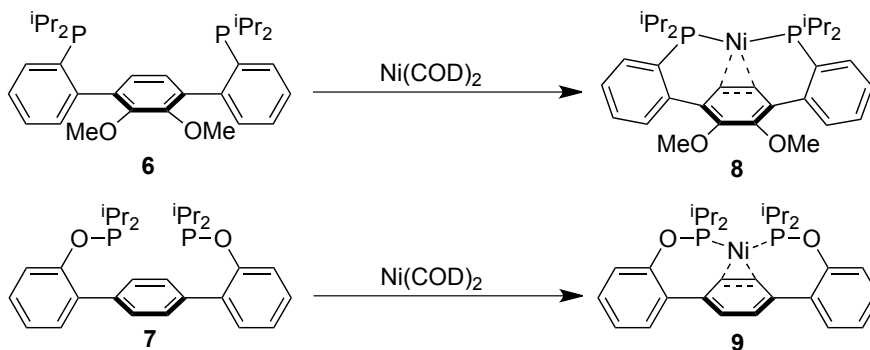
¹) (Scheme 2.1). The IR stretches are consistent with previously reported nickel(0) diphosphine monocarbonyl (1867-1996 cm⁻¹)²¹⁻²⁷ or monoisocyanide (1992-2094 cm⁻¹)^{28,29} complexes. Addition of more CO or CN^tBu led to formation of species exhibiting peaks corresponding to unbound phosphine by ³¹P NMR spectroscopy.

Two other terphenyl diphosphine ligands were designed and synthesized to explore electronic and steric effects on metal-arene interactions. Dimethoxy-substituted **6** and oxygen-linked **7** were metallated with Ni(COD)₂ to yield red mononickel complexes **8** and **9**, respectively (Scheme 2.2).

Scheme 2.1. Synthesis of M(0) Compounds 2-5.



Scheme 2.2. Synthesis of Ni(0) Compounds 8 and 9.



1.2. *Structural analysis.* Crystals of **2**, **3**, **4**, **5**, **8**, and **9** were grown and analyzed by XRD. All of these compounds display pseudo-C_s symmetry, with the metal bound by two

phosphines, two adjacent carbons of the central arene, and, for **4** and **5**, one exogenous ligand. The resulting alternation of short and long C–C bond lengths in the central arene can be understood as the result of localization of the double and single bonds so that one double bond can act as an olefinic ligand to the low-valent metal center.¹ In all cases, the bound C–C bond is elongated relative to the two unbound C–C double bonds. The extent of dearomatization in each compound can be gauged by the difference between the longest and shortest central arene C–C bond lengths (Δ_{CC} , Table 2.1). More dearomatization is expected to induce greater values of Δ_{CC} . The three three-coordinate Ni(0) compounds **2**, **8**, and **9** exhibit high Δ_{CC} values (>6.7 pm) that are similar to that of a previously reported *meta*-terphenyl diphosphine complex (7.0 pm).²¹ The particularly high value for **8** (8.3 pm) is due in part to the inherent asymmetry conferred by the methoxy substituents. For comparison, 1,2-dimethoxybenzene has been reported with $\Delta_{CC} = 3.4$ pm.³⁰ Ni generally binds better to π -acids than Pd. This difference is reflected in the low Δ_{CC} of **3** (3.6 pm).

Because **4** and **5** contain π -acidic ligands (L = CO, CN^tBu) competing with the central arene, the Δ_{CC} values are smaller than for **2**. Interestingly, although carbonyls and isonitriles are isoelectronic and similarly ranked ligands in the spectroelectrochemical series, **5** has a much larger Δ_{CC} than **4**. The bulky ^tBu group in **5** interacts with the phosphine substituents, forcing the angle between the Ni–(C=C) and Ni–L bonds to be less obtuse than the corresponding angle of the carbonyl ligand in **5** (99° vs. 106°). Because orthogonal π -acid ligands can participate in backbonding through different metal d-orbitals, backbonding in **5** is stronger than in **4**, and thus the Δ_{CC} of **5** is larger than that of **4**.

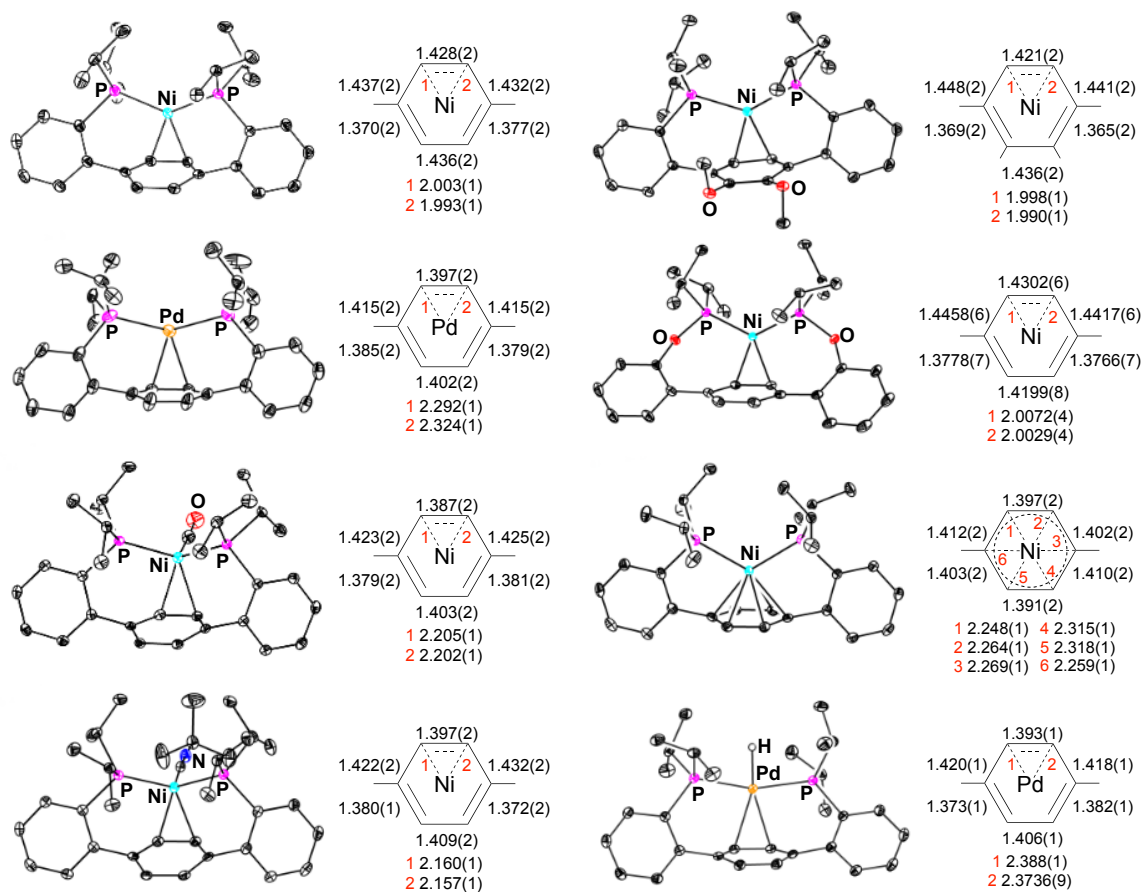


Figure 2.1. Solid-state structures of mononuclear *para*-terphenyl diphosphine complexes with central arene bond distances (Å). Left (from top to bottom): 2-5. Right: 8-11. Thermal ellipsoids are shown at 50% probability level. Non-hydride hydrogen atoms, solvent molecules, and outer-sphere anions are omitted for clarity.

Table 2.1. Central arene metrics for zero-valent complexes: Δ_{CC} (pm) and ^1H NMR peaks (samples at r.t. in C_6D_6 unless otherwise noted; δ (ppm))

	2	3	4	5	8	9	10 ^a	11 ^a
Δ_{CC}	6.7	3.6	4.6	6.0	8.3	6.9	2.2	4.7
^1H	5.42	6.73	6.72, 6.64	6.63, 6.21	4.52	5.82	^b	7.31

^a CD_3CN as NMR solvent. ^b paramagnetic species

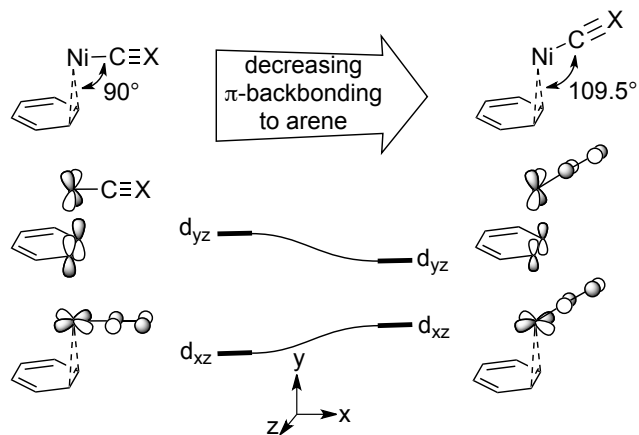


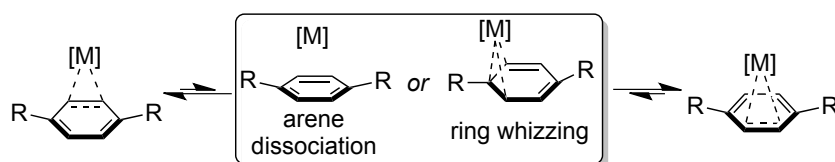
Figure 2.2. Arene π -backbonding vs. carbonyl/isonitrile relative binding angle.

The metal-arene interaction in **4** and **5** can also be interrogated by analysis of the exogenous π -acid ligand bond lengths. For **4**, the Ni-C(O) distance [1.778(2) Å] is longer than in comparable Ni(0)-phosphine-monocarbonyl complexes,^{23-26,31} and accordingly, the C-O distance [1.161(2) Å], is relatively short. For **5**, the Ni-C(N) bond length is longer than in a previously reported Ni(0)-phosphine-monoisonitrile complex [1.850(1) vs. 1.787(3) Å].²⁸ Instead, the Ni-C(N) bond length is more comparable to Ni(I) monoisonitrile complexes [Ni-C ~1.86 Å].²⁹ All of these bond lengths indicate that the arene acts as a weak π -acid, making the Ni center less electron rich and hence less tightly bound to the CO or CN^tBu.

1.3. Solution NMR spectroscopy. The metal-arene interaction can also be observed in solution by NMR spectroscopy. Dearomatization of the central arene disrupts ring current effects, and π -backbonding can increase the electron density of the central arene and induce diamagnetic shielding.³² Thus, the central arene ¹H NMR peaks appear in upfield areas of the spectrum typically reserved for olefinic moieties (Table 1). At room temperature, the three-coordinate complexes (**2**, **3**, **8**, and **9**) exhibit only one central arene ¹H NMR signal. Assuming fast rotation of the methoxy groups and the absence of non-interconverting isomers, this is expected for **8**. For **2**, **3**, and **10**, however, this feature reveals that the metal

center can rapidly exchange between two equivalent η^2 -binding sites: the front and back of the central arene (Scheme 2.3). In contrast, the four-coordinate species **4** and **5** exhibit two ^1H NMR central arene peaks integrating to two ^1H nuclei each,³³ suggesting that fluxionality of the metal-arene process is slow on the NMR time scale. To study the underlying fluxional processes governing these spectra, variable temperature (VT) NMR experiments were performed.

Scheme 2.3. Possible intermediates for central arene exchange



At room temperature, the central arene ^1H NMR peak of **2** is broad (half maximum full width = 93 Hz), suggesting that full line-shape analysis should be feasible. Thus, VT NMR study of **2** was conducted in d_8 -toluene (Figure 2.3). Below $-45\text{ }^\circ\text{C}$, sharp central arene singlets at 6.35 and 4.63 ppm suggest a C_s -symmetric structure, as observed in the solid state. At progressively increasing temperatures, these peaks broaden, coalesce at 5.42 ppm, and form a sharp singlet around $75\text{ }^\circ\text{C}$ (HMF_W = 10 Hz). This behavior is indicative of a degenerate exchange process involving coordination of the opposite pair of carbons of the central arene. Iterative line shape analysis of the central arene peaks (Figure 2.3) provides rate constants across this range of temperatures. The Eyring-Polanyi equation can then be used to determine the thermodynamic parameters of central arene inversion: $\Delta H^\ddagger = 13.07$ kcal/mol, $\Delta S^\ddagger = 3.08$ cal/mol·K.

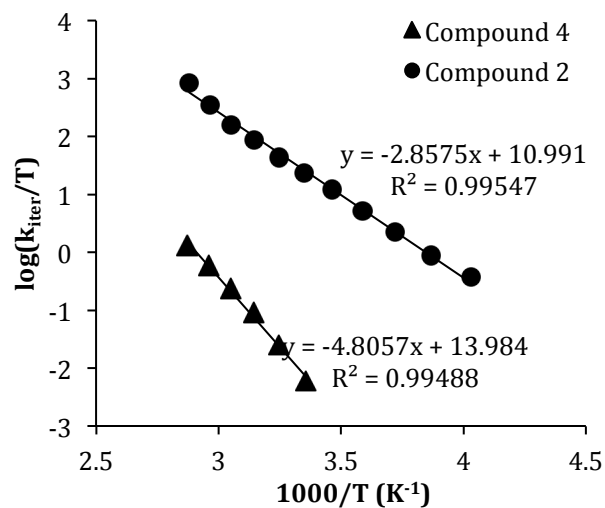
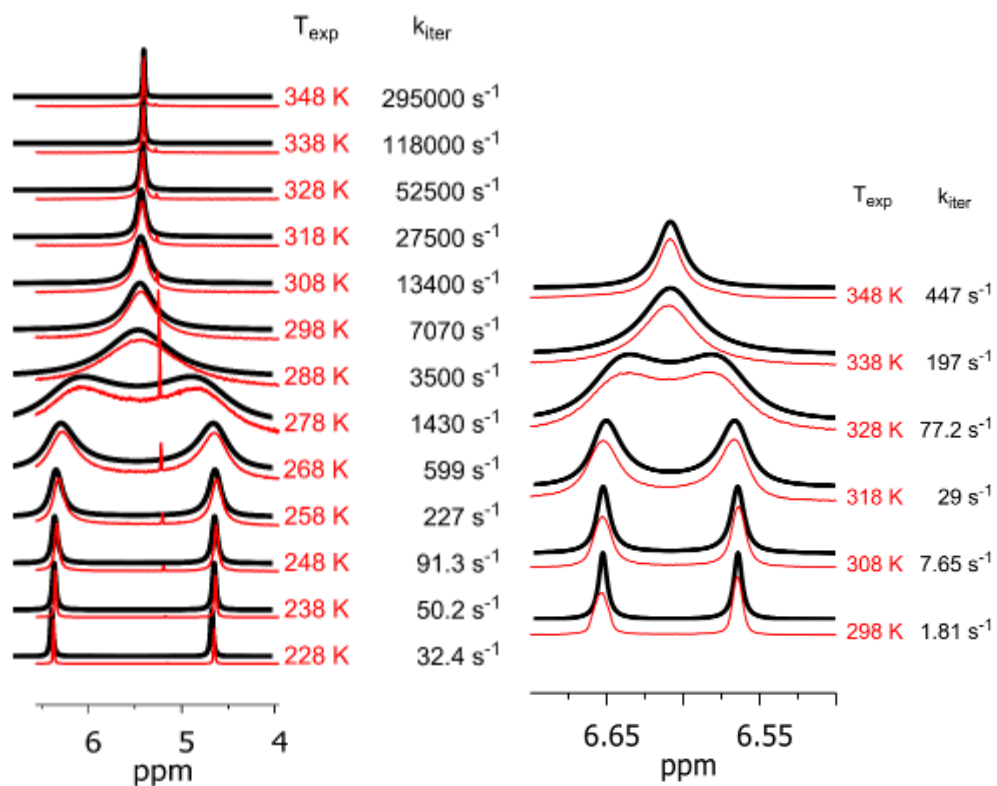


Figure 2.3. Top: VT ^1H NMR spectra (500 MHz, red), iteratively fit simulations (black), and corresponding rate constants for coalescence process (k_{iter}). 2 on left (d_8 -toluene), and 4 on right (C_6D_6). Bottom: corresponding Eyring-Polanyi plots.

One possible mechanism for the inversion of the central arene, involving η^3 -bound intermediates, is known as ring whizzing (Scheme 2.3). In other systems, ring whizzing³⁴ of monoarenes bound to Ni(0) is often too fast to resolve on the NMR timescale.³⁵⁻³⁷ For a bis(triethylphosphine)nickel•(1,2,4,5-tetrafluorobenzene) adduct, broad ¹H NMR spectra could not be fully decoalesced even at -90 °C, but the ring whizzing barrier was estimated to be 3.5 kcal/mol.³⁸ With the exception of interannular ring whizzing in nickel-polyacene adducts,³⁹⁻⁴¹ the exchange barrier in **2** is much larger than in previous Ni(0)-arene systems. This discrepancy could be accounted for by increased distortion of the terphenyl backbone in ring whizzing intermediates.

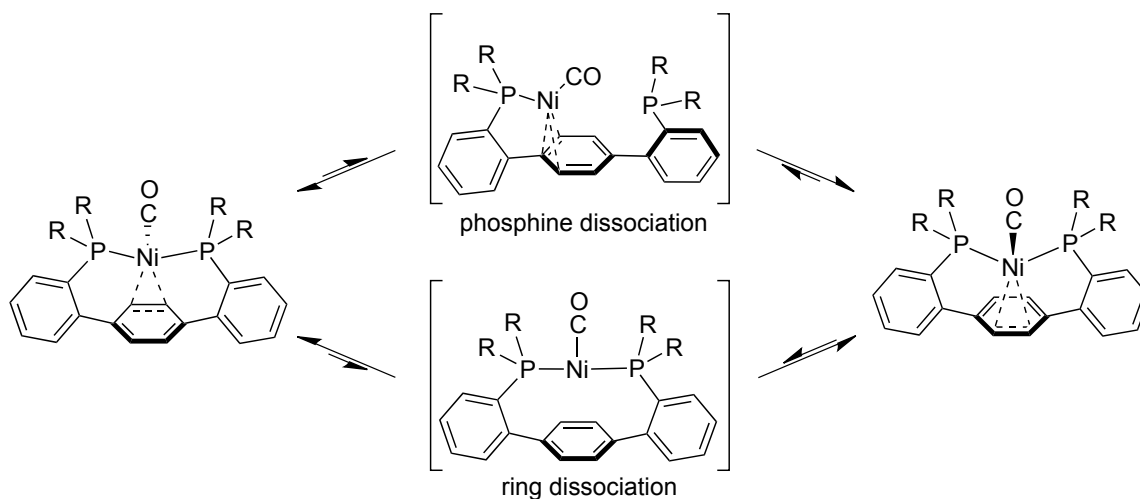
Alternatively, degenerate exchange could occur through arene dissociation (Scheme 2.3). Ni(0)-arene dissociation in various systems has been observed to be slow on the NMR timescale^{3,35,41} and calculated to be thermodynamically disfavored by >18 kcal/mol,⁴²⁻⁴⁴ markedly higher than the activation parameters for **2**. Because the central arene is tethered to the Ni center through the phosphine substituents, metal-arene dissociation in **2** would not unlock as many degrees of freedom as the previously studied systems with non-tethered arenes. So if arene dissociation were responsible for the fluxional behavior observed by ¹H NMR, the calculated enthalpy of activation would be over 18 kcal/mol. Thus, the VT NMR behavior of **2** is probably not the result of rapid central arene dissociation.

VT NMR study of **3** was also attempted, but the central arene ¹H signal remained a sharp singlet at temperatures as cold as -80 °C (*d*₈-toluene). Thus the exchange barrier is smaller for **3** than for **2**. This is consistent with the weaker π -interaction of Pd vs. Ni observed in the solid state.

VT NMR study of carbonyl complex **4** was performed. Coalescence occurs around 75 °C, but decomposition prevents observation of fast exchange at higher temperatures.

Iterative line shape analysis of the central arene peaks from 25 °C to 75 °C provides approximate rate constants for arene exchange (Figure 2.3, right), and an Eyring plot determines the thermodynamic parameters for molecular inversion: $\Delta H^\ddagger = 22.0$ kcal/mol, $\Delta S^\ddagger = 16.8$ cal/mol·K. The large positive entropy during inversion would be consistent with unlocking ~3-5 degrees of rotational conformational freedom in the inversion transition state.^{45,46} A transition state involving an unbound phosphine and ring whizzing (Scheme 2.4, top) could account for the large enthalpic and entropic parameters observed for **4**. An alternative exchange mechanism could be dissociation of the central arene, rotation of the Ni–CO bond perpendicular to the P–P vector, and recoordination of the central arene (Scheme 2.4, bottom). The latter pathway, which only unlocks rotation of the central arene and of the Ni–CO vector, may not account for the large observed ΔS^\ddagger , but has not been ruled out. Because the carbonyl ligand must move a large distance between the two conformations and the constrained geometry of the terphenyl diphosphine likely requires dissociation of a donor to facilitate degenerate exchange, overall the barrier for degenerated exchange is higher for **4** than for **2**.

Scheme 2.4. Phosphine dissociation-mediated ring whizzing



1.4. *Cyclic voltammetry.* The electrochemistry of complexes **2**, **3**, **8**, and **9** were examined with cyclic voltammetry. Ni(0) compounds **2** and **8** exhibit similar cyclic voltammograms (CVs) with two oxidation waves, assigned to Ni(0)/Ni(I) and Ni(I)/Ni(II) oxidations. The first waves are quasi-reversible, and **2** has a higher reduction potential ($E_{1/2}$) than **8** (-1.13 vs. -1.18 V; all potentials are referenced vs. $\text{FeCp}_2/[\text{FeCp}_2]^+$; Cp = cyclopentadienyl). The second oxidation waves are irreversible, although returning reduction waves are observed. Again, **2** is oxidized at a higher potential than **8** ($E_{\text{pa}} = -0.10$ vs. -0.18 V for 100 mV/s sweep rate). The relatively more negative reduction potentials of **8** can be rationalized by its more electron-rich central arene facilitating oxidation of the Ni center.

Terphenyl diphosphinite complex **9** exhibits one irreversible oxidative feature, assigned to a Ni(0)/Ni(I) transition, peaking at -0.98 V (100 mV/s sweep rate). The relatively higher oxidation potential of **9** vs. **2** agrees with phosphinite donors being less electron-rich than phosphine donors.⁴⁷

The CV of Pd(0) compound **3** is notably different from that of its Ni congener **2**. An oxidative wave near -0.45 V appears to be composed of two features at scan rates faster than 500 mV/s. The corresponding reduction wave, about equal in size to the sum of the oxidative features, appears singular at all scan rates. One explanation for these features is that **3** undergoes one-electron oxidation to a Pd(I) complex, which then disproportionates to **3** and a Pd(II) complex. If redox disproportionation occurs at an intermediate rate, then at slow scan rates very little Pd(I) should be oxidized by the electrode, and a single two-electron oxidative wave would be observed; and at fast scan rates unreacted Pd(I) complex would manifest as a second oxidative feature in the CV. Divalent d^8 -metal centers typically bind four ligands in a square planar geometry,⁴⁸ so the electrogenerated Pd(II) species may coordinate solvent. Thus the reductive wave, assigned as reduction of a Pd(II) solvent-

coordinated species, can appear as a single two-electron wave without violating microscopic reversibility.

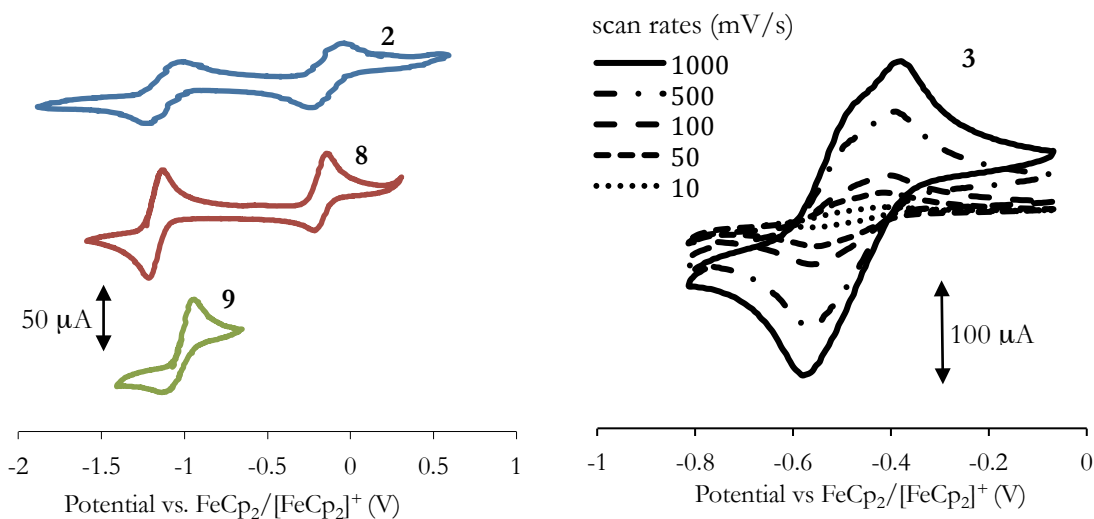
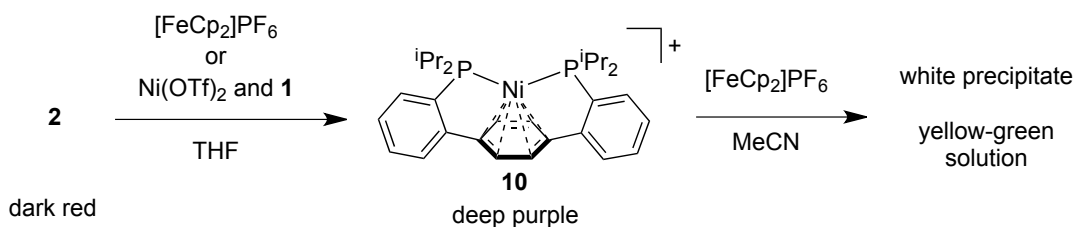


Figure 2.4. Cyclic voltammograms of (left, top to bottom; 100 mV/s scan rate) **2**, **8**, **9**, and (right) **3**. Data collected with 2 mM analyte in THF (100 mM Bu₄NPF₆).

2. Oxidized Mononuclear Complexes

2.1. Chemical oxidation of 2. The reversible first oxidative wave in the CV of **2** suggests the isolability of a Ni(I) complex. Indeed, **2** reacts with 1 equivalent of [FeCp₂]PF₆ in THF, yielding an orange solution with dark purple precipitate. ¹H NMR spectra of the homogenized reaction crude in CD₃CN show full conversion of **2** and generation of a sharp singlet at 4.18 ppm corresponding to ferrocene. Additionally, broad peaks at 11.31, 8.10, 4.04, and 0.16 ppm are observed. A purple compound, **10**-PF₆, exhibiting these broad NMR peaks can be isolated by triturating the reaction crude with toluene to remove ferrocene. A convenient alternative synthesis proceeds through comproportionation of a THF slurry of **1**, **2**, and Ni(OTf)₂ (OTf = triflate = trifluoromethanesulfonate) heated at 80 °C for 4 h, yielding two equivalents of **10**-OTf.

Scheme 2.5. Chemical oxidation of **2**



2.2. *Structure of 10.* After layering a MeCN solution of **10** over toluene, liquid diffusion afforded deep purple XRD-quality crystals. XRD analysis reveals that the nickel center is η^6 -bound by the central ring and that the triflate anion is not bound. The metal center is located 1.79 Å from the plane of the arene, with Ni–C distances ranging from 2.248(1) to 2.318(1) Å. The central arene retains aromaticity ($\Delta_{\text{CC}} = 2.1$ pm). The long Ni–C distances and smaller deformation of the central arene C–C bonds are reminiscent of cation-arene interactions.⁴⁶ The metal center's d^9 configuration, cationic charge, and relative positioning preclude strong π -backbonding to the central arene. Although diamagnetic Ni(0),^{3,49-52} Ni(II),⁵³⁻⁵⁷ or Ni(I)₂ complexes⁵⁸ with η^6 -arene ligands have been reported, **10** is the only known mononuclear Ni(I) η^6 -arene complex. The rarity of this motif is likely due in part to its formal 19 electron count.⁵⁸

2.3. *Electron Paramagnetic Resonance.* EPR spectra of **10** were collected in 1:1 MeCN/toluene. At 20 K, a broad rhombic spectrum is observed (Figure 2.5), and a suitable EPR simulation requires using large ³¹P hyperfine coupling constants, assuming equivalent phosphines ($g = [2.075, 2.440, 2.111]$; $A_{\text{p}} = [-2.75, 10.2, 135]$ G). Upon warming the EPR sample to room temperature, an isotropic signal ($g = 2.092$) is observed, again with very large ³¹P hyperfine coupling constants ($A_{\text{p}} = 188$ G). For reference, the previous highest reported A_{p} for a Ni(I) diphosphine complex, to the best of our knowledge, was 120 G.⁵⁹ Other Ni(I) diphosphine complexes have been reported with A_{p} between 5 and 100 G.^{21,60-63}

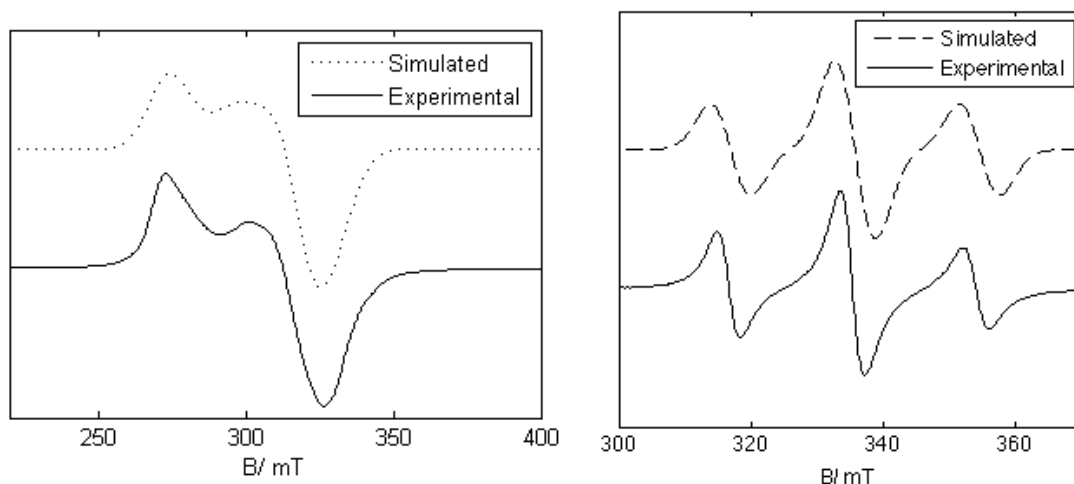


Figure 2.5. Experimental (X-band, solid black) and EasySpin-simulated (dashed) EPR spectra of **10** in 1:1 MeCN/toluene at 20 K (left) and room temperature (right).

EPR spectra of **10** (containing a perdeuterated central arene) exhibit identical spectra as **10**, suggesting that the unpaired electron spin is not strongly delocalized onto the central arene protons. Unrestricted density functional theory (DFT) was used to calculate the spin-density plot (Figure 2.6), and notable contributions are present from the phosphorous atoms (9% each) and *ipso*-carbon atoms of the central arene (8% each). The spin density plot also qualitatively correlates with the highest-occupied singly occupied orbital (SOMO).

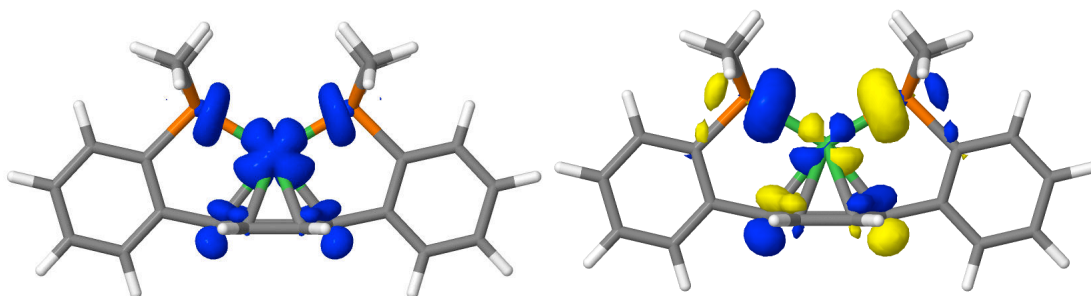


Figure 2.6. DFT-calculated isosurface plots of the spin density (left) and SOMO (right) (isovalue = 0.05) of **10**.

2.4. Accessing divalent complexes. According to the CVs of **2** and **3**, divalent Ni and Pd complexes should be accessible via chemical oxidation. Divalent d^8 -metal centers typically bind four ligands in a square planar geometry,⁴⁸ but the roles of the central arene, solvent

molecules, and weakly binding anions in that coordination sphere are not immediately obvious.

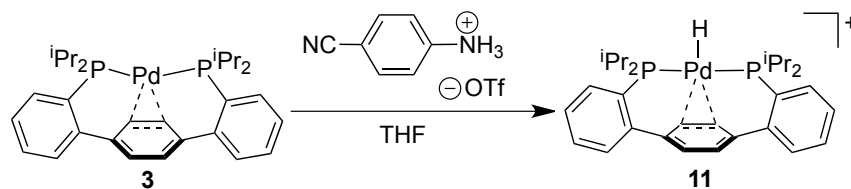
According to the CV of **2**, ferrocenium should oxidize **10**. Addition of $[\text{FeCp}_2]\text{PF}_6$ to **10** in MeCN results in formation of white precipitate out of a yellow-green solution (Scheme 2.5). These observations and NMR spectra of the reaction mixture are consistent with formation of insoluble $\text{Ni}(\text{PF}_6)_2$ and free **1**. As alternate routes to divalent nickel compounds, direct metallation of **1** with $\text{Ni}(\text{OTf})_2$ or $\text{NiCl}_2(\text{DME})$ (DME = 1,2-dimethoxyethane) does not show any signs of reaction. An explanation consistent with these observations and the irreversibility of the second oxidative wave in the CV of **2** is that a Ni(II) metal center may be too small to be stably bound by the rigid, trans-spanning diphosphine. If any Ni(II) compound is formed, phosphine(s) may dissociate, resulting in release of Ni(II) salts or formation of coordination polymers.

Similarly, accessing Pd(II) compounds is challenging. Chemical oxidations of **3** or metallations of **1** with Pd(II) precursors (e.g. $[\text{Pd}(\text{MeCN})_4](\text{BF}_4)_2$ or $\text{PdCl}_2(\text{COD})$) yield intractable mixtures of species with broad NMR features. These species in solution are unstable upon concentration and yield primarily insoluble orange precipitate. Although some mononuclear Pd(II) complexes have been crystallized by chance (see Appendix A), they have not been reliably reproduced. One possible explanation for the behavior of the proposed meta-stable Pd(II) complexes is phosphine dissociation followed by formation of an insoluble coordination polymer.

A strategy to disfavor formation of coordination polymers is minimization of steric repulsion between the terphenyl diphosphine framework and exogenous ligands that complete the square planar coordination sphere. For this purpose, installation of hydride ligands is ideal. Ni(II) hydride compounds can be accessed by protonation of **2**, but

discussion of their rich chemistry is reserved for Chapter 3. An analogous Pd hydride is synthesized by reaction of **3** with *p*-cyanoanilinium triflate in THF (Scheme 2.6). After triturating with benzene, the reaction mixture can be dissolved in MeCN and layered under Et₂O to yield pale yellow XRD-quality crystals of **11**.

Scheme 2.6. Protonation of 11



2.5. *Structural analysis of 11.* XRD analysis of **11** (Figure 2.1) shows that the Pd center is four-coordinate and square planar. The hydride ligand is positioned *trans* to a double bond of the central arene. The single and double bonds of the central arene are localized, and the resulting alternation of bond lengths is actually greater than for Pd(0) compound **3** ($\Delta_{CC} = 4.7$ vs. 3.6 pm).

While similar cationic palladium hydride complexes with monodentate phosphines,⁶⁴ bidentate diphosphines,^{65,66} and tridentate PXP pincer ligands (X = C, N, O)⁶⁷⁻⁷⁰ have been isolated, **11** is the first crystallographically characterized example of a palladium hydride bound to an unsaturated π -system. These species, which result from β -hydride elimination and precede olefin insertion in Pd-H bonds, have only previously been characterized by theory and spectroscopy.^{71,72} This rare motif is stabilized in **11** by (a) using an arene as the unsaturated π -system and (b) forcing the hydride to be *trans* to the arene by the topology of the tridentate terphenyl diphosphine framework. In contrast, the corresponding nickel hydride, discussed in detail in Chapter 3, is only meta-stable, and Ni-to-arene H-transfer is thermodynamically favored.

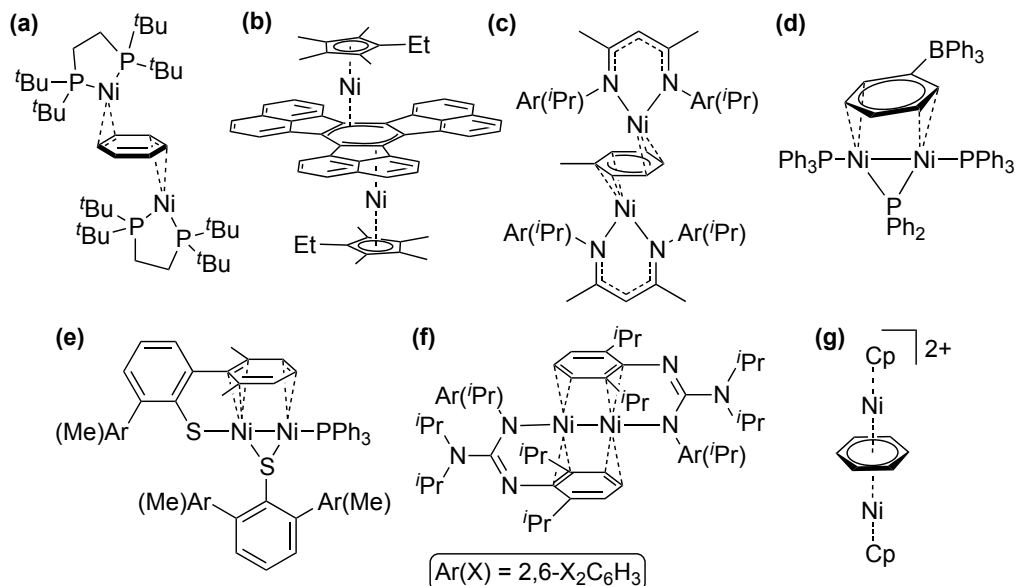
2.6. *Solution NMR spectroscopy.* NMR spectroscopy is a useful tool for identifying dearomatizing metal-arene interactions in oxidized mononuclear compounds. ^1H NMR spectra (CD_3CN) of **11** display a downfield triplet at -12.98 ppm that is assigned to Pd-H ($J_{\text{PH}} = 12$ Hz). A singlet at 7.31 ppm, assigned to the central arene protons, integrates to four nuclei. This singlet does not decoalesce at lower temperatures (-35 °C, CD_3CN). Thus, like Pd(0) complex **3**, exchange between the front and back of the central arene is facile and rapid on the NMR timescale. Although the central arene protons of **11** are relatively downfield vs. compounds **2-9**, the latter compounds are neutral and analyzed in a different NMR solvent. As a relative standard, the peripheral arene protons of **11** are all downfield of 7.66 ppm. Similarly, the ^{13}C NMR peaks corresponding to the central arene (124.9 and 118.4 ppm for *ipso*- and *ortho*-carbons, respectively) are well separated from the other aromatic carbons of **11** (148 through 128 ppm).

3. Dinuclear Complexes

Compounds 12-16 in this section were originally studied and reported by then-undergraduate Alexandra Velian.^{20,73} Their synthesis and structure are reproduced here to provide a comprehensive review of para-terphenyl diphosphine coordination chemistry and to segue into my study of their reactivity. We envisioned **1** as an excellent ligand for dinuclear moieties given the relatively rigid and large spacing of the two phosphines.⁷⁴ Furthermore, the central arene of **1** was expected to serve as a bridging ligand across two metals. There are several examples from the literature of dinickel compounds with bridging arenes that employ different ligands with different binding modes. Arenes can bridge two Ni(0) diphosphine fragments, binding as an $\mu\text{-}\eta^2\text{:}\eta^2\text{-}$ butadiene with an uncoordinated and localized double bond (Chart 2.2a).^{35,75} Arenes can also bridge Ni(I)₂ moieties, binding as $\mu\text{-}\eta^3\text{:}\eta^3\text{-}$ bisallyls (Chart 2.2b, c).^{4,76,77} Notably such complexes are often diamagnetic, suggesting either reduction of the arene with formation of Ni(II)₂ centers or antiferromagnetic coupling through arene-based orbitals. Furthermore,

arenes may bridge cofacial Ni(I)₂ moieties. Of the three previously known compounds to exhibit this characteristic, each has a different binding mode (Chart 2.2d-f).^{4,56,78} Finally, benzene has been shown to bridge two Ni(II) centers in a $\mu\text{-}\eta^6\text{:}\eta^6$ binding mode.⁷⁹

Chart 2.2. Dinickel complexes with bridging arenes.



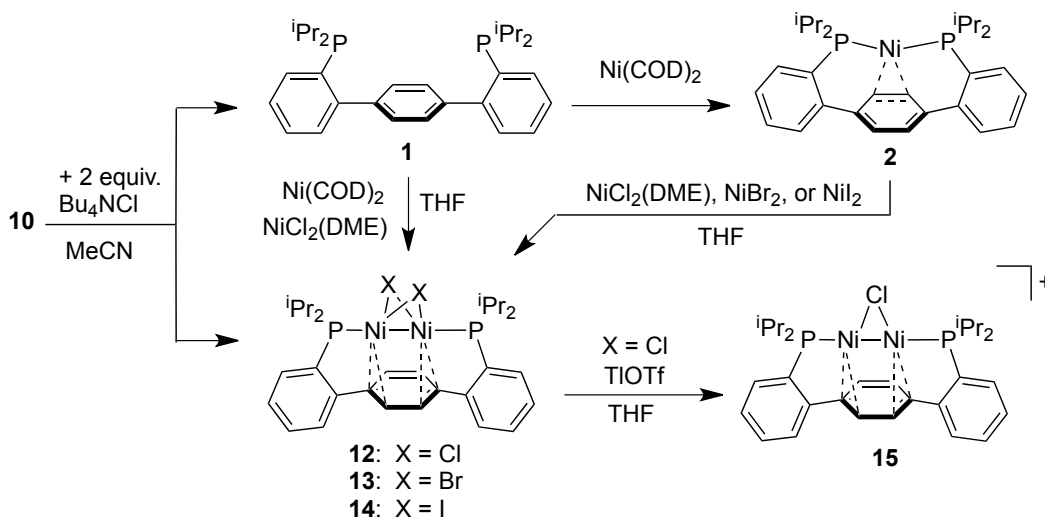
3.1. Synthesis. Comproportionation of Ni(COD)₂ and NiCl₂(DME) in the presence of **1** in THF solution (Scheme 2.7) yields a dark green solution displaying one ³¹P NMR singlet (47 ppm). The diamagnetic nature of this product is attributed to a Ni^I-Ni^I interaction. This same dark green mixture is observed upon reacting **2** and NiCl₂(DME). XRD studies of dark green crystals of **12** confirm its identity (*vide infra*). As an independent synthetic route, addition of 2 equiv. Bu₄NCl to cationic Ni(I) complex **10** cleanly yields a 1:1 mixture of **1** and **12**, as determined by ¹H and ³¹P NMR. This result suggests that the relatively rigid and widely spaced *para*-terphenyl diphosphine framework prefers to coordinate dimeric (Ni^ICl)₂ moieties over mononuclear Ni^ICl moieties.

Comproportionation of NiBr₂ or NiI₂ with **2** does not proceed at room temperature, perhaps owing to insolubility of the halide salts. However, heating the

reactions in THF at 70 °C cleanly yields halide congeners **13** (green-brown) or **14** (dark red), respectively. With these nickel(II) precursors, *in situ* comproportionation/metallation with **1** and Ni(COD)₂ yields complicated mixtures containing broad paramagnetically shifted peaks and a dark film on the reaction flask walls, possibly due to Ni(COD)₂ decomposition in heated THF (*vide infra*, synthesis of **8**). Compound **2** does not react with NiF₂ in refluxing THF.

A strategy to increase the reactivity of the dinickel moiety is halide abstraction. Adding TlOTf to a THF solution of **12** yields blue product **15** and insoluble white precipitate (presumably TlCl). Addition of excess TlOTf does not abstract a second chloride.

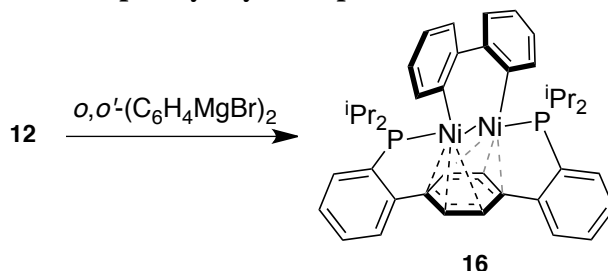
Scheme 2.7. Synthesis of dinickel(I) halide compounds 12-15.



In an effort to document redox organometallic reactivity at the dinuclear core of **12**, derivatives displaying hydrocarbyl ligands were targeted. Such complexes are expected to provide examples of reductive elimination or oxidative addition at a bimetallic nickel complex. Attempts to make a diphenyl complex by treating **12** with PhMgBr have led to the formation of biphenyl, presumably by reductive elimination from the *in situ* generated Ni^I₂Ph₂(PR₃)₂ target. Reaction of **12** with *o,o'*-biphenyldiyl

Grignard affords an isolable dinickel biphenyldiyl complex (**16**, Scheme 2.8), probably due to lack of facile decomposition pathways such as reductive or β -H elimination.

Scheme 2.8. Synthesis of biphenyldiyl complex 16



3.2. *Solid-state structures.* Single crystal X-ray diffraction (XRD) studies of **12-16** were performed. The structure of **12** reveals that the targeted Ni_2 moiety is coordinated by the phosphines in a nearly linear PNiNiP arrangement (Figure 2.7). To accommodate the coordination of both phosphines to the dinickel unit, the peripheral aryl rings are strained 16° downward relative to the plane of the central arene. The metal centers are bridged by chlorides and interact with a vicinal diene moiety of the central ring of the terphenyl framework ($\text{Ni}-\text{C} \sim 2.05$ to 2.10 \AA). The uncoordinated double bond of the central arene is noticeably contracted, with a Δ_{CC} of 9.7 pm . These metal–arene interactions are likely important for the stability and isolation of **3**. Dinuclear complexes stabilized by inter- and intramolecular interactions between an arene and the $\text{Ni}^{\text{I}}-\text{Ni}^{\text{I}}$ moiety have been reported recently (Chart 2.2).^{56,78}

Halide congeners **13** and **14** are essentially isostructural to **12**. The $\text{Ni}-\text{Ni}$ distance remains remarkably constant across this series ($2.3658(2)$ to $2.4071(2) \text{ \AA}$), despite the much larger radius of iodine vs. chloride. This is probably an effect of the constraining terphenyl backbone. For comparison, all other pairs of structurally characterized dinickel dihalide congeners (which are not constrained by a dinucleating ligand), exhibit much more variable $\text{Ni}-\text{Ni}$ distances (Figure 2.8).

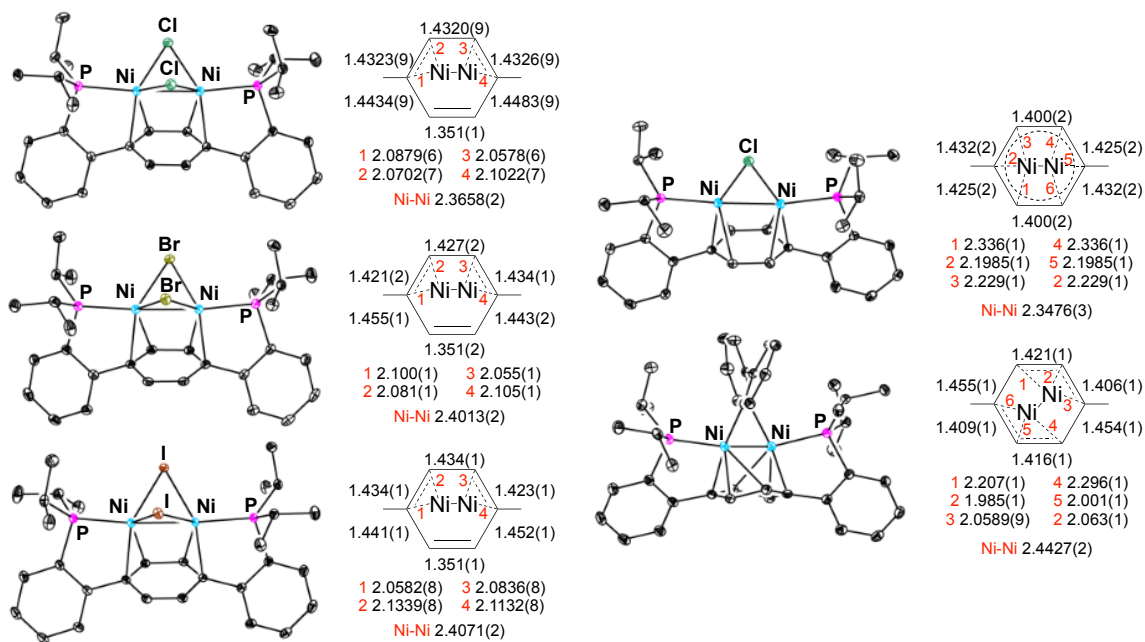


Figure 2.7. Solid-state structures of mononuclear *para*-terphenyl diphosphine complexes with central arene and Ni–Ni bond distances (Å). Left (from top to bottom): **12–14**. Right: **15, 16**. Thermal ellipsoids are shown at 50% probability level. Solvent molecules, hydrogen atoms, and outer-sphere anions are omitted for clarity.

Another effect of the coordination of the central arene is that the halides pucker together. The dihedral angle, φ , between the two Ni–Ni–Cl planes of **12** is 108.5°, whereas most structurally characterized Ni₂Cl₂ moieties are relatively planar geometries ($\varphi \sim 180$). Only one previously reported dinickel dichloride complex, which uses a third nickel center to pin the chlorides close together, has a more acute (Ni–Ni–Cl)(Ni–Ni–Cl) dihedral angle of 106.3°. ⁸⁰

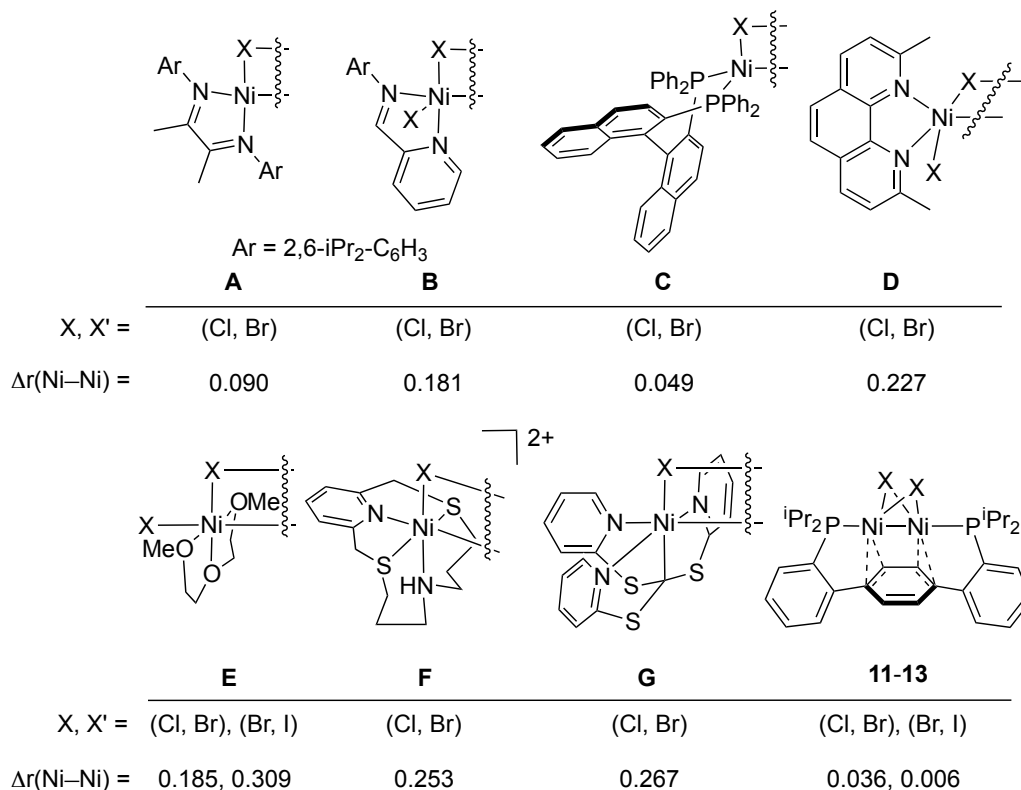


Figure 2.8. Differences in Ni–Ni bond length, $\Delta r(\text{Ni-Ni})$, between structurally characterized halide congener pairs (Ni_2X_2 and $\text{Ni}_2\text{X}'_2$): **A**^{81,82}, **B**⁸³, **C**⁸⁴, **D**,⁸⁵ **E**,^{86 87,88} **F**,⁸⁹ and **G**.⁹⁰

By losing a halide, the coordination motif of **15** changes noticeably (Figure 2.7). The triflate anion is outer-sphere, and the central arene binds to the dinickel moiety with all six carbons ($\text{Ni-C} \sim 2.20$ to 2.34 \AA) in a pseudo- C_{2v} geometry. Because of the symmetrical nature of the Ni_2 -arene interaction, **15** displays a relatively small Δ_{CC} of 3.2 pm. The Ni–Ni bond [$2.3476(3) \text{ \AA}$] is noticeably shorter than a previously reported μ^2 - η^2 : η^3 arene-supported dinickel(I) compound [$2.4238(4) \text{ \AA}$],⁵⁶ suggesting that a restoring force from the strained terphenyl backbone could play a role in the contracted Ni–Ni bond.

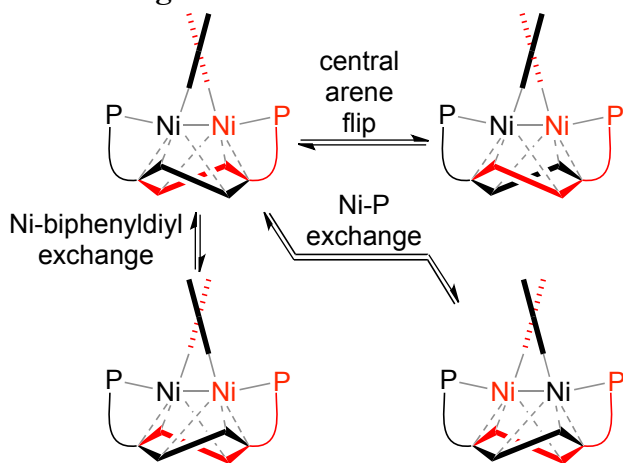
By replacing the bridging halides with a constraining biphenyldiyl ligand, the coordination geometry of **16** varies from all other complexes in this chapter (Figure 2.7). The biphenyldiyl ligand bridges the nickel centers in a $\mu\text{-}\eta^1\text{:}\eta^1$ binding mode. The nickel centers interact primarily with two non-vicinal double bonds of the central arene (Ni–C \sim 1.98 to 2.06 Å) and more weakly with the remaining two carbon atoms (2.20 to 2.30 Å). Compound **16** shows a significant distortion of the plane of the central ring toward a boat conformation. Previously reported $\mu^2\text{-}\eta^3\text{:}\eta^3$ arenes exhibit similar nonplanarity and C–C bond lengths and have been compared to a bisallyl moiety. Those complexes, containing two distant d^9 metal centers, are diamagnetic, suggesting two electron-reduction of the ring or antiferromagnetic coupling through the arene.^{4,76,77,91,92} Unlike previous “bisallyl-like” arene dinickel complexes, the two metal centers of **16** are on the same face of the ring. The Ni–Ni bond [2.4427(2) Å] is relatively long compared to previously reported dinickel(I) biphenyldiyl complexes (Ni–Ni: 2.35 to 2.40 Å⁹³⁻⁹⁷). This can be interpreted as partial reduction of the ring with the reducing electrons originating from a M–M bonding orbital. The strongly twisted C_2 structure of **16**, which is not observed in any other of the compounds supported by **1**, may be determined by the biphenyldiyl fragment. To minimize steric interaction with the ligand’s isopropyl groups, the biphenyldiyl axis prefers to lie in the plane roughly orthonormal to the P–P vector. Despite this unusual distortion of the central arene, the Δ_{CC} of **16** is only 4.9 pm.

3.3. Fluxional NMR behavior. Compounds **12-16** are diamagnetic and display NMR spectra with one ^1H NMR peak integrating to four nuclei that is assigned as to the central arene. The molecules thus all exhibit time-averaged C_{2v} symmetry. While expected for pseudo- C_{2v} symmetric **15**, this observation for halide species **12-14** (pseudo- C_s) and biphenyldiyl species **16** (pseudo- C_s) implies that the metal-arene

interactions are highly fluxional on the NMR timescale. Even at $-80\text{ }^{\circ}\text{C}$ (d_8 -toluene), the central arene peak of **12** and **16** remains a singlet. The fluxional behavior of **12-14** can be envisioned through dinuclear variations of low-barrier ring whizzing.

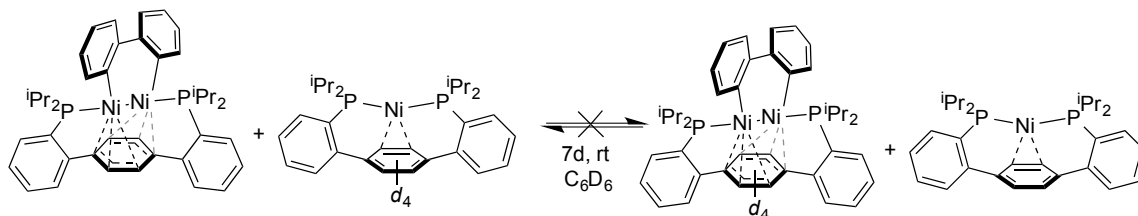
For **16**, however, pseudo- C_{2v} symmetry requires more than ring whizzing of the central arene due to the axial chirality of the biphenyldiyl ligand. There are three topologically distinct processes that could account for exchange of the four central arene protons while retaining the Ni–Ni bond (Scheme 2.9): (a) dissociation, flipping, and recoordination of the central arene, (b) ring whizzing and exchange of Ni–C(biphenyldiyl) bonds, or (c) ring whizzing and exchange of Ni–P bonds. Distinguishing between these processes experimentally would be very challenging.

Scheme 2.9. Potential exchange mechanisms that retain a Ni–Ni bond



A fourth exchange mechanism that could be active involves reversible cleavage of the Ni–Ni bond and release of **2** and a mononickel biphenyldiyl complex. To test for this possibility, an isotope-labelling crossover experiment was performed by mixing **16** with an equivalent of d_4 -**2** (with a perdeuterated central arene). No crossover was observed over one week at room temperature, so Ni–Ni dissociation does not account for the pseudo- C_{2v} symmetry of **12**.

Scheme 2.10. Isotope-labelling crossover experiment

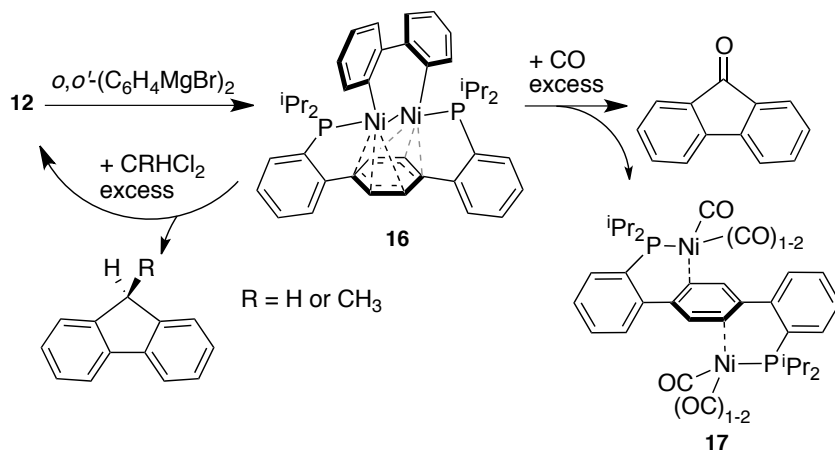


3.4. Reactivity of 16. Transition-metal catalyzed cross-coupling reactions have become some of the most widely used reactions in organic synthesis.⁹⁸ In the most common cases, C–C linkages are made using aryl halides as the electrophilic coupling partner. However, recent research, primarily with nickel catalysts, has extended the scope of starting materials to include alkyl halides. A variety of mononuclear mechanisms have been proposed with intermediate Ni oxidation states ranging from 0 to +4.⁹⁹⁻¹⁰² In light of contemporary results that Pd catalyzed C–heteroatom bond formation may proceed through via dinuclear species,¹⁰³ investigation of possible dinickel pathways in cross-coupling of alkyl halides was targeted. Thus, the C–C bond forming capability of **16** was explored.

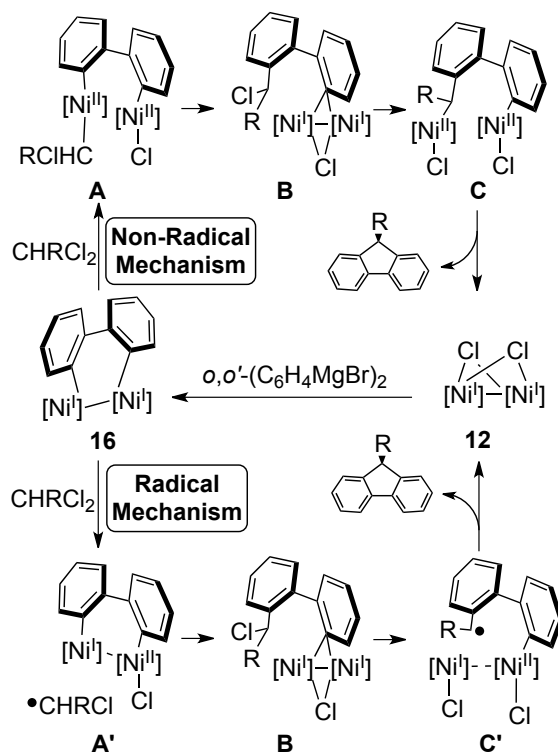
Complex **16** undergoes C–C bond formation with $CHRC_2$ or CO (Scheme 2.11). Upon addition of $CHRC_2$ to **16** ($R = H, Me$) formation of fluorene (or 9-methylfluorene) is observed, concomitant with reformation of dinickel dichloride complex **12**. A possible reaction mechanism (Scheme 2.12) initiates via oxidative addition of a C–Cl bond, yielding dinickel(II) intermediate **A**. C–C reductive elimination of the biphenyl and chloroalkyl moieties gives dinickel(I) species **B**. Intramolecular C–Cl oxidative addition results in dinickel(II) species **C**, and C–C reductive elimination releases fluorene and **12**. Alternatively, a radical based mechanism could be active. $1e^-$ transfer from **16** to substrate generates a Ni(I)-Ni(II) intermediate and an organic radical

(A'). The radical forms a C–C bond with the biphenyldiyl fragment, formally transferring the radical to the dinickel moiety (B). A second $1e^-$ transfer from the dinickel moiety results in scission of the now pendant C–Cl bond and formation of a benzylic radical tethered to a Ni(I)–Ni(II) moiety (C'). Recombination of the radical results in scission of the Ni–C(biphenyl) bond and yields fluorene and dinickel(I) product **12**. Thus, this C–C cross coupling reaction is proposed to go through a dinuclear mechanism accessing either Ni(I)–Ni(II) or Ni(II)–Ni(II) oxidation states. Oxidized dinickel species (including Ni(I)–Ni(III)) have previously been proposed in C–C bond formation pathways.¹⁰⁴

Scheme 2.11. Reactivity of biphenyldiyl complex 16.



Scheme 2.12. Mechanisms for reaction of 16 with dichloroalkanes.



In an alternative C–C bond formation, **16** reacts with CO. Fluorenone is formed, and dinickel(0) polycarbonyl species (**17**, Scheme 2.11 and Figure 2.9) are observed. Formation of fluorenone-like products have been previously observed from dinickel(I) biphenyldiyl complexes,^{97,105,106} but in this case the resulting organometallic products are also isolable. The reduced state of the product supports a CO coordination-insertion-reductive elimination mechanism for C–C bond formation. Upon addition of excess CO to **16**, more complex NMR spectra are observed, which match those observed upon addition of excess CO to mononickel monocarbonyl compound **4**. Thus, reaction of **16** with excess CO presumably liberates $\text{Ni}(\text{CO})_4$ and mononickel species. The reactivity of **16** with CHRCl_2 and CO suggests that the terphenyl diphosphine is capable of supporting Ni_2 oxidation states ranging from $\text{Ni}(0)_2$ to $\text{Ni}(\text{I})\text{Ni}(\text{II})$ or $\text{Ni}(\text{II})_2$, indicating the potential for three- or four-electron redox transformations.

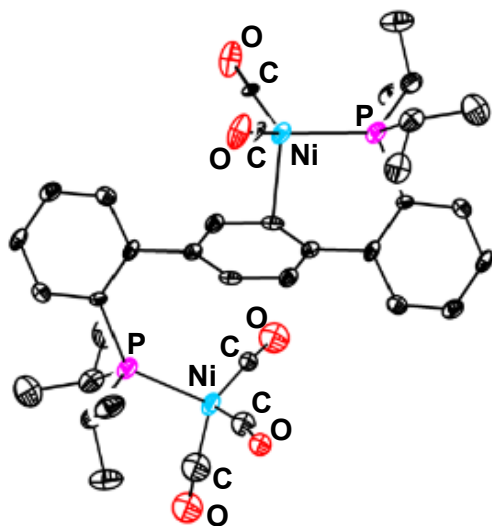


Figure 2.9. Solid-state structure of **17**. Thermal ellipsoids are shown at 50% probability level. The ratio of Ni(CO)₂ to Ni(CO)₃ moieties in the crystal is modeled as 80:20.

CONCLUSIONS

The terphenyl diphosphine ligand **1** can support a range of group 10 transition metal complexes. Low-valent and oxidized mononuclear compounds and a variety of dinickel compounds are shown in this chapter to display an assortment of metal-arene interactions in the solid state. The interactions are fluxional in solution, and aid the bischelating framework in holding two Ni centers together through three or four oxidation states. This work may influence future design of multinuclear complexes for multielectron chemistry.

EXPERIMENTAL SECTION

General considerations. All manipulations were carried out in an inert atmosphere glovebox or using standard Schlenk line techniques. [FeCp₂]PF₆ and CO (lecture bottle) were used as purchased from Aldrich. Ni(COD)₂, NiCl₂(DME), NiF₂, NiBr₂, NiI₂, NiOTf₂, Pd₂(dba)₃, PdCl₂(COD), [Pd(MeCN)₄](BF₄)₂, PtCl₂(COD), and

TfOH were used as purchased from Strem. Deuterated solvents were purchased from Cambridge Isotope Laboratories and vacuum transferred from sodium benzophenone (C_6D_6) or calcium hydride (CD_2Cl_2 , CD_3CN). Other organic reagents were dried by stirring over sodium metal or calcium hydride, degassed by three cycles of freeze-pump-thaw, and isolated via vacuum-transfer. Et_2O , toluene, THF, MeCN, and DCM were dried by the method of Grubbs.¹⁰⁷ All reagents, once degassed and dried, were stored in an inert atmosphere glovebox. 1H and ^{13}C NMR chemical shifts are reported relative to residual solvent peaks as reported in the literature.¹⁰⁸ ^{19}F and ^{31}P NMR chemical shifts are reported with respect to the instrument deuterated solvent lock. All NMR spectra were recorded at room temperature unless indicated otherwise. All non- 1H NMR spectra were recorded with 1H decoupling. Gas chromatography-mass spectrometry (GC-MS) analysis was performed upon filtering the sample through a plug of silica gel. High-resolution fast atom bombardment-mass spectrometry (FAB-MS) analysis was performed with a JEOL JMS-600H high-resolution mass spectrometer. Elemental analysis was conducted by Midwest Microlab, LLC (Indianapolis, IN; their glovebox EA service has since been discontinued). EPR spectra were recorded using an X-band Bruker EMX spectrometer and simulated using Easyspin 3.1.1. Cyclic voltammograms were performed using a Pine Biopotentiostat AFCBP1. The compounds **1**, **2**, **4**, **12-16** were originally studied by then-undergraduate Alexandra Velian, and some syntheses and characterizations have been published elsewhere.^{20,73} They are reproduced here for completeness. Compounds **6** and **8** were synthesized with undergraduate Christine Cheng.

Synthesis of 1,4-bis(2-bromophenyl)benzene. Suzuki coupling conditions were adapted from a previously published procedure.² 1,4-diiodobenzene (3.90 g, 11.82

mmol, 1 equiv), 2-bromo-phenylboronic acid (5.00 g, 24.89 mmol, 2.1 equiv), K_2CO_3 (9.80 g, 70.90 mmol, 6 equiv), 270 mL toluene, 65 mL ethanol, and 65 mL water were added to a 500 mL Schlenk tube fitted with a screw-in Teflon stopper. The mixture was degassed by two freeze-pump-thaw cycles, and $Pd(PPh_3)_4$ (685 mg, 0.59 mmol, 0.05 equiv) was added with a counterflow of nitrogen. The reaction vessel was placed in an oil bath preheated at 65 °C. After stirring for 18 h the mixture was allowed to cool to room temperature. Volatiles were removed via rotary evaporation and water was added. This mixture was extracted with CH_2Cl_2 (three times). The combined organic fractions were dried over $MgSO_4$, filtered, and concentrated via rotary evaporation. Recrystallization from $CH_2Cl_2/MeOH$ followed by filtration and drying garnered 2.8 g (60% yield, 11.07 mmol) of pale yellow crystals. 1H NMR (300 MHz, C_6D_6) δ : 7.49 (dd, $J = 8.0, 1.2$ Hz, 2H, aryl-*H*), 7.35 (s, 4H, central aryl-*H*), 7.08 (dd, $J = 8.0, 1.7$ Hz, 2H, aryl-*H*), 6.95 (td, $J = 7.5, 1.2$ Hz, 2H, aryl-*H*), 6.76 (td, $J = 7.5, 1.7$ Hz, 2H, aryl-*H*). ^{13}C NMR (75 MHz, C_6D_6) δ : 142.66, 140.72, 133.49, 131.71, 129.46, 129.03, 127.58, 123.01. The 1H NMR spectrum in $CDCl_3$ matched previously published data.³ MS (m/z): calcd, 387.9285 (M^+); found 388 (GC-MS, M^+), 387.9301 (FAB-MS, M^+).

Synthesis of 1,4-bis(2-(diisopropylphosphino)phenyl)benzene (1). A mixture of 1,4-bis(2-bromophenyl)benzene (2.25 g, 5.79 mmol, 1 equiv) and THF (40 mL) in a Schlenk tube fitted with a screw-in Teflon stopper was frozen in a cold well, in an inert atmosphere glove box. This mixture was allowed to thaw and $tBuLi$ solution (1.7 M in pentanes, 14 mL, 23.77 mmol, 4.1 equiv) was added via syringe while thawing. This purple-grey mixture was stirred for 30 min allowing it to reach room temperature. Chlorodiisopropylphosphine (1.86 g, 12.19 mmol, 2.1 equiv) was added via syringe to

the reaction mixture, which within minutes became a yellow-brown solution. After stirring at room temperature for 3 h, the volatiles were removed and the residue was dissolved in toluene and filtered through Celite. The volatiles were removed from the eluent under reduced pressure, and the resulting solids were washed with cold diethyl ether (20 ml) and filtered to yield 1.76 g (65% yield, 3.80 mmol) of spectroscopically pure **1** as a white solid. ^1H NMR (300 MHz, C_6D_6) δ : 7.55 (s, 4H, central aryl-*H*), 7.47 – 7.40 (m, 2H, aryl-*H*), 7.34 – 7.26 (m, 2H, aryl-*H*), 7.20-7.13 (m, 4H, aryl-*H*), 1.88 (m, 4H, $\text{CH}(\text{CH}_3)_2$), 1.05 – 0.88 (m, 24H, $\text{CH}(\text{CH}_3)_2$). $^{13}\text{C}\{^1\text{H}\}$ NMR (75 MHz, C_6D_6) δ : 150.81 (d, $J = 27.5$ Hz), 141.44 (d, $J = 5.5$ Hz), 135.17 (d, $J = 24.2$ Hz), 132.77 (d, $J = 2.9$ Hz), 131.01 (d, $J = 5.2$ Hz), 130.57 (d, $J = 5.1$ Hz), 128.66 (s), 126.77 (s), 24.88 (d, $J = 16.1$ Hz), 20.48 (d, $J = 20.0$ Hz), 19.85 (d, $J = 11.3$ Hz). $^{31}\text{P}\{^1\text{H}\}$ NMR (75 MHz, C_6D_6) δ : -4.7. MS (m/z): calcd, 462.2605 (M^+); found, 461 (GC-MS, M^+), 463.2665 and 479.2661 (FAB-MS, $[\text{M}+\text{H}]^+$ and $[\text{M}+\text{O}+\text{H}]^+$). Unfortunately, samples of **1** could not be subjected to FAB-MS under rigorously air-free conditions, and partial monooxygenation was observed.

Synthesis of 2. Upon addition of $\text{Ni}(\text{COD})_2$ (0.24 g, 0.864 mmol) to a colorless solution of **1** (0.4 g, 0.864 mmol) in THF (20 mL), the color of the mixture changed to deep red. The mixture was stirred at room temperature for 1 h. The volatiles were removed under reduced pressure to yield a deep red powder. X-ray quality crystals were grown in hexamethyldisiloxane at -35 °C. ^1H NMR (300 MHz, C_6D_6) δ : 7.61-7.60 (m, 2H, aryl-*H*), 7.35 (m, 2H, aryl-*H*), 7.22-7.19 (m, 4H, aryl-*H*), 5.52 (broad, 4H, central aryl-*H*), 2.02 (broad, 4H, $\text{CH}(\text{CH}_3)_2$), 1.14-1.09 (m, 12H, $\text{CH}(\text{CH}_3)_2$) and 1.2- 0.8 (m, 12H, $\text{CH}(\text{CH}_3)_2$). $^{13}\text{C}\{^1\text{H}\}$ NMR (75 MHz, C_6D_6) δ : 152.12 (t, $J = 8.1$ Hz), 132.86 (t, $J =$

2.2 Hz), 131.11 (s), 129.31 (s), 128.84 (s), 128.59 (s), 127.16 (t, $J = 2.1$ Hz), 126.65 (t, $J = 1.3$ Hz), 27.10 (t, $J = 6.8$ Hz), 20.40 (t, $J = 5.6$ Hz), 19.96 (s, broad). $^{31}\text{P}\{^1\text{H}\}$ NMR (75 MHz, C_6D_6) δ : 40.4. Anal. Calcd. For $\text{C}_{30}\text{H}_{40}\text{NiP}_2$ (%): C, 68.69; H, 7.61. Found: C, 69.12; H, 7.73. λ_{max} (THF, nm), ϵ ($\text{M}^{-1} \text{cm}^{-1}$): 256, 1.51×10^4 ; 396, 5.37×10^3 ; 494, 2.40×10^3 .

Synthesis of 3. Pd_2dba_3 (820 mg, 0.90 mmol) was added in portions in a solution of **1** (621 mg, 1.34 mmol) in 30 mL of THF. The reaction was stirred for 8 h, and volatiles were removed under vacuum. The crude was triturated in hexanes and filtered. The hexane eluent was concentrated under vacuum until precipitate became visible, and then chilled in a -35 °C freezer. Filtering the cold pentane solution through a Celite plug and concentrating the eluent yielded a more pure sample of **3** with dibenzylideneacetone impurities. Repeated chilling and filtering of pentane solutions eventually yielded **3** as a spectroscopically pure orange solid (566 mg, 1 mmol, 74%). XRD-quality crystals were grown from a concentrated pentane solution at -35 °C. ^1H NMR (300 MHz, C_6D_6) δ : 7.58 (m, 2H, aryl-*H*), 7.46 (m, 2H, aryl-*H*), 7.21 (m, 4H, aryl-*H*), 6.73 (s, 4H, central aryl-*H*), 1.96 (m, 4H, $\text{CH}(\text{CH}_3)_2$), 1.22 (app dd, 12H, $\text{CH}(\text{CH}_3)_2$), 0.90 (app dd, 12H, $\text{CH}(\text{CH}_3)_2$). $^{31}\text{P}\{^1\text{H}\}$ NMR (121 MHz, C_6D_6) δ : 43.4 ppm. ^{13}C NMR (101 MHz, C_6D_6) δ : 151.4 (t, $J = 9.1$ Hz, aryl-*C*), 132.4 (t, $J = 13.1$ Hz, aryl-*C*), 132.3 (m, aryl-*C*), 131.7 (s, aryl-*C*), 128.9 (s, aryl-*C*), 128.4 (s, aryl-*C*), 127.5 (s, aryl-*C*), 108.4 (s, central aryl-*C*), 28.2 (t, $J = 4.5$ Hz, $\text{CH}(\text{CH}_3)_2$), 21.6 (t, $J = 4.5$ Hz, $\text{CH}(\text{CH}_3)_2$), 20.7 (t, $J = 4.0$ Hz, $\text{CH}(\text{CH}_3)_2$). Anal. Calcd. For $\text{C}_{30}\text{H}_{40}\text{P}_2\text{Pd}$ (%): C, 63.32; H, 7.09. Found: C, 62.91; H, 6.70. High res. FAB-MS (m/z): calcd, 568.1640 M^+ ; found 568.1631 M^+ .
Alternate synthesis: Difficulty removing dibenzylideneacetone from the reaction crude in

the above synthesis led to the development of this alternative procedure. PdCl₂(COD) (242 mg, 0.847 mmol) was added as a THF slurry to **1** (392 mg, 0.847 mmol). The reaction homogenized while stirred for 30 minutes and was checked by ³¹P NMR for consumption of **1**. Then Ni(2,2'-bipyridine)(COD) (274 mg, 0.847 mmol) was added to the reaction mixture. After stirring for 30 minutes, the reaction mixture was filtered, and the filtrate was concentrated to yield spectroscopically pure **3** (450 mg, 93% yield).

Synthesis of 4. A calibrated volume gas bulb was used to condense ~1.1 equivalent of CO into a Schlenk flask containing a THF solution of **2** (250 mg, 0.479 mmol). The reaction changed in color from dark red to orange over minutes. After stirring for 1 h, the reaction was arrested by removing gas and solvent under vacuum. Redissolving the solids in benzene and sitting at room temperature afforded yellow crystals suitable for XRD (164 mg, 63% yield). ¹H NMR (300 MHz, C₆D₆, all peaks are broad) δ: 7.49 (m, 2H, aryl-*H*), 7.36 (m, 2H, aryl-*H*), 7.20 (m, 4H, aryl-*H*), 6.72 (br, 2H, central aryl-*H*), 6.64 (br, 2H, central aryl-*H*), 2.46 (m, 2H, CH(CH₃)₂), 1.61 (m, 2H, CH(CH₃)₂), 1.36 (m, 12H, CH(CH₃)₂), 0.69 (m, 6H, CH(CH₃)₂), 0.50 (m, 6H, CH(CH₃)₂). ¹H NMR (500 MHz, d₈-toluene, sharper peaks) δ: 7.45 (m, 2H, aryl-*H*), 7.32 (m, 2H, aryl-*H*), 7.23 – 7.15 (m, 4H, aryl-*H*), 6.66 (s, 2H, central aryl-*H*), 6.57 (s, 2H, central aryl-*H*), 2.42 (m, 2H, CH(CH₃)₂), 1.57 (m, 2H, CH(CH₃)₂), 1.30 (m, 12H, CH(CH₃)₂), 0.67 (m, 6H, CH(CH₃)₂), 0.48 (m, 6H, CH(CH₃)₂). ¹³C NMR (75 MHz, D₆D₆) δ: (Ni-CO not observed) 151.2 (m, aryl-*C*), 136.2 (s, aryl-*C*), 133.3 (m, aryl-*C*), 131.5 (s, aryl-*C*), 129.2 (s, aryl-*C*), 128.6 (s, aryl-*C*), 127.1 (s, aryl-*C*), 124.2 (s, aryl-*C*), 86.9 (Ni-*C*(aryl)), 30.1 (CH(CH₃)₂), 25.2 (m, CH(CH₃)₂), 19.9 (CH(CH₃)₂), 18.9 (m, CH(CH₃)₂), 18.3 (CH(CH₃)₂), 17.4 (CH(CH₃)₂). ³¹P NMR (121 MHz, C₆D₆) δ: 31.9. IR:

$\nu(\text{CO}) = 1926 \text{ cm}^{-1}$ (br). High res. FAB-MS (m/z): calcd, 520.1959 $[\text{M-CO}]^+$; found 520.1970 $[\text{M-CO}]^+$.

Synthesis of 5. A solution of CN^tBu (11.4 μL , 0.101 mmol) in Et_2O was added dropwise to a solution of **2** (52.5 mg, 0.101 mmol) in Et_2O (2 mL). After 2 h stirring, the reaction was concentrated under vacuum. The crude was washed with Et_2O through Celite. XRD-quality dark brown crystals of **6** (33 mg, 54%) were grown overnight from the Et_2O eluent in a $-35 \text{ }^\circ\text{C}$ freezer. The room temperature ^1H and ^{31}P NMR spectra (C_6D_6) of these crystals were broad and indicated the presence of multiple species. Features assigned to the major species, assumed to correspond to the crystallographically characterized **6** (or some fluxionality-averaged version thereof) are listed here. ^1H NMR (300 MHz, C_6D_6 , all peaks are broad) δ : 7.63 (2H, aryl- H), 7.47 (2H, aryl- H), 7.30 – 7.18 (4H, aryl- H), 6.63 (2H, central aryl- H), 6.21 (2H, central aryl- H), 2.55 (2H, $\text{CH}(\text{CH}_3)_2$), 1.75 (2H, $\text{CH}(\text{CH}_3)_2$), 1.29 (12H, $\text{CH}(\text{CH}_3)_2$), 1.04 – 0.90 (9H, CNCCH_3), 0.80 (6H, $\text{CH}(\text{CH}_3)_2$, 12H), 0.72 (6H, $\text{CH}(\text{CH}_3)_2$). ^{31}P NMR (121 MHz, C_6D_6) δ : 36.8 (br). No ^{13}C NMR peaks were observed. IR: $\nu(\text{CN}) = 2026 \text{ cm}^{-1}$ (br). High res. FAB-MS (m/z): calcd, 520.1934 $[\text{M-CN}^t\text{Bu}]^+$; found 520.1959 $[\text{M-CO}]^+$.

Synthesis of 2,3-dimethoxy-1,4-benzenediboronic acid bis(pinacol) ester.

Conditions were optimized from a previously published procedure.¹⁰⁹ An oven-dried 1 L Schlenk tube with Teflon screw stopper was cooled under N_2 . 1,2-dimethoxybenzene (10.0 mL, 78.5 mmol, 1 equiv) was added and degassed under vacuum for 30 min. Dried diethyl ether (500 mL) and dried tetramethylethylenediamine (31 mL, 207 mmol, 2.6 equiv) was added via cannula transfer. The mixture was cooled to $0 \text{ }^\circ\text{C}$, and $n\text{-BuLi}$ solution (100 mL, 2.5 M in hexane, 250 mmol, 3.2 equiv) was added via cannula

transfer. The Schlenk tube was sealed and heated to 40 °C for 4 h before being cooled to 0 °C. Trimethylborate (29 mL, 260 mmol, 3.3 equiv) was added, and the reaction mixture warmed to room temperature while stirring for 11 h. The reaction was chilled to 0 °C and aqueous HCl solution (250 mL, 6 M) was very slowly added with the aid of an addition funnel, and the mixture was stirred at room temperature for 1 h. The organic layer was separated, and the aqueous layer was extracted with diethyl ether three times. The combined organic layer was dried over magnesium sulfate, and volatiles were removed via rotary evaporation, leaving an off-white powder. This crude boronic acid was dissolved in toluene (60 mL), and pinacol (19.0 g, 161 mmol, 2 equiv) was added. The reaction mixture was refluxed with a Dean-Stark trap for 4 h. After the reaction was cooled to room temperature, volatiles were removed via rotary evaporation and the residue was purified by recrystallization from boiling hexanes to give white crystals (15.3 g, 50%), which, when dissolved in CDCl₃, displayed NMR spectra matching that previously reported in literature.¹⁰⁹ A ¹H NMR spectrum with better separated peaks was obtained using d⁶-acetone as the NMR solvent. ¹H NMR (300 MHz, d₆-acetone) δ: 7.31 (s, 2H, aryl-H), 3.80 (s, 6H, OCH₃), 1.34 (s, 24H, C(CH₃)₂) ppm. GC-MS (m/z): 390.2, calcd. 390.3, found.

Synthesis of 1,4-bis(2-bromophenyl)-2,3-dimethoxybenzene. Suzuki coupling conditions were adapted from a previously published procedure with similar starting materials.¹¹⁰ 2,3-Dimethoxy-1,4-benzenediboronic acid bis(pinacol) ester (15.3 g, 39.2 mmol, 1 equiv), K₂CO₃ (27.1 g, 196.1 mmol, 5 equiv), toluene (335 mL), H₂O (205 mL), EtOH (205 mL) were combined in a 500 mL Schlenk tube with screw-in Teflon stopper. The mixture was degassed by 10 exposures to static vacuum followed by 2 exposures to dynamic vacuum (~15 mTorr), and 2-bromiodobenzene (10.6 mL,

82.4 mmol, 2.1 equiv) and Pd(PPh₃)₄ (1.36 g, 0.12 mmol, 0.03 equiv) were added with a counterflow of N₂. The Schlenk tube was sealed and placed in an oil bath and heated to 75°C. After stirring for 12 h, the mixture was allowed to cool to room temperature and water was added. The aqueous and organic layers were separated, and the aqueous layer was extracted with dichloromethane five more times. The combined organic fractions were washed with brine and dried over MgSO₄, and volatiles were removed via rotary evaporation. The residue was heated in methanol to reflux and filtered through a short silica gel plug while hot, filtering off insoluble phosphorous-containing impurities. The filtrate was chilled in a -15 °C freezer to induce recrystallization from hot methanol to give white crystals. The mother liquor was concentrated with a rotavap until white precipitate crashed out of solution. The white crystals and precipitate were combined and found to be pure by NMR (11.0 g, 63%). ¹H NMR (300 MHz, CDCl₃) δ: 7.70 (d, *J* = 8.0 Hz, 2H, aryl-*H*), 7.39 (d, *J* = 5.5 Hz, 4H, aryl-*H*), 7.25 (m, 2H, aryl-*H*), 6.99 (s, 2H, central aryl-*H*), 3.70 (s, 6H, OCH₃) ppm. ¹³C NMR (75 MHz, CDCl₃) δ: 150.58, 139.44, 135.88, 132.74, 131.56, 129.07, 127.10, 125.33, 123.92, 60.97 ppm. GC-MS (*m/z*): 447.9, calcd. 447.9, 448.0, found.

Synthesis of 6. Conditions were adapted from a previously published procedure.²⁰ In a nitrogen glovebox, 1,4-bis(2-bromophenyl)-2,3-dimethoxybenzene (0.425 g, 0.95 mmol, 1 equiv) was dissolved with tetrahydrofuran (10 mL) in a scintillation vial equipped with stir bar. The reaction mixture was frozen in a cold well, and was allowed to thaw. While thawing, *t*-BuLi solution (2.6 mL, 1.5 M in *n*-pentane, 3.89 mmol, 4.1 equiv) was added via syringe. This brownish solution was stirred for 30 min, reaching room temperature and becoming lighter in color. Chlorodiisopropylphosphine (0.32 mL, 2 mmol, 2.1 equiv) was added via syringe, and the solution turned clear yellow. After stirring for 3 h, the volatiles were

pumped off, and the residue was dissolved in toluene and filtered through Celite twice. The volatiles were removed again, and the residue was washed with a minimal amount of cold hexane, yielding a white powder (0.177 g, 36%). ^1H NMR (300 MHz, C_6D_6) δ : 7.46 (m, 4H, aryl-*H*), 7.20 (m, 4H, aryl-*H*), 7.05 (s, 2H, central aryl-*H*), 3.61 (s, 6H, OCH_3), 1.94 (broad, 4H, $\text{CH}(\text{CH}_3)_2$), 1.05 (m, 24H, $\text{CH}(\text{CH}_3)_2$) ppm. $^{13}\text{C}\{^1\text{H}\}$ NMR (101 MHz, C_6D_6) δ : 150.5 (s, aryl-*C*), 146.9 (d, $J = 32.3$ Hz, aryl-*C*), 136.8 (m, aryl-*C*), 131.9 (d, $J = 4.0$ Hz, aryl-*C*), 130.3 (br s, aryl-*C*), 126.4 (s, aryl-*C*), 125.5 (br s, aryl-*C*), 59.5 (s, OCH_3), 25.5 (d, $J = 14.1$ Hz, $\text{CH}(\text{CH}_3)_2$), 24.1 (d, $J = 15.1$ Hz, $\text{CH}(\text{CH}_3)_2$), 20.2 (overlapping multiplets, $\text{CH}(\text{CH}_3)_2$), 19.1 (m, $\text{CH}(\text{CH}_3)_2$). ^{31}P NMR (121 MHz, C_6D_6) δ : -1.82 ppm.

Synthesis of 7. 1,4-bis(2-phenol)benzene was synthesized per literature procedures.¹¹¹ To a toluene (20 mL) solution of this (247 mg, 0.941 mmol) in a Schlenk tube was added ClP^iPr_2 (0.30 mL, 1.883 mmol), and 5 minutes later Et_3N (0.39 mL, 2.824 mmol) was added to the reaction mixture. The reaction changed from clear to cloudy within 10 minutes. The Schlenk tube was sealed with a Teflon screw cap and placed in a 100 °C oil bath for 3 h. The reaction was then cooled to room temperature and filtered through Celite. The filtrate was concentrated to a solid under vacuum and washed through Celite with pentanes. A persistent ~10% impurity by ^{31}P NMR could only be removed by dissolving the sample in minimal Et_2O and adding four volumetric equivalents of nitromethane. White precipitate (**7**) formed upon stirring and was collected via filtration (331 mg, 71% yield). ^1H NMR (400 MHz, C_6D_6) δ : 7.66 (overlapping peaks, 6H, aryl-*H* + cenral aryl-*H*), 7.35 (app d, 2H, aryl-*H*), 7.15 (m overlapping with $\text{C}_6\text{D}_5\text{H}$, 2H, aryl-*H*), 6.91 (app t, 2H, aryl-*H*), 1.70 (m, 4H, $\text{CH}(\text{CH}_3)_2$), 1.01 (m, 12H, $\text{CH}(\text{CH}_3)_2$), 0.93 (m, 12H, $\text{CH}(\text{CH}_3)_2$) ppm. ^{31}P NMR (121 MHz, C_6D_6) δ : 148.92 ppm. ^{13}C NMR peaks from HSQC and HMBC spectra (400 MHz, C_6D_6): 156.3 (aryl-

C), 137.5 (aryl-C), 132.1 (aryl-C), 130.9 (aryl-C), 129.4 (aryl-C), 129.0 (aryl-C), 121.8 (central aryl-ipso-C), 118.0 (central aryl-CH), 28.1 (CH(CH₃)₂), 16.9 (CH(CH₃)₂), 17.4 (CH(CH₃)₂).

Synthesis of 8. Conditions were adapted from a previously published procedure.²⁰ In a nitrogen glovebox, **6** (0.050 g, 0.10 mmol, 1 equiv) was dissolved with THF (2.5 mL), and Ni(COD)₂ (0.026 g, 0.10 mmol, 1 equiv) was added. The solution went from colorless to dark red in seconds and was stirred for 12 h. Volatiles were removed, and the residue was dissolved in hexane and filtered through Celite. Ni(COD)₂ was determined to be present by ¹H NMR spectroscopy, so the reaction mixture was redissolved in THF and heated at 70 °C for 6 h. A light film of dark precipitate formed on the reaction flask walls. Decomposition of Ni(COD)₂ was verified by again concentrating the reaction to a solid, redissolving in C₆D₆, and taking ¹H NMR spectra. Volatiles were again removed, and the residue was dissolved in minimal hexane and put in the freezer at -35 °C, yielding dark red XRD-quality crystals (0.031 g, 53% yield). ¹H NMR (300 MHz, C₆D₆) δ: 7.87 (m, 2H, aryl-H), 7.40 (m, 2H, aryl-H), 7.23 (m, 4H, aryl-H), 4.53 (m, 2H, central aryl-H), 3.60 (s, 6H, OCH₃), 2.04 (broad, 4H, CH(CH₃)₂), 1.27 (m, 6H, CH(CH₃)₂), 1.09 (m, 12H, CH(CH₃)₂), 0.80 (m, 6H, CH(CH₃)₂) ppm. ¹³C{¹H} NMR (75 MHz, C₆D₆) δ: 147.6 (t, *J* = 8.0 Hz, aryl-C), 146.7 (aryl-C), 131.2 (aryl-C), 129.5-129.1 (m, 3 types of aryl-C), 127.0 (aryl-C), 122.3 (aryl-C), 60.9 (t, *J* = 3.8 Hz, Ni-C), 60.2 (methoxy-C), 28.0 (t, *J* = 5.8 Hz, CH(CH₃)₂), 26.8 (t, *J* = 8.3 Hz, CH(CH₃)₂), 21.6 (t, *J* = 3.7 Hz, CH(CH₃)₂), 21.1 (t, *J* = 6.0 Hz, CH(CH₃)₂), 20.1 (t, *J* = 6.1 Hz, CH(CH₃)₂), 18.5 (CH(CH₃)₂). ³¹P NMR (121 MHz, C₆D₆) δ: 39.01 ppm. **8** changed color from dark red to yellow upon exposure to oxygen. It could not be analyzed by FAB-MS due to this air-sensitivity. Instead, **8** was treated with an equivalent of [dimethylformamide]•HOTf, and the resulting cationic species was analyzed by high res. FAB-MS (*m/z*): calcd, 581.2248 [**8**+H]⁺; found 581.2239 [**8**+H]⁺.

Synthesis of 9. In a nitrogen glovebox, **7** (91.5 mg, 0.185 mmol) was dissolved with THF (2.5 mL), and Ni(COD)₂ (50.9 mg, 0.185 mmol) was added. The solution went from colorless to dark red in seconds upon stirring. Several species were observed by ³¹P NMR after 24 h. Volatiles were removed, and the dark red/brown residue was dissolved in hexane and filtered through Celite. Volatiles were again removed, and the residue was dissolved in minimal hexane and put in the freezer at -35 °C, yielding red XRD-quality crystals (70 mg, 68% yield). ¹H NMR (400 MHz, C₆D₆) δ: 7.46 (2H, d, J = 7.6 Hz, aryl-H_a), 7.06 (4H, m, aryl-H_d + aryl-H_b), 6.96 (2H, m, aryl-H_c), 5.82 (4H, s, central aryl-H), 1.88 (4H, m, CH(CH₃)₂), 1.13 (12H, m, CH(CH₃)₂), 1.01 (12H, m, CH(CH₃)₂). ¹³C peaks (from HSQC and HMBC spectra on 400 MHz spectrometer, C₆D₆) d: 154.6 (C_f), 133.7 (C_e), 132.0 (C_g), 130.1 (C_a), 127.7 (C_d), 122.4 (C_b + C_c, overlapping), 94.5 (C_h + C_i, coalesced), 30.7 (CH(CH₃)₂), 18.0 (CH(CH₃)₂), 17.0 (CH(CH₃)₂). ³¹P NMR (162 MHz, C₆D₆) δ: 158.52 (s). High res. FAB-MS (m/z): calcd, 552.1857 M⁺; found 552.1890 M⁺.

Synthesis of 10. *With [FeCp₂]PF₆:* To a solution of **2** (10.0 mg, 0.02 mmol) in THF (2 mL) was added a suspension of FeCp₂PF₆ (6.4 mg, 0.02 mmol) in THF (1 mL). The solution turned dark within 5 minute. After washing with toluene to remove ferrocene byproduct, a ¹H NMR spectrum possessed the same broad paramagnetic peaks as in the synthesis of **10** via comproportionation. *Comproportionation synthesis:* A Schlenk tube fitted with a screw-in Teflon stopper was charged with **2** (50.0 mg, 0.10 mmol), **1** (50.0 mg, 0.11 mmol), Ni(OTf)₂ (38.6 mg, 0.11 mmol), MeCN (10 mL) and THF (3 mL). The tube was sealed and heated in an oil bath at 80 °C. After 4 h, the solution was dark purple. At 12 h, volatiles were removed under vacuum to yield a purple solid. The solid was triturated in THF and filtered through Celite, and then washed with MeCN. The MeCN eluent was concentrated under vacuum to

a purple solid (100.3 mg, 0.15 mmol, 78%). Purple XRD-quality crystals were formed by layering a MeCN solution of this product on toluene and allowing liquid diffusion to occur at -35 °C. ¹H NMR (300 MHz, CD₃CN) δ: 11.31 (br), 8.10 (br), 4.04 (br), 0.16 (br). EPR (50:50 MeCN/toluene, 20 K): g = [2.075, 2.440, 2.111]; for A_p = [-2.75, 10.2, 135] G. EPR (50:50 MeCN/toluene, ~298 K): g = 2.092; A_p = 188 G. Anal. Calcd. For C₃₁H₄₀F₃NiO₃P₂S (%): C, 55.54; H, 6.01. Found: C, 55.47; H, 5.99. High res. FAB-MS (m/z): calcd, 520.1959 [M-OTf]⁺; found 520.1948 [M-OTf]⁺.

Synthesis of 11. A solution of *p*-cyanoanilinium triflate (94.6 mg, 0.35 mmol) in THF (3 mL) was added dropwise to a stirring solution of **3** (200 mg, 0.35 mmol) in THF (3 mL). The reaction mixture changes from orange to yellow in a few minutes. The reaction mixture is concentrated under vacuum and washed with hexanes and then benzene. The remaining insolubles are then filtered through Celite using THF, and the eluent is concentrated to a yellow powder under vacuum. Pale yellow XRD-quality crystals were grown by layering a MeCN solution of the compound under Et₂O (212 mg, 0.29 mmol, 84%). ¹H NMR (400 MHz, C₆D₆) δ: 7.91 (2H, m, aryl-*H_d*), 7.83-7.66 (6H, m, aryl-*H_{b,d}*, overlapping) 7.31 (4H, s, central aryl-*H_b* + *H_i* coalesced), 1.96 (4H, m, CH(CH₃)₂), 1.11 (12H, m, CH(CH₃)₂), 0.99 (12H, m, CH(CH₃)₂), -12.98 (1H, t, *J_{PH}* = 12 Hz). ¹³C peaks (from HSQC and HMBC spectra on 400 MHz spectrometer, CD₃CN) δ: 147.5 (*C_f*), 137.6 (*C_g*), 132.5 (*C_a*), 131.7 (*C_b*), 129.2 (*C_c*), 128.7 (*C_d*), 124.9 (*C_e*), 118.4 (*C_b* + *C_e*, coalesced), 28.1 (CH(CH₃)₂), 19.4 (CH(CH₃)₂), 18.6 (CH(CH₃)₂). ³¹P{¹H} NMR (162 MHz, C₆D₆) δ: 45.4 (apparent doublet due to incomplete ¹H decoupling of the far upfield hydride). High res. FAB-MS (m/z): calcd, 581.1719 [M-OTf]⁺; found 581.1745 [M-OTf]⁺.

Synthesis of 12. Upon addition of Ni(COD)₂ (0.332 g, 1.51 mmol) and NiCl₂(DME) (0.416 g, 1.51 mmol) to a colorless solution of **1** (0.700 g, 1.51 mmol) in

THF (50 mL), the color of the mixture changes first to red and then to green. The mixture is stirred at room temperature for 30 min, and the volatiles removed under reduced pressure. Recrystallization from a concentrated benzene solution procured X-ray quality crystals of **3** • C₆H₆. Alternatively, recrystallization from THF/pentane at -35 °C gave **3** in 90% yield. ¹H NMR (300 MHz, C₆D₆) δ: 7.24 (d, *J* = 7.5 Hz, 2H, aryl-*H*), 6.99 (app t, 2H, aryl-*H*), 6.87 (app t, 2H, aryl-*H*), 6.74 (s, 4H, central aryl-*H*), 6.69 (br d, 2H, aryl-*H*), 1.5 (m, 4H, CH(CH₃)₂), 1.25 (app d, 12H, CH(CH₃)₂), 0.91 (app d, 12H, CH(CH₃)₂). ¹³C{¹H} NMR (75 MHz, C₆D₆) δ: 154.1 (t, *J* = 10.0 Hz, aryl-*C*), 133.7 (t, *J* = 16.4 Hz, aryl-*C*), 130.6 (s, aryl-*C*), 130.4 (s, aryl-*C*), 129.7 (s, aryl-*C*), 126.9 (s, aryl-*C*), 104.4 (s, central aryl ipso-*C*), 89.8 (s, central aryl-*CH*), 23.1 (t, *J* = 8.6 Hz, CH(CH₃)₂), 19.0 (s, CH(CH₃)₂), 18.1 (s, CH(CH₃)₂). ³¹P{¹H} NMR (75 MHz, C₆D₆) δ: 47.3. Anal. Calcd. For C₃₀H₄₀Cl₂Ni₂P₂ (%): C, 55.36; H, 6.19. Found: C, 54.92; H, 6.47. λ_{max} (THF, nm), ε (M⁻¹ cm⁻¹): 249, 3.75 x 10⁴; 318, 3.21 x 10⁴; 375, 8.01 x 10³; 446, 8.52 x 10³; 739, 7.68 x 10².

Synthesis of 12 from 2. NiCl₂(DME) (0.042 g, 0.15 mmol) was added to a red solution of **2** (0.033 g, 0.15 mmol) in THF (5 mL) and stirred for 30 minutes to give a dark green solution. Volatiles were removed under reduced pressure, and ¹H and ³¹P NMR spectroscopy identified the sole product as **3**.

Synthesis of 13. Using NiBr₂ instead of NiCl₂(DME), **13** was synthesized from **2** using the same procedure as for **12**. After removal of reaction solvent, the reaction crude was washed with hexanes and filtered through Celite with benzene. The benzene filtrate yielded a green-brown powder upon removal of volatiles. ¹H NMR (300 MHz, C₆D₆) δ 7.20 (app d, 2H, aryl-*H*), 6.99 (app t, 2H, aryl-*H*), 6.87 (app t, 2H, aryl-*H*), 6.79 (s, 4H, central aryl-*H*),

6.71 (m, 2H, aryl-*H*), 1.49 (m, 4H, $\text{CH}(\text{CH}_3)_2$), 1.24 (m, 12H, $\text{CH}(\text{CH}_3)_2$), 0.93 (m, 12H, $\text{CH}(\text{CH}_3)_2$). ^{31}P NMR (121 MHz, C_6D_6) δ 50.8. ^{13}C NMR (75 MHz, C_6D_6) δ 153.8 (app t, aryl-*C*), 133.8 (app t, aryl-*C*), 130.6 (s, aryl-*C*), 130.4 (s, aryl-*C*), 129.5 (s, aryl-*C*), 127.0 (s, aryl-*C*), 105.5 (s, central aryl-*CH*), 91.0 (s, central aryl ipso-*C*), 23.5 (m, $\text{CH}(\text{CH}_3)_2$), 19.2 (s, $\text{CH}(\text{CH}_3)_2$), 18.0 (s, $\text{CH}(\text{CH}_3)_2$). Anal. Calcd. For $\text{C}_{30}\text{H}_{40}\text{Br}_2\text{Ni}_2\text{P}_2$ (%): C, 48.71; H, 5.45. Found: C, 48.83; H, 5.38.

Synthesis of 14. Using NiI_2 instead of $\text{NiCl}_2(\text{DME})$, **14** was synthesized from **2** using the same procedure as for **12**. The dark red reaction crude was placed under vacuum to remove volatiles. The crude was washed with hexanes and filtered through Celite with benzene, leaving behind purple-gray insoluble matter. The benzene filtrate yielded a bronze powder after concentration under vacuum. ^1H NMR (300 MHz, C_6D_6) δ 7.19 (m, 2H, aryl-*H*), 7.06 (m, 2H, aryl-*H*), 6.94 (s, 4H, aryl-*H*), 6.80 (m, 2H, aryl-*H*), 1.67 (m, 4H, $\text{CH}(\text{CH}_3)_2$), 1.25 (m, 12H, $\text{CH}(\text{CH}_3)_2$), 1.00 (m, 12H, $\text{CH}(\text{CH}_3)_2$). ^{31}P NMR (121 MHz, C_6D_6) δ 63.9. ^{13}C NMR (400 MHz HSQC, HMBC, C_6D_6) δ 152.6 (aryl-*C*), 133.2 (aryl-*C*), 129.8 (aryl-*C*), 129.6 (aryl-*C*), 128.6 (aryl-*C*), 126.6 (aryl-*C*), 107.1 (central aryl-*CH*), 93.8 (central aryl ipso-*C*), 24.0 (m, $\text{CH}(\text{CH}_3)_2$), 18.8 (s, $\text{CH}(\text{CH}_3)_2$), 17.6 (s, $\text{CH}(\text{CH}_3)_2$). Anal. Calcd. For $\text{C}_{30}\text{H}_{40}\text{I}_2\text{Ni}_2\text{P}_2$ (%): C, 43.22; H, 4.84. Found: C, 42.90; H, 4.85.

Synthesis of 15. A THF solution of **12** (500 mg, 0.768 mmol) was added over solid TiOTf (272 mg, 0.768 mmol). The mixture changed from dark green to deep blue with light precipitate in seconds upon stirring. After stirring for 10 minutes, the solution was filtered through Celite and layered underneath toluene, yielding blue-gray XRD-quality crystals (463 mg, 79% yield) by liquid diffusion. ^1H NMR (300 MHz, C_6D_6) δ 7.69-7.46 (m, 8H, aryl-*H*), 6.19 (s, 4H, central aryl-*H*), 2.25 (m, 4H, $\text{CH}(\text{CH}_3)_2$), 1.25 (m, 12H, $\text{CH}(\text{CH}_3)_2$), 1.10 (m, 12H, $\text{CH}(\text{CH}_3)_2$). ^{31}P NMR (121 MHz, C_6D_6) δ 53.0. ^{13}C NMR

(75 MHz, C₆D₆; due to poor solubility, some quaternary carbons were not observed) δ 138.5 (s, aryl-C), 132.7 (s, aryl-C), 132.6 (s, aryl-C), 131.3 (s, aryl-C), 130.2 (s, aryl-C), 102.6 (s, central aryl-CH), 94.0 (s, central aryl ipso-C), 25.3 (m, CH(CH₃)₂), 19.7 (s, CH(CH₃)₂), 19.2 (s, CH(CH₃)₂).

Synthesis of 16. Magnesium turnings (100 mg), 2,2'-dibromobiphenyl (101 mg, 0.32 mmol, 1 equiv), and THF (15 mL) were heated in a Schlenk flask at 40 °C. After 4h, an aliquot was quenched with D₂O, dried with MgSO₄, and filtered through silica gel. GC-MS analysis of the aliquot showed the absence of starting 2,2'-dibromobiphenyl and the presence of *d*₂-biphenyl, indicating the complete conversion of starting material to Grignard. The solution was filtered through Celite to remove magnesium particles. Solvent was removed under reduced pressure to yield an off-white powder that was suspended in toluene (50 mL) and frozen in a cold well. A solution of **3** (234.3 mg, 0.32 mmol, 1 equiv) in toluene (15 mL) was chilled to -35 °C and layered on top of the frozen Grignard solution. The reaction mixture was frozen solid, then allowed to thaw and stir for 40 minutes, during which the solution gradually changed from dark green to dark brown. Volatile materials were removed under reduced pressure, and the residue was dissolved in hexanes (50 mL) and filtered through Celite. The filtrate was concentrated under reduced pressure, and the residue was washed with hexanes (20 mL). The wash was discarded by filtration, while the remaining residue was dissolved in hexanes (50 mL) and filtered again. The filtrate was concentrated to a residue under reduced pressure, and lyophilized in benzene to obtain a brown powder (39.1 mg, 0.05 mmol, 27%). A concentrated solution of **4** in hexanes was chilled to -35 °C for 1 day to yield X-ray quality crystals. ¹H NMR (300 MHz, C₆D₆) δ : 7.56 (d, 2H, aryl-H), 7.43 (d,

2H, aryl-*H*), 7.23 (d, 2H, aryl-*H*), 7.07-6.90 (m, 10H, aryl-*H*), 5.26 (s, 4H, central aryl-*H*), 1.92 (m, 4H, CH(CH₃)₂), and 0.69 (m, 24H, CH(CH₃)₂). ¹³C{¹H} NMR (300 MHz, C₆D₆) δ: 164.18 (s), 163.40 (t, J = 3.4 Hz), 152.24 (t, J = 15.2 Hz), 138.93 (s), 138.62 (t, J = 12.5 Hz), 131.35 (s), 129.69 (s), 128.88 (t, J = 5.8 Hz), 127.46 (s), 123.92 (s), 123.38 (s), 121.72 (s), 92.18 (s), 88.92 (s), 25.25 (s), and 17.89 (s). ³¹P{¹H} NMR (300 MHz, C₆D₆) δ: 36.9. Anal. Calcd. For C₃₀H₄₀Cl₂Ni₂P₂ (%): C, 68.90; H, 6.61. Found: C, 69.01; H, 6.54. λ_{max} (C₆H₆, nm), ε (M⁻¹ cm⁻¹): 439, 3.9 x 10²; 518, 2.6 x 10²; 665, 7.2 x 10¹.

Reaction of 16 with CH₂Cl₂. A C₆D₆ (0.6 mL) solution of **4** (10 mg, 0.01 mmol) was transferred to a J. Young NMR tube. 5 drops of CH₂Cl₂ were added and the reaction was followed by ³¹P NMR spectroscopy. At 3.75 h, the reaction was complete and had changed from dark brown to dark green in color. ¹H and ³¹P NMR spectra identified **3** as the major organometallic species in solution. GC-MS analysis of the crude mixture indicated that fluorene was the only organic species present.

Reaction of 16 with CO to form 17. A 100 mL Schlenk flask was charged with a stir bar and a solution of **4** (98 mg, 0.13 mmol) in C₆H₆ (15 mL) inside a nitrogen-atmosphere glovebox and covered with a rubber septum. The flask was brought out of the box, and CO (19.3 mL, 0.80 mmol) was injected into the solution with a syringe and long metal needle. Over 15 min the reaction mixture changed from dark brown to pale green-yellow. The reaction was placed under a positive nitrogen pressure while the septum was replaced with a greased glass stopper, and then volatiles were removed under vacuum. The solid was dissolved in hexanes and filtered through Celite. Volatiles were again removed under vacuum, and the resultant yellow solid was triturated in hexanes and filtered through Celite. The filtrate was found by ¹H-NMR and GC-MS to contain fluorenone. The filter cake was collected by washing with more hexanes. NMR

spectra of the filter cake were complex but contained well-defined features. ^1H NMR (300 MHz, C_6D_6) δ : 8.34 – 8.20 (m, 2.33H), 8.09 – 8.01 (m, 0.22H), 7.86 (d, $J = 7.3$ Hz, 0.60), 7.13 (s, 5.44H), 7.10 – 6.76 (m, 15.09H), 6.71 (app d, 0.75H), 5.85 (s, 1.00H), 5.65 (s, 0.13H), 4.56 (s, 0.12H), 3.58 (m, 0.13H), 2.32 (m, 1.65H), 2.10 (m, 6.02H), 1.04 (d, $J = 6.7$ Hz, 11.50H), 0.98 (d, $J = 6.7$ Hz, 10.03H), 0.81 (d, $J = 6.9$ Hz, 11.25H), 0.76 (d, $J = 6.9$ Hz, 8.03H). $^{31}\text{P}\{^1\text{H}\}$ NMR (300 MHz, C_6D_6) δ : 75.0 (broad), 51.1, 50.1, 38.1 (broad), 37.1, 35.6. Hexanes was layered on a concentrated solution of this mixture in Et_2O to yield yellow-orange crystals that were found to be a mixture of nickel carbonyls, **17**: ca. 80% of the phosphines are bound to nickel dicarbonyl and the remaining phosphines are bound to nickel tricarbonyl.

Table 2.2. Crystal and refinement data for complexes **2**, **3**, **4**, **5**, **8**, **9**, **10**, **11**.

	2	3	4	5	8	9	10	11
CCDC Number	745169	790176	790173	782790	--	--	790177	810418
Empirical formula	C ₃₀ H ₄₀ P ₂ Ni	C ₃₀ H ₄₀ P ₂ Pd	C ₃₁ H ₄₀ OP ₂ Ni • C ₆ H ₆	C ₃₅ H ₄₉ NP ₂ Ni	C ₃₂ H ₄₄ NiO ₂ P ₂ • 1/2 (C ₆ H ₆)	C ₃₀ H ₄₀ NiO ₂ P ₂	[C ₃₀ H ₄₀ P ₂ Ni] [CF ₃ O ₃ S]	[C ₃₀ H ₄₁ P ₂ Pd] [CF ₃ O ₃ S]
Formula weight	521.27	568.96	627.39	604.40	620.38	553.27	670.34	719.04
T (K)	100(2)	100(2)	100(2)	100(2)	100(2)	100(2)	100(2)	100(2)
<i>a</i> , Å	8.5770(3)	8.6107(4)	9.8042(4)	11.7303(4)	23.157(2)	8.1130(3)	12.0523(4)	10.4060(5)
<i>b</i> , Å	14.8684(5)	11.5616(6)	9.9171(4)	19.7927(7)	8.4778(6)	11.0794(4)	14.5265(5)	17.7393(8)
<i>c</i> , Å	21.6483(7)	14.4906(8)	16.7675(6)	14.0216(5)	17.241(1)	17.2216(6)	17.6176(5)	17.9098(8)
α , deg	90	94.311(3)	98.712(2)	90	90	76.340(20)	90	90
β , deg	90	99.673(3)	90.901(2)	92.024(2)	109.382(4)	86.346(2)	90	101.955(2)
γ , deg	90	99.378(3)	95.213(2)	90	90	70.436(2)	90	90
Volume, Å ³	2760.73(16)	1395.25(12)	1604.10(11)	3253.4(2)	3192.8(4)	1417.17(9)	3084.5(2)	3234.4(3)
Z	4	2	2	4	4	2	4	4
Crystal system	Orthorhombic	Triclinic	Triclinic	Monoclinic	Monoclinic	Triclinic	Orthorhombic	Monoclinic
Space group	P2 ₁ 2 ₁ 2 ₁	P-1	P-1	P 2 ₁ / <i>n</i>	P12 ₁ / <i>c</i> 1	P-1	P2 ₁ 2 ₁ 2 ₁	P2 ₁ / <i>n</i>
<i>d</i> _{calc} , g/cm ³	1254	1354	1229	1296	1291	1297	1444	1480
θ range, deg	1.66–35.07	1.80–36.32	2.09–35.36	1.78–32.63	1.86–36.62	2.00–51.11	4.33–34.55	2.30–38.77
μ , mm ⁻¹	0.835	0.796	0.733	0.718	0.738	0.822	0.850	0.785
Abs. Correction	None	Integration	None	Gaussian	Multi-scan	Multi-scan	None	None
GOF	1.311	1.388	2.791	1.721	1.016	0.982	1.431	1.816
R ₁ , ^a	0.0302,	0.0346,	0.0544,	0.0326,	0.0624,	0.0275,	0.0301,	0.0264,
wR ₂ , ^b	0.0568	0.0482	0.0777	0.0516	0.1496	0.0760	0.0417	0.0429
[I>2s(I)]								

^a R₁ = $\sum ||F_o| - |F_c|| / \sum |F_o|$. ^b wR₂ = $[\sum [w(F_o^2 - F_c^2)^2] / \sum [w(F_o^2)^2]]^{1/2}$.

Table 2.3. Crystal and refinement data for complexes **12**, **13**, **14**, **15**, **16**, **17**

	12	13	14	15	16	17
CCDC Number	702807	790175	790174	790172	745065	767040
Empirical formula	$C_{30}H_{40}P_2Cl_2Ni_2 \cdot C_6H_6$	$C_{30}H_{40}Br_2P_2Ni_2 \cdot C_6H_6$	$C_{30}H_{40}I_2P_2Ni_2$	$[C_{30}H_{40}ClP_2Ni_2][CF_3O_3S]$	$C_{42}H_{48}P_2Ni_2 \cdot \frac{1}{2}(C_6H_{14})$	$0.80(C_{34}H_{40}O_4P_2Ni_2) \cdot 0.20(C_{36}H_{40}O_6P_2Ni_2)$
Formula weight	728.99	817.91	833.78	764.50	775.25	703.36
T (K)	100(2)	100(2)	100(2)	100(2)	100(2)	100(2)
<i>a</i> , Å	9.6730(5)	11.1574(5)	15.2390(7)	28.192(1)	11.7255(5)	7.1846(13)
<i>b</i> , Å	12.8755(6)	25.621(1)	17.1554(8)	14.9782(5)	13.1876(5)	25.477(4)
<i>c</i> , Å	14.3392(7)	12.2369(5)	23.999(1)	19.6646(8)	14.7366(6)	9.4217(16)
α , deg	102.753(3)	90	90	90	105.066(2)	90
β , deg	99.036(3)	95.900(2)	90	127.104(3)	97.410(2)	100.794(11)
γ , deg	91.500(3)	90	90	90	115.216(2)	90
Volume, Å ³	1716.76(15)	3479.5(3)	6274.0(5)	6622.4(4)	1814.32(13)	1694.1(5)
Z	2	4	8	8	2	2
Crystal system	Triclinic	Monoclinic	Orthorhombic	Monoclinic	Triclinic	Monoclinic
Space group	P-1	P2 ₁ / <i>n</i>	<i>Pbca</i>	C2/ <i>c</i>	P-1	P2 ₁ / <i>n</i>
<i>d</i> _{calc} , g/cm ³	1410	1672	1765	1534	1345	1379
θ range, deg	1.93–45.99	1.85–36.39	1.70–40.86	1.63–36.96	1.49–39.07	2.34–26.37
μ , mm ⁻¹	1.37	3.495	3.288	3168	1.098	1.242
Abs. Correction	Semi-empirical	Integration	Integration	Semi-empirical	None	Semi-empirical
GOF	2.237	1.197	1.298	2.087	1.747	1.248
<i>R</i> ₁ ^a	0.0270,	0.0254,	0.0200,	0.0337,	0.0334,	0.0651,
<i>wR</i> ₂ ^b	0.0532	0.0349	0.0260	0.0568	0.0565	0.0634
[I>2s(I)]						

^a $R_1 = \sum ||F_o| - |F_c|| / \sum |F_o|$. ^b $wR_2 = [\sum [w(F_o^2 - F_c^2)^2] / \sum [w(F_o^2)^2]]^{1/2}$.

Refinement details.

In each case, crystals were mounted on a glass fiber and placed on the diffractometer under a nitrogen stream. Low temperature (100 K) X-ray data were obtained on a Bruker APEXII CCD based diffractometer (Mo sealed X-ray tube, $K_{\alpha} = 0.71073 \text{ \AA}$). All diffractometer manipulations, including data collection, integration and scaling were carried out using the Bruker APEXII software.¹¹² Absorption corrections were applied using SADABS.¹¹³ Space groups were determined on the basis of systematic absences and intensity statistics and the structures were solved by direct methods using XS¹¹⁴ (incorporated into SHELXTL) and refined by full-matrix least squares on F^2 . All non-hydrogen atoms were refined using anisotropic displacement parameters. Hydrogen atoms were placed in idealized positions and refined using a riding model. The structure was refined (weighted least squares refinement on F^2) to convergence. Graphical representation of structures with 50% probability thermal ellipsoids was generated using Diamond visualization software.¹¹⁵

Special refinement details for 3. Two of the isopropyl groups are disordered. The disorder was modeled and refined without restraints.

Special refinement details for 8. The sample appeared to be multiple plates, and two domains were found by the program CellNow. The second domain was rotated from first domain by 177.8 degrees about the b axis. Absorption correction was performed with the TwinABS program. The structure was solved using only the composite data points. Details are contained in the .cif file.

Special refinement details for 15. The crystal is a twin with two domains related by a two-fold rotation around the 1 0 1 axis. Refinement included both domains with a refined batch

scale factor of 0.08 (HKLF 5 file). There are two-half molecules in the asymmetric unit, each sitting at a unique center of symmetry.

Special refinement details for 17. The molecule sits at a center of symmetry AND is disordered between two distinctly different molecular formulas in an 80:20 ratio. The major component has two carbonyl ligands bonded to Ni and the Ni interacting with C10 of the central ring. In the minor component the Ni no longer interacts with C10 but now has three carbonyl ligands. The parameters of the minor component were refined with restraints to maintain somewhat reasonable geometry due to significant overlap of the atomic positions of C1 and C2A and of O2 and O3A. Minor component parameters were then fixed for the final least-squares cycles.

REFERENCES

- (1) Muetterties, E. L.; Bleeke, J. R.; Wucherer, E. J.; Albright, T. *Chem. Rev.* **1982**, *82*, 499.
- (2) Braga, D.; Dyson, P. J.; Grepioni, F.; Johnson, B. F. G. *Chem. Rev.* **1994**, *94*, 1585.
- (3) Lee, C. H.; Laitar, D. S.; Mueller, P.; Sadighi, J. P. *J. Am. Chem. Soc.* **2007**, *129*, 13802.
- (4) Jones, C.; Schulten, C.; Fohlmeister, L.; Stasch, A.; Murray, K. S.; Moubaraki, B.; Kohl, S.; Ertem, M. Z.; Gagliardi, L.; Cramer, C. J. *Chem. Eur. J.* **2011**, *17*, 1294.
- (5) Pfirrmann, S.; Yao, S.; Ziemer, B.; Stösser, R.; Driess, M.; Limberg, C. *Organometallics* **2009**, *28*, 6855.
- (6) Otten, E.; Batinas, A. A.; Meetsma, A.; Hessen, B. *J. Am. Chem. Soc.* **2009**, *131*, 5298.
- (7) Montag, M.; Leitus, G.; Shimon, L. J. W.; Ben-David, Y.; Milstein, D. *Chem. Eur. J.* **2007**, *13*, 9043.
- (8) Nesmeyanov, A. N.; Krivykh, V. V.; Rybinskaya, M. I. *J. Organomet. Chem.* **1979**, *164*, 159.
- (9) Singewald, E. T.; Mirkin, C. A.; Stern, C. L. *Angew. Chem. Int. Ed.* **1995**, *34*, 1624.
- (10) Singewald, E. T.; Shi, X.; Mirkin, C. A.; Schofer, S. J.; Stern, C. L. *Organometallics* **1996**, *15*, 3062.
- (11) Werner, H. *Dalton Trans.* **2003**, 3829.
- (12) Vigalok, A.; Uzan, O.; Shimon, L. J. W.; Ben-David, Y.; Martin, J. M. L.; Milstein, D. *J. Am. Chem. Soc.* **1998**, *120*, 12539.
- (13) Winter, W. *Angew. Chem. Int. Ed.* **1976**, *15*, 241.
- (14) Dani, P.; Karlen, T.; Gossage, R. A.; Smeets, W. J. J.; Spek, A. L.; van Koten, G. *J. Am. Chem. Soc.* **1997**, *119*, 11317.
- (15) Fages, F.; Desvergne, J. P.; Bouas-Laurent, H.; Marsau, P.; Lehn, J. M.; Kotzyba-Hibert, F.; Albrecht-Gary, A. M.; Al-Joubbeh, M. *J. Am. Chem. Soc.* **1989**, *111*, 8672.
- (16) Howarth, O. W.; Nelson, J.; McKee, V. *Chem. Commun.* **2000**, 21.
- (17) Stepień, M.; Latos-Grażyński, L.; Szterenberga, L.; Panek, J.; Latajka, Z. *J. Am. Chem. Soc.* **2004**, *126*, 4566.
- (18) Ribas, X.; Calle, C.; Poater, A.; Casitas, A.; Gómez, L.; Xifra, R. I.; Parella, T.; Benet-Buchholz, J.; Schweiger, A.; Mitrikas, G.; Solà, M.; Llobet, A.; Stack, T. D. *J. Am. Chem. Soc.* **2010**, *132*, 12299.
- (19) Barder, T. E.; Biscoe, M. R.; Buchwald, S. L. *Organometallics* **2007**, *26*, 2183.
- (20) Velian, A.; Lin, S.; Miller, A. J. M.; Day, M. W.; Agapie, T. *J. Am. Chem. Soc.* **2010**, *132*, 6296.

- (21) Herbert, D. E.; Lara, N. C.; Agapie, T. *Chem. Eur. J.* **2013**, *19*, 16453.
- (22) Kelley, P.; Lin, S.; Edouard, G.; Day, M. W.; Agapie, T. *J. Am. Chem. Soc.* **2012**, *134*, 5480.
- (23) Fryzuk, M. D.; MacNeil, P. A. *J. Am. Chem. Soc.* **1984**, *106*, 6993.
- (24) Ekici, S.; Nieger, M.; Glaum, R.; Niecke, E. *Angew. Chem. Int. Ed.* **2003**, *42*, 435.
- (25) Ghilardi, C. A.; Sabatini, A.; Sacconi, L. *Inorg. Chem.* **1976**, *15*, 2763.
- (26) Cecconi, F.; Ghilardi, C. A.; Innocenti, P.; Mealli, C.; Midollini, S.; Orlandini, A. *Inorg. Chem.* **1984**, *23*, 922.
- (27) Ferguson, G. S.; Wolczanski, P. T. *Organometallics* **1985**, *4*, 1601.
- (28) Hou, H.; Gantzel, P. K.; Kubiak, C. P. *Organometallics* **2003**, *22*, 2817.
- (29) MacBeth, C. E.; Thomas, J. C.; Betley, T. A.; Peters, J. C. *Inorg. Chem.* **2004**, *43*, 4645.
- (30) Gerzain, M.; Buchanan, G. W.; Driega, A. B.; Facey, G. A.; Enright, G.; Kirby, R. A. *J. Chem. Soc., Perkin Trans. 2* **1996**, 2687.
- (31) Hou, H.; Rheingold, A. L.; Kubiak, C. P. *Organometallics* **2004**, *24*, 231.
- (32) Price, J. T.; Sorensen, T. S. *Can. J. Chem.* **1968**, *46*, 515.
- (33) NMR spectra of the dissolved crystals of **6** indicate the presence of multiple species. The major species, with analogous NMR features to **5**, is assigned as a species corresponding to **6**.
- (34) Silvestre, J.; Albright, T. A. *J. Am. Chem. Soc.* **1985**, *107*, 6829.
- (35) Bach, I.; Porschke, K.-R.; Goddard, R.; Kopsike, C.; Kruger, C.; Rufinska, A.; Seevogel, K. *Organometallics* **1996**, *15*, 4959.
- (36) Browning, J.; Cundy, C. S.; Green, M.; Stone, F. G. A. *J. Chem. Soc. A.* **1971**, 448.
- (37) Browning, J.; Green, M.; Spencer, J. L.; Stone, F. G. A. *J. Chem. Soc., Dalton Trans.* **1974**, 97.
- (38) Johnson, S. A.; Mroz, N. M.; Valdizon, R.; Murray, S. *Organometallics* **2011**, 441.
- (39) Stanger, A.; Vollhardt, K. P. C. *Organometallics* **1992**, *11*, 317.
- (40) Scott, F.; Krüger, C.; Betz, P. *J. Organomet. Chem.* **1990**, *387*, 113.
- (41) Benn, R.; Mynott, R.; Topalovic, I.; Scott, F. *Organometallics* **1989**, *8*, 2299.
- (42) Atesjin, T. I. A.; Li, T.; Lachaize, S. b.; García, J. J.; Jones, W. D. *Organometallics* **2008**, *27*, 3811.
- (43) Li, J.; Lin, Z. *Organometallics* **2009**, *28*, 4231.
- (44) Nova, A.; Reinhold, M.; Perutz, R. N.; Macgregor, S. A.; McGrady, J. E. *Organometallics* **2010**, *29*, 1824.
- (45) Page, M. I.; Jencks, W. P. *Proc. Natl. Acad. Sci. USA* **1971**, *68*, 1678.

- (46) Anslyn, E. V.; Dougherty, D. A. *Modern Physical Organic Chemistry*; 4th ed.; University Science Books: Sausalito, California, 2006.
- (47) Tolman, C. A. *Chem. Rev.* **1977**, *77*, 313.
- (48) Albright, T. A.; Burdett, J. K.; Whangbo, M. H. *Orbital Interactions in Chemistry*; 1st ed.; John Wiley & Sons, Inc.: New York, 1985.
- (49) Nickel, T.; Goddard, R.; Krüger, C.; Pörschke, K.-R. *Angew. Chem. Int. Ed.* **1994**, *33*, 879.
- (50) Meltzer, A.; Präsang, C.; Milsmann, C.; Driess, M. *Angew. Chem. Int. Ed.* **2009**, *48*, 3170.
- (51) Watanabe, C.; Inagawa, Y.; Iwamoto, T.; Kira, M. *Dalton Trans.* **2010**, *39*, 9414.
- (52) Henning, J.; Wesemann, L. *Angew. Chem. Int. Ed.* **2012**, *51*, 12869.
- (53) Radonovich, L. J.; Koch, F. J.; Albright, T. A. *Inorg. Chem.* **1980**, *19*, 3373.
- (54) Priego, J. L.; Doerrer, L. H.; Rees, L. H.; Green, M. L. H. *Chem. Commun.* **2000**, 779.
- (55) Campora, J.; del Mar Conejo, M.; Reyes, M. L.; Mereiter, K.; Passaglia, E. *Chem. Commun.* **2003**, 78.
- (56) Ito, M.; Matsumoto, T.; Tatsumi, K. *Inorg. Chem.* **2009**, *48*, 2215.
- (57) Wright, A. M.; Wu, G.; Hayton, T. W. *Inorg. Chem.* **2011**, *50*, 11746.
- (58) Serrano, O.; Hoppe, E.; Fettingner, J. C.; Power, P. P. *J. Organomet. Chem.* **2011**, *696*, 2217.
- (59) Kraikivskii, P. B.; Saraev, V. V.; Meusinger, R.; Bocharova, V. V.; Ushakov, I. A.; Petrovskii, S. K. *J. Organomet. Chem.* **2012**, *715*, 43.
- (60) Mindiola, D. J.; Waterman, R.; Jenkins, D. M.; Hillhouse, G. L. *Inorg. Chim. Acta* **2003**, *345*, 299.
- (61) Kitiachvili, K. D.; Mindiola, D. J.; Hillhouse, G. L. *J. Am. Chem. Soc.* **2004**, *126*, 10554.
- (62) Ingleson, M. J.; Fullmer, B. C.; Buschhorn, D. T.; Fan, H.; Pink, M.; Huffman, J. C.; Caulton, K. G. *Inorg. Chem.* **2007**, *47*, 407.
- (63) Marlier, E. E.; Tereniak, S. J.; Ding, K.; Mulliken, J. E.; Lu, C. C. *Inorg. Chem.* **2011**, *50*, 9290.
- (64) Sommovigo, M.; Pasquali, M.; Leoni, P.; Sabatino, P.; Braga, D. *J. Organomet. Chem.* **1991**, *418*, 119.
- (65) Perez, P. J.; Calabrese, J. C.; Bunel, E. E. *Organometallics* **2000**, *20*, 337.
- (66) Fanjul, T.; Eastham, G.; Fey, N.; Hamilton, A.; Orpen, A. G.; Pringle, P. G.; Waugh, M. *Organometallics* **2010**, *29*, 2292.
- (67) Steinke, T.; Shaw, B. K.; Jong, H.; Patrick, B. O.; Fryzuk, M. D. *Organometallics* **2009**, *28*, 2830.

- (68) Gregor, L. C.; Chen, C.-H.; Fafard, C. M.; Fan, L.; Guo, C.; Foxman, B. M.; Gusev, D. G.; Ozerov, O. V. *Dalton Trans.* **2010**, *39*, 3195.
- (69) Zhu, Y.; Chen, C.-H.; Fafard, C. M.; Foxman, B. M.; Ozerov, O. V. *Inorg. Chem.* **2011**, *50*, 7980.
- (70) Derrah, E. J.; Martin, C.; Mallet-Ladeira, S.; Miqueu, K.; Bouhadir, G.; Bourissou, D. *Organometallics* **2013**, *32*, 1121.
- (71) Koga, N.; Obara, S.; Kitaura, K.; Morokuma, K. *J. Am. Chem. Soc.* **1985**, *107*, 7109.
- (72) López-Serrano, J.; Duckett, S. B.; Aiken, S.; Almeida Leñero, K. Q.; Drent, E.; Dunne, J. P.; Konya, D.; Whitwood, A. C. *J. Am. Chem. Soc.* **2007**, *129*, 6513.
- (73) Velian, A. Undergraduate Thesis, California Institute of Technology, 2009.
- (74) Konrad, T. M.; Fuentes, J. A.; Slawin, A. M. Z.; Clarke, M. L. *Angew. Chem. Int. Ed.* **2010**, *49*, 9197.
- (75) Johnson, S. A.; Taylor, E. T.; Cruise, S. J. *Organometallics* **2009**, *28*, 3842.
- (76) Bai, G.; Wei, P.; Stephan, D. W. *Organometallics* **2005**, *24*, 5901.
- (77) Schneider, Jörg J.; Spickermann, D.; Bläser, D.; Boese, R.; Rademacher, P.; Labahn, T.; Magull, J.; Janiak, C.; Seidel, N.; Jacob, K. *Eur. J. Inorg. Chem.* **2001**, *2001*, 1371.
- (78) Chen, Y.; Sui-Seng, C.; Zargarian, D. *Angew. Chem. Int. Ed.* **2005**, *44*, 7721.
- (79) Priego, J. L.; Doerrer, L. H.; Rees, L. H.; Green, M. L. H. *Chem. Commun.* **2000**, 779.
- (80) Higgs, T. C.; Carrano, C. J. *Inorg. Chem.* **1997**, *36*, 298.
- (81) Shao, Q.; Sun, H.; Shen, Q.; Zhang, Y. *Appl. Organomet. Chem.* **2004**, *18*, 289.
- (82) Meinhard, D.; Reuter, P.; Rieger, B. *Organometallics* **2007**, *26*, 751.
- (83) Laine, T. V.; Klinga, M.; Leskelä, M. *Eur. J. Inorg. Chem.* **1999**, *1999*, 959.
- (84) Ge, S.; Hartwig, J. F. *J. Am. Chem. Soc.* **2011**, *133*, 16330.
- (85) Butcher, R. J.; Sinn, E. *Inorg. Chem.* **1977**, *16*, 2334.
- (86) Petriček, S.; Demšar, A. *Polyhedron* **2010**, *29*, 3329.
- (87) A crystal structure of $[(\kappa^3\text{-di(2-methoxy)ether})\text{NiBr}_2]_2$ is available from the Cambridge Crystallographic Data Centre: deposition 725331.
- (88) Crochet, A.; Fromm, Katharina M. *Z. Anorg. Allg. Chem.* **2010**, *636*, 1484.
- (89) Tamayo, A.; Casabó, J.; Escriche, L.; Lodeiro, C.; Covelo, B.; Brondino, C. D.; Kivekäs, R.; Sillampää, R. *Inorg. Chem.* **2006**, *45*, 1140.
- (90) Kuwamura, N.; Kitano, K. i.; Hirotsu, M.; Nishioka, T.; Teki, Y.; Santo, R.; Ichimura, A.; Hashimoto, H.; Wright, L. J.; Kinoshita, I. *Chem. Eur. J.* **2011**, *17*, 10708.
- (91) Konze, W. V.; Scott, B. L.; Kubas, G. J. *J. Am. Chem. Soc.* **2002**, *124*, 12550.

- (92) Thomas, J. C.; Peters, J. C. *J. Am. Chem. Soc.* **2003**, *125*, 8870.
- (93) Buchalski, P.; Grabowska, I.; Karaskiewicz, A.; Suwińska, K.; Jerzykiewicz, L. *Organometallics* **2008**, *27*, 3316.
- (94) Buchalski, P.; Koziol, A.; Pasynkiewicz, S.; Pietrzykowski, A.; Suwinska, K.; Zdziemborska, M. *J. Organomet. Chem.* **2006**, *691*, 4080.
- (95) Keen, A. L.; Doster, M.; Johnson, S. A. *J. Am. Chem. Soc.* **2007**, *129*, 810.
- (96) Keen, A. L.; Johnson, S. A. *J. Am. Chem. Soc.* **2006**, *128*, 1806.
- (97) Ramakrishna, T. V. V.; Sharp, P. R. *Organometallics* **2004**, *23*, 3079.
- (98) Suzuki, A. *Angew. Chem. Int. Ed.* **2011**, *50*, 6722.
- (99) Frisch, A. C.; Beller, M. *Angew. Chem. Int. Ed.* **2005**, *44*, 674.
- (100) Netherton, M. R.; Fu, G. C. *Adv. Synth. Catal.* **2004**, *346*, 1525.
- (101) Rudolph, A.; Lautens, M. *Angew. Chem. Int. Ed.* **2009**, *48*, 2656.
- (102) Terao, J.; Kambe, N. *Acc. Chem. Res.* **2008**, *41*, 1545.
- (103) Powers, D. C.; Lee, E.; Ariafard, A.; Sanford, M. S.; Yates, B. F.; Canty, A. J.; Ritter, T. *J. Am. Chem. Soc.* **2012**, *134*, 12002.
- (104) Beck, R.; Johnson, S. A. *Chem. Commun.* **2011**, *47*, 9233.
- (105) Edelbach, B. L.; Lachicotte, R. J.; Jones, W. D. *Organometallics* **1999**, *18*, 4040.
- (106) Eisch, J. J.; Piotrowski, A. M.; Han, K. I.; Kruger, C.; Tsay, Y. H. *Organometallics* **1985**, *4*, 224.
- (107) Pangborn, A. B.; Giardello, M. A.; Grubbs, R. H.; Rosen, R. K.; Timmers, F. J. *Organometallics* **1996**, *15*, 1518.
- (108) Fulmer, G. R.; Miller, A. J. M.; Sherden, N. H.; Gottlieb, H. E.; Nudelman, A.; Stoltz, B. M.; Bercaw, J. E.; Goldberg, K. I. *Organometallics* **2010**, *29*, 2176.
- (109) Ikeda, C.; Sakamoto, N.; Nabeshima, T. *Org. Lett.* **2008**, *10*, 4601.
- (110) Albrecht, M.; Schneider, M. *Synthesis* **2000**, *2000*, 1557.
- (111) Shukla, R.; Lindeman, S. V.; Rathore, R. *Chem. Commun.* **2009**, 5600.
- (112) APEX2, Version 2 User Manual, M86-E01078, Bruker Analytical X-ray Systems, Madison, WI, June 2006.
- (113) Sheldrick, G.M. "SADABS (version 2008/1): Program for Absorption Correction for Data from Area Detector Frames", University of Göttingen, 2008.
- (114) Sheldrick, G.M. (2008). *Acta Cryst. A* *64*, 112-122.
- (115) Brandenburg, K. (1999). DIAMOND. Crystal Impact GbR, Bonn, Germany.

CHAPTER 3

INTRAMOLECULAR DEAROMATIZATION REACTIONS OF MONONICKEL TERPHENYL DIPHOSPHINE COMPOUNDS

Published in part as:

Lin, S., Day, M. W., Agapie, T. *J. Am. Chem. Soc.*, **2011**, *133*, 3828-3831.

ABSTRACT

Nickel hydrides supported by a terphenyl diphosphine are synthesized and found to undergo intramolecular nickel-to-arene H-transfers. Some of the resulting complexes also undergo the reverse (C-to-Ni) H-migration indicating the potential for storing H-equivalents in this type of pincer ligand. NMR spectroscopy, single crystal X-ray diffraction, and isotopic labeling studies investigating the mechanism of these processes are discussed. Reactivity of nickel-bound central arene is then extended to arene hydrogenation with Shvo's catalyst, which does not typically hydrogenate aromatic substrates. Although other complexes of the terphenyl diphosphine framework are tested for susceptibility to hydrogenation, no other complexes are found to be reactive. One possibility is that the reactivity of the nickel complex may result from steric strain of its terphenyl backbone.

INTRODUCTION

Metal hydrides are intermediates in a wide variety of catalytic transformations. Improved understanding of the parameters that affect hydride reactivity is of interest in developing effective catalysts for proton reduction, CO₂ reduction, hydrosilylation, hydroboration, heterocycle activation, arene reduction and olefin hydrogenation and isomerization.¹⁻¹⁸ Furthermore, molecular designs for shuttling of hydrogen equivalents are of importance in biological transformations such as dioxygen activation and reduction. A diphosphine-arene pincer ligand was recently reported to support mononuclear and dinuclear nickel complexes that exhibit strong nickel-arene interactions.^{19,20} This chapter discusses two kinds of reactivity of these compounds: (1) These complexes provide access to a new class of nickel hydrides supported by arene π -interactions. We report on the reactivity of these species and a series of H-migration processes relevant to arene hydrogenation and to potential storage of H-equivalents in the ligand backbone. (2) We then extend the studies toward hydrogenation of nickel-bound arenes catalyzed by external catalysts.

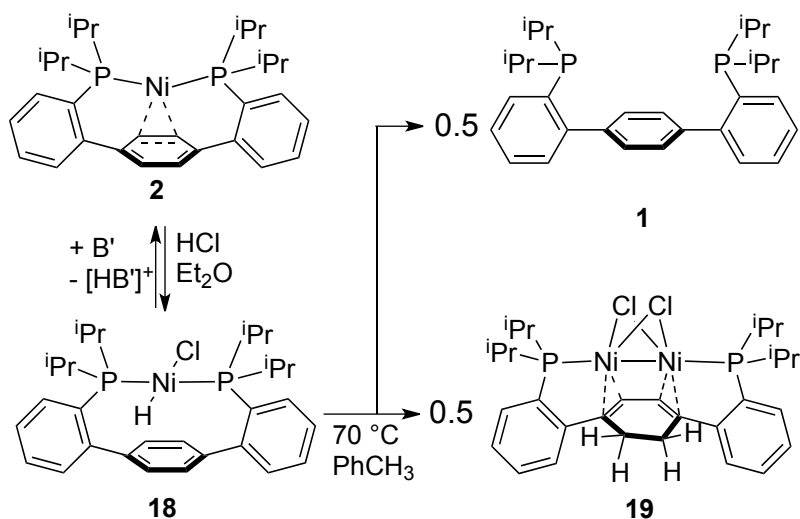
RESULTS AND DISCUSSION

1. Nickel-to-Arene Hydrides Transfers

1.1. Synthesis and reactivity of nickel hydride chloride 18. Treatment of Ni(0) diphosphine **2** with one equivalent of HCl/Et₂O (Scheme 3.1) generates a new species that displays a triplet at -29.0 ppm ($J_{\text{PH}} = 79$ Hz) in the ¹H NMR spectrum and a doublet in the ³¹P NMR spectrum, consistent with formation of a nickel hydride complex with two equivalent phosphines.^{5,8,11,21-24} Two singlets are observed in the ¹H NMR spectrum corresponding to the central ring, supporting a C_s-symmetric structure (**18**). In THF, compound **18** is 22% deprotonated by one equivalent of dimethylbenzylamine (DMBA) to reform **2**, indicating

that **18** is slightly less acidic than [DMBA]-H⁺ (p*K*_a approx. 16.79 in MeCN^{25,26}). This result also indicates that protonation of **2** is a reversible process. The single-crystal X-ray diffraction (XRD) difference map of **18** shows, in addition to a chloride and two phosphines, a smaller electron density peak in proximity to nickel (*r* = 1.33(2) Å). This peak was assigned as a hydride ligand to complete a square planar coordination environment around the metal center. Consistent with this geometry, the Ni–C(arene) distances are long (> 2.5 Å), indicating weak interaction between the metal and the π-system of the arene. Further, only a slight variation in the C–C bond lengths of the central arene is observed, with a difference between the longest and the shortest bonds of less than 0.02 Å (**18**, Figure 3.1). In contrast, the Ni–C bond lengths of **2** are about 1.99 Å, and the C–C bonds show differences of up to 0.07 Å.

Scheme 3.1. Synthesis and Ligand Disproportionation of **18**



Heating a C₆H₆ solution of **18** at 70 °C leads to clean generation of equimolar amounts of a new nickel-containing species (**19**, Scheme 3.1) and free diphosphine (**1**). The ¹H NMR spectrum of **19** shows a singlet corresponding to only two hydrogens in the olefinic region. Additionally, two new peaks that integrate to two hydrogens each are present in the

aliphatic region. An XRD study reveals that **19** possesses a Ni₂Cl₂ core that interacts with four carbons of the central ring (Figure 3.1). The remaining two central ring carbons are 1.519(1) Å apart, indicative of a single bond. Thus the present system provides a well-defined architecture to further our understanding of arene hydrogenation and H-migration from metals to arenes.⁸

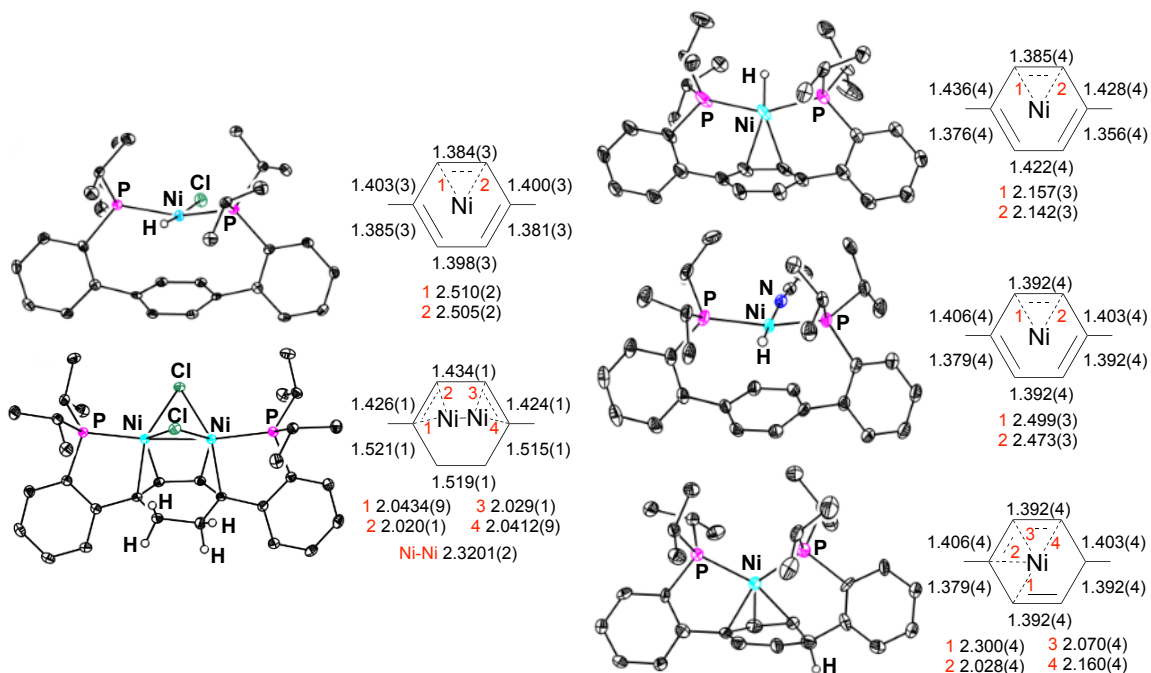


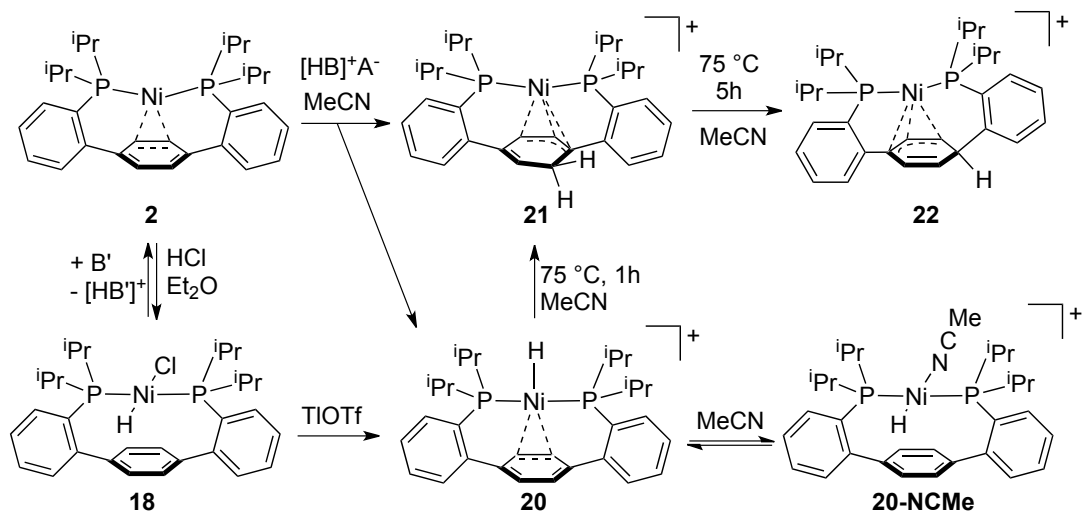
Figure 3.1. Solid-state structures of (top to bottom, left column then right): **18**, **19**, **20-OTf**, **20-MeCN-OTf**, and **22-BArF₂₄** and selected C-C and Ni-C distances. Solvent molecules, anions, and select hydrogen atoms have been cropped for clarity.

Furthermore, “non-innocent” aromatic ligands that can store H-equivalents by incorporation into a π -system are of interest and have been recently described in the context of transformations such as water splitting into dioxygen and dihydrogen.²⁷⁻³¹

1.2. Synthesis and reactivity of cationic nickel hydride. To study the H-migration process, a cationic hydride variant was prepared by halide abstraction of **18** with TlOTf (Scheme 3.2).

XRD studies of crystals obtained from acetonitrile solution reveal the presence of two co-crystallized cationic species in the solid state. One species (**20**) is a nickel-hydride supported by two phosphines and a double bond of the central arene. The Ni–C distances (2.142(3)–2.157(3) Å) are shorter than in **18**, indicating that displacement of the halide to generate a cationic species leads to a stronger interaction of the metal center with the arene (Figure 1). The central arene C–C bond lengths indicate similar dearomatization as in **2** (variation up to 0.06 Å). The second species has acetonitrile coordinated to the site previously occupied by chloride (**20-NCMe**). Similar to **18**, the Ni–C distances are long (> 2.4 Å). Peaks in the XRD difference map are assigned to hydrides of **20** and **20-NCMe** and complete pseudo-square planar coordination environments around the metal centers. On the NMR time scale, a single species is detected in an acetonitrile solution of **20**, with a Ni–H signal at –25.1 ppm. In CD₂Cl₂, the Ni–H peak is at –17.6 ppm. Titration of this solution with acetonitrile leads to a gradual shift of the Ni–H peak towards the chemical shift in acetonitrile. This behavior suggests that coordination of acetonitrile to **20** is rapid and reversible in solution. Assuming that in acetonitrile the chemical shift of the hydride corresponds to **20-MeCN**, the equilibrium constant for acetonitrile dissociation from **20-MeCN** is calculated to be 1.13 M. In THF, **20** is 26% deprotonated by one equivalent of DMBA, suggesting that it is of comparable acidity to **18**.

Scheme 3.2. Synthesis, Acetonitrile Coordination, and Ni-to-Arene H-Transfer of 20

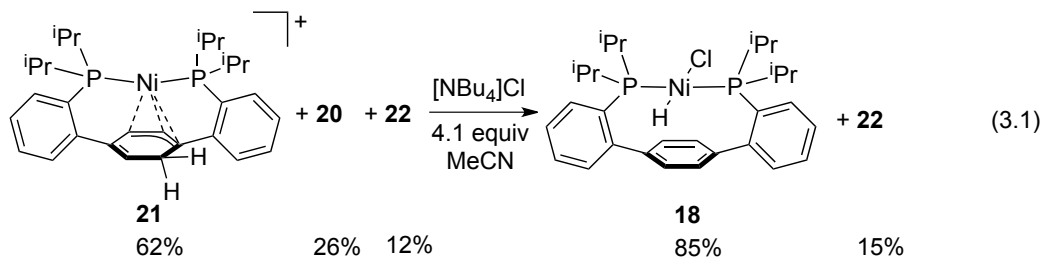


Handling of **20** in solvents such as THF or DCM at room temperature leads to the formation of two new species displaying no upfield ^1H NMR signals indicative of a metal hydride over several days. As determined by various NMR correlation experiments, one species (**21**) possesses three olefinic protons and two methylene protons on its central ring (see Experimental). A pair of doublets ($J_{\text{pp}} = 10.9$ Hz) is observed by ^{31}P NMR spectroscopy. While reliable crystallographic information has not been obtained for compound **21**, NMR data is consistent with H-migration to the central ring at the position *ortho* to an aryl-aryl linkage (Scheme 3.2).

The species (**22**) observed in mixture with **21** possesses two olefinic ^1H peaks and a pair of ^{31}P doublets ($J_{\text{pp}} = 1.4$ Hz). XRD characterization of **22** shows that the two arene-arene linkages display different angles, with one being significantly removed from coplanarity with respect to the central ring. The C–C bonds of the central ring adjacent to this aryl-aryl linkage are elongated (> 1.47 Å). The nickel center displays close contacts to only three carbons of the central ring (< 2.2 Å), reminiscent of a metal-allyl interaction. Consistent with this bonding description, a double bond appears to be localized between the

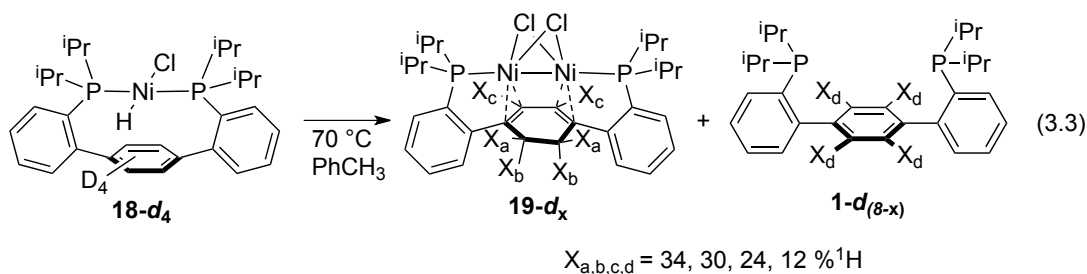
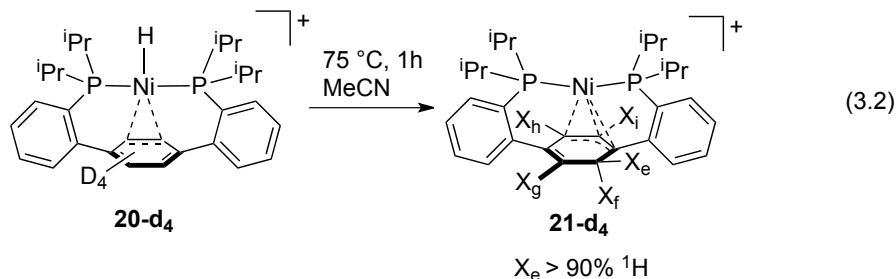
remaining two carbons of the central ring.³²⁻³⁴ The crystallographic and NMR data is consistent with H-migration to the *ipso*-carbon of the central ring (Scheme 3.2).

To further explore the potential of the arene pincer for reversible storage of H-equivalents, the cationic products (**21** and **22**) of Ni-to-C H-migration were investigated. Heating of **20** in THF was interrupted when a mixture of **21** (62%), **20** (26%), and **22** (12%) was generated (eq 3.1). Addition of chloride to this mixture leads to the formation of **18** (85%) and **22** (15%), which is consistent with the quantitative conversion of **21** and **20** into **18**. Treatment of the mixture of **20**, **21**, and **22** with 1,8-diazabicyclo[5.4.0]undec-7-ene (DBU) leads to the formation of **2**. While generation of **18** from **20** by coordination of chloride is expected, the generation of **18** from **21** is less mechanistically obvious. In an acid-base mechanism, chloride could act as a base to deprotonate **21**, generating **1** and HCl as intermediates toward **18**. This explanation is inconsistent with the stability of **22** toward chloride and the weak basicity of chloride (predicted $pK_a(\text{HCl}) = 10.30$ in MeCN³⁵). In an alternate mechanism, chloride could bind to nickel and weaken metal-carbon interactions, leading to more reactive methylene C–H bonds that would be prone to undergo C-to-Ni H-transfer. Intramolecular H-migration between a metal center and a delocalized p-bound ligand has been proposed previously, for example, for the hydrogenation of arene by cobalt hydrides and for isotopic scrambling in the reductive elimination of alkane from bis(pentamethylcyclopentadienyl)zirconium derivatives.^{36,37} Direct deprotonation of arenium moiety by added base cannot be ruled out especially for stronger bases, however, given that both **21** and **22** are converted to **2** by DBU ($pK_a([\text{DBU}]\text{-H}^+) = 24.34$ in MeCN²⁶).



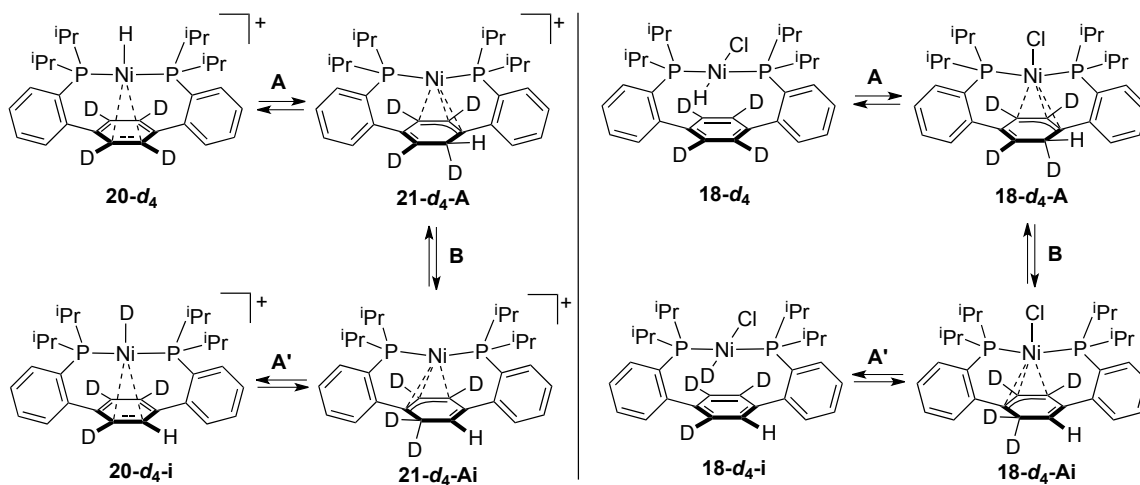
The H-migration processes were studied in detail. Heating of **20** for 1h at 75 °C in CD₃CN leads initially to formation of **21** with little generation of **22**; further heating converts **21** to **22** (Scheme 3.2). These observations are consistent with H-migration from the metal center to the less substituted carbon of the central arene, under kinetic control to first generate intermediate **21**. Further H-migration around the ring to the *ipso*-carbon gives the thermodynamic product **22**. Calculations have suggested that *ipso* protonation is thermodynamically disfavored *vs.* *ortho* or *para* protonation of biphenyl,³⁸ but the relative stability of **22** might be due to release of terphenyl strain that is present in all other mononuclear complexes of ligand **1** (**2**, **18**, **20** and **21**). Protonations of **2** with [H(OEt₂)] [B(C₆H₃(CF₃)₂)₄] or [H₃NC₆H₄CN] [OTf] (OTf = triflate) in acetonitrile at room temperature lead to **20** and **21** upon mixing (Scheme 3.2). The fast formation of **21** suggests that **20** is not an intermediate in this case. Hence, direct intermolecular protonation at the carbon is a viable mechanistic pathway in these systems. Again, formation of **22** is kinetically unfavorable.

1.3. Deuterium isotope labeling studies. Isotopic labeling studies have provided further mechanistic insight into these processes. Nickel complexes of **1-d₄** (perdeuterated at the central arene) were prepared. Complex **20-d₄** converts to **21-d₄** with ¹H incorporation primarily at the *endo* methylene position of the central ring (X_c, eq. 3.2). No ¹H incorporation occurs at the olefinic positions (X_g, X_h, or X_i). Unreacted **20-d₄** (during the conversion to **21-d₄**) showed no label scrambling.



Lack of ^1H incorporation at the olefinic positions indicates that after H-transfer from metal to carbon (similar to process A, Scheme 3.3), 1,2-H shifts (process B) from methylene to methine do not occur on the timescale of the experiment.^{39,40} ^1H incorporation at the *endo* methylene position suggests an intramolecular mechanism for conversion of **20** to **21**. The rate of formation of **21** from **20** is solvent dependent, suggesting that coordination of nitrile to **20** inhibits H-migration. The nickel interaction with the π -system, which is stronger in the absence of acetonitrile, may be a determining factor for ring activation toward H-transfer.

Scheme 3.3. Isotope Scrambling Mechanisms for **20** (left) and **18** (right)



Upon heating, **18-d₄** leads to significant label distribution to all positions of the ring in **19** (% ¹H incorporation at aliphatic positions X_a and X_b, and olefinic position X_c is 34:30:24, eq. 3.3) but also into free phosphine, **1** (X_d, 12%). Analysis of unreacted **18-d₄** at 50% conversion shows ~60% of ¹H scrambled into the aromatic positions. Label scrambling in **18-d₄** suggests a mechanism similar to the conversion of **20** to **21** (process A, Scheme 3.3), but followed by either 1,2-H-shift from methylene to methine (process B) and then migration of H(D) back to nickel (process A'), or intermolecular H-transfer back to metal to give isotopomer **18-d₄-i**. This scrambling further attests to the reversible H-shuttling potential of pincer arenes. As with **20** in acetonitrile, compound **18** requires heating for H-migration to occur; this, again, may be a consequence of a weaker interaction between nickel and the central arene. This proposal is consistent with the difference in the isotopic label scrambling between the cationic and neutral hydrides; a weaker interaction between the halide-coordinated nickel and the π-system may allow for facile 1,2-H shifts if an arenium moiety is formed. In contrast, assuming that the π-system of **21** is localized as in **22** (as a strong nickel-allyl-like interaction adjacent to a double bond), 1,2-H shifts are less accessible for the cationic species.

The sequence of steps subsequent to H-migration leading to the dinuclear species **19** and free phosphine are not clear. Nevertheless, isotopic scrambling into **18-d₄** (eq. 3.3) explains the incorporation of ¹H at all positions on the central ring of **19** and **1**; the lower than expected statistical ¹H content in the resulting free phosphine, however, suggests an isotope effect for subsequent steps that favors ¹H incorporation into the partially reduced arene of **19**. The driving force for this reaction may be the formation of a Ni¹₂Cl₂ moiety, which has been observed in a few reactions with this ligand. A combination of bridging

halides, Ni–Ni bonding, and Ni–arene interactions may render **19** as the thermodynamic product.

2. Hydrogenation of Nickel-Bound Arenes

2.1 Introduction. Arenes are relatively less reactive than alkenes and dienes due to aromatic stabilization. One strategy to activate arenes for olefin-like reactivity is transition metal coordination. Transition metals act as a π -base and bind η^2 to aromatics, inducing partial localization of single and double bonds about the arene ring. These partially localized double bonds may be susceptible to traditional alkene and diene chemistry. Harman and Taube⁴¹ studied landmark complexes of the form $[\text{Os}(\text{NH}_3)_5(\eta^2\text{-arene})]^{2+}$, and Harman later reported other low-valent octahedral d^6 metal (Re(I), Mo(0), W(0)) complexes that bind and activate a range of η^2 -arenes.^{42,43} The four unbound carbons of the arenes were shown by x-ray diffraction (XRD) studies to resemble butadiene; accordingly, the butadiene-like fragments were able to undergo protonation, hydrogenation, electrophilic addition, or Diels-Alder reactions. Unfortunately these dearomatization agents do not readily release bound product due to the thermodynamic and kinetic stability of d^6 octahedral compounds, precluding catalytic turnover. For instance, hydrogenation of $[\text{Os}(\text{NH}_3)_5(\eta^2\text{-benzene})]^{2+}$ yields $[\text{Os}(\text{NH}_3)_5(\eta^2\text{-cyclohexene})]^{2+}$, but oxidation of the metal center is necessary to release cyclohexene.⁴¹ Lewis acids have been used as substoichiometric dearomatization agents, allowing for hydrogenation of arenes under mild conditions.⁴⁴ Unfortunately, Lewis acids could be incompatible with polar functional groups, limiting the substrate scope of Lewis acid dearomatization agents. While other transition metals have been observed

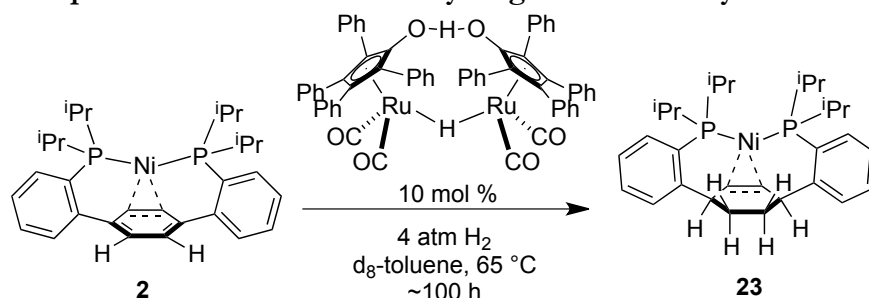
to bind and activate arenes, few studies of these metals as (potentially catalytic) dearomatization agents have been reported.

Group 10 metal-arene interactions, as demonstrated and discussed throughout Chapter 2, are relatively labile. As a proof of principle that these labile late transition metal-arene interactions can facilitate dearomatization reactions, **2** was chosen as a favorable test substrate because the nickel-arene interaction is enforced by phosphine chelation.

2.2. Hydrogenation of 2. Using a multi-well stainless steel reactor, various hydrogenation catalysts (~10 wt%) were screened for reactivity with **2** in toluene under 7 atm H₂. The reactions were evaluated by ³¹P NMR of the crude mixture after 16 h at 100 °C. Reactions with RhCl(PPh₃)₃, IrCl(PPh₃)₃, and Shvo's catalyst^{45,46} each displayed peaks downfield of the starting material that may be hydrogenation products of **2**. However, the former two catalysts also facilitated complete decomposition of **2** to **1** ($\delta_{31\text{P}} = -4.7$ ppm). Because of the amenability of homogeneous catalysts toward mechanistic study, Shvo's catalyst was chosen for further optimization of hydrogenation conditions (Scheme 3.4). Of note, Shvo's catalyst has not been reported to hydrogenate arenes, and typical reaction conditions include toluene as solvent.⁴⁷

Hydrogenation of **2** by Shvo's catalyst (10 mol%) under 3.9 atm H₂ at 65 °C over 100 h leads to a new species (**23**) that exhibits one ³¹P NMR peak (s, 46.6 ppm). By ¹H NMR spectroscopy, **23** possesses four aromatic peaks and six aliphatic or olefinic peaks that integrate to two protons each. These integrations are consistent with double hydrogenation of the central arene to a cyclohexene moiety. Fast atom bombardment MS (FAB-MS) of a solution of **23** shows a peak corresponding to doubly hydrogenated ligand (m/z [**23**-Ni+H]⁺ calcd. 467.2996; found 467.2978).

Scheme 3.4. Optimized Conditions for Hydrogenation of **2** by Shvo's Catalyst



To support our assignment of **23**, ¹H-¹H COSY spectra were recorded. Based on the crosspeaks observed, the ¹H NMR spectrum could be assigned for the olefinic and aliphatic peaks H_a through H_f (Figure 3.2). Multiplets at 2.44 and 2.20 ppm show crosspeaks to methyl signals from 1.30 to 1.00 ppm, and are assigned as the isopropyl methine protons. The multiplet at 3.73 ppm shows cross peaks with the multiplets at 1.91 and 1.81 ppm, revealing the former to be benzylic/allylic H_d and the latter pair of multiplets to be aliphatic H_b and H_c. That leaves the singlet with no crosspeaks at 3.03 to be assigned as H_a. The lack of a crosspeak between H_a and H_b can be explained by the magnitude of vicinal couplings vanishing near dihedral angles of 90°.⁴⁸ Although no structural data is available for **23**, for reference, the *ipso*- and *ortho*- central arenium protons of **22** do not display a crosspeak.

To distinguish the germinal *endo*- and *exo*- protons of the central ring (H_c and H_b, respectively), 1D selective Nuclear Overhauser Effect (NOE) experiments were performed. An inverted peak at 3.74 ppm upon excitation at 1.85 ppm indicates through-space interaction between H_d and H_b. Excitation at 1.95 ppm (H_c) did not result in any non-geminal NOE transfers. Ultimately, upon assignment of the central ring protons of **23**, their ¹H NMR chemical shifts match well with literature comparisons. (Figure 3.3)

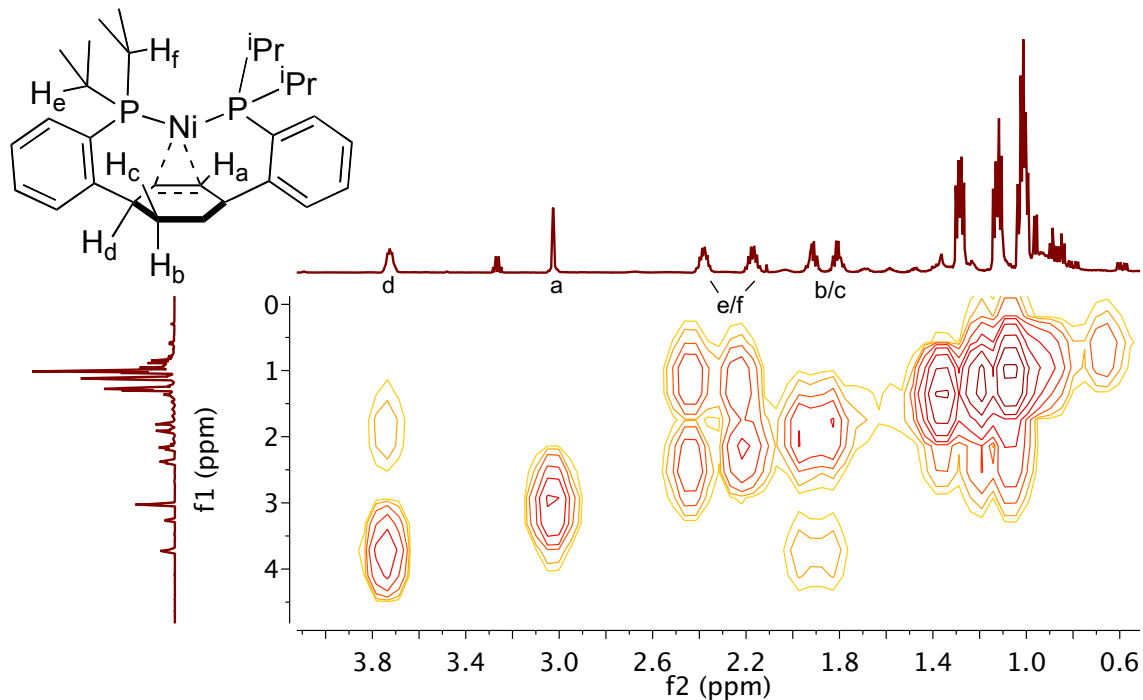


Figure 3.2. Olefinic and aliphatic region of a gradient COSY spectrum of **23**.

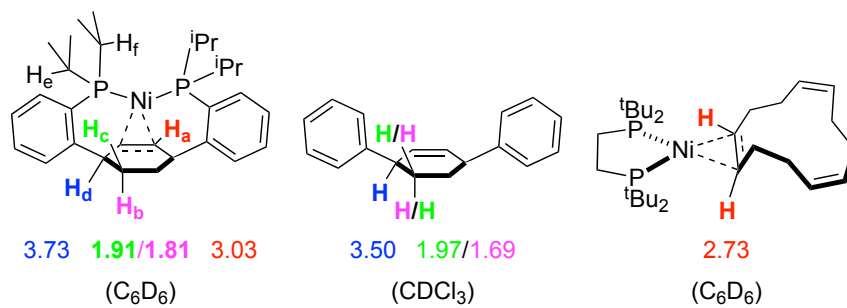
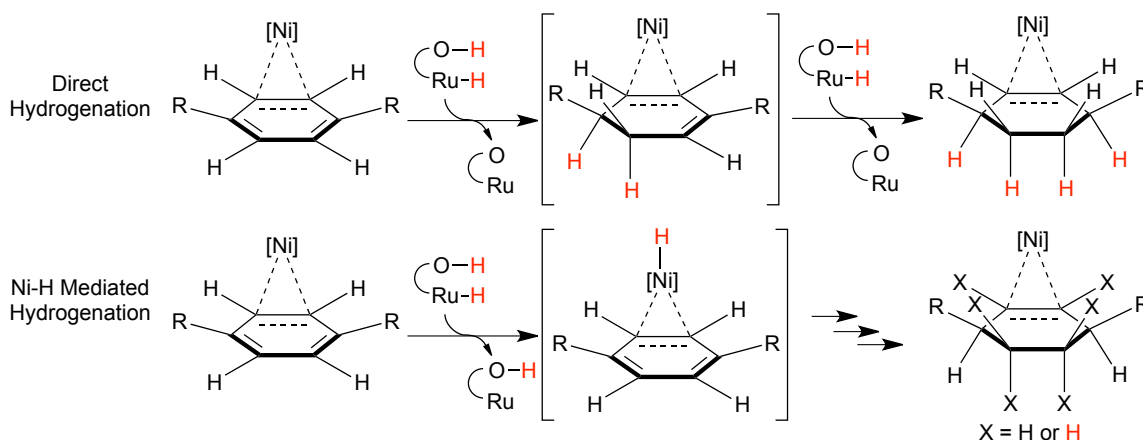


Figure 3.3. Comparison of select ¹H NMR chemical shifts (δ , ppm) of **6**, *cis*-3,6-diphenylcyclohexene,⁴⁹ and (1,2-bis(di-*tert*-butylphosphino)ethane)Ni(η^2 -*cis,cis,cis*-cyclododeca-1,5,9-triene).⁵⁰

Hydrogenation presumably starts via net hydrogenolysis of Shvo's catalyst into monoruthenium hydride species.⁴⁷ Then two routes could account for hydrogenation of the ring: (a) direct hydrogenation of the central ring by ruthenium species or (b)

sequential Ru-to-Ni, Ni-to-arene, and Ru-to-arenium H-transfers (Scheme 3.5). Deuterium labeling studies were designed to distinguish these two mechanisms. Alternatively, heterogeneous ruthenium from Shvo's catalyst decomposition could serve as the catalyst.

Scheme 3.5. Two Mechanisms for Hydrogenation of 2.



A variant of **2** with a perdeuterated central arene (**2-d₄**) was subjected to hydrogenation conditions. The resulting product (**23-d₄**) was found to differ from **23** by missing two peaks in the ¹H NMR spectrum (Figure 3.4): an olefinic singlet at 3.03 (H_a) and an aliphatic multiplet at 1.81 ppm (H_c). The remaining two ¹H NMR peaks of **23-d₄** corresponding to central ring protons were shown to couple through space via Nuclear Overhauser Effect (H_b, H_d). Thus, central ring ¹H nuclei in **23-d₄** are all located on the *exo* face, suggesting that direct *exo* hydrogenation by ruthenium species may be the active mechanism. Putative monohydrogenated intermediates are not observed. They could be minor species in solution at all times, slowly generated and quickly hydrogenated to form **6** upon loss of aromaticity.

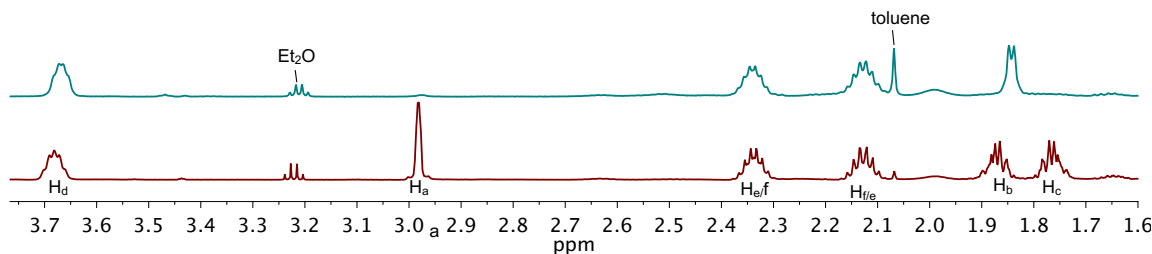


Figure 3.4. Olefinic and aliphatic region of ^1H NMR (600 MHz, C_6D_6) spectra of **23-d₄** (top) and **23** (bottom).

2.3. Hydrogenation of other group 10 metal-arene complexes. Extension of metal coordination-assisted hydrogenation of arenes to other substrates was explored. As a preliminary control, Shvo's catalyst does not hydrogenate **1** under the optimized conditions. Complexes of **1** were then screened for hydrogenation under the optimized reaction conditions. **3**, **7**, **8**, and **12** showed no hydrogenation, despite all exhibiting strong dearomatization of the central arene in the solid state. The other compounds of **1** (reported in Chapter 2) are all thermally unstable or insoluble in toluene. Attempts to hydrogenate these compounds in THF or acetonitrile were unsuccessful.

One explanation for the unique reactivity of **2** is that it combines strong central arene dearomatization with steric accessibility. For instance, although **8** and **9** are similarly dearomatized, the methoxy groups of the former and the unstrained terphenyl backbone of the latter hinder hydrogenation. To increase steric accessibility, hydrogenation of (2-biphenyl)di-*tert*-butylphosphine by Shvo's catalyst was attempted with $\text{Pd}_2(\text{dba})_3$ as an additive (Figure 3.5). By ^{31}P NMR (300 MHz, d_0 -toluene, ref. vs external H_3PO_4), starting phosphine and a new product are observed at 17.9 and 12.9 ppm, respectively. Upon dissolution of the reaction crude in CDCl_3 , the ^1H and ^{31}P NMR spectra of the product align with those reported for trihydrogenated product,

previously synthesized through an independent route⁵¹. The trihydrogenated product was also observed by GC-MS. No *d*₈-1-methylcyclohexane, the product of toluene hydrogenation, was observed by NMR spectroscopy or GC-MS. Although control reactions removing either Shvo's catalyst or Pd₂(dba)₃ did not yield hydrogenated product, hydrogenation by heterogeneous catalysis with Ru or Pd nanoparticles is a possible mechanism given the instability of Pd₂(dba)₃ and the heterogeneous appearance of the reaction mixture.⁵² Nevertheless, the hydrogenation selectivity in an aromatic solvent suggests that the pendant arene is activated toward hydrogenation, perhaps via tethered metal-arene interactions.⁵³

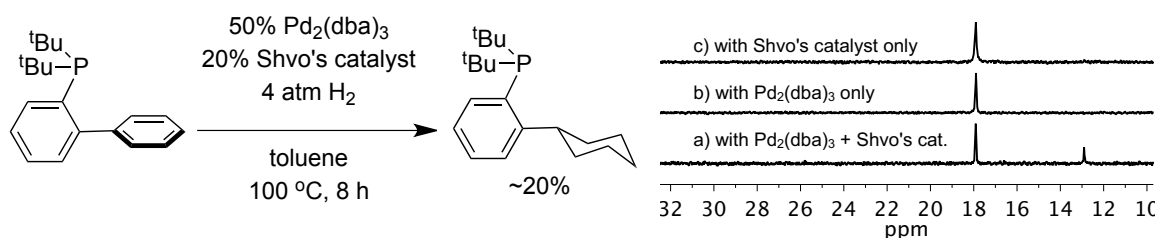


Figure 3.5. Hydrogenation of JohnPhos with Shvo's catalyst and Pd₂(dba)₃. Left: reaction conditions. Right: ³¹P NMR (300 MHz, *d*₀-toluene, ref. vs external H₃PO₄) of reaction crude and control reactions.

CONCLUSIONS

In summary, metal-arene interactions enforced by a terphenyl diphosphine scaffold have been shown to facilitate a variety of H-transfers to the arene. Neutral and cationic nickel-hydride complexes supported by a terphenyl diphosphine have been synthesized. The neutral nickel-hydride has been shown to partially hydrogenate the pincer arene in a stoichiometric manner. The H-migration was studied in detail using isotopic labeling and characterization of intermediates observed with the cationic hydrides. Metal-to-arene H-

migration was found to be reversible by isotopic labeling; chloride addition to a nickel-bound arenium species results in H-migration from carbon back to metal.

The metal-arene interaction was also used to facilitate hydrogenation of **2** by Shvo's catalyst. Through isotope-labeling studies, the hydrogenation was found to occur exclusively from the *exo*-face. Although no other metal compounds of **1** were hydrogenated under similar conditions, a proof-of-principle hydrogenation reaction of a biaryl monophosphine has been shown with Shvo's catalyst and Pd₂(dba)₃. These results suggest that future development of arene functionalization via catalytic transition-metal dearomatization agents may be possible.

EXPERIMENTAL SECTION

General considerations. All manipulations were carried out in an inert atmosphere glovebox or using standard Schlenk line techniques. [H(OEt₂)₂][B(C₆H₃(CF₃)₂)₄] (Brookhart's acid) was synthesized as previously reported.⁵⁴ HCl/Et₂O and HOTf were used as purchased from Aldrich. Shvo's catalyst, (2-biphenyl)di-*tert*-butylphosphine, and Pd₂(dba)₃ were used as purchased from Strem. Deuterated solvents were purchased from Cambridge Isotope Laboratories and vacuum transferred from sodium benzophenone (C₆D₆) or calcium hydride (CD₂Cl₂, CD₃CN). Other organic reagents were dried by stirring over sodium metal or calcium hydride, degassed by three cycles of freeze-pump-thaw, and isolated via vacuum-transfer. Et₂O, toluene, THF, MeCN, and DCM were dried by the method of Grubbs.⁵⁵ All reagents, once degassed and dried, were stored in an inert atmosphere glovebox. ¹H and ¹³C NMR chemical shifts are reported relative to residual solvent peaks as reported in the literature.⁵⁶ ¹⁹F and ³¹P NMR chemical shifts are reported with respect to the instrument

deuterated solvent lock. All NMR spectra were recorded at room temperature unless indicated otherwise. All non- ^1H NMR spectra were recorded with ^1H decoupling unless otherwise noted. Gas chromatography-mass spectrometry (GC-MS) analysis was performed upon filtering the sample through a plug of silica gel. High-resolution fast atom bombardment-mass spectrometry (FAB-MS) analysis was performed with a JEOL JMS-600H high-resolution mass spectrometer. Elemental analysis was conducted by Midwest Microlab, LLC (Indianapolis, IN; their glovebox EA service has since been discontinued).

Synthesis of 18. A Schlenk flask was charged with **2** (650 mg, 1.25 mmol) and 30 mL of Et_2O . A syringe was used to add 0.69 mL of 2.0 M $\text{HCl}/\text{Et}_2\text{O}$ (1.37 mmol) to the reaction, which changed from dark red to orange color in seconds. After 30 minutes, the reaction was concentrated to a powder and sequentially washed and filtered with 10 mL of hexanes, Et_2O , and toluene. The product was obtained by concentration of the toluene fraction to a light orange powder (470 mg, 0.84 mmol, 67%), which was pure by NMR spectroscopy. Orange XRD-quality crystals were grown by layering pentane on a toluene solution of the product for 2 days at room temperature. ^1H NMR (300 MHz, C_6D_6) δ 8.44 (s, 2H, central aryl- H , $^1J_{\text{CH}} = 172.8$ Hz), 7.47 (app d, 2H, aryl- H), 7.22 (m, 4H, aryl- H), 7.09 (m, 2H, aryl- H), 6.93 (s, 2H, central aryl- H , $^1J_{\text{CH}} = 161.6$ Hz), 2.68 (br m, 2H, $\text{CH}(\text{CH}_3)_2$), 1.63 (m, 14H, $\text{CH}(\text{CH}_3)_2$ and $2[\text{CH}(\text{CH}_3)_2]$), 0.92 (app dd, 6H, $\text{CH}(\text{CH}_3)_2$), 0.48 (app dd, 6H, $\text{CH}(\text{CH}_3)_2$), -28.97 (t, $J_{\text{P-H}} = 79.0$ Hz, 1H, Ni- H). $^{13}\text{C}\{^1\text{H}\}$ NMR (101 MHz, C_6D_6) δ : 150.15 (t, $J = 6.7$ Hz), 137.15 (app t), 131.77 (s), 130.78 (t, $J = 16.1$ Hz), 129.66 (s), 126.88 (s), 121.86 (s), 29.33 (br t), 26.56 (br t), 19.59 (s), 19.37 (s), 19.00 (s), 17.78 (s). $^{31}\text{P}\{^1\text{H}\}$ NMR (121 MHz, C_6D_6) δ : 23.4 (dd, $J_{\text{P-H}} = 74.7$ Hz, $J_{\text{P-P}} = 5.3$ Hz). Anal. Calcd. for $\text{C}_{30}\text{H}_{41}\text{ClNiP}_2$ (%): C, 64.60; H, 7.41. Found: C,

63.91; H, 7.26. MS (m/z): calcd, 556.1726 (M^+); found 556.1750 (FAB-MS, M^+). λ_{\max} (benzene, nm), ϵ ($M^{-1} \text{ cm}^{-1}$): 322, 6.36×10^2 ; 425, 1.72×10^2 .

Conversion of 18 to 1 and 19. A stock solution of **18** (32.6 mg, 0.058 mmol) in 1.6 mL d_8 -toluene was prepared. A J. Young NMR tube was charged with 0.5 mL of this 36.5 mM stock solution. The complete conversion of **18** to **19** (0.5 equiv.) and **1** (0.5 equiv.) was observed over 3 h in an NMR spectrometer that was preequilibrated to 90 °C. The two products were separated by removing volatiles under vacuum and washing the resultant powder with hexanes. **1** dissolves in hexanes, leaving mostly **19**. Dark purple XRD-quality crystals of **19** could be isolated by vapor diffusion of pentane into a toluene solution of **19** (5.0 mg, 0.009 mmol, 84% yield). ^1H NMR (300 MHz, C_6D_6) δ : 7.40 (app d, 2H, aryl-*H*), 7.05 (app t, 2H, aryl-*H*), 6.96 (app t, 2H, aryl-*H*), 6.80 (m, 2H, aryl-*H*), 4.64 (s, 2H, olefin-*H*), 2.30 (d, $J = 11.4$ Hz, 2H, CH_aH), 1.94 (m, 2H, $\text{CH}(\text{CH}_3)_2$), 1.79 (d, $J = 11.4$ Hz, 2H, CHH_b), 1.63 (m, 2H, $\text{CH}(\text{CH}_3)_2$), 1.32 (m, 12H, $\text{CH}(\text{CH}_3)_2$), 0.96 (m, 12H, $\text{CH}(\text{CH}_3)_2$). ^{31}P NMR (121 MHz, C_6D_6) δ : 52.7. MS (m/z): calcd, 652.0816 (M^+); found 652.0827 (FAB-MS, M^+). λ_{\max} (benzene, nm), ϵ ($M^{-1} \text{ cm}^{-1}$): 327, 1.71×10^3 ; 392, 5.78×10^2 ; 508, 4.25×10^2 ; 670, 8.44×10^1 . A 1D NOE experiment showed interaction between the aliphatic peak at 1.79 ppm and an aromatic peak at 7.40 ppm. Thus, based on H—H distances observed in the XRD-derived structure, that peak was assigned to the H_b (*exo*) protons of the central ring; the peak at 2.30 ppm did not exhibit 1D NOE cross-peaks with aromatic protons and was assigned to the H_a (*endo*) protons of the central ring.

Synthesis of 1,4-diiodo-2,3,5,6-tetradeuterobenzene. This synthesis was adapted from a literature procedure.⁵⁷ An oven-dried three-necked flask was charged

with NaIO₄ (3.050 g, 14.26 mmol), freshly ground I₂ (10.85 g, 42.78 mmol), AcOH (50 mL), and Ac₂O (25 mL) under a counterflow of nitrogen. A thermometer was inserted through a septum such that the tip was submerged in the reaction, taking care to not interfere with the stir bar. Subsequent temperature measurements were taken using this thermometer. The red suspension was chilled to 5-10 °C using an ice water bath. With vigorous stirring, H₂SO₄ (13.3 mL) was added dropwise slowly enough to keep the temperature between 5-10 °C. Dry C₆D₆ (3.17 mL, 35.65 mmol) was added, and the reaction was allowed to reach room temperature. Reaction progress was monitored by GC-MS over 4h. The reaction was quenched by pouring a solution of Na₂SO₃ (20g in 1 L H₂O) into the reaction flask. The crude was filtered and washed with H₂O and then Et₂O to yield a white solid, the purity of which was checked by TLC and identified by GC-MS as the desired product (7.12 g, 21.3 mmol, 60%) MS (m/z): calcd, 333.8653 (M⁺); found 334 (GC-MS, M⁺).

Synthesis of deuterated compounds. All deuterated compounds were made from 1,4-diiodo-2,3,5,6-tetradeuterobenzene in the same manner as the all protio analogues are synthesized from 1,4-diiodo-2,3,5,6-tetradeuterobenzene.

Thermal conversion of 18-*d*₄ to partially deuterated 19 and 1. A stock solution of 18-*d*₄ (20.0 mg, 0.0356 mmol) in toluene (1.6 mL) was prepared. A J. Young NMR tube was charged with 0.5 mL of this 22.2 mM solution and suspended in a preheated 90 °C oil bath for 3 hours. The complete conversion of 18 to 19 (*ca.* 0.5 equiv.) and 1 (*ca.* 0.5 equiv.) was confirmed by ³¹P NMR. (Attempts to perform this reaction in *d*₈-toluene and track the deuterium distribution by ¹H NMR in the J Young tube were precluded by overlapping peaks between the products and residual protio toluene.) The two products were separated by removing volatiles under vacuum and

washing the resultant powder with hexanes. ^1H NMR spectroscopy (600MHz, C_6D_6) of the hexanes-soluble materials showed 1 peak with diminished integration relative to **1** (d_0). Assigning the multiplet at 6.95 ppm an integration value of 2 showed that the peak at 7.35 ppm integrated to 0.49 instead of 4. Likewise, ^1H NMR spectroscopy of the hexanes-insoluble materials showed 3 peaks with diminished integration relative to **19** (d_0). Assigning the multiplet at 1.63 ppm an integration value of 2 showed that the peaks at 4.64, 2.30, and 1.79 ppm integrated to 0.24, 0.60, and 0.70 respectively, instead of 2.

Synthesis of 20·OTf and 20-NCMe·OTf. To an orange suspension of **18** (107.9 mg, 0.193 mmol) in MeCN (5 mL) was added a solution of TiOTf (68.4 mg, 0.193 mmol) in MeCN (5 mL). In minutes, the reaction was light yellow in color and white powder had precipitated out of solution. The reaction was filtered through a plug of Celite, and volatiles were removed under vacuum to yield spectroscopically pure product as a light yellow powder. Yellow XRD-quality crystals were grown by layering a MeCN solution of the product over Et_2O and storing the layered solution at $-35\text{ }^\circ\text{C}$ overnight. Prior to elemental analysis and mass spectrometry, these crystals were crushed to a powder and left under vacuum for 3h (94.5 mg, 0.141 mmol, 73% yield). Via XRD, the crystal was determined to have an asymmetric unit consisting of one molecule each of **20·OTf** and **20-NCMe·OTf**. ^1H NMR (300 MHz, CD_3CN) δ : 7.79 – 7.70 (m, 4H, aryl-*H*), 7.66 (app t, 2H, aryl-*H*), 7.56 (app t, 2H, aryl-*H*), 7.38, (br s, 4H, central aryl-*H*, $^1J_{\text{CH}} = 161.4\text{ Hz}$), 2.41 (m, 4H, $\text{CH}(\text{CH}_3)_2$), 1.10 (app dd, 12H, $\text{CH}(\text{CH}_3)_2$), 0.93 (app dd, 12H, $\text{CH}(\text{CH}_3)_2$), -25.12 (t, $J_{\text{P-H}} = 67.9\text{ Hz}$, 1H, Ni-*H*). ^{31}P NMR (121 MHz, CD_3CN) δ : 35.56 (app m). $^{13}\text{C}\{^1\text{H}\}$ NMR (151 MHz, CD_3CN) δ : 149.35 (t, $J = 6.3\text{ Hz}$), 138.02 (app t), 132.75 (s), 131.55 (s), 129.01 (t, $J = 2.4\text{ Hz}$), 128.94 (t, $J = 19.2\text{ Hz}$), 128.74 (t, $J = 2.9\text{ Hz}$), 123.68 (s), 27.92 (t, $J = 11.6\text{ Hz}$), 19.41 (t,

$J = 2.8$ Hz), 18.37 (s). λ_{\max} (THF, nm), ϵ ($M^{-1} \text{ cm}^{-1}$): 307, 9.12×10^2 ; 345, 7.59×10^2 .
Anal. Calcd. for $C_{31}H_{41}F_3NiO_3P_2S$ (%): C, 55.46; H, 6.16. Found: C, 55.04; H, 5.88. MS
(m/z): calcd, 521.2037 ($M^+[-OTf]$); found 521.2011 (FAB-MS, $M^+[-OTf]$).

NMR of 20·OTf in CD_2Cl_2 . 20·OTf could not be isolated cleanly in CD_2Cl_2 without traces of 21·OTf or 22·OTf. 1H NMR (300 MHz, CD_2Cl_2) δ : 7.87 – 7.44 (m, 8H, aryl-*H*), 6.87, (br s, 4H, central aryl-*H*), 2.45 (m, 4H, $CH(CH_3)_2$), 1.19 – 0.96 (app m, 24H, $CH(CH_3)_2$), -17.57 (t, $J_{P-H} = 67.8$ Hz, 1H, Ni-*H*). ^{31}P NMR (121 MHz, CD_3CN) δ : 38.87 (app m).

Thermal conversion of 20·OTf to 21·OTf and 22·OTf. To a stirring suspension of 2 (9.5 mg, 0.017 mmol) in minimal CD_3CN was added $TfOTf$ (6.0 g, 0.017 mmol) with the aid of 0.3 mL CD_3CN . After stirring for 30 min, the reaction was filtered through a plug of glass filter paper into a J. Young NMR tube and diluted to a previously demarcated volume of 0.5 mL with more CD_3CN . The purity of 20·OTf in solution was verified by room temperature 1H and ^{31}P NMR. A 400 MHz Varian NMR Spectrometer was equilibrated to 75 °C, the sample was inserted into the probe, and locked and shimmed. 1H NMR spectra were collected every 3 minutes. After 1h, the two major species in solution were 20·OTf and 21·OTf. After 5h, 20·OTf and 21·OTf were mostly consumed, and 22·OTf was the major species. At the end of 11h, the sample was ejected, and a dark metallic mirror on the NMR tube wall was evident, suggesting that decomposition may have contributed to the broad unidentified peaks that grew throughout the experiment. Crystallization of 22·OTf from MeCN/ Et_2O yielded light yellow crystals. 22·OTf Anal. Calcd. for $C_{31}H_{41}F_3NiO_3P_2S$ (%): C, 55.46; H, 6.16. Found: C, 55.12; H, 5.97.

NMR characterization of 21·OTf. Species **21** could not be isolated. Numerous attempts to crystallize mixtures of **20** and **21** resulted in either crystals of **22** or disordered crystals that upon dissolving in CD₃CN, were identified by ³¹P NMR as a mixture of **20**, **21**, and **22**. Aromatic and isopropyl ¹H NMR peaks of **21** could not be differentiated from those of **20** or **22**, but various correlation experiments were used to assign the protons from the central ring of **21**. 2D gradient COSY revealed the connectivity of the central ring protons. The shapes of the peaks were more complicated than expected, but simplified upon broadband ³¹P decoupling using a GARP waveform centered at 55 ppm, indicating the presence of large $J_{\text{P-H(central ring)}}$. To differentiate between H_c (*exo*) and H_d (*endo*) of the sp³ central ring carbon, 1D NOE experiments were conducted. Irradiation of the peak at 1.78 ppm transferred to an aromatic doublet. This observation was assigned to the NOE between the *exo* proton and the *ortho* proton of the neighboring arene. **21·OTf** ¹H NMR (300 MHz, CD₂Cl₂) δ: 7.56 (1H, H_i), 5.76 (1H, H_a), 5.70 (1H, H_b), 5.18 (1H, H_c), 2.85 (1H, H_d), 1.78 (1H, H_e). ³¹P NMR (121 MHz, CD₃CN) δ: 61.11 (*d*, J_{pp} = 10.9 Hz), 35.45 (*d*, J_{pp} = 10.9 Hz).

Protonation of 2 and isolation of 22·BArF₂₄. To a red solution of **1** (30.4 mg, 0.06 mmol) in THF (2 mL) was added [H(OEt₂)] [B(C₆H₃(CF₃)₂)₄] (59.0 mg, 0.06 mmol). ³¹P NMR at this stage indicates that a mixture of **20·BArF₂₄**, **21·BArF₂₄**, and **22·BArF₂₄** was present. After stirring for 30 minutes at room temperature, volatiles were removed under vacuum. The crude product was washed with hexanes to remove trace unreacted **2**, and then filtered through Celite as a Et₂O solution. The filtrate was concentrated under vacuum to a solid. A DCM solution of this solid was layered under pentane, and dark brown XRD-quality crystals of **22·BArF₂₄** (58.0 mg, 72% yield) were formed at -35 °C over three days. ¹H NMR (400 MHz, CD₃CN) δ: 7.91 (m, 2H, aryl-*H*), 7.69 (br s,

8H, BArF-*H*), 7.67 (br s, 4H, BArF-*H*), 7.56 (m, 4H, aryl-*H*), 7.39 (m, 2H, aryl-*H*), 5.86 (d, $J = 8.1$ Hz, 2H, H_c and H_c' , $^1J_{CH} = 175.6$ Hz), 5.12 (m, 2H, H_b and H_b' , $^1J_{CH} = 167.6$ Hz), 2.59 (m, 5H, $CH(CH_3)_2$ and H_a), 1.10 (m, 24H, $CH(CH_3)_2$). ^{31}P NMR (121 MHz, CD_3CN) δ : 58.80 (*d*, $J_{PP} = 1.6$ Hz), 50.44 (*d*, $J_{PP} = 1.6$ Hz). ^{13}C NMR (101 MHz, CD_2Cl_2 , not all carbons were observed) δ : 163.06 (s), 162.57 (s), 162.07 (s), 161.58 (s), 135.289 (d, $J = 19.1$ Hz), 133.15 (m), 132.57 (m), 131.20 (app d), 129.30 (app q), 127.87 (br s), 126.53 (s), 118.16 (d, $J = 22.5$ Hz), 97.32 (br m), 97.105 (app d), 30.31 (s), 27.32 (m), 25.94 (m), 20.23 (m), 19.52 (m), 18.89 (m), 18.57 (m). The chemical shift of H_a was determined to overlap with the methine protons by integration of 1H NMR data (see Figure S20) and by a COSY experiment that showed correlation with H_b .

Thermal conversion of 20- d_4 -OTf to partially deuterated 21-OTf. To a suspension of **18- d_4** (7.2 mg, 0.0128 mmol) in CD_3CN (0.4 mL) was added TlOTf (4.5 mg, 0.0128 mmol). The solution was allowed to stir for 30 min and then filtered thru a plug of Celite into a J. Young NMR tube. The vial and filter were washed with CD_3CN into the NMR tube until a predemarcated total volume of 0.5 mL was reached. The NMR tube was sealed and placed in a 75 °C oil bath. The reaction was monitored by NMR over 24h, after which it was determined that sufficient conversion had occurred. Due to the formation of a partial mirror on the NMR tube walls, the reaction mixture was filtered through Celite, volatiles were removed, and the crude was redissolved in CD_2Cl_2 in a clean NMR tube, which allows for better resolution of the aliphatic 1H NMR peaks. A major doublet was observed at 2.85 ppm (*endo* proton of **21**), and a minor multiplet was present at ~1.78 ppm. Assuming that the multiplet at 1.78 corresponded to the *exo* proton and not an impurity, the ratio of *endo:exo* 1H incorporation is 90:10.

Chloride addition to a mixture of 20·OTf, 21·OTf, and 22·OTf. A solution of **20·OTf** (9.4 mg, 0.0140 mmol) in THF (0.5 mL) was loaded in a J. Young NMR tube and placed in a 70 °C oil bath. After 1h, the NMR tube was washed with hexanes to remove oil and allowed to cool to room temperature. ³¹P NMR indicated a mixture of **20·OTf**, **21·OTf**, and **22·OTf** in solution. Volatiles were removed under vacuum, and the resulting solids were redissolved in CD₂Cl₂. An initial ¹H NMR spectrum was collected. Then NBu₄Cl (4.3 mg, 0.0154 mmol) was added to the mixture and an intermediate spectrum was recorded. Finally, another portion of NBu₄Cl (11.7 mg, 0.042 mmol) was added and a final spectrum was recorded. Integration of ¹H NMR peaks at 6.82 and -28.90 ppm and regions 5.90-5.60 and 5.26-5.05 ppm were used to determine to relative concentrations of **18**, **20·OTf**, **21·OTf**, and **22·OTf** throughout the reaction. It was determined that a 62:26:12 mixture of **21·OTf**, **20·OTf**, and **22·OTf** was transformed into a 85:15 mixture of **18** and **22·OTf**.

1,8-Diazabicyclo[5.4.0]undec-7-ene addition to a mixture of 20·OTf, 21·OTf, and 22·OTf. A solution of **20·OTf** (7.0 mg, 0.0104 mmol) in THF (0.5 mL) was loaded in a J. Young NMR tube and placed in a 70 °C oil bath. After 1h, the NMR tube was washed with hexanes to remove oil and allowed to cool to room temperature. ³¹P NMR indicated a mixture of **20·OTf**, **21·OTf**, and **22·OTf** in solution. Volatiles were removed under vacuum, and the resulting solids were redissolved in CD₃CN. Initial ¹H and ³¹P NMR spectra were collected. Then 1,8-diazabicyclo[5.4.0]undec-7-ene (DBU, 2.34 μL, 0.0155 mmol) was added to the mixture, and an intermediate spectrum was recorded, indicating full consumption of **21·OTf** and **22·OTf**. **20·OTf** persisted, however, even 30 min after addition of more DBU (10.0 μL, 0.0662 mmol). However

after 12h, colorless crystals were formed the NMR tube, and NMR of the solution indicated full conversion of **21·OTf** to **2**.

Determination of equilibrium dissociation constant of MeCN to 20·OTf. A solution of **20·OTf** (7.6 mg, 0.0113 mmol) in CD₂Cl₂ (0.4 mL) was loaded in a septum-capped NMR tube. A starting ¹H NMR spectrum was collected, and then a microsyringe was used to inject increments of 1:1 MeCN/CD₂Cl₂ or neat MeCN. The chemical shift of the hydride peak shifted upon addition of more MeCN. Assuming that δ(Ni-H) in neat CD₃CN corresponds to **20-NCMe**, a normalized measure of the relative concentrations of [**20-NCMe**] and [**5**] is definable as $\Delta\delta = [\delta(\text{Ni-H}) - \delta(\text{Ni-H})_{\text{CD}_2\text{Cl}_2}] / [\delta(\text{Ni-H})_{\text{CD}_3\text{CN}} - \delta(\text{Ni-H})_{\text{CD}_2\text{Cl}_2}] = [\mathbf{20-NCMe}] / [\mathbf{5}]_{\text{total}}$. Because $K_d = [\mathbf{5}][\text{MeCN}] / [\mathbf{20-NCMe}]$, then $\Delta\delta = [\text{MeCN}] / ([\text{MeCN}] + K_d)$, and fitting 1/Δδ vs. 1/[MeCN] yields $K_d = 1.13 \text{ M}$.

Deprotonation of hydride complexes with dimethylbenzylamine. A stock solution of **18** (21.8 mg, 0.0391 mmol) in THF (1.6 mL) was prepared. 0.5 mL of this orange solution (0.0122 mmol **18**) was transferred into an NMR tube. A coaxial insert was loaded with a saturated THF solution of 1,2-bisdiphenylphosphinoethane (dppe) and placed in the same NMR tube. A preliminary ³¹P NMR spectrum was collected. One equivalent of dimethylbenzylamine (DMBA, 1.8 μL, 0.0122 mmol) was added to the NMR tube, causing the emergence of a deep red color upon mixing. Another ³¹P NMR spectrum was taken and indicated the generation of **2**. The relative integrations of the signals for **18** and dppe were used to calculate 22% deprotonation of **18**. An identical procedure was used to determine 26% deprotonation of **20·OTf** by 1 equivalent of DMBA.

Hydrogenation of 2 with Shvo's catalyst and characterization of 23. A J. Young NMR tube was charged with **2** (5.8 mg, 0.011 mmol), Shvo's catalyst (1.2 mg, 0.001 mmol), and *d*₈-toluene (0.5 mL). The solution was degassed by 5 freeze-pump-thaw cycles. The NMR tube was opened to a Schlenk line, mercury bubbler-limited to ~1 atm of flowing H₂ (298 K). The open NMR tube was then chilled with LN₂, allowing for 1 atm H₂ (77 K) to concentrate in the tube. The J. Young valve was closed, and the tube was warmed to room temperature, resulting in 3.9 atm H₂ ($P_1/T_1 = P_2/T_2$). Preliminary NMR spectra were collected, and then the tube was placed in a preheated 65 °C oil bath. The reaction was monitored by NMR spectroscopy over 100 h and then stopped with a minor amount of NiP₂ still present. Volatiles were removed under vacuum. The resulting powder was dissolved in hexanes and filtered through Celite. Upon concentrating the filtrate under vacuum, an orange solid resulted (6.7 mg). While multiple species appear to be present, there is one major species (**23**) by NMR spectroscopy. Several attempts to purify this compound via crystallization at room temperature or -35 °C led to decomposition to an NMR-silent, benzene-insoluble green solid. ¹H NMR (C₆D₆, 300 MHz) δ: 7.55 (app t, 2H, aryl-*H*), 7.22 (app d, 2H, aryl-*H*), 7.19 (app t, 2H, aryl-*H*), 7.14 (app d, 2H, aryl-*H*), 3.73 (m, 2H, H_a – see below for assignment diagram), 3.03 (app s, 2H, H_b), 2.39 (m, 2H, CH(CH₃)₂), 2.15 (m, 2H, CH(CH₃)₂), 1.91 (m, 2H, H_c), 1.81 (m, 2H, H_d), 1.28 (app dd, 6H, CH(CH₃)₂), 1.12 (app dd, 6H, CH(CH₃)₂), 1.03 (m, 12H, CH(CH₃)₂). ³¹P NMR (C₆D₆, 121 MHz) δ: 46.6 (s). MS (m/z): calcd, 467.2996 ([M-Ni+H]⁺), 483.2946 ([M-Ni+O+H]⁺), 499.2895 ([M-Ni+2O+H]⁺); found 467.2978, 483.2937, 499.2907 (FAB-MS, +).

Hydrogenation of (2-biphenyl)di-*tert*-butylphosphine (JohnPhos) with Shvo's catalyst and Pd₂(dba)₃. The reaction was set up in the same way as for

hydrogenation of **2**, except with d_0 -toluene as the reaction solvent. The reaction was heated at 100 °C for 8 h. Upon cessation of the reaction, analysis with GC-MS, and recording ^1H and ^{31}P NMR spectra in CDCl_3 , the sole phosphine product was determined to be (2-cyclohexylphenyl)di-*tert*-butylphosphine.⁵¹

Table 3.1. Crystal and refinement data for complexes **12**, **13**, **14**, **15**, **16**, **17**

	18	19	20·OTf + 20-MeCN·OTf	22·BArF₂₄
CCDC Number	782511	800343	800346	800345
Empirical formula	C ₃₀ H ₄₁ ClP ₂ Ni	C ₃₀ H ₄₂ P ₂ Cl ₂ Ni ₂	[C ₃₀ H ₄₀ P ₂ NiH] ⁺ [C ₃₂ H ₄₃ NP ₂ NiH] ⁺ 2[CF ₃ O ₃ S] ⁻	[C ₃₀ H ₄₁ P ₂ Ni] ⁺ [C ₃₂ H ₁₂ BF ₂₄] ⁻
Formula weight	557.73	652.9	691.88	1385.5
T (K)	100(2)	100(2)	100(2)	100(2)
<i>a</i> , Å	8.6569(3)	10.9521(4)	27.7671(12)	18.8883(8)
<i>b</i> , Å	23.2021(8)	16.7037(7)	12.6722(6)	18.2168(8)
<i>c</i> , Å	14.5399(5)	17.0594(7)	20.3587(9)	19.5092(8)
α , deg	90	90	90	90
β , deg	106.911(2)	106.816(2)	112.212(2)	116.405(2)
γ , deg	90	90	90	90
Volume, Å ³	2794.17(17)	2987.4(2)	6632.0(5)	6012.5(4)
Z	4	4	8	4
Crystal system	Monoclinic	Monoclinic	Monoclinic	Monoclinic
Space group	P 2 ₁ / <i>n</i>	P 2 ₁ / <i>n</i>	P 2 ₁ / <i>c</i>	P 2 ₁ / <i>c</i>
<i>d</i> _{calc} , g/cm ³	1326	1452	1386	1531
θ range, deg	1.71 to 26.43	1.74 to 36.01	1.79 to 30.57	2.09 to 30.56
μ , mm ⁻¹	0.922	1.565	0.794	0.491
Abs. Correction	Gaussian	None	None	None
GOF	1.759	1.552	2.908	1.7
R ₁ , ^a wR ₂ ^b [I>2s(I)]	0.0302, 0.0476	0.0268, 0.0426	0.1001, 0.0925	0.0479, 0.0568

$$^a R_1 = \sum ||F_o| - |F_c|| / \sum |F_o|. \quad ^b wR_2 = [\sum [w(F_o^2 - F_c^2)^2] / \sum [w(F_o^2)]^{1/2}.$$

Refinement details.

In each case, crystals were mounted on a glass fiber and placed on the diffractometer under a nitrogen stream. Low temperature (100 K) X-ray data were obtained on a Bruker APEXII CCD based diffractometer (Mo sealed X-ray tube, $K_{\alpha} = 0.71073 \text{ \AA}$). All diffractometer manipulations, including data collection, integration and scaling were carried out using the Bruker APEXII software.⁵⁸ Absorption corrections were applied using SADABS.⁵⁹ Space groups were determined on the basis of systematic absences and intensity statistics and the structures were solved by direct methods using XS⁶⁰ (incorporated into SHELXTL) and refined by full-matrix least squares on F^2 . All non-hydrogen atoms were refined using anisotropic displacement parameters. Hydrogen atoms were placed in idealized positions and refined using a riding model. The structure was refined (weighted least squares refinement on F^2) to convergence. Graphical representation of structures with 50% probability thermal ellipsoids was generated using Diamond visualization software.⁶¹

REFERENCES

- (1) Benson, E. E.; Kubiak, C. P.; Sathrum, A. J.; Smieja, J. M. *Chem. Soc. Rev.* **2009**, *38*, 89.
- (2) Rakowski Dubois, M.; Dubois, D. L. *Acc. Chem. Res.* **2009**, *42*, 1974.
- (3) Breitenfeld, J.; Vechorkin, O.; Corminboeuf, C. m.; Scopelliti, R.; Hu, X. *Organometallics* **2010**, *29*, 3686.
- (4) Chakraborty, S.; Zhang, J.; Krause, J. A.; Guan, H. J. *Am. Chem. Soc.* **2010**, *132*, 8872.
- (5) Chakraborty, S.; Krause, J. A.; Guan, H. *Organometallics* **2008**, *28*, 582.
- (6) Tran, B. L.; Pink, M.; Mindiola, D. J. *Organometallics* **2009**, *28*, 2234.
- (7) Tolman, C. A. J. *Am. Chem. Soc.* **1972**, *94*, 2994.
- (8) Laird, M. F.; Pink, M.; Tsvetkov, N. P.; Fan, H.; Caulton, K. G. *Dalton Trans.* **2009**, 1283.
- (9) Schmeier, T. J.; Hazari, N.; Incarvito, C. D.; Raskatov, J. A. *Chem. Commun.* **2011**, *47*, 1824.
- (10) Bach, I.; Goddard, R.; Kopiske, C.; Seevogel, K.; Porschke, K.-R. *Organometallics* **1998**, *18*, 10.
- (11) Iluc, V. M.; Hillhouse, G. L. *Tetrahedron* **2006**, *62*, 7577.
- (12) Iluc, V. M.; Hillhouse, G. L. *J. Am. Chem. Soc.* **2010**, *132*, 11890.
- (13) Curtis, C. J.; Miedaner, A.; Raebiger, J. W.; DuBois, D. L. *Organometallics* **2003**, *23*, 511.
- (14) Vicic, D. A.; Jones, W. D. *J. Am. Chem. Soc.* **1997**, *119*, 10855.
- (15) Vicic, D. A.; Jones, W. D. *J. Am. Chem. Soc.* **1999**, *121*, 7606.
- (16) Muetterties, E. L.; Bleeke, J. R. *Acc. Chem. Res.* **1979**, *12*, 324.
- (17) Muetterties, E. L.; Hirsekorn, F. J. *J. Am. Chem. Soc.* **1974**, *96*, 4063.
- (18) Lee, C. H.; Cook, T. R.; Nocera, D. G. *Inorg. Chem.* **2011**, *50*, 714.
- (19) Velian, A.; Lin, S.; Miller, A. J. M.; Day, M. W.; Agapie, T. *J. Am. Chem. Soc.* **2010**, *132*, 6296.
- (20) Muetterties, E. L.; Bleeke, J. R.; Wucherer, E. J.; Albright, T. *Chem. Rev.* **1982**, *82*, 499.

- (21) Liang, L.-C.; Chien, P.-S.; Lee, P.-Y. *Organometallics* **2008**, *27*, 3082.
- (22) Aresta, M.; Quaranta, E.; Dibenedetto, A.; Giannoccaro, P.; Tommasi, I.; Lanfranchi, M.; Tiripicchio, A. *Organometallics* **1997**, *16*, 834.
- (23) Steinke, T.; Shaw, B. K.; Jong, H.; Patrick, B. O.; Fryzuk, M. D. *Organometallics* **2009**, *28*, 2830.
- (24) Boro, B. J.; Duesler, E. N.; Goldberg, K. I.; Kemp, R. A. *Inorg. Chem.* **2009**, *48*, 5081.
- (25) Teitel'baum, A. B.; Kudryavtseva, L. A.; Bel'skii, V. E.; Ivanov, B. E. *Russ. Chem. Bull.* **1980**, *29*, 1571.
- (26) Kaljurand, I.; Kütt, A.; Sooväli, L.; Rodima, T.; Mäemets, V.; Leito, I.; Koppel, I. A. *J. Org. Chem.* **2005**, *70*, 1019.
- (27) Ben-Ari, E.; Leitus, G.; Shimon, L. J. W.; Milstein, D. *J. Am. Chem. Soc.* **2006**, *128*, 15390.
- (28) Steinke, T.; Shaw, B. K.; Jong, H.; Patrick, B. O.; Fryzuk, M. D.; Green, J. C. *J. Am. Chem. Soc.* **2009**, *131*, 10461.
- (29) Gunanathan, C.; Gnanaprakasam, B.; Iron, M. A.; Shimon, L. J. W.; Milstein, D. *J. Am. Chem. Soc.* **2010**, *132*, 14763.
- (30) Khaskin, E.; Iron, M. A.; Shimon, L. J. W.; Zhang, J.; Milstein, D. *J. Am. Chem. Soc.* **2010**, *132*, 8542.
- (31) Kohl, S. W.; Weiner, L.; Schwartzburd, L.; Konstantinovski, L.; Shimon, L. J. W.; Ben-David, Y.; Iron, M. A.; Milstein, D. *Science* **2009**, *324*, 74.
- (32) Keane, J. M.; Chordia, M. D.; Mocella, C. J.; Sabat, M.; Trindle, C. O.; Harman, W. D. *J. Am. Chem. Soc.* **2004**, *126*, 6806.
- (33) Harman, W. D. *Chem. Rev.* **1997**, *97*, 1953.
- (34) Harman, W. D. *Coord. Chem. Rev.* **2004**, *248*, 853.
- (35) Kütt, A.; Rodima, T.; Saame, J.; Raamat, E.; Mäemets, V.; Kaljurand, I.; Koppel, I. A.; Garlyauskayte, R. Y.; Yagupolskii, Y. L.; Yagupolskii, L. M.; Bernhardt, E.; Willner, H.; Leito, I. *J. Org. Chem.* **2010**, *76*, 391.
- (36) Hirsekorn, F. J.; Rakowski, M. C.; Muetterties, E. L. *J. Am. Chem. Soc.* **1975**, *97*, 237.
- (37) McAlister, D. R.; Erwin, D. K.; Bercaw, J. E. *J. Am. Chem. Soc.* **1978**, *100*, 5966.

- (38) Necula, A.; Racoveanu-Schiketanz, A.; Gheorghiu, M. D.; Scott, L. T. *J. Org. Chem.* **1995**, *60*, 3448.
- (39) Kuck, D. *Int. J. Mass Spectrom.* **2002**, *213*, 101.
- (40) Olah, G. A.; Schlosberg, R. H.; Porter, R. D.; Mo, Y. K.; Kelly, D. P.; Mateescu, G. D. *J. Am. Chem. Soc.* **1972**, *94*, 2034.
- (41) Harman, W. D.; Taube, H. *J. Am. Chem. Soc.* **1988**, *110*, 7906.
- (42) Keane, J. M.; Harman, W. D. *Organometallics* **2005**, *24*, 1786.
- (43) Chordia, M. D.; Smith, P. L.; Meiere, S. H.; Sabat, M.; Harman, W. D. *J. Am. Chem. Soc.* **2001**, *123*, 10756.
- (44) Deshmukh, R. R.; Lee, J. W.; Shin, U. S.; Lee, J. Y.; Song, C. E. *Angew. Chem.* **2008**, *120*, 8743.
- (45) Shvo, Y.; Czarkie, D.; Rahamim, Y.; Chodosh, D. F. *J. Am. Chem. Soc.* **1986**, *108*, 7400.
- (46) Blum, Y.; Czarkie, D.; Rahamim, Y.; Shvo, Y. *Organometallics* **1985**, *4*, 1459.
- (47) Conley, B. L.; Pennington-Boggio, M. K.; Boz, E.; Williams, T. J. *Chem. Rev.* **2010**, *110*, 2294.
- (48) Friebolin, H. *Basic One- and Two-Dimensional NMR Spectroscopy*; 4th ed.; Wiley-VCH: Weinheim, Germany, 2005.
- (49) Wu, T. C.; Xiong, H.; Rieke, R. D. *J. Org. Chem.* **1990**, *55*, 5045.
- (50) Chernyshova, E. S.; Goddard, R.; Pörschke, K.-R. *Organometallics* **2007**, *26*, 4872.
- (51) Wolfe, J. P.; Tomori, H.; Sadighi, J. P.; Yin, J.; Buchwald, S. L. *J. Org. Chem.* **2000**, *65*, 1158.
- (52) Zaleskiy, S. S.; Ananikov, V. P. *Organometallics* **2012**, *31*, 2302.
- (53) Christmann, U.; Vilar, R.; White, A. J. P.; Williams, D. J. *Chem. Commun.* **2004**, 1294.
- (54) Brookhart, M.; Grant, B.; Volpe, A. F. *Organometallics* **1992**, *11*, 3920.
- (55) Pangborn, A. B.; Giardello, M. A.; Grubbs, R. H.; Rosen, R. K.; Timmers, F. J. *Organometallics* **1996**, *15*, 1518.
- (56) Fulmer, G. R.; Miller, A. J. M.; Sherden, N. H.; Gottlieb, H. E.; Nudelman, A.; Stoltz, B. M.; Bercaw, J. E.; Goldberg, K. I. *Organometallics* **2010**, *29*, 2176.
- (57) Lulinski, P.; Skulski, L. *Bull. Chem. Soc. Jpn.* **2000**, *73*, 951.

- (58) APEX2, Version 2 User Manual, M86-E01078, Bruker Analytical X-ray Systems, Madison, WI, June 2006.
- (59) Sheldrick, G.M. "SADABS (version 2008/1): Program for Absorption Correction for Data from Area Detector Frames", University of Göttingen, 2008.
- (60) Sheldrick, G.M. (2008). *Acta Cryst.* A64, 112-122.
- (61) Brandenburg, K. (1999). DIAMOND. Crystal Impact GbR, Bonn, Germany.

CHAPTER 4

DIPALLADIUM(I) TERPHENYL DIPHOSPHINE COMPLEXES AS MODELS FOR TWO-SITE ADSORPTION AND ACTIVATION OF ORGANIC MOLECULES

Published in part as:

Lin, S., Herbert, D. E., Velian, A., Day, M. W., Agapie, T. J. *Am. Chem. Soc.*, **2013**, *135*,
15830-15840.

ABSTRACT

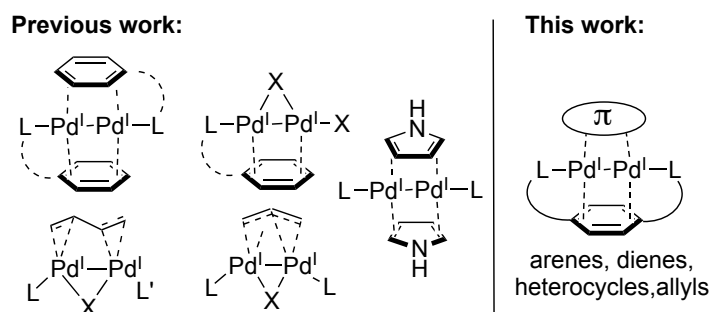
Well-defined models for binding of organic molecules across two metal centers are relatively rare. A *para*-terphenyl diphosphine was employed to support a dipalladium(I) moiety. Unlike previously reported dipalladium(I) species, the present system provides a single molecular hemisphere for binding of ligands across two metal centers, enabling the characterization and comparison of the binding of a wide variety of saturated and unsaturated organic molecules. The dipalladium(I) terphenyl diphosphine toluene-capped complex was synthesized from a dipalladium(I) hexaacetonitrile precursor in the presence of toluene. The palladium centers display interactions with the π -systems of the central ring of the terphenyl unit and that of the toluene. Exchange of toluene for anisole, 1,3-butadiene, 1,3-cyclohexadiene, thiophenes, pyrroles, or furans resulted in well-defined π -bound complexes which were studied by crystallography, nuclear magnetic resonance (NMR) spectroscopy, and density functional theory. Several of the complexes exhibit rare μ^2 - η^2 : η^2 or μ^2 - η^2 : η^1 (O or S) bridging motifs. Hydrogenation of the thiophene and benzothiophene adducts was demonstrated to proceed at room temperature. The relative binding strength of the neutral ligands was determined by competition experiments monitored by NMR spectroscopy. The relative equilibrium constants (K_{eq}) for ligand substitution span over 13 orders of magnitude. This represents the most comprehensive analysis to date of the relative binding of heterocycles and unsaturated ligands to bimetallic sites. Binding interactions were computationally studied with electrostatic potentials and molecular orbital analysis. Anionic ligands were also demonstrated to form π -bound complexes.

INTRODUCTION

The majority of organometallic studies have focused on mononuclear compounds, but reactions at surfaces, clusters, and homogeneous catalysts may involve multiple metal centers. Reactions involving aromatic systems such as hydrogenation or cross-coupling often invoke intermediates with the π -systems coordinating to one or more metals on the surface.¹⁻
³ Additionally in petroleum refining, removal of sulfur and nitrogen impurities (hydrodesulfurisation and hydrodenitrification, respectively) requires binding and activation of nitrogen and sulfur-containing heterocycles.⁴ Heteroatom-containing molecules are known to inhibit these processes,⁵ but very few organometallic models for multinuclear binding of heterocycles are known.⁶ In this context, structural models and quantitative evaluation of binding with π -interactions and heteroatoms to multimetallic sites are of interest.

The Pd(I)–Pd(I) moiety with a metal–metal π -bond has been shown to be stable without support from bridging ligands and binds a variety of π -systems.⁷⁻⁹ Numerous homogeneous dinuclear palladium complexes displaying bridging arenes,¹⁰⁻¹⁸ butadienes,¹⁹⁻²¹ allyls²²⁻²⁷, and recently pyrroles⁵ have been reported (Chart 4.1). In these complexes there is significant variation in the nature of the ancillary ligands (L, L', X). This is due to the mode of synthesis that typically coordinates two identical π -systems to a Pd₂ unit. We have designed a diphosphine supporting ligand that allows for systematic studies of single ligand binding to a Pd₂ unit (Chart 4.1, right).

Chart 4.1. Representation of dipalladium(I) compounds. Dashed arcs indicate ligands with or without covalent linkages.



Herein, we report the synthesis of dipalladium(I) complexes supported by a common *p*-terphenyl diphosphine framework. This platform has been synthesized with capping arenes, heterocycles, and other organic ligands. The coordination modes, dynamic processes, relative binding strengths, and reactivity were investigated by single crystal X-ray diffraction (XRD), solution nuclear magnetic resonance spectroscopy (NMR), and density functional theory (DFT) calculations. The present study provides insight into the coordination of common ligands spanning a relative binding window of over 13 orders of magnitude.

RESULTS AND DISCUSSION

For organizational purposes, the insights into dipalladium complexes are discussed in eight sections: (1) arene adducts, (2) diene adducts, (3) heterocycle adducts, (4) hydrogenation of S-heterocycle adducts, (5) anionic ligand-capped complexes, (6) binding equilibria, (7) computational guide to binding, and (8) molecular orbital theory.

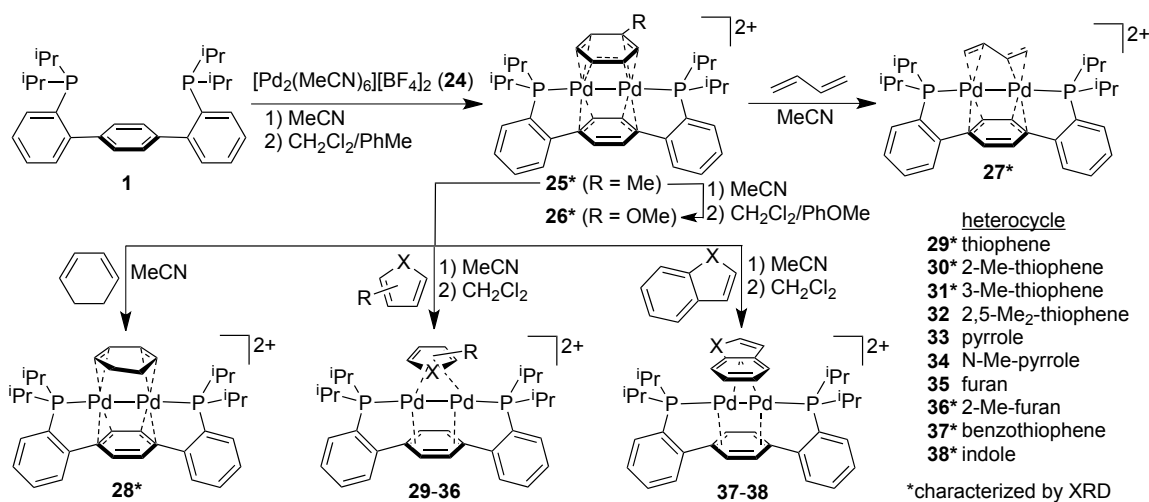
1. Synthesis and Characterization of Arene Adducts.

Terphenyl diphosphines have been employed as trans-spanning ligands for supporting mono- and bimetallic complexes.²⁸⁻³¹ In particular, diphosphine **1** (Scheme 4.1)

was shown to coordinate a Ni^I-Ni^I moiety with phosphine coordination roughly along the metal-metal vector.²⁸ The central arene was found to have interactions with the metal centers and to coordinatively and sterically saturate one hemisphere of the bimetallic unit. An analogous motif was targeted for palladium.

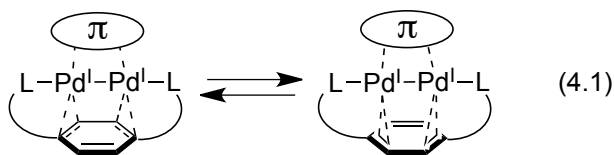
The M^{II}/M⁰ *in situ* comproportionation reaction, employed for nickel, was not successful for palladium. An alternate synthetic strategy was tested, utilizing preformed dipalladium precursor [Pd₂(MeCN)₆][BF₄]₂ (**24**).⁷ As the two reagents are not soluble in the same solvents, a solution of **24** in MeCN was added to solid diphosphine **1** with rapid stirring. The initial dark red suspension became more homogeneous after stirring for ~10 minutes. Upon removal of volatile materials, the dark red residue was recrystallized by reconstitution with CH₂Cl₂ and layering under toluene to give toluene adduct **25** (Scheme 4.1).

Scheme 4.1. Synthesis of dipalladium(I) diphosphine compounds 25-38 with BF₄ counterions.



¹H NMR spectra of these crystals in CD₂Cl₂ displayed a singlet and a multiplet significantly upfield from the aromatic region (6.21 and 6.19 ppm, respectively). The singlet

was assigned to the protons of the central arene of the terphenyl backbone. The chemical shift suggests coordination of the π -system of the central arene to the palladium centers, as previously observed for the nickel analogs.²⁸ ^1H - ^{13}C 2D NMR experiments (HSQC and HMBC) identified the multiplet as corresponding to a bound toluene molecule. The carbons *ortho*-, *meta*-, and *para*- to the toluene methyl are shielded (104.7, 91.3, and 100.9 ppm, respectively), consistent with π -coordination to a metal center and disruption of aromaticity. The methyl group of toluene is expected to be located away from the P–P vector due to steric reasons, which would make the molecule pseudo- C_s symmetric and show two peaks for the central arene in the slow exchange limit. The observation of a singlet for the central arene protons indicates a fast exchange process on the NMR time scale that involves the toluene ligand. Addition of excess toluene to an NMR sample of **25** allowed observation of peaks corresponding to bound and free toluene instead of an averaged spectrum, indicating that degenerate ligand substitution is slow on the NMR timescale. These findings are consistent with the toluene rotating 180° on the NMR time scale. Additionally, the Pd_2 unit exchanges quickly between coordination to π -electrons in the “front” and “back” (as drawn) of the central ring (eq 4.1):



Crystals of **25** were further studied by XRD (Figure 4.1). The two palladium(I) centers are sandwiched between the central ring of the terphenyl backbone and a capping toluene molecule. The central ring is bound $\mu\text{-}\eta^2\text{:}\eta^2$ through two adjacent, partially localized double bonds. These central arene bonds are elongated (1.409(3) and 1.420(3) Å), while the third, uncoordinated double bond of the central ring is noticeably shorter (1.360(2) Å)

relative to a typical aromatic C–C bond. The toluene molecule is bound $\mu\text{-}\eta^2\text{:}\eta^2$ (using a Pd–C cutoff distance of 2.5 Å to assign bonds), and two phosphines complete the coordination sphere. The terphenyl unit adopts a convex geometry to accommodate the bimetallic core. Interestingly, the Pd–Pd distance of 2.7091(2) Å is a close match for nearest-neighbor Pd–Pd distances of bulk Pd (2.75 Å).^{32,33}

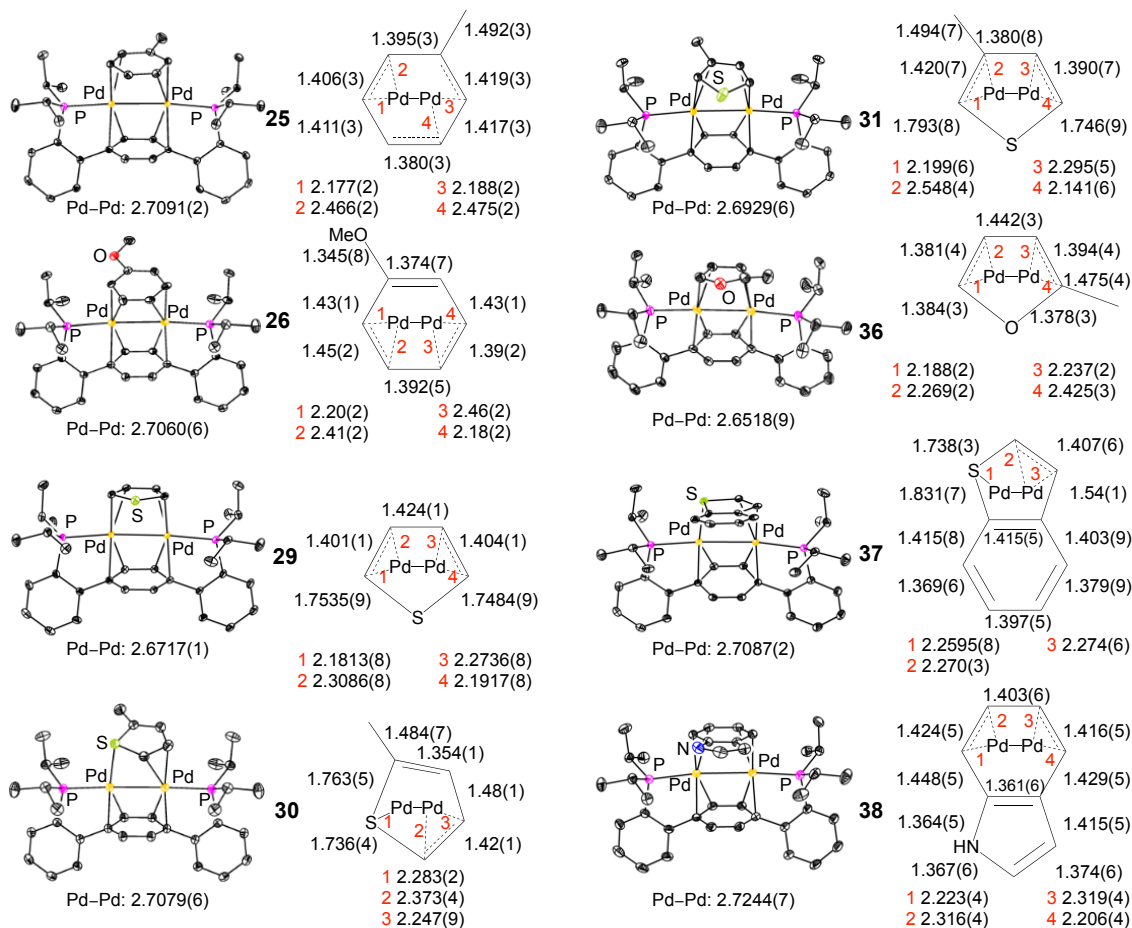


Figure 4.1. Structures of **25**, **26**, **29-31**, **36-38** as determined by single-crystal X-ray diffraction. Thermal ellipsoids generated at the 50% probability level.³⁴ Outer-sphere anions, solvent molecules, and hydrogen atoms are not shown. Bond distances (Å) for the capping ligands are shown.

^1H NMR spectra in CD_3CN revealed the lability of toluene from **25**. A new singlet at 5.96 ppm is assigned as the central arene protons. Peaks corresponding to free toluene³⁵ are also observed. Dissolution of **25** in CH_3CN followed by removal of volatiles under vacuum shows by ^1H NMR analysis (CD_2Cl_2) that the toluene has been exchanged for two acetonitrile ligands (2.56 ppm, *cf.* 1.97 ppm for free CH_3CN in CD_2Cl_2 ³⁵).

Furthermore, layering of this acetonitrile-capped species in DCM under anisole yielded red crystals of anisole-capped species **26** (Scheme 4.1). XRD analysis revealed a π -binding mode similar to that of toluene (Figure 4.1). In the solid-state, the methoxy group is nearly coplanar with the anisole ring (dihedral angle, $\varphi = 3^\circ$). The π -coordination of anisole in solution is supported by NMR spectra (CD_3NO_2) of **26** exhibiting features analogous to those of **25**: ^1H NMR olefinic singlet and multiplet (6.21 and 5.96 ppm, respectively) and shielded *ortho*-, *meta*-, and *para*- ^{13}C NMR anisole signals (86.7, 94.7, and 87.4 ppm).

2. Synthesis and Characterization of Diene Adducts.

The lability of toluene in **25** raised the question if neutral non-aromatic dienes or diene analogues could serve as more strongly binding ligands. Upon exposure of **25** to 1 atm of 1,3-butadiene (Scheme 4.1), the reaction mixture became light orange. Light yellow crystals of the resultant species **27** were obtained from acetonitrile solution layered under diethyl ether (Et_2O), and XRD revealed a $\mu\text{-}\eta^2\text{:}\eta^2\text{-}(s\text{-trans})$ -butadiene capping two Pd centers that are 2.8379(8) Å apart (Figure 4.10). This motif mirrors that proposed for 1,3-butadiene on Pd(110) between nearest-neighbor surface atoms based on STM image analysis.³⁶ The Pd–Pd distance enforced by the terphenyl framework contrasts with a Pd–Pd separation of 3.19 Å reported for a bis(butadiene) sandwich.¹⁹ The present Pd–Pd distance is closer to that in one atom-bridged systems (Figure 4.1,

bottom left, X = halide, $r(\text{Pd-Pd}) = 2.58$ to 2.70 Å),^{20,37} suggesting that the terphenyl diphosphine compresses the distance between the two metals.

While crystallographic disorder of the butadiene ligand³⁸ obscures accurate determination of the structural parameters corresponding to bonding with the metal centers, the NMR data provides information about the dynamics of the Pd₂-butadiene interaction in solution. The central arene protons of **27** are represented by two ¹H NMR doublets ($\delta = 6.10, 5.83$ ppm; $J = 7.8$ Hz). One ³¹P NMR peak ($\delta = 78.8$ ppm) is observed. These observations are consistent with the pseudo-C₂ symmetric solid-state structure persisting in solution on the NMR timescale, indicating that the Pd₂ unit exchanges quickly relative to the central ring (eq. 4.1). The diene binding, however, is not fluxional on the NMR time scale. The lack of butadiene displacement by MeCN is consistent with the plethora of stable *s-trans*-diene-bridged dipalladium compounds in the literature.^{19,20,39}

In contrast, 1,3-cyclohexadiene (CHD), an *s-cis*-diene, has rarely been isolated bridging between two adjacent metal centers.^{19,20} No crystal structures have been published previously. The present terphenyl diphosphine framework was thus employed to characterize such an adduct. Addition of 10 equiv. CHD to a CD₃CN solution of **25** formed a new species (**28**) nearly quantitatively within minutes (Scheme 4.1). By ¹H NMR spectroscopy, **28** exhibits two singlets (6.35, 5.45 ppm) and one multiplet (4.78 ppm) in the olefinic region, all with approximately the same integration. A ¹H-¹H 2D NMR experiment (COSY) showed the multiplet being correlated with a second multiplet at 7.18 ppm. The olefinic singlets are attributed to the central arene, and the multiplets are assigned to CHD.⁴⁰ This data is consistent with a $\mu\text{-}\eta^2\text{:}\eta^2\text{-CHD}$ adduct in solution, where rotation of the CHD adduct atop the two metal centers and CHD dissociation are slow on the NMR time scale. Similar to butadiene, these suggest that

the interaction with the diene moiety is strong. Yellow crystals were grown via vapor diffusion of Et₂O into a MeCN solution of **28**, and an XRD study yielded the structure suggested by NMR data, albeit with significant disorder (Figure 4.8). This is the first reported structure of CHD bound to any dipalladium moiety. While no surface studies of CHD adsorption on Pd have been reported, a study of CHD adsorption on Pt(111) predicted the present μ^2 motif to be unstable and a μ^3 binding mode to be lower in energy.⁴¹ However, the present motif may be important on lower coordinate faces [e.g. (110), (210), etc.] and defect sites.

3. Synthesis and Characterization of Heterocycle Adducts.

The well-defined ligation of olefins and arenes indicated that the dipalladium moiety supported by terphenyl diphosphine, **1**, may allow for binding of a much broader spectrum of substrates. Dipalladium species bridged by thiophenes, pyrroles, and furans were explored.

3.1 Thiophenes. Adding 10 equivalents of thiophene to a red solution of **25** in CD₃CN did not result in any changes observable by NMR spectroscopy. To limit competitive binding from excess acetonitrile, reaction in CH₂Cl₂ was attempted, but found to be slow due to the low solubility of **25**. Thus, **25** was first treated with acetonitrile to exchange away toluene, then volatiles were removed under vacuum. This material readily dissolved in CH₂Cl₂ and reacted upon addition of excess thiophene, resulting in orange precipitate of **29** within seconds (Scheme 4.1). XRD-quality crystals of **29** were grown by diffusion of Et₂O vapor into a nitromethane solution (Figure 4.1). In the solid-state, thiophene is $\mu\text{-}\eta^2\text{:}\eta^2$ -bound, with the C=C double bonds (1.401(1), 1.404(1) Å) and the C–S bonds (1.7535(9) and 1.7484(9) Å) elongated relative to free thiophene.⁴² These metrics suggest that aromaticity in

thiophene is disrupted by the interaction of the metal centers with the double bonds. While mononuclear adducts of η^2 -thiophene are well-known⁴³⁻⁴⁷ and higher hapticity mononuclear adducts have precedent,⁴⁸⁻⁵¹ dinuclear adducts of thiophene are rare. In most examples, cleavage of a C–S bond occurs (perhaps through a mononuclear intermediate) and polynuclear adducts of C–S cleaved fragments are observed.⁵²⁻⁵⁴ In the nearest precedent to **29**, 3,4-bis(trifluoromethyl)-S-methyl-thiophenium was reported to be μ - η^2 : η^2 -bound to a dimolybdenum moiety.⁵⁵

Nickel and palladium have been extensively used to cross-couple thiophene groups, but prior to **29**, no π -adducts were structurally characterized. Organonickel thiophene π -adducts have been proposed to play a role in various processes, such as precursors to C–S oxidative addition⁵⁶ and propagating species in nickel-catalyzed polymerization of 3-alkylthiophenes.⁵⁷ Analogous thiophene π -adducts in organopalladium chemistry have yet to be widely considered.

EXAFS studies have found thiophene monolayers to bind parallel to Pd(111) and (100) surfaces.⁵⁸ The initially proposed adsorption models had the carbons bound essentially η^4 -atop one Pd center with unusually long Pd–C bonds (>2.5 Å c.f. ~ 2.16 Å in Pd(COD)₂⁵⁹). A later DFT study of thiophene on Pd(100) explored six adsorption geometries and found an energy minimum with the double bonds bridging three metal centers and sulfur binding a fourth metal center.⁶⁰ A thiophene-surface adsorption model in which the double bonds are μ^2 - η^2 : η^2 -bound to two Pd centers, as in **29**, has never been discussed in the literature, to the best of our knowledge.⁶¹

To determine the effect of substitution on the thiophene binding mode, the synthesis of 2-methylthiophene and 3-methylthiophene complexes was attempted.

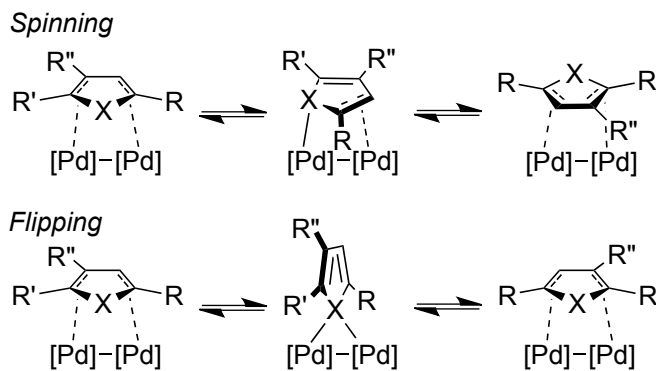
Analogous procedures to that for thiophene afforded XRD-quality crystals of **30** and **31**, respectively (Scheme 4.1). 3-Methylthiophene in **31** is $\mu\text{-}\eta^2\text{:}\eta^2$ -bound, similar to thiophene in **29**, but 2-methylthiophene in **30** is $\mu\text{-}\eta^2\text{:}\eta^1(\text{S})$ -bound (Figure 4.1). Prior to this work, this latter cofacial bridging mode of thiophene had not been crystallographically characterized and nor analyzed in computational studies of thiophene on metal surfaces. The only previously reported co-facial $\mu\text{-}\eta^2\text{:}\eta^1(\text{S})$ -heterocycle adducts were enforced by C–H activation of the 2-position by a third metal center in a trismium cluster.^{62,63} The observed differences in the binding modes are likely due to the steric interactions. Binding of 2-methylthiophene similar to thiophene would direct the methyl group toward the isopropyl substituents. The methyl group of 3-methylthiophene, however, does not have unfavorable steric interactions and thus binds like thiophene.

To examine the persistence and fluxionality of these binding modes in solution, **29**–**31** and 2,5-dimethylthiophene adduct **32** were studied by NMR spectroscopy (CD_3NO_2 , 25 °C). Atypical ^1H chemical shifts attributed to the thiophene moiety in **29** are similar to those attributed to olefinic protons of π -bound CHD in **28**.^{40,64} Compounds **29**–**32** each exhibit a ^1H NMR peak between 6.25 and 6.11 ppm corresponding to the four equivalent central arene protons, but the shape of this peak at room temperature varies from a sharp singlet (full width at half maximum (FWHM) \sim 1 Hz) for **29** to a very broad peak (FWHM = 146 Hz) for **31**. ^1H NMR spectra of **29** collected at -20 °C show broadening of the central arene signal but not decoalescence into two peaks. This indicates that for **29**, fluxional processes occur rapidly on the NMR timescale, at room temperature, to generate pseudo- C_{2v} symmetry in solution. In contrast, for **31**, partial decoalescence of the central arene ^1H signal into two peaks is observed at -18 °C, and coalescence to a sharp ^1H singlet is observed only upon heating at 90 °C. While the lack of full decoalescence at temperatures above the solvent

freezing point precludes precise calculation, ΔG^\ddagger at 25 °C for fluxional processes in **31** is equal to or greater than 13 kcal/mol.

Two mechanisms may be responsible for the fluxional processes in π -coordinated thiophenes and other heterocycles (Scheme 4.2). The central arene of the diphosphine is assumed to exchange rapidly as discussed previously (eq. 4.1). Additionally, “spinning” of the heterocycle may occur to exchange the atoms ligated to the metal centers. This mechanism could also be responsible for the exchange processes in arenes in **25** and **26**. Alternatively, the binding mode of the heterocycle may change from the π -system to a dative interaction from the lone pairs on the heteroatom. Re-coordination, or “flipping”, to the heterocycle π -system may result in a different orientation relative to the central arene. For heterocycles that have C_{2v} symmetry in free form (e.g. thiophene, 2,5-dimethylthiophene), both spinning and flipping mechanisms could account for observation of one singlet for the four central arene protons. However, for heterocycles with only C_s symmetry, the spinning mechanism could not make all four central ring protons equivalent. Therefore, flipping would be responsible for the exchange.

Scheme 4.2. Fluxional processes for heterocycle adducts



3.2. *Pyrroles*. Pyrrole and *N*-methylpyrrole adducts **33** and **34** were synthesized and isolated in an analogous procedure to **29** (Scheme 4.1). Both complexes exhibit two multiplets between 3.22 and 3.02 ppm and a downfield ¹H NMR multiplet (8.89 and 8.62 ppm, respectively). The two aliphatic multiplets correspond to two isopropyl methine environments and the downfield multiplet corresponds to the α-H nuclei (α-Hs) of the heterocycle. These features are consistent with a C_s-symmetric structure. Given that the 1- and 4-Hs in CHD adduct **28** and α-Hs of thiophene adduct **29** are also shifted conspicuously downfield (7.18 and 8.80 ppm, respectively), the binding modes of pyrrole and *N*-methylpyrrole are likely structurally analogous, i.e. μ²-η²:η².⁶⁴

Dipalladium(I) complexes sandwiched by two μ-η²:η²-pyrroles were recently reported⁶ but due to their high symmetry could not be easily used to elucidate the fluxionality of π-bound pyrroles. In **33** and **34**, the asymmetric sandwich motif facilitates the study of fluxional processes. The ¹H NMR spectrum of **33** displays central arene signals (6.24 and 6.15 ppm, FWHM = 8.4 Hz) that are broader than those of **34** (6.28 and 6.17 ppm, FWHM = 3.6 Hz), suggesting that pyrrole spinning occurs and is faster than *N*-methylpyrrole spinning. A variable temperature ¹H NMR study of **33** shows coalescence of the central arene signals and isopropyl methine signals near 50 °C. Flipping is not possible in this case, as the nitrogen center does not have an accessible lone pair in contrast to sulfur in thiophene.

3.3. *Furans*. Furan and 2-methylfuran adducts **35** and **36** were accessed in a procedure analogous to **29** (Scheme 4.1). The ¹H NMR spectrum of **35** exhibits two doublets in the olefinic region (6.32, 6.27 ppm; J = 1.4 Hz) and two multiplets downfield and upfield of the aromatic region (9.42, 6.41 ppm, respectively), all with approximately the same integration.⁴⁰

These features, mirroring those of **28** and **34**, suggest that furan is $\mu\text{-}\eta^2\text{:}\eta^2$ -bound and not rapidly fluxional on the NMR timescale. In contrast, 2-methylfuran adduct **36** exhibits three ^1H NMR multiplets between 6.38 and 6.08 ppm (integrating 2:1:1) and ^{31}P NMR doublets at 60.9 and 57.4 ppm ($J_{\text{PP}} = 162$ Hz). The ^1H NMR multiplets, corresponding to the central arene protons, and the asymmetric phosphines support a time-averaged C_1 -symmetric structure for **36**. Such a structure could be realized with $\mu\text{-}\eta^2\text{:}\eta^2$ or $\mu\text{-}\eta^2\text{:}\eta^1(\text{O})$ binding modes for 2-methylfuran. Given the large difference in ^{13}C NMR chemical shift between the α -Cs of the bound heterocycle ($\text{OCCH}_3 = 179.8$; $\text{OCH} = 65.5$ ppm), $\mu\text{-}\eta^2\text{:}\eta^1(\text{O})$ binding was initially suspected. However, XRD study of **36** revealed a $\mu\text{-}\eta^2\text{:}\eta^2$ binding mode (Figure 4.1). Asymmetric binding of the α -Cs ($\Delta r(\text{Pd-C}) = 0.24$ Å) may account for their dissimilar chemical shifts. Theoretical studies of furan on Pd(111) surfaces indicated low-energy binding modes across three metal centers,⁶⁵ but the $\mu^2\text{-}\eta^2\text{:}\eta^2$ motif from **35** and **16** may be present on lower-coordinate surfaces. Such furan binding modes have not been crystallographically characterized previously, although trans-facial $\mu^2\text{-}\eta^2\text{:}\eta^2$ binding of furan to two Re(I) centers has been proposed.⁴⁴

To explore if furan spinning or flipping is thermally accessible, a variable temperature NMR study of **35** was conducted. The difference in chemical shift of the central arene peaks ($\Delta\delta$) was recorded near the freezing temperature of the NMR solvent (CD_3NO_2). From -25 °C to 90 °C, $\Delta\delta$ decreased from 0.11 to 0.02 ppm, suggesting that an exchange process occurs but is slow on the NMR timescale.

3.4. Benz ζ -derivatives: Benz ζ thiophene, Indole, and 4,6-Dimethyldibenz ζ thiophene. Perhaps due to the large number of surface conformations and atoms, theoretical adsorption models of benzothiophene and indole on surfaces have been less developed than for five-membered

heterocycles. Thus, benzothiophene- and indole-bridged species **37** and **38** were synthesized, purified, and crystallized in an analogous manner to **29** (Scheme 4.1). XRD analysis reveals benzothiophene to be bound $\mu\text{-}\eta^2\text{:}\eta^1(\text{S})$, whereas indole binds $\mu\text{-}\eta^2\text{:}\eta^2$ through its carbocyclic ring (Figure 4.1). The only previously reported co-facial $\mu\text{-}\eta^2\text{:}\eta^1(\text{S})$ -benzothiophene adducts were enforced by C–H activation of the 2-position by a third metal center in a trinuclear cluster,^{62,63} but the all-carbon binding mode of indole in **38** mirrors that in a recently reported bisindole dipalladium(I) sandwich complex.⁶

The asymmetry of the present terphenyl diphosphine environment again allows analysis of the fluxionality of benzothiophene and indole ligands that would be difficult in a symmetric sandwich compound. At room temperature, ¹H NMR spectra of **37** exhibit four peaks spanning 5.75–6.13, and ³¹P NMR spectra show doublets at 67.3 and 65.9 ppm (*J* = 168 Hz). In contrast, ¹H NMR spectra of **38** exhibits two broad peaks at 6.42 and 5.57 ppm, and ³¹P NMR spectra show one broad peak at 64.7 ppm. The ¹H NMR features, attributed to the central arene protons, and the ³¹P NMR spectra indicate that benzothiophene, bound through its heterocyclic ring, does not spin or flip rapidly on the NMR timescale, but indole, bound through its carbocyclic ring, may be able to rapidly spin on the NMR timescale. Coincidental overlap of the central arene ¹H and phosphine ³¹P signals, rather than fast exchange processes, could not be ruled out.

4,6-Dimethyldibenzothiophene is considered to be an especially recalcitrant heterocycle toward hydrodesulfurization.⁶⁶ Crystallographically characterized models for multinuclear binding have not been previously reported. Targeting such a model, 4,6-dimethyldibenzothiophene adduct **39** was synthesized and studied (Figure 4.2). XRD analysis show that the heterocycle is bound $\mu^2\text{-S}$, perpendicular relative to the central arene, in contrast to the parallel heterocycles in **29–38**. The S–C bonds are elongated 0.02 Å relative to

free 4,6-dimethyldibenzothiophene.⁶⁷ This is the first crystallographically characterized example of a μ^2 -S bound dibenzothiophene. The perpendicular binding mode is likely the result of steric interactions with the ligand isopropyl groups for the parallel coordination; on a palladium surface, the methyl groups might interfere with perpendicular binding, and parallel π -coordination might be preferred. Perpendicular σ -binding is proposed to precede C–S bond cleavage in hydrodesulfurization over Ni–MoS₂/ γ -Al₂O₃.⁶⁶

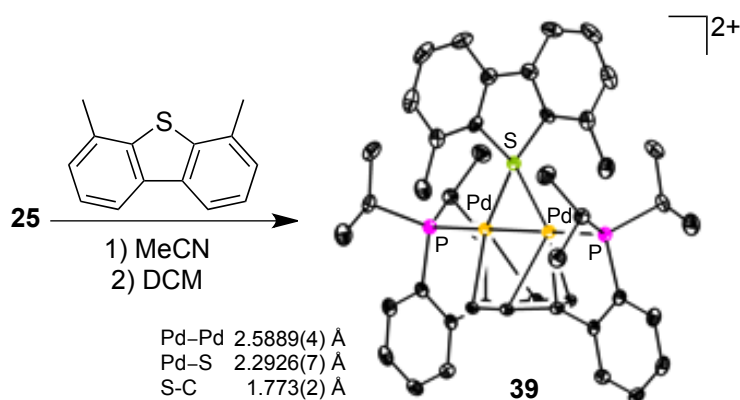


Figure 4.2. Synthesis and solid-state structure of 4,6-dimethyldibenzothiophene adduct **39** with 50% thermal ellipsoids. Outer-sphere anions, solvent molecules, and hydrogen atoms not shown.

3.5. Comparison of Fluxional Processes of S-, N-, and O-Heterocycle Adducts. In the above observations of compounds **29-36**, generally, the fluxionality of bound thiophenes is greater than bound pyrroles, which in turn are more fluxional than furans. Energetically similar Pd–heteroatom and Pd–(C=C) interactions are expected to lead to small barriers for fluxional processes depicted in Scheme 4.2. According to hard-soft acid-base theory,⁶⁸ sulfur is a soft, better-matched, ligand for palladium than nitrogen or oxygen. Thus, the spinning and flipping intermediates illustrated in Scheme 4.2 are expected to be more readily accessible for

bound thiophene. In fact, the solid-state structures of **30**, **31**, and **37** are models for spinning intermediates and that of **39** is a model for a flipping intermediate. Accordingly, the central arene and isopropyl methine protons of **29** appear as single resonances in room temperature ^1H NMR spectra. Nitrogen is a worse matched ligand than sulfur, and a μ^2 -N flipping intermediate is not possible for pyrroles, which do not have a lone pair on the heteroatom that is not part of the π -system. Correspondingly, by ^1H NMR the central arene protons of **33** have coalesced to one peak, but the isopropyl methine protons remain two distinct peaks at room temperature. The apparent fluxionality of indole in **38** should be attributed to the fact that no Pd–N bond needs to be formed during spinning about the carbocyclic ring.

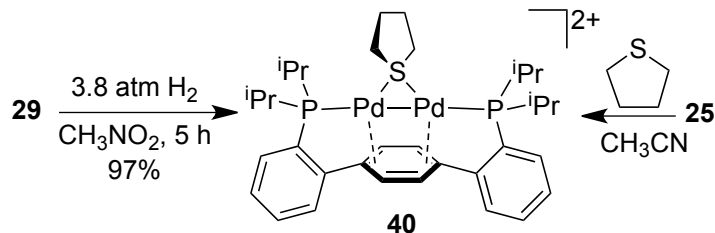
Finally, oxygen is a hard Lewis base, and spinning or flipping intermediates displaying Pd–O bonds are expected to be prohibitively uphill. The relatively static behavior of furan in **35** and the μ^2 - η^2 : η^2 coordination mode of 2-methylfuran in **36**, despite steric repulsion from the isopropyl groups (*cf.* **30**), support this trend. Consistent with the above explanations, rings with higher aromaticity are expected to have lower barriers to exchange. In agreement, the order of aromaticity of heterocycles (thiophene > pyrrole > furan) matches the observed qualitative exchange rates.⁶⁹

4. Hydrogenation of S-Heterocycle Adducts.

Palladium has been explored as a component of next-generation deep hydrodesulfurization catalysts.^{70,71} Initial π -coordination on Pd surfaces is proposed to facilitate subsequent cleavage of otherwise unreactive C–S bonds.^{72,73} To study this process, **29** in CH_3NO_2 was sealed with 3.8 atm H_2 in a J. Young NMR tube (Scheme 4.3). Over 5 h at room temperature, **29** was fully converted to a new species **40** by ^{31}P ($\delta = 69.8$ ppm) and some black precipitate was formed. This species was precipitated from MeCN by addition of

excess Et₂O and exhibited a singlet in the region for central arene protons and two new aliphatic multiplets (6.09, 3.55, and 2.43 ppm) integrating 1:1:1. Thus, **40** was assigned to contain one bridging tetrahydrothiophene (THT) ligand (97% isolated yield). The constitution of **40** was further confirmed by gas chromatography-mass spectrometry (GC-MS) of the reaction mixture, which showed a match for THT. An independent synthesis by addition of THT to **25** released toluene and directly formed **40** (Figure 4.3), supporting the above assignment. Under identical hydrogenation conditions, benzothiophene adduct **37** was observed to convert to a more symmetric species with one ³¹P NMR signal (72.8 ppm, s), which could be a κS-dihydrobenzothiophene adduct. GC-MS of the reaction mixture confirmed the presence of 2,3-dihydrobenzothiophene. No intermediates were observed in significant amounts during these hydrogenation reactions. No hydrogenation/hydrogenolysis products were observed under similar reaction conditions with 4,6-dimethyldibenzothiophene adduct **39**.

Scheme 4.3. Hydrogenation and direct routes to tetrahydrothiophene adduct 40



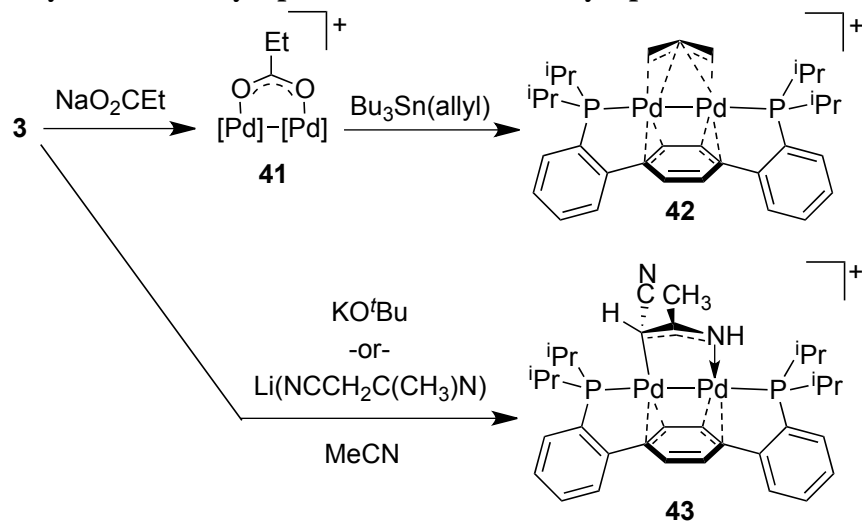
Under hydrogenation conditions, small amounts of black precipitate were observed, suggesting some reduction to Pd(0). Hydrogenation of thiophene by heterogeneous palladium, which has previously been reported for η²-thiophene tungsten compounds,⁴⁵ cannot be ruled out. However, the hydrogenation of free thiophene with heterogeneous palladium catalysts has been reported under strongly acidic conditions or at elevated

temperatures.⁷⁴ In the present system, the π -coordination of thiophene may activate it towards hydrogenation, although the exact mechanism is currently unclear.

5. Synthesis and Characterization of Anionic-Bridged Complexes.

Bridging anionic allyl species have been proposed in hydrocracking and hydrogenation mechanisms on heterogeneous Pd⁷⁵ and have been recently discovered to exhibit reactivity toward CO₂ in a homogeneous system.²⁴ To test if such ligands could be supported on the present dipalladium motif, **25** was initially treated with sodium *n*-propanoate to form a red, putative carboxylate complex (**41**, Scheme 4.4). Subsequent transmetalation with tributylallyl tin yielded a yellow species **42**, which exhibited two inequivalent central arene singlets (6.23, 5.55 ppm) in the ¹H NMR spectrum, suggesting slow or no rotation of the bridging allyl on the NMR time scale. Crystals of **42** were grown from a CH₃CN solution layered under Et₂O and analyzed by XRD. The solid-state structure shows the allyl moiety to bridge symmetrically the two metal centers (Figure 4.3).

Scheme 4.4. Synthesis of allyl species **42** and heteroallyl species **43**.



A related heteroallyl species **43** was synthesized by reaction of **25** with KO^tBu in MeCN (Scheme 4.4). NMR spectra of **43** showed broad ¹H peaks corresponding to the CH and CH₃ moieties (4.51 and 2.32 ppm) of an iminobutanenitrilyl anion and broad ³¹P peaks at 50.2 and 49.2 ppm. FAB-MS found a major species with m/z = 757.1390 (calcd. BF₄⁻ dissociated cation: 757.1132). Although **43** could not be isolated cleanly, its assignment was supported through an alternate synthesis by treating **25** with a pre-formed diacetoneitrilyl anion.⁷⁶ Crystals grown from a CH₂Cl₂ solution layered under Et₂O were studied by XRD, and revealed the dipalladium moiety capped by a μ-κC:κN-NCCHC(CH₃)NH moiety (Figure 4.3). Such diacetoneitrilyl anions have not structurally characterized in this particular tautomer or binding motif.⁷⁷ While the allyl carbons in **42** lie in a plane canted toward that of the central arene, the three atoms of the heteroallyl in **43** are tilted away from the central arene. ($\varphi(\text{allyl}, \text{central arene}) = 20.6^\circ$; $\varphi(\text{heteroallyl}, \text{central arene}) = -19.4^\circ$). Thus allyl binds μ-η²:η², but diacetoneitrilyl binds μ-κC:κN.

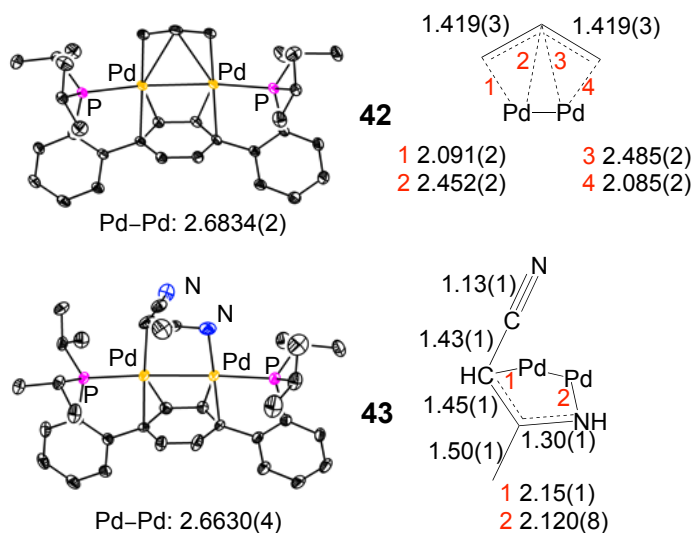
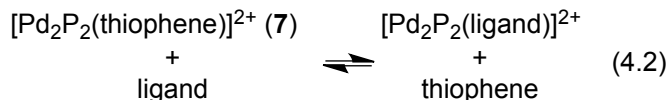


Figure 4.3. Structures of **42** and **43** as determined by single-crystal x-ray diffraction, with 50% prob. thermal ellipsoids. Outer-sphere anions, solvent molecules, and hydrogen atoms are not shown. Bond distances for the capping ligands are shown.

6. Experimentally Determined Relative Binding Strength of Ligands.

The capping arenes, furans, and thiophenes in **25**, **26**, **29-32**, **35-37**, and **39** are all quantitatively displaced by acetonitrile (determined by ^1H NMR) upon dissolution of the compound in CD_3CN . In contrast, capping dienes, N-heterocycles, and THT in **27**, **28**, **33**, **34**, **38**, and **40** are persistent in CD_3CN . With access to this series of diverse, yet structurally related compounds we proceeded to measure the relative binding strengths of a variety of ligands to a Pd_2 moiety. To compare the binding of these ligands, equilibrium experiments starting with thiophene adduct **29** and a free diene, arene, or heterocycle were performed (eq. 4.2):



All species (except for THT adduct **40**) in the equilibrium mixture did not exhibit peak shifting, broadening, or coalescence, which indicates slow intermolecular exchange on the NMR timescale. The relative concentrations were determined by integration of ^1H NMR spectra (CD_3NO_2 , 25 °C). The resulting equilibrium constants were found to span greater than 13 orders of magnitude (Figure 4.4). To our knowledge, this is the first study that has allowed the measurement of quantitative binding affinities of such a broad class of substrates relevant to many catalytic transformations involving π -systems.⁷⁸ N-heterocycles are more strongly bound than the S-heterocycles, which are more strongly bound than O-heterocycles. On Pd surfaces, experimental measurement of desorption energy of heterocycles is complicated by C-heteroatom cleavage,⁷⁹ but the same order of heterocycle binding affinity has been reported with thermal desorption spectroscopy of pyrrole, thiophene, and furan on $\text{Cu}(100)$.⁸⁰

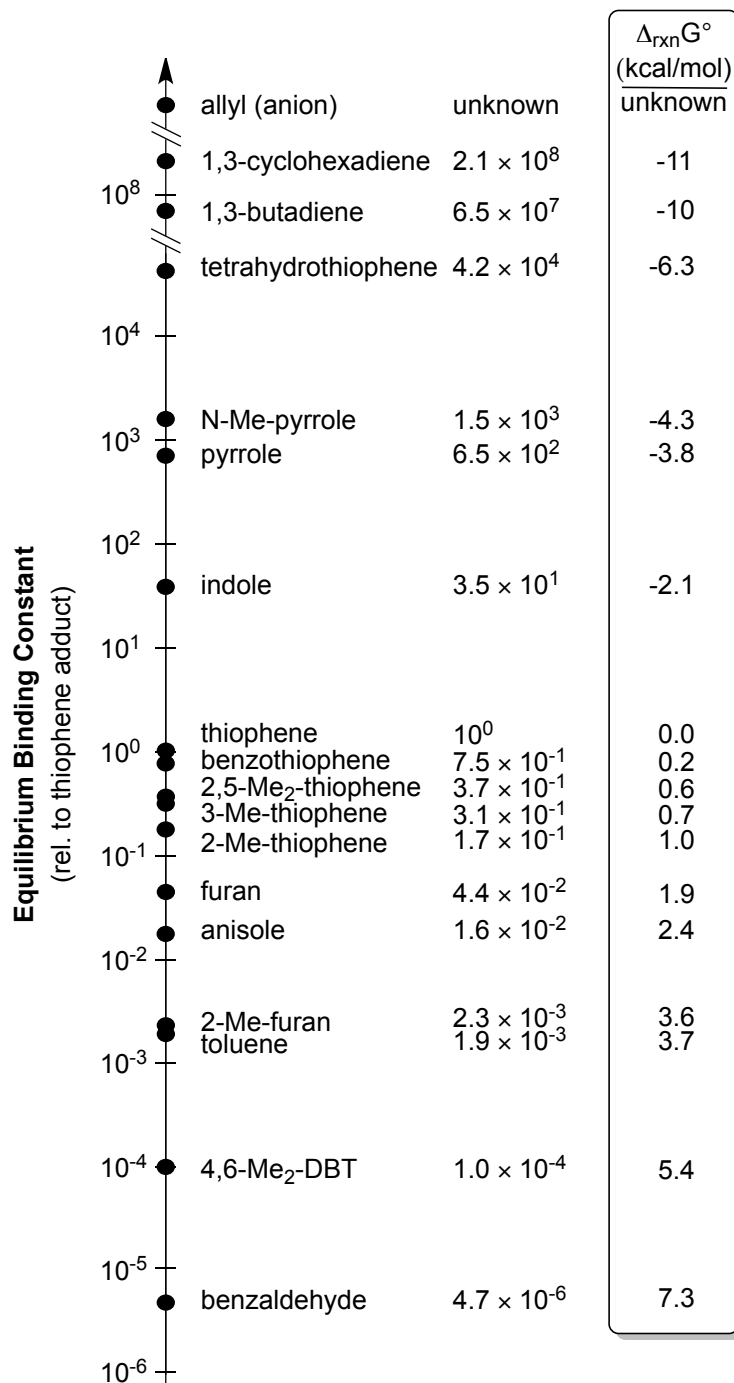


Figure 4.4. Equilibrium binding constants and relative standard Gibbs free energy of reaction of various arenes and heterocycles (eq. 4.2).

Sterics play a role in binding affinity to dipalladium(I). Substitution of the thiophenes and furans weakens binding, but only by less than one order of magnitude. This effect is likely due to steric repulsion between the heterocycle substituents and phosphine groups. In the case of 4,6-Me₂-DBT, the substitution precludes π -binding, and the resulting μ^2 -S binding is so weak (10⁴ fold weaker than thiophene) that an equilibrium constant could not be determined directly against **29** but had to be determined against toluene adduct **25** instead.

THT quantitatively displaces thiophene from **29**, so its relative binding affinity was determined against the *N*-methylpyrrole adduct **34**. Similarly, butadiene quantitatively displaces *N*-methylpyrrole from **34**; therefore its binding affinity was determined against THT, and that of CHD, the strongest binding neutral ligand in this study, was determined relative to butadiene. Because of broadening of ¹H NMR signals and the overlapping of other ¹H NMR features, equilibria involving THT and **40** (vs *N*-methylpyrrole and butadiene) were determined by integration of ³¹P NMR spectra.

Exposure of allyl adduct **42** to 4 atm butadiene did not induce any reaction. Anionic ligands are probably not displaced by neutral ligands for Coulombic reasons. Allyl is thus very tightly bound to dipalladium(I) and could not be quantitatively placed on the relative binding affinity scale.

Two potential ligands which did not measurably react with toluene adduct **25** were tetrahydrofuran and PhCF₃, even at 100 equivalents. A benzaldehyde adduct was observed in equilibrium with **25** by NMR in CD₃NO₂ (¹H: 9.38 ppm, s, CHO vs 9.99 ppm for free benzaldehyde; ³¹P: 70.2 ppm, s), but could not be isolated. Compared to toluene, electron deficient benzaldehyde binds *ca.* 1000 times more weakly, while more electron rich anisole bind greater than 10 times more strongly.

7. Computational Guide to Relative Binding Affinities.

The observed relative binding affinity of arenes (PhOMe, PhMe, PhCHO, PhCF₃) is correlated with arene electron-richness, which has been tabulated for various substituted benzenes using empirically-derived Hammett parameters or related resonance effect parameters (e.g., σ_p or R).⁸¹

The strong binding of pyrrole mirrors the greater electron density of pyrrole relative to thiophene and furan. For example, weak electrophiles such as benzenediazonium cation and nitrous acid are known to induce rapid electrophilic aromatic substitution with pyrrole but do not react with thiophene and furan.⁶⁹ Qualitatively, electrostatic potential (ESP) plots reveal the regions of greatest electron density in the ground state of heterocycles, and have been predictive for cation- π interactions.^{82,83} The ESPs of pyrrole, thiophene, furan, indole, and benzothiophene were mapped onto their molecular electron density isosurfaces (Figure 4.5) using the GaussView program.⁸⁴ As expected, pyrrole has the most electron-rich (red) π -system. While ESPs of thiophene and furan look similar to each other, the electron density of thiophene is spread across the four binding carbons, whereas in furan, the alpha carbons are less electron rich (yellow/green), accounting for furan's weaker binding affinity. Previous studies of Na⁺- π interactions found the same trend in binding affinity and ESPs for pyrrole, thiophene, and furan.⁸³

The ESPs at the η^3 - vs η^4 -binding sites of indole and benzothiophene predict the regioselectivity of the observed adducts. For indole, the four carbons from the carbocyclic ring have more negative charge than the three atoms from the heterocyclic ring, while for benzothiophene, the heterocyclic ring is less positively charged (blue) than the carbocyclic ring. These contrasting electron distributions are reflected in the observed complementary

binding modes of indole and benzothiophene. Previous studies of cation-indole (or tryptophan) interactions have also found preferential binding to the carbocyclic ring.⁸² However, the electrostatic potential of benzothiophene has not previously been discussed in the context of cation- π -system binding. Although pure Pd(0) would not be expected to exhibit significant electrostatic interactions, palladium sulfides or hydrides present during catalysis may induce surface polarization⁸⁵ and, subsequently, cation- π -like interactions.

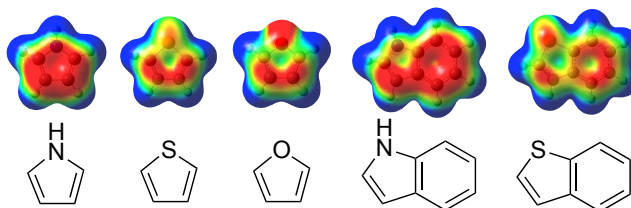


Figure 4.5. Electrostatic potentials (above) plotted onto electron density isosurfaces (isovalued = 0.004) of unbound heterocycles (below). Red represents a potential energy lower or equal to -0.02 Hartrees (electron-rich), and blue a potential energy higher or equal to +0.02 Hartrees (electron-poor).

8. Molecular Orbital Interactions in μ - η^2 : η^2 Binding.

Although simple electrostatics can be predictive for similar ligands in these complexes (*vide supra*), the interactions between the dipalladium unit and a capping diene have a covalent component as described by bonding molecular orbitals derived from Pd d-orbitals and diene π -system. The μ - η^2 : η^2 -binding mode of two π -systems in sandwich dipalladium(I) complexes has been previously examined by others.^{6,19,86} Diene binding is described through two key interactions: donation of the diene HOMO to the Pd-Pd [$d\sigma$ - $d\sigma$]* antibonding orbital (Figure 4.6a) and back-donation of the Pd-Pd $d\sigma$ - $d\sigma$ bonding orbital to the diene LUMO (Figure 4.6b).

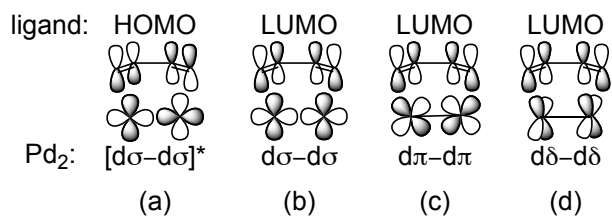


Figure 4.6. Bonding interactions between (a) diene HOMO and unfilled Pd₂-based orbital and (b-d) diene LUMO and filled Pd₂-based orbitals.

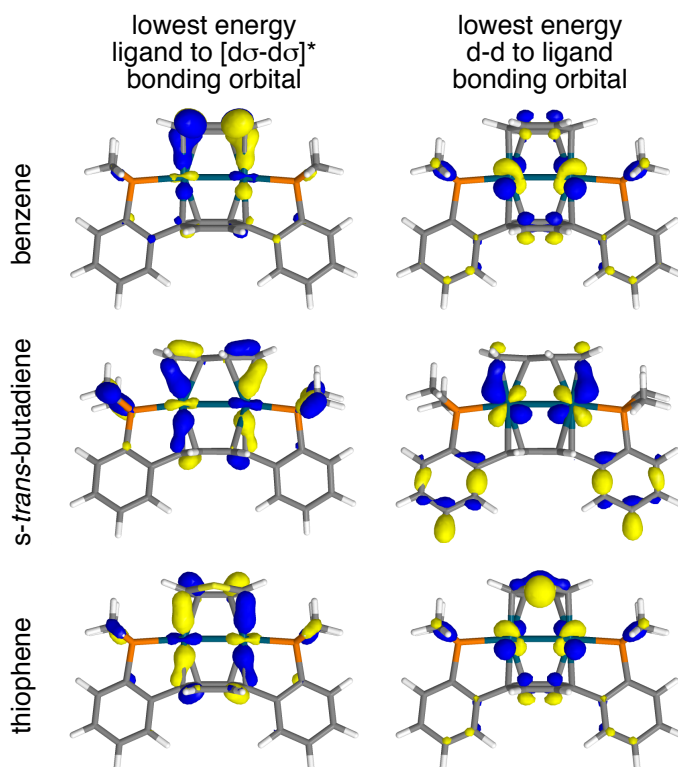


Figure 4.7. Lowest energy Pd₂-ligand bonding orbitals (isosurface = 0.05) with [dσ-dσ]* Pd₂ component (left) and mixed dπ-dπ/dδ-dδ Pd₂ component (right). Lower energy molecular orbitals involving less than 20% Pd₂ contribution are not shown.

This established bonding model was compared with DFT calculations of a series of model complexes of the form [Pd₂L(μ-η²:η²-ligand)]²⁺ (L = Me-for-^tPr variant of **1**; ligand = benzene, *s-trans*-butadiene, 1,3-cyclohexadiene, thiophene, furan) and [Pd₂L(allyl)]⁺. For

illustrative purposes, select MOs from the benzene, butadiene, and thiophene adducts are presented in Figure 4.7. The ligand-HOMO-to- $[d\sigma-d\sigma]^*$ donation is consistent across all of the complexes (Figure 4.7, left). However, the constitution of the Pd_2 -to-ligand back-bond varies.

The LUMO of a generic *s-cis*-diene is symmetric with respect to reflection in the plane perpendicular to the molecule (i.e. transforms as the a' irreducible representation in the C_s point group). There are six filled metal/phosphine-based frontier orbitals for the $[Pd_2L]^{2+}$ fragment of the same symmetry (Figure 4.8), and any of these could back-donate into the diene LUMO. The $d\sigma-d\sigma$ orbital has the best energy match to donate to a ligand-based orbital, and indeed is observed participating in a strong interaction in $[Pd_2L(allyl)]^+$ (Figure 4.9). For dienes, however, the $d\sigma-d\sigma$ lobes are directed at nodes in the diene LUMO. Instead, the primary metal-based orbital for back-donation to dienes has $d\pi-d\pi$ character, as seen with *s-trans*-butadiene (Figure 4.6c; Figure 4.7, middle right). For *s-cis*-dienes (e.g. benzene, thiophene), some $d\delta-d\delta$ character is also mixed into the back-bonding interaction to accommodate the arrangement of the diene LUMO (Figure 4.6d; Figure 4.7, right)

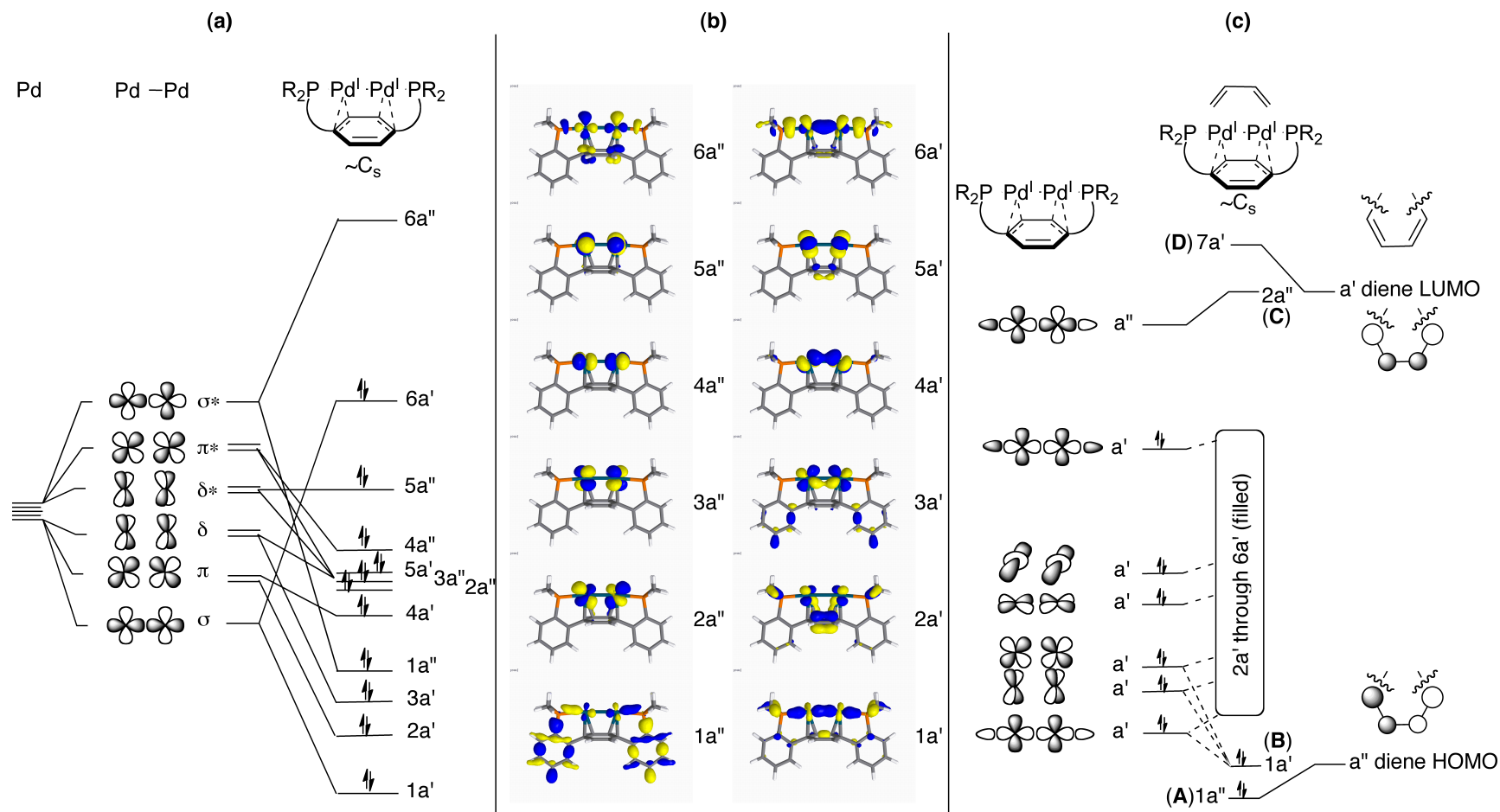


Figure 4.8. Qualitative MO bonding analysis. (a) Frontier orbitals of a C_s -symmetric dipalladium diphosphine fragment (b) DFT-calculated orbitals of a dipalladium diphosphine fragment (c) Interaction diagram of frontier orbitals with those of a diene, assuming C_s symmetry.

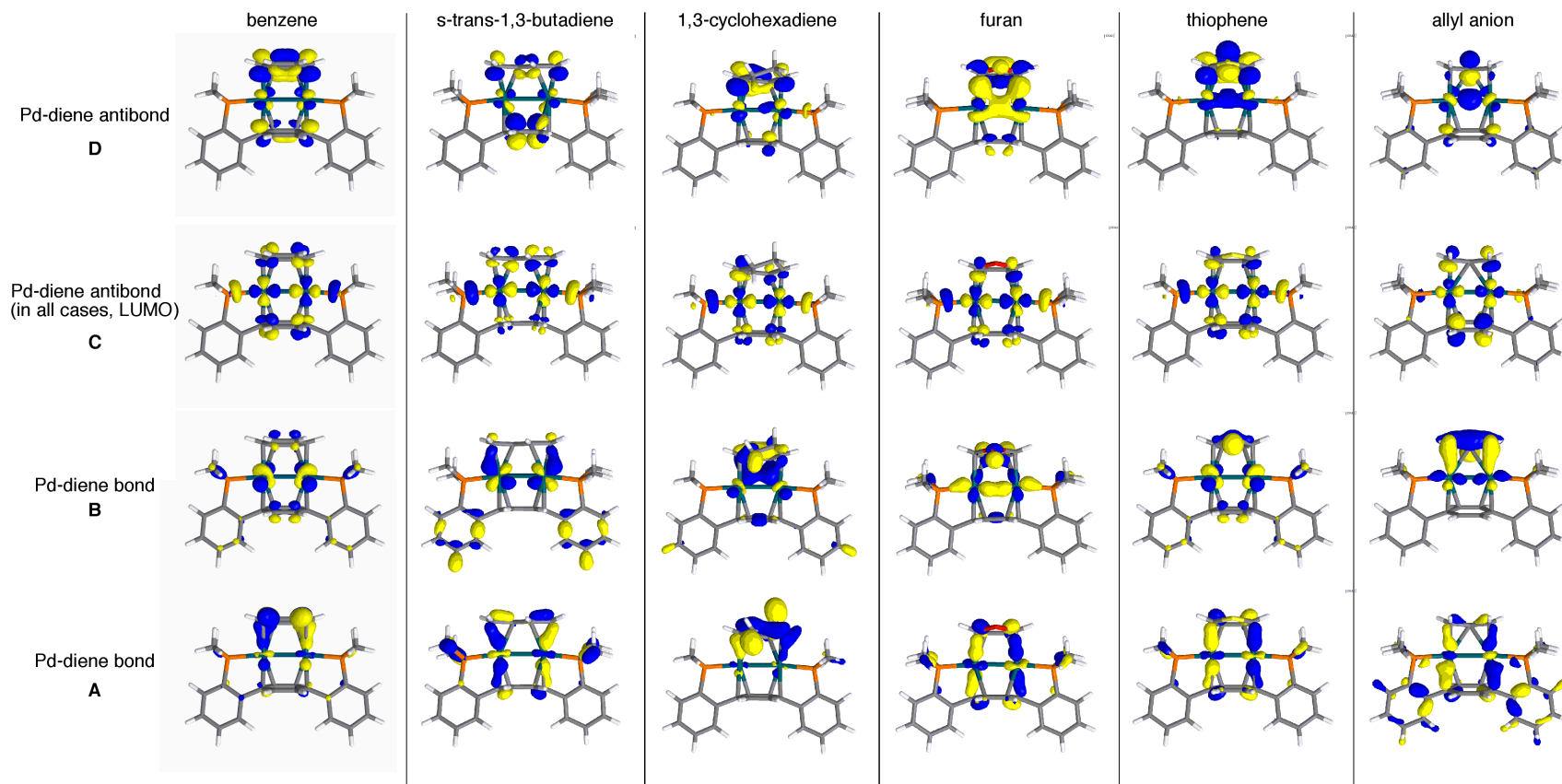


Figure 4.9. Examples of molecular orbitals displaying bonding interactions between $[\text{Pd}_2\text{L}]^{2+}$ and various capping ligands, corresponding to MOs **A-D** in Figure 4.8c.

CONCLUSIONS

A novel dipalladium(I) terphenyl diphosphine framework has been used to study well-defined π -bound complexes of toluene, anisole, 1,3-butadiene, 1,3-cyclohexadiene, thiophenes, pyrroles, and furans across two metal centers using crystallography, NMR spectroscopy, and DFT. σ -bound complexes of tetrahydrothiophene and 4,6-dimethyldibenzothiophene and π -complexes of allyl and diacetonitrilyl anions are also described. Of note, the first crystallographically characterized μ - η^2 : η^2 1,3-cyclohexadiene, thiophene, and furan adducts and μ - η^2 : η^1 (S) benzothiophene adduct are reported. The thiophene and benzothiophene adducts undergo hydrogenation to yield tetrahydrothiophene and dihydrobenzothiophene adducts. Unlike in previous systems, the multidentate framework allows substitution of only one bridging ligand, or a single molecular hemisphere. The resulting asymmetry of the complex allows for analysis of bonding dynamics by NMR spectroscopy. Capping aromatics and thiophenes undergo rapid flipping or spinning processes at room temperature, while such processes are slow for 1,3-cyclohexadiene, pyrrole, furan, and allyl ligands. Importantly, the common binding framework also allows for determination of relative binding strengths by NMR spectroscopy. Competition experiments revealed a scale of relative binding affinities spanning over 13 orders of magnitude. The general trends observed in this study were found to relate to the electron density of the π -systems. Increasing binding affinity in the order furan < thiophene < pyrrole is rationalized based on the electrostatic potentials at the binding atoms. Complementary binding modes of benzothiophene and indole are also explained through similar analysis. Unlike pure cation- π interactions, these binding interactions are shown by DFT calculations to involve Pd-Pd $d\sigma$ - $d\sigma$, $d\pi$ - $d\pi$, and $d\delta$ - $d\delta$ orbitals. Overall, the present system offers a platform to study

binding and reactivity at two adjacent metal centers. To our knowledge this is the only system that has afforded quantitative determination of relative equilibrium binding affinities for a wide variety of organic molecules coordinating via π -systems to transition metal centers. These studies provide structural, thermodynamic, and electronic insight into the binding of such substrates to homogeneous or heterogeneous bimetallic sites.

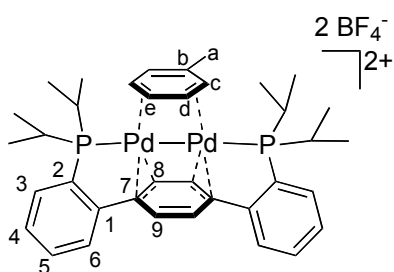
EXPERIMENTAL SECTION

General considerations. All manipulations were carried out in an inert atmosphere glovebox or using standard Schlenk line techniques. Diphosphine **1** and dipalladium complex **24** were synthesized as previously reported.^{7,28} 1,4-Butadiene was used as purchased from Aldrich. Other organic reagents were dried by stirring over sodium metal or calcium hydride, degassed by 3 cycles of freeze-pump-thaw, and isolated via vacuum-transfer. Et₂O, toluene, THF, MeCN, and DCM were dried by the method of Grubbs.⁸⁷ Deuterated solvents were purchased from Cambridge Isotope Laboratories and vacuum transferred from calcium hydride. All reagents, once degassed and dried, were stored in an inert atmosphere glovebox. ¹H and ¹³C NMR chemical shifts are reported relative to residual solvent peaks: CD₃NO₂ (¹H: 4.33; ¹³C: 61.39 ppm) and others as reported in the literature.³⁵ ¹⁹F and ³¹P NMR chemical shifts are reported with respect to the instrument solvent lock. All NMR spectra were recorded at room temperature unless indicated otherwise. Gas chromatography-mass spectrometry (GC-MS) analysis was performed upon filtering the sample through a plug of silica gel. Fast atom bombardment-mass spectrometry (FAB-MS) analysis was performed with a JEOL JMS-600H high resolution mass spectrometer. Elemental analysis was conducted by Complete Analysis Laboratories (Parsippany, NJ).

Computational details. All calculations were performed with DFT as implemented in Gaussian 09 Revision C.01.⁸⁴ Geometry optimizations and electronic structure calculations were performed with the TPSSh hybrid functional^{88,89} that, incorporating 10% exact exchange (c.f. BLYP 0% and B3LYP 20%), has been shown to be effective for calculating transition metal-containing compounds.⁹⁰⁻⁹² The LANL2DZ basis set and effective core potential⁹³ for Pd atoms and the 6-31++G(d,p) basis set⁹⁴ for all other atoms was used. No solvent corrections were used. All optimizations of palladium complexes were performed ignoring molecular symmetry starting from a crystallographic set of coordinates and as singlet dications. The benzene adduct, although input as an $\eta^3:\eta^3$ structure from the experimentally obtained toluene adduct, always optimized to an $\eta^2:\eta^2$ minimum. Energetic minima were confirmed with a subsequent frequency calculation that did not return imaginary frequency vibrations $< -10 \text{ cm}^{-1}$. All molecular orbital illustrations are depicted with a 0.05 isosurface value. The orbitals of “dipalladium diphosphine fragment” in the following figure were calculated based on the geometry from the benzene adduct with a single point energy calculation. L = a computational variant of the experimentally used diphosphine **1**, with methyls in place of isopropyls. Mulliken charges of heterocycles were calculated from geometry-optimized unbound heterocycles, and H atoms were summed into the nearest heavy atoms. While primitive, ground-state Mulliken charge calculations have been shown to be predictive, for instance, for relative pK_a s of substituted benzoic acids, phenols, and anilines.^{1,2,95} Electrostatic potentials were mapped using GaussView, the GUI component of the Gaussian software package, onto the 0.004 electron density isosurface. Red indicates potential energy lower or equal to -0.02 Hartrees, and blue

signifies potential energy higher or equal to +0.02 Hartrees. Atomic coordinates of optimized structures are published⁹⁶ and not reproduced in this thesis.

Synthesis of **25**



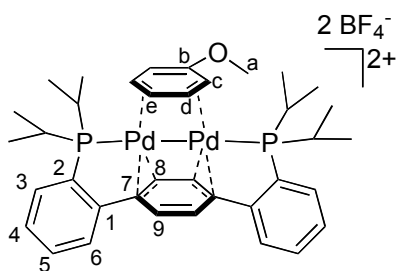
A solution of **24** (628.9 mg, 0.99 mmol) in MeCN (10 mL) was transferred over solid **1** (424.0 mg, 0.99 mmol) with stirring. After 2 h, volatiles were removed under vacuum. The solids were triturated with THF and filtered through Celite with minimal DCM (~8 mL).

Toluene (6 mL) was layered on the DCM eluent. Red crystals formed and were rinsed with minimal DCM to yield pure **25** (668.1 mg, 80%). Substituting Pd₂(dba)₃ for Pd₂(dba)₃•CHCl₃ in the synthesis of **24** led to less pure **25**, as determined by crude ³¹P NMR spectroscopy. ¹H NMR (400 MHz, CD₂Cl₂) δ: 7.85 - 7.70 (m, Ar-H_{4,6}, 6H), 7.46 (app d, *J* = 7.4 Hz, Ar-H₃, 2H), 7.27 (br d, H_c, 2H), 7.21 (br t, H_d, 2H), 6.21 (s, Ar-H₈ + Ar-H₉, 4H), 6.19 (m, H_e, 1H), 3.13 (m, CH(CH₃)₂, 4H), 1.97 (s, CH₃, 3H), 1.34 (m, CH(CH₃)₂, 24H). ¹⁹F{¹H} NMR (376 MHz, CD₂Cl₂) δ: -151.9 (s). ³¹P{¹H} NMR (162 MHz, CD₂Cl₂) δ: 64.4 (s). ¹³C{¹H} NMR (101 MHz, CD₂Cl₂) δ: 146.0 (t, *J* = 11.5 Hz, Ar-C₁), 142.5 (s, tol-C_b), 133.7 (s, Ar-C₄), 132.9 (s, Ar-C₅), 132.1 (t, *J* = 8.0 Hz, Ar-C₃), 130.5 (s, Ar-C₆), 128.5 (d, *J* = 40.4 Hz, Ar-C₂), 115.0 (s, Ar-C₇), 112.9 - 109.9 (br, Ar-C₈ and Ar-C₉), 104.7 (s, tol-C_c), 100.9 (s, tol-C_e), 91.3 (s, tol-C_d), 27.8 (t, *J* = 10.1 Hz, CH(CH₃)₂), 21.4 (s, tol-CH₃), 18.4 (s, CH(CH₃)₂), 17.7 (s, CH(CH₃)₂). Anal. Calcd. for C₃₇H₄₈B₂F₈P₂Pd₂ (%): C, 47.22; H, 5.14. Found: C, 47.13; H, 5.27.

Isolation of toluene-free, acetonitrile-exchanged 25. *Method A:* A sample of **25** was dissolved in minimal MeCN, precipitated with Et₂O (5:1 vs MeCN), and

collected by filtration. This procedure was repeated 3 times, yielding toluene-free (as determined by ^1H NMR) **25**. *Method B*: A solution of **24** (136.8 mg, 0.216 mmol) in 10 mL and added over **1** (100.0 mg, 0.216 mmol). The mixture was stirred for 45 min, then filtered. Et_2O (50 mL) was added to precipitate out an orange powder, which was collected by filtration (150.2 mg, 55% yield assuming two acetonitrile ligands). ^1H NMR (300 MHz, CD_3CN) δ : 7.81-7.63 (m, 6H, aryl-*H*), 7.56 (app d, 2H, aryl-*H*), 5.99 (s, 4H, central aryl-*H*), 2.82 (m, 4H, $\text{CH}(\text{CH}_3)_2$), 1.32-1.15 (m, 24H, $\text{CH}(\text{CH}_3)_2$). $^{31}\text{P}\{^1\text{H}\}$ NMR (121 MHz, CD_3CN) δ : 62.0 (s). To observe the bound acetonitrile ligands, a ^1H NMR spectrum was also recorded in CD_2Cl_2 . ^1H NMR (300 MHz, CD_2Cl_2) δ : 7.83 – 7.59 (m, 6H, aryl-*H*), 7.50 (app d, 2H, aryl-*H*), 5.96 (s, 4H, central aryl-*H*), 2.91 – 2.68 (m, 4H, $\text{CH}(\text{CH}_3)_2$), 2.56 (s, 6H, NCCH_3), 1.47 – 1.16 (m, 24H, $\text{CH}(\text{CH}_3)_2$).

Synthesis of anisole-capped species **26**

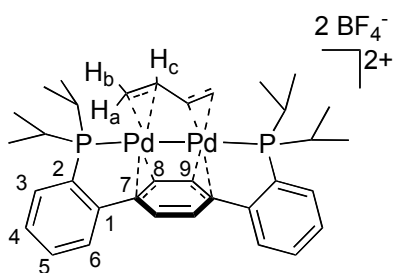


A solution of **25** (42 mg, mmol) in MeCN was concentrated under vacuum to a red-orange oil. This oil was reconstituted with DCM and layered under anisole. Red crystals were observed on the vial walls.

The mother liquor was decanted and washed with Et_2O , and the crystals were collected by filtration. Recrystallization from vapor diffusion of Et_2O into a MeNO_2 solution yielded clean **26** (27 mg, 63%). ^1H NMR (600 MHz, CD_3NO_2) δ : 7.97 (m, 2H, Ar- H_o), 7.86 (app t, 2H, Ar- H_s), 7.81 (app t, 2H, Ar- H_t), 7.60 (app d, 2H, Ar- H_3), 7.31 (app t, 2H, Ar- H_d), 6.95 (app d, 2H, H_c), 6.21 (br s, 4H, Ar- H_8 + Ar- H_9), 5.96 (app t, 1H, H_e), 3.51 (s, 3H, H_a), 3.32 (m, 4H, $\text{CH}(\text{CH}_3)_2$), 1.34 (m, 24H, $\text{CH}(\text{CH}_3)_2$). $^{31}\text{P}\{^1\text{H}\}$ NMR (162 MHz, CD_3NO_2) δ : 65.8 (br s) $^{19}\text{F}\{^1\text{H}\}$ NMR (376 MHz, CD_3NO_2) δ : -152.7 (s). $^{13}\text{C}\{^1\text{H}\}$ NMR (CD_3NO_2 , shifts determined

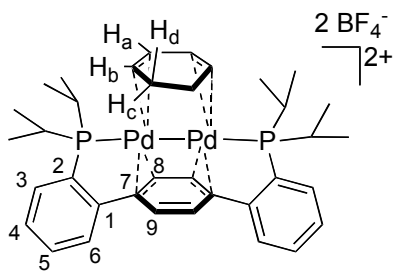
from HSQC and HMBC 2D spectra): 162.6 (C_b), 145.8 (Ar- C_1), 133.2 (Ar- C_6), 133.3 (Ar- C_5), 131.7 (Ar- C_3), 130.1 (Ar- C_4), 130.0 (Ar- C_2), 114.8 (Ar- C_7), (Ar- $C_{8/9}$), 94.7 (C_d), 87.4 (C_e), 86.7 (C_c), 55.9 (C_a), 27.2 ($CH(CH_3)_2$), 17.1 ($CH(CH_3)_2$). Ar- $C_{8/9}$ not observed by 1H - ^{13}C 2D NMR due to broadness of Ar- $H_{8/9}$ signal.

Synthesis of butadiene-capped species 27



A mixture of **25** (8.2 mg, 8.7 mmol) in CD_3CN (0.5 mL) was transferred into a J. Young NMR tube. The mixture was degassed by three freeze-pump-thaw cycles. With the aid of a manometer and calibrated gas bulb, the tube was pressurized with 3.9 atm of butadiene. The reaction turned yellow in seconds upon shaking. Reaction was confirmed by NMR, and the product was crystallized by layering the crude mixture under Et_2O to yield yellow crystals. 1H NMR (400 MHz, CD_3CN) δ : 8.03 (m, 2H, Ar- H), 7.88 (m, 4H, Ar- H), 7.75 (app d, 2H, Ar- H), 6.10 (d, $J = 7.2$ Hz, 2H, central aryl- H), 5.85 (d, $J = 7.2$ Hz, 2H, central aryl- H), 5.33 (m, 2H, butadiene- H_b), 3.36 (m, 2H, $CH(CH_3)_2$), 3.19 (m, 2H, $CH(CH_3)_2$), 3.12 (app d, $J = 13.8$ Hz, 2H, butadiene- H_a), 2.71 (m, butadiene- H_c), 1.50-0.86 (m, 24H, $CH(CH_3)_2$). $^{19}F\{^1H\}$ NMR (282 MHz, CD_3CN) δ : -151.6 (s). $^{31}P\{^1H\}$ NMR (121 MHz, CD_3CN) δ : 78.8 (s). $^{13}C\{^1H\}$ NMR (101 MHz, toluene) δ : 146.7 (app t, Ar- C_1), 136.7 (app t, Ar- C_2), 134.6 (br, Ar- $C_6 + Ar-C_5$), 133.9 (app t, Ar- C_3), 131.5 (s, Ar- C_4), 116.7 (app t, Ar- C_7), 111.3 (s, Ar- $C_{8/9}$), 109.1 (s, Ar- $C_{9/8}$), 89.4 (s, $CHCH_2$), 62.2 (s, $CHCH_2$), 29.8 (app dd, $CH(CH_3)_2$), 19.4 (s, $CH(CH_3)_2$), 18.8 (s, $CH(CH_3)_2$). Anal. Calcd. for $C_{34}H_{46}B_2F_8P_2Pd_2$ (%): C, 45.22; H, 5.13. Found: C, 45.18; H, 5.02.

Synthesis of 1,3-cyclohexadiene-capped species 28

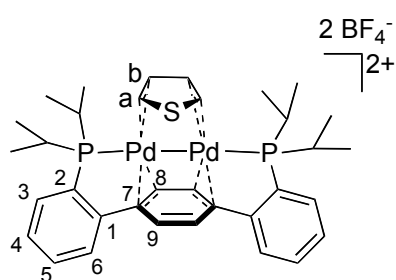


To a mixture of **25** (84.2 mg, 0.09 mmol) in MeCN (4 mL) was added 1,3-cyclohexadiene (10.4 mL, 0.11 mmol). The reaction quickly changed from red to light yellow in color. After stirring for 15 minutes, the reaction was concentrated under vacuum and washed with benzene to remove excess cyclohexadiene. The resultant solid was redissolved in MeCN and crystallized by vapor diffusion of Et₂O to yield yellow-orange crystals (73.8 mg, 89%). ¹H NMR (300 MHz, CD₃CN) δ: 8.00-7.76 (m, 8H, H₃₋₆), 7.20 (br, 2H, H_b), 6.37 (s, 2H, Ar-H₉), 5.46 (s, 2H, Ar-H₈), 4.80 (m, 2H, H_a), 3.25 (m, 2H, CH(CH₃)₂), 3.12 (m, 2H, CH(CH₃)₂), 1.97 (m, 2H, H_d), 1.47 (m, 12H, CH(CH₃)₂), 0.98 (m, 12H, CH(CH₃)₂), 0.29 (app dd, 2H, H_c). ³¹P{¹H} NMR (121 MHz, CD₃CN) δ: 66.4 (s). ¹⁹F{¹H} NMR (282 MHz, CD₃CN) δ: -151.6 (s). ¹³C{¹H} NMR (101 MHz, CD₃CN) δ: 146.7 (app t, Ar-C₁), 137.0 - 135.9 (app t, Ar-C₂), 134.5 (s, Ar-C₆), 134.4 (s, Ar-C₅), 133.8 (app t, Ar-C₃), 131.4 (s, Ar-C₄), 122.3 (s, Ar-C₉), 117.6 (app t, Ar-C₇), 97.4 (s, Ar-C₈), 83.0 (s, CH=CH-CH=CH), 81.6 (s, CH=CH-CH=CH), 28.9 (s, CH(CH₃)₂), 28.2 (app d, CH(CH₃)₂), 23.9 (s, CH=CH-CH₂), 19.7 (s, CH(CH₃)₂), 19.1 (s, CH(CH₃)₂), 18.0 (app t, J = 2.4 Hz, CH(CH₃)₂), 17.9 (s, CH(CH₃)₂). Anal. Calcd. for C₃₆H₄₈B₂F₈P₂Pd₂ (%): C, 46.53; H, 5.21. Found: C, 46.46; H, 5.19.

Synthesis of species 29-39. The procedure to synthesize **29** is described. This procedure was general for the synthesis of species **29-39**. To a solution of acetonitrile-exchanged **25** (112.0 mg, 0.12 mmol) in DCM (5 mL) was added slowly added excess thiophene (1 mL). The reaction changed from red to orange in color with fine precipitate in seconds. After stirring for 1 h, the suspension was filtered over Celite and washed with DCM to remove excess thiophene. The orange solids were washed through

Celite with CH_3NO_2 . Orange crystals (109.1 mg, 98%) were grown from vapor diffusion of Et_2O into a CH_3NO_2 solution of this compound. For **32**, **36-39**, the product did not precipitate out of DCM. Instead, the product was crashed out of DCM by addition of Et_2O , collected by filtration, and purified by repeated cycles of dissolution in DCM, addition of excess heterocycle ligand, and precipitation with Et_2O . Crystals were similarly grown by vapor diffusion of Et_2O into CH_3NO_2 .

Thiophene-capped species 29



2BF_4^- ^1H NMR (400 MHz, CD_3NO_2) δ : 8.80 (m, H_a , 2H), 7.98 (m, Ar- H_6 , 2H), 7.88 (m, Ar- H_5 , 2H), 7.82 (m, Ar- H_4 , 2H), 7.65 (app d, Ar- H_3 , 2H), 6.49 (app t, H_b , 2H), 6.25 (s, Ar- H_{8+9} , 2H), 3.30 (m, $\text{CH}(\text{CH}_3)_2$, 4H) , 1.36 (m,

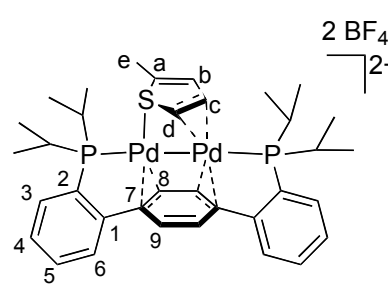
$\text{CH}(\text{CH}_3)_2$, 24H). ^{19}F NMR (376 MHz, CD_3NO_2) δ : -152.3 (s). ^{31}P NMR (162 MHz, CD_3NO_2) δ : 65.1 (s). ^{13}C NMR (101 MHz, CD_3NO_2) δ : 146.1 (app t, Ar- C_1), 134.3 (app t, Ar- C_2), 133.7 (s, Ar- C_6), 133.5 (s, Ar- C_5), 132.3 (app t, Ar- C_3), 130.2 (app t, Ar- C_4), 116.4 (app t, Ar- C_7), 111.6 (br s, Ar- C_{8+9}), 99.0 (app t, C_b), 89.2 (s, C_a), 27.2 (app td, $\text{CH}(\text{CH}_3)_2$), 17.7 (app t, $\text{CH}(\text{CH}_3)_2$), 17.1 (s, $\text{CH}(\text{CH}_3)_2$). Anal. Calcd. for $\text{C}_{34}\text{H}_{44}\text{B}_2\text{F}_8\text{S}_2\text{P}_2\text{Pd}_2(\%)$: C, 43.76; H, 4.75. Found: C, 43.66; H, 4.69.

Synthesis of 2,5-dideuterothiophene. This procedure was adapted from a literature procedure.⁹⁷ A ~6M solution of D_2SO_4 in D_2O (3 mL) was added to neat thiophene (1 mL) in a Schlenk tube with a magnetic stir bar. The tube was sealed with a Teflon screw-cap and heated to 100 °C with vigorous stirring. After 10 h, the organic phase from the reaction was separated from the aqueous phase, initially dried over MgSO_4 , further dried over Na, degassed via freeze-pump-thaw, and isolated via vacuum transfer. GC-MS data confirmed dideuterated thiophene to be the major product with

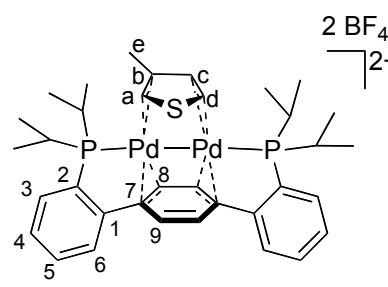
trace amounts of trideuterated product. By ^1H NMR (C_6D_6) the multiplet at 6.92 ppm in natural abundance thiophene is nearly absent relative to the multiplet at 6.82 ppm. This mixture of isotopomers was used without further purification.

Synthesis of thiophene-capped species d_2 -29. Synthesis was analogous to that for **7**, but with 2,5-dideuteriothiophene in place of natural abundance thiophene. ^1H NMR(CD_3NO_2 , 300 MHz): The multiplet present in **7** at 8.80 ppm was absent in d_2 -29.

2-Me-Thiophene-capped species **30**

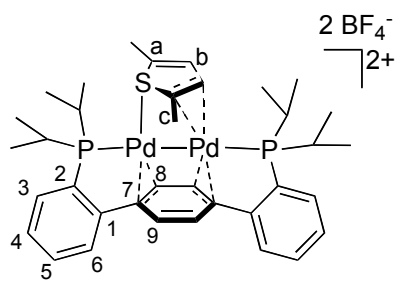
 2BF_4^- ^1H NMR (400 MHz, CD_3NO_2) δ : 8.01 (m, 2H, Ar- H_6), 7.87 (m, 2H, Ar- H_5), 7.83 (m, 2H, Ar- H_4), 7.74 – 7.69 (app d, 2H, Ar- H_3), 7.65 (m, 1H, H_c), 7.02 (m, 1H, H_d) 6.11 (s, 4H, Ar- H_8 + Ar- H_9), 4.98 (m, 1H, H_b), 3.32 (br, 2H, $\text{CH}(\text{CH}_3)_2$), 3.22 (br, 2H, $\text{CH}(\text{CH}_3)_2$) 2.16 (s, 3H, H_e), , 1.53 – 1.28 (m, 24H, $\text{CH}(\text{CH}_3)_2$). ^{31}P NMR (121 MHz, CD_3NO_2) δ : 68.3 (s). ^{19}F NMR (376 MHz, CD_3NO_2) δ : -152.4 (s). ^{13}C NMR (CD_3NO_2 , shifts determined from HSQC and HMBC 2D spectra): 149.9 (Ar- C_a), 145.9 (Ar- C_1), 134.9 (Ar- C_2), 133.6 (Ar- C_6), 133.5 (Ar- C_5), 132.3 (Ar- C_3), 132.0 (C_d), 130.0 (Ar- C_4), 117.5 (Ar- C_8 + Ar- C_9), 111.8 (Ar- C_7), 81.1 (C_c), 78.5 (C_b), 28.0 ($\text{CH}(\text{CH}_3)_2$), 27.6 ($\text{CH}(\text{CH}_3)_2$), 17.6 ($\text{CH}(\text{CH}_3)_2$), 17.1 ($\text{CH}(\text{CH}_3)_2$), 14.3 (C_e)

3-Me-Thiophene-capped species **31**

 2BF_4^- ^1H NMR (300 MHz, CD_3NO_2) δ : 8.29 (app t, 1H, H_a), 8.11 (app td, $J_{\text{Hc}} = 3.4$ Hz, 1H, H_d), 8.04 – 7.92 (m, 2H, Ar- H_6), 7.86 (m, 2H, Ar- H_5), 7.82 (m, 2H, Ar- H_4), 7.64 (m, 2H, Ar- H_3), 6.91 (d, $J = 3.4$ Hz, 1H, H_c), 6.24 (br s, 4H, Ar- H_8 + Ar- H_9), 3.28 (m, 4H, $\text{CH}(\text{CH}_3)_2$), 2.24 (s, 3H, H_e), 1.66 – 1.17 (m, 24H, $\text{CH}(\text{CH}_3)_2$). ^{31}P NMR (162 MHz, CD_3NO_2) δ : 65.9 (s). ^{19}F NMR (376 MHz, CD_3NO_2) δ :

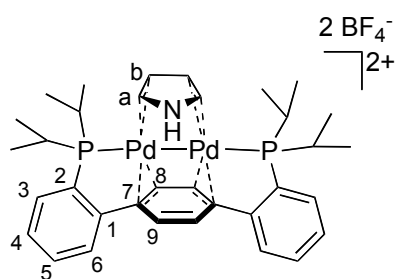
-152.7 (s). ^{13}C NMR (CD_3NO_2 , shifts determined from HSQC and HMBC 2D spectra): 146.2 (Ar- C_1), 133.5 (Ar- C_6 + Ar- C_5), 133.2 (Ar- C_2), 132.0 (Ar- C_3), 130.3 (Ar- C_4), 127.5 (C_b), 119.5 (Ar- C_7), 115.4 (Ar- C_8 + Ar- C_9), 100.0 (C_c), 87.9 (C_a), 87.3 (C_d), 27.3 ($\text{CH}(\text{CH}_3)_2$), 17.1 ($\text{CH}(\text{CH}_3)_2$), 17.0 ($\text{CH}(\text{CH}_3)_2$), 16.5 (C_e).

2,5-Me₂-Thiophene-capped species 32



2BF_4^- ^{1}H NMR (400 MHz, CD_3NO_2) δ : 8.02 (app t, 2H, Ar- H_6), 7.85 (m, 4H, Ar- H_4 + Ar- H_5), 7.79-7.55 (br m, 2H, Ar- H_3), 7.09 (s, 2H, H_b), 6.15 (br s, 4H, Ar- H_8 + Ar- H_9), 3.28 (m, 4H, $\text{CH}(\text{CH}_3)_2$), 2.73 (s, 6H, H_c), 1.60 – 1.17 (m, 24H, $\text{CH}(\text{CH}_3)_2$). ^{31}P NMR (121 MHz, CD_3NO_2) δ : 70.1 (d, $J = 175$ Hz), 65.6 (d, $J = 175$ Hz). ^{19}F NMR (376 MHz, CD_3NO_2) δ : -152.7 (s) ^{13}C NMR (CD_3NO_2 , shifts determined from HSQC and HMBC 2D spectra): 145.9 (Ar- C_1), 133.7 (Ar- C_5), 133.2 (Ar- C_6), 132.2 (Ar- C_2), 131.5 (Ar- C_3), 129.9 (Ar- C_4), 126.1 (Ar- C_7), 124.3 (C_a), 108.4 (Ar- C_8 + Ar- C_9), 108.4 (C_b), 27.7 ($\text{CH}(\text{CH}_3)_2$), 17.5 ($\text{CH}(\text{CH}_3)_2$), 17.4 ($\text{CH}(\text{CH}_3)_2$), 15.4 (C_c).

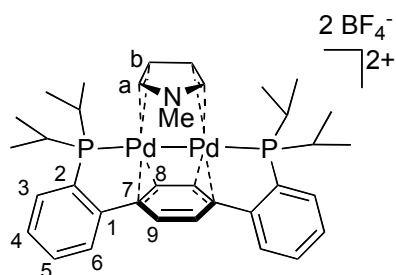
Pyrrole-capped species 33



2BF_4^- ^{1}H NMR (500 MHz, CD_3NO_2) δ : 9.76 (br s, 1H, N- H), 8.89 (m, 2H, H_a), 7.93 (m, 2H, Ar- H_6), 7.81 (m, 2H, Ar- H_5), 7.76 (m, 2H, Ar- H_4), 7.59 (app d, 2H, Ar- H_3), 6.24 (br s, 2H, Ar- $H_{8/9}$), 6.15 (br s, 4H, Ar- $H_{8/9}$ + H_b). 3.21 (br m, 2H, $\text{CH}(\text{CH}_3)_2$), 3.04 (br m, 2H, $\text{CH}(\text{CH}_3)_2$), 1.55-1.37 (m, 12H, $\text{CH}(\text{CH}_3)_2$), 1.19 (m, 12H, $\text{CH}(\text{CH}_3)_2$). $^{31}\text{P}\{^1\text{H}\}$ NMR (121 MHz, CD_3NO_2) δ : 60.2 (s) $^{19}\text{F}\{^1\text{H}\}$ NMR (376 MHz, CD_3NO_2) δ : -152.7 (s) ^{13}C NMR (CD_3NO_2 , shifts determined from HSQC and HMBC 2D spectra): 146.3 (Ar- C_1), 135.2 (Ar- C_2), 133.4 (Ar- C_6), 132.9 (Ar- C_5), 132.0 (Ar- C_3), 129.7 (Ar- C_4), 105.2 (C_a), 79.2 (C_b), 117.0 (Ar- $C_{8/9}$), 111.7 (Ar- C_7) 103.5

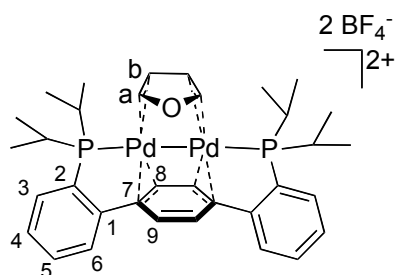
(Ar- $C_{8/9}$), 27.2 ($CH(CH_3)_2$), 26.1 ($CH(CH_3)_2$), 18.3 ($CH(CH_3)_2$), 17.5 ($CH(CH_3)_2$), 16.8, ($CH(CH_3)_2$), 16.6 ($CH(CH_3)_2$).

N-Me-Pyrrole-capped species 34



$2 BF_4^-$ 1H NMR (400 MHz, CD_3NO_2) δ : 8.62 (s, 2H, H_a), 7.94 (m, 2H, Ar- H_6), 7.82 (m, 2H, Ar- H_5), 7.77 (m, 2H, Ar- H_4), 7.62 (app d, 2H, Ar- H_3), 6.28 (s, 2H, Ar- $H_{8/9}$), 6.17 (s, 2H, Ar- $H_{8/9}$), 6.09 (s, 2H, H_b), 3.22 (br m, 2H, $CH(CH_3)_2$), 3.02 (br m, 2H, $CH(CH_3)_2$), 1.55-1.37 (m, 12H, $CH(CH_3)_2$), 1.19 (m, 12H, $CH(CH_3)_2$). ^{31}P NMR (121 MHz, CD_3NO_2) δ : 58.5 (s) ^{19}F NMR (376 MHz, CD_3NO_2) δ : -152.7 (s). ^{13}C NMR (CD_3NO_2 , shifts determined from HSQC and HMBC 2D spectra): 145.5 (Ar- C_1), 134.3 (Ar- C_2), 133.4 (Ar- C_6), 132.9 (Ar- C_5), 132.0 (Ar- C_3), 129.6 (Ar- C_4), 115.6 (Ar- $C_{8/9}$), 111.5 (Ar- C_7), 103.6 (Ar- $C_{8/9}$), 109.4 (C_a), 78.8 (C_b), 35.5 (N- CH_3), 27.2 ($CH(CH_3)_2$), 26.2 ($CH(CH_3)_2$), 18.6 ($CH(CH_3)_2$), 17.5 ($CH(CH_3)_2$), 16.7 ($CH(CH_3)_2$), 16.6 ($CH(CH_3)_2$).

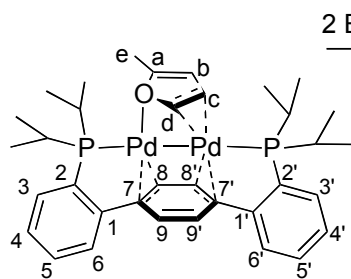
Furan-capped species 35



$2 BF_4^-$ 1H NMR (400 MHz, CD_3NO_2) δ : 9.42 (m, H_a , 2H), 7.96 (m, Ar- H_6 , 2H), 7.87 (m, Ar- H_5 , 2H), 7.81 (m, Ar- H_4 , 2H), 7.68 (app d, Ar- H_3 , 2H), 6.41 (m, H_b , 2H), 6.32 (d, $J = 1.4$ Hz, Ar- H_9 , 2H), 6.27 (d, $J = 1.4$ Hz, Ar- H_8 , 2H), 3.27 (m, $CH(CH_3)_2$, 2H), 3.06 (m, $CH(CH_3)_2$, 2H), 1.54 (app dd, $CH(CH_3)_2$, 6H), 1.44 (app dd, $CH(CH_3)_2$, 6H), 1.19 (app dd, $CH(CH_3)_2$, 6H), 1.14 (app dd, $CH(CH_3)_2$, 6H). $^{19}F\{^1H\}$ NMR (376 MHz, CD_3NO_2) δ : -152.5 (s). $^{31}P\{^1H\}$ NMR (162 MHz, CD_3NO_2) δ : 61.5 (s). $^{13}C\{^1H\}$ NMR (101 MHz, CD_3NO_2) δ : 145.4 (app t, Ar- C_1), 134.6 (app t, Ar- C_2), 133.9 (s, Ar- C_6), 133.4 (s, Ar- C_5), 132.3 (app t, Ar- C_3), 130.4 (app t, Ar- C_4), 120.8 (s,

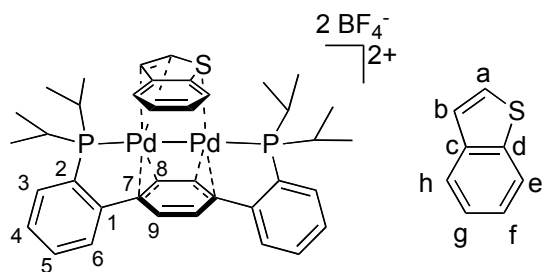
C_a), 119.1 (app t, Ar- C_9), 114.8 (app t, Ar- C_7), 103.3 (s, Ar- C_8), 83.0 (m, C_b), 27.7 (app td, CH(CH₃)₂), 26.4 (app t, CH(CH₃)₂), 18.8 (app t, CH(CH₃)₂), 17.6 (app t, CH(CH₃)₂), 16.8 (app t, CH(CH₃)₂), 16.6 (app t, CH(CH₃)₂). Anal. Calcd. for C₃₄H₄₄B₂F₈OP₂Pd₂(%): C, 44.53; H, 4.84. Found: C, 44.40; H, 4.64.

2-Me-Furan-capped species 36



$2 BF_4^-$ 1H NMR (400 MHz, CD₃NO₂) δ : 9.25 (app t, 1H, H_c), 8.02 – 7.92 (m, 2H, Ar- H_6 + Ar- H_6'), 7.91 – 7.74 (m, 4H, Ar- H_5 + Ar- H_5' + Ar- H_4 + Ar- H_4'), 7.73 – 7.60 (m, 2H, Ar- H_3 + Ar- H_3'), 7.28 (m, 1H, H_d), 6.38 – 6.25 (m, 2H, Ar- $H_{8/9/8'/9'}$), 6.21 (app dd, 1H, Ar- $H_{8/9/8'/9'}$), 6.08 (app dd, 1H, Ar- $H_{8/9/8'/9'}$), 5.61 (s, 1H, H_b), 3.33 (m, 1H, CH(CH₃)₂), 3.17 (m, 1H, CH(CH₃)₂), 3.04 (m, 2H, CH(CH₃)₂), 2.78 (d, J = 2.1 Hz, 3H, H_e), 1.70 – 1.03 (m, 24H, CH(CH₃)₂). ^{31}P NMR (162 MHz, CD₃NO₂) δ : 60.9 (d, J = 162 Hz), 57.4 (d, J = 162 Hz). ^{19}F NMR (376 MHz, CD₃NO₂) δ : -152.7 (s). ^{13}C NMR (CD₃NO₂, shifts determined from HSQC and HMBC 2D spectra): 179.8 (C_a), 145.7 (Ar- $C_{1/1'}$), 145.5 (Ar- $C_{1/1'}$), 135.0 (Ar- $C_{2/2'}$), 134.0 (Ar- $C_{2/2'}$), 133.6 (Ar- C_6 + Ar- C_6'), 133.4 (Ar- $C_{5/5'}$), 133.2 (Ar- $C_{5/5'}$), 130.2 (Ar- $C_{4/4'}$), 130.1 (Ar- $C_{4/4'}$), 132.3 (Ar- $C_{3/3'}$), 131.8 (Ar- $C_{3/3'}$), 117.0 (Ar- $C_{8/9/8'/9'}$), 115.6 (Ar- $C_{8/9/8'/9'}$), 107.0 (Ar- $C_{8/9/8'/9'}$), 102.9 (C_c), 98.4 (Ar- $C_{8/9/8'/9'}$), 85.6 (C_b), 65.5 (C_d), 27.5 (CH(CH₃)₂), 26.2 (CH(CH₃)₂), 26.1 (2C, CH(CH₃)₂), 19.9 (C_e), 18.6 (CH(CH₃)₂), 18.3 (CH(CH₃)₂), 18.0 (CH(CH₃)₂), 17.7 (CH(CH₃)₂), 17.1 (CH(CH₃)₂), 17.0 (CH(CH₃)₂), 16.9 (CH(CH₃)₂), 16.2 (CH(CH₃)₂).

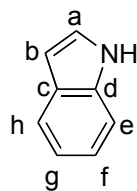
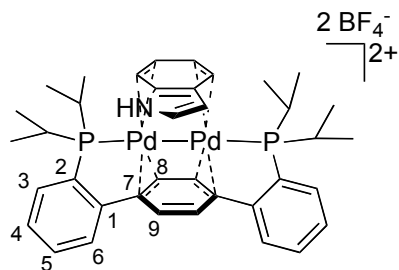
Benzothiophene-capped species 37



Recrystallization by vapor diffusion of Et₂O into a MeNO₂ solution yielded XRD-quality orange prisms (80.2 mg, 80%). ¹H NMR (400 MHz, CD₃NO₂) δ: 8.26 (app q, H_b,

1H), 8.09 – 7.96 (overlapping multiplets, H_f and one each of Ar-H₃₋₆ and Ar-H_{3'-6'}, 3H), 7.92 – 7.78 (overlapping multiplets, H_g and two each of Ar-H₃₋₆ and Ar-H_{3'-6'}, 5H), 7.73 – 7.68 (app d, one of Ar-H₃₋₆ or Ar-H_{3'-6'}, 1H), 7.61 (app d, one of Ar-H₃₋₆ or Ar-H_{3'-6'}, 1H), 7.57 (app td, H_h, 1H), 7.49 (app td, H_e, 1H), 6.13 (dd, J = 8.0, 2.0 Hz, Ar-H₉, 1H), 6.09 (dd, J = 8.0, 1.6 Hz, Ar-H₉, 1H), 5.99 (dd, J = 7.2, 2.0 Hz, Ar-H₈, 1H), 5.75 (dd, J = 7.2, 1.6 Hz, Ar-H₈, 1H), 5.18 (app t, H_a, 1H), 3.72 (m, CH(CH₃)₂, 1H), 3.31 (m, CH(CH₃)₂, 3H), 1.89 – 1.66 (m, CH(CH₃)₂, 9H), 1.66 – 1.56 (m, CH(CH₃)₂, 3H), 1.36 – 1.22 (m, CH(CH₃)₂, 3H), 1.13 – 0.92 (m, CH(CH₃)₂, 9H). ¹⁹F NMR (376 MHz, CD₃NO₂) δ: -152.5 (s). ³¹P{¹H} NMR (162 MHz, CD₃NO₂) δ: 67.3 (d, J = 168 Hz), 65.9 (d, J = 168 Hz). ¹³C NMR (101 MHz, CD₃NO₂) δ: 145.8 (overlapping multiplets, Ar-C₁ and Ar-C_{1'}), 139.6 (s, C₂), 138.8 (s, C₄), 134.7 (overlapping multiplets, Ar-C₂ and Ar-C_{2'}), 133.6 (s, Ar-C₆ or Ar-C_{6'}), 133.5 (s, Ar-C₆ or Ar-C_{6'}), 133.4 (s, Ar-C₅ and Ar-C_{5'}), 132.5 (app d, Ar-C₃ or Ar-C_{3'}), 132.1 (app d, Ar-C₃ or Ar-C_{3'}), 130.4 (app t, Ar-C₄ and Ar-C_{4'}), 130.0 (s, C_b), 129.5 (s, C_e), 127.5 (s, C_f), 125.5 (s, C_g), 119.0 (s, C₉), 117.4 (s, C_{9'}), 114.1 (t, C₇), 111.3 (t, C_{7'}), 99.5 (s, C₈), 97.4 (s, C_{8'}), 76.7 (s, C_b), 70.2 (s, C_a), 28.6 (m, CH(CH₃)₂), 27.7 (m, CH(CH₃)₂), 27.5 (m, CH(CH₃)₂), 27.2 (m, CH(CH₃)₂), 19.0 (br s, two of CH(CH₃)₂), 18.1 (app d, CH(CH₃)₂), 17.9 (br s, CH(CH₃)₂), 17.3 (br s, two of CH(CH₃)₂), 16.8 (app d, CH(CH₃)₂), 16.7 (app d, CH(CH₃)₂). Anal. Calcd. for C₃₈H₄₆B₂F₈P₂Pd₂S (%): C, 46.42; H, 4.72. Found: C, 46.30; H, 4.60.

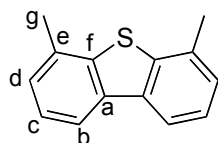
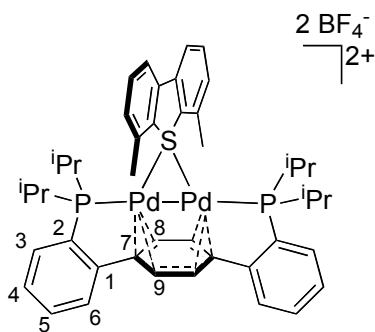
Indole-capped species 38



^1H NMR (400 MHz, CD_3NO_2) δ : 9.93 (br s, 1H, H_a), 9.09 (br s, 1H, N-H), 8.74 (m, 1H, H_h), 8.71 (m, 1H, H_e), 7.94 (br s, 2H, Ar- H_6), 7.84 (m, 2H, Ar- H_5), 7.81 (m, 2H, Ar- H_4), 7.52 (m, 2H, Ar- H_3), 7.14 (m, 1H, H_b), 6.48 (m, 2H, Ar- $H_{8/9}$), 5.97 (t, 1H, H_f), 5.87 (t, 1H, H_g), 5.57 (br s, 2H, Ar- $H_{8/9}$), 3.65 (m, 2H, $\text{CH}(\text{CH}_3)_2$), 3.23 (m, 2H, $\text{CH}(\text{CH}_3)_2$), 1.74 (m, 6H, $\text{CH}(\text{CH}_3)_2$), 1.09 (m, 6H, $\text{CH}(\text{CH}_3)_2$), 0.95 (m, 6H, $\text{CH}(\text{CH}_3)_2$).

^{31}P NMR (121 MHz, CD_3NO_2) δ : 64.7 (br s). ^{19}F NMR (376 MHz, CD_3NO_2) δ : -152.7 (s). ^{13}C NMR (CD_3NO_2 , shifts determined from HSQC and HMBC 2D spectra): 146.1 (Ar- C_1), 133.6 (Ar- $C_{5/4}$), 133.1 (Ar- C_6), 131.7 (Ar- C_3), 130.4 (C_a), 129.6 (Ar- $C_{5/4}$), 128.0 (C_b), 127.7 (Ar- C_2), 124.4 (C_d), 123.4 (Ar- $C_{8/9}$), 113.7 (Ar- C_7), 105.3 (Ar- $C_{8/9}$), 105.2 (C_c), 95.8 (Ar- $C_{8/9}$), 86.6 ($C_{f/g}$), 86.5 ($C_{f/g}$), 76.0 (C_h), 71.1 (C_e), 27.8 ($\text{CH}(\text{CH}_3)_2$), 26.2 ($\text{CH}(\text{CH}_3)_2$), 18.5 ($\text{CH}(\text{CH}_3)_2$), 17.7 ($\text{CH}(\text{CH}_3)_2$), 16.1 ($\text{CH}(\text{CH}_3)_2$), 16.0 ($\text{CH}(\text{CH}_3)_2$).

4,6-Dimethyldibenzothiophene-capped species 39

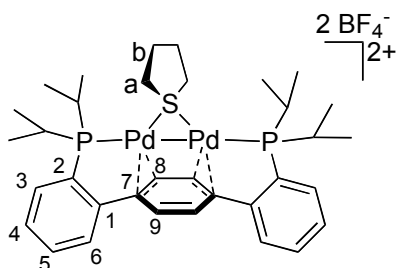


^1H NMR (400 MHz, CD_3NO_2) δ : 8.36 (app d, 2H, H_b), 7.95-7.78 (m, 10H, H_c + Ar- H_{3-6}), 7.50 (app d, 2H, H_d), 6.63 (s, 4H, Ar- H_8 + Ar- H_9), 2.66 (m, 4H, $\text{CH}(\text{CH}_3)_2$), 2.20

(s, 4H, H_g), 1.07 (app dd, 12H, $\text{CH}(\text{CH}_3)_2$), 0.90 (app dd, 12H, $\text{CH}(\text{CH}_3)_2$). ^{31}P (121 MHz, CD_3NO_2) δ : 75.3 (s). ^{19}F (376 MHz, CD_3NO_2) δ : -152.8 (s). ^{13}C NMR (CD_3NO_2 , shifts determined from HSQC and HMBC 2D spectra): 144.5 (Ar- C_1), 138.5 (C_a), 136.8 (Ar- C_2), 135.7 (C_e), 133.2 (C_c), (133.1, 132.3, 130.4), [overlapping peaks for (Ar- C_6), (Ar-

C_5), (Ar- C_3), (Ar- C_4], 132.0 (C_d), 126.3 (C_f), 122.9 (C_b), 113.3 (Ar- C_8 + Ar- C_9), 112.1 (Ar- C_7), 26.5 ($\text{CH}(\text{CH}_3)_2$), 21.4 (C_g), 18.4 ($\text{CH}(\text{CH}_3)_2$), 18.2($\text{CH}(\text{CH}_3)_2$).

Synthesis of tetrahydrothiophene-capped species **40**

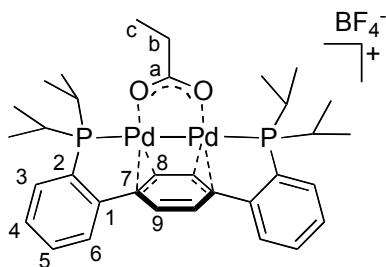


Method A: **32** (75.8 mg, 0.08 mmol) was dissolved in CH_3NO_2 in a J. Young NMR tube. The solution was degassed with three cycles of freeze-pump-thaw, chilled with LN_2 , and sealed under a ~ 1 atm stream of H_2 (regulated at r.t. with a Hg bubbler). The tube was warmed back up to r.t. and then continuously inverted. The reaction was monitored by ^{31}P NMR and complete after 5h. The heterogeneous reaction mixture was filtered through Celite and volatiles were removed. The solids were triturated with THF, then filtered through Celite as a MeCN solution. Volatiles were removed again, yielding **40** an orange powder (75.0 mg, 99%).

Method B: **40** was prepared from **25** (78.1 mg, 0.08 mmol) in the same manner as **29** (vide supra). The resulting orange solids (74.8 mg, 96%) were analytically pure.

Characterization: ^1H NMR (300 MHz, CD_3CN) δ : 7.93 – 7.65 (m, Ar- $H_{3,6}$, 8H), 6.09 (s, Ar- H_{8+9} , 4H), 3.55 (app t, H_a , 4H), 2.81 (m, $\text{CH}(\text{CH}_3)_2$, 4H), 2.43 (m, H_b , 4H), 1.25 (app dd, $\text{CH}(\text{CH}_3)_2$, 12H), 1.10 (app dd, $\text{CH}(\text{CH}_3)_2$, 12H). ^{19}F NMR (282 MHz, CD_3CN) δ : -151.6 (s). $^{31}\text{P}\{^1\text{H}\}$ NMR (121 MHz, CD_3CN) δ : 69.8 (s). $^{13}\text{C}\{^1\text{H}\}$ NMR (101 MHz, CD_3CN) δ : 146.2 (app t, Ar- C_1), 138.1 (app t, Ar- C_2), 134.6 (s, Ar- C_6), 133.9 (s, Ar- C_5), 133.6 (app t, Ar- C_3), 131.2 (s, Ar- C_4), 112.3 (s, Ar- C_{8+9}), 110.3 (app t, Ar- C_7), 46.2 (br s, C_a), 31.3 (s, C_b), 27.6 (m, $\text{CH}(\text{CH}_3)_2$), 20.4 (app q, $\text{CH}(\text{CH}_3)_2$), 19.4 (app d, $\text{CH}(\text{CH}_3)_2$).
Anal. Calcd. for $\text{C}_{34}\text{H}_{48}\text{B}_2\text{F}_8\text{P}_2\text{Pd}_2\text{S}$ (%): C, 43.57; H, 5.16. Found: C, 43.59; H, 5.09.

Synthesis of carboxylate-capped species **41**

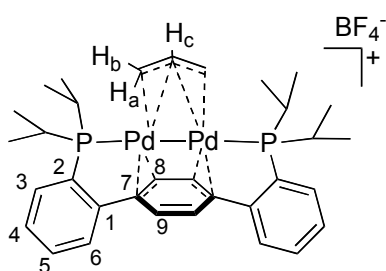


A solution of **25** (23.4 mg, 0.025 mmol) in MeCN (3 mL) was added over NaO₂CEt (2.4 mg, 0.025 mmol).

The ruby red solution did not appear to change color, but a reaction was evidenced by NMR spectroscopy. An orange precipitate was obtained by adding Et₂O to the

crude MeCN mixture (18.5 mg, 89%) ¹H NMR (300 MHz, CD₃CN) δ: 7.74-7.46 (m, 8H, aryl-*H*₃₋₆), 5.89 (s, 4H, Ar-*H*₈₊₉), 2.65 (m, 4H, CH(CH₃)₂), 2.41 (q, *J* = 7.6 Hz, 2H, *H*_b), 1.29 (app dd, 12H, CH(CH₃)₂), 1.19-1.09 (m, 12H + 3H, CH(CH₃)₂ + *H*_c). ¹⁹F{¹H} NMR (282 MHz, CD₃CN) δ: -152.2 (s). ³¹P{¹H} NMR (121 MHz, CD₃CN) δ: 53.6 (s). ¹³C{¹H} NMR (101 MHz, CD₃CN) δ: 203.6 (app t, *J* = 4.8 Hz, *C*_a), 148.6 (app t, *J* = 13.8 Hz, Ar-*C*₁), 135.3 (t, *J* = 17.3 Hz, Ar-*C*₂), 133.9 (s, Ar-*C*₆), 133.2 (s, Ar-*C*₅), 132.2 (t, *J* = 8.7 Hz, Ar-*C*₃), 130.6 (s, Ar-*C*₄), 104.8 (s, Ar-*C*₈₊₉), 92.9 (t, *J* = 2.2 Hz, Ar-*C*₇), 32.9 (s, *C*_b), 26.8 (t, *J* = 9.1 Hz, CH(CH₃)₂), 19.4 (s, CH(CH₃)₂), 19.2 (t, *J* = 3.3 Hz, CH(CH₃)₂), 10.4 (s, *C*_c).

Synthesis of allyl-capped species **42**

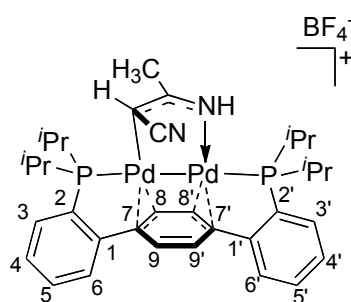


To a red solution of **41** (10.6 mg, 0.0128 mmol) in MeCN (1 mL) was added tributylallyltin (4.0 μL, 0.0128 mmol). A yellow color evolved in less than a minute.

After 10 minutes, the reaction mixture was filtered. The filtrate was concentrated under vacuum and washed with benzene. The remaining solid was redissolved in MeCN, filtered, and layered under Et₂O. XRD-quality yellow crystals were grown at -35 °C (8.1 mg, 79% yield). ¹H NMR (600 MHz, CD₃CN) δ: 7.88 (m, 2H, Ar-*H*₃), 7.70 (app t, 2H, Ar-*H*₄), 7.65 (app t, 2H, Ar-*H*₅), 7.58 (app d, 2H, Ar-*H*₆), 6.24 (s, 2H, Ar-*H*_{8/9}), 5.55 (s, 2H, Ar-*H*_{9/8}), 3.90 (m, 2H, allyl-*H*_{a/b}), 2.94 (m, 2H, CH(CH₃)₂),

2.76 (m, 2H, CH(CH₃)₂), 2.40 (m, 1H, allyl-H_c), 1.26-1.15 (m, 12H + 2H, CH(CH₃)₂ + allyl-H_{b/a}), 1.07 (app dd, 6H, CH(CH₃)₂), 1.02 (app dd, 6H, CH(CH₃)₂). ¹⁹F{¹H} NMR (282 MHz, CD₃CN) δ: -152.2 (s). ³¹P{¹H} NMR (121 MHz, CD₃CN) δ: 50.5 (s). ¹³C{¹H} NMR (101 MHz, CD₃CN) δ: 149.8 (app t, J = 13.5 Hz, Ar-C₁), 140.9 – 140.3 (app t, Ar-C₂), 134.2 (s, Ar-C₃), 133.5 (app t, J = 7.1 Hz, Ar-C₆), 132.7 (s, Ar-C₄), 130.0 (s, Ar-C₅), 120.4 (s, Ar-C_{8/9}), 117.0 (app t, J = 2.4 Hz, Ar-C₇), 97.3 (s, Ar-C_{9/8}), 70.5 (s, allyl-CH), 31.0 (s, allyl-CH₂), 27.4 (app t, J = 10.2 Hz, CH(CH₃)₂), 27.2 (t, J = 9.7 Hz, CH(CH₃)₂), 19.6 (t, J = 2.8 Hz, CH(CH₃)₂), 19.3 (t, J = 3.2 Hz, CH(CH₃)₂), 19.1 (s, CH(CH₃)₂), 18.9 (s, CH(CH₃)₂). Anal. Calcd. for C₃₃H₄₅BF₄P₂Pd₂ (%): C, 49.34; H, 5.65. Found: C, 49.27; H, 5.58.

Synthesis of diacetonitrile anion capped species **43**



Method A: To a solution of **25** (200 mg, 0.212 mmol) in CH₃CN (10 mL) was added KO^tBu (23.8 mg, 0.212 mmol). The solution remained dark brown in color over 3 hours at room temperature. Volatiles were removed under vacuum, and the waxy solids were washed with hexanes,

Et₂O, benzene, THF, and CH₂Cl₂ (separately, in that order). The solids were insoluble in hexanes and Et₂O, but some yellow color eluted with the benzene wash. THF washings initially eluted an intense dark brown color, but most of the crude material remained insoluble. The remaining crude was dissolved in CH₂Cl₂ and filtered through Celite. Crystallization of the eluent in CH₂Cl₂/Et₂O yielded some XRD-quality crystals, but the mixture of solids was not pure **43**. **Method B:** To a solution of **25** (63.7 mg, 0.07 mmol) in CH₃CN (10 mL) was added [Li{N(H)C(Me)=C(H)CN}]_n (18.1 mg, 0.07 mmol).⁷⁶ The same purification procedures as in Method A yielded 41 mg of relatively

clean **43**. *Characterization*: FAB-MS (-BF₄-dissociated cation; m/z: 757.1390; calcd.: 757.1132). ¹H NMR (600 MHz, CD₃CN) δ: 7.86 – 7.21 (m, Ar-H₂₋₆ + Ar-H_{2'-6'}, 8H), 6.24 – 5.95 (broad, Ar-H_{8/9}, 2H), 5.81 (broad, NH, 1H) 5.80 – 5.38 (broad, Ar-H_{9/8}, 2H), 4.61 – 4.41 (broad, NCCH, 1H), 3.22 – 2.45 (broad, CH(CH₃)₂, 4H), 2.45 – 2.20 (broad, HNCCH₃, 3H), 1.76 – 0.50 (broad, CH(CH₃)₂, 24H). ³¹P{¹H} NMR (121 MHz, CD₃CN) δ: 50.2, 49.2 (1:1, broad).

Table 4.1. Crystal and refinement data for 25-31, 36-39, 42, 43

	25	26	27	28	29	30	31	36	37	38	39	42	43
CCDC no.	702664	944713	944714	944715	944716	944717	944718	944719	944720	944721	944722	944723	944724
Empirical formula	C ₃₇ H ₄₈ B ₂ F ₈ P ₂ Pd ₂	C ₃₇ H ₄₈ B ₂ F ₈ OP ₂ Pd ₂	C ₃₄ H ₄₂ B ₂ F ₈ P ₂ Pd ₂	C ₃₆ H ₄₈ B ₂ F ₈ P ₂ Pd ₂	C ₃₄ H ₄₄ B ₂ F ₈ P ₂ Pd ₂ S	C ₃₅ H ₄₆ B ₂ F ₈ P ₂ Pd ₂ S	C ₃₅ H ₄₆ B ₂ F ₈ P ₂ Pd ₂ S	C ₃₅ H ₄₆ B ₂ F ₈ OP ₂ Pd ₂	C ₃₉ H ₄₉ B ₂ F ₈ NO ₂ P ₂ Pd ₂ S	C ₃₈ H ₄₇ B ₂ F ₈ NP ₂ Pd	C ₄₄ H ₅₂ B ₂ F ₈ P ₂ Pd ₂ S	C ₃₃ H ₄₅ B F ₄ P ₂ Pd ₂	C ₃₄ H ₄₅ B F ₄ N ₂ P ₂ Pd ₂
Formula wt	941.11	957.11	899.04	929.10	933.11	947.14	947.14	931.08	1044.21	966.13	1061.27	803.24	843.27
a, Å	13.1190(6)	18.020(4)	15.2809(8)	11.8911(5)	19.2900(11)	17.950(4)	18.338(4)	11.880(2)	9.9974(4)	31.050(6)	19.395(1)	8.6364(3)	14.6826(6)
b, Å	15.2041(7)	15.340(3)	12.8833(6)	13.5564(6)	16.1824(9)	15.271(3)	15.222(3)	19.070(4)	14.9331(6)	15.190(3)	11.1339(6)	15.3772(6)	13.1786(5)
c, Å	18.3188(9)	13.560(3)	18.3268(9)	23.4012(11)	23.3891(13)	13.363(3)	13.065(3)	16.440(3)	28.042(1)	20.770(4)	20.589(1)	25.239(1)	17.8342(7)
a, °	90.00	90.00	90.00	90.00	90.00	90.00	90.00	90.00	90.00	90.00	90.00	90.00	90.00
b, °	90.00	90.00	90.062(3)	100.514(2)	90.00	90.00	90.00	90.00	98.53(3)	94.887(2)	121.85(3)	103.026(2)	91.591(2)
c, °	90.00	90.00	90.00	90.00	90.00	90.00	90.00	90.00	90.00	90.00	90.00	90.00	90.00
Volume, Å ³	3653.9(3)	3748.3(13)	3608.0(3)	3708.9(3)	7301.1(7)	3663(1)	3647(1)	3683.3(13)	4171.2(3)	8321(3)	4331.5(4)	3350.6(2)	3441.1(2)
Z	4	4	4	4	8	4	4	4	4	8	4	4	4
Cryst syst	Orthorhombic	Orthorhombic	Monoclinic	Monoclinic	Orthorhombic	Orthorhombic	Orthorhombic	Monoclinic	Monoclinic	Monoclinic	Monoclinic	Monoclinic	Monoclinic
Space group	P2 ₁ 2 ₁ 2 ₁	Pnma	P2 ₁ /c	P2 ₁ /c	Pbca	Pnma	Pnma	P2 ₁ /c	P2 ₁ /n	C 2/c	C 2/c	P2 ₁ /c	P2 ₁ /c
d _{calcd} (g/cm ³)	1.711	1.696	1.655	1.664	1.698	1.717	1.725	1.679	1.663	1.542	1.627	1.592	1.628
q range, °	1.71 to 33.00	1.93 to 33.57	1.58 to 27.53	1.74 to 27.10	3.48 to 99.28	1.95 to 31.37	1.96 to 31.37	1.69 to 33.63	3.992 to 55.14	1.59 to 32.43	2.03 to 27.52	1.55 to 40.23	1.92 to 30.62
m, mm ⁻¹	1.141	1.115	1.151	1.123	1.196	1.193	1.199	1.133	1.061	1.005	1.019	1.213	1.187
Absorption correction	Semi-empirical	Empirical	Semi-empirical	Semi-empirical	Empirical	Empirical	Empirical	Empirical	Empirical	Empirical	Empirical	Empirical	Semi-empirical
GoF ^a	1.558	1.106	1.026	1.097	1.060	1.069	0.781	1.113	1.111	1.159	1.667	1.072	1.056
R1 ^b , wR2 ^c	0.0250,	0.0242,	0.0711,	0.1656,	0.0269,	0.0333,	0.0376,	0.0406,	0.0214,	0.0377,	0.0322,	0.0398,	0.0509,
[I>2σ(I)]	0.0421	0.0651	0.1838	0.3240	0.0624	0.0880	0.1086	0.1093	0.0479	0.1010	0.0614	0.0807	0.1012
Type of diffractometer	Bruker	SSRL	Bruker	Bruker	Bruker	SSRL	SSRL	SSRL	Bruker	SSRL	Bruker	Bruker	Bruker

^a GoF = S = { S[w(F_o²-F_c²)²] / (n-p) }^{1/2}

^b R1 = S | |F_o| - |F_c| | / S |F_o|

^c wR2 = { S[w(F_o²-F_c²)²] / S[w(F_o²)²] }^{1/2}

Refinement details.

In each case, crystals were mounted on a glass fiber or nylon loop using Paratone oil, then placed on the diffractometer under a nitrogen stream. Low temperature (100 K) X-ray data were obtained on a Bruker APEXII CCD based diffractometer (Mo sealed X-ray tube, $K_{\alpha} = 0.71073 \text{ \AA}$) or at Beamline 12-2 at the Stanford Synchrotron Radiation Lightsource (SSRL; DECTRIS PILATUS 6M detector, $K_{\alpha} = 0.72930 \text{ \AA}$). Loop-mounted samples sent to SSRL were submerged in LN_2 during transport (~ 1 day). All diffractometer manipulations, including data collection, integration and scaling were carried out using the Bruker APEXII software.⁹⁸ Absorption corrections were applied using SADABS.⁹⁹ Space groups were determined on the basis of systematic absences and intensity statistics and the structures were solved by direct methods using XS¹⁰⁰ (incorporated into SHELXTL) and refined by full-matrix least squares on F^2 . All non-hydrogen atoms were refined using anisotropic displacement parameters. Hydrogen atoms were placed in idealized positions and refined using a riding model. The structure was refined (weighted least squares refinement on F^2) to convergence. Graphical representation of structures with 50% probability thermal ellipsoids was generated using Diamond visualization software.³⁴

Special refinement details for 25. The largest disagreements in structure factors indicate twinning and the Flack parameter suggests a racemic twin ratio of 0.546:0.454. The refined coordinates suggest the higher symmetry space group $Pnma$. However, although there is 98% agreement between the coordinates and the higher symmetry, the diffraction intensities do not support that assignment. Therefore the correct space group assignment is as assigned, $P2_12_12_1$. Hydrogen atoms were refined from the difference map without constraints.

Special refinement details for 26. A solution in $Pnma$ was elusive at first, so structure refinement was performed in $P-1$ space group. Reduction of the solution to $Pnma$ using PLATON's Addsym function gave an instructions file with the proper unit cell. Reprocessing the raw hkl file with $Pnma$ space group, using the PLATON output, and refining led to the final solution. Anisole was disordered over two sites and modeled with the PART -1 instruction.

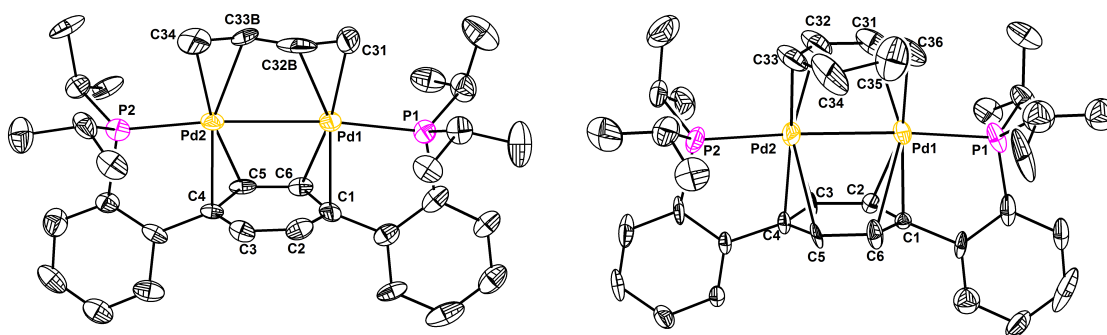


Figure 4.10. Structural drawings of **27** (left) and **28** (right) with 50% probability ellipsoids. Outer-sphere tetrafluoroborate ions and hydrogen atoms are not shown for clarity.

Special refinement details for 27. The dataset was twinned and disorder in the butadiene fragment precludes accurate determination of the butadiene structure. The solution was obtained in monoclinic $P2_1/c$; attempted solutions in orthorhombic $Pnma$ gave worse R values and esds.

Special refinement details for 28. A yellow parallelepiped block of suitable size (0.40 x 0.23 x 0.16 mm) was selected from a representative sample of crystals of the same habit using an optical microscope and mounted onto a glass fiber. Low temperature (100 K) X-ray data were obtained on a Bruker APEXII CCD based diffractometer (Mo sealed X-ray tube, $K_\alpha = 0.71073 \text{ \AA}$). All diffractometer manipulations, including data collection, integration and

scaling were carried out using the Bruker APEXII software. While the crystals diffracted very well, the data could not be solved to give a satisfactory model. This is likely due to the crystal beginning to undergo a phase transition resulting in loss of symmetry and possible twinning that could not be accounted for. The systematic absence violations listed by XPREP for a 2_1 axis are [$N = 58$, $N(I > 3\sigma) = 9$, $\langle I \rangle = 0.1$, $\langle I/\sigma \rangle = 1.5$] and for a c-glide plane [$N = 3325$, $N(I > 3\sigma) = 1501$, $\langle I \rangle = 0.6$, $\langle I/\sigma \rangle = 4.5$] (for comparison, lattice exceptions for all reflections, $N = 156641$, $N(I > 3\sigma) = 113930$, $\langle I \rangle = 5.2$, $\langle I/\sigma \rangle = 9.6$). Despite the weakening or destruction of the c-glide, the structure refinement behaves better in $P2_1/c$ than in $P2_1$. While the $P2_1/c$ model does not produce accurate bond lengths and bond angles, this represents the best solution and no additional symmetry elements or changes were recommended by PLATON. The presented model does show with certainty the presence of the targeted cyclohexadiene adduct, which was also confirmed by multiple spectroscopic techniques (*vide supra*). Not all non-hydrogen atoms could be satisfactorily refined by using anisotropic displacement parameters. Hydrogen atoms were placed in idealized positions and refined using a riding model. The final least-squares refinement converged to $R_1 = 0.1656$ ($I > 2\sigma(I)$, 7869 data; $R(\text{int}) = 0.0360$) and $wR_2 = 0.3258$ (F^2 , 8182 data, 415 parameters, 0 restraint).

Special refinement details for 30. The capping 2-methylthiophene was disordered and modeled as an exact 50:50 mixture of mirror conformations across the molecular mirror plane using the “PART -1” card in SHELX. Attempts to allow the relative population or geometries of the two conformations to float did not improve refinement statistics or significantly alter geometries.

Special refinement details for 31. The capping 3-methylthiophene was disordered and modeled as an exact 50:50 mixture of mirror conformations across the molecular mirror

plane using the “PART -1” card in SHELX. Attempts to allow the relative population or geometries of the two conformations to float did not improve refinement statistics or significantly alter geometries.

Special refinement details for 36. The capping 2-methylfuran was modeled in only one conformation. A minor Q peak possibly corresponding to the methyl group of a mirror image 2-methylfuran was observed during refinement, but other binding conformations could not be modeled. Attempting to switch the positions of O1 and C1 resulted in unreasonable structures with worse refinement indicators.

Special refinement details for 37. An outer-sphere nitromethane molecule and tetrafluoroborate anions were disordered and modeled in two conformations. The capping benzothiophene was disordered and initially modeled in two “SADI”-related conformations. Upon relaxation of these constraint, a 60:40 mixture of internally dissimilar benzothiophenes resulted.

Special refinement details for 38. Outer-sphere electron density could not be accurately modeled and was analyzed using PLATON’s squeeze algorithm. Four voids of 181.5 \AA^3 ($\sim 68 e^-$) are left in the unit cell, which would correspond with either one indole ($62 e^-$) or two molecules of nitromethane ($70 e^-$) per dipalladium unit. Free indole and nitromethane were present in the crystallization conditions and observed in NMR spectra of freshly crystallized material.

Special refinement details for 39. Atom S1 lies along a C_2 axis of symmetry and thus was modeled in the asymmetric unit with 0.5 relative population.

Special refinement details for 42. An outer-sphere tetrafluoroborate ion was disordered and modeled in two conformations.

Special refinement details for 43. Outer-sphere tetrafluoroborate ions were disordered and modeled in two conformations. The capping diacetonitrilyl was disordered and initially modeled in two internally “SADI”-related conformations with fixed populations. Upon relaxation of these constraint, a 60:40 mixture of internally dissimilar diacetonitrilyls resulted.

REFERENCES

- (1) Hafner, J. *Monatsh. Chem.* **2008**, *139*, 373.
- (2) Biffis, A.; Zecca, M.; Basato, M. *J. Mol. Catal. A: Chem.* **2001**, *173*, 249.
- (3) Augustine, R. L.; O'Leary, S. T. *J. Mol. Catal. A: Chem.* **1995**, *95*, 277.
- (4) Prins, R.; Egorova, M.; Röthlisberger, A.; Zhao, Y.; Sivasankar, N.; Kukula, P. *Catal. Today* **2006**, *111*, 84.
- (5) Girgis, M. J.; Gates, B. C. *Ind. Eng. Chem. Res.* **1991**, *30*, 2021.
- (6) Murahashi, T.; Kimura, S.; Takase, K.; Ogoshi, S.; Yamamoto, K. *Chem. Commun.* **2013**, *49*, 4310.
- (7) Murahashi, T.; Nagai, T.; Okuno, T.; Matsutani, T.; Kurosawa, H. *Chem. Commun.* **2000**, 1689.
- (8) Murahashi, T.; Kurosawa, H. *Coord. Chem. Rev.* **2002**, *231*, 207.
- (9) Paton, R. S.; Brown, J. M. *Angew. Chem. Int. Ed.* **2012**, *51*, 10448.
- (10) Allegra, G.; Tettamanti Casagrande, G.; Immirzi, A.; Porri, L.; Vitulli, G. *J. Am. Chem. Soc.* **1970**, *92*, 289.
- (11) Dupont, J.; Pfeffer, M.; Rotteveel, M. A.; De Cian, A.; Fischer, J. *Organometallics* **1989**, *8*, 1116.
- (12) Sommovigo, M.; Pasquali, M.; Leoni, P.; Braga, D.; Sabatino, P. *Chem. Ber.* **1991**, *124*, 97.
- (13) Åkerstedt, J.; Gorlov, M.; Fischer, A.; Kloo, L. *J. Organomet. Chem.* **2010**, *695*, 1513.
- (14) Dotta, P.; Kumar, P. G. A.; Pregosin, P. S.; Albinati, A.; Rizzato, S. *Organometallics* **2004**, *23*, 4247.
- (15) Barder, T. E. *J. Am. Chem. Soc.* **2005**, *128*, 898.
- (16) Christmann, U.; Pantazis, D. A.; Benet-Buchholz, J.; McGrady, J. E.; Maseras, F.; Vilar, R. n. *J. Am. Chem. Soc.* **2006**, *128*, 6376.
- (17) Murahashi, T.; Takase, K.; Oka, M.; Ogoshi, S. *J. Am. Chem. Soc.* **2011**, *133*, 14908.
- (18) Murahashi, T.; Fujimoto, M.; Oka, M.; Hashimoto, Y.; Uemura, T.; Tatsumi, Y.; Nakao, Y.; Ikeda, A.; Sakaki, S.; Kurosawa, H. *Science* **2006**, *313*, 1104.

- (19) Murahashi, T.; Otani, T.; Mochizuki, E.; Kai, Y.; Kurosawa, H.; Sakaki, S. *J. Am. Chem. Soc.* **1998**, *120*, 4536.
- (20) Murahashi, T.; Kanehisa, N.; Kai, Y.; Otani, T.; Kurosawa, H. *Chem. Commun.* **1996**, 825.
- (21) Leoni, P.; Pasquali, M.; Sommovigo, M.; Albinati, A.; Lianza, F.; Pregosin, P. S.; Ruegger, H. *Organometallics* **1993**, *12*, 4503.
- (22) Werner, H.; Kühn, A.; Tune, D. J.; Krüger, C.; Brauer, D. J.; Sekutowski, J. C.; Tsay, Y.-h. *Chem. Ber.* **1977**, *110*, 1763.
- (23) Werner, H.; Kraus, H.-J.; Schubert, U.; Ackermann, K. *Chem. Ber.* **1982**, *115*, 2905.
- (24) Hruszkewycz, D. P.; Wu, J.; Green, J. C.; Hazari, N.; Schmeier, T. J. *Organometallics* **2011**, *31*, 470.
- (25) Kobayashi, Y.; Iitaka, Y.; Yamazaki, H. *Acta Crystallogr. Sect. B* **1972**, *28*, 899.
- (26) Sui-Seng, C.; Enright, G. D.; Zargarian, D. J. *Am. Chem. Soc.* **2006**, *128*, 6508.
- (27) Markert, C.; Neuburger, M.; Kulicke, K.; Meuwly, M.; Pfaltz, A. *Angew. Chem. Int. Ed.* **2007**, *46*, 5892.
- (28) Velian, A.; Lin, S.; Miller, A. J. M.; Day, M. W.; Agapie, T. *J. Am. Chem. Soc.* **2010**, *132*, 6296.
- (29) Lin, S.; Day, M. W.; Agapie, T. *J. Am. Chem. Soc.* **2011**, *133*, 3828.
- (30) Chao, S. T.; Lara, N. C.; Lin, S.; Day, M. W.; Agapie, T. *Angew. Chem. Int. Ed.* **2011**, *50*, 7529.
- (31) Kelley, P.; Lin, S.; Edouard, G.; Day, M. W.; Agapie, T. *J. Am. Chem. Soc.* **2012**, *134*, 5480.
- (32) Kaye, G. W. C.; Laby, T. H. *Tables of Physical and Chemical Constants*; 15th ed.; Longman: London, UK, 1993.
- (33) Efremenko, I. *J. Mol. Catal. A: Chem.* **2001**, *173*, 19.
- (34) Brandenburg, K. (1999). DIAMOND. Crystal Impact GbR, Bonn, Germany.
- (35) Fulmer, G. R.; Miller, A. J. M.; Sherden, N. H.; Gottlieb, H. E.; Nudelman, A.; Stoltz, B. M.; Bercaw, J. E.; Goldberg, K. I. *Organometallics* **2010**, *29*, 2176.
- (36) Katano, S.; Ichihara, S.; Ogasawara, H.; Kato, H. S.; Komeda, T.; Kawai, M.; Domen, K. *Surf. Sci.* **2002**, *502-503*, 164.
- (37) Murahashi, T.; Kurosawa, H. *J. Organomet. Chem.* **1999**, *574*, 142.

- (38) Reiß, G. J.; Konietzny, S. J. *Chem. Soc., Dalton Trans.* **2002**, 862.
- (39) Tatsumi, Y.; Naga, T.; Nakashima, H.; Murahashi, T.; Kurosawa, H. *Chem. Commun.* **2004**, 1430.
- (40) The unusual downfield-shifted multiplet was confirmed to belong to the bridging diene by two-dimensional ^1H - ^1H NMR correlation spectroscopy (COSY). This feature is consistently found in **5-8** as the protons bound to the two carbons of the diene closest to Pd. The protons bound to the two internal carbons of the diene moiety are consistently shifted upfield.
- (41) Saeys, M.; Reyniers, M. F.; Neurock, M.; Marin, G. B. *Surf. Sci.* **2006**, *600*, 3121.
- (42) Harshbarger, W. R.; Bauer, S. H. *Acta Crystallogr. Sect. B* **1970**, *26*, 1010.
- (43) Harman, W. D. *Coord. Chem. Rev.* **2004**, *248*, 853.
- (44) Keane, J. M.; Harman, W. D. *Organometallics* **2005**, *24*, 1786.
- (45) Delafuente, D. A.; Myers, W. H.; Sabat, M.; Harman, W. D. *Organometallics* **2005**, *24*, 1876.
- (46) Ateşin, T. A.; Jones, W. D. *Organometallics* **2007**, *27*, 53.
- (47) Ateşin, T. A.; Jones, W. D. *Organometallics* **2008**, *27*, 3666.
- (48) Hachgenei, J. W.; Angelici, R. J. *Organometallics* **1989**, *8*, 14.
- (49) Angelici, R. J. *Organometallics* **2001**, *20*, 1259.
- (50) Janak, K. E.; Tanski, J. M.; Churchill, D. G.; Parkin, G. J. *Am. Chem. Soc.* **2002**, *124*, 4182.
- (51) Sattler, A.; Janak, K. E.; Parkin, G. *Inorg. Chim. Acta* **2011**, *369*, 197.
- (52) Vicić, D. A.; Jones, W. D. *J. Am. Chem. Soc.* **1999**, *121*, 7606.
- (53) Jones, W. D.; Chin, R. M.; Hoaglin, C. L. *Organometallics* **1999**, *18*, 1786.
- (54) Jones, W. D.; Chin, R. M. *Organometallics* **1992**, *11*, 2698.
- (55) Capon, J.-F.; Schollhammer, P.; Pétilion, F. B. Y.; Talarmin, J.; Muir, K. W. *Organometallics* **1999**, *18*, 2055.
- (56) Grochowski, M. R.; Li, T.; Brennessel, W. W.; Jones, W. D. *J. Am. Chem. Soc.* **2010**, *132*, 12412.
- (57) Iovu, M. C.; Sheina, E. E.; Gil, R. R.; McCullough, R. D. *Macromolecules* **2005**, *38*, 8649.

- (58) Terada, S.; Yokoyama, T.; Sakano, M.; Imanishi, A.; Kitajima, Y.; Kiguchi, M.; Okamoto, Y.; Ohta, T. *Surf. Sci.* **1998**, *414*, 107.
- (59) Schwalbe, M.; Walther, D.; Schreer, H.; Langer, J.; Görls, H. *J. Organomet. Chem.* **2006**, *691*, 4868.
- (60) Orita, H.; Itoh, N. *Surf. Sci.* **2004**, *550*, 177.
- (61) Such a motif (with S bound to a third metal) has been proposed in a DFT study of thiophene on Pt(111): Zhu, H.; Guo, W.; Li, M.; Zhao, L.; Li, S.; Li, Y.; Lu, X.; Shan, H. *ACS Catal.* **2011**, *1*, 1498.
- (62) Adams, R. D.; Qu, X. *Organometallics* **1995**, *14*, 2238.
- (63) Kabir, S. E.; Miah, M. A.; Sarker, N. C.; Golzar Hussain, G. M.; Hardcastle, K. I.; Nordlander, E.; Rosenberg, E. *Organometallics* **2005**, *24*, 3315.
- (64) The ¹H NMR multiplet at 8.80 ppm was absent when **3** was treated with 2,5-d²-thiophene.
- (65) Knight, M. J.; Allegretti, F.; Kröger, E. A.; Polcik, M.; Lamont, C. L. A.; Woodruff, D. P. *Surf. Sci.* **2008**, *602*, 2524.
- (66) Wang, H.; Prins, R. *J. Catal.* **2009**, *264*, 31.
- (67) Meille, V.; Schulz, E.; Lemaire, M.; Faure, R.; Vrinat, M. *Tetrahedron* **1996**, *52*, 3953.
- (68) Pearson, R. G. *J. Am. Chem. Soc.* **1963**, *85*, 3533.
- (69) Joule, J. A.; Mills, K. *Heterocyclic Chemistry*; 4th ed.; Blackwell Publishing: Ames, Iowa, 2000.
- (70) Stanislaus, A.; Marafi, A.; Rana, M. S. *Catal. Today* **2010**, *153*, 1.
- (71) Fu, W.; Zhang, L.; Tang, T.; Ke, Q.; Wang, S.; Hu, J.; Fang, G.; Li, J.; Xiao, F.-S. *J. Am. Chem. Soc.* **2011**, *133*, 15346.
- (72) Yu, K.; Li, H.; Watson, E. J.; Virkaitis, K. L.; Carpenter, G. B.; Sweigart, D. A. *Organometallics* **2001**, *20*, 3550.
- (73) Baldovino-Medrano, V. G.; Giraldo, S. A.; Centeno, A. b. *J. Mol. Catal. A: Chem.* **2009**, *301*, 127.
- (74) Mozingo, R.; Harris, S. A.; Wolf, D. E.; Hoffhine, C. E.; Easton, N. R.; Folkers, K. *J. Am. Chem. Soc.* **1945**, *67*, 2092.
- (75) Rooney, J. J.; Gault, F. G.; Kemball, C. *Proc. Chem. Soc.* **1960**, 407.

- (76) Avent, A. G.; Frankland, A. D.; Hitchcock, P. B.; Lappert, M. F. *Chem. Commun.* **1996**, 2433.
- (77) A similar (deprotonated) tautotmer and binding motif has been reported bound to a phosphido-palladium two-centered moiety: Braunstein, P.; Matt, D.; Dusausoy, Y.; Fischer, J. *Organometallics* **1983**, *2*, 1410.
- (78) Ligand exchange kinetics have been studied for π -adducts of mononuclear d^6 octahedral compounds, but thermodynamic binding experiments have not been reported to the authors' knowledge. See: C. J. Mocella, D. A. Delafuente, J. M. Keane, G. R. Warner, L. A. Friedman, M. Sabat, W. D. Harman, *Organometallics* **2004**, *23*, 3772-3779.
- (79) Caldwell, T. E.; Land, D. P. *Polyhedron* **1997**, *16*, 3197.
- (80) Sexton, B. A. *Surf. Sci.* **1985**, *163*, 99.
- (81) Hansch, C.; Leo, A.; Taft, R. W. *Chem. Rev.* **1991**, *91*, 165.
- (82) Mecozzi, S.; West, A. P.; Dougherty, D. A. *Proc. Natl. Acad. Sci. USA* **1996**, *93*, 10566.
- (83) Ma, J. C.; Dougherty, D. A. *Chem. Rev.* **1997**, *97*, 1303.
- (84) Gaussian 09, Revision C.01, Frisch, M. J.; Trucks, G. W.; Schlegel, H. B.; Scuseria, G. E.; Robb, M. A.; Cheeseman, J. R.; Scalmani, G.; Barone, V.; Mennucci, B.; Petersson, G. A.; Nakatsuji, H.; Caricato, M.; Li, X.; Hratchian, H. P.; Izmaylov, A. F.; Bloino, J.; Zheng, G.; Sonnenberg, J. L.; Hada, M.; Ehara, M.; Toyota, K.; Fukuda, R.; Hasegawa, J.; Ishida, M.; Nakajima, T.; Honda, Y.; Kitao, O.; Nakai, H.; Vreven, T.; Montgomery, Jr., J. A.; Peralta, J. E.; Ogliaro, F.; Bearpark, M.; Heyd, J. J.; Brothers, E.; Kudin, K. N.; Staroverov, V. N.; Kobayashi, R.; Normand, J.; Raghavachari, K.; Rendell, A.; Burant, J. C.; Iyengar, S. S.; Tomasi, J.; Cossi, M.; Rega, N.; Millam, J. M.; Klene, M.; Knox, J. E.; Cross, J. B.; Bakken, V.; Adamo, C.; Jaramillo, J.; Gomperts, R.; Stratmann, R. E.; Yazyev, O.; Austin, A. J.; Cammi, R.; Pomelli, C.; Ochterski, J. W.; Martin, R. L.; Morokuma, K.; Zakrzewski, V. G.; Voth, G. A.; Salvador, P.; Dannenberg, J. J.; Dapprich, S.; Daniels, A. D.; Farkas, Ö.; Foresman, J. B.; Ortiz, J. V.; Cioslowski, J.; Fox, D. J. Gaussian, Inc., Wallingford CT, 2009.
- (85) Theoretical study of chemisorbed H on Pd surfaces suggests that formation of an H—Pd bond is accompanied by transfer of *ca.* 0.2 electrons from Pd to H. See: D. Tománek, Z. Sun, S. G. Louie, *Physical Review B* **1991**, *43*, 4699-4713.
- (86) Kurosawa, H. *J. Organomet. Chem.* **2004**, *689*, 4511.
- (87) Pangborn, A. B.; Giardello, M. A.; Grubbs, R. H.; Rosen, R. K.; Timmers, F. J. *Organometallics* **1996**, *15*, 1518.

- (88) Tao, J.; Perdew, J. P.; Staroverov, V. N.; Scuseria, G. E. *Phys. Rev. Lett.* **2003**, *91*, 146401.
- (89) Staroverov, V. N.; Scuseria, G. E.; Tao, J.; Perdew, J. P. *The Journal of Chemical Physics* **2003**, *119*, 12129.
- (90) Jensen, K. P. *Inorg. Chem.* **2008**, *47*, 10357.
- (91) Bühl, M.; Kabrede, H. *Journal of Chemical Theory and Computation* **2006**, *2*, 1282.
- (92) Waller, M. P.; Braun, H.; Hojdis, N.; Bühl, M. *Journal of Chemical Theory and Computation* **2007**, *3*, 2234.
- (93) Hay, P. J.; Wadt, W. R. *The Journal of Chemical Physics* **1985**, *82*, 270.
- (94) Ditchfield, R.; Hehre, W. J.; Pople, J. A. *The Journal of Chemical Physics* **1971**, *54*, 724.
- (95) Saeys, M.; Reyniers, M.-F. B.; Neurock, M.; Marin, G. B. *The Journal of Physical Chemistry B* **2003**, *107*, 3844.
- (96) Lin, S.; Herbert, D. E.; Velian, A.; Day, M. W.; Agapie, T. J. *Am. Chem. Soc.* **2013**, *135*, 15830.
- (97) Dawson, R.; Gillis, R. *Aust. J. Chem.* **1972**, *25*, 1221.
- (98) APEX2, Version 2 User Manual, M86-E01078, Bruker Analytical X-ray Systems, Madison, WI, June 2006.
- (99) Sheldrick, G.M. "SADABS (version 2008/1): Program for Absorption Correction for Data from Area Detector Frames", University of Göttingen, 2008.
- (100) Sheldrick, G.M. (2008). *Acta Cryst. A* **64**, 112-122.

CHAPTER 5

COMPUTATIONAL AND ISOTOPIC LABELING STUDIES ON NICKEL-MEDIATED HYDROGENOLYSIS OF C-O BONDS OF ARYL ALKYL ETHERS

Published in part as:

Kelley, P., Lin, S., Edouard, G., Day, M. W., and Agapie, T. *J. Am. Chem. Soc.* **2012**, *134*,
5480-5483.

ABSTRACT

A recent mechanistic study of aryl alkyl ether cleavage in a model *meta*-terphenyl diphosphine proposed that net hydrogenolysis of the aryl-O bond can proceed from a nickel-aryl-alkoxide intermediate through β -H elimination of the alkoxide ligand rather than cleavage of the Ni-O bond by H₂; the final aryl-H bond does not incorporate H₂ nuclei. This chapter (a) shows that a similar mechanism is operative in catalytic hydrogenolysis of isotopically labeled substrates and (b) computationally examines the electronic effect of different substituents in the model system.

INTRODUCTION

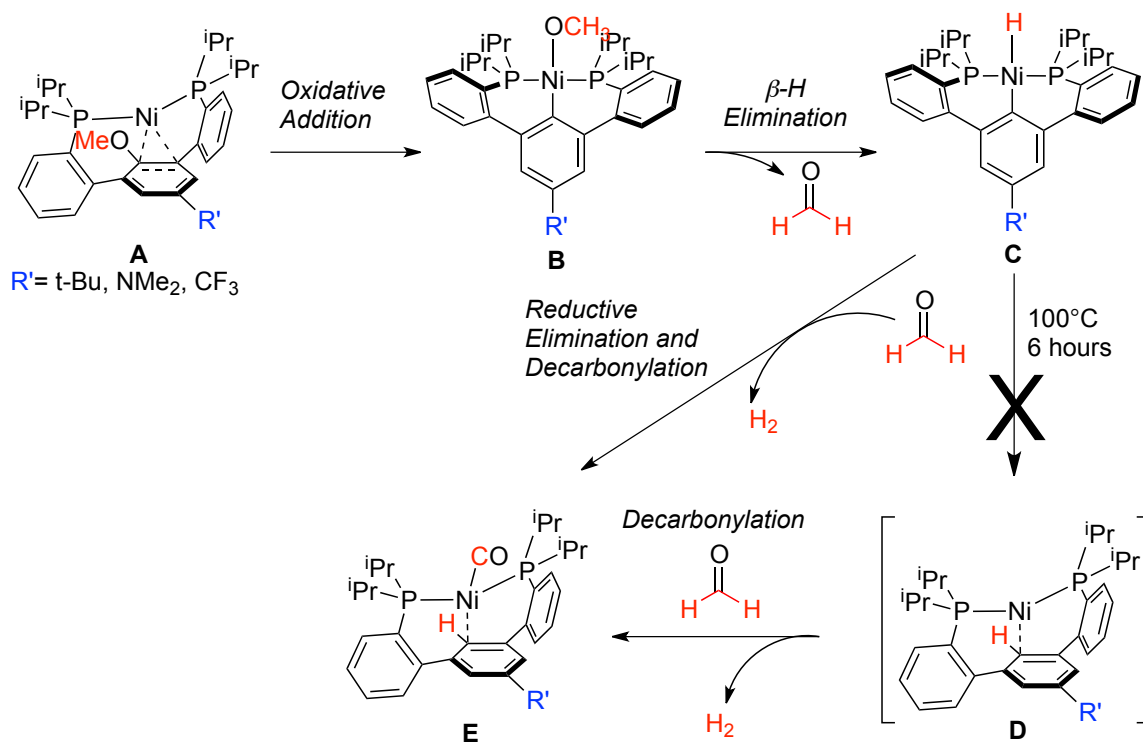
The previous chapters' results with chelated metal-arene interactions suggest that normally unstable species can be isolated and studied using a terphenyl diphosphine framework. Toward this end, other members of the Agapie Group synthesized a *meta*-terphenyl diphosphine variant with a methyl ether on the central arene. From this framework, they elucidated a mechanism for reduction of aryl C–O bonds (*vide infra*).

The elaboration of the aryl C–O bond to a variety of functional groups has emerged as a versatile synthetic tool in organic methodology,¹ as phenol precursors are readily available and synthetic modification of the aromatic ring is facile. The strong aryl C–O bond, however is typically difficult to activate. Nickel-based catalysts have proven versatile in the conversion of substrates with aryl C–O²⁻¹³ or C–S¹⁴⁻¹⁶ bonds. Although cross-coupling of phenolic substrates tends to require prior conversion to the more reactive sulfonates,² recent advances show that aryl phosphates, aryl esters, aryl carbamates, aryl ethers and even free phenols can be used as electrophiles in cross-coupling reactions.³⁻¹³ In a complementary approach, the conversion of aryl C–O to aryl-H bonds has been recognized as a valuable strategy for removing oxygen-based directing groups from aryl rings. Silanes have been utilized as a hydride source for this transformation.^{10,11} Additionally, stoichiometric intramolecular aryl C–O activation has been reported with rhodium and palladium pincer complexes.^{17,18} In the context of biomass conversion to alternative fuels and chemicals, the depolymerization of lignin, a significant component of biomass containing aryl ether linkages, is a considerable challenge.¹⁹⁻²¹ Recently, an appealing strategy involving the cleavage of lignin-like aryl C–O bonds via nickel-catalyzed hydrogenolysis was reported by Hartwig *et al.*²² Given the general interest in the conversion of aryl C–O bonds, detailed

mechanistic insight, including the nature of the intermediates, is instrumental in developing practical catalysts.

Previous computational investigations of C-O bond activation in cross-coupling of phenol derivatives predict that an intermediate displaying η^2 -interactions between a Ni(0) center and the double bond adjacent to the oxygen preceded C-O bond activation.^{8,23} Paul Kelley and Guy Edouard designed a *meta*-terphenyl diphosphine ligand where the central arene is functionalized with an alkyl ether, and metal complexes thereof have been determined to display η^2 -interactions adjacent to the ether moiety. The nickel complexes proved amenable to mechanistic study of C-O bond activation, and intermediates along the pathway to formation of a C-H bond were isolated and characterized (A-E, Scheme 5.1).

Scheme 5.1. Mechanism for Ni-Mediated Cleavage of a Model Aryl Alkyl Ether, by Kelley and Edouard



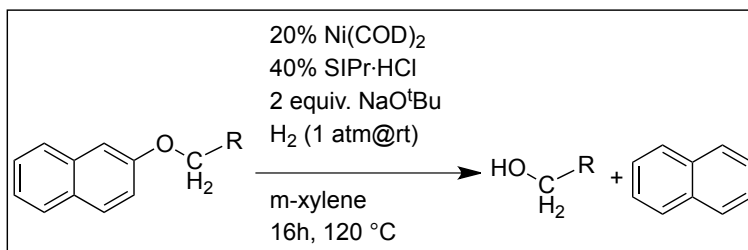
The generation of **E** and the intermediates characterized above map out a potential pathway for the cleavage of aryl alkyl ethers. Notably, this process does not require dihydrogen. Two questions related to this process are discussed in this chapter: (1) Is such a mechanism also operative in catalytic systems, and (2) what electronic effect do electron-donating and electron-withdrawing substituents have on C-O bond cleavage?

RESULTS AND DISCUSSION

1. Mechanistic Investigations of Catalytic Aryl Alkyl Ether Hydrogenations

To investigate the relevancy of this process for the catalytic reaction, aryl alkyl ethers were subjected to hydrogenolysis under reported reaction conditions (Scheme 5.2).²² 2-Methoxynaphthalene and 2-hexyloxynaphthalene were selected as substrates. 1,3-Bis(2,6-diisopropylphenyl)-imidazolium chloride (SIPr·HCl), NaO^tBu, and Ni(COD)₂ in *m*-xylene generate the catalytic species *in situ*. Heating to 120 °C for 16h under 1 atm of H₂ leads to the formation of naphthalene and corresponding aliphatic alcohol (hexyl silyl ether analyzed upon derivatization). In order to elucidate the origin of the hydrogen delivered to the naphthyl group, four types of products were explored: (a) naphthalene obtained from from hydrogenolysis of protic substrates under D₂, (b) naphthalene obtained from partially deuterated substrates under H₂, (c) hexyl silyl ether derived from reaction products, and (d) products obtained in the absence of dihydrogen.

Scheme 5.2. Representative Catalytic Hydrogenolysis of Aryl Alkyl Ethers



1.1. *Naphthalene from hydrogenolysis of protic substrates under D₂*. Hydrogenolysis of NaphOCH₃ and NaphO(CH₂)₅CH₃, Naph=2-naphthyl) were performed under D₂. Various isotopologues of naphthalene were observed in the reaction mixtures (*d*₀₋₃ as major constituents; Figure 5.1 middle row). However, as a control, natural abundance naphthalene (Figure 5.1 top row) was submitted to the reaction conditions, and *d*₀₋₅ isotopologues of naphthalene were observed. Scrambling of aromatic C-H bonds under D₂ thus limits the applicability of this approach.

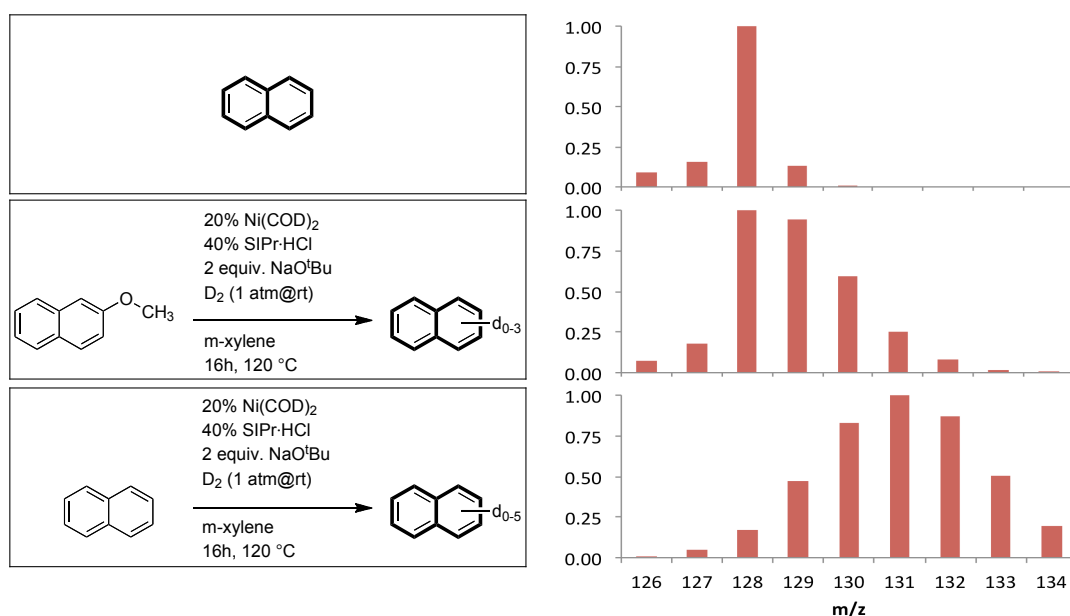


Figure 5.1. Reaction conditions (left) and normalized GC-MS traces of resulting naphthalene isotopologues.

1.2. *Naphthalene from hydrogenolysis of partially deuterated substrates under H₂*. To limit the impact of H/D scrambling, hydrogenolysis of partially deuterated substrates (NaphOCD₃ and NaphOCD₂(CH₂)₄CH₃, Naph=2-naphthyl) was targeted. H/D scrambling of the aromatic C-H bonds of the starting materials would have no effect on the final isotopologue distribution. H₂ scrambling into NaphD produced during the reaction would have a 7/8 chance of undergoing degenerate H/H exchange, assuming equal probability of scrambling

into the α and β positions of naphthalene. Thus, the isotopologue distribution resulting from hydrogenolysis of partially deuterated substrates under H_2 should be less time-dependent and provide more meaningful mechanistic insights.

NaphOCD₃ was synthesized by protection of NaphOH with commercially available CD₃I under basic conditions, with excellent isotopic retention (Figure 5.2, first *vs.* second rows). An analogous reaction between NaphOH and CH₃(CH₂)₄CD₂I (obtained by reduction of ethyl hexanoate with commercially available LiAlD₄) produced NaphOCD₂(CH₂)₄CH₃ (Figure 5.2, third *vs.* fourth rows).

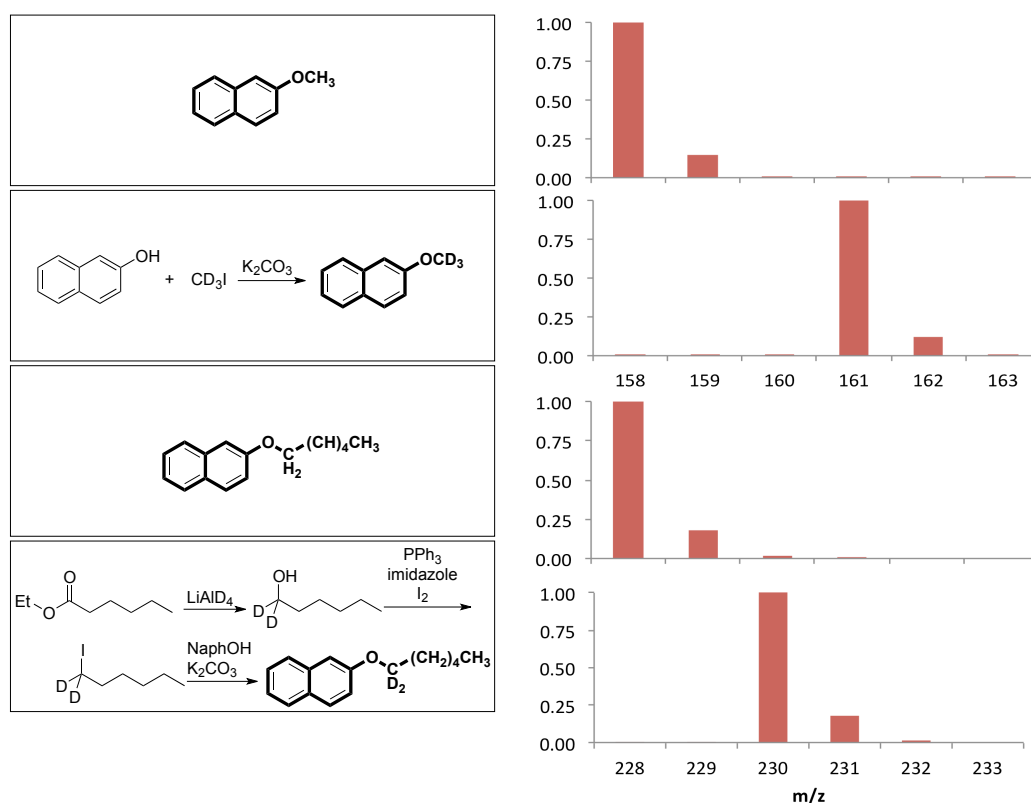


Figure 5.2. Reaction conditions (left) and normalized GC-MS traces of resulting 2-alkoxy naphthalene isotopologues.

With the deuterated substrates in hand, hydrogenolysis under H_2 was performed. In each case, the naphthalene isotopologues were $>90\%$ d_1 -naphthalene by GC-MS (Figure

5.3). ^2H NMR confirmed that NaphD was the exclusive isotopmer, with no D incorporation at the alpha position. These results support extension of the $\beta\text{-H}$ elimination mechanism from the model system (Scheme 5.1) to the catalytic system.

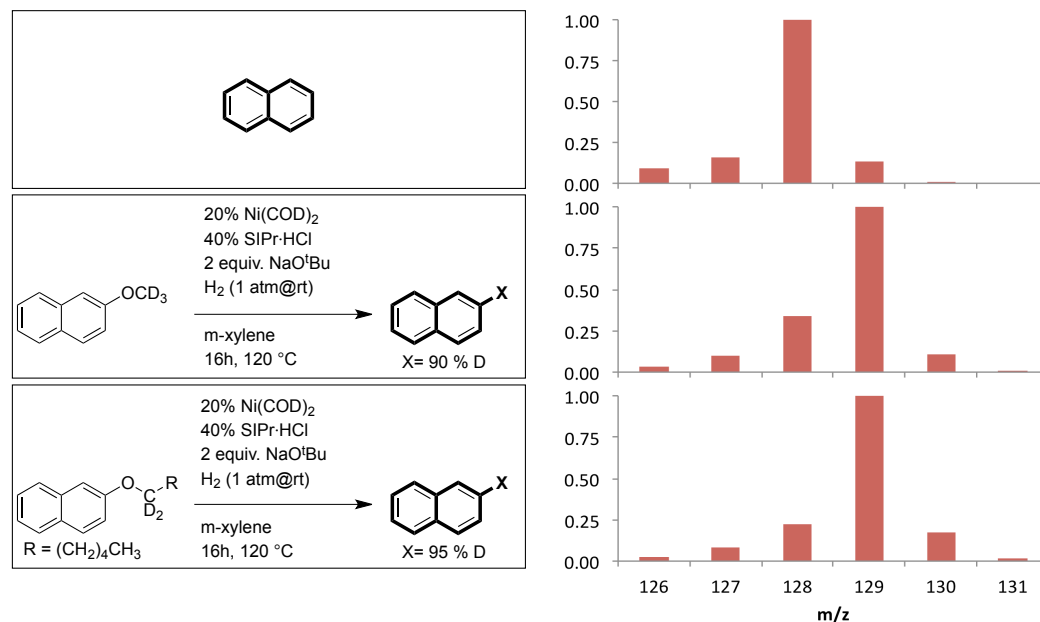


Figure 5.3. Reaction conditions (left) and normalized GC-MS traces of resulting naphthalene isotopologues.

1.3. *Derivatized hexanol from isotope labeling experiments.* To support the results drawn from the naphthalene isotopologue distribution, similar analysis of the alcohol co-product was attempted. For 2-methoxynaphthalene, the resulting methanol is volatile and could be difficult to isolate and characterize. Thus, reactions with 2-hexyloxynaphthalene were targeted for alcohol analysis. Upon completion of the hydrogenolysis reaction, the xylene-soluble organic products were filtered through a MgSO_4 plug into a Schlenk tube. Excess *N*-methyl-*N*-(trimethylsilyl)trifluoroacetamide was added, and the tube was sealed and heated to 60 °C for 1 h prior to GC-MS analysis of the crude reaction mixture.

For hexanol derivatives from $\text{NaphO}(\text{CH}_2)_5\text{CH}_3$ under D_2 , a mixture of d_{0-4} isotopologues was observed (Figure 5.4, middle row; 7% d_0 , 25% d_1 , 36% d_2 , 25% d_3 , 7% d_4) indicating prevalent D_2 scrambling into the product. Similarly, hexanol derivatives from $\text{NaphOCD}_2(\text{CH}_2)_4\text{CH}_3$ under H_2 showed H_2 scrambling (Figure 5.4, bottom row; 70% d_0 , 27% d_1 , 3% d_2).

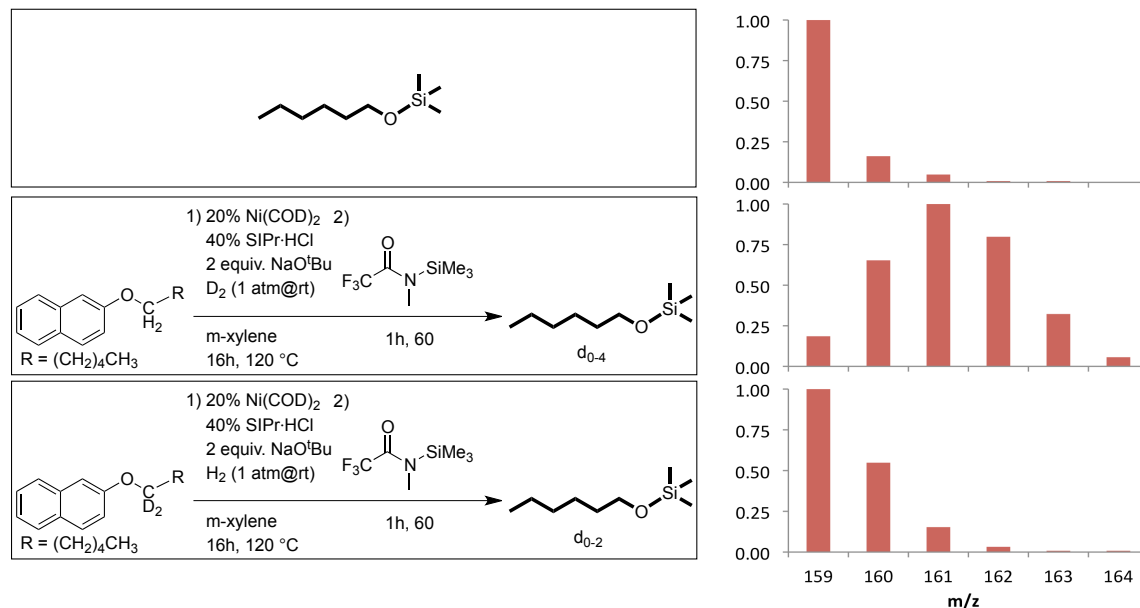


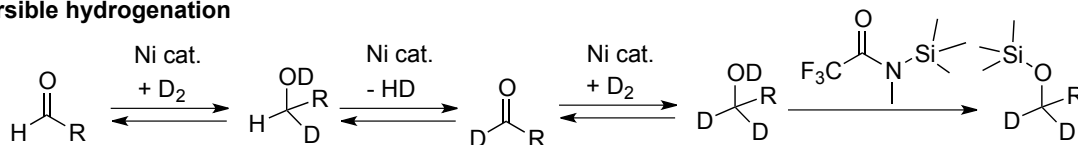
Figure 5.4. Reaction conditions (left) and normalized GC-MS traces of resulting hexyloxytrimethylsilane isotopologues.

If the alcohol remained an alcohol throughout the reaction, then scrambling of the acidic O-H moiety would be expected, but that nuclei would be removed upon derivatization. To account for the high scrambling rates, re-examination of the mechanism from the model system shows that the alcohol likely results from hydrogenation of aldehyde released from β -H elimination from **B** to **C** (Scheme 5.1). Aldehydes can undergo isotopic scrambling at the β -position through reversible enolate formation. Additionally, if aldehyde hydrogenation is reversible, then further isotopic scrambling can occur at the α -position. Taking these two processes into account, access to d_0 - through d_4 -isotopologues from

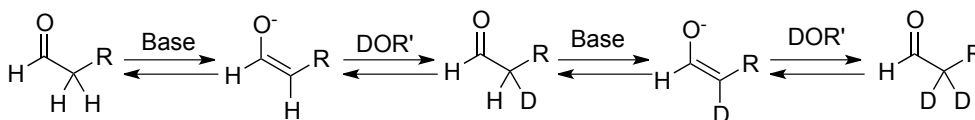
NaphO(CH₂)₅CH₃ under D₂ can be rationalized (Scheme 5.3). Indeed, subsection of natural abundance isotope hexanol to the reaction conditions also generated *d*₀- through *d*₄- isotopologues of hexyl trimethylsilyl ether. Importantly, this proposal also accounts for the lack of *d*₅- or higher isotopologues.

Scheme 5.3. Isotope Scrambling Into Hexyloxytrimethylsilane

reversible hydrogenation



enolate scrambling



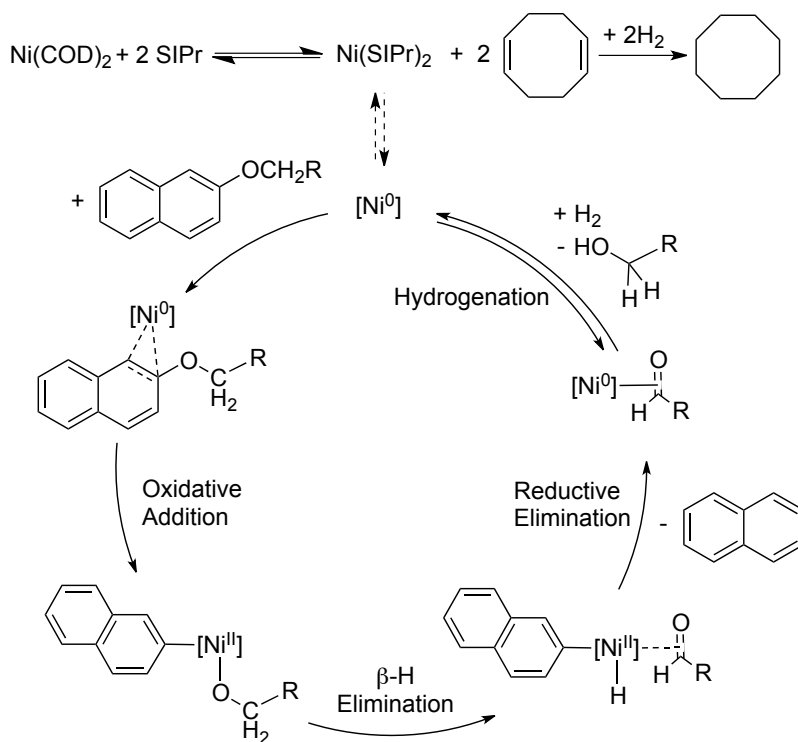
1.4. Role of dihydrogen. The isotopic labeling studies support a unified C-O bond cleavage mechanism for the catalytic system and the *meta*-terphenyl diphosphine model system. However, the latter system occurs in the absence of H₂. Furthermore, the conversion of **A** to **E** under D₂ does not display any evidence of D-incorporation. Thus, a catalytic system, too, might be operative in the absence of H₂. Running the reaction conditions from Scheme 5.2 *sans* H₂ yielded only trace amounts of naphthalene (< 5%).

It has been reported that Ni(COD)₂/N-heterocyclic carbene mixtures are in equilibrium.²⁴ Therefore hydrogenation of COD to cyclooctane (observed in reaction mixtures by GC-MS) could drive formation of an active catalyst, and account for the necessity of H₂. Thus, a mixture of 1,3-bis(2,6-diisopropylphenyl)-imidazolium chloride (SIPr·HCl), NaO^tBu, and Ni(COD)₂ in toluene was heated under H₂, concentrated under vacuum to a dark red wax, reconstituted with *m*-xylene, and treated with aryl ether substrate under N₂. Ether conversion to arene was observed, albeit in lower yields (ca. 50%) compared

to standard conditions (ca. 75%). These experiments support the hypothesis that H₂ is necessary for the formation of the active catalyst, but not for the actual catalytic transformation.

On the basis of these isotope labeling and preactivation experiments, a mechanism can be proposed for the catalytic system (Scheme 5.4). Ni(COD)₂ and SIPr form an active reduced nickel species, [Ni⁰], driven by hydrogenation of COD to cyclooctane. Coordination of substrate, C-O oxidative addition, alkoxide β-H elimination, and reductive elimination release free arene. The remaining aldehyde can be hydrogenated to form alcohol and turn over the system.

Scheme 5.4. Mechanisms for catalytic conversion of aryl alkyl ethers to arenes.



1.5. Comparison of dihydrogen and silane. Silanes have been utilized as a hydride source for reduction of aryl ether C-O to C-H bonds.^{10,11} In those cases, the authors concluded from isotope labeling studies that full incorporation of the silane hydrogen occurs. Thus, we

were interested in using Et₃SiH in place of H₂ in the N-heterocyclic carbene-supported system. The reduction of 2-methoxynaphthalene with silanes proved to be effective, but isotope labeling studies were unclear (Table 5.1). In all four H/D permutations of NaphOCX₃ and Et₃SiX, over 80% of the naphthalene product was the *d*₀-isotopologue. These isotopic labeling studies suggest that hydrogen atoms from moieties other than OCX₃ and SiX are incorporated into the arene product. Possible sources of ¹H nuclei in the reaction of NaphOCD₃ and Et₃SiD include Ni(COD), SIPr·HCl, KO^tBu, and *meta*-xylene.

Table 5.1. Results of various labeling studies with triethylsilane

Substrate	Silane	Naphthalene yield (%)	<i>d</i> ₀ (% vs <i>d</i> ₁)
NaphOCD ₃	2 equiv. Et ₃ SiH	81	95
NaphOCH ₃	2 equiv. Et ₃ SiD	56	> 95
NaphOCH ₃	8.3 equiv. Et ₃ SiD	85	81*
NaphOCD ₃	2 equiv. Et ₃ SiD	68	85*

*Schlenk tube was successively rinsed three times with D₂O under N₂ and flame-dried under vacuum prior to use for this reaction.

2. Effects of Electron-Donating and -Withdrawing Substituents on C-O Bond Cleavage

Because C-O bond cleavage proceeds through oxidative addition, electron-withdrawing substituents on the arene should enhance reactivity. For example, phenol derivatives with electron-withdrawing substituents undergo cross-coupling more readily.⁶ However, this is not observed in the model system. Instead, Paul Kelley has shown nickel complexes containing a variety of electronic substituents *para*- to the methoxy group undergo oxidative addition at very similar rates (Figure 5.5):²⁵

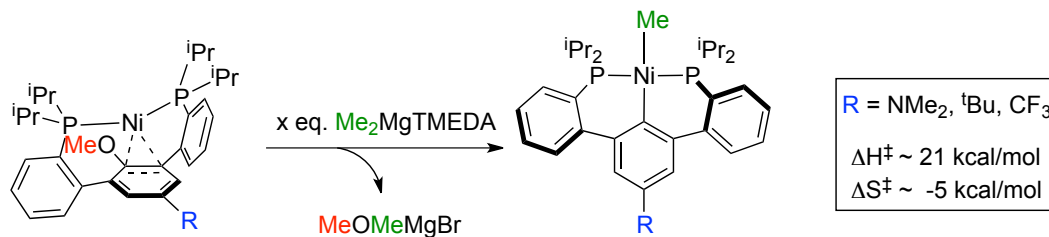


Figure 5.5. Experimentally observed rates of C-O bond cleavage (Kelley).

To understand this difference between the catalytic and model systems, computational study of the model system was performed. Previous computational studies of catalytic systems are available for comparison.^{8,23} To simplify the system and avoid having to model many rotational isomers, the ligand isopropyl groups were truncated to methyl groups. Structures for Ni(COD)₂, COD, and **44**^R through **47**^R (Scheme 5.5; R = H, NMe₂, ^tBu, CF₃, ⁺NMe₃) were optimized and confirmed to be local minima (or a first-order saddle point for **46**^R) by frequency calculations, and plotted by their relative Gibbs free energies (Figure 5.6).

The reaction energy plot shows why Ni(0) adducts containing electron-withdrawing groups, such as **45**^{+NMe₃}, do not undergo more facile oxidative addition: the Ni(0) adduct is too stabilized (i.e. ΔG of metallation is too negative). Conversely, adducts with electron-donating substituted arenes, such as **45**^{NMe₂}, are not significantly stabilized vs. Ni(COD)₂ and free ligand **44**^{NMe₂}. Thus, the barrier to oxidative addition is very similar (in some cases, even slightly lower) with electron-donating groups *vs.* electron-withdrawing groups.

This result seems to contradict the trends observed for intermolecular C-O activation during cross-coupling of phenol derivatives.⁶ However, aryl ethers from catalytic systems, which lack the additional stability afforded by diphosphine chelation, traverse a qualitatively different reaction energy landscape. Unless the aryl ether is very electron-deficient, the formation of an arene adduct analogous to **45**^R is thermodynamically uphill.

For instance, Ni(COD)₂ dissolved in neat *d*₆-benzene does not show any signs of free COD by ¹H NMR. Even if the arene is substituted with a heteroatom directing group, such as a carbamate or an ester, coordination of nickel has been calculated to be thermodynamically uphill relative to Ni(PCy₃)₂ starting material.⁸ A non-chelated system in which metal π-coordination is a downhill process is coordination of electron-deficient alkenes.²⁶

Scheme 5.5. Computational Models for Stoichiometric C-O Activation

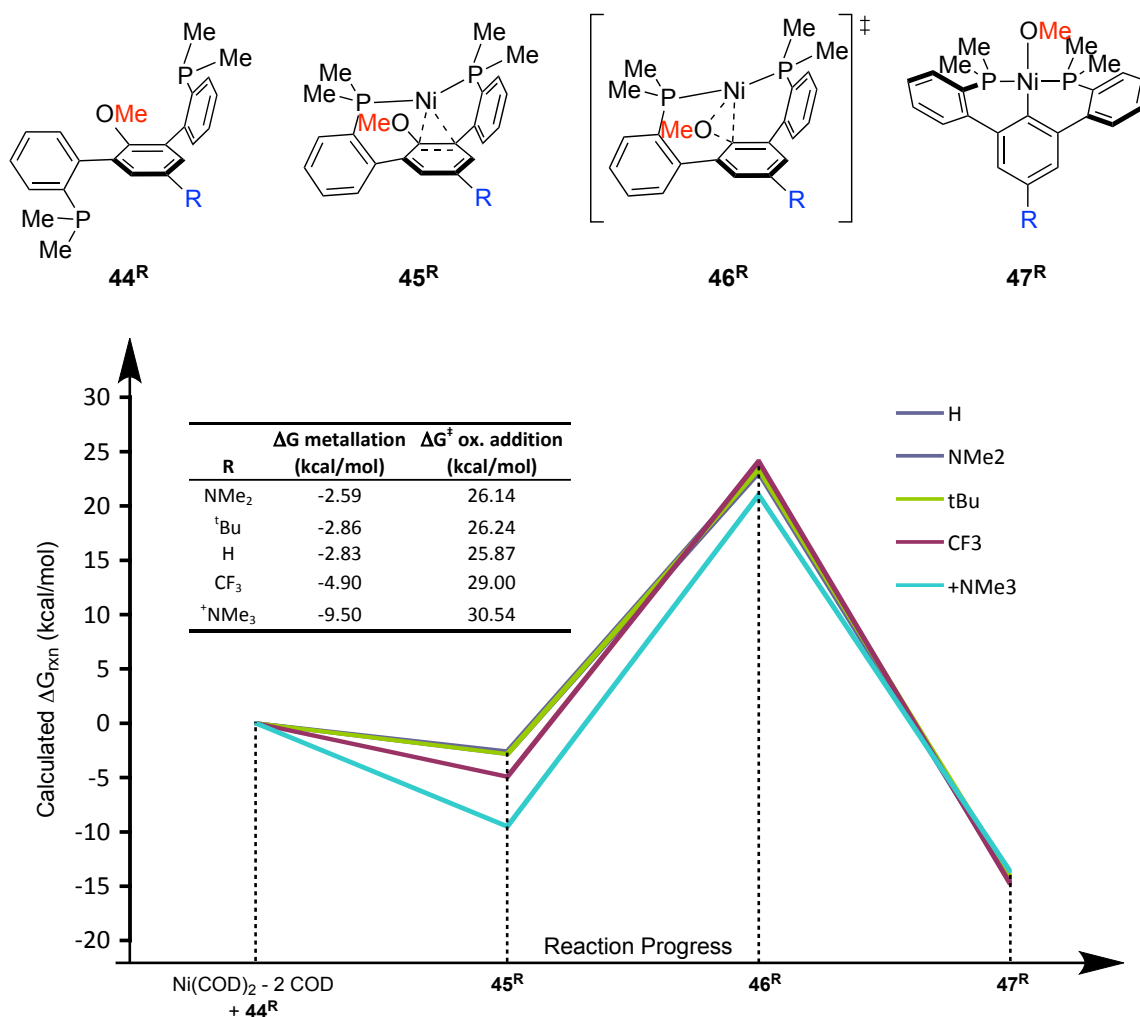


Figure 5.6. Reaction energy plot for 44^R through 47^R.

The result of having a positive ΔG of metallation is that the metallation now adds to the overall barrier of oxidative addition, whereas for the terphenyl diphosphine system, the

negative ΔG of metallation did not affect oxidative addition. The difference between these two reaction energy landscapes is diagrammed in Figure 5.7. The effects of electron-donating and -withdrawing groups on ΔG^\ddagger (oxidative addition) are clearly shown.

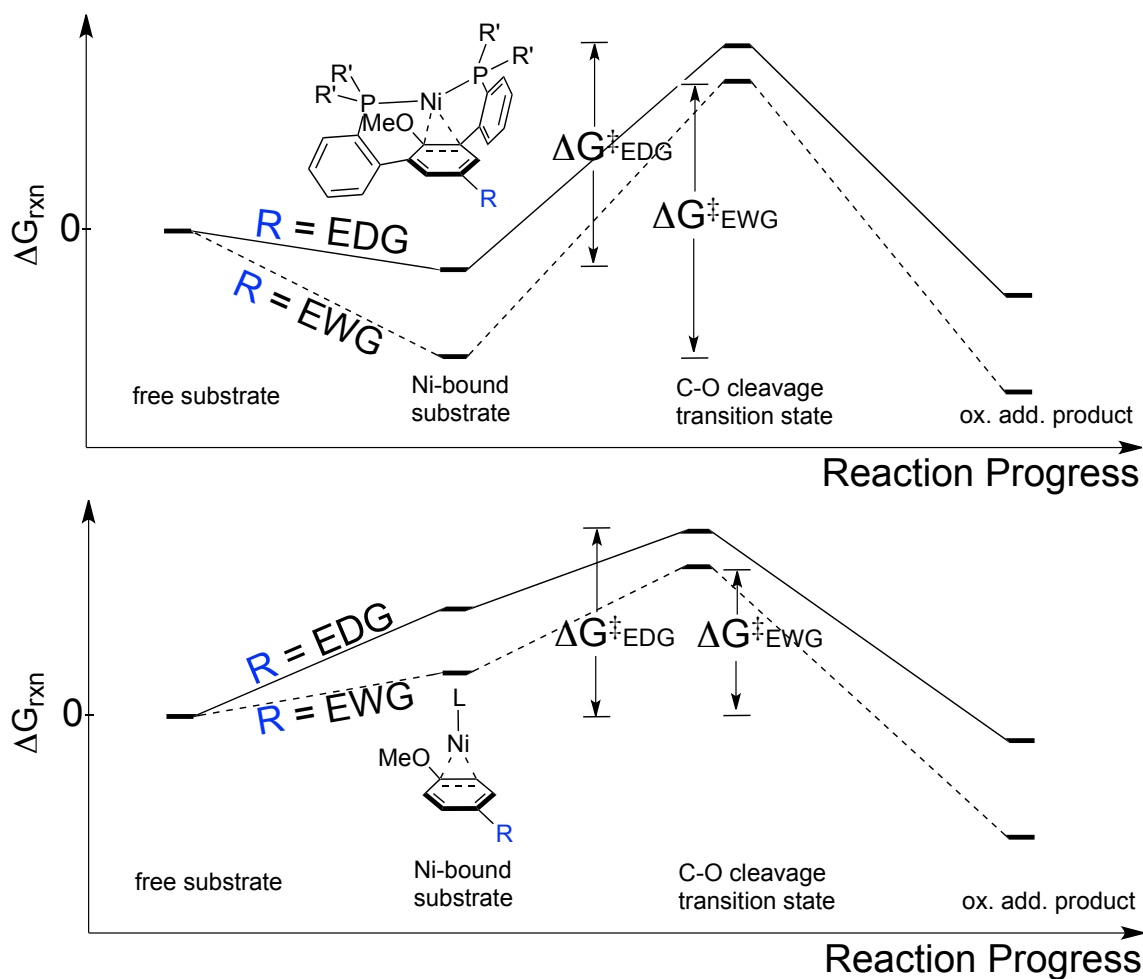


Figure 5.7. Qualitative reaction energy diagrams for C-O bond cleavage with terphenyl diphosphine ether (top) and typical non-chelated aryl ether substrate (bottom).

CONCLUSION

Recently reported mechanistic insights from a *meta*-terphenyl diphosphine ether into Ni/NHC-catalyzed aryl alkyl ether C-O bond cleavage have been studied. Isotopic labeling studies have shown that the hydrogen for the resulting C-H bond does not

originate from H₂, but from the alkyl ether moiety through β -H elimination from a putative Ni(II)-alkoxide intermediate. A proof-of-principle conversion of 2-methoxynaphthalene to naphthalene in the absence of H₂ was demonstrated, utilizing H₂ only to generate the catalytically active nickel species. The similar reaction rates for electronically dissimilar variants of the model system have been computationally studied. Because of the chelation of nickel with tethered phosphines, the effect of electron-donating vs. -withdrawing groups on ΔG of metallation is nullified. Thus, ΔG^\ddagger (oxidative addition) is relatively similar across a wide range of arene substituents. Overall, these studies demonstrate that mechanistic lessons derived from model systems with enforced metal-arene interactions can be extended to catalytic systems with transient metal-arene intermediates. In the future, development of custom multidentate platforms bearing chelated substrates may be utilized to elucidate other catalytic mechanisms.

EXPERIMENTAL SECTION

General considerations. Syntheses of 2-(trideutromethoxy)naphthalene,⁹ 2-(hexyloxy)naphthalene,¹⁰ 1,1-dideuteriodohexane,¹¹ and 1,3-bis(2,6-diisopropylphenyl)-imidzolinium chloride¹² (SIPr·HCl) were performed as described in the literature. *Meta*-xylene was dried with sodium benzophenone ketyl and stored in an inert atmosphere glovebox. Hexanol was dried with sodium, distilled, and used in an inert atmosphere glovebox.

Synthesis of 2-(1,1-dideuterohexyloxy)naphthalene. The following procedure was adapted from the literature.¹⁰ A Schlenk tube was charged with a stir bar, 2-hydroxynaphthalene (0.72 g, 5.0 mmol), K₂CO₃ (1.05 g, 7.6 mmol), 1,1-dideuteriodohexane (1.65 g, 7.7 mmol), and acetone (7.5 mL) under an N₂

counterflow. The tube was sealed with a Teflon screw-stopper and heated at 70 °C for 14h. The reaction mixture was washed with hexanes and the combined organic washes were concentrated under vacuum to an orange oil. The organics were run through a silica gel plug with hexanes and concentrated under vacuum to obtain the pure product as a colorless oil (1.04 g, 91%). ¹H NMR (300 MHz, CDCl₃) δ: 7.80-7.67 (m, 3H), 7.47-7.39 (app td, 1H), 7.35-7.29 (app td, 1H), 7.18-7.11 (m, 2H), 1.84 (app t, 2H), 1.59-1.31 (m, 8H), 1.02-0.81 (m, 3H). GC-MS (m/z): calcd, 230.16 (M⁺); found 230.2.

Synthesis of 2-deuteronaphthalene. A Schlenk tube was charged with 2-bromonaphthalene (100 mg, 0.780 mmol), a stir bar, and Et₂O (10 mL) and stirred at -78 °C under N₂. A solution of 1.7 M ^tBuLi (0.96 mL, 1.638 mmol) was added dropwise. After 30 min, the reaction mixture was allowed to warm to room temperature over 10 min. Then D₂O (0.16 mL, 7.8 mmol) was added to the reaction. The reaction mixture was washed with H₂O, extracted with DCM, dried with MgSO₄, and filtered. After removing volatiles via rotary evaporation and redissolution in DCM, the mixture was analyzed by GC-MS and ²H NMR. GC-MS (m/z): calcd, 129.07 (M⁺); found 129.1. ²H NMR (74 MHz, CH₂Cl₂ with internal CD₂Cl₂ standard): 7.52 (s).

Hydrogenolysis of 2-methoxynaphthalene (and deuterated variants). The following procedure was adapted from the literature.¹⁰ In a N₂-atmosphere glovebox, a Schlenk tube was carefully charged with a stir bar, SIPr·HCl (27.5 mg, 0.062 mmol), and NaO^tBu (37.5 mg, 0.389 mmol) with the aid of weighing paper and an anti-static bar. Ni(COD)₂ (8.5 mg, 0.031 mmol) was affected by static too much to consistently transfer as a solid, so for reproducibility, a suspension in minimal hexanes was employed for addition to the reaction vessel. Immediately thereafter, the reaction flask was placed under vacuum to remove the hexanes. A solution (0.8 mL) of 2-

methoxynaphthalene (23.5 mg, 0.149 mmol) and tetradecane (8.1 μ L, 0.031 mmol) in *m*-xylene was added with a pipette. The reaction mixture was sealed with a Teflon screw-stopper and stirred for 10 minutes at room temperature. The mixture was degassed with two freeze-pump-thaw cycles, warmed to room temperature, and treated with 1 atm H₂ (as regulated by a mercury bubbler). The reaction mixture was once again sealed with a Teflon screw-stopper and placed in a 120 °C oil bath for 16h. The reaction flask was removed from heat, allowed to cool to room temperature, and quenched with 1 mL of Et₂O and 1.5 mL of 1M HCl aqueous solution. After 5 minutes of vigorous stirring, the top organic phase was separated via pipet. The aqueous phase was washed with 1 mL of Et₂O. The combined organic solutions were pushed through successive MgSO₄ and Celite plugs, and analyzed by GC-MS and GC. Naphthalene yield relative to internal tetradecane standard (GC FID): 74%. Analogous reactions with 2-(trideuteromethoxy)naphthalene or D₂ were performed by the same procedure.

Hydrogenolysis of 2-(n-hexyloxy)naphthalene (and deuterated variants).

The following procedure was adapted from the literature.¹⁰ In a N₂-atmosphere glovebox, a Schlenk tube was carefully charged with a stir bar, SIPr·HCl (25.8 mg, 0.060 mmol), and NaO^tBu (37.4 mg, 0.389 mmol) with the aid of weighing paper and an anti-static bar. Ni(COD)₂ (8.5 mg, 0.031 mmol) was affected by static too much to consistently transfer as a solid, so for reproducibility, a suspension in minimal hexanes was employed to add to the reaction mixture. Immediately thereafter, the reaction flask was placed under vacuum to remove hexanes. A solution (0.8 mL) of 2-(n-hexyloxy)naphthalene (33.9 mg, 0.148 mmol) and tetradecane (8.1 μ L, 0.031 mmol) in *m*-xylene was added with a pipette. The reaction mixture was sealed with a Teflon screw-stopper and stirred for 10 minutes at room temperature. The mixture was

degassed with two freeze-pump-thaw cycles, warmed to room temperature, and treated with 1 atm H₂ (as regulated by a mercury bubbler). The reaction mixture was once again sealed with a Teflon screw-stopper and placed in a 120 °C oil bath for 16h. The reaction flask was removed from heat, allowed to cool to room temperature, and quenched with 1 mL Et₂O and 1.5 mL 1M HCl aqueous solution. After 5 minutes of vigorous stirring, the top organic phase was separated via pipet. The aqueous phase was washed with 1 mL Et₂O. The combined organic solutions were pushed through successive MgSO₄ and Celite plugs and analyzed by GC and GC-MS. Naphthalene yield relative to internal tetradecane standard (GC FID): 98%. ²H NMR spectra (74 MHz, CH₂Cl₂ with CD₂Cl₂ internal standard), although broad, indicated ²H incorporation at the 2-position of naphthalene product. Analogous reactions with 2-(trideuteromethoxy)naphthalene or D₂ were performed by the same procedure.

Exposure of naphthalene to hydrogenolysis conditions under D₂.

Naphthalene was submitted to hydrogenolysis conditions under D₂ (*vide supra*) in place of alkyl-naphthylether substrate. The reaction mixture was analyzed by GC and GC-MS.

Derivatization of hexanol byproducts. A procedure was adapted from the literature.¹⁰ Authentic hexanol or the organic extracts from hydrogenolysis of 2-(n-hexyloxy)naphthalene (and deuterated variants) were pushed through a MgSO₄ plug into a Schlenk tube under N₂ counterflow. N-methyl-N-(trimethylsilyl)trifluoroacetamide (0.10 mL) was added to the tube. The tube was sealed and heated to 60 °C for 1h to derivatize hexanol into (n-hexyloxy)trimethylsilane. The reaction mixture was analyzed by GC-MS and GC without further purification. The base peak in the mass spectrum of (n-hexyloxy)trimethylsilane (for *d*₀, *m/z* = 159) corresponds to loss of a methyl group from the molecular ion. Near quantitative methyl fragmentation is also observed for this

compound in the NIST database reference spectrum. It is assumed that the fragmented methyl group is not ^2H -enriched. Products derived from under D_2 display d_{0-4} -isotopologues. Two C-D bonds could be formed from reversible hydrogenation of an aldehyde intermediate. Another two C-D bonds could be formed from β -position deuteration via enolates formed from an aldehyde intermediate under the basic reaction conditions.

Reaction of 2-methoxynaphthalene under hydrogenolysis conditions with H_2 pre-activation. In an N_2 -atmosphere glovebox, a Schlenk tube was carefully charged with a stir bar, $\text{SiPr}\cdot\text{HCl}$ (27.5 mg, 0.0618 mmol), and NaO^tBu (37.5 mg, 0.3894 mmol) with the aid of weighing paper and an anti-static bar. $\text{Ni}(\text{COD})_2$ (8.5 mg, 0.0309 mmol) was transferred as a suspension in minimal toluene (ca. 1 mL) to the reaction mixture. The reaction mixture was sealed with a Teflon screw-stopper and stirred for 10 minutes at room temperature. The mixture was degassed with two freeze-pump-thaw cycles, warmed to room temperature, and treated with 1 atm H_2 (as regulated by a mercury bubbler). The reaction mixture was once again sealed with a Teflon screw-stopper and placed in a 120 °C oil bath for 5h. The reaction mixture was placed under vacuum, removing all volatiles and leaving a dark red crude mixture. The reaction flask was brought back into a glovebox, and a solution (0.8 mL) of 2-methoxynaphthalene (23.5 mg, 0.1485 mmol) and tetradecane (8.1 μL , 0.0309 mmol) in *m*-xylene was added with a pipette. The reaction mixture was then sealed and placed in a 120 °C oil bath for 16h. The reaction flask was removed from heat, allowed to cool to room temperature, and quenched with 1 mL Et_2O and 1.5 mL 1M HCl aqueous solution. After 5 minutes of vigorous stirring, the top organic phase was separated via pipet. The aqueous phase

was washed with 1 mL Et₂O. The combined organic solutions were pushed through successive MgSO₄ and Celite plugs, and analyzed by GC-MS and GC. Naphthalene yield relative to internal tetradecane standard: 49% (GC FID).

Reductive cleavage studies with triethylsilane. A procedure was adapted from the literature.¹⁰ In a N₂-atmosphere glovebox, a Schlenk tube was carefully charged with a stir bar, SIPr·HCl (25.8 mg, 0.062 mmol), and NaO^tBu (37.4 mg, 0.389 mmol) with the aid of weighing paper and an anti-static bar. Ni(COD)₂ (8.5 mg, 0.031 mmol) was affected by static too much to consistently transfer as a solid, so for reproducibility, a suspension in minimal hexanes was employed to add to the reaction mixture. Immediately thereafter, the reaction flask was placed under vacuum to remove hexanes. A solution (0.8 mL) of 2-methoxynaphthalene (23.6 mg, 0.149 mmol) and tetradecane (8.1 μL, 0.031 mmol) in *m*-xylene was added with a pipette. Then Et₃SiD (48.9 mL, 0.297 mmol) was added via microsyringe. The reaction mixture was sealed with a Teflon screw-stopper and placed in a 120 °C oil bath for 24h. The reaction flask was removed from heat, allowed to cool to room temperature, and quenched with 1 mL Et₂O and 1.5 mL 1M HCl aqueous solution. After 5 minutes of vigorous stirring, the top organic phase was separated via pipet. The aqueous phase was washed with 1 mL Et₂O. The combined organic solutions were pushed through successive MgSO₄ and Celite plugs, and analyzed by GC-MS and GC. These isotopic labeling studies suggest that hydrogens from moieties other than OCX₃ and SiX (X = H or D) are incorporated into the arene product.

Computational details. All calculations were performed with DFT as implemented in Gaussian 09 Revision C.01.²⁷ Geometry optimizations and electronic structure calculations were performed with the TPSSh hybrid functional^{28,29} that,

incorporating 10% exact exchange (c.f. BLYP 0% and B3LYP 20%), has been shown to be effective for calculating transition metal-containing compounds.³⁰⁻³² The LANL2DZ basis set and effective core potential³³ for Ni atoms and the 6-31++G(d,p) basis set³⁴ for all other atoms was used. No solvent corrections were used. All optimizations of nickel complexes were performed with restricted spin and ignoring molecular symmetry after starting from a crystallographic set of coordinates. Energetic minima were confirmed with a subsequent frequency calculation that did not return imaginary frequency vibrations $< -10 \text{ cm}^{-1}$. Thermochemistry was calculated at standard temperature and pressure. Atomic coordinates for **44^R** through **47^R** are listed below in .xyz format. Transition states **46^R** were found by starting from the atomic coordinates for **45^R** and optimizing the geometry at increasing, fixed C-O bond lengths. A maximum in energy was observed near $r(\text{C-O}) = 1.95 \text{ \AA}$. Subsequently, the transition states were located by standard saddlepoint-locating algorithms and verified to contain exactly one imaginary vibrational mode.

52

44-H

P	3.88194	-1.37488	0.08165
P	-3.04710	1.59860	0.53188
C	-0.20581	-0.19923	-0.01119
O	-0.43011	0.38825	-1.24128
C	-3.48326	-0.03493	-0.23714
C	3.41922	0.41528	-0.15939
C	-1.24971	-0.94003	0.57710
C	1.03020	-0.02307	0.64333
C	4.36243	1.35128	-0.62546
H	5.38865	1.03737	-0.79792
C	2.09044	0.85391	0.06600
C	-2.55895	-1.10442	-0.12774
C	-4.68431	-0.26058	-0.93085
H	-5.40596	0.54330	-1.03859
C	4.01636	2.67815	-0.88320
H	4.76805	3.37618	-1.24188
C	1.74750	2.19249	-0.21177
H	0.72284	2.51142	-0.04725
C	-2.88070	-2.35926	-0.66817
H	-2.16733	-3.17304	-0.56383
C	-1.02634	-1.54498	1.82419
H	-1.82631	-2.12367	2.27871
C	2.69699	3.09816	-0.68093
H	2.41077	4.12670	-0.88228
C	1.20845	-0.63055	1.89747
H	2.14453	-0.47628	2.42654
C	0.19721	-1.39469	2.48110
C	-4.98415	-1.50827	-1.48866
H	-5.92049	-1.65031	-2.02158
C	-4.08423	-2.56633	-1.34897
H	-4.31018	-3.54206	-1.76980
C	-3.58032	1.26675	2.29227
C	-4.47873	2.66807	0.00902
C	5.04965	-1.63860	-1.35099
C	5.15333	-1.20490	1.44049
H	5.42644	-2.66532	-1.29175
H	5.90743	-0.95689	-1.36027
H	4.50350	-1.53446	-2.29336
H	5.65708	-2.16779	1.57729
H	4.66025	-0.94497	2.38196
H	5.90386	-0.43852	1.21430
H	-3.52330	2.20353	2.85729
H	-2.89123	0.55318	2.75202
H	-4.60077	0.87207	2.35103
H	-4.35417	3.64135	0.49507
H	-5.45837	2.26523	0.29275

H	-4.45375	2.83239	-1.07275
C	0.11788	-0.34105	-2.34913
H	-0.11237	0.24864	-3.23780
H	-0.35001	-1.32992	-2.42717
H	1.20402	-0.45079	-2.24782
H	0.35621	-1.85814	3.45034

53

45-H

Ni	-0.25116	0.78497	0.52421
P	1.59511	1.64965	-0.27685
P	-2.31576	1.48325	0.54843
C	0.28492	-1.02470	0.01321
O	0.39953	-0.98845	-1.39063
C	-3.04757	0.02426	-0.31845
C	2.99138	0.42500	-0.26845
C	-1.02659	-1.16894	0.62448
C	1.46624	-1.28749	0.80237
C	4.26964	0.77617	-0.73119
H	4.44032	1.76984	-1.13970
C	2.78877	-0.87537	0.26632
C	-2.29626	-1.16567	-0.18822
C	-4.24781	0.01867	-1.04600
H	-4.82490	0.93339	-1.15471
C	5.34166	-0.11868	-0.67350
H	6.31950	0.17779	-1.04283
C	3.87974	-1.76289	0.32797
H	3.71800	-2.75873	0.73271
C	-2.79055	-2.34651	-0.76477
H	-2.23267	-3.27092	-0.64074
C	-1.07590	-1.75685	1.93679
H	-2.05458	-1.96040	2.36592
C	5.14423	-1.39325	-0.13303
H	5.96833	-2.09930	-0.07869
C	1.34469	-1.80998	2.08423
H	2.23902	-1.94900	2.68650
C	0.06914	-2.08006	2.63909
H	-0.00647	-2.51041	3.63359
C	-4.71203	-1.15845	-1.64093
H	-5.63786	-1.15190	-2.20973
C	-3.98415	-2.34391	-1.49326
H	-4.34477	-3.26425	-1.94464
C	-3.34482	1.58841	2.09475
C	-2.98698	2.93691	-0.39018
C	2.39389	3.14829	0.47421
C	1.52541	2.13996	-2.06273
H	1.67560	3.97354	0.43710
H	3.30976	3.45032	-0.04592

H	2.62971	2.94510	1.52250
H	0.82332	2.97188	-2.17427
H	1.15344	1.28622	-2.63360
H	2.50565	2.44336	-2.44735
H	-3.07595	2.49658	2.64383
H	-3.12603	0.72433	2.72737
H	-4.41617	1.60729	1.86616
H	-2.62324	3.85351	0.08476
H	-4.08268	2.96526	-0.40658
H	-2.61120	2.90981	-1.41683
C	0.74681	-2.25191	-1.97872
H	0.77764	-2.08199	-3.05680
H	-0.01017	-3.01067	-1.74737
H	1.72909	-2.59370	-1.63130

53

46-H

Ni	-0.03882	0.92808	-0.48107
P	1.92312	1.64465	0.19158
P	-2.01515	1.58313	0.33096
C	-0.02732	-0.83652	0.20060
C	-3.11379	0.19547	-0.14162
C	3.06735	0.24217	-0.10341
C	-1.26008	-1.40496	0.63667
C	1.20520	-1.37911	0.66550
C	4.37350	0.40766	-0.59461
H	4.75907	1.40727	-0.77225
C	2.56622	-1.06522	0.12609
C	-2.58713	-1.11024	0.01455
C	-4.38604	0.36515	-0.71020
H	-4.79468	1.36369	-0.83588
C	5.19775	-0.68962	-0.85748
H	6.20300	-0.53614	-1.24002
C	3.41820	-2.15639	-0.13702
H	3.03632	-3.16252	0.01239
C	-3.37372	-2.20316	-0.38918
H	-2.96708	-3.20530	-0.28487
C	-1.24215	-2.35110	1.67423
H	-2.19072	-2.72929	2.04759
C	4.71452	-1.97949	-0.62398
H	5.33581	-2.84599	-0.83224
C	1.16086	-2.33234	1.70947
H	2.10252	-2.68062	2.12661
C	-0.04114	-2.80127	2.22975
C	-5.14859	-0.73357	-1.11814
H	-6.12973	-0.57982	-1.55900
C	-4.63925	-2.02353	-0.95328
H	-5.21586	-2.88694	-1.27318

C	-2.91573	3.09674	-0.24013
C	-2.26952	1.68861	2.16633
C	2.80894	3.11381	-0.50858
C	2.14345	1.94264	2.01135
H	2.18761	3.99594	-0.32702
H	2.92834	2.99895	-1.58952
H	3.78986	3.27761	-0.04772
H	3.19816	2.08960	2.26894
H	1.75550	1.07960	2.55866
H	1.56766	2.82658	2.30315
H	-3.92038	3.17663	0.19067
H	-2.98709	3.09841	-1.33142
H	-2.33409	3.97179	0.06541
H	-1.89188	0.77144	2.62616
H	-3.32942	1.80747	2.41639
H	-1.70241	2.53636	2.56353
H	-0.04542	-3.51784	3.04564
O	-0.28284	-0.52326	-1.70959
C	0.74385	-1.10016	-2.49631
H	0.34552	-1.17864	-3.51751
H	0.99587	-2.11149	-2.14560
H	1.66117	-0.49713	-2.52399

53

47-H

Ni	0.00419	-0.91535	0.08007
P	1.61679	-0.61856	1.50764
P	-1.70089	-0.97488	-1.29345
C	-0.04294	1.01419	-0.08777
C	-2.93042	-0.14326	-0.22138
C	2.88558	0.06653	0.38383
C	-1.25086	1.75087	0.05938
C	1.13722	1.75247	-0.38623
C	4.17850	-0.46877	0.29079
H	4.48585	-1.26094	0.96733
C	2.47960	1.10283	-0.49768
C	-2.54915	1.08352	0.37973
C	-4.17653	-0.71244	0.07968
H	-4.46760	-1.65432	-0.37518
C	5.08339	-0.00139	-0.66818
H	6.07904	-0.43097	-0.73075
C	3.40377	1.55199	-1.45715
H	3.10009	2.32283	-2.16009
C	-3.44892	1.69298	1.27151
H	-3.15858	2.61953	1.75928
C	-1.27412	3.14884	-0.12030
H	-2.21888	3.68219	-0.04866
C	4.68846	1.00853	-1.54791

H	5.37287	1.36819	-2.31115	H	4.42203	-4.17913	-1.39183
C	1.09337	3.15386	-0.53780	C	1.52890	-2.39684	-1.29356
H	2.01430	3.70096	-0.72349	H	0.50078	-2.42779	-1.64136
C	-0.10733	3.85154	-0.41712	C	-2.91594	1.06474	2.12409
C	-5.05767	-0.08770	0.96842	H	-2.15861	1.67370	2.61246
H	-6.01605	-0.54605	1.19464	C	-0.87262	1.94018	-0.06022
C	-4.68814	1.11819	1.56743	H	-1.60593	2.72988	0.04954
H	-5.35500	1.60723	2.27203	C	2.40545	-3.43727	-1.60492
C	-1.74874	-0.04048	-2.88599	H	2.05952	-4.27951	-2.19606
C	-2.42507	-2.60545	-1.72496	C	1.30581	1.11311	-0.73505
C	2.35548	-2.09056	2.31624	H	2.28499	1.26630	-1.17357
C	1.46317	0.59152	2.89334	C	0.39828	2.15895	-0.58863
H	1.58975	-2.52682	2.96300	C	-5.12988	0.10317	2.09920
H	3.23741	-1.83366	2.91277	H	-6.10715	-0.03129	2.55338
H	2.61121	-2.83692	1.56163	C	-4.16897	0.90655	2.71942
H	0.72714	0.21728	3.61133	H	-4.38966	1.40085	3.66067
H	1.11355	1.54725	2.49757	C	-4.71589	-0.67147	-2.34318
H	2.42617	0.73062	3.39478	C	-3.60584	-2.93672	-1.03005
H	-1.06472	-0.51184	-3.59821	C	3.07190	-0.05134	2.55066
H	-1.41787	0.98504	-2.70753	C	5.63607	-0.25343	1.35768
H	-2.76089	-0.03088	-3.30258	H	3.46747	0.67114	3.27204
H	-1.75913	-3.09275	-2.44250	H	3.24762	-1.06361	2.92895
H	-3.41999	-2.51331	-2.17251	H	1.99503	0.11627	2.46054
H	-2.45556	-3.22105	-0.82315	H	6.01988	0.51048	2.04136
H	-0.13206	4.92989	-0.54612	H	6.27827	-0.25540	0.47242
O	0.04215	-2.78737	0.28700	H	5.69666	-1.22689	1.85614
C	0.79931	-3.46687	-0.67186	H	-4.66669	-1.14855	-3.32755
H	1.87878	-3.21182	-0.64965	H	-4.72757	0.41214	-2.49416
H	0.72063	-4.55328	-0.49458	H	-5.65226	-0.97045	-1.85985
H	0.46872	-3.28188	-1.71528	H	-3.56084	-3.49783	-1.96921
				H	-4.60170	-3.06642	-0.59256
				H	-2.85757	-3.34828	-0.34819
				C	-0.12822	-2.22823	1.75863
				H	-0.55627	-3.22596	1.85022
				H	-0.39122	-1.62776	2.63579
				H	0.95802	-2.29891	1.65240
				C	1.22633	3.51051	-2.49458
				H	2.05606	2.82171	-2.63747
				H	0.35781	3.17507	-3.06065
				H	1.51941	4.51935	-2.78972
				C	2.05309	3.94968	-0.19930
				H	2.83484	3.19696	-0.29998
				H	2.39725	4.92124	-0.55846
				H	1.73720	4.01086	0.84194
				C	-0.21983	4.58238	-0.84749
				H	-1.08334	4.31961	-1.45780
				H	-0.49244	4.63902	0.20554
				H	0.19571	5.53531	-1.17586

64

44-NMe3

P	3.90527	0.23717	0.90799
P	-3.19385	-1.15630	-1.38204
C	-0.31432	-0.40741	0.21422
O	-0.72940	-1.65964	0.57537
C	-3.57702	-0.38022	0.26888
C	3.29648	-1.22613	-0.06807
C	-1.24748	0.64463	0.32914
C	0.97535	-0.18493	-0.32241
C	4.15873	-2.28773	-0.39743
H	5.18781	-2.27416	-0.05509
C	1.95748	-1.28770	-0.54346
C	-2.60638	0.42395	0.91059
C	-4.83017	-0.52515	0.88777
H	-5.59304	-1.13791	0.41474
C	3.72637	-3.37901	-1.15718

N 0.84941 3.53406 -1.02565

65

45-+NMe3

Ni -0.24221 -0.79574 -0.74848
P 1.60001 -2.01763 -0.84237
P -2.31174 -1.34276 -1.27858
C 0.27319 0.09327 0.88339
O 0.36804 -0.89632 1.85993
C -3.06033 -0.87884 0.34258
C 2.98658 -1.15174 0.03243
C -1.03985 0.62414 0.51260
C 1.45350 0.81017 0.46524
C 4.26071 -1.73149 0.13586
H 4.43822 -2.72177 -0.27650
C 2.77950 0.14307 0.57292
C -2.31879 0.06586 1.08558
C -4.26803 -1.37785 0.85446
H -4.84039 -2.10927 0.29093
C 5.32040 -1.05996 0.75194
H 6.29593 -1.53175 0.82034
C 3.85477 0.81228 1.18438
H 3.68778 1.79786 1.61204
C -2.81831 0.50971 2.31968
H -2.25882 1.24635 2.89080
C -1.08648 1.97365 0.00988
H -2.07016 2.41201 -0.11308
C 5.11610 0.22023 1.27447
H 5.93083 0.75106 1.75772
C 1.35131 2.08124 -0.09135
H 2.25733 2.55504 -0.45741
C 0.07272 2.66945 -0.26559
C -4.74399 -0.94392 2.09507
H -5.67521 -1.34074 2.48812
C -4.01927 0.00332 2.82597
H -4.38686 0.34385 3.78952
C -3.33591 -0.40321 -2.50955
C -2.89309 -3.07245 -1.58217
C 2.37150 -2.47423 -2.46301
C 1.52863 -3.64765 0.02578
H 1.65791 -3.07921 -3.03053
H 3.29840 -3.04354 -2.33900
H 2.58497 -1.56659 -3.03399
H 0.82680 -4.30050 -0.50138
H 1.16315 -3.48424 1.04207
H 2.50816 -4.13487 0.06278
H -3.03147 -0.68487 -3.52233
H -3.16416 0.66889 -2.38091

H -4.40332 -0.61112 -2.38351
H -2.50015 -3.40994 -2.54591
H -3.98526 -3.14957 -1.60668
H -2.50409 -3.72986 -0.80023
C 0.76692 -0.42537 3.16323
H 0.75293 -1.30262 3.81055
H 0.05606 0.32037 3.53620
H 1.77665 -0.00170 3.13529
C 0.62179 4.08386 -2.22539
H 0.57552 5.10188 -2.61701
H 1.65425 3.74518 -2.17073
H 0.03854 3.40130 -2.84272
C 0.81928 5.00701 0.05946
H 1.84853 4.65818 0.10926
H 0.77739 6.01183 -0.36511
H 0.37091 4.98413 1.05220
N 0.02742 4.07213 -0.83111
C -1.37296 4.61932 -0.92993
H -1.95139 3.99644 -1.61082
H -1.82236 4.62540 0.06232
H -1.30448 5.63536 -1.32007

65

46-+NMe3

Ni 0.03807 -1.71665 -0.15937
P -1.90754 -2.00290 0.86440
P 2.01292 -1.92178 0.93180
C 0.01885 0.13595 -0.36602
C 3.11102 -0.91308 -0.13113
C -3.06281 -0.93589 -0.07628
C 1.24951 0.85698 -0.27212
C -1.21286 0.85468 -0.25436
C -4.36944 -1.33414 -0.40541
H -4.74868 -2.28543 -0.04570
C -2.57535 0.30851 -0.55231
C 2.58686 0.29967 -0.64330
C 4.39145 -1.32955 -0.52806
H 4.80064 -2.25884 -0.14433
C -5.20171 -0.53118 -1.18915
H -6.20555 -0.86526 -1.43311
C -3.43232 1.10395 -1.33798
H -3.05576 2.03838 -1.74653
C 3.37864 1.05568 -1.52641
H 2.96886 1.96836 -1.95163
C 1.23964 2.20560 0.12074
H 2.19894 2.69319 0.24441
C -4.72784 0.69548 -1.65927
H -5.35310 1.32299 -2.28710

C	-1.17725	2.20778	0.13695	C	-0.52863	2.99870	-0.19721
H	-2.12947	2.70307	0.30537	C	-1.00405	-2.81479	0.41482
C	0.03138	2.86861	0.33949	C	1.14266	1.11798	0.21087
C	5.16073	-0.56926	-1.41319	C	0.92092	-1.26283	-0.20264
H	6.14663	-0.91496	-1.70887	C	-1.64961	-4.05218	0.27611
C	4.65023	0.62923	-1.91545	H	-2.52712	-4.27328	0.87585
H	5.22816	1.22120	-2.61864	C	0.14624	-2.53237	-0.36798
C	2.89866	-3.52875	1.14389	C	0.60293	2.48505	0.48685
C	2.22156	-1.15365	2.60674	C	-0.97168	4.29984	0.08204
C	-2.77041	-3.63004	1.01214	H	-1.83930	4.69903	-0.43322
C	-2.05493	-1.34580	2.59167	C	-1.18851	-5.01022	-0.63301
H	-2.12697	-4.29826	1.59190	H	-1.70790	-5.95844	-0.73077
H	-2.91521	-4.07162	0.02263	C	0.58573	-3.50398	-1.28289
H	-3.73577	-3.54782	1.52269	H	1.43497	-3.28396	-1.92514
H	-3.09519	-1.34608	2.93302	C	1.24185	3.30238	1.43472
H	-1.66566	-0.32458	2.61663	H	2.08345	2.90523	1.99697
H	-1.44979	-1.96309	3.26242	C	2.54739	0.99974	0.14321
H	3.89126	-3.40371	1.58920	H	3.14348	1.89904	0.24113
H	2.99254	-4.03429	0.17910	C	-0.07261	-4.72895	-1.42256
H	2.29833	-4.16175	1.80391	H	0.27862	-5.45150	-2.15295
H	1.82882	-0.13367	2.58015	C	2.32268	-1.37984	-0.22621
H	3.27432	-1.12712	2.90614	H	2.75864	-2.36810	-0.34361
H	1.64846	-1.72655	3.34221	C	3.12237	-0.24844	-0.07083
O	0.30037	-1.03972	-1.92324	C	-0.31943	5.09937	1.02667
C	-0.73794	-0.94154	-2.88694	H	-0.68544	6.10025	1.23331
H	-0.33226	-1.35585	-3.81886	C	0.78868	4.59569	1.70894
H	-1.01743	0.10629	-3.06737	H	1.29030	5.19705	2.46101
H	-1.63736	-1.50785	-2.61397	C	-0.40020	1.86102	-2.88128
C	-0.69402	4.38633	2.15901	C	-2.93831	2.78853	-1.85204
H	-1.70681	4.00071	2.06100	C	-3.31385	-2.02799	2.07319
H	-0.12790	3.77452	2.86066	C	-0.64060	-1.42280	2.97762
H	-0.71324	5.42978	2.47965	H	-3.74704	-1.19798	2.63711
C	-0.76556	5.15585	-0.18934	H	-3.22904	-2.90821	2.71849
H	-1.78669	4.78736	-0.26360	H	-3.97762	-2.23435	1.23201
H	-0.76135	6.19012	0.15970	H	-1.02403	-0.64230	3.64131
H	-0.26567	5.06768	-1.15338	H	0.38986	-1.17896	2.71019
N	-0.00744	4.30561	0.81031	H	-0.66663	-2.38619	3.49590
C	1.36890	4.90316	0.96234	H	-0.90139	1.24677	-3.63514
H	1.92721	4.32952	1.70091	H	0.57511	1.41990	-2.66294
H	1.87373	4.88394	-0.00263	H	-0.26297	2.87420	-3.27128
H	1.24616	5.93221	1.30149	H	-3.45199	2.19077	-2.60925
				H	-2.70493	3.76896	-2.27872
65				H	-3.60077	2.88199	-0.98898
47-+NMe3				O	-3.48830	0.33081	0.05640
Ni	-1.62858	0.16141	0.00728	C	-4.17953	-0.32820	-0.97208
P	-1.68427	-1.47129	1.45539	H	-4.06653	-1.42963	-0.94659
P	-1.42729	1.88598	-1.34538	H	-5.25384	-0.10876	-0.87293
C	0.28908	-0.00221	0.01387	H	-3.86979	-0.01342	-1.98814

C	5.37257	0.87535	0.03243
H	5.08468	1.55568	-0.76811
H	5.13557	1.30232	1.00593
H	6.43823	0.65289	-0.02903
C	5.02004	-1.01041	-1.47276
H	4.54158	-1.98062	-1.58870
H	4.67821	-0.32946	-2.25164
H	6.10589	-1.11803	-1.49864
N	4.62581	-0.42464	-0.13180
C	5.07731	-1.35582	0.97580
H	4.58990	-2.32019	0.84782
H	6.16137	-1.46714	0.91474
H	4.78500	-0.91311	1.92748

55

44-CF3

P	3.73040	0.05378	1.24217
P	-3.21193	-1.01026	-1.49540
C	-0.26676	-0.53983	0.21387
O	-0.54229	-1.86331	0.46985
C	-3.56878	-0.66858	0.29471
C	3.32068	-1.15377	-0.11694
C	-1.27436	0.41475	0.47142
C	0.97939	-0.16276	-0.32328
C	4.25395	-2.10550	-0.56956
H	5.26262	-2.10330	-0.16525
C	2.01648	-1.17862	-0.67125
C	-2.58522	0.00215	1.06293
C	-4.76459	-1.04411	0.92988
H	-5.53313	-1.56809	0.37014
C	3.91730	-3.06632	-1.52457
H	4.66067	-3.78710	-1.85416
C	1.67990	-2.16128	-1.62124
H	0.67112	-2.17465	-2.02305
C	-2.83966	0.31278	2.40774
H	-2.07988	0.84135	2.97803
C	-1.00673	1.76285	0.21163
H	-1.77108	2.50627	0.41823
C	2.61993	-3.09866	-2.04737
H	2.34339	-3.84604	-2.78557
C	1.20830	1.19551	-0.58997
H	2.14986	1.49811	-1.03429
C	0.23027	2.15113	-0.31654
C	-4.99955	-0.75426	2.27823
H	-5.93400	-1.06018	2.74074
C	-4.03884	-0.06398	3.01950
H	-4.21487	0.17578	4.06418
C	-3.75976	0.61504	-2.23762

C	-4.67113	-2.05210	-1.99390
C	4.89348	-0.95692	2.29338
C	4.99603	1.12533	0.38346
H	5.21536	-0.32778	3.13003
H	5.78718	-1.30813	1.76532
H	4.36264	-1.81986	2.70671
H	5.46926	1.77315	1.12904
H	4.50776	1.76737	-0.35520
H	5.77041	0.53412	-0.11876
H	-3.75901	0.51840	-3.32868
H	-3.04658	1.39966	-1.97027
H	-4.76050	0.90839	-1.90226
H	-4.58316	-2.24439	-3.06822
H	-5.64054	-1.57414	-1.80950
H	-4.63941	-3.01796	-1.48020
C	0.04117	-2.37708	1.67917
H	-0.22779	-3.43353	1.71059
H	-0.37405	-1.85969	2.55180
H	1.13141	-2.27068	1.66489
C	0.47134	3.60462	-0.60673
F	1.73564	3.85321	-1.03568
F	-0.36946	4.08306	-1.57091
F	0.26458	4.38865	0.48923

56

45-CF3

Ni	-0.24091	-0.81467	-0.76350
P	1.60937	-1.99056	-0.81827
P	-2.31232	-1.28138	-1.31251
C	0.29835	0.10155	0.86022
O	0.43148	-0.88875	1.84795
C	-3.03672	-0.89705	0.34328
C	3.00669	-1.09353	0.01153
C	-1.02566	0.61926	0.53612
C	1.46495	0.86001	0.46156
C	4.29169	-1.65480	0.08168
H	4.46878	-2.64914	-0.32241
C	2.79774	0.20746	0.54000
C	-2.28572	0.02241	1.10995
C	-4.23147	-1.42462	0.85687
H	-4.81003	-2.13553	0.27299
C	5.36247	-0.96205	0.65343
H	6.34605	-1.42121	0.69776
C	3.88608	0.89802	1.10460
H	3.71879	1.89137	1.51291
C	-2.76929	0.41471	2.36758
H	-2.21033	1.14272	2.94938
C	-1.10160	1.95680	0.02284

H	-2.08233	2.40025	-0.11999
C	5.15738	0.32463	1.16085
H	5.98095	0.87643	1.60515
C	1.32512	2.12481	-0.08427
H	2.20298	2.65700	-0.43849
C	0.03368	2.69075	-0.26467
C	-4.68751	-1.04553	2.12310
H	-5.60954	-1.46445	2.51656
C	-3.95668	-0.12070	2.87615
H	-4.31108	0.18413	3.85693
C	-3.32453	-0.22912	-2.46211
C	-2.98438	-2.96191	-1.71550
C	2.38252	-2.51371	-2.42212
C	1.56764	-3.59285	0.10862
H	1.66489	-3.13878	-2.96271
H	3.31072	-3.07839	-2.28164
H	2.59175	-1.62780	-3.02795
H	0.86668	-4.27152	-0.38700
H	1.20831	-3.39106	1.12017
H	2.55392	-4.06716	0.15565
H	-3.04911	-0.46038	-3.49607
H	-3.10249	0.82436	-2.27403
H	-4.39746	-0.40259	-2.32545
H	-2.62263	-3.25041	-2.70726
H	-4.08000	-2.99039	-1.72380
H	-2.60962	-3.68700	-0.98774
C	0.82003	-0.38342	3.13669
H	0.82149	-1.24506	3.80678
H	0.10005	0.36154	3.49494
H	1.82235	0.05886	3.10138
C	-0.06895	4.07860	-0.80986
F	0.56518	4.21492	-2.01557
F	0.51304	5.00737	0.01051
F	-1.35223	4.48501	-1.00152

56

46-CF3

Ni	-0.00210	-1.71312	-0.17679
P	-1.94057	-1.95487	0.84381
P	1.96968	-1.93032	0.88067
C	0.01379	0.15513	-0.39840
C	3.08531	-0.95563	-0.19551
C	-3.08733	-0.87855	-0.09596
C	1.25888	0.84907	-0.29622
C	-1.20626	0.88156	-0.25845
C	-4.39973	-1.25497	-0.42694
H	-4.79276	-2.20487	-0.07702
C	-2.57849	0.36219	-0.55872

C	2.57917	0.27023	-0.69359
C	4.35153	-1.39867	-0.60838
H	4.74499	-2.33914	-0.23388
C	-5.22137	-0.42818	-1.19770
H	-6.23160	-0.74288	-1.44372
C	-3.42778	1.18537	-1.32309
H	-3.04176	2.12887	-1.69919
C	3.37893	1.01960	-1.57368
H	2.98901	1.95355	-1.96900
C	1.26599	2.17968	0.13851
H	2.21877	2.68275	0.27353
C	-4.73094	0.80087	-1.64476
H	-5.35159	1.45362	-2.25176
C	-1.14463	2.22148	0.17556
H	-2.07297	2.75109	0.36393
C	0.07123	2.86493	0.39208
C	5.12720	-0.64671	-1.49586
H	6.10342	-1.00993	-1.80470
C	4.63808	0.56929	-1.97779
H	5.22542	1.16109	-2.67392
C	2.85105	-3.53845	1.12940
C	2.19442	-1.13161	2.53975
C	-2.85986	-3.54704	1.05564
C	-2.05061	-1.24728	2.55558
H	-2.23894	-4.21283	1.66257
H	-3.01916	-4.02251	0.08391
H	-3.82336	-3.41239	1.55987
H	-3.08502	-1.22205	2.91514
H	-1.64876	-0.23094	2.54080
H	-1.43965	-1.85163	3.23329
H	3.84987	-3.40703	1.56043
H	2.93274	-4.07096	0.17781
H	2.25348	-4.14968	1.81246
H	1.81755	-0.10685	2.48983
H	3.24872	-1.11352	2.83580
H	1.61293	-1.67906	3.28846
O	0.24817	-1.02108	-1.94038
C	-0.78493	-0.86818	-2.89955
H	-0.39587	-1.27922	-3.84106
H	-1.02699	0.19224	-3.05924
H	-1.70554	-1.40551	-2.63643
C	0.10646	4.25481	0.94689
F	0.20572	4.27559	2.31400
F	-1.01029	4.96967	0.64392
F	1.17206	4.96958	0.48848

56

47-CF3

Ni	-1.57774	0.37782	0.02047	C	-4.18664	0.22386	-0.90845
P	-1.78917	-1.22841	1.47281	H	-4.21127	-0.88398	-0.86218
P	-1.12594	2.02494	-1.35819	H	-5.22802	0.57436	-0.81019
C	0.30397	-0.05611	-0.00547	H	-3.85254	0.47487	-1.93632
C	-0.10547	3.02422	-0.21157	C	4.54230	-1.01886	-0.13371
C	-1.35782	-2.64969	0.40607	F	5.03237	-1.25299	1.12233
C	1.30035	0.94011	0.19709	F	5.29934	-0.01116	-0.64850
C	0.75228	-1.38597	-0.24629	F	4.81961	-2.13460	-0.86078
C	-2.18428	-3.77599	0.28531				
H	-3.07187	-3.86495	0.90479	60			
C	-0.19624	-2.53247	-0.40064	44-NMe2			
C	0.94501	2.36478	0.47604	P	3.71209	0.31088	1.21237
C	-0.38182	4.37112	0.06469	P	-3.19922	-1.08015	-1.44723
H	-1.18946	4.87667	-0.45556	C	-0.25847	-0.41289	0.18042
C	-1.88643	-4.79146	-0.62931	O	-0.51210	-1.72494	0.54282
H	-2.53971	-5.65491	-0.71418	C	-3.55266	-0.53574	0.29283
C	0.08086	-3.56140	-1.31687	C	3.32827	-1.00438	-0.05042
H	0.95098	-3.47414	-1.96181	C	-1.25432	0.56288	0.35833
C	1.68253	3.09467	1.42375	C	0.98035	-0.05683	-0.38212
H	2.47307	2.59423	1.97646	C	4.27845	-1.98292	-0.40068
C	2.66800	0.62510	0.12282	H	5.27930	-1.93638	0.02081
H	3.41220	1.40855	0.23013	C	2.03474	-1.08585	-0.62360
C	-0.75302	-4.67711	-1.43656	C	-2.56750	0.21280	0.98484
H	-0.51866	-5.44848	-2.16452	C	-4.75018	-0.83991	0.96322
C	2.12551	-1.68957	-0.29073	H	-5.51828	-1.41973	0.46092
H	2.45016	-2.71513	-0.43588	C	3.96784	-3.02751	-1.27241
C	3.07964	-0.68613	-0.12202	H	4.72257	-3.76814	-1.52332
C	0.36423	5.07981	1.01218	C	1.72540	-2.15485	-1.48650
H	0.13042	6.12019	1.21835	H	0.72272	-2.21504	-1.89883
C	1.39797	4.43597	1.69467	C	-2.82698	0.66445	2.28849
H	1.97603	4.96898	2.44407	H	-2.06556	1.24834	2.79976
C	-0.09286	1.83068	-2.87649	C	-0.99947	1.89057	-0.01114
C	-2.49968	3.11389	-1.89847	H	-1.78781	2.61768	0.14881
C	-3.45130	-1.56218	2.17076	C	2.67942	-3.11804	-1.81099
C	-0.68026	-1.34735	2.94367	H	2.42064	-3.93231	-2.48210
H	-3.72894	-0.69599	2.77692	C	1.20638	1.27163	-0.76559
H	-3.46369	-2.46466	2.79097	H	2.15903	1.50700	-1.22551
H	-4.18092	-1.64494	1.36319	C	0.22745	2.27398	-0.59547
H	-0.90424	-0.52115	3.62513	C	-4.98831	-0.40645	2.27199
H	0.35973	-1.26456	2.62155	H	-5.92409	-0.66063	2.76264
H	-0.82775	-2.29979	3.46247	C	-4.02764	0.35842	2.93610
H	-0.66116	1.27065	-3.62529	H	-4.20426	0.70818	3.94941
H	0.81002	1.26796	-2.62922	C	-3.62966	0.49283	-2.36104
H	0.18723	2.80673	-3.28493	C	-4.72570	-2.06291	-1.86315
H	-3.07196	2.58426	-2.66502	C	4.85999	-0.61087	2.35991
H	-2.14048	4.05956	-2.31683	C	5.00252	1.30047	0.28907
H	-3.15824	3.28515	-1.04403	H	5.17031	0.08266	3.14890
O	-3.40755	0.81037	0.09489	H	5.76073	-1.00327	1.87476

H	4.32185	-1.43841	2.83197
H	5.46668	2.01107	0.98175
H	4.53006	1.87269	-0.51471
H	5.78324	0.66472	-0.14500
H	-3.61590	0.28542	-3.43666
H	-2.86924	1.25049	-2.15326
H	-4.61492	0.88314	-2.08200
H	-4.65104	-2.34842	-2.91774
H	-5.66178	-1.50924	-1.72218
H	-4.75673	-2.98419	-1.27304
C	-0.06767	-2.06333	1.86343
H	-0.30913	-3.11901	2.00073
H	-0.59371	-1.46176	2.61486
H	1.01458	-1.91472	1.96221
C	1.81113	3.99288	-1.33892
H	2.49822	3.89484	-0.48251
H	2.20417	3.39771	-2.16975
H	1.79845	5.03663	-1.65870
C	-0.44737	4.63036	-0.53921
H	-0.44820	4.72056	0.55963
H	-0.13400	5.58441	-0.96733
H	-1.47336	4.44004	-0.87056
N	0.44902	3.58738	-1.01968

61

45-NMe2

Ni	-0.21502	-0.71202	-0.80165
P	1.66786	-1.82335	-0.84088
P	-2.26792	-1.23876	-1.26808
C	0.25998	0.26263	0.84668
O	0.37906	-0.74467	1.82388
C	-3.03216	-0.77062	0.34748
C	3.02046	-0.91361	0.05385
C	-1.03849	0.78140	0.48440
C	1.42599	1.01180	0.45947
C	4.31091	-1.45350	0.17516
H	4.52178	-2.44094	-0.22978
C	2.76557	0.37708	0.58670
C	-2.31129	0.21383	1.05866
C	-4.22668	-1.28318	0.87748
H	-4.78051	-2.04593	0.33636
C	5.34499	-0.74937	0.79830
H	6.33387	-1.19228	0.87999
C	3.81752	1.07949	1.20386
H	3.61454	2.06514	1.61516
C	-2.83202	0.69487	2.27074
H	-2.29760	1.47671	2.80429
C	-1.10869	2.10386	-0.07718

H	-2.10009	2.49701	-0.27337
C	5.09579	0.52803	1.30930
H	5.88959	1.08886	1.79513
C	1.30556	2.26886	-0.11680
H	2.21130	2.75726	-0.45790
C	0.02770	2.86607	-0.35020
C	-4.71474	-0.82160	2.10369
H	-5.63548	-1.23004	2.51156
C	-4.01903	0.17530	2.79642
H	-4.39909	0.54570	3.74477
C	-3.30052	-0.27576	-2.48100
C	-2.91278	-2.95211	-1.58054
C	2.53044	-2.32428	-2.41000
C	1.63660	-3.43701	0.07161
H	1.85031	-2.95911	-2.98683
H	3.46193	-2.87300	-2.22997
H	2.75113	-1.43141	-3.00172
H	0.96948	-4.12756	-0.45352
H	1.23693	-3.25315	1.07156
H	2.63195	-3.88856	0.14998
H	-3.01032	-0.55282	-3.49970
H	-3.10460	0.79101	-2.34398
H	-4.37067	-0.46702	-2.34382
H	-2.53534	-3.29036	-2.55055
H	-4.00800	-3.00179	-1.59705
H	-2.53285	-3.62842	-0.80957
C	0.66364	-0.24003	3.13753
H	0.70119	-1.11202	3.79385
H	-0.12808	0.43992	3.47395
H	1.62958	0.27941	3.15956
C	-1.36539	4.64592	-1.28384
H	-1.28031	5.68934	-1.59551
H	-1.76609	4.05644	-2.12765
H	-2.08508	4.60006	-0.46057
C	1.07616	4.72625	-1.57234
H	1.30941	4.15785	-2.48890
H	0.84736	5.75747	-1.85098
H	1.96898	4.74820	-0.94148
N	-0.06050	4.18338	-0.83721

61

46-NMe2

Ni	0.01090	-1.58545	-0.15490
P	-1.94343	-1.87157	0.77866
P	1.98591	-1.83084	0.84650
C	0.01986	0.30123	-0.32802
C	3.08945	-0.78913	-0.18424
C	-3.07439	-0.74270	-0.12515

C	1.25002	1.00380	-0.18658	H	-1.93511	4.48850	1.80696
C	-1.19330	1.02326	-0.16110	H	-0.96319	5.96175	1.81898
C	-4.38056	-1.10104	-0.49976	C	1.32187	5.02163	1.20694
H	-4.77881	-2.06843	-0.20823	H	1.62908	5.26152	0.17491
C	-2.55971	0.52193	-0.51244	H	1.17686	5.95588	1.75351
C	2.57396	0.45805	-0.61722	H	2.13753	4.47751	1.69241
C	4.35641	-1.20194	-0.62624	N	0.08612	4.25176	1.26769
H	4.75736	-2.15834	-0.30356				
C	-5.19059	-0.23634	-1.24087	61			
H	-6.19582	-0.53899	-1.52101	47-NMe2			
C	-3.39680	1.38159	-1.25028	Ni	0.28672	-1.46479	0.01311
H	-3.00177	2.34169	-1.57087	P	1.84340	-1.01911	1.46030
C	3.36585	1.25460	-1.46275	P	-1.39893	-1.66176	-1.36956
H	2.96566	2.20373	-1.80873	C	-0.10157	0.43615	0.04957
C	1.25387	2.30603	0.33148	C	-2.74233	-1.17492	-0.22358
H	2.21808	2.77667	0.48792	C	2.94772	0.00085	0.41864
C	-4.69360	1.01412	-1.61566	C	-1.41090	0.94079	0.26345
H	-5.30353	1.69610	-2.20156	C	0.90991	1.40971	-0.16799
C	-1.14489	2.33597	0.35666	C	4.31416	-0.27905	0.27099
H	-2.09307	2.82142	0.55820	H	4.77166	-1.06826	0.86062
C	0.06253	2.98935	0.65708	C	2.34656	1.03268	-0.34905
C	5.12476	-0.40171	-1.47726	C	-2.57297	0.03111	0.50388
H	6.10168	-0.74345	-1.80829	C	-3.86577	-1.98153	0.01118
C	4.62643	0.83422	-1.89468	H	-3.99436	-2.90772	-0.54079
H	5.20668	1.46372	-2.56364	C	5.10279	0.44048	-0.63324
C	2.90386	-3.43071	1.02086	H	6.15826	0.20679	-0.73926
C	2.22224	-1.10334	2.53843	C	3.15691	1.73647	-1.25700
C	-2.88058	-3.46754	0.87962	H	2.70508	2.50645	-1.87630
C	-2.11795	-1.25802	2.52315	C	-3.55313	0.37760	1.45016
H	-2.27598	-4.17133	1.45962	H	-3.42009	1.28367	2.03499
H	-3.02005	-3.88559	-0.12130	C	-1.69302	2.31954	0.22919
H	-3.85508	-3.35801	1.36965	H	-2.72390	2.63527	0.34487
H	-3.16616	-1.24165	2.84177	C	4.51661	1.44680	-1.40352
H	-1.70672	-0.24666	2.57845	H	5.11093	2.00003	-2.12548
H	-1.54019	-1.90466	3.19093	C	0.62376	2.78831	-0.17648
H	3.90382	-3.30161	1.45098	H	1.44574	3.48298	-0.30789
H	2.98722	-3.92100	0.04686	C	-0.68158	3.27690	0.02217
H	2.32109	-4.08126	1.68009	C	-4.83033	-1.61594	0.95623
H	1.81901	-0.08730	2.53944	H	-5.69048	-2.25631	1.12922
H	3.28086	-1.07308	2.81882	C	-4.66895	-0.43232	1.67907
H	1.66655	-1.69843	3.27028	H	-5.40094	-0.14354	2.42829
O	0.27433	-0.81526	-1.89373	C	-1.61978	-0.57333	-2.84561
C	-0.73736	-0.61976	-2.86506	C	-1.85045	-3.32752	-1.99592
H	-0.33636	-1.00615	-3.81251	C	2.85461	-2.40732	2.10669
H	-0.96471	0.44851	-2.99567	C	1.49987	-0.01173	2.96860
H	-1.66962	-1.15343	-2.63699	H	2.19614	-3.03373	2.71433
C	-1.14461	5.03033	1.27861	H	3.69693	-2.06145	2.71561
H	-1.50817	5.27551	0.26600	H	3.21123	-3.01832	1.27509

H	0.84895	-0.58397	3.63657
H	0.98507	0.90589	2.67715
H	2.43045	0.23702	3.48858
H	-0.86349	-0.82823	-3.59425
H	-1.47898	0.46703	-2.54456
H	-2.61825	-0.69931	-3.27632
H	-1.13398	-3.60141	-2.77524
H	-2.85969	-3.35321	-2.41974
H	-1.74977	-4.04529	-1.17859
O	0.64565	-3.31480	0.03481
C	1.48713	-3.76995	-0.98369
H	2.50686	-3.33354	-0.94894
H	1.60283	-4.86449	-0.89923
H	1.10646	-3.56104	-2.00542
C	-2.34336	5.07630	-0.07189
H	-2.81690	4.75161	-1.01389
H	-2.93386	4.68579	0.76275
H	-2.37992	6.16639	-0.02033
C	0.04122	5.55779	-0.51385
H	0.97801	5.49321	0.04843
H	0.25885	5.35601	-1.57640
H	-0.32830	6.58113	-0.42183
N	-0.95481	4.65130	0.04190

64

44-tBu

P	3.74972	-0.00838	1.24422
P	-3.20507	-1.04656	-1.49408
C	-0.29088	-0.53615	0.21798
O	-0.56019	-1.86950	0.46382
C	-3.58025	-0.66526	0.28443
C	3.29189	-1.18020	-0.13062
C	-1.28476	0.42312	0.47257
C	0.95716	-0.15223	-0.30927
C	4.21094	-2.13371	-0.61005
H	5.22345	-2.15005	-0.21392
C	1.98366	-1.17348	-0.67340
C	-2.60546	0.02268	1.05015
C	-4.78463	-1.02890	0.91083
H	-5.54481	-1.56608	0.35210
C	3.85686	-3.07118	-1.58053
H	4.58884	-3.79377	-1.93133
C	1.62936	-2.13766	-1.63776
H	0.61664	-2.13212	-2.02964
C	-2.88261	0.36025	2.38458
H	-2.12987	0.89950	2.95441
C	-1.00494	1.77716	0.21863
H	-1.78860	2.49846	0.42856

C	2.55327	-3.07769	-2.09035
H	2.26030	-3.80797	-2.83951
C	1.18798	1.20754	-0.55869
H	2.14673	1.48471	-0.98996
C	0.22814	2.19844	-0.29759
C	-5.03985	-0.71068	2.24913
H	-5.98042	-1.00852	2.70471
C	-4.09007	-0.00323	2.98820
H	-4.28038	0.25824	4.02535
C	-3.69351	0.58392	-2.26745
C	-4.69161	-2.04692	-2.00055
C	4.69537	-1.15429	2.37532
C	5.19887	0.87240	0.46119
H	5.08585	-0.56162	3.20966
H	5.53422	-1.66869	1.89283
H	4.01204	-1.90356	2.78657
H	5.69574	1.48325	1.22250
H	4.84196	1.54074	-0.32831
H	5.92958	0.17891	0.02944
H	-3.66985	0.47559	-3.35732
H	-2.96419	1.34927	-1.98806
H	-4.69345	0.90855	-1.95875
H	-4.59968	-2.24651	-3.07334
H	-5.64824	-1.53997	-1.82636
H	-4.69313	-3.01149	-1.48332
C	-0.08079	-2.33959	1.73144
H	-0.33687	-3.39949	1.77398
H	-0.57382	-1.80465	2.55222
H	1.00635	-2.21766	1.80931
C	0.54717	3.67333	-0.59465
C	0.84895	3.84287	-2.10313
H	1.70268	3.23245	-2.41497
H	-0.01503	3.54842	-2.70887
H	1.08455	4.89064	-2.32565
C	1.78575	4.10887	0.22409
H	2.66451	3.50434	-0.02204
H	2.02668	5.15795	0.01375
H	1.59906	4.00533	1.29823
C	-0.62168	4.60807	-0.23084
H	-1.52392	4.37418	-0.80720
H	-0.86817	4.55313	0.83545
H	-0.34305	5.64365	-0.45528

65

45-tBu

Ni	-0.24353	-0.84181	-0.78337
P	1.61465	-1.99876	-0.83972
P	-2.30858	-1.30871	-1.29956

C	2.91865	-3.49124	1.19186
C	2.21486	-1.08515	2.57013
C	-2.82452	-3.57908	1.04886
C	-2.09176	-1.24792	2.53360
H	-2.20858	-4.23002	1.67670
H	-2.95695	-4.06846	0.07990
H	-3.80069	-3.45103	1.53053
H	-3.13849	-1.22521	2.85656
H	-1.69642	-0.22894	2.51583
H	-1.50083	-1.83758	3.24144
H	3.91314	-3.33436	1.62508
H	3.01465	-4.03449	0.24762
H	2.33048	-4.10570	1.88024
H	1.82364	-0.06645	2.50626
H	3.26874	-1.04905	2.86726
H	1.63996	-1.63188	3.32453
O	0.30234	-1.07276	-1.90808
C	-0.71335	-0.95359	-2.88885
H	-0.30990	-1.39878	-3.80885
H	-0.95111	0.10110	-3.09000
H	-1.63964	-1.47966	-2.62273
C	-0.00618	4.33537	0.88581
C	-0.72441	4.38060	2.25629
H	-1.74939	4.00224	2.18398
H	-0.19055	3.77174	2.99428
H	-0.76956	5.41158	2.62867
C	1.40334	4.93061	1.06247
H	1.99405	4.36572	1.79233
H	1.95481	4.95389	0.11586
H	1.32101	5.96106	1.42623
C	-0.78041	5.22250	-0.11852
H	-1.81026	4.87523	-0.25237
H	-0.81956	6.25765	0.24217
H	-0.29184	5.21817	-1.09903

65

47-tBu

Ni	-1.64365	0.19216	0.02461
P	-1.66133	-1.43426	1.46634
P	-1.36532	1.87512	-1.34868
C	0.28232	-0.00352	0.01855
C	-0.47632	3.00003	-0.20892
C	-1.04530	-2.78927	0.40444
C	1.15578	1.09434	0.22705
C	0.89766	-1.26467	-0.21748
C	-1.72335	-4.00931	0.26579
H	-2.60089	-4.21309	0.87277
C	0.10287	-2.52020	-0.38620

C	0.63927	2.47180	0.49066
C	-0.90689	4.30999	0.04787
H	-1.76455	4.71348	-0.48179
C	-1.28997	-4.97274	-0.65133
H	-1.82981	-5.91004	-0.75044
C	0.51447	-3.49963	-1.30668
H	1.37145	-3.29615	-1.94287
C	1.28272	3.29563	1.43066
H	2.12163	2.89476	1.99295
C	2.55773	0.93915	0.16607
H	3.17548	1.82395	0.28491
C	-0.17043	-4.71033	-1.44370
H	0.16566	-5.43993	-2.17523
C	2.29863	-1.39328	-0.24596
H	2.72081	-2.38595	-0.38559
C	3.15960	-0.30068	-0.06903
C	-0.25084	5.11260	0.98730
H	-0.60253	6.12238	1.17819
C	0.84660	4.59957	1.68149
H	1.35642	5.20540	2.42544
C	-0.29805	1.78314	-2.85433
C	-2.83689	2.80570	-1.93042
C	-3.27451	-1.97969	2.14718
C	-0.56266	-1.41616	2.95034
H	-3.66502	-1.16103	2.75727
H	-3.18054	-2.88298	2.75943
H	-3.97932	-2.14421	1.33004
H	-0.89364	-0.62150	3.62577
H	0.46246	-1.20709	2.63768
H	-0.59984	-2.37845	3.47083
H	-0.78546	1.14597	-3.59853
H	0.66303	1.33847	-2.58700
H	-0.13613	2.78019	-3.27630
H	-3.33629	2.20564	-2.69599
H	-2.56765	3.77518	-2.36211
H	-3.52796	2.92726	-1.09329
O	-3.51576	0.39961	0.08590
C	-4.22198	-0.25244	-0.92901
H	-4.13786	-1.35826	-0.89199
H	-5.29487	-0.00907	-0.84035
H	-3.90528	0.03858	-1.95230
C	4.68315	-0.49999	-0.12800
C	5.11912	-1.48361	0.98454
H	4.62993	-2.45707	0.87610
H	6.20337	-1.64443	0.94409
H	4.86724	-1.08699	1.97419
C	5.45418	0.81874	0.06814
H	5.20590	1.55288	-0.70660

H	5.24974	1.26670	1.04715
H	6.53084	0.62354	0.01031
C	5.07754	-1.08665	-1.50469
H	4.59294	-2.05180	-1.68529
H	4.78973	-0.40690	-2.31423
H	6.16236	-1.24074	-1.55437

REFERENCES

- (1) Rosen, B. M.; Quasdorf, K. W.; Wilson, D. A.; Zhang, N.; Resmerita, A.-M.; Garg, N. K.; Percec, V. *Chem. Rev.* **2010**, *111*, 1346.
- (2) Zim, D.; Lando, V. R.; Dupont, J.; Monteiro, A. L. *Org. Lett.* **2001**, *3*, 3049.
- (3) Dankwardt, J. W. *Angew. Chem. Int. Ed.* **2004**, *43*, 2428.
- (4) Johnstone, R. A. W.; Neil McLean, W. *Tetrahedron Lett.* **1988**, *29*, 5553.
- (5) Guan, B.-T.; Xiang, S.-K.; Wu, T.; Sun, Z.-P.; Wang, B.-Q.; Zhao, K.-Q.; Shi, Z.-J. *Chem. Commun.* **2008**, 1437.
- (6) Tobisu, M.; Shimasaki, T.; Chatani, N. *Angew. Chem. Int. Ed.* **2008**, *47*, 4866.
- (7) Quasdorf, K. W.; Tian, X.; Garg, N. K. *J. Am. Chem. Soc.* **2008**, *130*, 14422.
- (8) Quasdorf, K. W.; Antoft-Finch, A.; Liu, P.; Silberstein, A. L.; Komaromi, A.; Blackburn, T.; Ramgren, S. D.; Houk, K. N.; Snieckus, V.; Garg, N. K. *J. Am. Chem. Soc.* **2011**, *133*, 6352.
- (9) Guan, B.-T.; Wang, Y.; Li, B.-J.; Yu, D.-G.; Shi, Z.-J. *J. Am. Chem. Soc.* **2008**, *130*, 14468.
- (10) Álvarez-Bercedo, P.; Martin, R. *J. Am. Chem. Soc.* **2010**, *132*, 17352.
- (11) Tobisu, M.; Yamakawa, K.; Shimasaki, T.; Chatani, N. *Chem. Commun.* **2011**, *47*, 2946.
- (12) Wenkert, E.; Michelotti, E. L.; Swindell, C. S. *J. Am. Chem. Soc.* **1979**, *101*, 2246.
- (13) Antoft-Finch, A.; Blackburn, T.; Snieckus, V. *J. Am. Chem. Soc.* **2009**, *131*, 17750.
- (14) Vacic, D. A.; Jones, W. D. *J. Am. Chem. Soc.* **1997**, *119*, 10855.
- (15) Vacic, D. A.; Jones, W. D. *J. Am. Chem. Soc.* **1999**, *121*, 7606.
- (16) Torres-Nieto, J.; Brennessel, W. W.; Jones, W. D.; García, J. J. *J. Am. Chem. Soc.* **2009**, *131*, 4120.
- (17) van der Boom, M. E.; Liou, S.-Y.; Ben-David, Y.; Shimon, L. J. W.; Milstein, D. *J. Am. Chem. Soc.* **1998**, *120*, 6531.
- (18) van der Boom, M. E.; Liou, S.-Y.; Ben-David, Y.; Vigalok, A.; Milstein, D. *Angew. Chem. Int. Ed.* **1997**, *36*, 625.
- (19) Rinaldi, R.; Schuth, F. *Energy Environ. Sci.* **2009**, *2*, 610.

- (20) Zakzeski, J.; Bruijninx, P. C. A.; Jongerius, A. L.; Weckhuysen, B. M. *Chem. Rev.* **2010**, *110*, 3552.
- (21) Hicks, J. C. *J. Phys. Chem. Lett.* **2011**, *2*, 2280.
- (22) Sergeev, A. G.; Hartwig, J. F. *Science* **2011**, *332*, 439.
- (23) Li, Z.; Zhang, S.-L.; Fu, Y.; Guo, Q.-X.; Liu, L. *J. Am. Chem. Soc.* **2009**, *131*, 8815.
- (24) Louie, J.; Gibby, J. E.; Farnworth, M. V.; Tekavec, T. N. *J. Am. Chem. Soc.* **2002**, *124*, 15188.
- (25) Paul Kelley, unpublished results.
- (26) Zenkina, O. V.; Karton, A.; Shimon, L. J. W.; Martin, J. M. L.; van der Boom, M. E. *Chem. Eur. J.* **2009**, *15*, 10025.
- (27) Gaussian 09, Revision C.01, Frisch, M. J.; Trucks, G. W.; Schlegel, H. B.; Scuseria, G. E.; Robb, M. A.; Cheeseman, J. R.; Scalmani, G.; Barone, V.; Mennucci, B.; Petersson, G. A.; Nakatsuji, H.; Caricato, M.; Li, X.; Hratchian, H. P.; Izmaylov, A. F.; Bloino, J.; Zheng, G.; Sonnenberg, J. L.; Hada, M.; Ehara, M.; Toyota, K.; Fukuda, R.; Hasegawa, J.; Ishida, M.; Nakajima, T.; Honda, Y.; Kitao, O.; Nakai, H.; Vreven, T.; Montgomery, Jr., J. A.; Peralta, J. E.; Ogliaro, F.; Bearpark, M.; Heyd, J. J.; Brothers, E.; Kudin, K. N.; Staroverov, V. N.; Kobayashi, R.; Normand, J.; Raghavachari, K.; Rendell, A.; Burant, J. C.; Iyengar, S. S.; Tomasi, J.; Cossi, M.; Rega, N.; Millam, J. M.; Klene, M.; Knox, J. E.; Cross, J. B.; Bakken, V.; Adamo, C.; Jaramillo, J.; Gomperts, R.; Stratmann, R. E.; Yazyev, O.; Austin, A. J.; Cammi, R.; Pomelli, C.; Ochterski, J. W.; Martin, R. L.; Morokuma, K.; Zakrzewski, V. G.; Voth, G. A.; Salvador, P.; Dannenberg, J. J.; Dapprich, S.; Daniels, A. D.; Farkas, Ö.; Foresman, J. B.; Ortiz, J. V.; Cioslowski, J.; Fox, D. J. Gaussian, Inc., Wallingford CT, 2009.
- (28) Tao, J.; Perdew, J. P.; Staroverov, V. N.; Scuseria, G. E. *Phys. Rev. Lett.* **2003**, *91*, 146401.
- (29) Staroverov, V. N.; Scuseria, G. E.; Tao, J.; Perdew, J. P. *The Journal of Chemical Physics* **2003**, *119*, 12129.
- (30) Jensen, K. P. *Inorg. Chem.* **2008**, *47*, 10357.
- (31) Bühl, M.; Kabrede, H. *Journal of Chemical Theory and Computation* **2006**, *2*, 1282.
- (32) Waller, M. P.; Braun, H.; Hojdis, N.; Bühl, M. *Journal of Chemical Theory and Computation* **2007**, *3*, 2234.
- (33) Hay, P. J.; Wadt, W. R. *The Journal of Chemical Physics* **1985**, *82*, 270.
- (34) Ditchfield, R.; Hehre, W. J.; Pople, J. A. *The Journal of Chemical Physics* **1971**, *54*, 724.

APPENDIX A

TOWARD HETERODINUCLEAR ACTIVATION OF SMALL MOLECULES SUPPORTED BY A
NOVEL CATECHOL-DIPHOSPHINE LIGAND

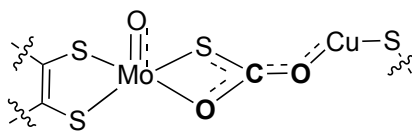
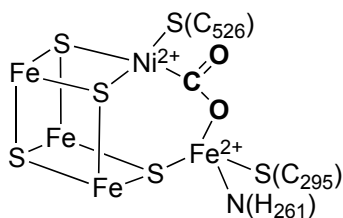
ABSTRACT

To develop heterodinuclear frameworks for small molecule activation, a catechol-diphosphine ligand structurally related to *para*-terphenyl diphosphine **1** was designed and synthesized. Metallation of the diphosphine moiety with a variety of late transition metals was compared to analogous coordination chemistry with **1**. Metallation of the catecholate moiety was also attempted, but in many cases found to be difficult to control, resulting in a variety of unexpected crystal structures. Motivations of this work toward a CO dehydrogenase mimic is discussed.

INTRODUCTION

Although mononuclear organometallic chemistry can provide useful models for studying fundamental chemistry, many important reactions are catalyzed by multinuclear catalysts. For example, biological CO₂ reduction to CO is efficiently catalyzed by CO dehydrogenases (CODHs) with Ni-Fe or Cu-Mo active sites (Chart A.1).¹⁻³ Industrially, the water-gas shift reaction is catalyzed by a poorly defined heterogeneous catalysts containing mixed oxides of Cu, Zn, Al, Fe, and Cr.⁴ The water-gas shift reaction (eq. A.1) is important for several industrial processes such as steam reformation of hydrocarbons and controlling the H₂/CO ratio for Fischer Tropsch feedstocks. Studying the mechanism of this reaction, in addition to being of fundamental interest, may lead to catalysts that are active at lower temperatures, which could be used to increase the efficiency of hydrogen fuel cells by simultaneously scavenging deleterious CO and producing H₂.⁵⁻⁷

Chart A.1. Proposed active sites for Ni-Fe (left) and Cu-Mo (right) CODH.^{1,2}



To this end, homogeneous activation of CO₂ is a growing field of research. Early results by Floriani and coworkers utilized nucleophilic Co(II) and alkali cations to bifunctionally fixate CO₂. More recently, bifunctional activation of CO₂ has been studied using Cu-B,⁸ Co-Zr,⁹ Re-K,¹⁰ and Ni-B¹¹ paired systems (among many more not cited here).

The Agapie research group has had a long-standing interest in synthesizing and studying biomimetic multinuclear complexes.¹²⁻¹⁴ Thus, to target CO₂ activation via a CODH model, a framework was designed to hold a nickel center and an iron center (or copper and molybdenum centers) near each other while allowing space for intervening CO and bridging CO₂ ligands. Based on structural characterization of nickel carbonyl complex **4**, a dinuclear complex was imagined, in which a pendant iron center could be attached through an *ortho*-dihydroxy-functionalized central arene, or catechol (Figure A.1).

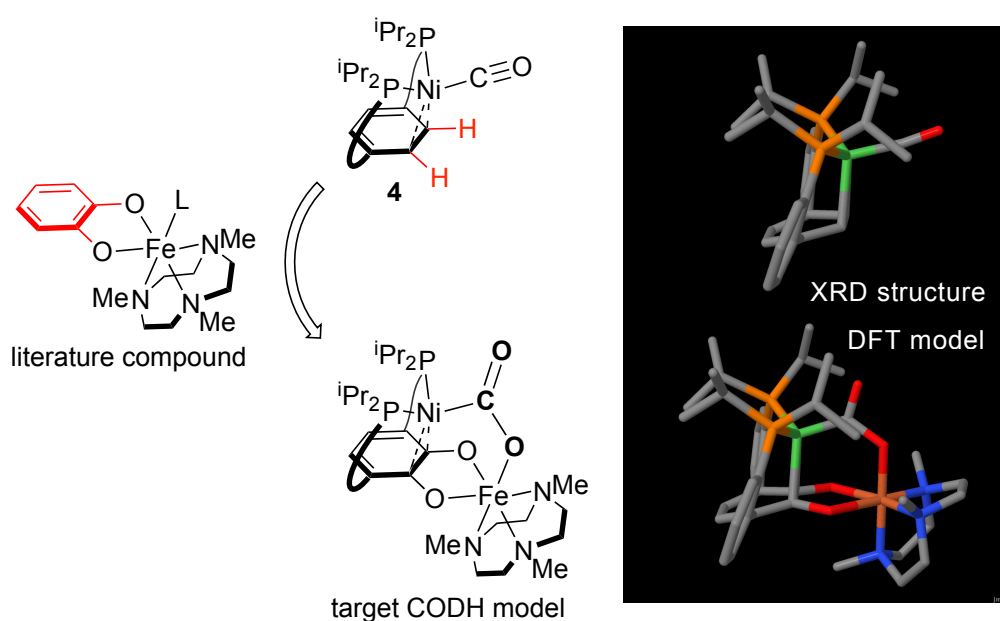


Figure A.1. Design of catechol-diphosphine to support a Ni-Fe CODH model schematically (left) and with atomic coordinates (right).

Iron catecholate complexes have been previously synthesized and studied as catechol dioxygenase models,¹⁵ and occur naturally in iron-transporting proteins such as enterobactin.¹⁶ Additionally, a number of dinuclear complexes have been characterized with a catecholate ligand bridging between a σ -bound metal and a π -bound metal,¹⁷⁻²⁷ albeit only a few of these are heterobimetallic.¹⁷⁻²⁰ As an alternative, the catechol could,

instead of binding a second transition metal, serve as a reservoir of protons and electrons for multielectron chemistry²⁸ or a hydrogen-bond donor for potential.^{28,29}

RESULTS AND DISCUSSION

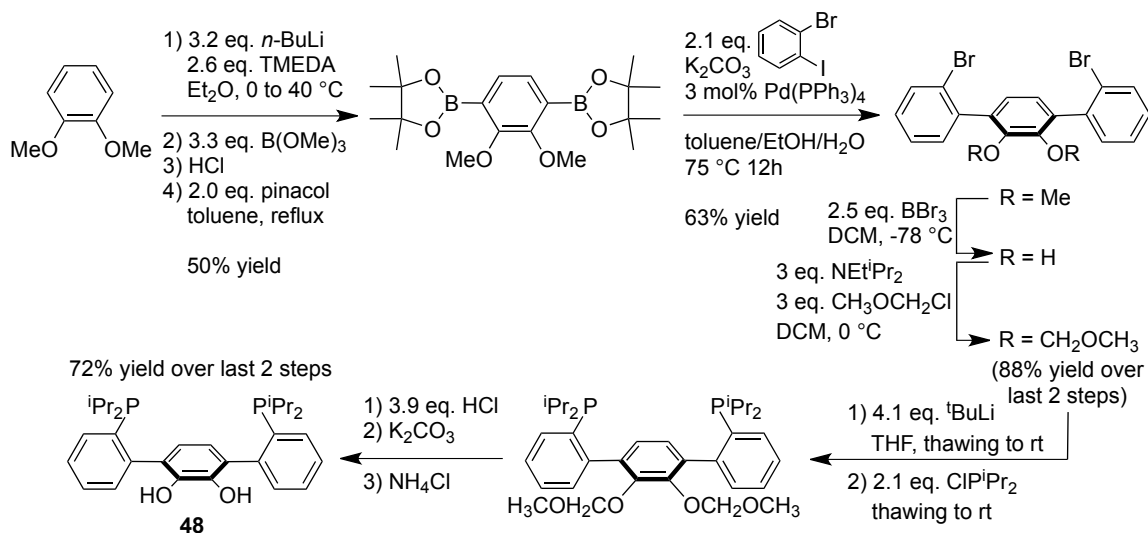
1. Ligand Synthesis and Characterization.

Undergraduate Christine Cheng initially targeted a catechol diphosphine through deprotection of dimethoxy diphosphine **6**. This strategy was unsuccessful possibly due to irreversible Al-P or B-P adduct formation. A modified synthesis changing the methoxy groups for more labile methoxymethyl (MOM) protecting groups before phosphination was adopted. A catechol diphosphine was synthesized in six steps from veratrole (Scheme A.1). For convenience, the initial dilithiation reaction was optimized to utilize a full 100 mL bottle of 2.5 M ⁿBuLi solution and yield 50% product (vs. veratrole) after boronation/deprotection/pinacol ester formation. The optimized dilithiation conditions use much less excess ⁿBuLi (3.2 equiv. total) vs. previously published conditions (5.0 equiv. total),³⁰ resulting in higher reaction throughput and easier product workup. The optimization of this step in the synthesis was conducted with Justin Henthorn.

Subsequent Suzuki coupling with 2-iodobromobenzene yielded 1,4-bis(2-bromophenyl)-2,3-dimethoxybenzene in 63% yield. Deprotection with BBr₃ and re-protection with MOMCl yielded 88% 1,4-bis(2-bromophenyl)-2,3-bis(methoxymethyl)benzene. Lithium-halogen exchange followed by quenching with chlorophosphine yields a diMOM diphosphine, and deprotection with HCl followed by neutralization/pH balancing with K₂CO₃ and NH₄Cl yield **48** in 72% yield. Overall, **48**

was synthesized in six steps with 20% yield on a multigram scale starting from one 100 mL bottle of 2.5 M n -BuLi.

Scheme A.1. Six-step synthesis of catechol-diphosphine **48**.



¹H and ³¹P NMR spectra of **48** are broad and solvent dependent. For instance, ³¹P NMR spectra of **48** in THF show a broad doublet near 1 ppm. This doublet coalesces at higher temperatures. In contrast, a ³¹P NMR spectrum of **48** in CD₂Cl₂ is a broad singlet at room temperature. These complications are likely the result of hindered rotation along the terphenyl axis and intramolecular hydrogen bonding interactions.

2. Late Transition Metal Complexes of **48**.

Attempts to selectively metallate the catechol moiety first, using oxophilic transition metal complexes, led to a mixture of ³¹P NMR peaks, many of which indicated P-metal bonding. However, selective metallation of the diphosphine moiety of **48** was well-behaved for a number of late transition metal precursors.

2.1. Nickel Complexes. Reaction of **48** with 1 equivalent of Ni(COD)₂ in THF yielded a dark red solution over the course of a day (Scheme A.2). The product, **49**, was

characterized by $^{31}\text{P}\{^1\text{H}\}$ nuclear magnetic resonance (NMR) spectroscopy, revealing two doublets at 64.0 and 47.6 ppm ($J_{\text{PP}} = 19.6$ Hz). In the ^1H NMR spectrum, one broad peak at 6.60 ppm, integrating as one proton relative to the rest of the spectrum, can be washed out by addition of H_2O and was assigned as a hydroxyl proton. Three multiplets of similar integration value to the hydroxyl peak are observed at 4.31, 3.73, and 3.29 ppm. $^1\text{H}\{^{31}\text{P}\}$ NMR spectroscopy with a GARP waveform decoupler centered at 56 ppm simplified the multiplets to a doublet, a doublet of doublets, and a broad singlet, respectively. A gradient-enhanced ^1H - ^1H correlated spectroscopy (COSY) experiment identified cross-peaks between the first pair of peaks, the last pair of peaks, but not the between the first and last peaks. Finally, a 1D Nuclear Overhauser effect (NOE) experiment showed a crosspeak between the multiplet at 3.29 and a doublet at 7.29 ppm. All of this NMR data indicated an asymmetric (C_1) complex with only one hydroxyl group. Single crystals of **49** were grown from a hexanes/toluene layering stored at -20 °C. Preliminary structural characterization through x-ray diffraction (XRD), revealed a keto-enol isomer of catechol, with Ni bound η^4 to the remaining two C-C double bonds of the central ring. (Figure A.3). The solid-state structure is consistent with all of the NMR data. Additionally, the splitting patterns, ^{31}P -coupling, COSY, and 1D NOE cross-peaks described above parallel those of a previously reported mononickel complex **22**,³¹ that is isostructural to **49**.

Scheme A.2. Well-characterized phosphine metallations of 48

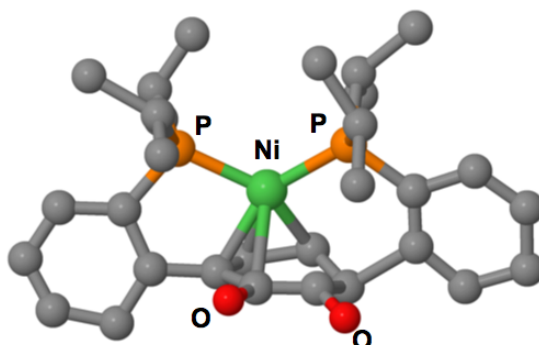
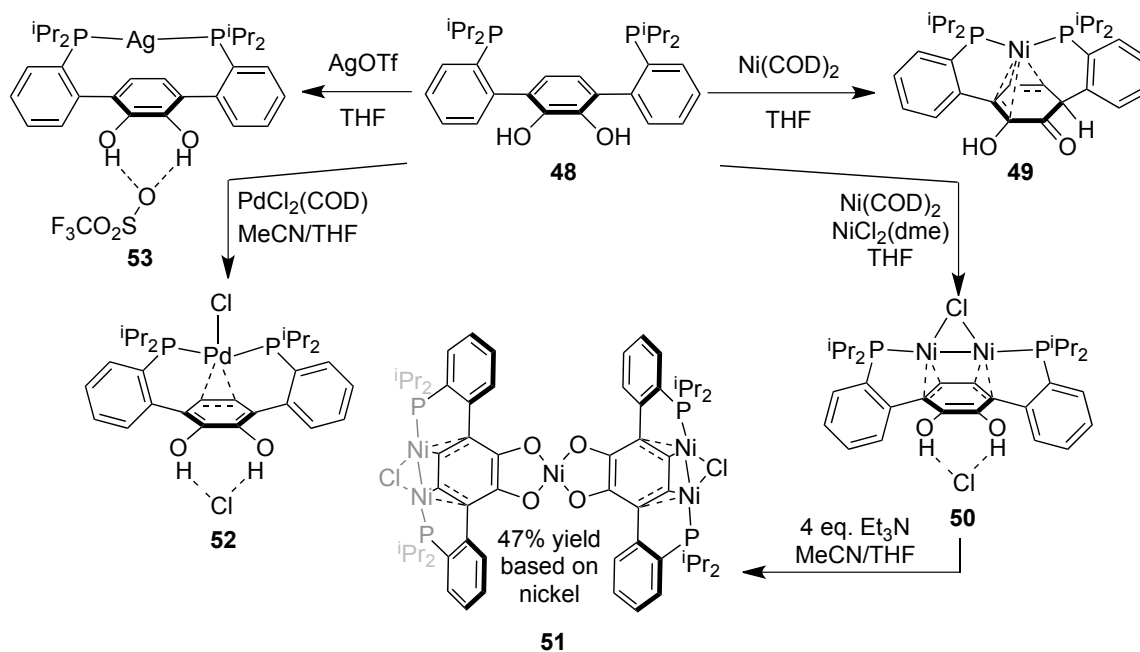


Figure A.2. Preliminary crystal structure of 49.

Reaction of 48 with one equivalent each of Ni(COD)_2 and $\text{NiCl}_2(\text{dme})$ in THF (Scheme A.2) yielded a dark green solution in minutes, mirroring the previously reported metallation of 1 to yield 12. However, the reaction mixture became an orange solution with dark green precipitate over hours. This precipitate was insoluble in THF and sparingly soluble in DCM and MeCN. $^{31}\text{P}\{^1\text{H}\}$ NMR spectra of this compound display a singlet at 56.0 ppm. ^1H NMR spectra are broad, but peaks at 10.35, 5.38, 2.31, and 2.21 ppm integrate to two protons each, and can be assigned as the catechol O-H,

catechol *C-H*, and two isopropyl methine protons from a C_s -symmetric species on the NMR timescale. Crystals were grown from DCM/hexanes layering, and an XRD study revealed that the product, **50**, contains a dinickel(I) core with one bound chloride and another dissociated chloride located within 3.0 Å from each oxygen atom, likely stabilized by hydrogen-bonding interactions (Figure A.3). Examination of the unit cell packing showed that the environment around the dissociated chloride also includes isopropyl groups from other molecules in the crystal.

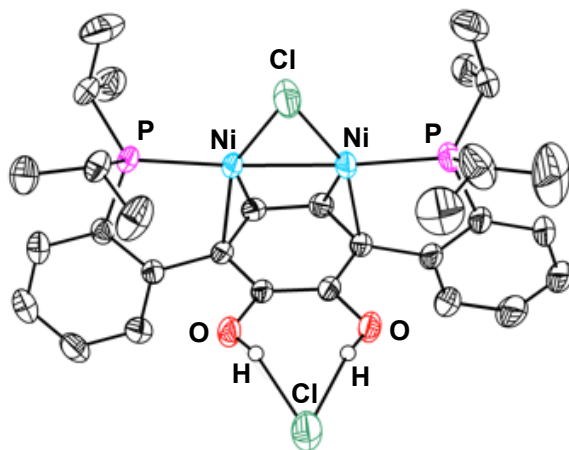


Figure A.3. Solid-state structure of **50**. Thermal ellipsoids are shown at 50% probability level. Hydrogen atoms not involved in hydrogen bonding are omitted for clarity.

Addition of one equivalent of Et_3N to **50** in MeCN yielded a brown-green solution. The reaction mixture displayed clean generation of a new singlet in the ^{31}P NMR spectrum at 51.5 ppm. Addition of 3 more equivalents of Et_3N lead to the formation of brown insolubles, and ^{31}P NMR of the heterogeneous mixture indicated a slight shift of the singlet to 51.3 ppm and a major decrease in intensity. The reaction mixture was filtered through Celite with the aid of THF, leaving behind white insolubles. The filtrate was concentrated under vacuum and washed with Et_2O . The remaining brown-green solid was soluble in C_6D_6 , and now displayed one broad singlet

in ^{31}P NMR spectra at 98.8 ppm. The ^1H NMR spectrum was broad and could not be assigned, but the number of peaks indicated that the product was possibly C_s -symmetric on the NMR timescale. Crystals were grown from vapor diffusion of Et_2O into a benzene solution, and single-crystal XRD data identified the product as pentanickel species **51** (Figure A.4). One nickel is bound by the four oxygen atoms of two quinonoids in a square-planar geometry. The dinickel-chloride-diphosphine moieties are situated trans to each other across the central nickel atom, and bind to their respective π -systems in a twisted fashion, so that the two Ni atoms in each dinickel moiety are inequivalent. Overall the solid-state structure is pseudo- C_i symmetric. Although the stoichiometry for this reaction is currently unclear, the isolated yield of 47% indicates that this reaction should be reproducible on a larger scale for full characterization.

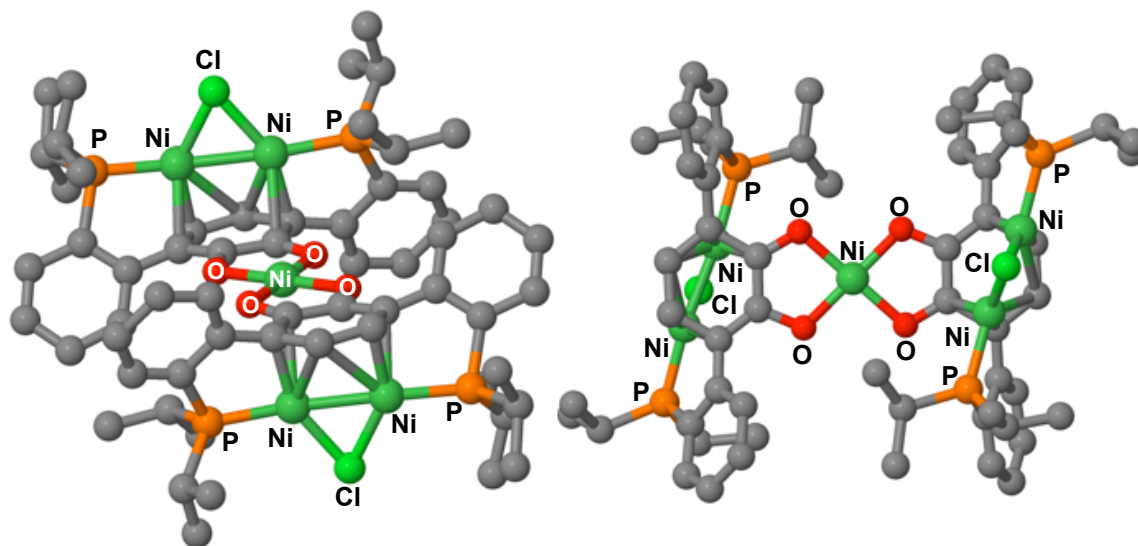


Figure A.4. Preliminary XRD structure of **51**. Left: side view. Right: top view.

2.2. Other late transition metal complexes. To access palladium chemistry, a yellow suspension of $\text{PdCl}_2(\text{COD})$ in THF was added to a solution of **48** in THF (Scheme A.2), immediately yielding a dark red, seemingly homogeneous mixture, paralleling attempted metallations of **1** with $\text{PdCl}_2(\text{COD})$. After a couple of minutes, the reaction mixture was

orange and noticeably less homogeneous. The red-orange solid product **52** was isolated by filtration and sparingly soluble in MeCN and DCM. ^{31}P NMR spectroscopy shows one singlet at 34.2 ppm. The ^1H NMR spectrum, between the typical aromatic and aliphatic regions ($\sim 2\text{-}7$ ppm), displays a triplet, a singlet, and two multiplets each integrating to two protons. Including the relatively clean aromatic and aliphatic peaks, the NMR data are consistent with a C_s -symmetric molecule on the NMR timescale. The triplet assigned as catechol C-H protons (6.25 ppm) is coupled to two equivalent ^{31}P nuclei ($J_{\text{HP}} = 4.0$ Hz), perhaps indicating strong Pd-catechol π -interactions. Crystals of **52** were grown from DCM solution, and single-crystal XRD data indicates that the Pd center is bound by two phosphines, one chloride, and a double bond of the catechol in a square planar coordination environment (Figure A.5). A dissociated chloride is stabilized by hydrogen bonding interactions with the catechol, similar to the motif in **50**.

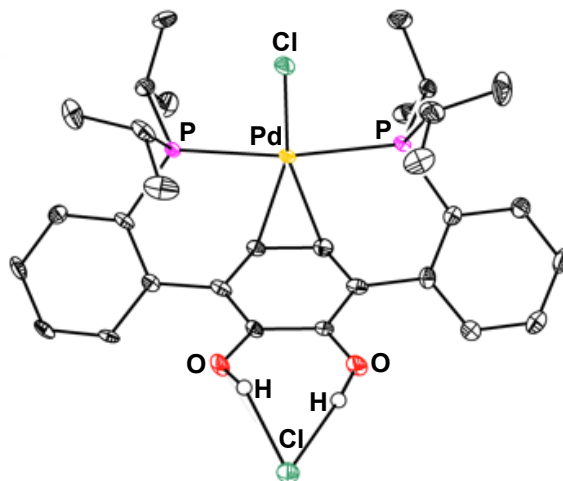


Figure A.5. Solid-state structure of **52**. Thermal ellipsoids are shown at 50% probability level. Hydrogen atoms not participating in hydrogen bonding are not shown for clarity.

Metallation of **48** with AgOTf yielded a Ag(I) complex (**53**, Scheme A.2). XRD analysis shows that the triflate appears to be hydrogen-bound to the catechol (Figure A.6). In

all other spectroscopic and structural aspects, **53** is analogous to the related AgOTf complex of **1**.³²

Attempts to metallate compounds **49-53** with a second metal center between the catechol oxygens was met with varying success. The only compounds that crystallized displayed unexpected solid-state structures, likely the result of decomposition of the targeted heterobifunctional complexes. The observed structures, containing titanium pentamethylcyclopentadienyl moieties, are shown in Figure A.6.

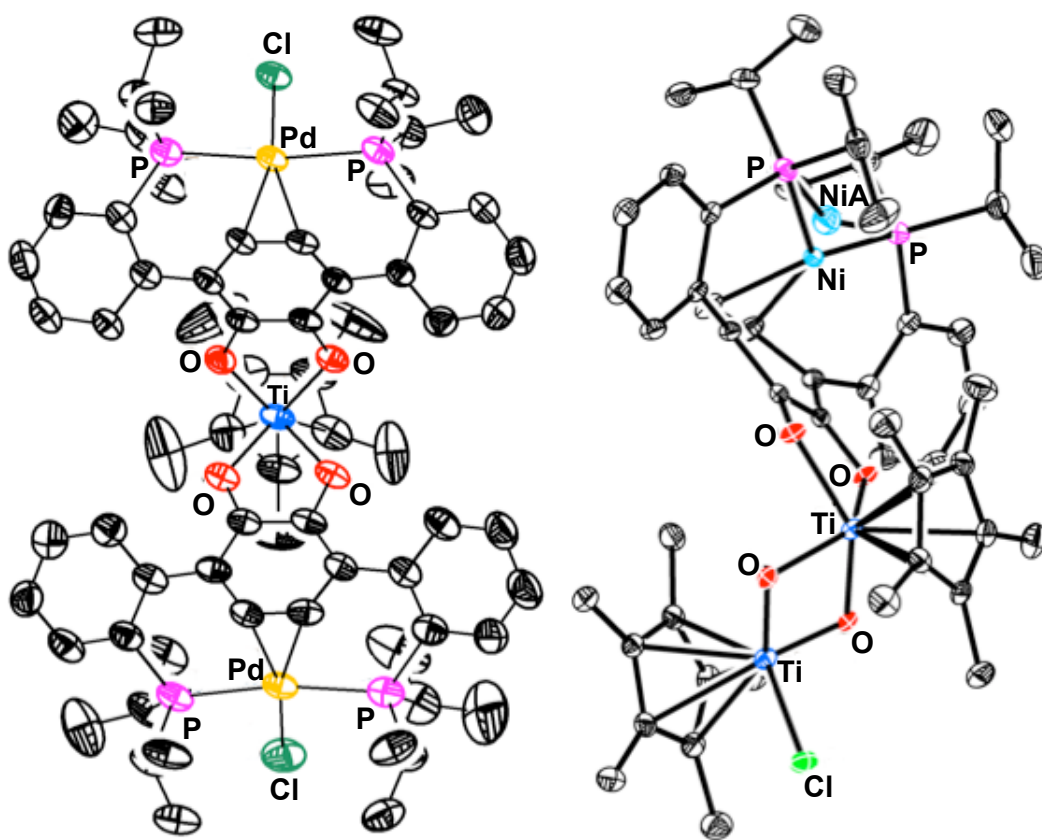


Figure A.6. Unexpected trinuclear complexes crystallized from reaction mixtures in which a second metal center was attempted to be bound to the catecholate moiety. Thermal ellipsoids are shown at 50% probability level. Hydrogen atoms are omitted for clarity.

3. Metal-Carbonyl Complexes of Functionalized Variants of **48**.

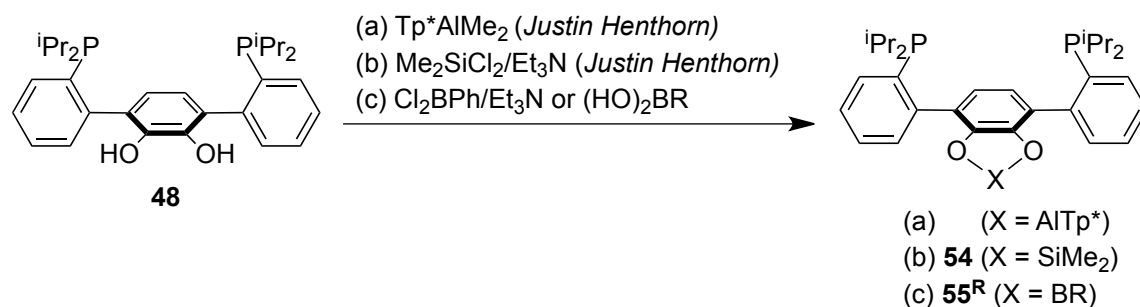
Mid transition metal-carbonyl compounds offer complementary access to study of CO₂ chemistry. Whereas late transition metals are often installed without carbonyl ligands and then reacted with CO, transition metals from the middle of the periodic table are often most metallated from polycarbonyl precursors. Once a metal carbonyl complex is obtained, study of oxidative CO chemistry (i.e. CO₂ chemistry) or reductive H₂ chemistry (i.e. Fischer Tropsch chemistry^{33,34}) would be accessible.

Attempts at direct metallation of **48** with Re(CO)₅X (X = Cl, Br, OTf) were very low yielding, with most of the reaction mixture becoming irreversibly insoluble, speculatively due to formation of a coordination polymer. No crystal structures from those reactions were obtained. It was hypothesized that pre-functionalization of the catechol moiety might facilitate isolation of metal carbonyl complexes. Thus, a variety of “protecting groups” for the catechol moiety were explored, and preliminary metallations with metal carbonyls is discussed.

3.1. Synthesis of protected catecholate ligands. Three routes have been determined to yield clean, selective functionalization of the oxygen atoms of **48**: alumination with Tp*AlMe₂, silylation with Me₂SiCl₂/Et₃N, and borylation with Cl₂BPh/Et₃N or, more synthetically versatile, borylation via condensation of boronic acids (HO)₂BR to yield **55^R**. The former two methods, developed by Justin Henthorn, will not be detailed herein. In all cases, the broad peak attributed to the catechol OH protons in **48** (~6.5 ppm) is no longer present. Borylation with Cl₂BPh/Et₃N or (HO)₂BPh were confirmed yield the same product, **55^{Ph}**, by ¹H NMR spectroscopy. To incorporate diverse electronic and steric profiles, boronic acid condensation has also been used to synthesize **55^{Me}**, **55^{Mes}**, and **55^{CF₃Ph}** (Mes = 2,4,6-trimethylphenyl; CF₃Ph = *para*-

trifluoromethyl-phenyl). Attempts to selectively functionalize the oxygen atoms of **48** with early transition metals were unsuccessful.

Scheme A.3. Protecting groups for catechol functionality.



3.2. *Products from reaction with cobalt carbonyl.* **55^{CF3PH}** was metallated with 1 equiv. $\text{Co}_2(\text{CO})_8$ at 130 °C in m-xylene (Scheme A.4). After 20 h, the reaction was stopped, volatiles were removed under vacuum and the crude was fractionated into hexanes (orange-brown), benzene (dark green-brown), and THF (dark brown). The benzene fraction yielded two types of crystals after sitting in the NMR tube for 1 d: dark chunks along the solvent line (minor) and red-brown needles that grew vertically along the NMR tube walls. XRD-diffraction of these two crystal morphologies indicated very different products (Figure A.7). The dark chunks (**56^{CF3PH}**) were determined to be pentacobalt species with two equivalents of terphenyl, one of which is C-H activated to act as a μ_4 -benzyne ligand. The red-brown needles (**57^{CF3PH}**) were determined to be $\text{Co}_2(\text{CO})_4$ adducts of the intact ligand framework. This structural motif contrasts that observed upon reaction of $\text{Co}_2(\text{CO})_8$ with **1**, in which a $\text{Co}_2(\text{CO})_3$ adduct was observed as the only product. In that case, a pronounced twisting about the terphenyl axis was present, and perhaps the substitution of the central arene in **55^{CF3Ph}** precludes such a binding geometry, causing retention of a fourth CO ligand.

Scheme A.4. Cobalt metallation.

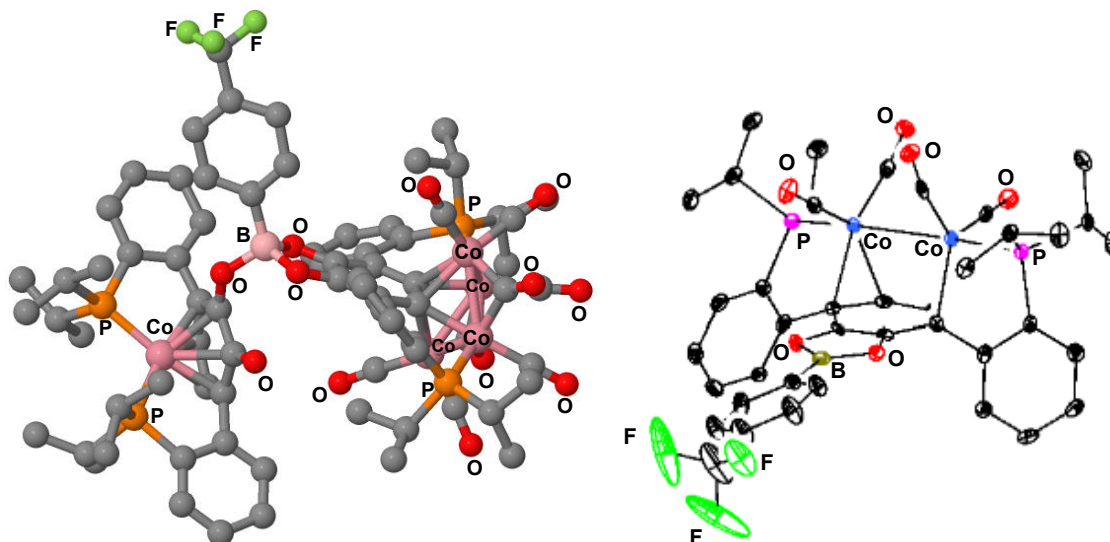
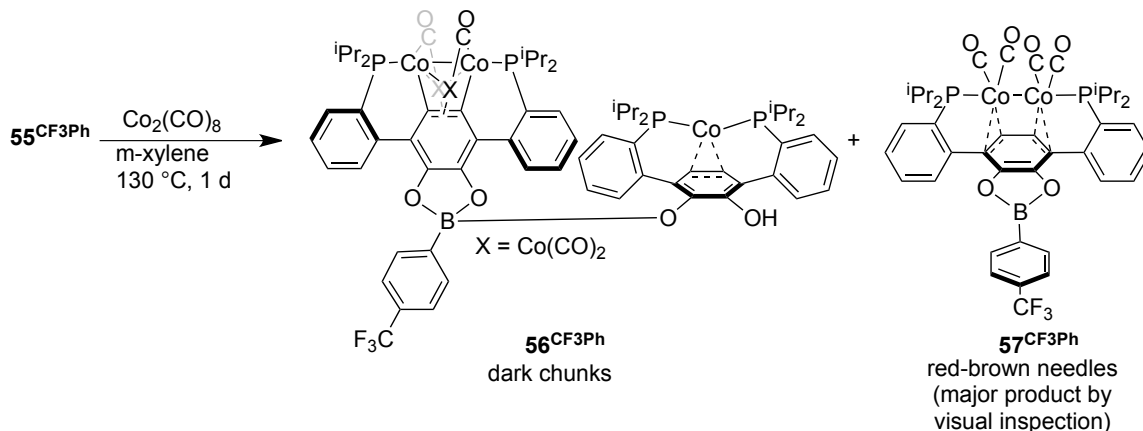
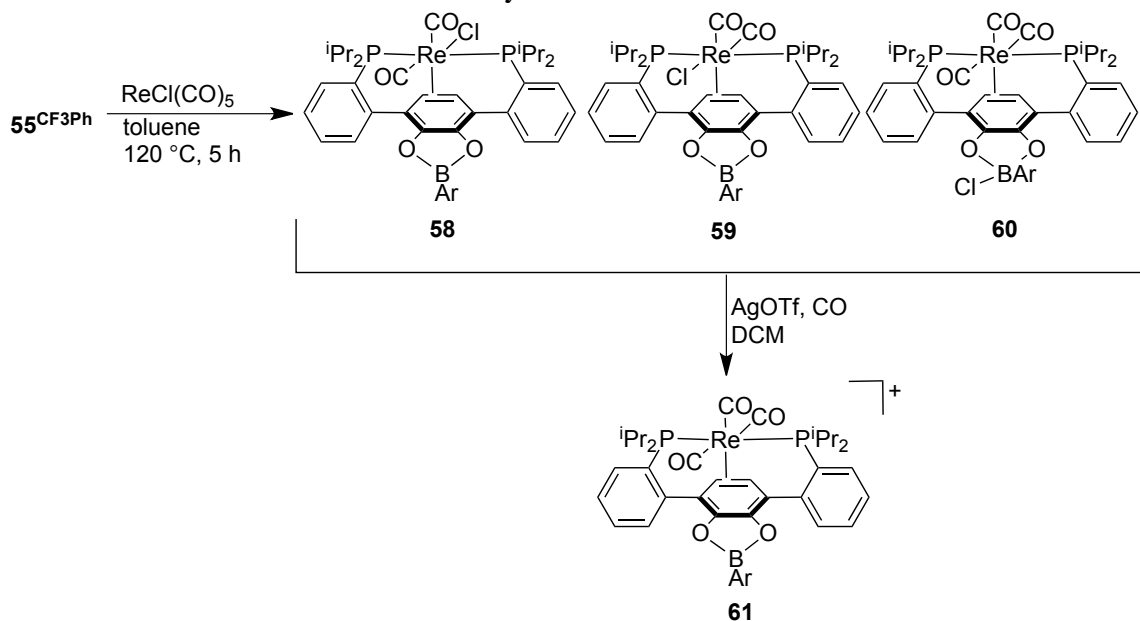


Figure A.7. Solid-state structures of cobalt metallation products **56**^{CF₃PH} (left) and **57**^{CF₃PH} (right)

3.3. Rhenium metallation. **55**^{CF₃Ph} was heated with 1 equiv. $\text{ReCl}(\text{CO})_5$ in toluene at 120 °C over 5h (Scheme A.5). The reaction progress was confirmed by ³¹P NMR spectroscopy to show total consumption of starting phosphine and the rise of two singlets at 12.5 and 10.1 ppm consistent with two metallation isomers. It is unclear if the isomers are dicarbonyl chloride adducts with the chloride pointing away from or toward the boron (**58**^{CF₃PH} and **59**^{CF₃PH}, respectively), or a rhenium tricarbonyl adduct

with a chloride bound at the boron (**60**^{CF3PH}). The products were washed with hexanes and filtered through Celite with dichloromethane as a bright yellow solution.

Scheme A.4. Rhenium Pentacarbonyl Chloride Metallation.



Access to cationic species would facilitate nucleophilic attack of metal carbonyls, so chloride abstraction of the **58-60**^{CF3PH} product mixture in DCM under an atmosphere of CO was performed by AgOTf. Of note, TlOTf is not strong enough to drive this reaction forward, and the product appears to be one species, **61**^{CF3PH}, which polymerizes THF upon dissolution in neat THF. By IR spectroscopy, **61**^{CF3PH} has two CO stretches at 1956 and 1924 cm^{-1} .

Unfortunately, upon addition of hydrides, no rhenium formyls are observed by NMR or IR spectroscopy. One possibility is that the nucleophile is intercepted by the Lewis acidic boron center. In a previous report, a strong Lewis acid was able to form a stable outer-sphere hydride without modifying a rhenium tetracarbonyl complex in solution.³⁵ Although ^1H and ^{11}B NMR were not clear toward the possibility of a borohydride, analogous reaction with nucleophilic methyl could be characterized

crystallographically, and indeed the nucleophile is bound to boron on the opposite face of the molecule from the metal center (Figure A.8).

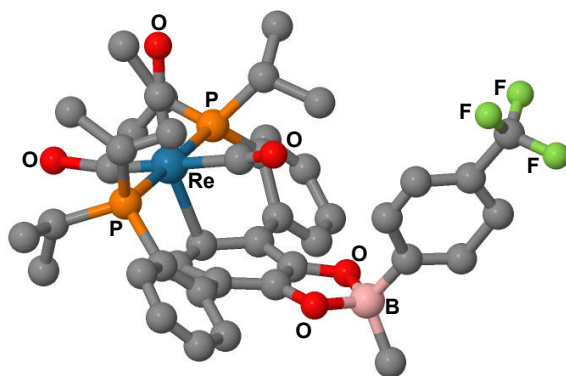
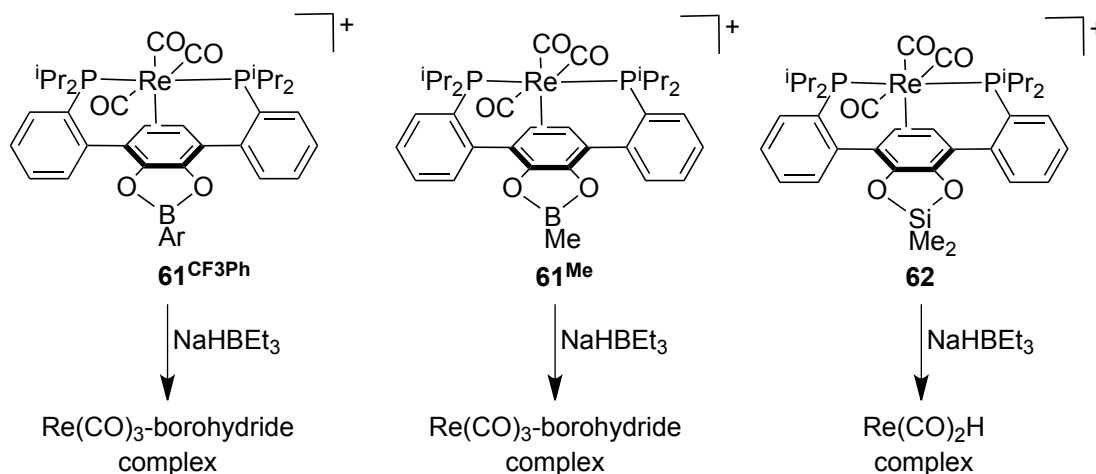


Figure A.8. Solid-state structure of a product from addition of MeMgBr to $61^{\text{CF}_3\text{PH}}$.

To attenuate the Lewis acidity of the boron center, a more electron-rich ligand, 55^{Me} was synthesized. Again, addition of hydride sources to the $\text{Re}(\text{CO})_3$ adduct of 55^{Me} (with an outer-sphere triflate) yielded no spectroscopic signatures of formyls, and formation of a stable borohydride was suspected to have occurred due to similar ^1H NMR splitting patterns compared to reactions with $61^{\text{CF}_3\text{PH}}$ (Scheme A.5).

Scheme A.5. Reactions of cationic rhenium tricarbonyl complexes with hydrides.

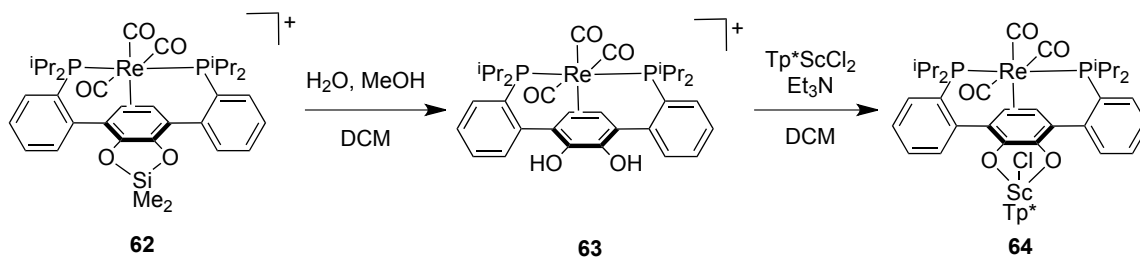


Analogous procedures with dimethylsilyl ligand 54 yielded a cationic rhenium tricarbonyl 62 . In this case, the pendant dimethylsilyl moiety is a weak Lewis acid, and

rather than intercepting hydrides or stabilizing rhenium formyl products, it appears to act as a spectator while hydride displaces a carbonyl ligand to cleanly yield a rhenium hydride ($^1\text{H NMR}$: -5.68 ppm, t, $J_{\text{PH}} = 33.3$ Hz).

The dimethylsilyl group of **62** could be removed upon treatment with H_2O and MeOH in DCM to yield **63** (Scheme A.6). Upon workup, $^1\text{H NMR}$ spectra confirm loss of silyl methyl peaks and introduction of a broad peak around 8.4 ppm that is assigned to the catechol OH protons. In an attempt to install a Lewis acidic group, **63** was treated with ScCl_2Tp^* and Et_3N at room temperature. In this case, although the crude NMR spectra had very little, if any signal, at least two crystal morphologies were observed after a DCM/hexane layering. The yellow blocks (minor morphology) were determined by XRD to be species **64** (Figure A.9). If **64** can be remade cleanly, then chloride abstraction followed by hydride addition may result in scandium-stabilized rhenium formyl species to model and study Fischer Tropsch processes. A very weak data set collected on the other morphology yellow crystals show two chlorides bound to rhenium, suggesting that higher yielding routes to **64** maybe possible with excess base, stronger bases (e.g. KBn), or higher reaction temperatures.

Scheme A.6. Deprotection and Scandium Attachment of **62**



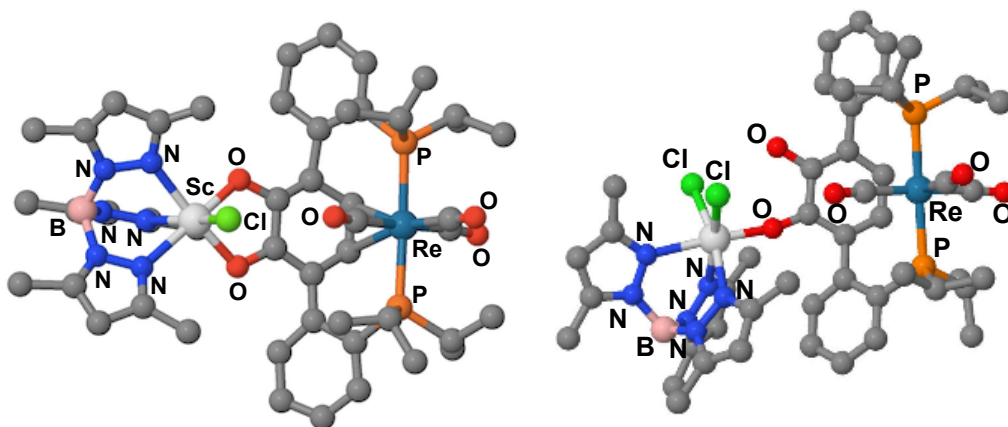


Figure A.9. Preliminary crystal structures of **64** (left) and a co-crystallized product **65** in which both chlorides are still attached to scandium (right). In the right structure, an outer-sphere triethylammonium triflate is not shown.

CONCLUSIONS

The catechol-diphosphine framework **48** is a promising system upon which to develop heterobimetallic complexes. In particular, metal carbonyl compounds developed by our group with para-terphenyl diphosphine **1** can be functionalized with a pendant reactive metal center to study oxidative and reductive transformations of carbonyls.

EXPERIMENTAL SECTION

General considerations. All manipulations were carried out in an inert atmosphere glovebox or using standard Schlenk line techniques. Liquid organic reagents were dried by stirring over sodium metal or calcium hydride, degassed by 3 cycles of freeze-pump-thaw, and isolated via vacuum-transfer. Et₂O, toluene, THF, MeCN, and DCM were dried by the method of Grubbs.³⁶ Deuterated solvents were purchased from Cambridge Isotope Laboratories and vacuum transferred from calcium hydride. All

reagents, once degassed and dried, were stored in an inert atmosphere glovebox. ^1H and ^{13}C NMR chemical shifts are reported relative to residual solvent peaks: CD_3NO_2 (^1H : 4.33; ^{13}C : 61.39 ppm) and others as reported in the literature.³⁷ ^{19}F and ^{31}P NMR chemical shifts are reported with respect to the instrument solvent lock. All NMR spectra were recorded at room temperature unless indicated otherwise. Gas chromatography-mass spectrometry (GC-MS) analysis was performed upon filtering the sample through a plug of silica gel. Fast atom bombardment-mass spectrometry (FAB-MS) analysis was performed with a JEOL JMS-600H high-resolution mass spectrometer.

Computational details. All calculations were performed with DFT as implemented in Gaussian 09 Revision C.01.³⁸ Geometry optimizations and electronic structure calculations were performed with the TPSSh hybrid functional^{39,40} that, incorporating 10% exact exchange (c.f. BLYP 0% and B3LYP 20%), has been shown to be effective for calculating transition metal-containing compounds.⁴¹⁻⁴³ The LANL2DZ basis set and effective core potential⁴⁴ for transition metal atoms and the 6-31++G(d,p) basis set⁴⁵ for all other atoms was used. No solvent corrections were used. Energetic minima were confirmed with a subsequent frequency calculation that did not return imaginary frequency vibrations $< -10\text{ cm}^{-1}$.

Synthesis of 2,3-dimethoxy-1,4-benzenediboronic acid bis(pinacol) ester. Conditions were optimized from a previously published procedure.³⁰ An oven-dried 1 L Schlenk tube with Teflon screw stopper was cooled under N_2 . 1,2-dimethoxybenzene (10.0 mL, 78.5 mmol, 1 equiv) was added and degassed under vacuum for 30 min. Dried diethyl ether (500 mL) and dried tetramethylethylenediamine (31 mL, 207 mmol, 2.6 equiv) was added via cannula transfer. The mixture was cooled to $0\text{ }^\circ\text{C}$, and *n*-BuLi solution (100 mL, 2.5 M in hexane, 250 mmol, 3.2 equiv) was added via cannula

transfer. The Schlenk tube was sealed and heated to 40 °C for 4 h before being cooled to 0 °C. Trimethylborate (29 mL, 260 mmol, 3.3 equiv) was added, and the reaction mixture warmed to room temperature while stirring for 11 h. The reaction was chilled to 0 °C and aqueous HCl solution (250 mL, 6 M) was very slowly added with the aid of an addition funnel, and the mixture was stirred at room temperature for 1 h. The organic layer was separated, and the aqueous layer was extracted with diethyl ether three times. The combined organic layer was dried over magnesium sulfate, and volatiles were removed via rotary evaporation, leaving an off-white powder. This crude boronic acid was dissolved in toluene (60 mL), and pinacol (19.0 g, 161 mmol, 2 equiv) was added. The reaction mixture was refluxed with a Dean-Stark trap for 4 h. After the reaction was cooled to room temperature, volatiles were removed via rotary evaporation and the residue was purified by recrystallization from boiling hexanes to give white crystals (15.3 g, 50%), which displayed a ¹H NMR spectrum matching that previously reported in literature.³⁰ ¹H NMR (300 MHz, *d*₆-acetone) δ: 7.31 (s, 2H, aryl-*H*), 3.80 (s, 6H, OCH₃), 1.34 (s, 24H, C(CH₃)₂) ppm.

Synthesis of 1,4-bis(2-bromophenyl)-2,3-dimethoxybenzene. Suzuki coupling conditions were adapted from a previously published procedure.⁴⁶ 2,3-Dimethoxy-1,4-benzenediboronic acid bis(pinacol) ester (15.3 g, 39.2 mmol, 1 equiv), K₂CO₃ (27.1 g, 196.1 mmol, 5 equiv), toluene (335 mL), H₂O (205 mL), EtOH (205 mL) were combined in a 500 mL Schlenk tube with screw-in Teflon stopper. The mixture was degassed by 10 exposures to static vacuum followed by 2 exposures to dynamic vacuum (~15 mTorr), and 2-bromoiodobenzene (10.6 mL, 82.4 mmol, 2.1 equiv) and Pd(PPh₃)₄ (1.36 g, 0.12 mmol, 0.03 equiv) were added with a counterflow of N₂. The Schlenk tube was sealed and placed in an oil bath and heated to 75 °C. After

stirring for 12 h, the mixture was allowed to cool to room temperature and water was added. The aqueous and organic layers were separated, and the aqueous layer was extracted with dichloromethane five more times. The combined organic fractions were washed with brine and dried over MgSO_4 , and volatiles were removed via rotary evaporation. The residue was heated in methanol to reflux and filtered through a short silica gel plug while hot, filtering off insoluble phosphorous-containing impurities. The filtrate was chilled in a $-15\text{ }^\circ\text{C}$ freezer to induce recrystallization from hot methanol to give white crystals. The mother liquor was concentrated with a rotavap until white precipitate crashed out of solution. The white crystals and precipitate were combined and found to be pure by NMR (11.0 g, 63%). ^1H NMR (300 MHz, CDCl_3) δ : 7.70 (d, $J = 8.0$ Hz, 2H, aryl-*H*), 7.39 (d, $J = 5.5$ Hz, 4H, aryl-*H*), 7.25 (m, 2H, aryl-*H*), 6.99 (s, 2H, central aryl-*H*), 3.70 (s, 6H, OCH_3) ppm. ^{13}C NMR (75 MHz, CDCl_3) δ : 150.58, 139.44, 135.88, 132.74, 131.56, 129.07, 127.10, 125.33, 123.92, 60.97 ppm.

Synthesis of 1,4-di(2-bromophenyl)-2,3-dihydroxybenzene. In a Schlenk flask under N_2 counterflow, 1,4-di(2-bromophenyl)-2,3-dimethoxybenzene (6.305 g, 14.07 mmol) was dissolved in minimal benchtop DCM with stirring. The flask was fitted with a septum and chilled in a dry ice/acetone bath. BBr_3 (3.4 mL neat, 35.17 mmol) was added to the flask dropwise via syringe over 5 min. The reaction was allowed to warm to room temperature over 12 h. The reaction was then quenched by slow dropwise addition of H_2O until bubbling ceased. The reaction mixture was further diluted with H_2O until no more solids dissolved. Organics were extracted with DCM, dried with MgSO_4 , filtered, and concentrated via rotary evaporation to product as a white powder (~95% yield), which was utilized in the next step without further purification. ^1H NMR (400 MHz, CDCl_3) δ : 7.75 (app d, 2H), 7.46 (app s, 2H), 7.44

(app s, 2H), 7.34-7.27 (m, 2H), 6.84 (s, 2H, central aryl-*H*), 5.34 (br s, 2H, *OH*).¹³C{¹H} NMR (101 MHz, CDCl₃) δ: 140.9 (s), 138.1 (s), 133.2 (s), 132.1 (s), 129.7 (s), 127.9 (s), 127.7 (s), 124.0 (s), 121.9 (s).

Synthesis of 1,4-di(2-bromophenyl)-2,3-di(methoxymethylether)benzene.

A Schlenk flask was charged with 1,4-di(2-bromophenyl)-2,3-dihydroxybenzene (assuming 100% yield from previous step, 14.07 mmol) dissolved in minimal dried DCM (~42 mL). Diisopropylethylamine (7.36 mL, 42.21 mmol) was added to the flask under N₂ counterflow. The flask was then chilled in an ice/water bath, and a 2.1 M solution of chloromethyl methyl ether in toluene (20.1 mL, 42.21 mmol)⁴⁷ was added dropwise, evolving a white vapor, which dissipated after 10 min. The reaction was allowed to stir for 12 h, then quenched by addition of H₂O and extracted with DCM. The combined organic extracts were washed with saturated NaHCO₃, dried with MgSO₄, and concentrated under rotary evaporation to yield a white powder. Trituration and filtration with cold MeOH yielded spectroscopically pure product (6.283 g, 88% yield over the last two steps). ¹H NMR (300 MHz, CDCl₃) δ: 7.68 (app d, 2H), 7.51-7.34 (m, 4H), 7.25-7.19 (m, 2H), 7.07 (s, 2H, central aryl-*H*), 5.01-4.85 (br app d, 4H, CH₂OCH₃), 2.93 (s, 6H, CH₂OCH₃).¹³C{¹H} NMR (75 MHz, CDCl₃) δ: 147.8 (s), 139.4 (s), 136.6 (s), 132.6 (s), 132.3 (s), 129.0 (s), 127.0 (s), 126.0 (s), 124.2 (s), 99.2 (s), 56.7 (s).

Synthesis of 1,4-bis(2-(diisopropylphosphino)phenyl)-2,3-di(methoxymethylether)benzene. In an N₂-atmosphere glovebox, a round-bottom flask was charged with 1,4-di(2-bromophenyl)-2,3-di(methoxymethylether)benzene (6.283 g, 12.36 mmol), THF (90 mL), and a stir bar. The reaction mixture was placed in an LN₂-chilled cold well until frozen and then placed back at room temperature. While

the mixture was thawing with slow stirring, a 1.7 M solution of ^tBuLi (29.8 mL, 50.69 mmol) in pentanes was added dropwise. A light yellow color appeared in seconds, and as the reaction was allowed to stir for 30 min at room temperature, a darker orange color evolved. The reaction mixture was once again frozen in a LN₂-chilled cold well and placed back at room temperature. While the mixture was thawing with slow stirring, chlorodiisopropylphosphine (4.13 mL, 25.96 mmol) was added to the reaction mixture, inducing a light yellow color. After stirring for 1h, volatiles were removed under vacuum. The solids were suspended in a dilute aqueous solution of NaHCO₃, and organics were extracted with DCM. The organics were dried with MgSO₄, filtered, and concentrated under vacuum to a white powder. By NMR spectroscopy, the major species (ca. 90%) was the desired product, and the crude was carried forward in the synthesis without further purification. Impurities in the NMR may simply be rotamers that could funnel to the same product after the next step. ¹H NMR (300 MHz, CDCl₃) δ: 7.58 – 7.50 (m, 2H, aryl-*H*), 7.47 – 7.29 (m, 6H, aryl-*H*), 6.90 (s, 2H, central aryl-*H*), 4.94 (d, *J* = 5.7 Hz, 2H, CH₂OCH₃), 4.81 (d, *J* = 5.7 Hz, 2H, CH₂OCH₃), 2.87 (s, 6H, CH₂OCH₃), 2.17 (m, 2H, CH(CH₃)₂), 1.85 (m, 2H, CH(CH₃)₂), 1.16 – 0.95 (m, 12H, CH(CH₃)₂), 0.91 – 0.75 (m, 12H, CH(CH₃)₂). ³¹P{¹H} (121 MHz, CDCl₃) δ: -1.0 (s). ¹³C{¹H} (75 MHz, CDCl₃) δ: 147.2 (s), 146.8 (d, *J*_{PC} = 31.2 Hz), 137.4 (d, *J*_{PC} = 6.3 Hz), 136.6 (d, *J*_{PC} = 21.6 Hz), 132.1 (d, *J*_{PC} = 3.5 Hz), 130.7 (d, *J*_{PC} = 5.3 Hz), 128.2 (s), 126.6 (s), 125.6 (s), 98.6 (s), 56.7 (s), 25.6 (d, *J*_{PC} = 15.7 Hz), 23.3 (d, *J*_{PC} = 14.4 Hz), 20.7-20.0 (m), 18.5 (d, *J*_{PC} = 5.9 Hz).

Synthesis of 1,4-bis(2-(diisopropylphosphino)phenyl)-2,3-dihydroxybenzene (48). A 1:9 (v/v) mixture of concentrated HCl (~12 M) and MeOH was dynamically degassed under vacuum. Then 41.2 mL of this solution (~49.4 mmol

HCl) was then added to a stirring solution of 1,4-bis(2-(diisopropylphosphino)phenyl)-2,3-di(methoxymethylether)benzene (12.36 mmol assuming full conversion in the previous step) in 90 mL DCM. The reaction was tracked with ^{31}P NMR, and within an hour, one major species was apparent. After 2 h, the reaction was quenched with excess NaHCO_3 . The homogeneous organic phase was extracted with DCM (3 x 130 mL), washed with saturated $\text{K}_2\text{CO}_3/\text{H}_2\text{O}$ to yield an organic phase with fine white precipitate, separated, and then washed with saturated $\text{NH}_4\text{Cl}/\text{H}_2\text{O}$, re-homogenizing the organic phase. The combined organics were dried with MgSO_4 , filtered, and concentrated under vacuum while heated in a 50 °C oil bath for 6 h to ensure removal of water. The crude was washed with hexanes, in which the major product was poorly soluble. The remaining crude was washed with toluene, yielding the product as a white precipitate (4.376 g, 72% yield over last two steps). The product seemed to be most soluble in Et_2O and THF and only sparingly soluble in benzene and MeCN. NMR spectra recorded in C_6D_6 exhibited poor signal-to-noise due to solubility limitations. ^1H NMR (300 MHz, CD_2Cl_2) δ : 7.57 (m, 2H), 7.48-7.34 (m, 6H), 6.77 (s, 2H, central aryl-H), 6.41 (br s, 2H, OH), 2.30 (m, 2H, $\text{CH}(\text{CH}_3)_2$), 1.99 (m, 2H, $\text{CH}(\text{CH}_3)_2$), 1.49-0.69 (m, 24H, $\text{CH}(\text{CH}_3)_2$). $^{31}\text{P}\{^1\text{H}\}$ (121 MHz, CD_2Cl_2) δ : 1.90 (br s).

Synthesis of 49. $\text{Ni}(\text{COD})_2$ (30.0, 0.109 mmol) was added to **48** (54.0 mg, 0.109 mmol) with the assistance of THF (3 mL). The reaction mixture became dark red in 10 minutes. The reaction progress was tracked by ^{31}P NMR and determined to be complete after 24 h. Volatiles were removed under vacuum. The remaining crude was washed sequentially with hexanes, Et_2O , and toluene. The toluene fraction was isolated by filtration and layered underneath hexanes in a -20 °C freezer to yield dark red XRD-quality rod-like crystals (47.1 mg, 78% yield) (Spectra included in Appendix C).

Synthesis of 50. Ni(COD)₂ (69.7 mg, 0.254 mmol) was added to **48** (125.4 mg, 0.254 mmol) with the aid of THF (5 mL). The reaction was stirred for 10 minutes, and then NiCl₂(dme) (55.7 mg, 0.254 mmol) was added with the aid of minimal THF. After 5 h of stirring, the dark green precipitate was collected by filtration, washed with THF, and redissolved in DCM. The DCM solution was layered under hexanes and chilled in a -20 °C freezer to yield turquoise crystals (148.1 mg, 85% yield) (Spectra included in Appendix C).

Synthesis of 51. To **50** (14.2 mg, 0.0208 mmol) in minimal MeCN in a J. Young Tube was added Et₃N (2.9 mL, 0.0208 mmol). A ³¹P NMR was recorded, and then more Et₃N (9 mL, 0.0624 mmol) was added to the reaction mixture. Brownish precipitate formed on the NMR tube walls. The precipitate was dissolved upon addition of minimal THF, and the reaction mixture was concentrated under vacuum. The resulting crude was washed sequentially with hexanes, Et₂O, and benzene. The benzene fraction was then subjected to vapor diffusion of Et₂O to yield brown/green XRD-quality crystals (5.3 mg, 47% yield based on total available nickel in reaction) (Spectra included in Appendix C).

Synthesis of 52. To **48** (30.0 mg, 0.0607 mmol) in 3 mL THF, was added dropwise PdCl₂(COD) (17.3 mg, 0.0607 mmol) suspended in minimal THF. The reaction mixture immediately turned dark red and seemingly homogeneous. However, after two minutes, orange precipitate begins to form. After 30 minutes, the solid was isolated by filtration, washed with THF, and dissolved with DCM. XRD quality crystals were grown in DCM at room temperature the course of 3 days. No isolated yield has been determined for this reaction, but by NMR spectroscopy, this reaction has good conversion and yield (Spectra included in Appendix C).

Synthesis of 55^{CF3Ph}. A Schlenk tube was loaded with catechol **48** (1.53 g, 3.09 mmol), 4-trifluoromethylphenylboronic acid (0.588 g, 3.09 mmol), MgSO₄ (1 g) and deoxygenated m-xylene (10 mL). The tube was sealed with a Teflon screw cap and stirred at 120 °C for 3 h. Within the first 15 minutes, the white solids were stuck the reaction flask walls, indicating generation of water and absorption by MgSO₄. After heating, the solution was cooled to room temperature and volatiles were removed with vacuum. The solid product was then further dried under vacuum while heated to 100 °C for 1 h. The solids were washed sequentially with hexanes, Et₂O, and benzene through Celite. The white solids isolated by concentration of the benzene fraction were clean by ¹H NMR spectroscopy (900 mg, 45% yield) (Spectra included in Appendix C).

Synthesis of cobalt complexes 56 and 57. A Schlenk tube was charged with **55^{CF3Ph}** (10.2 mg, 0.016 mmol), Co₂(CO)₈ (5.4 mg, 0.016 mmol), and 1 mL m-xylene. The reaction mixture was heated at 130 °C for 20 h. The crude was sequentially washed with hexanes, Et₂O, benzene, and THF. The benzene fraction was the largest fraction (6.9 mg). It was analyzed by NMR spectroscopy, and crystals grew in the NMR tube overnight (C₆D₆) (Spectra included in Appendix C).

Synthesis of rhenium chloride complexes (two isomers out of 58, 59, and 60). A Schlenk tube was charged with **55^{CF3Ph}** (147 mg, 0.23 mmol), Re(CO)₅Cl (82 mg, 0.23 mmol), and 20 mL toluene. The reaction vessel was placed in a 120 °C oil bath such that while open to an N₂ bubbler, toluene could reflux and condense on the sides of the reaction vessel. Heating while open to an N₂ bubbler was found to greatly accelerate the reaction vs. decarbonylation in a sealed reaction flask. The reaction was complete by 5 h, as determined by consumption of starting material and appearance of two singlets in the ³¹P NMR spectrum: 12.5 and 10.0 ppm. The solvent was removed

under vacuum. The crude was washed with hexanes to remove any trace xylenes. Then the product was filtered through a Celite plug using DCM. Upon removal of DCM, a bright yellow solid was obtained (196 mg, 92% yield) (Spectra included in Appendix C).

Chloride abstraction from 58-60 to yield tricarbonyl 61. AgOTf (2.9 mg, 0.011 mmol) was added to a solution of 58-60 (10.3 mg, 0.011 mmol) in THF (3 mL). White precipitate was noticeable in minutes. After 20 minutes, the reaction was filtered through Celite. This product, presumably a dicarbonyl triflate, appeared to be one isomer by ^1H and ^{31}P NMR, but was not stable in DCM, yielding DCM-insoluble tan powder over time (Spectra included in Appendix C). To avoid this problem and consolidate reaction set up time, halide abstraction was set up, degassed, and repressurized with 1 atm CO. Run on a larger scale (168 mg, 0.181 mmol of 58-60), this procedure yielded 201 mg of light yellow material that initially dissolved in benzene but, upon removal of volatiles under vacuum, was not resolvable in benzene. This presumed tricarbonyl triflate species polymerizes THF and could only be handled in DCM or PhCl as long-term solvents (Spectra included in Appendix C).

Synthesis of dimethylsilyl-protected rhenium tricarbonyl cation 62. A Schlenk tube was charged with **54** (64 mg, 0.116 mmol) and $\text{Re}(\text{CO})_5\text{OTf}$ (55 mg, 0.116 mmol) with 2 mL m-xylene. The tube was sealed with a Teflon screw cap and heated at 130 C for °C for 30 h. Lots of yellow insolubles were apparent in the reaction mixture. Solvents were removed under vacuum, and the resultant solid was washed sequentially with hexanes, benzene, and DCM. The DCM fraction was intense yellow and, upon concentration to a solid, weighed 88 mg (78% yield). This solid was not very resolvable in DCM (Spectra included in Appendix C).

Deprotection of 62 to release catechol 63. A septum-screw cap NMR tube was charged with **62** (16.6 mg, 0.017 mmol) and CD₂Cl₂ (~0.5 mL). A degassed and nitrogen-sparged source of MeOH and microsyringe were used to add 6 μL of MeOH to the reaction mixture. This may have released free catechol, but ¹H NMR spectra were inconclusive, so degassed DI water (6 μL) was also added to the reaction mixture. The reaction was confirmed to be complete by ¹H NMR. The NMR tube was then brought into a water-tolerant glovebox. There was no visible loss of CD₂Cl₂ through the grease-patched septum piercing while the tube was in the vacuum antechamber (~1 h). Excess MgSO₄ was added directly into the NMR tube to bind any water. The reaction was then filtered through a pipet filter, and volatiles were pumped off under vacuum. The solids were washed with benzene to remove trace methyl silyl species (Spectra included in Appendix C).

Attachment of ScTp* moiety to 63 to form 64. An NMR tube was loaded with **63** (9.5 mg, 0.0103 mmol) in minimal CD₂Cl₂. Then 29 mL of a 10 volume % solution Et₃N in CD₂Cl₂ was added to tube. The dark brown color of the solution of **63** turned yellow in seconds. Then Tp*ScCl₂(THF) was added to the reaction mixture. The reaction crude looked messy but seemed to contain one major product, **64**. ¹H NMR (300 MHz, C₆D₆) δ: 8.69 (app d, 2H, aryl-*H*), 7.35 (m, 2H, aryl-*H*), 7.24 (app t, 2H, aryl-*H*), 7.07 (app t, 2H, aryl-*H*), 5.56 (s, 2H, anti-pyrazolyl-*H*), 5.50 (s, 1H, syn-pyrazolyl-*H*), 5.44 (t, *J*_{PH} = 6.3 Hz, 2H, central aryl-*H*), 3.11 (s, 3H, syn-pyrazolyl-CH₃), 2.75 (s, 6H, anti-pyrazolyl-CH₃), 2.33 (s, 3H, syn-pyrazolyl-CH₃), 2.15 (m, 6H, anti-pyrazolyl-CH₃), 1.20 (m, 6H, CH(CH₃)₂), 1.04 (m, 6H, CH(CH₃)₂), 0.91 (m, 6H, CH(CH₃)₂), 0.78 (m, 6H, CH(CH₃)₂). (virtual septets typically observed for isopropyl methine protons are not visible).

REFERENCES

- (1) Jeoung, J.-H.; Dobbek, H. *Science* **2007**, *318*, 1461.
- (2) Dobbek, H.; Gremer, L.; Kiefersauer, R.; Huber, R.; Meyer, O. *Proc. Natl. Acad. Sci. USA* **2002**, *99*, 15971.
- (3) Can, M.; Armstrong, F. A.; Ragsdale, S. W. *Chem. Rev.* **2014**.
- (4) Newsome, D. S. *Catalysis Reviews* **1980**, *21*, 275.
- (5) Gottesfeld, S.; Pafford, J. J. *Electrochem. Soc.* **1988**, *135*, 2651.
- (6) Kwak, J. H.; Kovarik, L.; Szanyi, J. *ACS Catalysis* **2013**, *3*, 2094.
- (7) Zugic, B.; Zhang, S.; Bell, D. C.; Tao, F.; Flytzani-Stephanopoulos, M. *J. Am. Chem. Soc.* **2014**.
- (8) Laitar, D. S.; Müller, P.; Sadighi, J. P. *J. Am. Chem. Soc.* **2005**, *127*, 17196.
- (9) Krogman, J. P.; Foxman, B. M.; Thomas, C. M. *J. Am. Chem. Soc.* **2011**, *133*, 14582.
- (10) Smieja, J. M.; Benson, E. E.; Kumar, B.; Grice, K. A.; Seu, C. S.; Miller, A. J. M.; Mayer, J. M.; Kubiak, C. P. *Proc. Natl. Acad. Sci. USA* **2012**, *109*, 15646.
- (11) González-Sebastián, L.; Flores-Alamo, M.; García, J. J. *Organometallics* **2013**, *32*, 7186.
- (12) Lionetti, D.; Day, M. W.; Agapie, T. *Chemical Science* **2013**, *4*, 785.
- (13) Kanady, J. S.; Tsui, E. Y.; Day, M. W.; Agapie, T. *Science* **2011**, *333*, 733.
- (14) Tsui, E. Y.; Kanady, J. S.; Agapie, T. *Inorg. Chem.* **2013**, *52*, 13833.
- (15) Costas, M.; Mehn, M. P.; Jensen, M. P.; Que, L. *Chem. Rev.* **2004**, *104*, 939.
- (16) Raymond, K. N.; Carrano, C. J. *Acc. Chem. Res.* **1979**, *12*, 183.
- (17) Oh, M.; Carpenter, G. B.; Sweigart, D. A. *Organometallics* **2003**, *22*, 1437.
- (18) Moussa, J.; Rager, M. N.; Chamoreau, L. M.; Ricard, L.; Amouri, H. *Organometallics* **2009**, *28*, 397.
- (19) Damas, A. I.; Ventura, B.; Axet, M. R.; Esposti, A. D.; Chamoreau, L.-M.; Barbieri, A.; Amouri, H. *Inorg. Chem.* **2010**, *49*, 10762.
- (20) Blasberg, F.; Bolte, M.; Lerner, H.-W.; Wagner, M. *Organometallics* **2012**, *31*, 3213.

- (21) Asato, E.; Kyan, A.; Madanbashi, T.; Tamura, T.; Tadokoro, M.; Mizuno, M. *Chem. Commun.* **2010**, *46*, 1227.
- (22) Takemoto, S.; Ogura, S.-i.; Kamikawa, K.; Matsuzaka, H. *Inorg. Chim. Acta* **2006**, *359*, 912.
- (23) Paw, W.; Keister, J. B.; Lake, C. H.; Churchill, M. R. *Organometallics* **1995**, *14*, 767.
- (24) Bauer, G.; Englert, C.; Nieger, M.; Gudat, D. *Inorg. Chim. Acta* **2011**, *374*, 240.
- (25) Bohle, D. S.; Carron, K. T.; Christensen, A. N.; Goodson, P. A.; Powell, A. K. *Organometallics* **1994**, *13*, 1355.
- (26) Bohle, D. S.; Christensen, A. N.; Goodson, P. A. *Inorg. Chem.* **1993**, *32*, 4173.
- (27) Fox, G. A.; Pierpont, C. G. *J. Chem. Soc., Chem. Commun.* **1988**, 806.
- (28) Wang, W.-H.; Muckerman, J. T.; Fujita, E.; Himeda, Y. *ACS Catalysis* **2013**, *3*, 856.
- (29) Hull, J. F.; Himeda, Y.; Wang, W.-H.; Hashiguchi, B.; Periana, R.; Szalda, D. J.; Muckerman, J. T.; Fujita, E. *Nat Chem* **2012**, *4*, 383.
- (30) Ikeda, C.; Sakamoto, N.; Nabeshima, T. *Org. Lett.* **2008**, *10*, 4601.
- (31) Lin, S.; Day, M. W.; Agapie, T. *J. Am. Chem. Soc.* **2011**, *133*, 3828.
- (32) Velian, A. Undergraduate Thesis, California Institute of Technology, 2009.
- (33) Miller, A. J. M.; Labinger, J. A.; Bercaw, J. E. *J. Am. Chem. Soc.* **2008**, *130*, 11874.
- (34) Miller, A. J. M.; Labinger, J. A.; Bercaw, J. E. *Organometallics* **2011**, *30*, 4308.
- (35) Miller, A. J. M.; Labinger, J. A.; Bercaw, J. E. *Organometallics* **2010**, *29*, 4499.
- (36) Pangborn, A. B.; Giardello, M. A.; Grubbs, R. H.; Rosen, R. K.; Timmers, F. J. *Organometallics* **1996**, *15*, 1518.
- (37) Fulmer, G. R.; Miller, A. J. M.; Sherden, N. H.; Gottlieb, H. E.; Nudelman, A.; Stoltz, B. M.; Bercaw, J. E.; Goldberg, K. I. *Organometallics* **2010**, *29*, 2176.
- (38) Gaussian 09, Revision C.01, Frisch, M. J.; Trucks, G. W.; Schlegel, H. B.; Scuseria, G. E.; Robb, M. A.; Cheeseman, J. R.; Scalmani, G.; Barone, V.; Mennucci, B.; Petersson, G. A.; Nakatsuji, H.; Caricato, M.; Li, X.; Hratchian, H. P.; Izmaylov, A. F.; Bloino, J.; Zheng, G.; Sonnenberg, J. L.; Hada, M.; Ehara, M.; Toyota, K.; Fukuda, R.; Hasegawa, J.; Ishida, M.; Nakajima, T.; Honda, Y.; Kitao, O.; Nakai, H.; Vreven, T.; Montgomery, Jr., J. A.; Peralta, J. E.; Ogliaro, F.; Bearpark, M.; Heyd, J. J.; Brothers, E.; Kudin, K. N.; Staroverov, V. N.; Kobayashi, R.; Normand, J.; Raghavachari, K.; Rendell, A.; Burant, J. C.;

- Iyengar, S. S.; Tomasi, J.; Cossi, M.; Rega, N.; Millam, J. M.; Klene, M.; Knox, J. E.; Cross, J. B.; Bakken, V.; Adamo, C.; Jaramillo, J.; Gomperts, R.; Stratmann, R. E.; Yazyev, O.; Austin, A. J.; Cammi, R.; Pomelli, C.; Ochterski, J. W.; Martin, R. L.; Morokuma, K.; Zakrzewski, V. G.; Voth, G. A.; Salvador, P.; Dannenberg, J. J.; Dapprich, S.; Daniels, A. D.; Farkas, Ö.; Foresman, J. B.; Ortiz, J. V.; Cioslowski, J.; Fox, D. J. Gaussian, Inc., Wallingford CT, 2009.
- (39) Tao, J.; Perdew, J. P.; Staroverov, V. N.; Scuseria, G. E. *Phys. Rev. Lett.* **2003**, *91*, 146401.
- (40) Staroverov, V. N.; Scuseria, G. E.; Tao, J.; Perdew, J. P. *The Journal of Chemical Physics* **2003**, *119*, 12129.
- (41) Jensen, K. P. *Inorg. Chem.* **2008**, *47*, 10357.
- (42) Bühl, M.; Kabrede, H. *Journal of Chemical Theory and Computation* **2006**, *2*, 1282.
- (43) Waller, M. P.; Braun, H.; Hojdis, N.; Bühl, M. *Journal of Chemical Theory and Computation* **2007**, *3*, 2234.
- (44) Hay, P. J.; Wadt, W. R. *The Journal of Chemical Physics* **1985**, *82*, 270.
- (45) Ditchfield, R.; Hehre, W. J.; Pople, J. A. *The Journal of Chemical Physics* **1971**, *54*, 724.
- (46) Albrecht, M.; Schneider, M. *Synthesis* **2000**, *2000*, 1557.
- (47) Berliner, M. A.; Belecki, K. *J. Org. Chem.* **2005**, *70*, 9618.

APPENDIX B

NOVEL COORDINATION COMPOUNDS OF PARA-TERPHENYL DIPHOSPHINES

ABSTRACT

In developing the extensive chemistry discussed in the previous chapters, several unexpected coordination compounds were observed crystallographically. This appendix organizes and highlights these compounds.

INTRODUCTION

In the previous chapters, the *para*-terphenyl diphosphine framework has been shown to stably coordinate one or two metal centers. However, some coordination compounds have eluded reproducible syntheses or were not followed up on. In some cases, crystals of the material were obtained and examined by XRD. This short appendix organizes and highlights some unusual coordination modes that *para*-terphenyl diphosphine metal complexes can adapt.

RESULTS AND DISCUSSION

Monopalladium(II) or monoplatinum(II) complexes of **1** generally have eluded characterization due to irreversible precipitation of compounds from solution over time. One possibility for this observation is the formation of coordination polymers. Metallation of **1** with Pd(MeCN)₄(BF₄)₂ in MeCN yielded a complex reaction mixture, but upon layering under Et₂O, yellow crystals of **66** were obtained. Compound **67**, on the other hand, was isolated fortuitously from the ecomplex reaction mixture of Pd(0) compound **3** and Pd(COD)Cl₂. Concomittant formation of a mirror on the reaction vessel walls was consistent with decomposition of a “Pd(COD)” equivalent. Crystals of monopalladium(II) compounds **66** and **67** have been studied by XRD. As expected for d⁸ metal centers, the metal centers are square planar, four-coordinate (Figure B.1).

Chart B.1. Unexpected Compounds Characterized by XRD

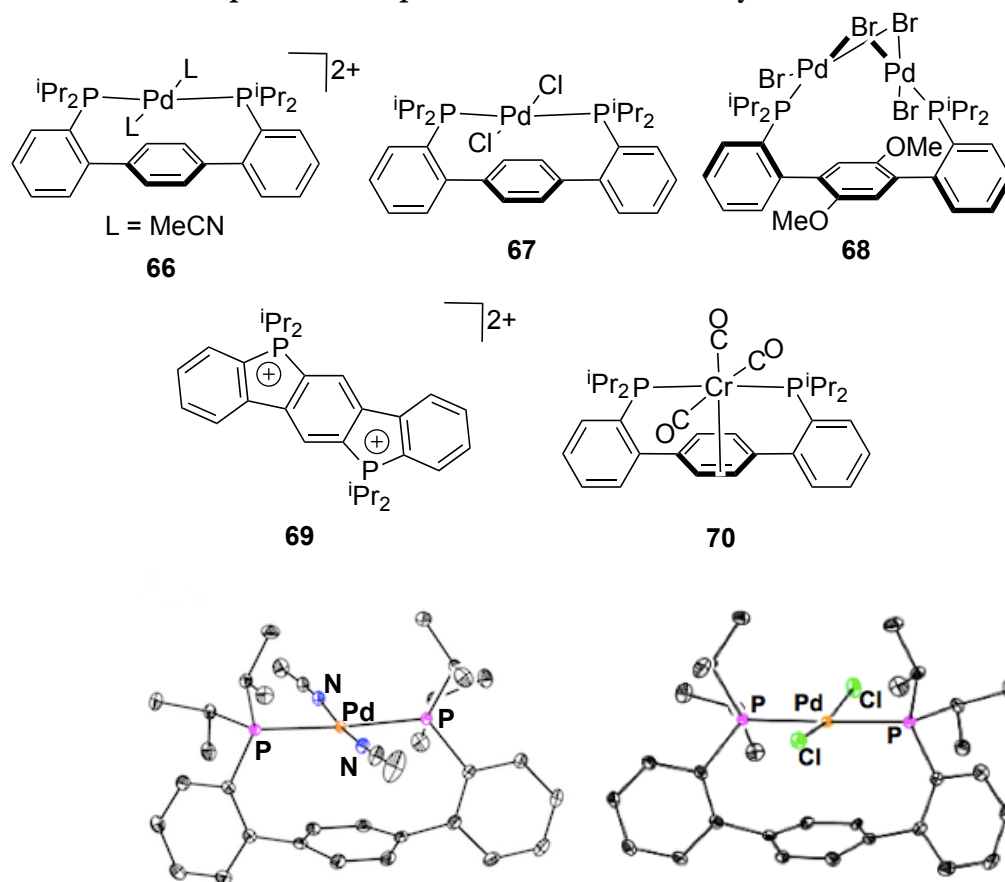


Figure B.1. Preliminary solid-state structures of **66** and **67**. Hydrogen atoms and outer-sphere tetrafluoroborates are not shown.

Relating to dipalladium complexes, a CuBr-contaminated variant ligand with para-dimethoxy-substituted central arene (since isolated cleanly by Kyle Horak via an alternative synthesis) was used for metallation with PdCl₂(COD). In this case, crystals of a dipalladium tetrabromide were characterized (**68**, Figure B.2). This is the only case of a dipalladium(II) complex being characterized on the terphenyl diphosphine framework. Attempting to exchange the capping toluene ligand of **25** with p-benzoquinone, which in theory could also lead to a dipalladium(II) complex with a capping para-catecholate ligand, also led to an unusual complex. A diphosphonium salt showing evidence of two C-H activations and loss of both palladium centers was isolated (**69**).

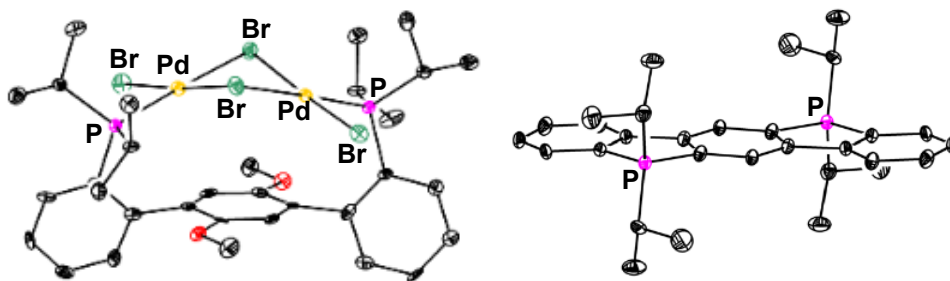


Figure B.2. Preliminary solid-state structures of **68** and **69**. Hydrogen atoms and outer-sphere tetrafluoroborates are not shown.

Finally, **1** has shown rich coordination chemistry for a variety of middle transition metals. Notably missing, however, was a coordination compound of chromium. Reacting chromium tris(acetonitrile) tris(carbonyl) with **1** in refluxing m-xylene for three days led to the formation of tricarbonyl compound **70**, characterized by NMR spectroscopy and preliminary crystallographic data. This is isostructural to a molybdenum compound that is currently being investigated in the Agapie group for small-molecule activation.

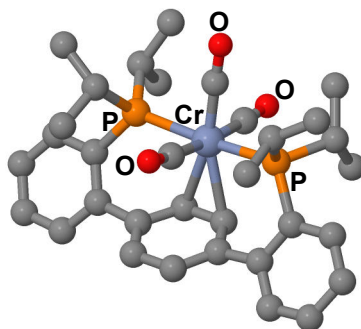


Figure B.3. Preliminary solid-state structure of **70**.

CONCLUSION

A variety of unusual coordination modes of para-terphenyl diphosphines were crystallographically characterized. The structures are shared in this appendix to serve as a reference for future researchers using this ligand motif.

APPENDIX C

NMR SPECTRA

Chapter 2

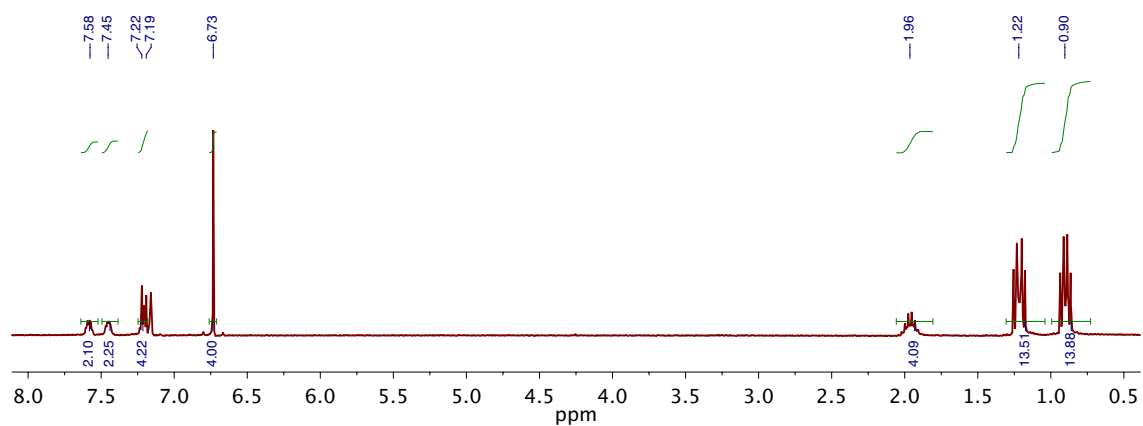
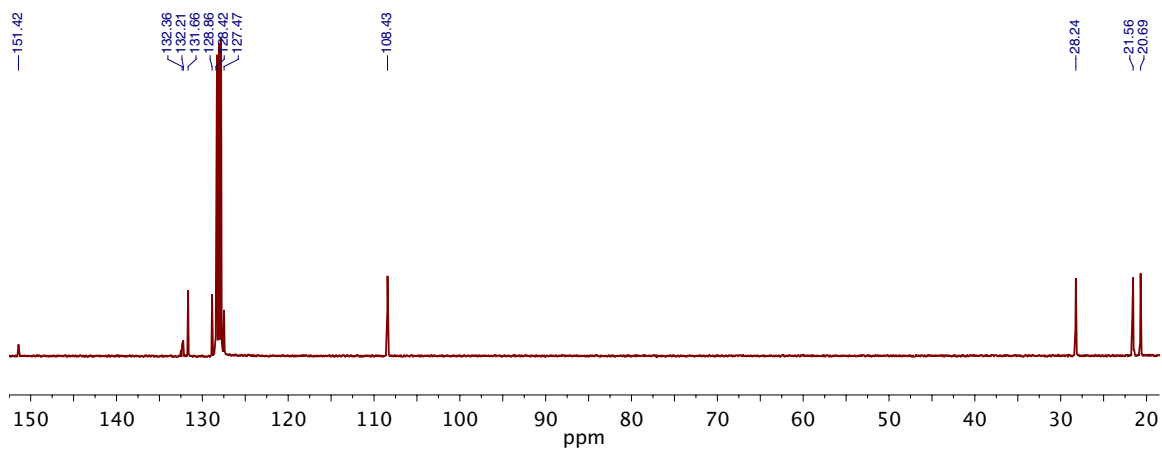


Figure C.1. ^1H NMR spectrum (300 MHz, C_6D_6) of **3**.



$^{13}\text{C}\{^1\text{H}\}$ NMR spectrum (101 MHz, C_6D_6) of **3**

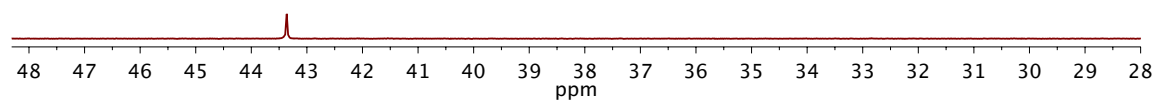


Figure C.2. $^{31}\text{P}\{^1\text{H}\}$ NMR spectrum (121 MHz, C_6D_6) of **3**.

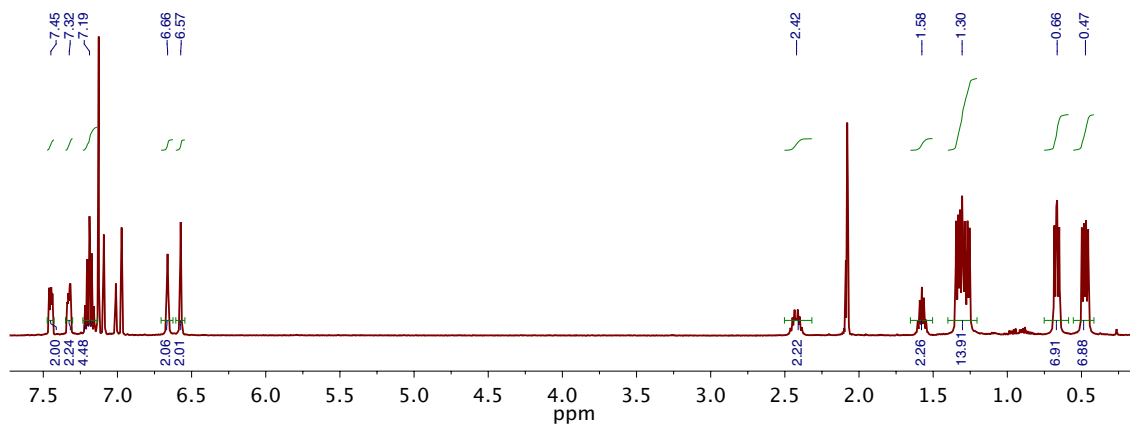


Figure C.3. ^1H NMR spectrum (500 MHz, d_8 -toluene) of 4.

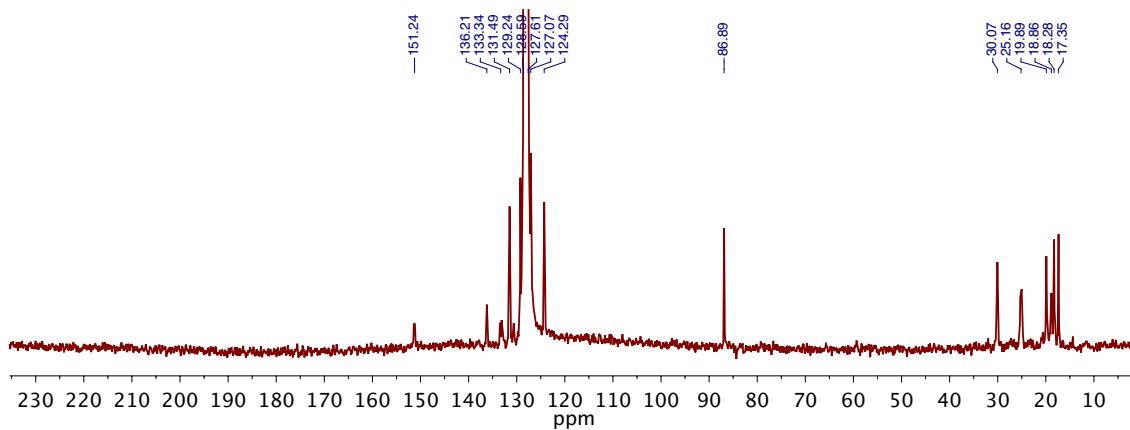


Figure C.4. $^{13}\text{C}\{^1\text{H}\}$ NMR spectrum (75 MHz, C_6D_6) of 4.

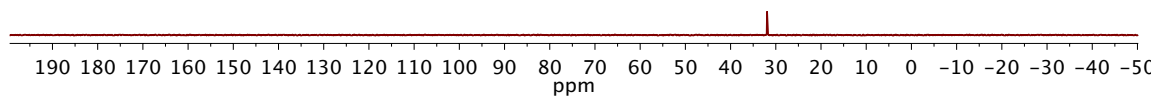


Figure C.5. $^{31}\text{P}\{^1\text{H}\}$ NMR spectrum (121 MHz, C_6D_6) of 4.

SL2080e_H
NiP2 + 1x CNTBu
brown xtals from cold
E122

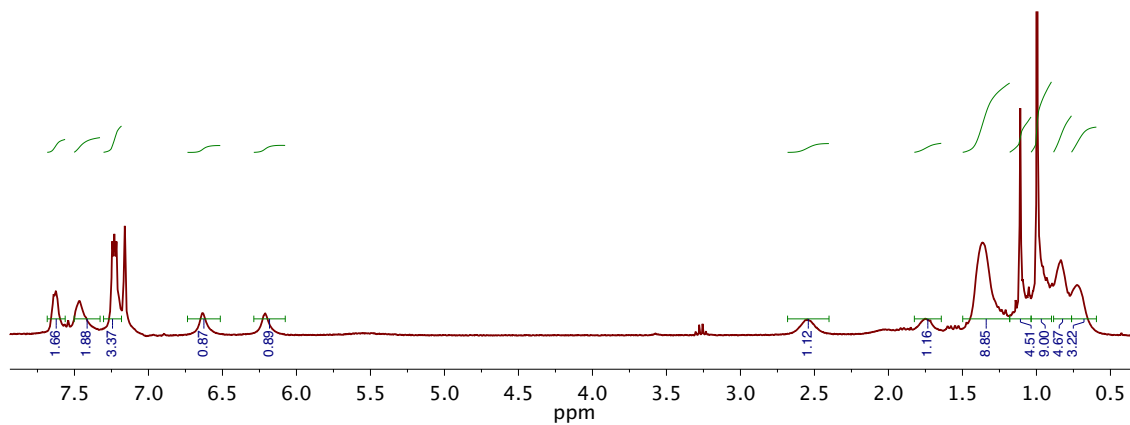


Figure C.6. ^1H NMR spectrum (300 MHz, C_6D_6) of 5.

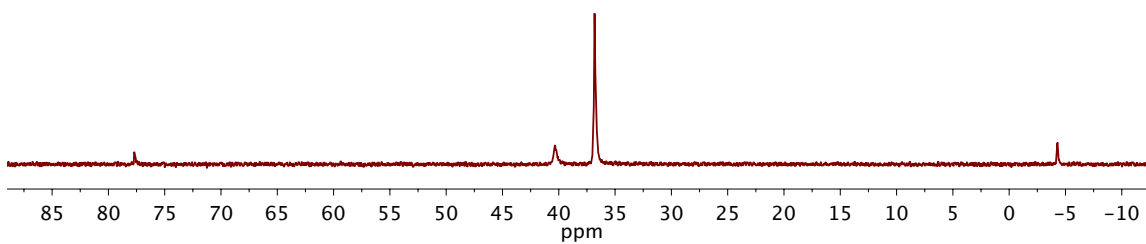


Figure C.7. ^{31}P $\{^1\text{H}\}$ NMR spectrum (121 MHz, C_6D_6) of 5.

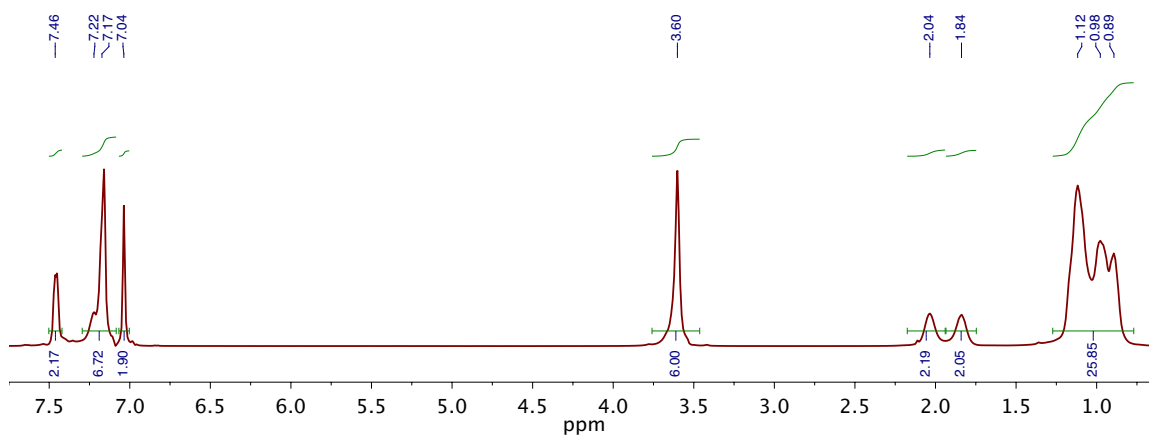


Figure C.8. ^1H NMR spectrum (400 MHz, C_6D_6) of **6**.

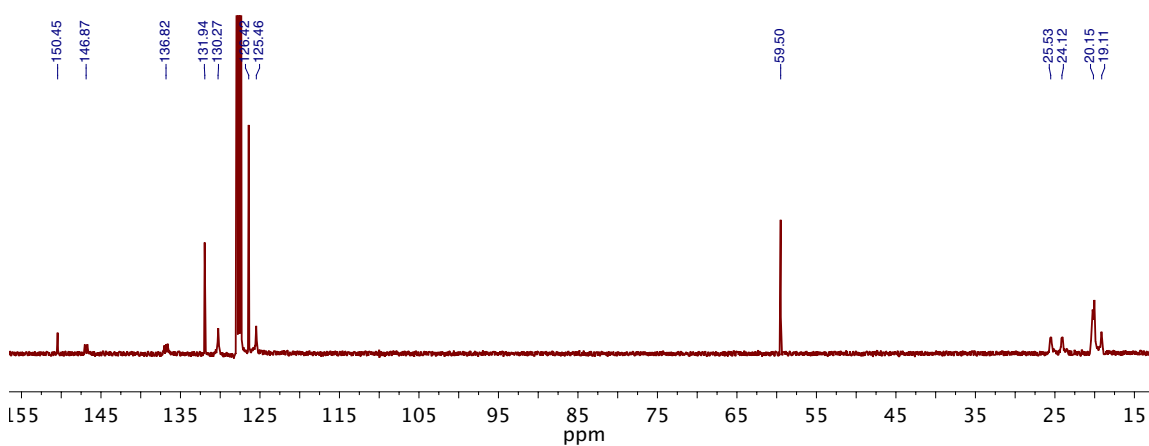


Figure C.9. $^{13}\text{C}\{^1\text{H}\}$ NMR spectrum (101 MHz, C_6D_6) of **6**.

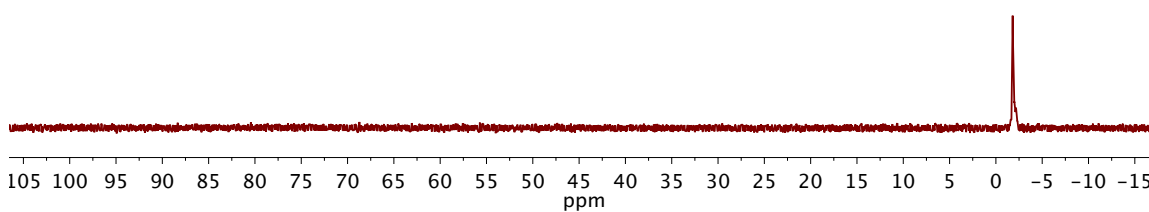


Figure C.10. $^{31}\text{P}\{^1\text{H}\}$ NMR spectrum (121 MHz, C_6D_6) of **6**.

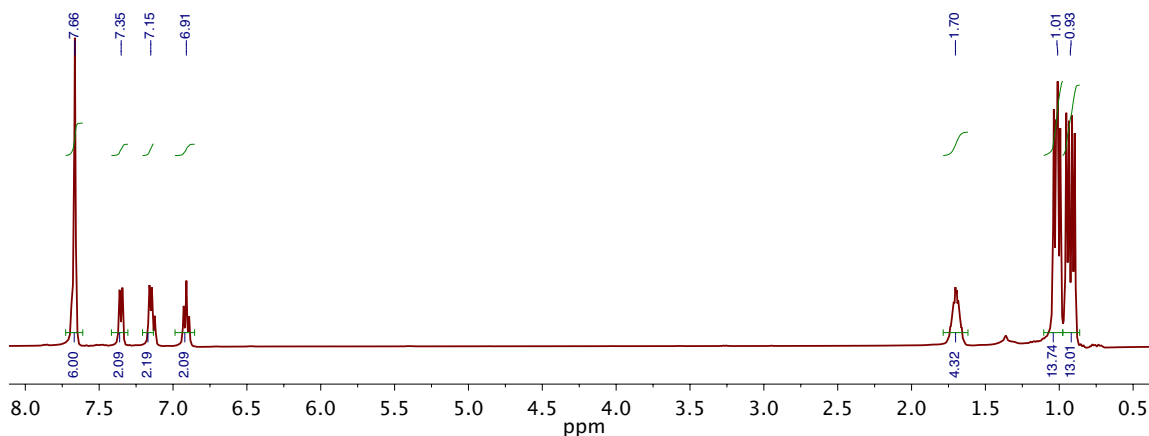


Figure C.11. ^1H NMR spectrum (400 MHz, C_6D_6) of **7** (“POTOP”).

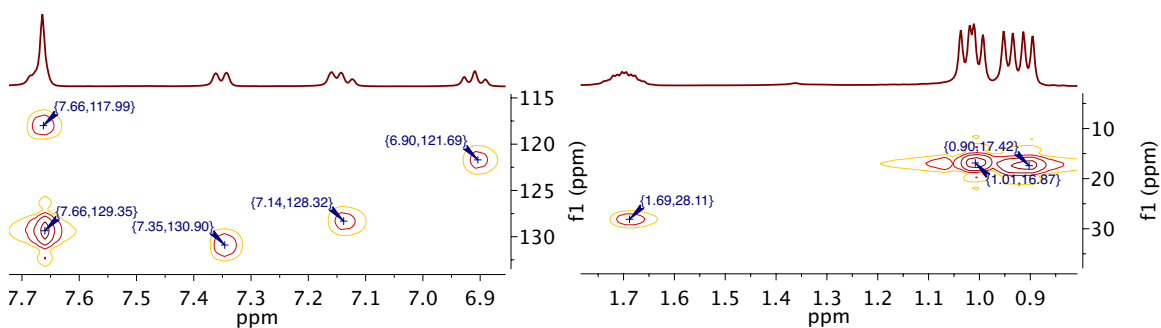


Figure C.12. HSQC NMR spectrum (400 MHz, C_6D_6) of **7**.

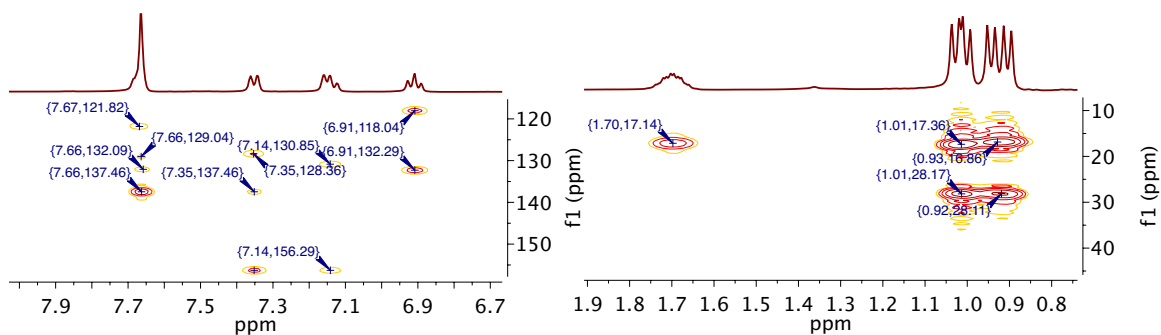


Figure C.13. HMBC NMR spectrum (400 MHz, C_6D_6) of **7**.

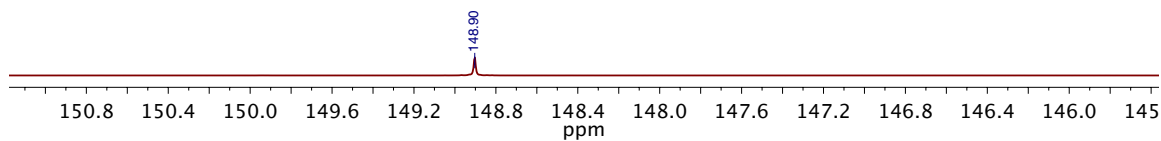


Figure C.14. $^{31}\text{P}\{^1\text{H}\}$ NMR spectrum (121 MHz, C_6D_6) of **7**.

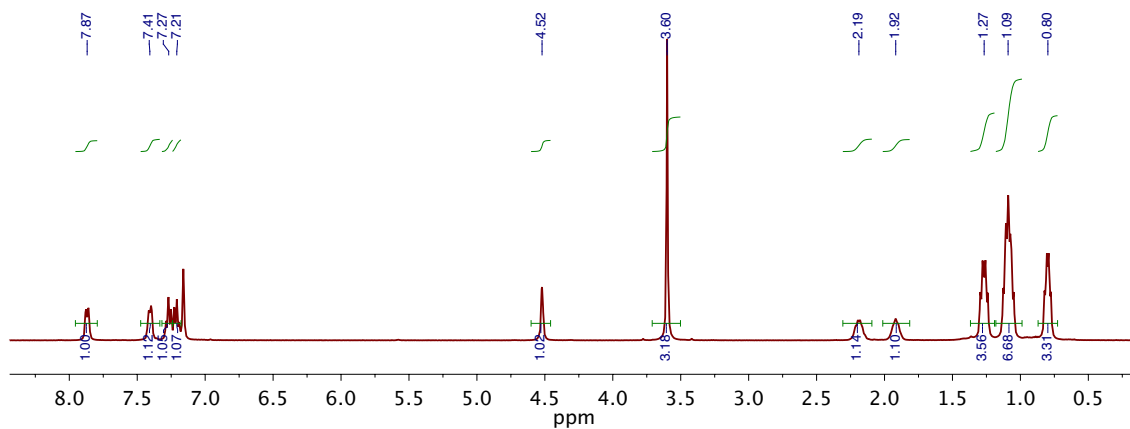


Figure C.15. ^1H NMR spectrum (400 MHz, C_6D_6) of **8**.

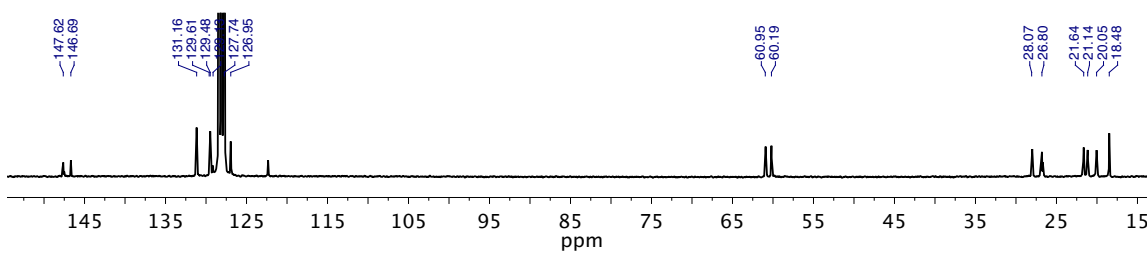


Figure C.16. $^{13}\text{C}\{^1\text{H}\}$ NMR spectrum (101 MHz, C_6D_6) of **8**.

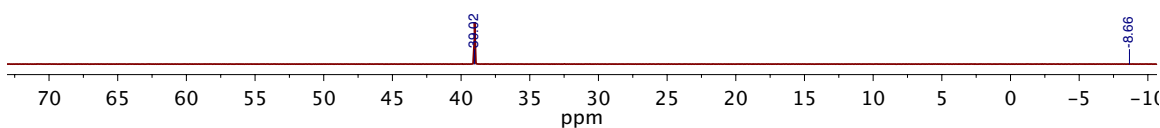


Figure C.17. $^{31}\text{P}\{^1\text{H}\}$ NMR spectrum (121 MHz, C_6D_6) of **8**.

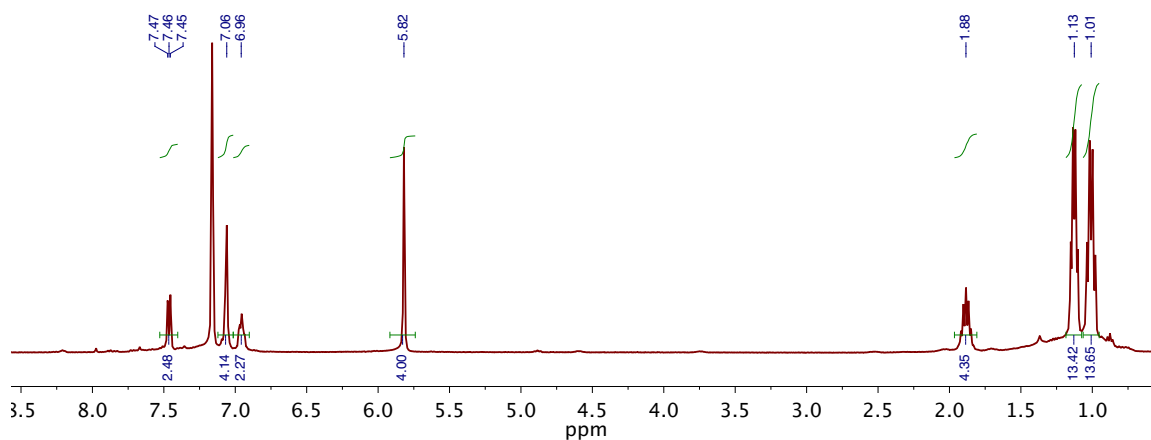


Figure C.18. ^1H NMR spectrum (400 MHz, C_6D_6) of **9**.

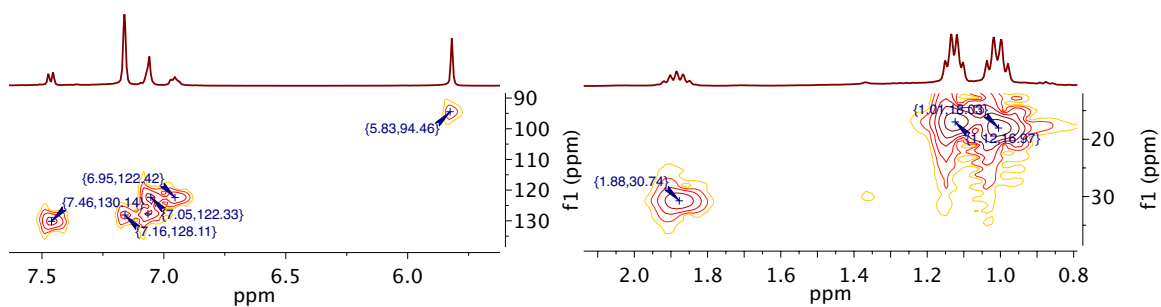


Figure C.19. HSQC NMR spectrum (400 MHz, C_6D_6) of **9**.

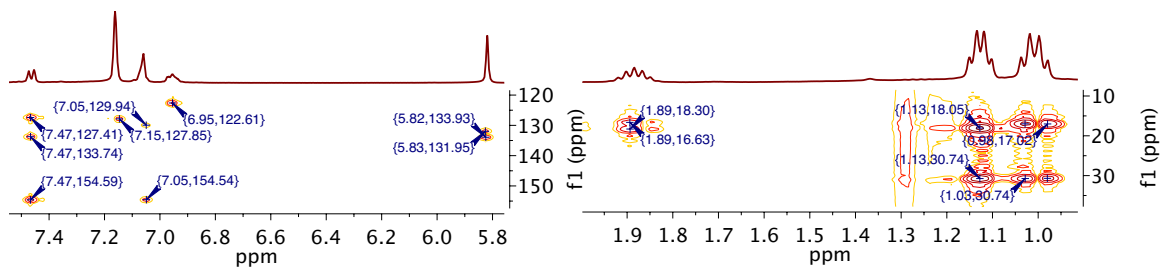


Figure C.20. HMBC NMR spectrum (400 MHz, C_6D_6) of **9**.

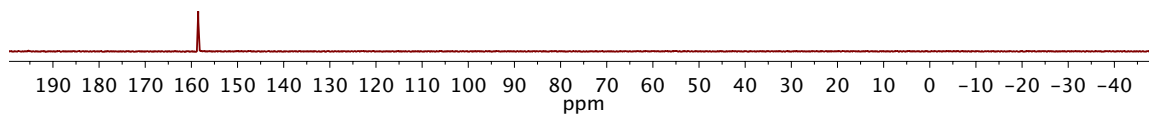


Figure C.21. $^{31}\text{P}\{^1\text{H}\}$ NMR spectrum (162 MHz, C_6D_6) of **9**.

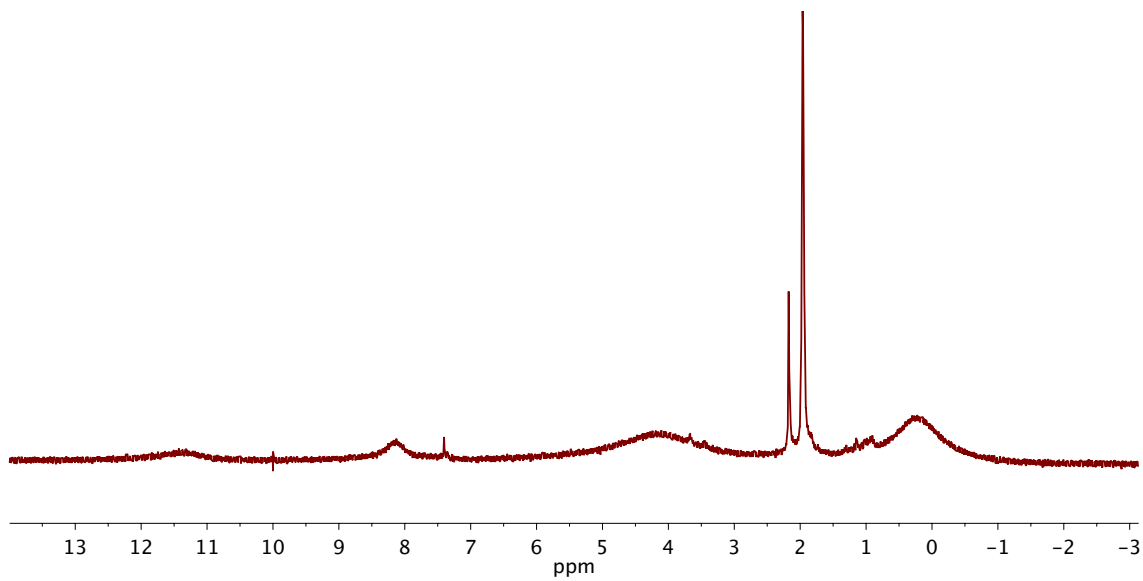


Figure C.22. Paramagnetically shifted ¹H NMR spectrum (300 MHz, CD₃CN) of **10**.

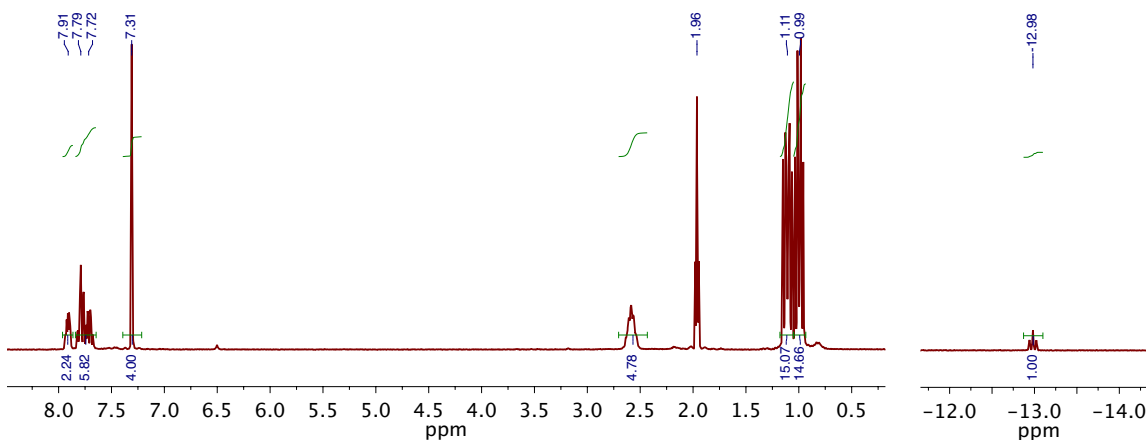


Figure C.23. ^1H NMR spectrum (400 MHz, CD_3CN) of **11**.

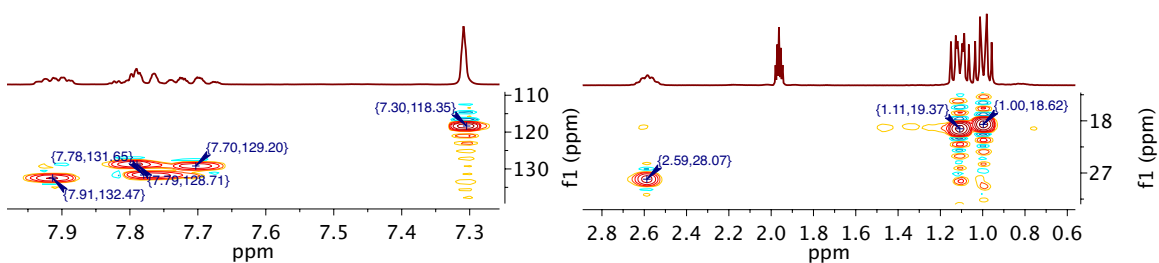


Figure C.24. HSQC NMR spectrum (400 MHz, C_6D_6) of **11**.

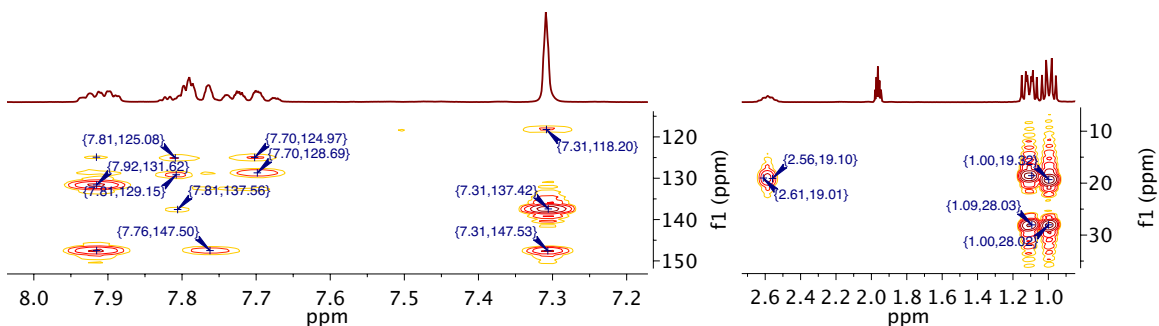


Figure C.25. HMBC NMR spectrum (400 MHz, C_6D_6) of **11**.

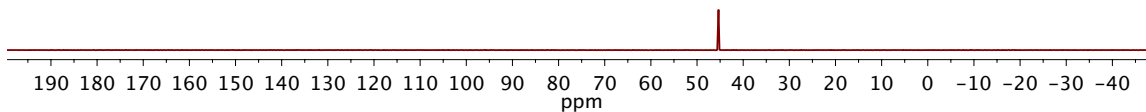


Figure C.26. $^{31}\text{P}\{^1\text{H}\}$ NMR spectrum (162 MHz, CD_3CN) of **11**.

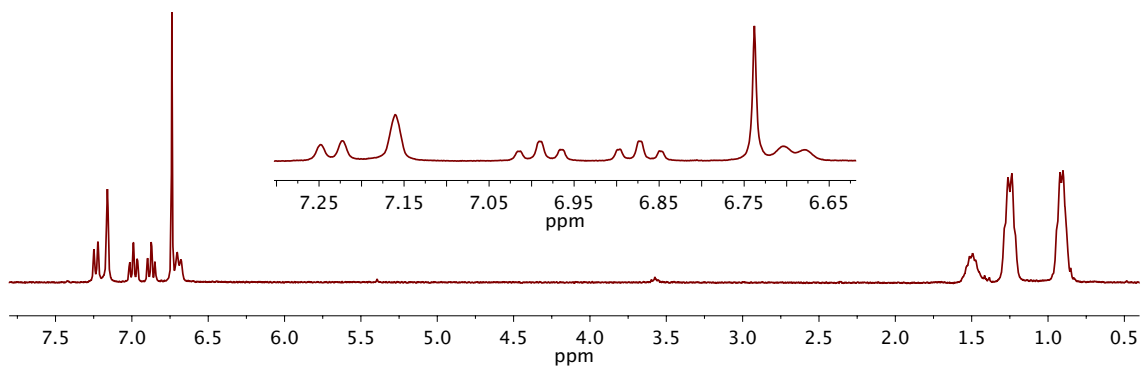


Figure C.27. ^1H NMR spectrum (300 MHz, C_6D_6) of **12**.

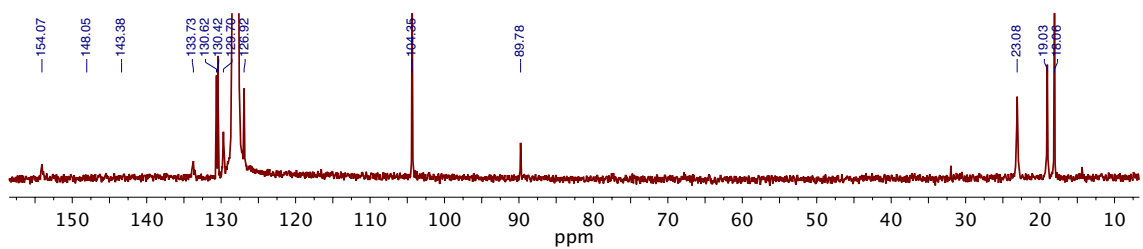


Figure C.28. $^{13}\text{C}\{^1\text{H}\}$ NMR spectrum (75 MHz, C_6D_6) of **12**.

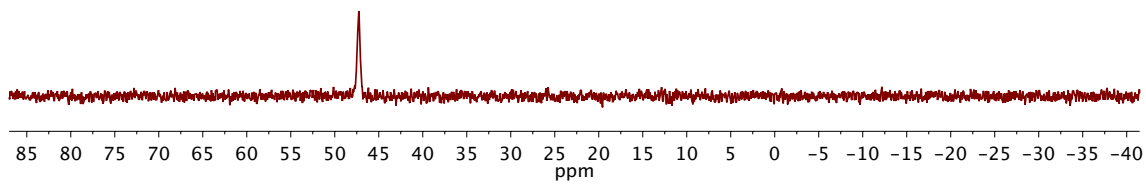


Figure C.29. $^{31}\text{P}\{^1\text{H}\}$ NMR spectrum (121 MHz, C_6D_6) of **12**.

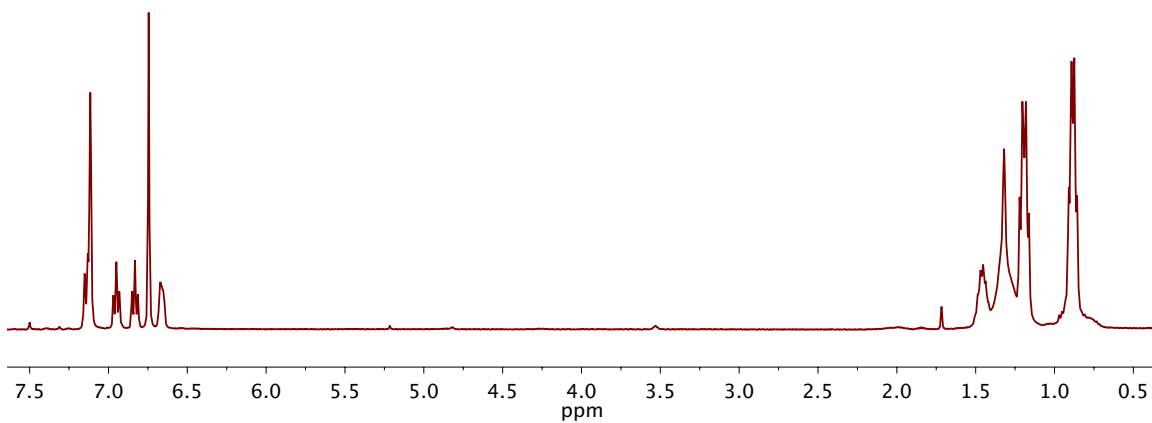


Figure C.30. ^1H NMR spectrum (400 MHz, C_6D_6) of **13**.

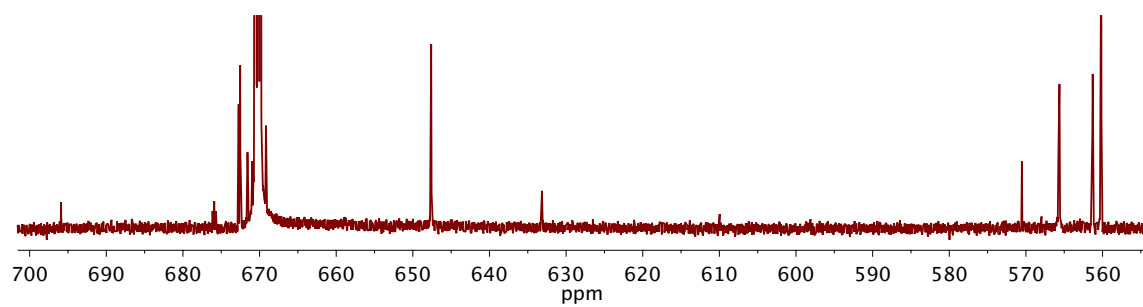


Figure C.31. $^{13}\text{C}\{^1\text{H}\}$ NMR spectrum (75 MHz, C_6D_6) of **13**.

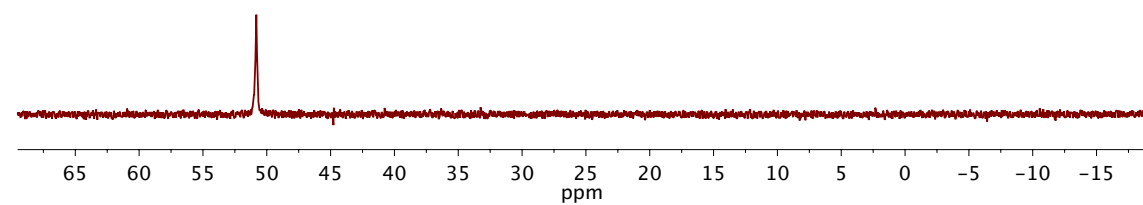


Figure C.32. $^{31}\text{P}\{^1\text{H}\}$ NMR spectrum (121 MHz, C_6D_6) of **13**.

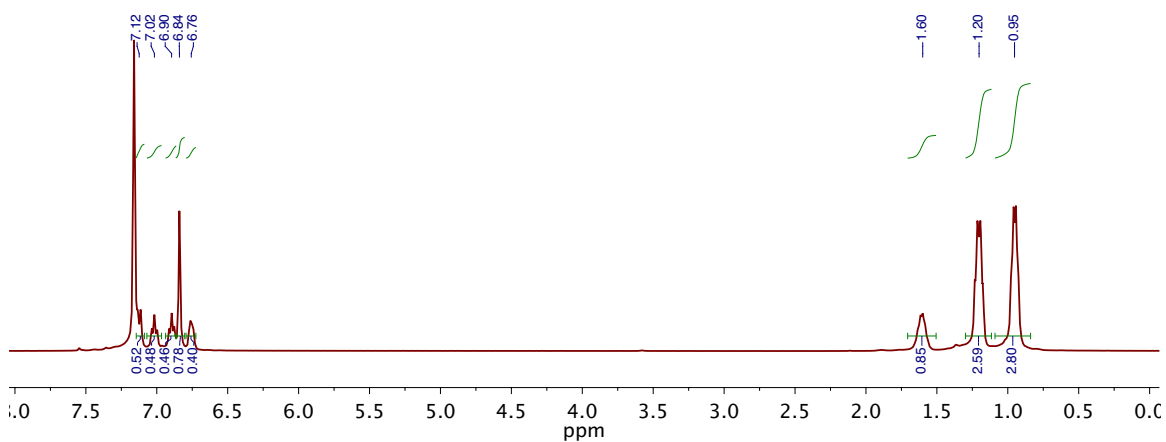


Figure C.33. ^1H NMR spectrum (400 MHz, C_6D_6) of **14**.

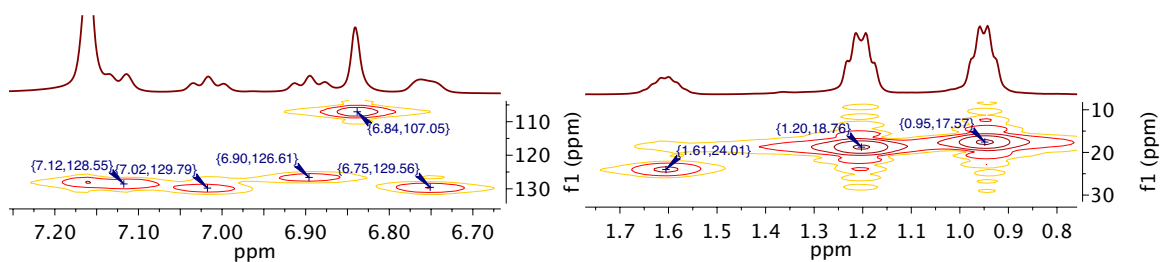


Figure C.34. HSQC NMR spectrum (400 MHz, C_6D_6) of **14**.

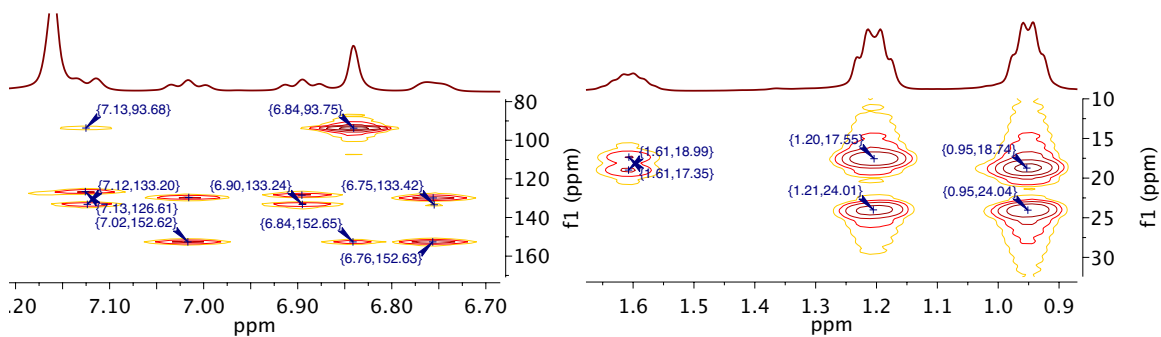


Figure C.35. HMBC NMR spectrum (400 MHz, C_6D_6) of **14**.

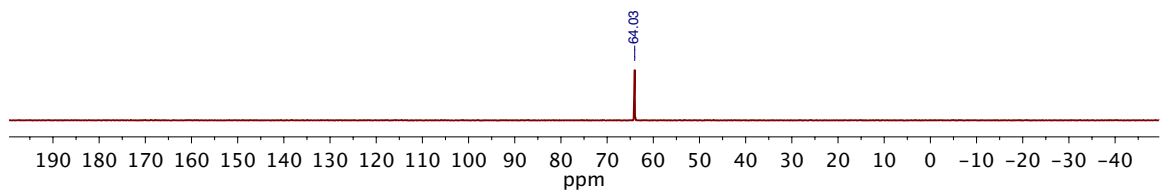


Figure C.36. ^{31}P $\{^1\text{H}\}$ NMR spectrum (162 MHz, C_6D_6) of **14**.

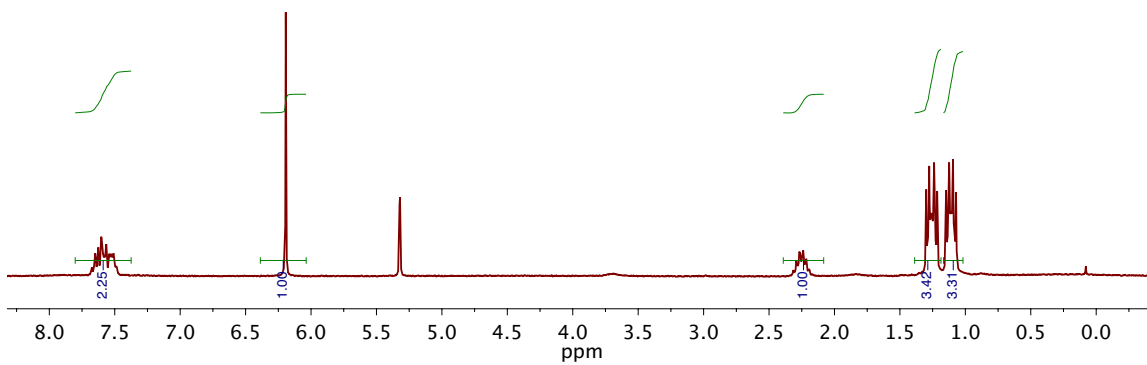


Figure C.37. ^1H NMR spectrum (300 MHz, CD_2Cl_2) of **15**.

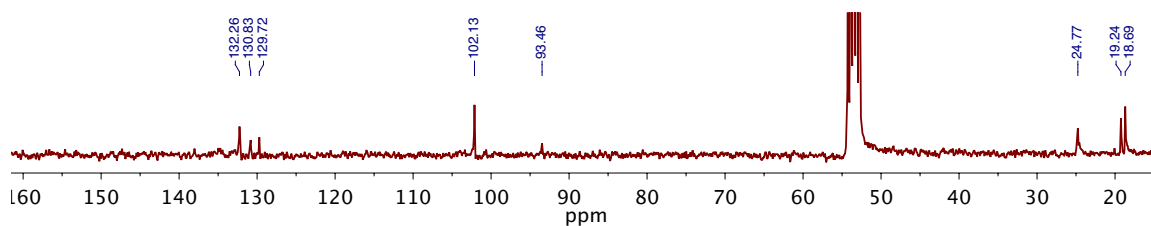


Figure C.38. ^{13}C NMR spectrum (75 MHz, CD_2Cl_2) of **15**.

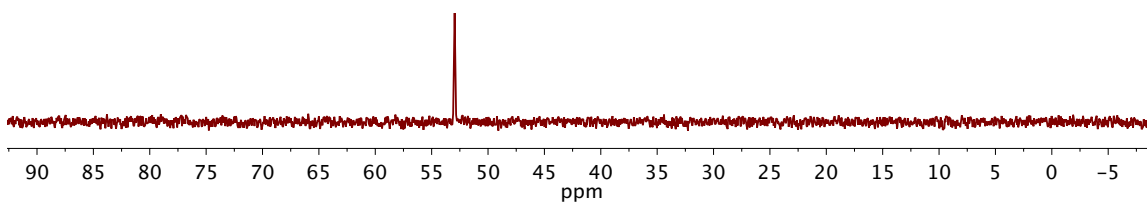


Figure C.39. ^{31}P NMR spectrum (121 MHz, CD_2Cl_2) of **15**.

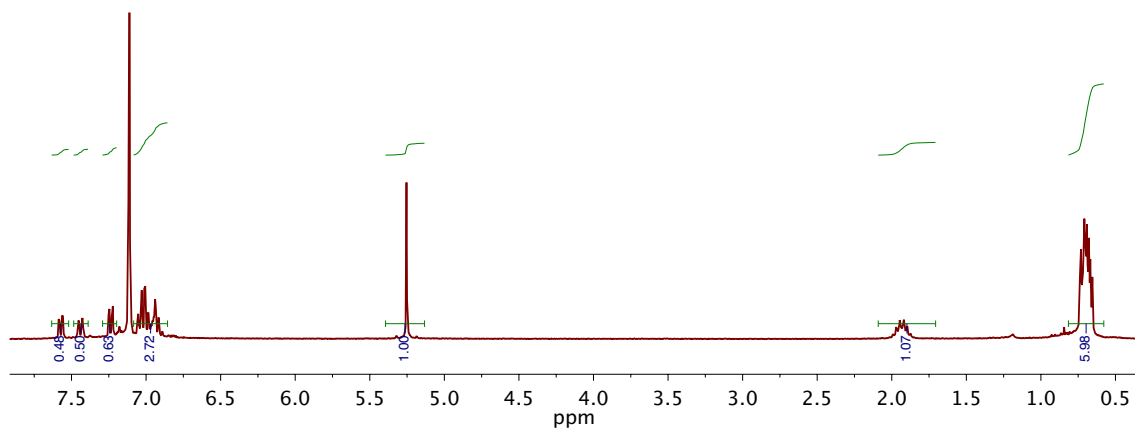


Figure C.40. ^1H NMR spectrum (300 MHz, C_6D_6) of **16**.

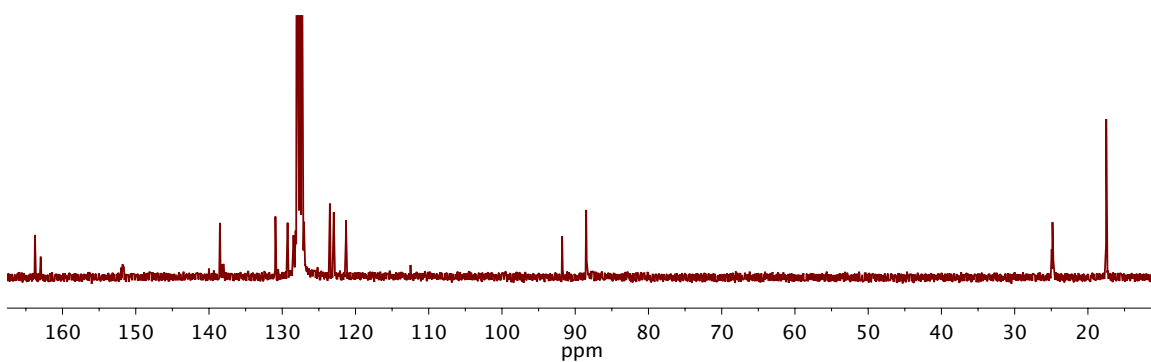


Figure C.41. ^{13}C NMR spectrum (75 MHz, C_6D_6) of **16**.

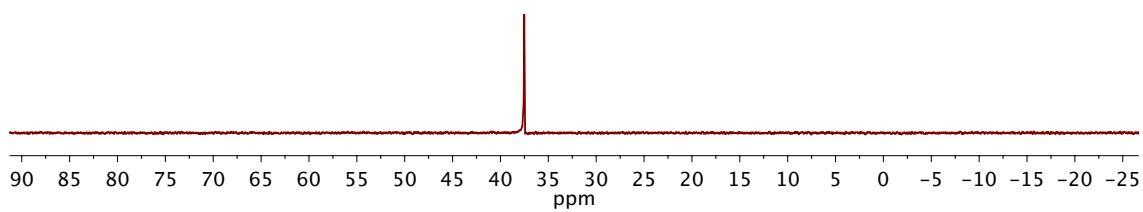


Figure C.42. ^{31}P NMR spectrum (121 MHz, C_6D_6) of **16**.

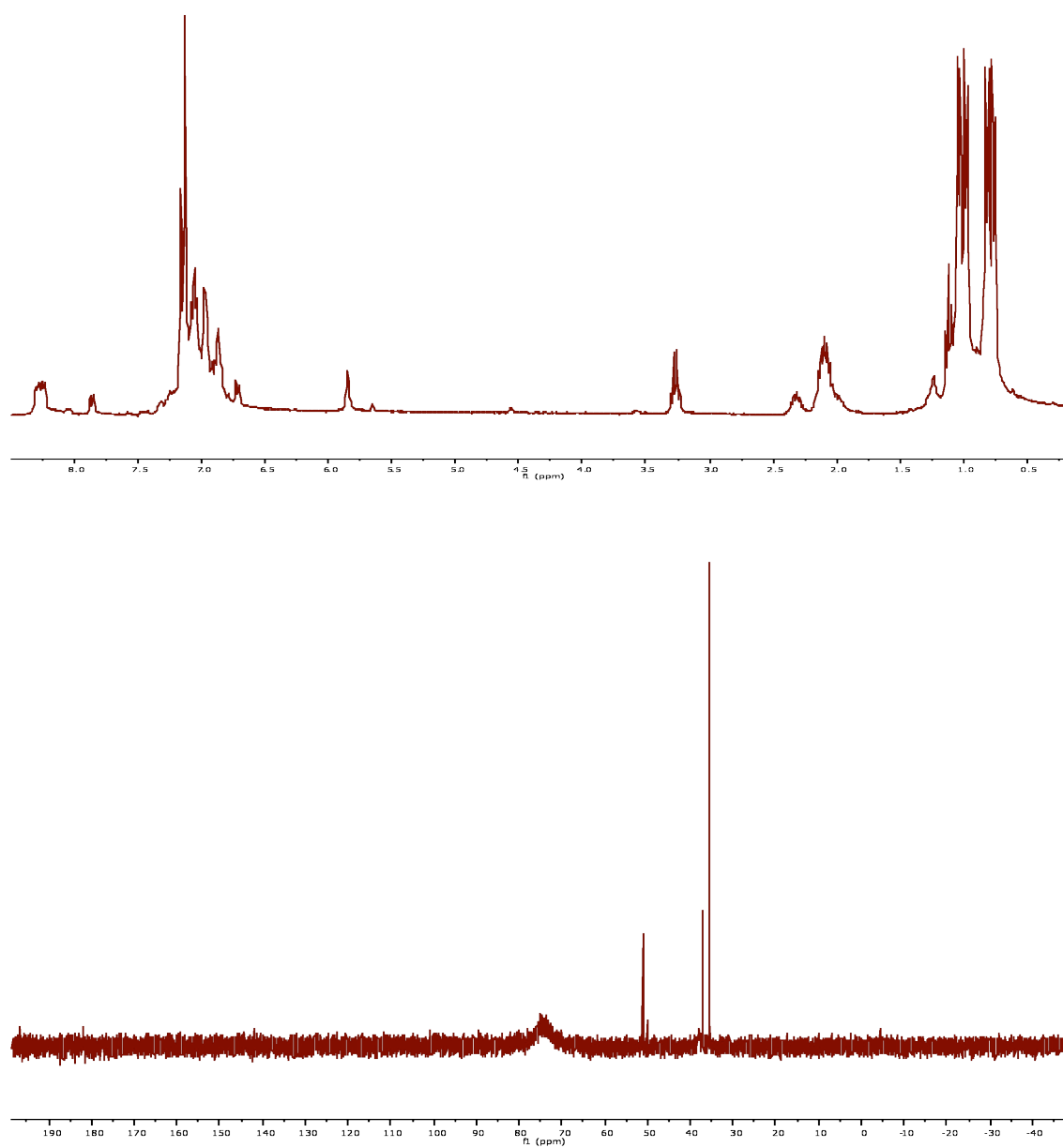


Figure C.43. ^1H NMR spectrum (C_6D_6 , 300 MHz, top) and ^{31}P NMR spectrum (C_6D_6 , 121 MHz, bottom) of the mixture derived from the reaction of **16** and 6 equivalents of CO (primarily compound **17**).

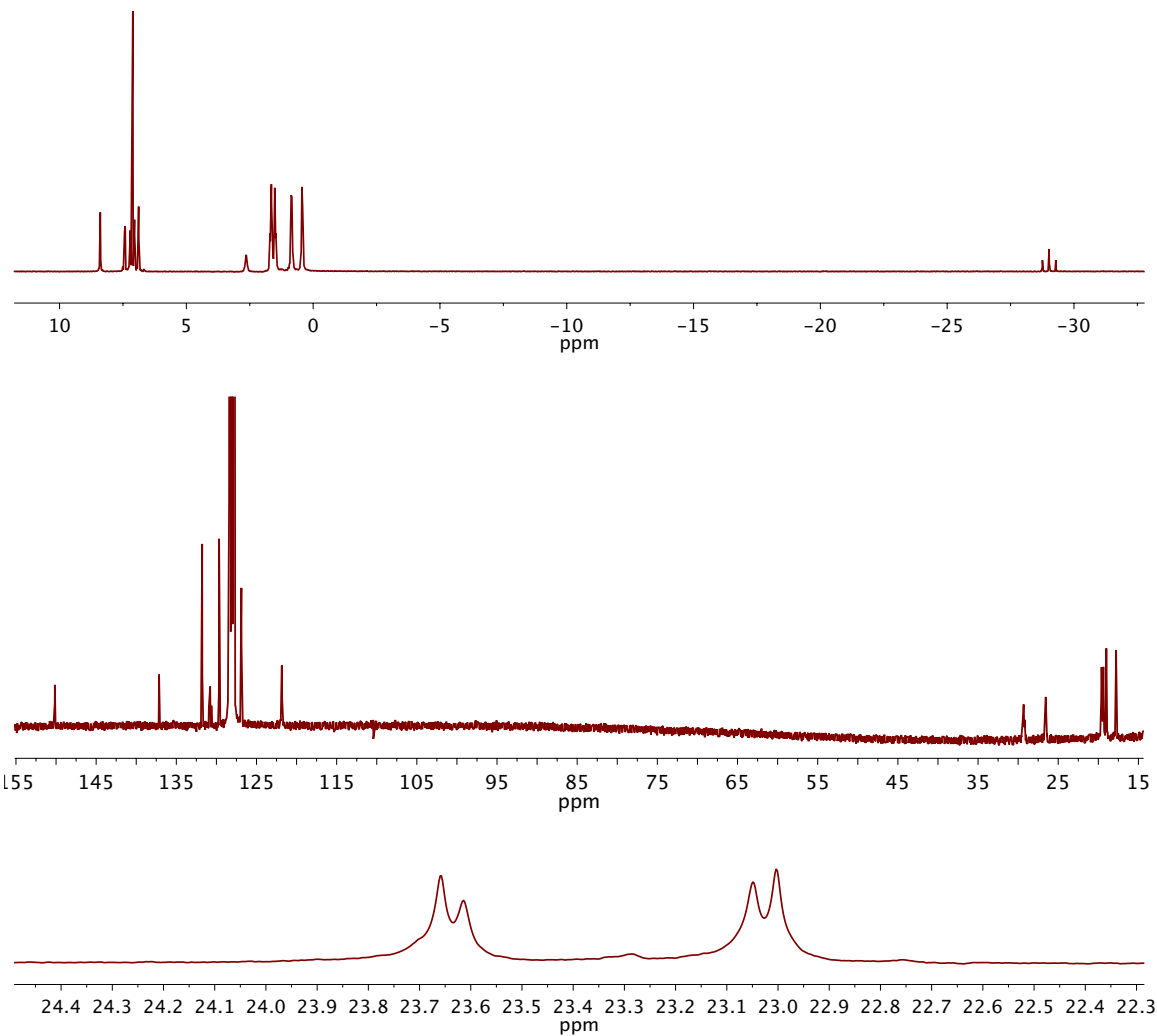


Figure C.44. ^1H NMR (C_6D_6 , 300 MHz, top), $^{13}\text{C}\{^1\text{H}\}$ NMR (C_6D_6 , 75 MHz, middle), and ^{31}P NMR (C_6D_6 , 121 MHz, bottom) spectra of **18**. Note the incomplete ^1H decoupling in the ^{31}P spectrum due to the far upfield location of the hydride signal.

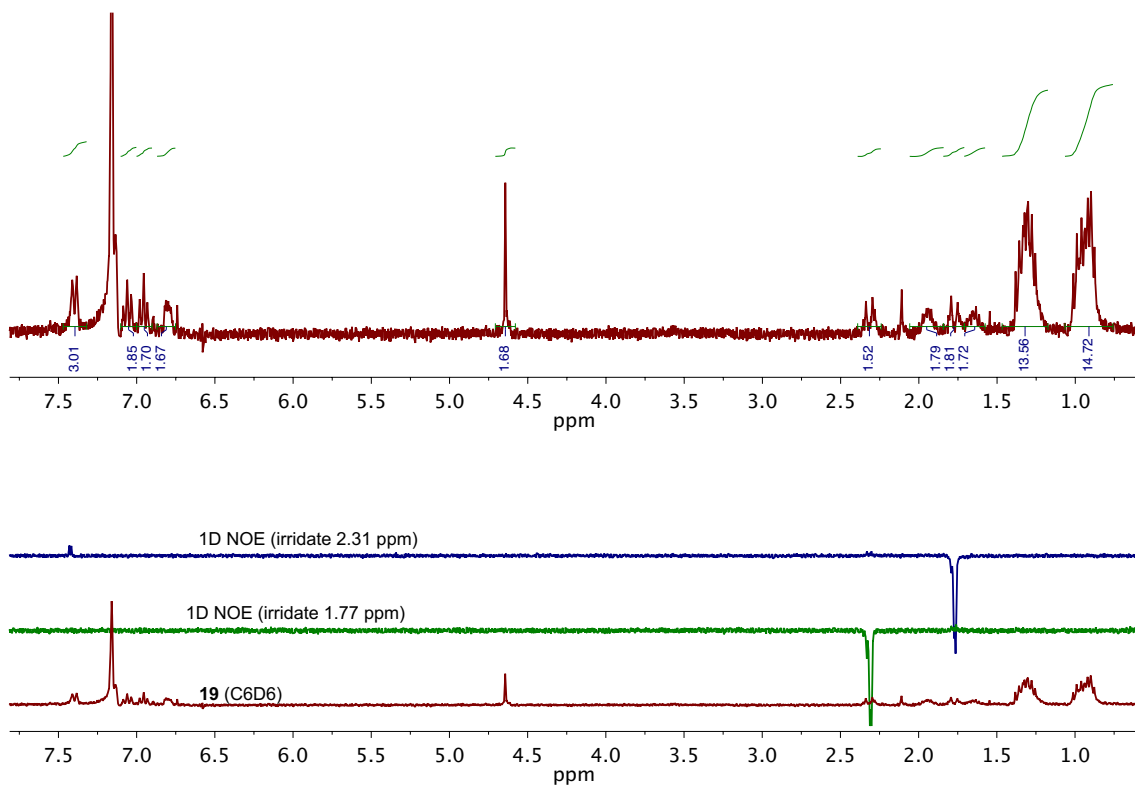


Figure C.45. ^1H NMR (C_6D_6 , 300 MHz, top) and related 1D NOE experiments (bottom) of **19**.

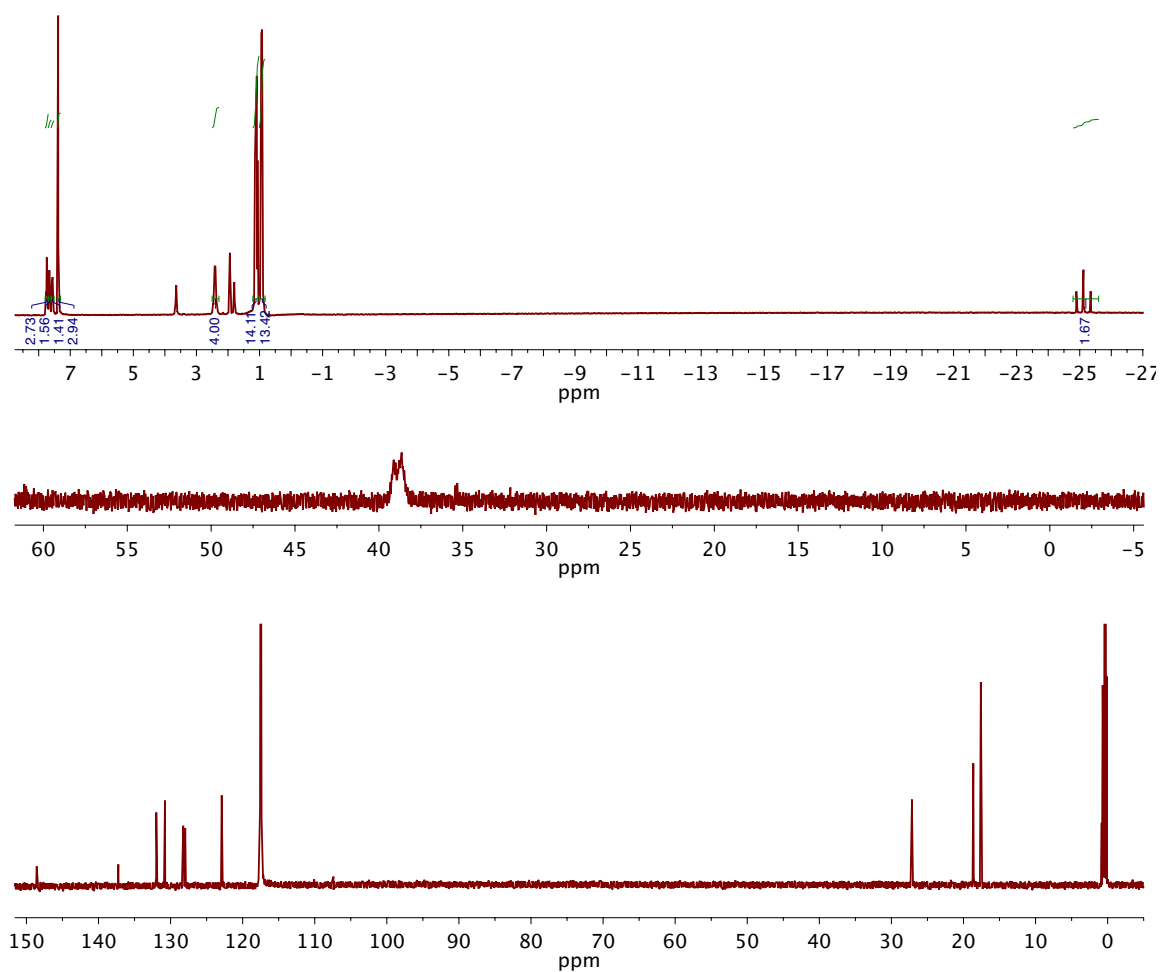


Figure C.46. ^1H NMR (CD_2Cl_2 , 300 MHz, top), ^{31}P NMR (CD_2Cl_2 , 121 MHz, middle), and ^{13}C NMR (CD_3CN , 75 MHz, bottom) spectra of **20-OTf**. Note the incomplete ^1H decoupling in the ^{31}P spectrum due to the far upfield location of the hydride signal.

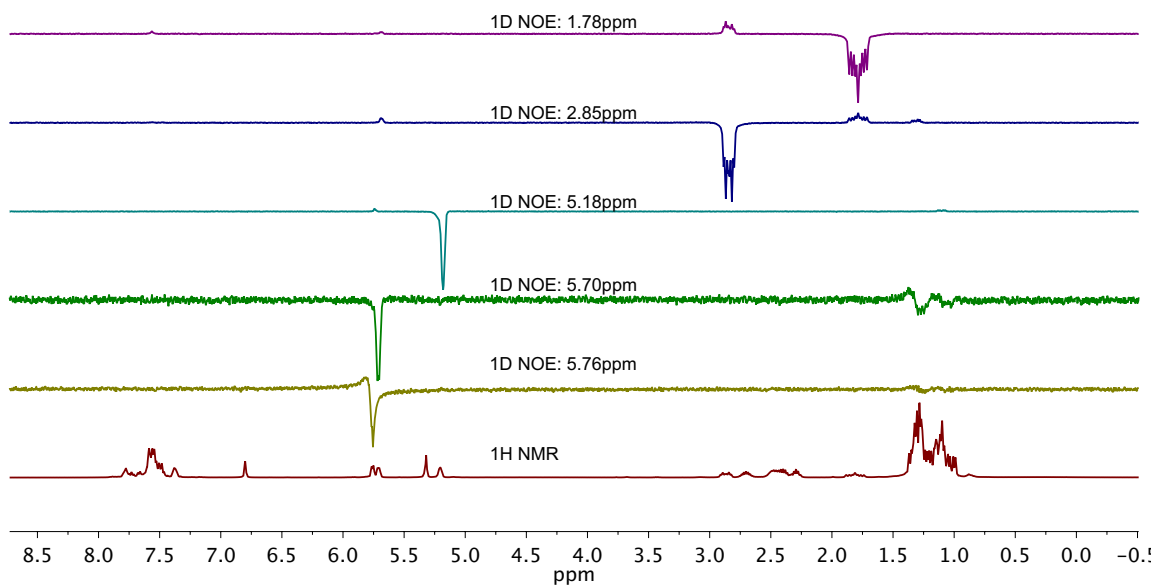


Figure C.47. ^1H NMR and 1D NOE spectra of a mixture of **20-OTf** and **21-OTf** (CD_2Cl_2 , 400 MHz)

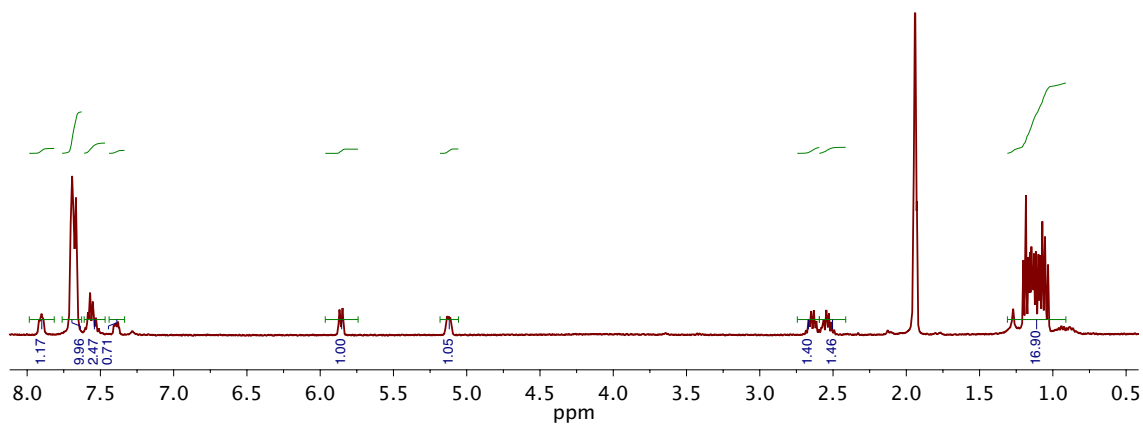


Figure C.48. ^1H NMR spectrum of $22 \cdot \text{BAr}_{\text{F}24}$ (CD_3CN , 600 MHz).

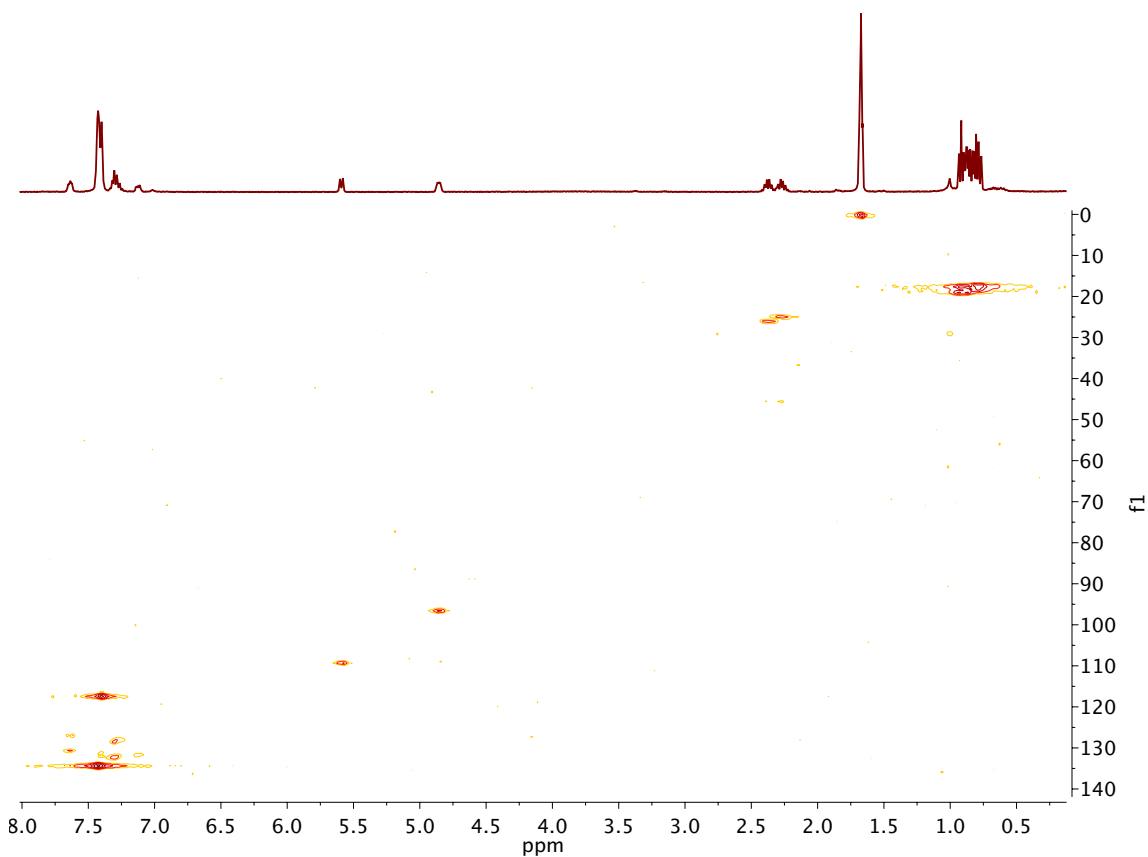


Figure C.49. HSQC NMR spectrum of $22 \cdot \text{BAr}_{\text{F}24}$ (CD_3CN , 600 MHz).

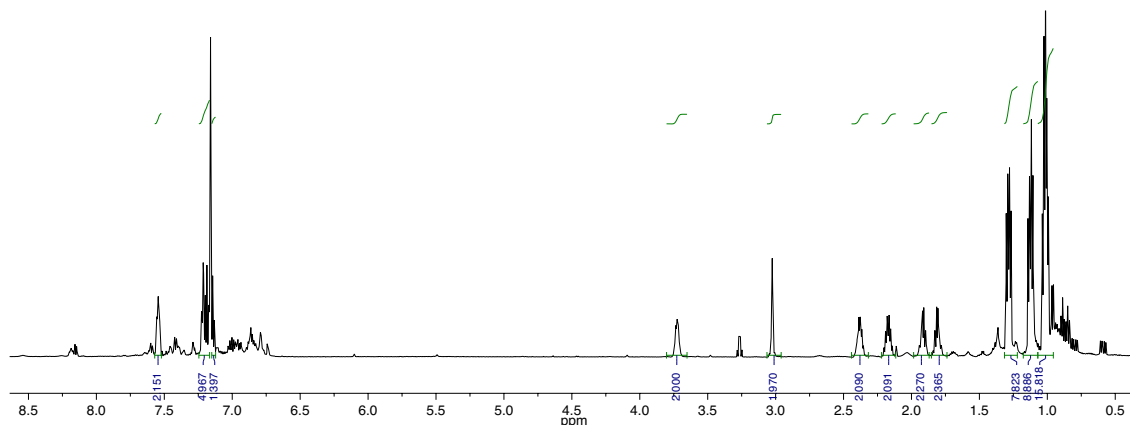


Figure C.50. ^1H NMR spectrum of **23** (C_6D_6 , 600 MHz).

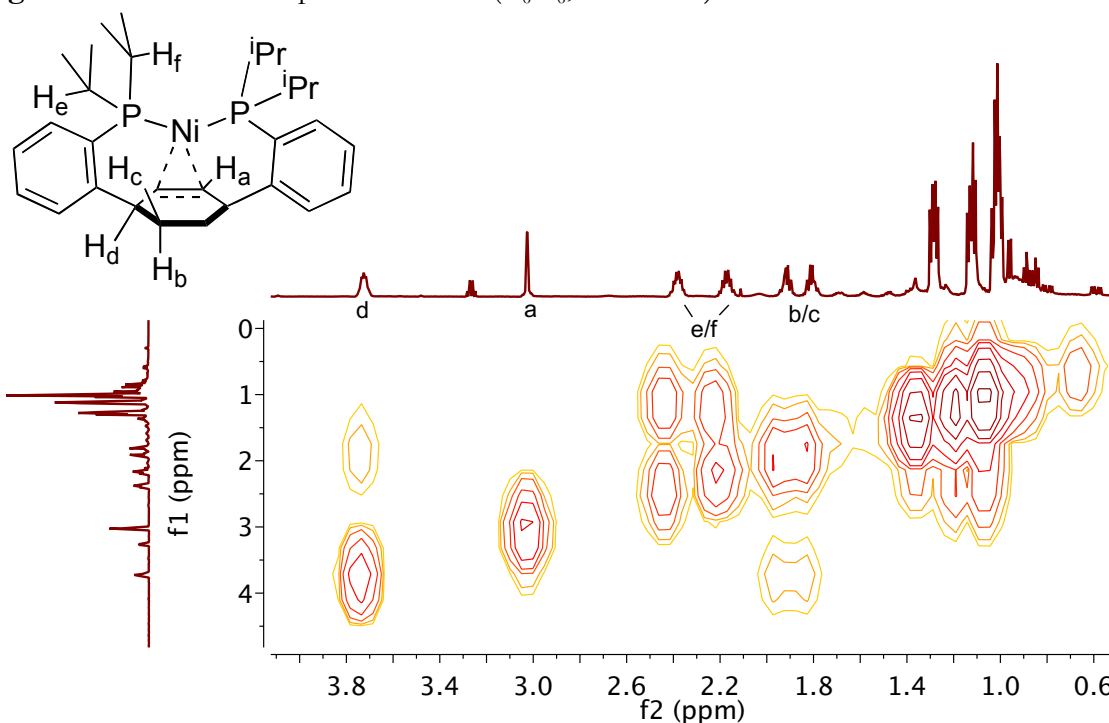


Figure C.51. Olefinic and aliphatic region of gradient COSY spectrum of **23** (C_6D_6 , 600 MHz).

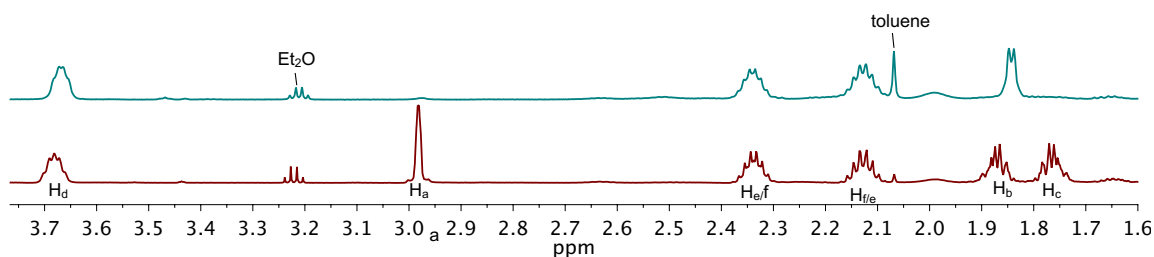


Figure C.52. Stacked olefinic-aliphatic region of ^1H NMR spectra of **23** (bottom) and **23-d₄** (top).

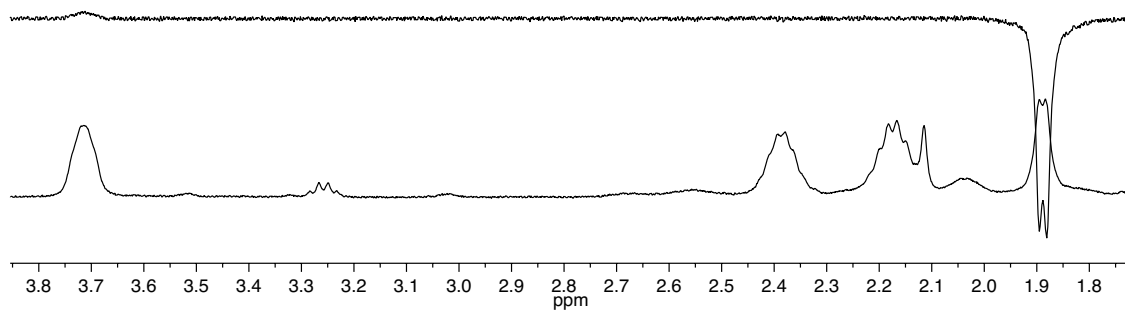


Figure C.53. 1D NOE experiment on **23-d₄** showing through-space dipolar coupling between H_b and H_d.

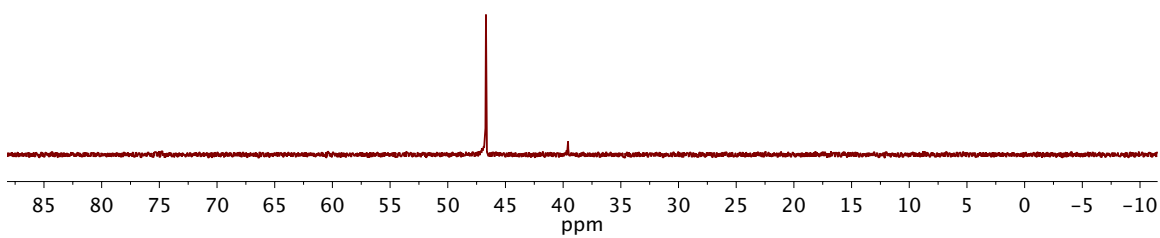


Figure C.54. ³¹P{¹H} NMR spectrum of **23**.

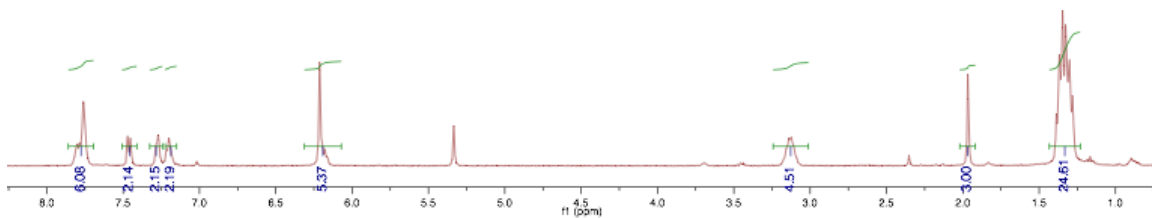


Figure C.55. ^1H NMR (CD_2Cl_2 , 400 MHz) spectrum of **25**.

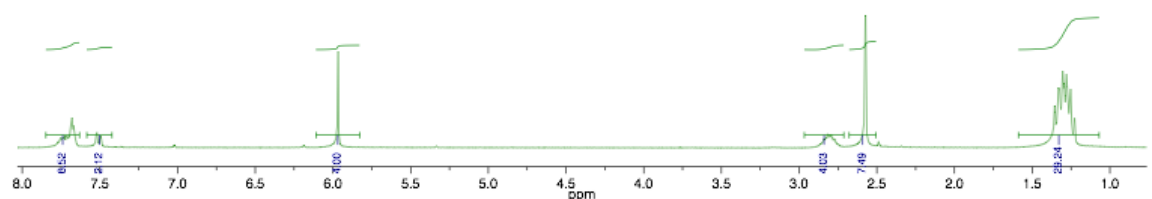


Figure C.56. ^1H NMR (CD_2Cl_2 , 300 MHz) spectrum of toluene-free, acetonitrile-exchanged **25**.

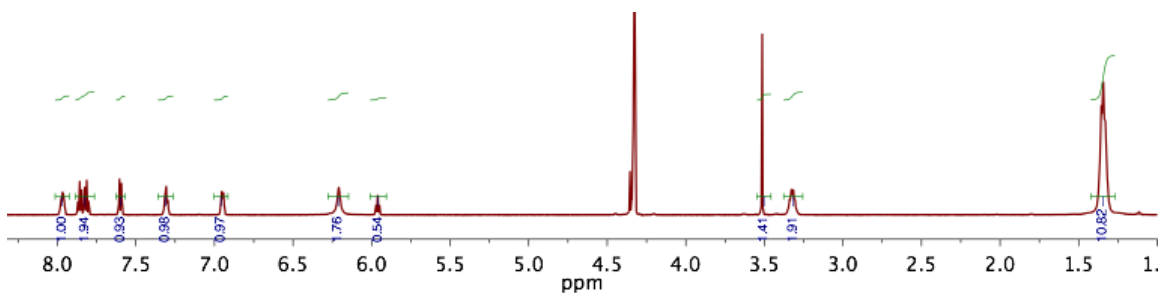


Figure C.57. ^1H NMR (CD_3NO_2 , 400 MHz) spectrum of anisole complex **26**.

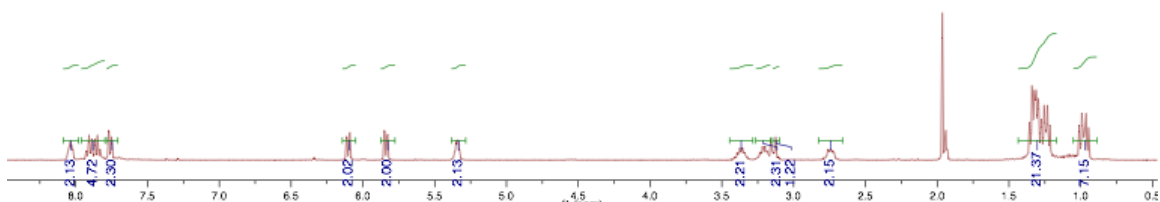


Figure C.58. ^1H NMR (CD_3CN , 400 MHz) spectrum of butadiene complex **27**.

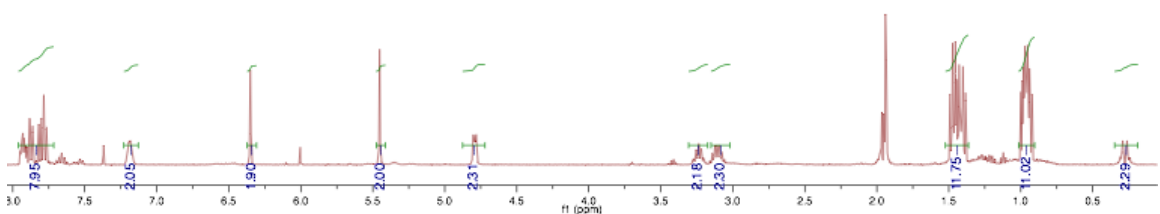


Figure C.59. ^1H NMR (CD_3CN , 400 MHz) spectrum of 1,3-cyclohexadiene complex **28**.

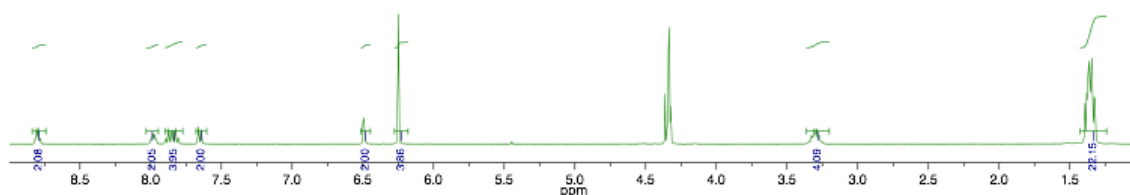


Figure C.60. ^1H NMR (CD_3NO_2 , 400 MHz) spectrum of thiophene complex **29**.

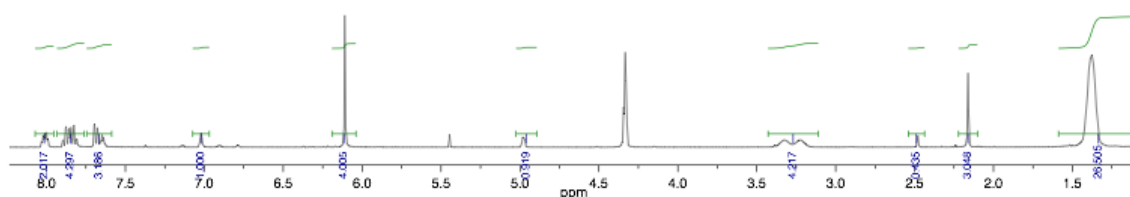


Figure C.61. ^1H NMR (CD_3NO_2 , 400 MHz) spectrum of 2-methylthiophene complex **30**.

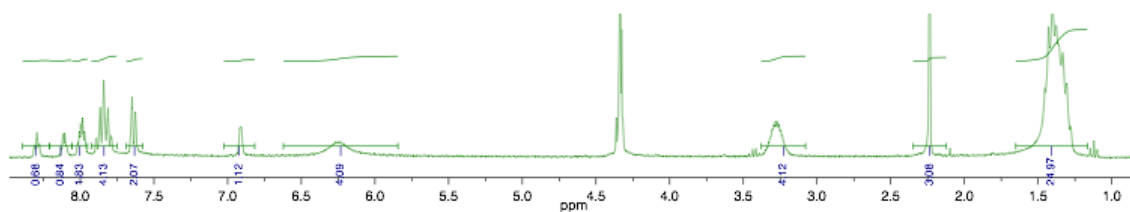


Figure C.62. ^1H NMR (CD_3NO_2 , 400 MHz) spectrum of 3-methylthiophene complex **31**.

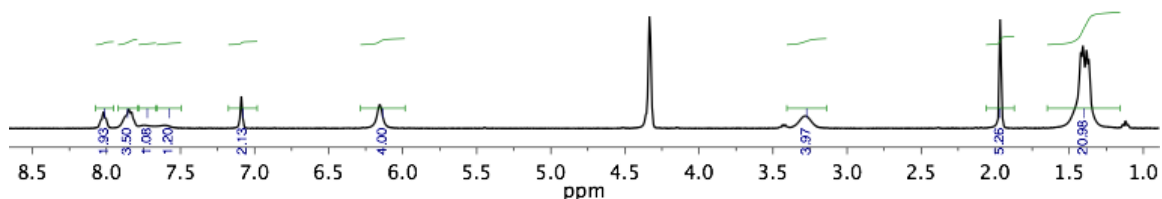


Figure C.63. ^1H NMR (CD_3NO_2 , 400 MHz) spectrum of 2,5-dimethylthiophene complex **32**.

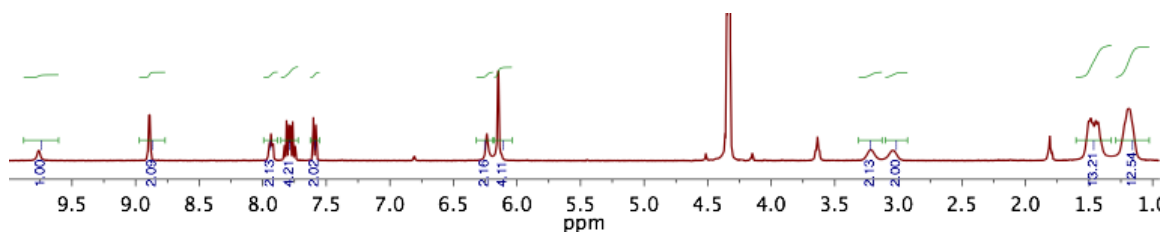


Figure C.64. ^1H NMR (CD_3NO_2 , 400 MHz) spectrum of pyrrole complex **33**.

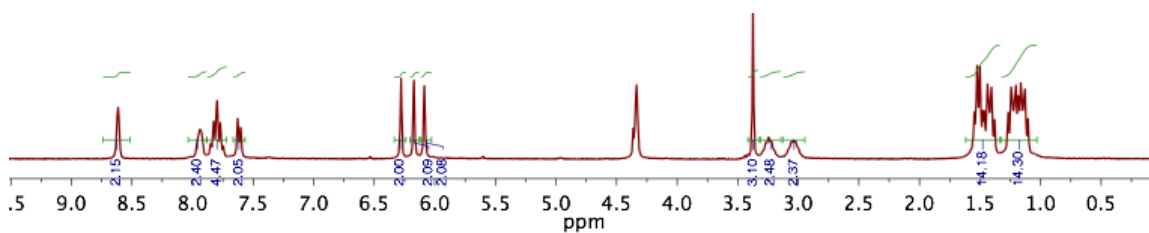


Figure C.65. ^1H NMR (CD_3NO_2 , 400 MHz) spectrum of N-methylpyrrole complex **34**.

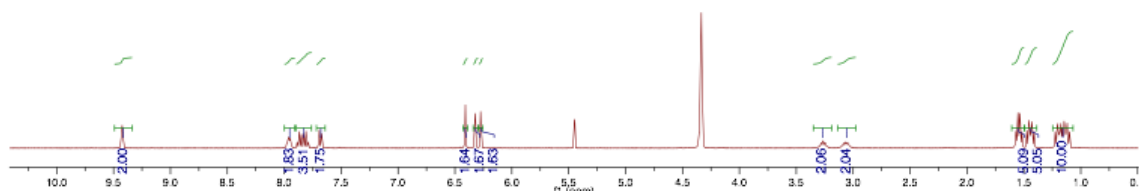


Figure C.66. ^1H NMR (CD_3NO_2 , 400 MHz) spectrum of furan complex **35**.

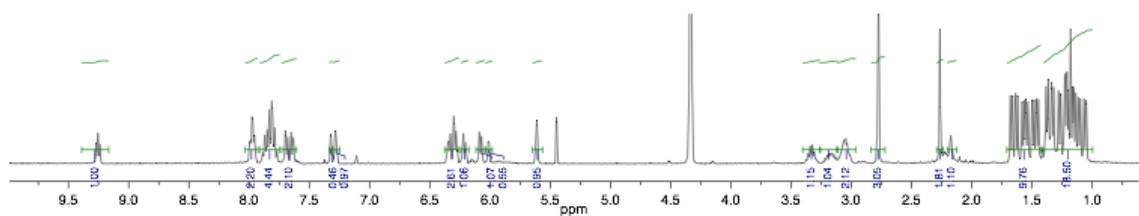


Figure C.67. ^1H NMR (CD_3NO_2 , 400 MHz) spectrum of 2-methylfuran complex **36**.

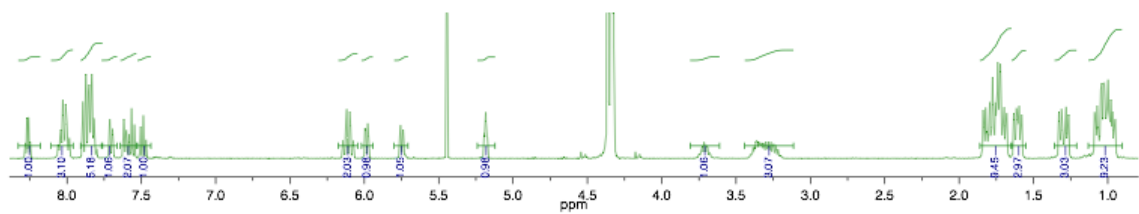


Figure C.68. ^1H NMR (CD_3NO_2 , 400 MHz) spectrum of benzothiophene complex **37**.

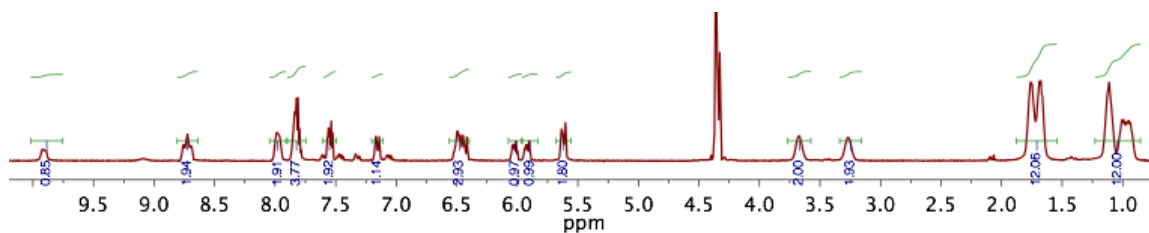


Figure C.69. ^1H NMR (CD_3NO_2 , 400 MHz) spectrum of indole complex **38**.

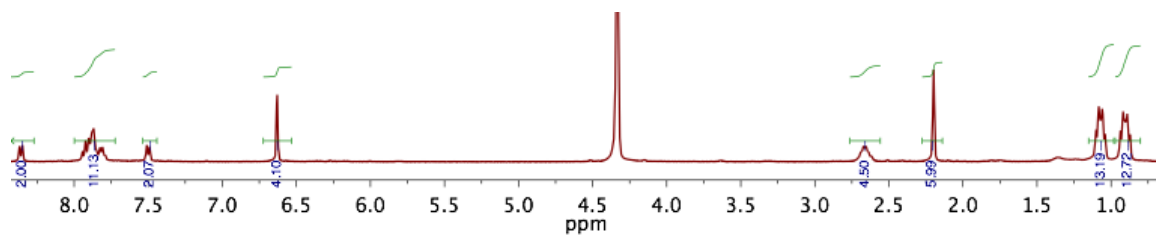


Figure C.70. ^1H NMR (CD_3NO_2 , 400 MHz) spectrum of 4,6-dimethyldibenzothiophene complex **39**.

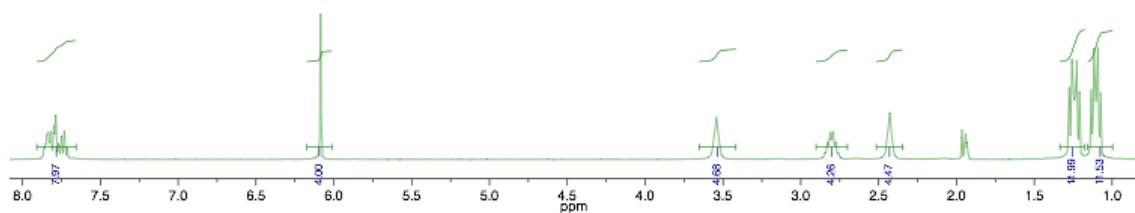


Figure C.71. ^1H NMR (CD_3NO_2 , 400 MHz) spectrum of tetrahydrothiophene complex **40**.

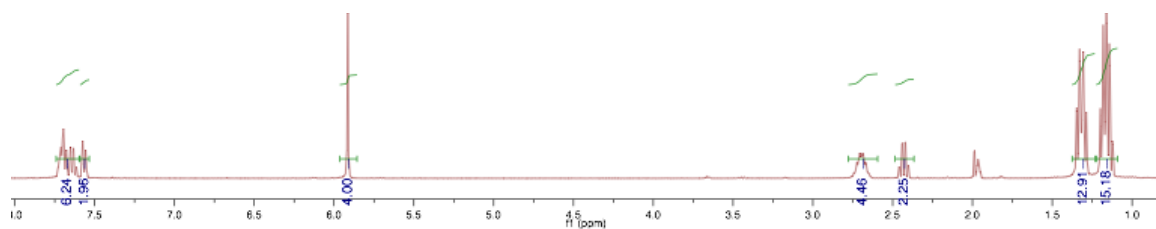


Figure C.72. ^1H NMR (CD_3CN , 400 MHz) spectrum of propanoate complex **41**.

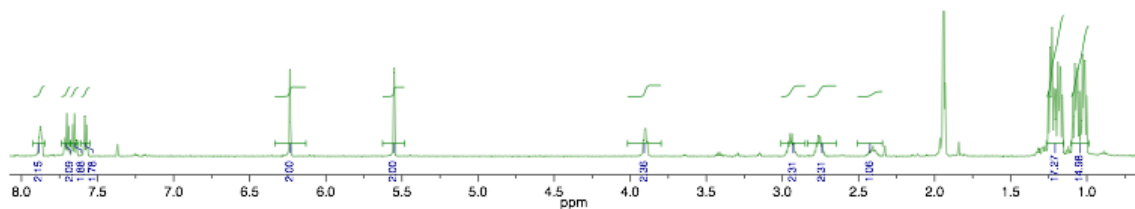


Figure C.73. ^1H NMR (CD_3CN , 400 MHz) spectrum of allyl complex **42**.

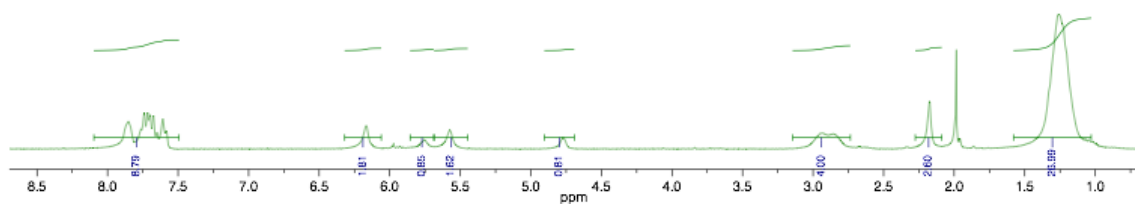


Figure C.74. ^1H NMR (CD_3CN , 400 MHz) spectrum of diacetonitril complex **43**.

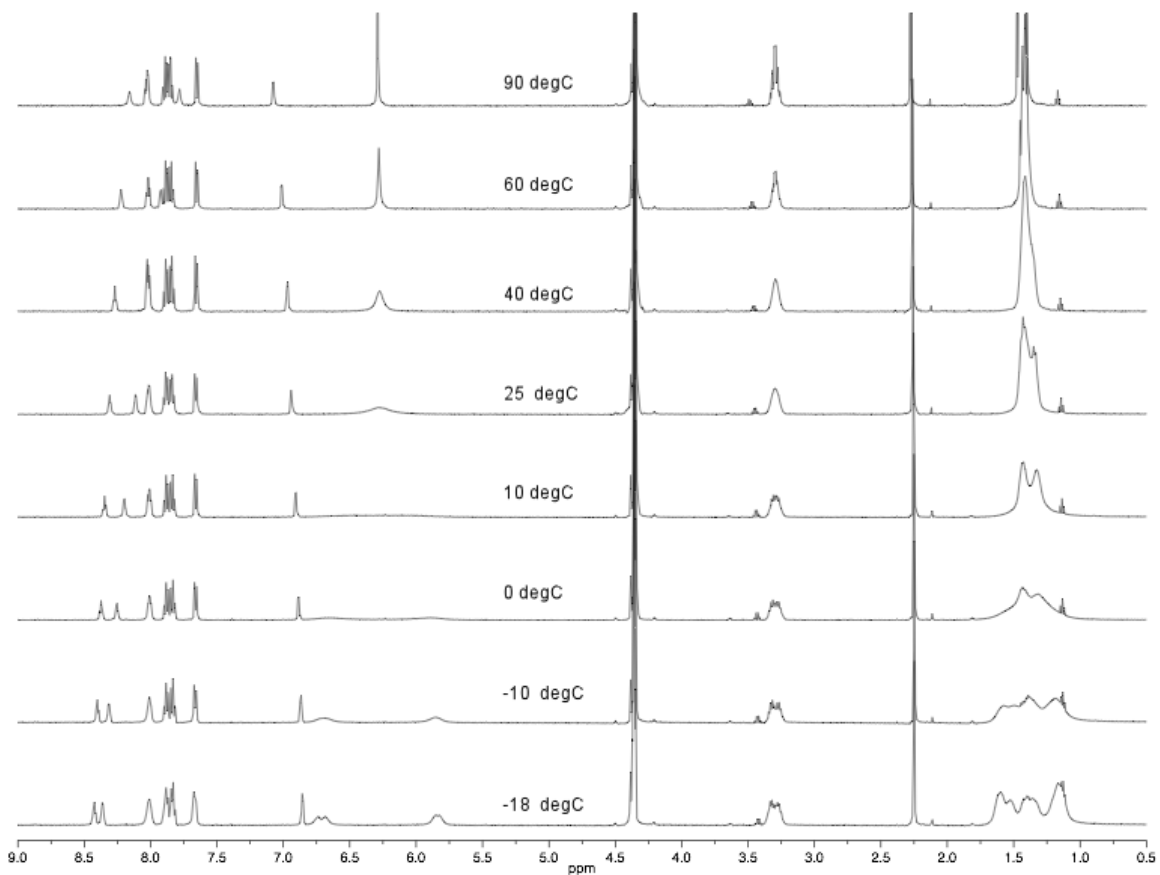


Figure C.75. VT ¹H NMR (CD₃NO₂, 500 MHz) spectra of 2-methylthiophene adduct **31**.

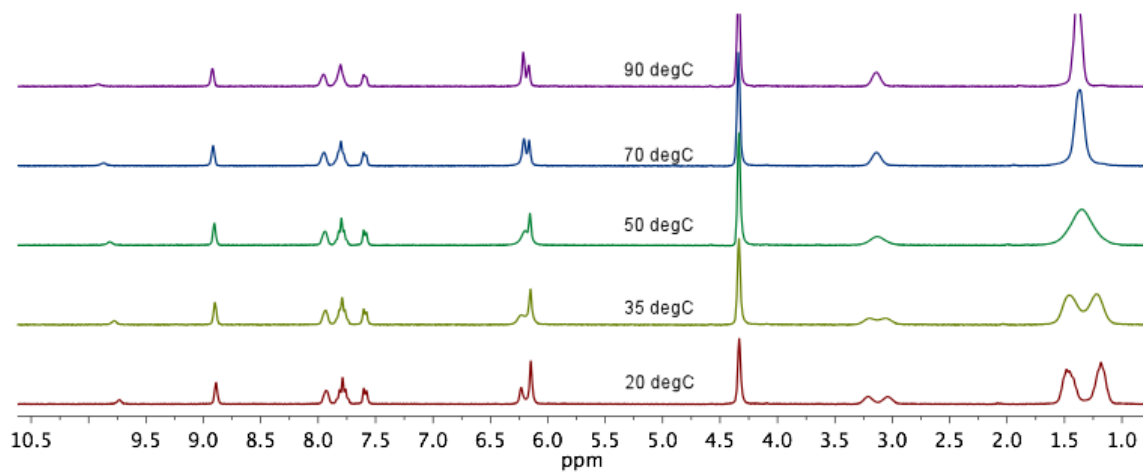


Figure C.76. VT ¹H NMR (CD₃NO₂, 300 MHz) spectra of pyrrole adduct **33**.

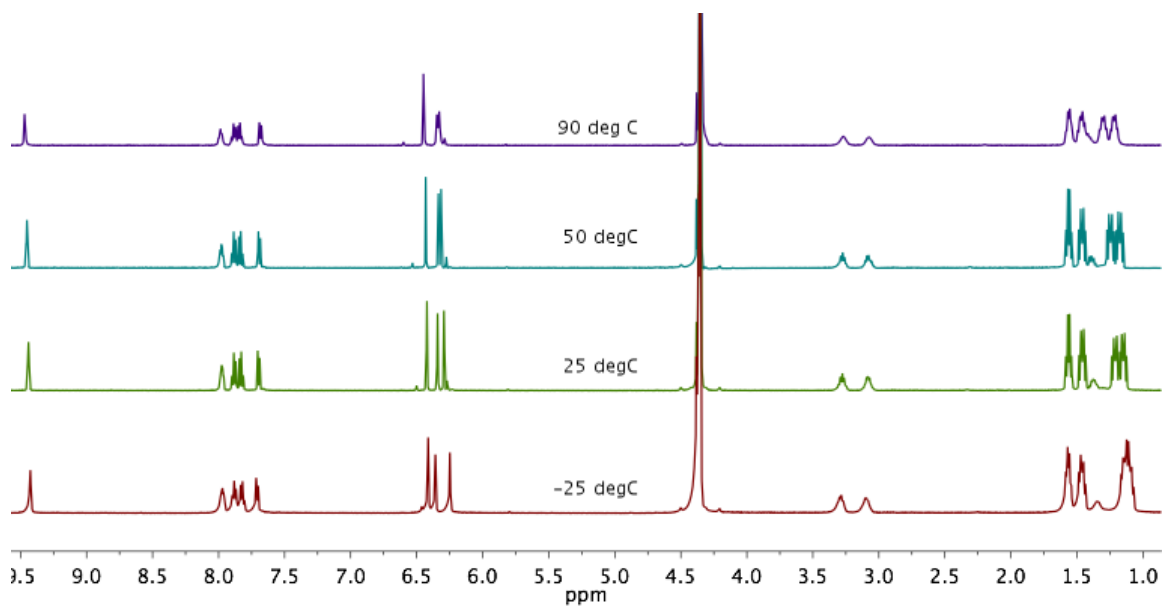


Figure C.77. VT ^1H NMR (CD_3NO_2 , 500 MHz) spectra of furan adduct **35**.

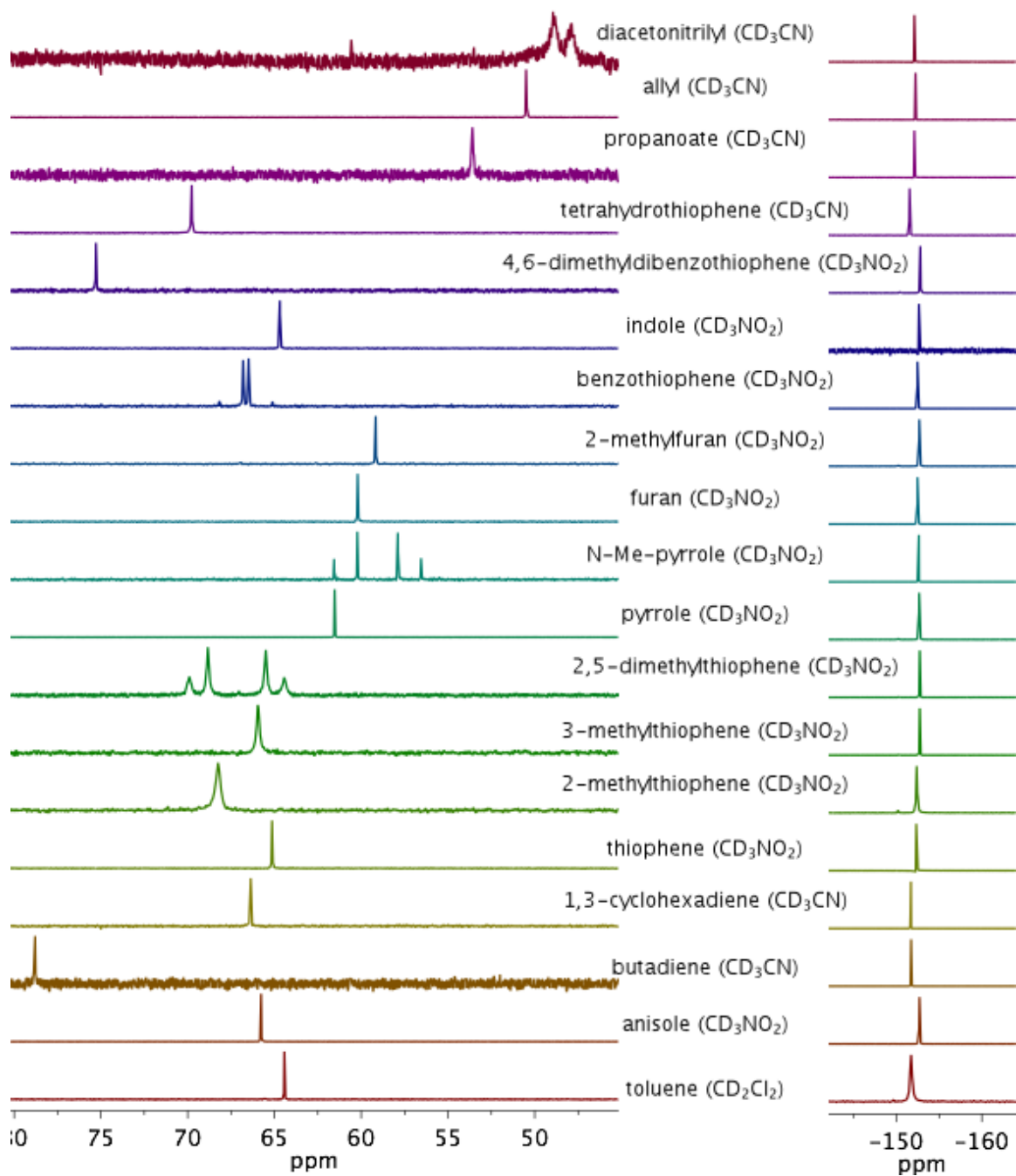


Figure C.78. $^{31}\text{P}\{^1\text{H}\}$ (left) and $^{19}\text{F}\{^1\text{H}\}$ (right) NMR spectra of **25-43** (ordered bottom to top).

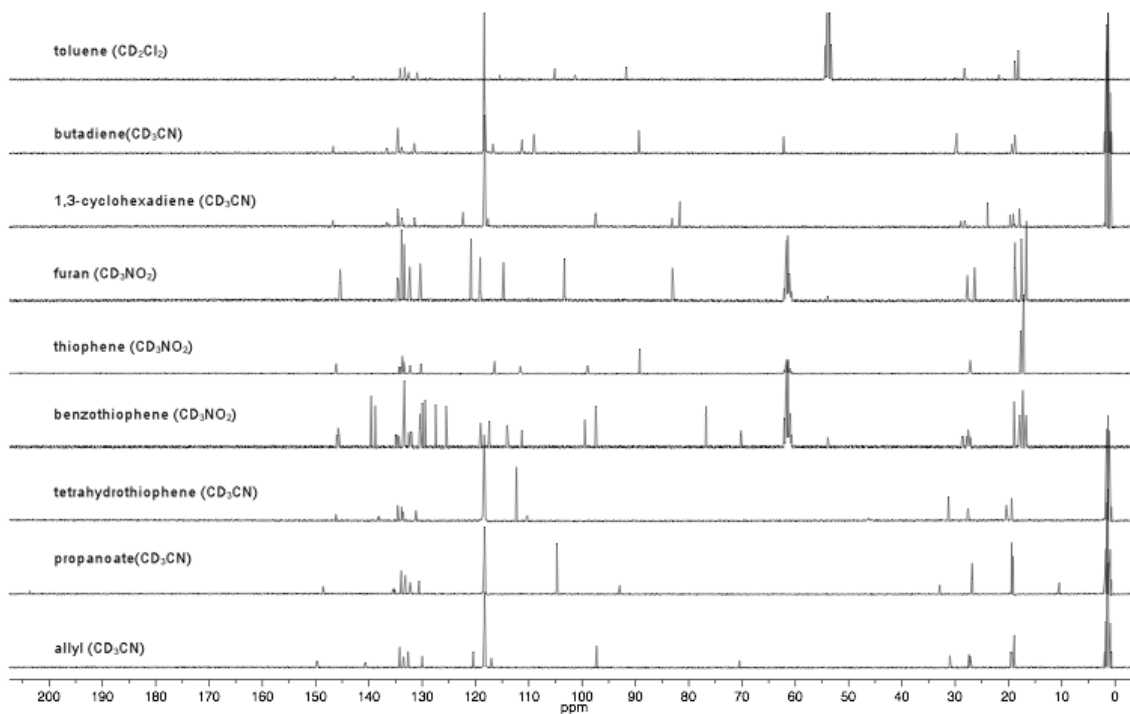


Figure C.79. Stacked $^{13}\text{C}\{^1\text{H}\}$ NMR spectra of 25, 27-29, 35, 37, 40-42.

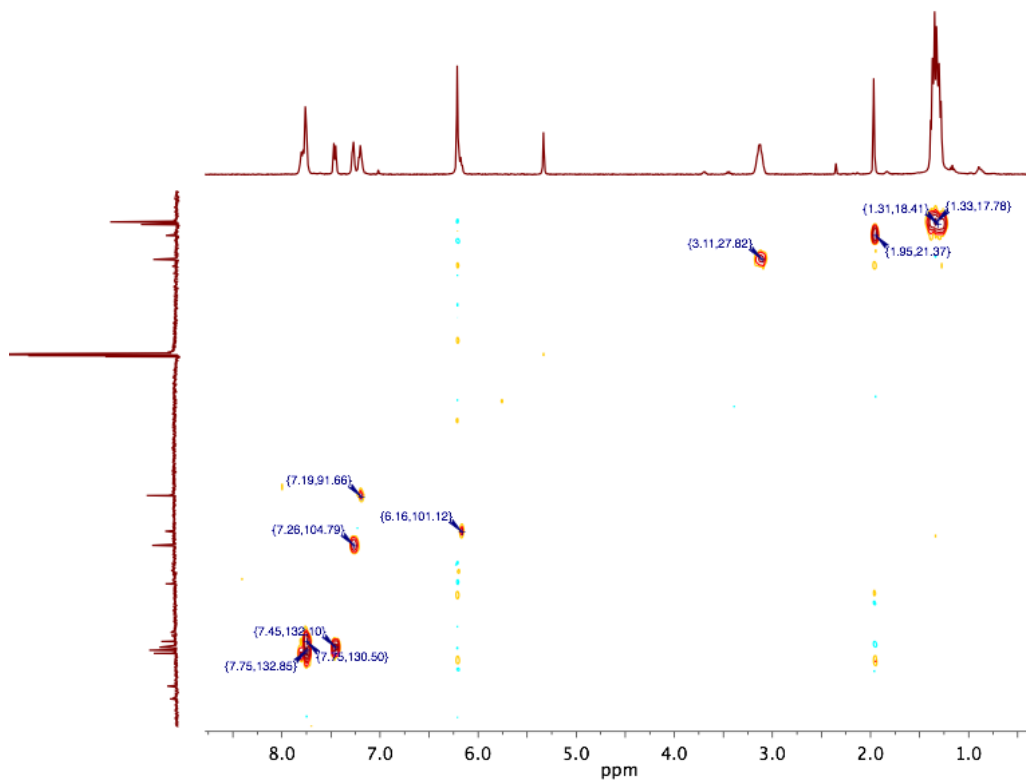


Figure C.80. HSQC spectrum (CD₂Cl₂, 400 MHz) for toluene adduct **25**.

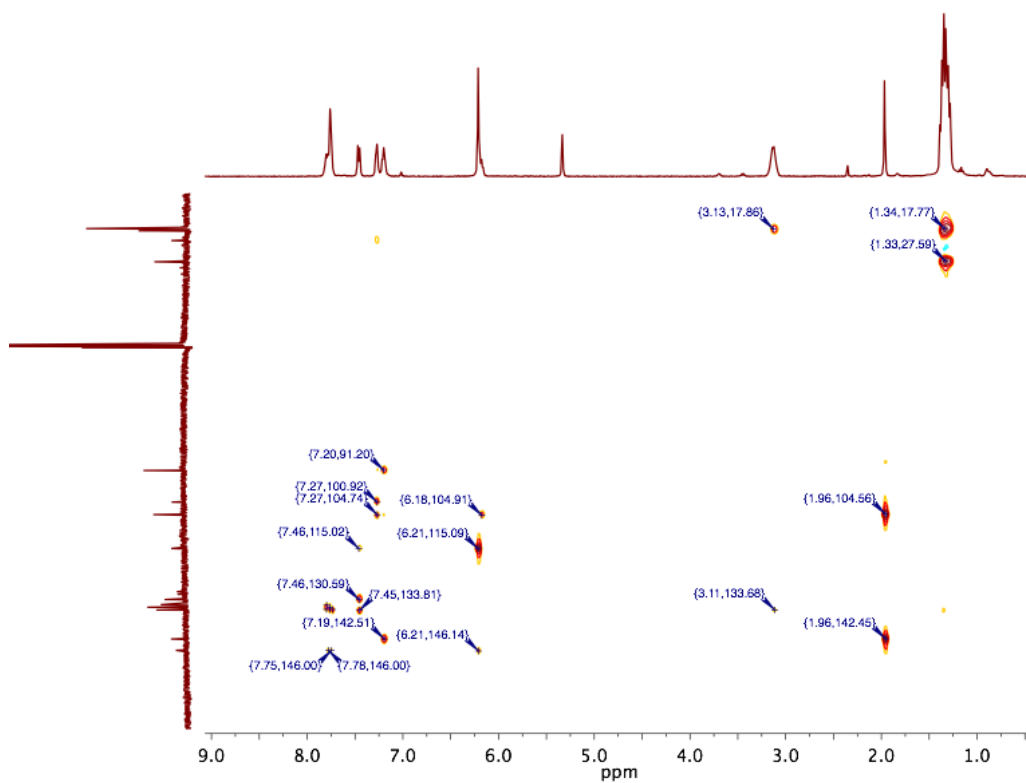


Figure C.81. HMBC spectrum (CD₂Cl₂, 400 MHz) for toluene adduct **25**.

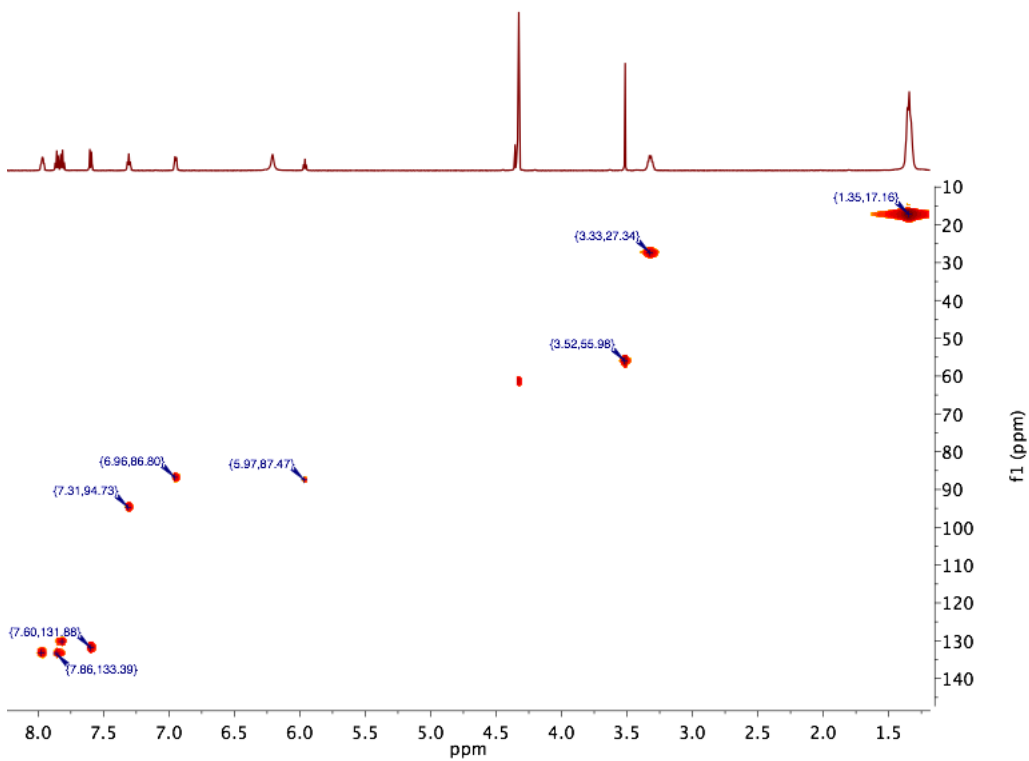


Figure C.82. HSQC spectrum (CD_3NO_2 , 400 MHz) for anisole adduct **26**.

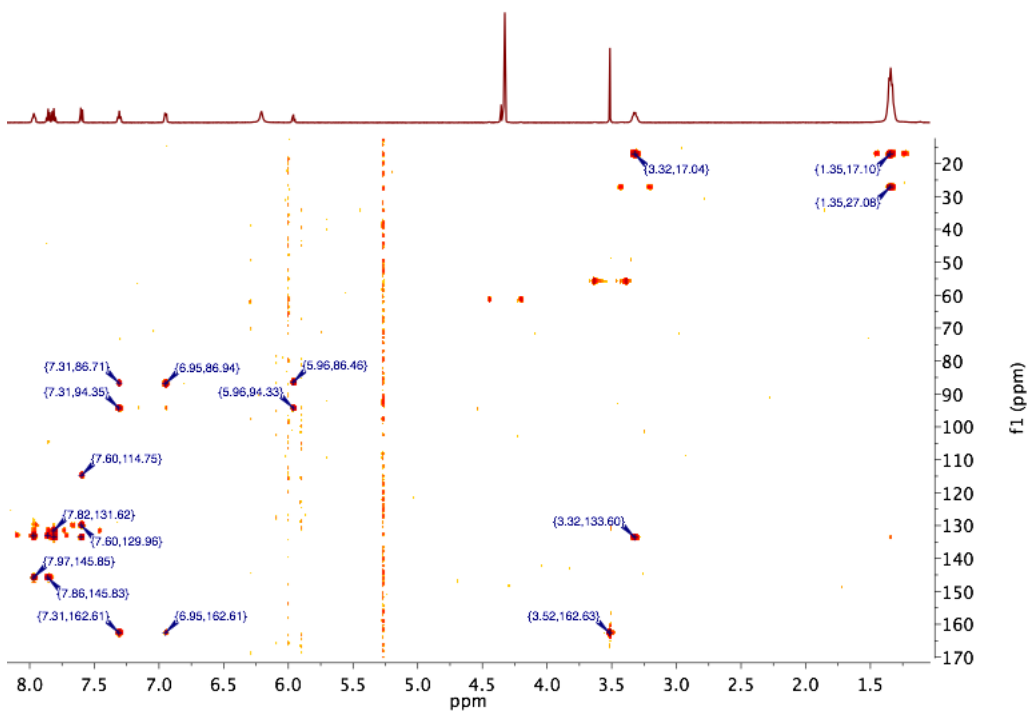


Figure C.83. HMBC spectrum (CD_3NO_2 , 400 MHz) for anisole adduct **26**.

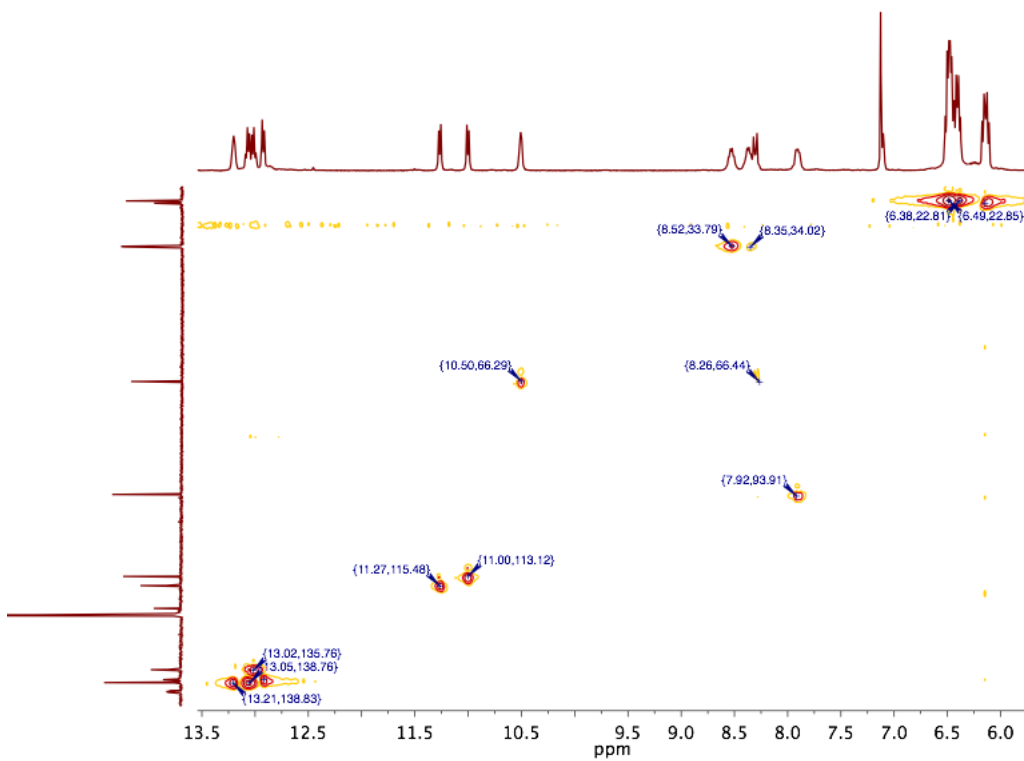


Figure C.84. HSQC spectrum (CD₃CN, 400 MHz) for butadiene adduct **27**.

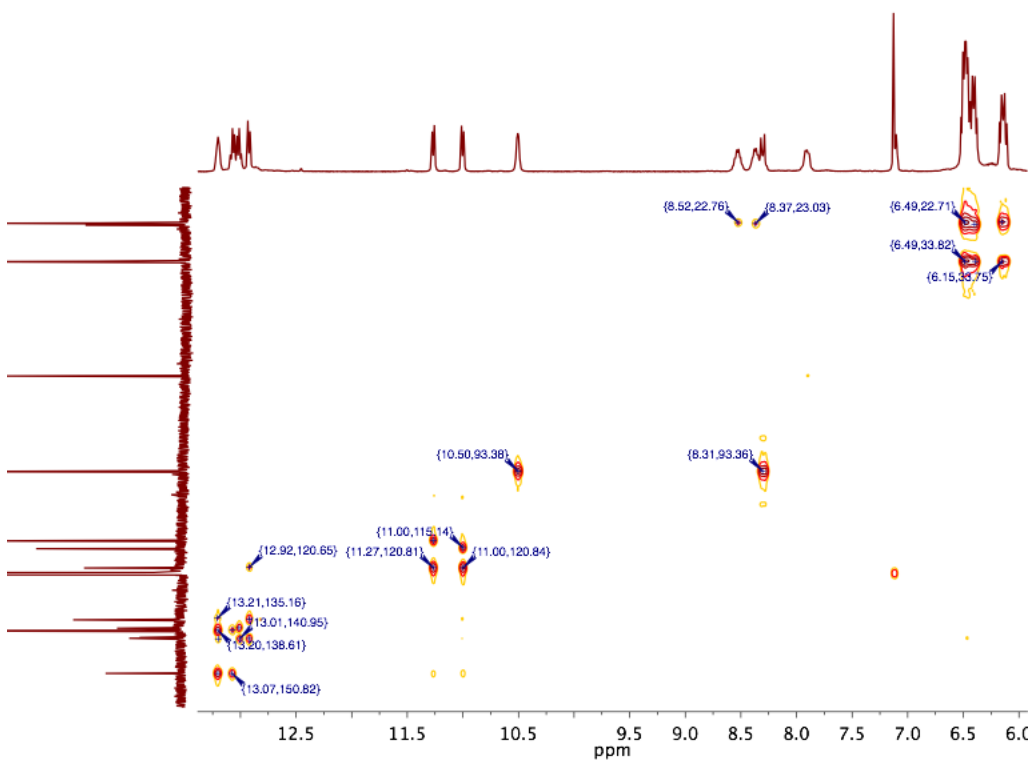


Figure C.85. HMBC spectrum (CD₃CN, 400 MHz) for butadiene adduct **27**.

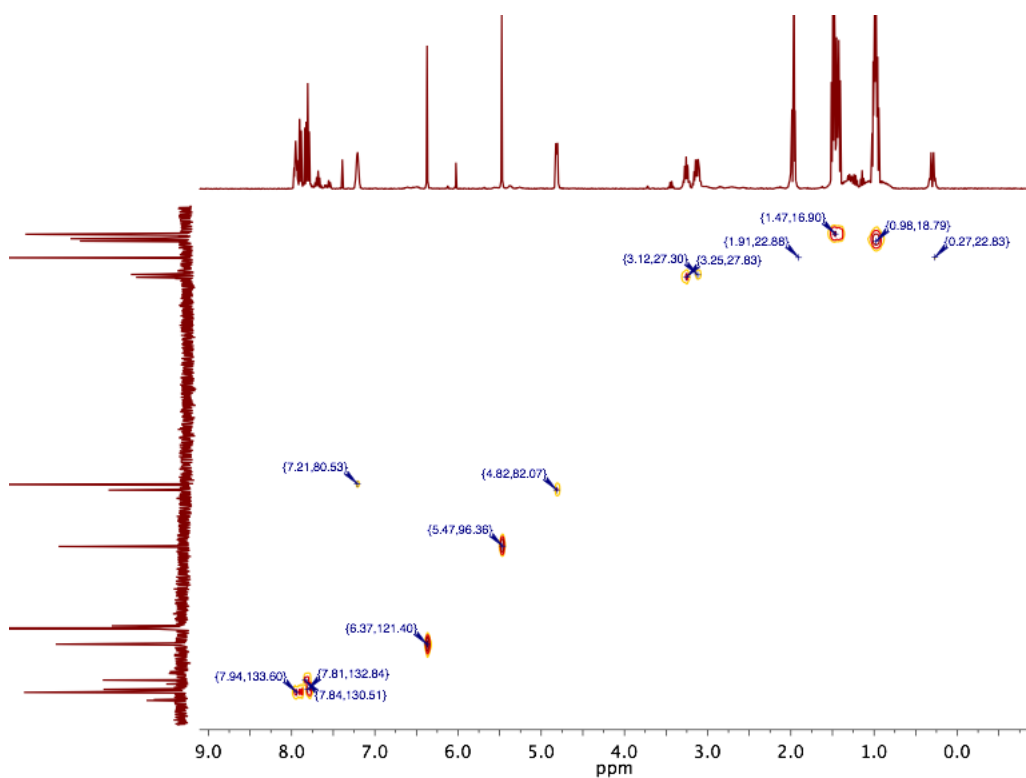


Figure C.86. HSQC spectrum (CD₃CN, 400 MHz) for 1,3-cyclohexadiene adduct **28**.

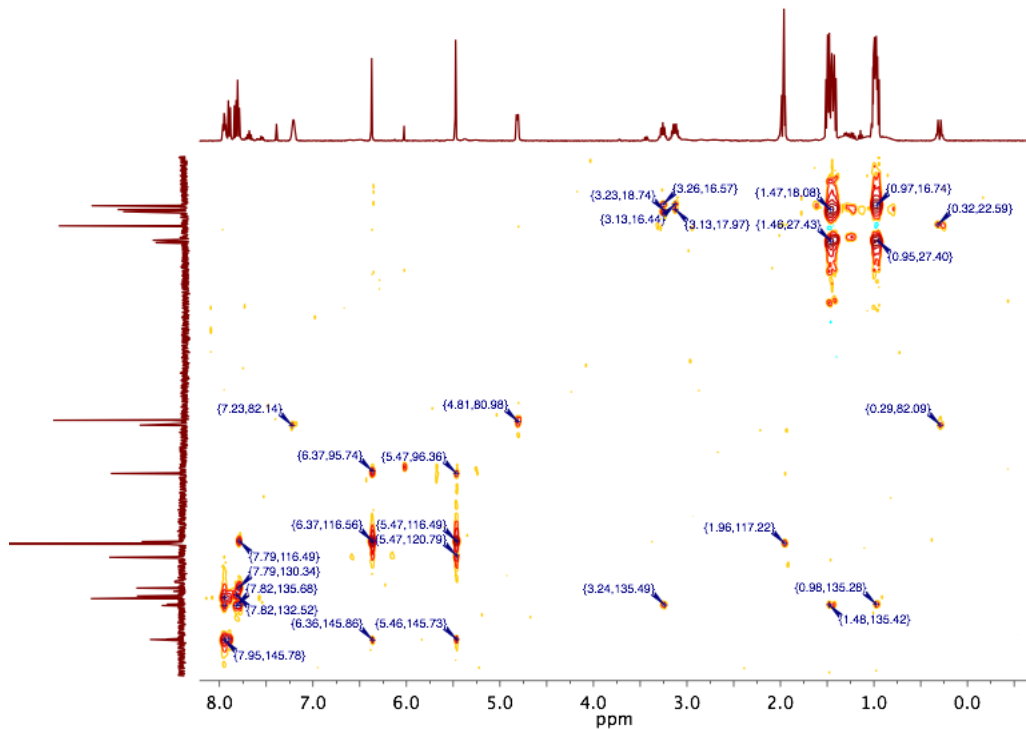


Figure C.87. HMBC spectrum (CD₃CN, 400 MHz) for 1,3-cyclohexadiene adduct **28**.

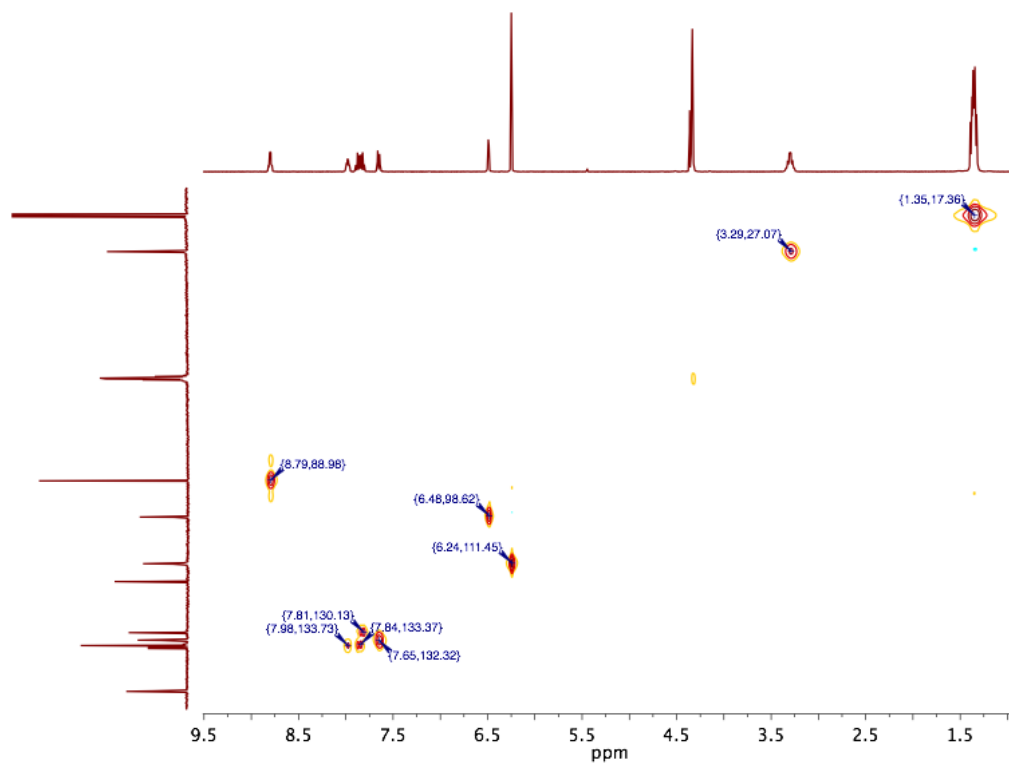


Figure C.88. HSQC spectrum (CD₃NO₂, 400 MHz) for thiophene adduct **29**.

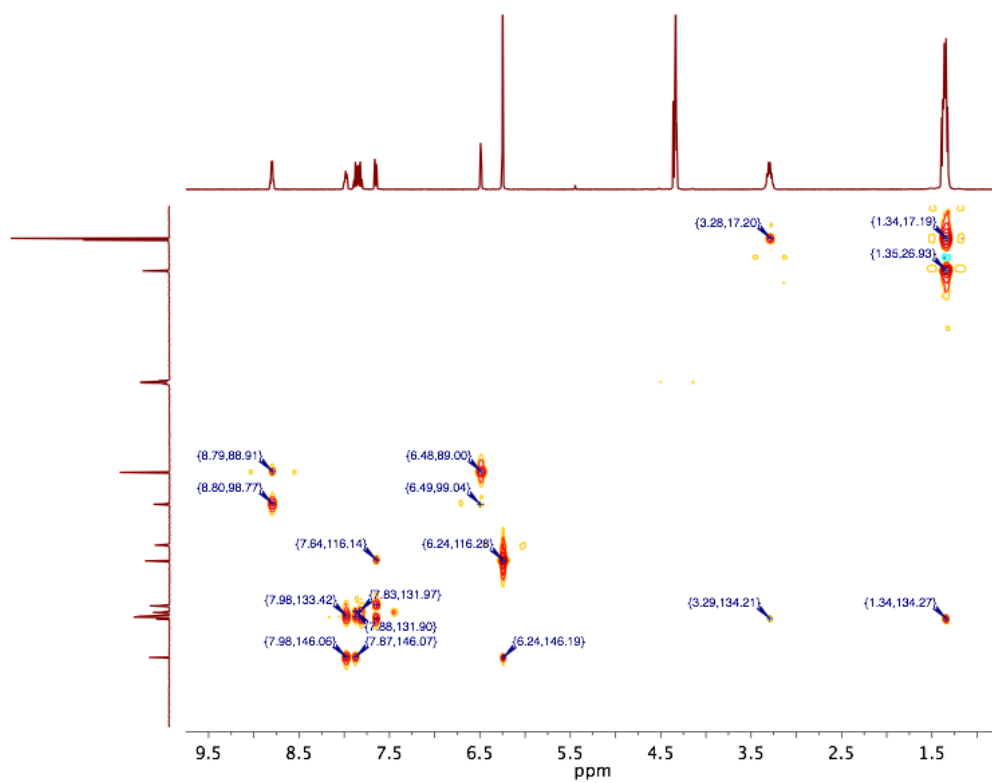


Figure C.89. HMBC spectrum (CD₃NO₂, 400 MHz) for thiophene adduct **29**.

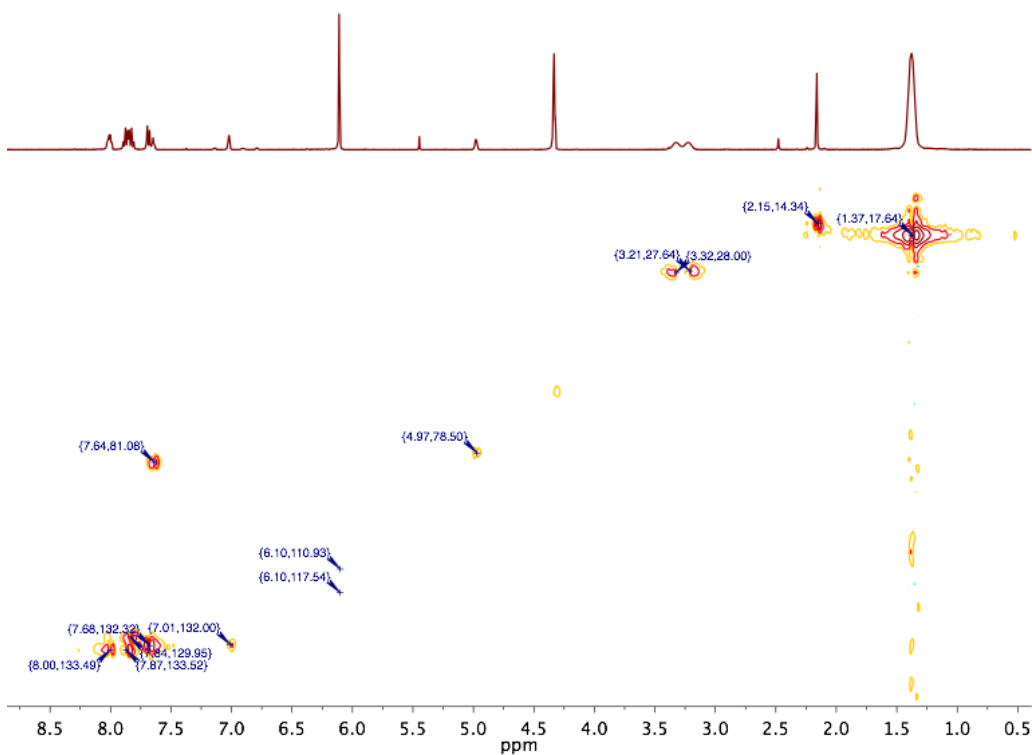


Figure C.90. HSQC spectrum (CD₃NO₂, 400 MHz) for 2-methylthiophene adduct **30**.

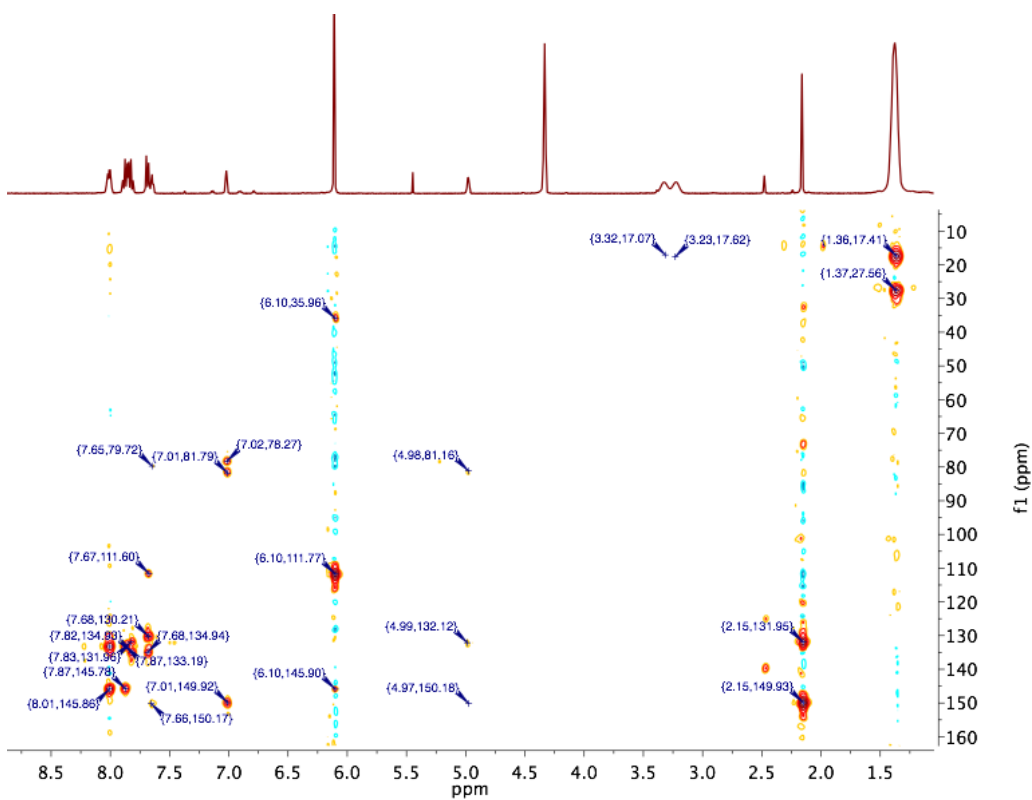


Figure C.91. HMBC spectrum (CD₃NO₂, 400 MHz) for 2-methylthiophene adduct **30**.

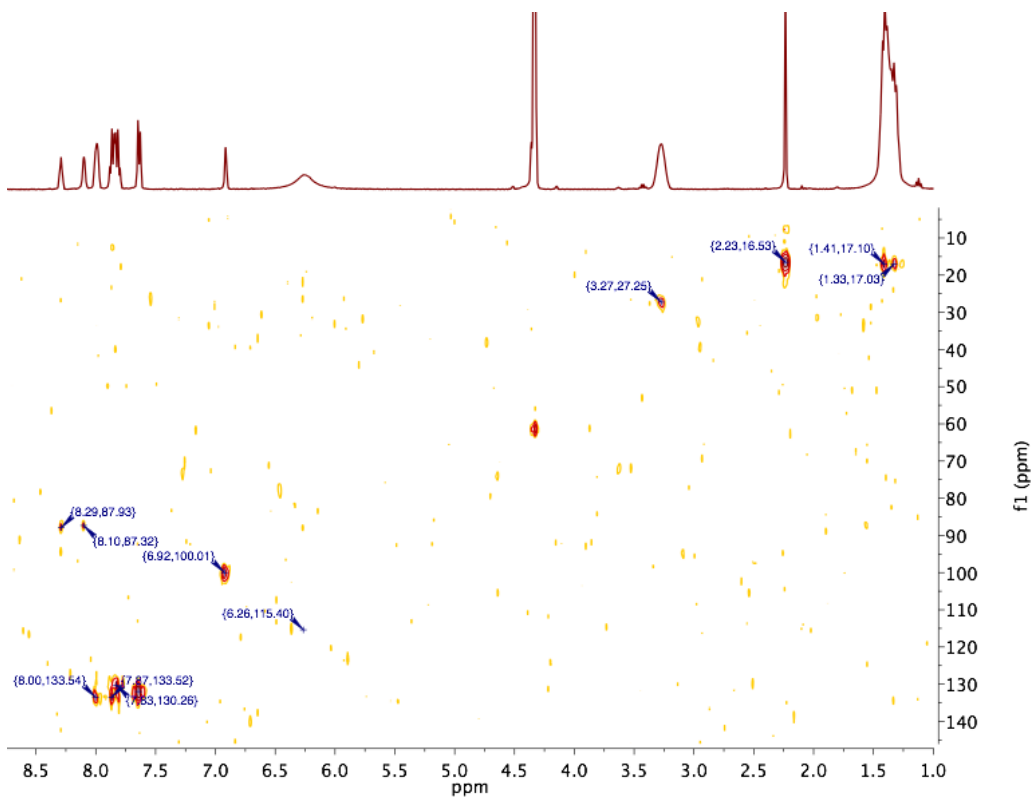


Figure C.92. HSQC spectrum (CD₃NO₂, 400 MHz) for 3-methylthiophene adduct **31**.

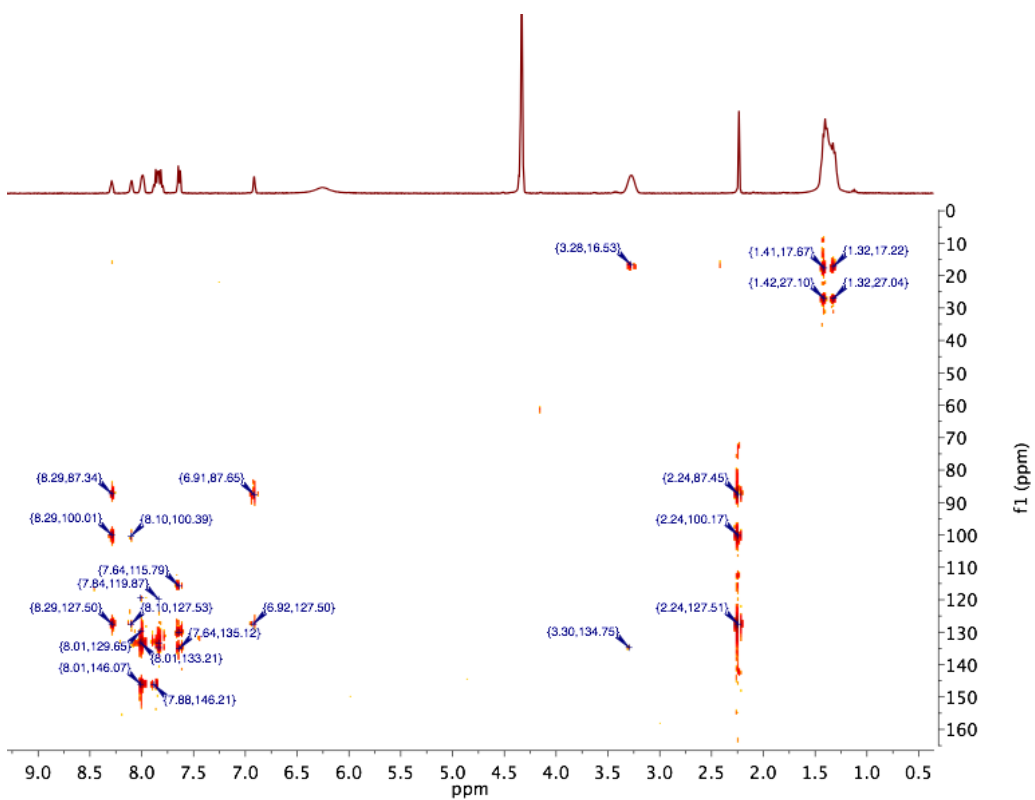


Figure C.93. HMBC spectrum (CD₃NO₂, 400 MHz) for 3-methylthiophene adduct **31**.

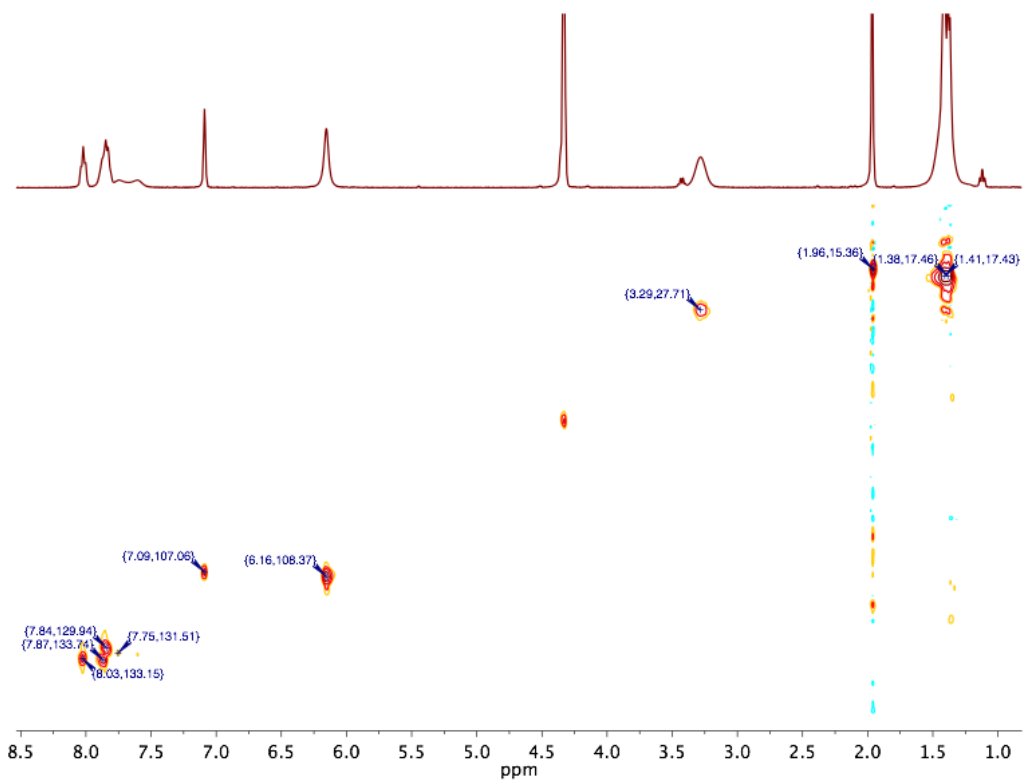


Figure C.94. HSQC spectrum (CD_3NO_2 , 400 MHz) for 2,5-dimethylthiophene adduct **32**.

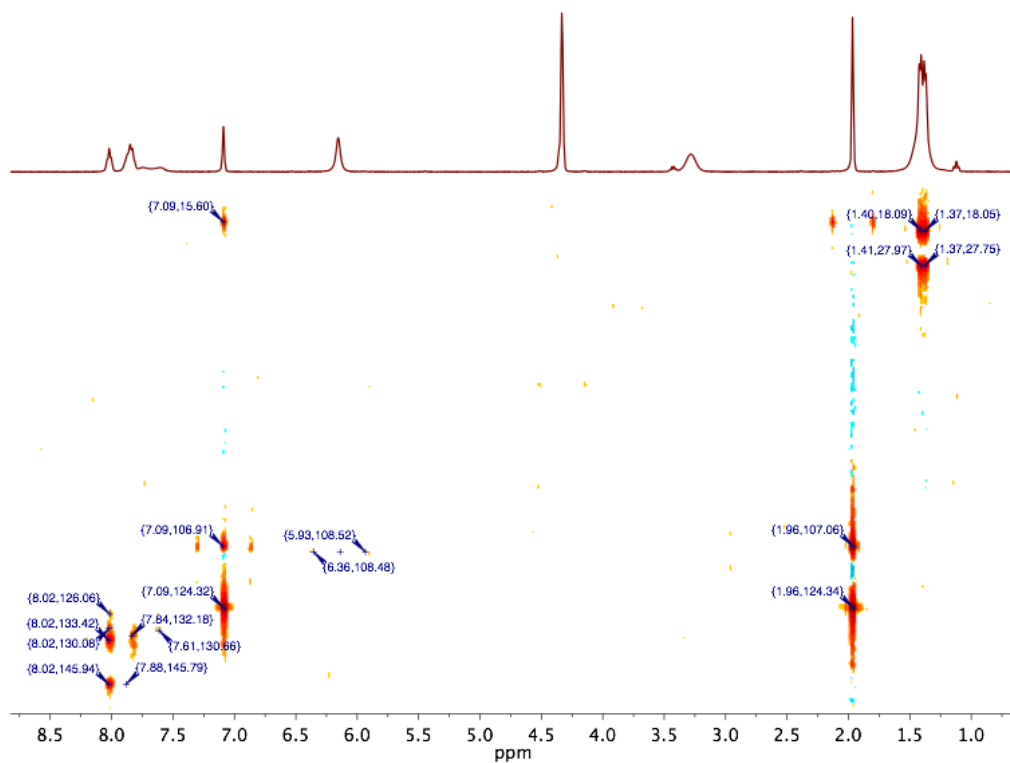


Figure C.95. HMBC spectrum (CD_3NO_2 , 400 MHz) for 2,5-dimethylthiophene adduct **32**.

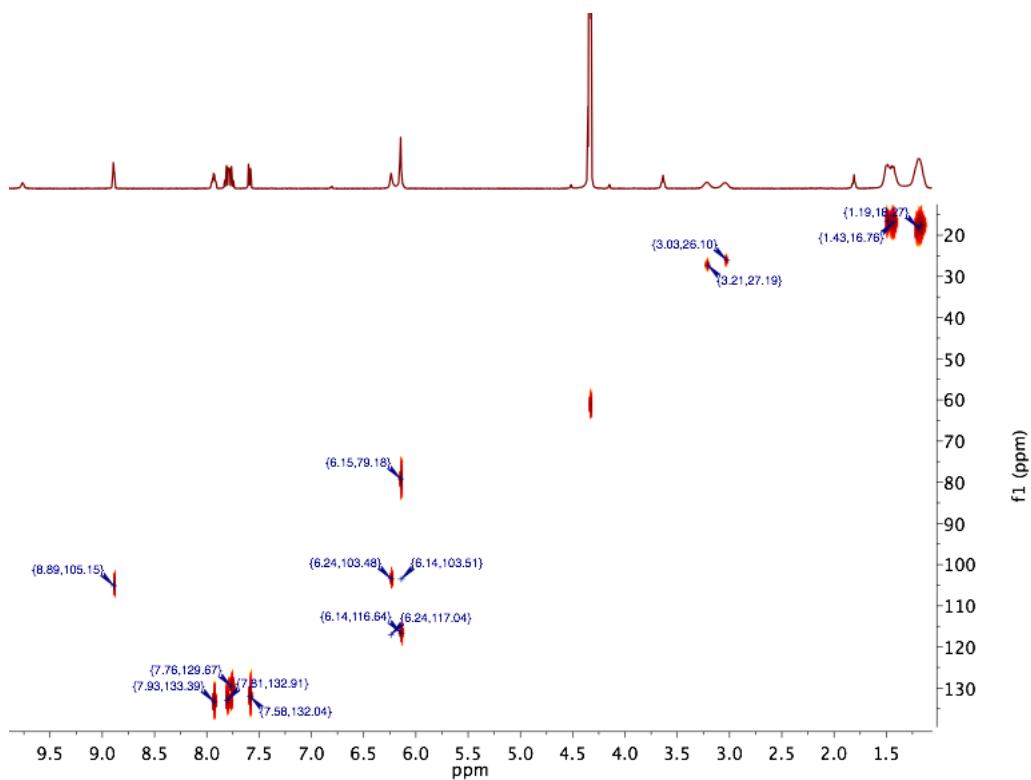


Figure C.96. HSQC spectrum (CD₃NO₂, 400 MHz) for pyrrole adduct **33**.

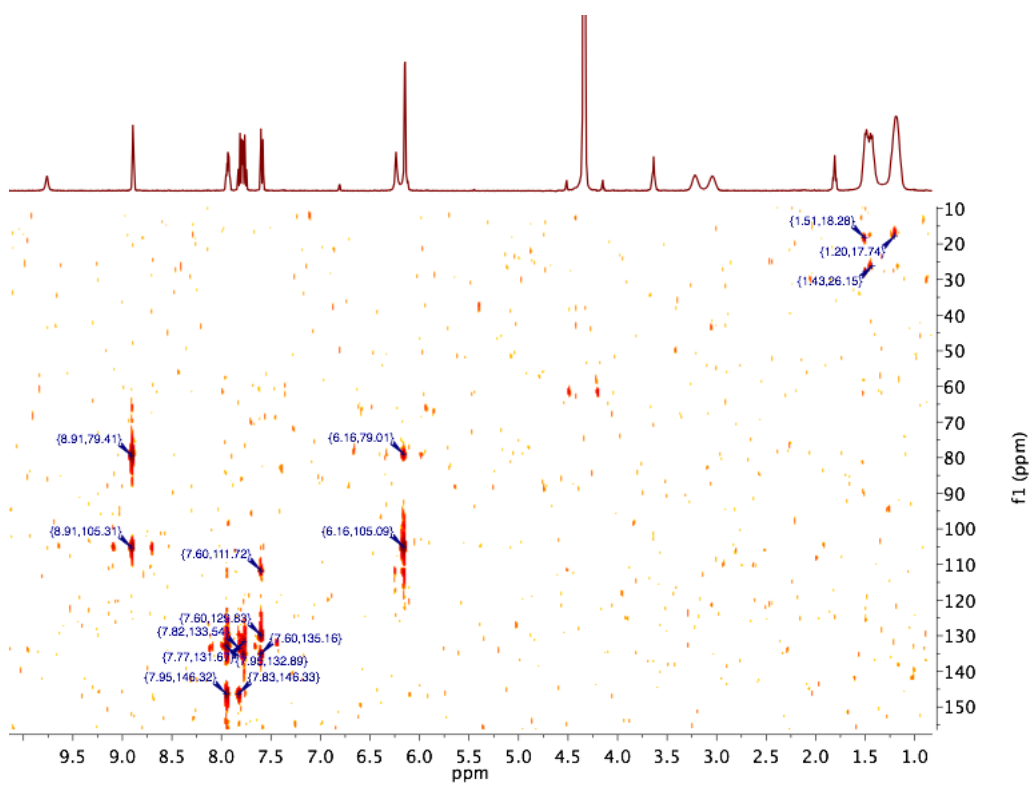


Figure C.97. HMBC spectrum (CD₃NO₂, 400 MHz) for pyrrole adduct **33**.

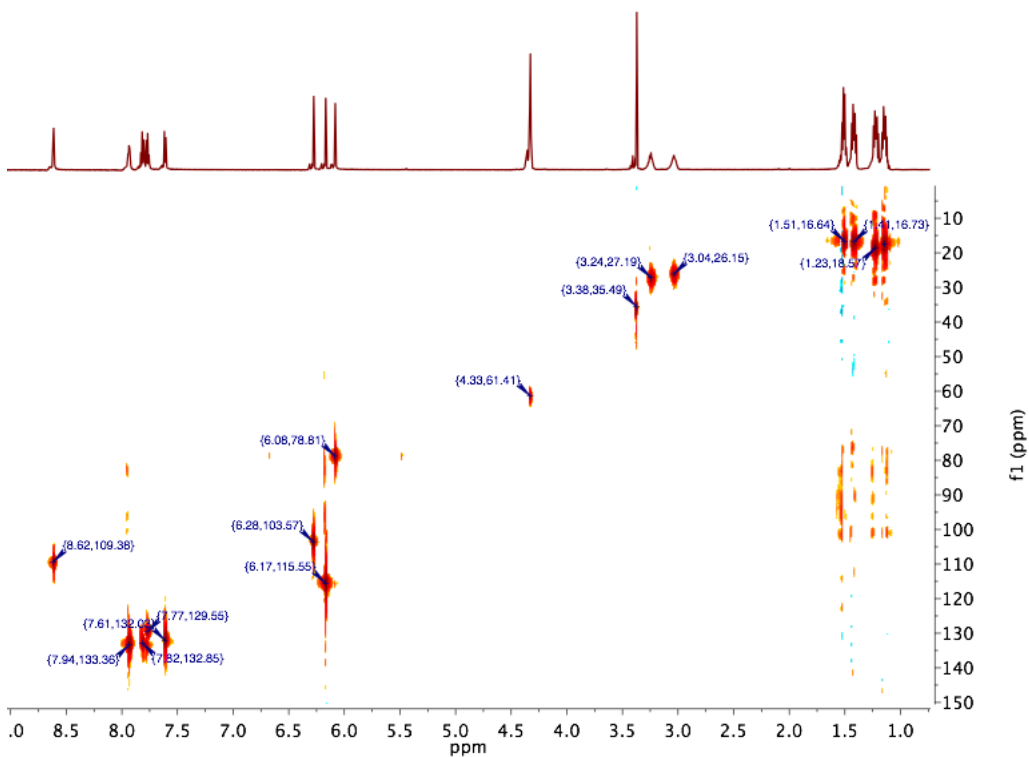


Figure C.98. HSQC spectrum (CD_3NO_2 , 400 MHz) for N-Me-pyrrole adduct 34.

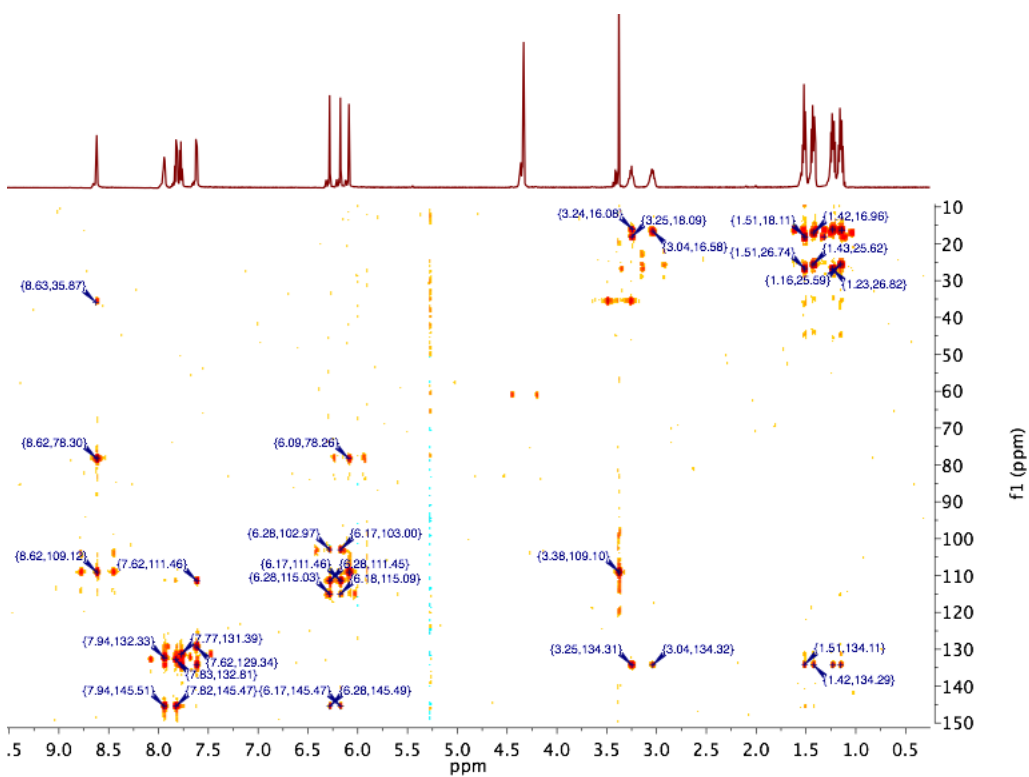


Figure C.99. HMBC spectrum (CD_3NO_2 , 400 MHz) for N-Me-pyrrole adduct 34.

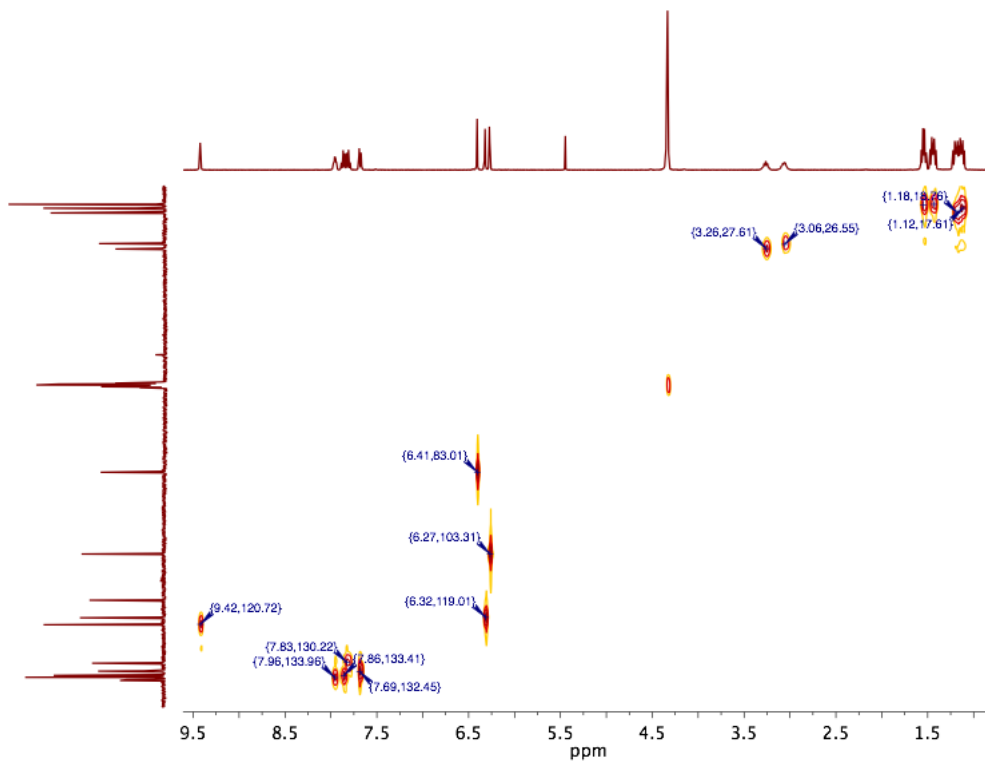


Figure C.100. HSQC spectrum (CD₃NO₂, 400 MHz) for furan adduct 35.

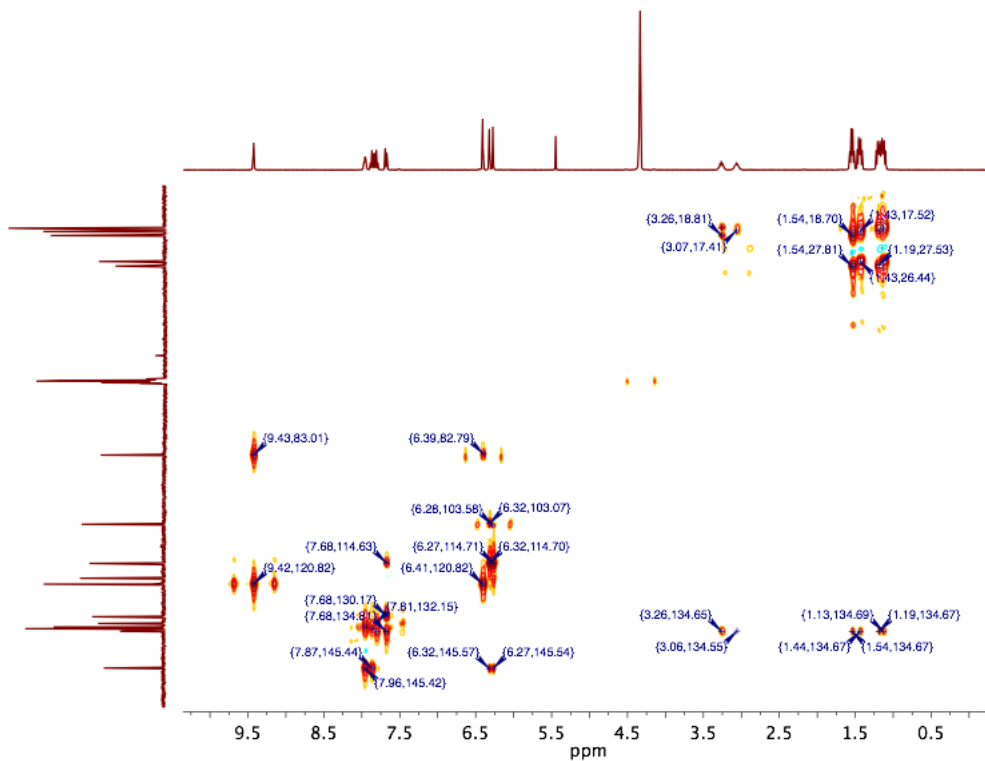


Figure C.101. HMBC spectrum (CD₃NO₂, 400 MHz) for furan adduct 35.

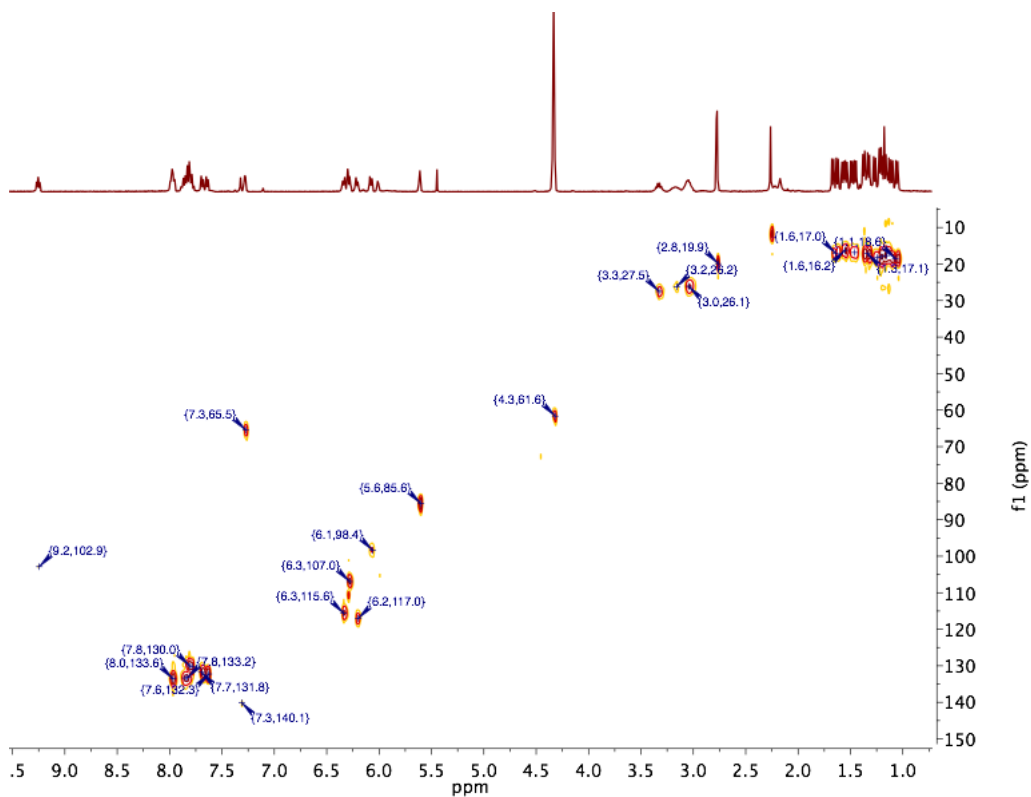


Figure C.102. HSQC spectrum (CD₃NO₂, 400 MHz) for 2-methylfuran adduct **36**.

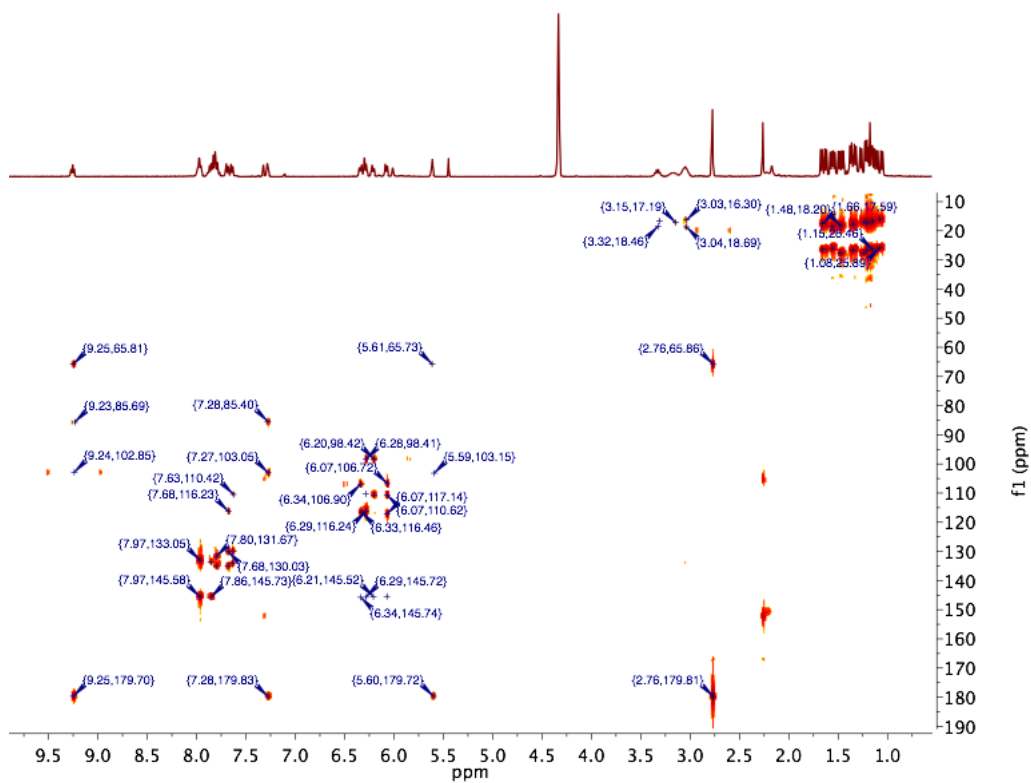


Figure C.103. HMBC spectrum (CD₃NO₂, 400 MHz) for 2-methylfuran adduct **36**.

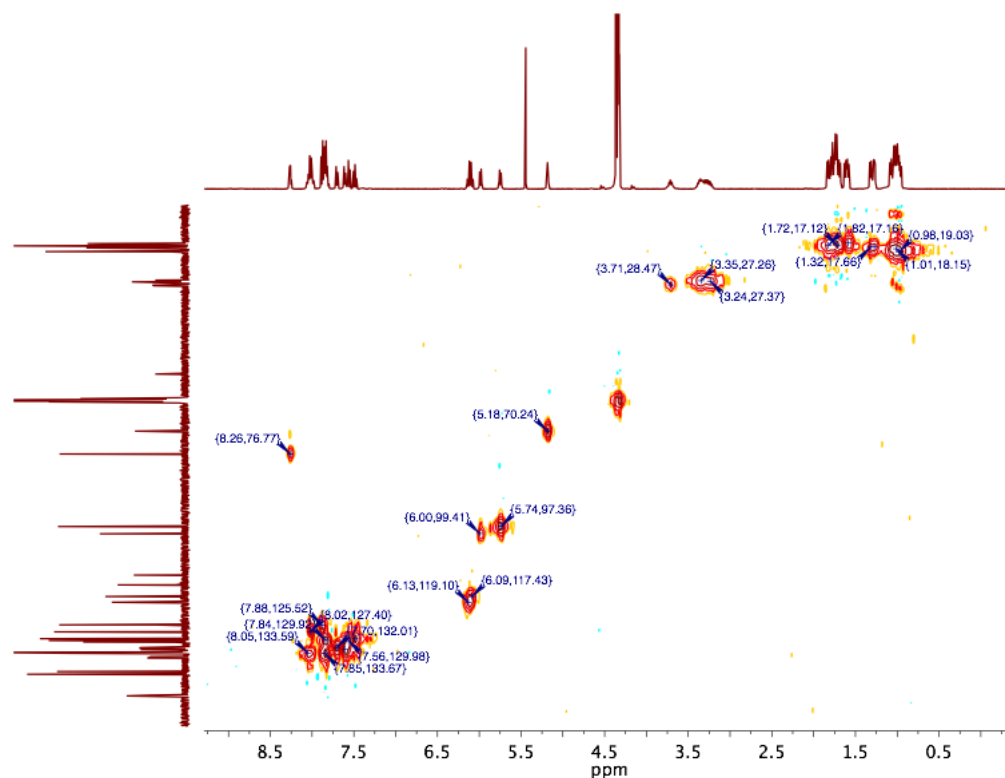


Figure C.104. HSQC spectrum (CD₃NO₂, 400 MHz) for benzothiophene adduct **37**.

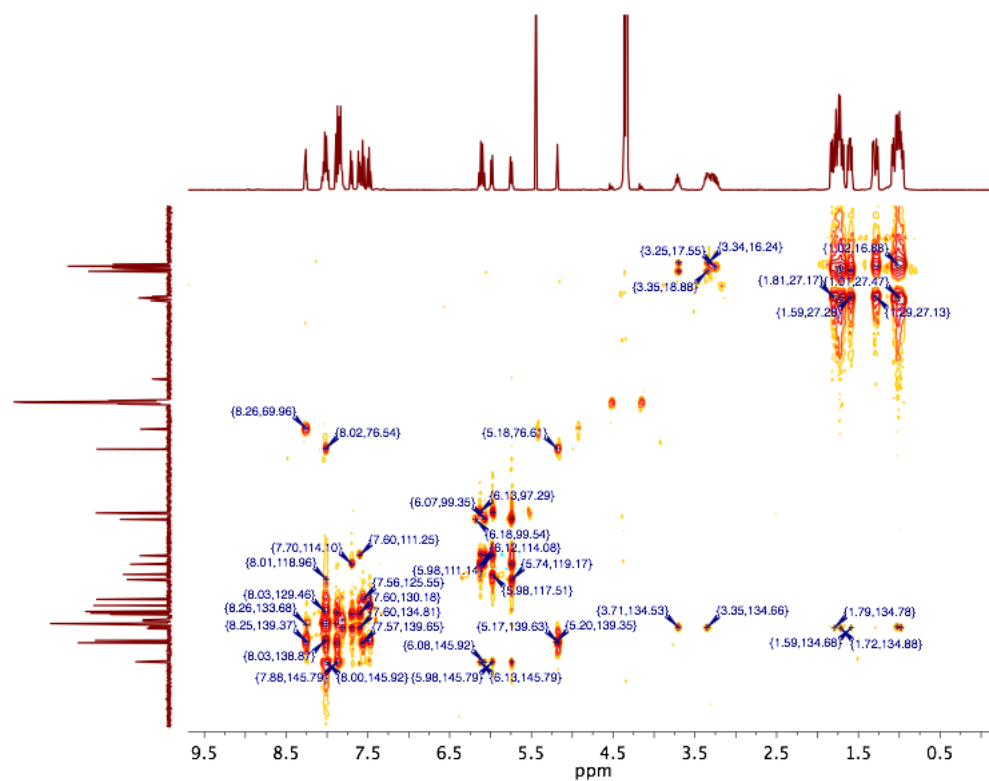


Figure C.105. HMBC spectrum (CD₃NO₂, 400 MHz) for benzothiophene **37**.

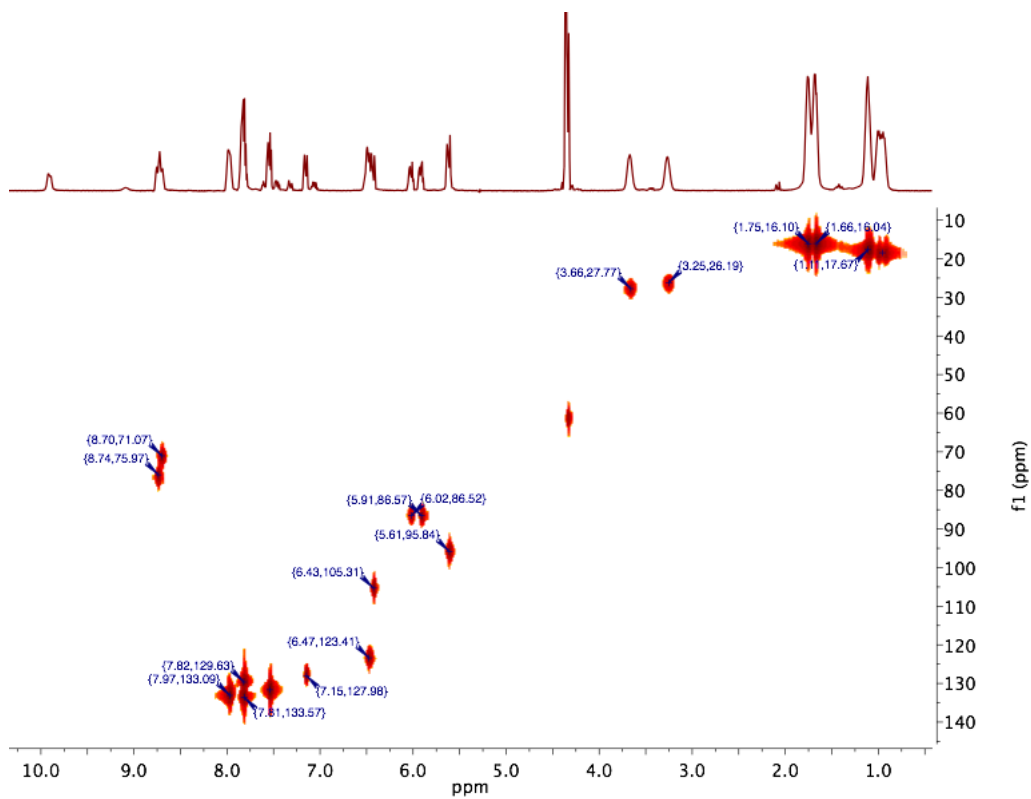


Figure C.106. HSQC spectrum (CD₃NO₂, 400 MHz) for indole adduct 38.

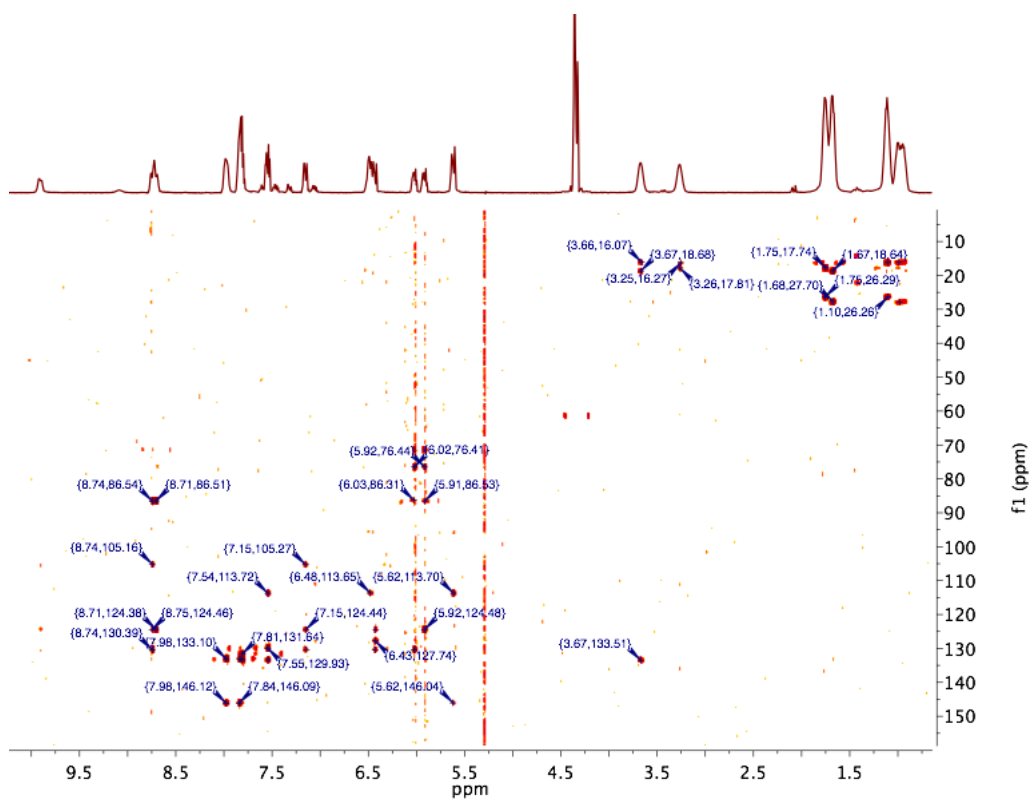


Figure C.107. HMBC spectrum (CD₃NO₂, 400 MHz) for indole adduct 38.

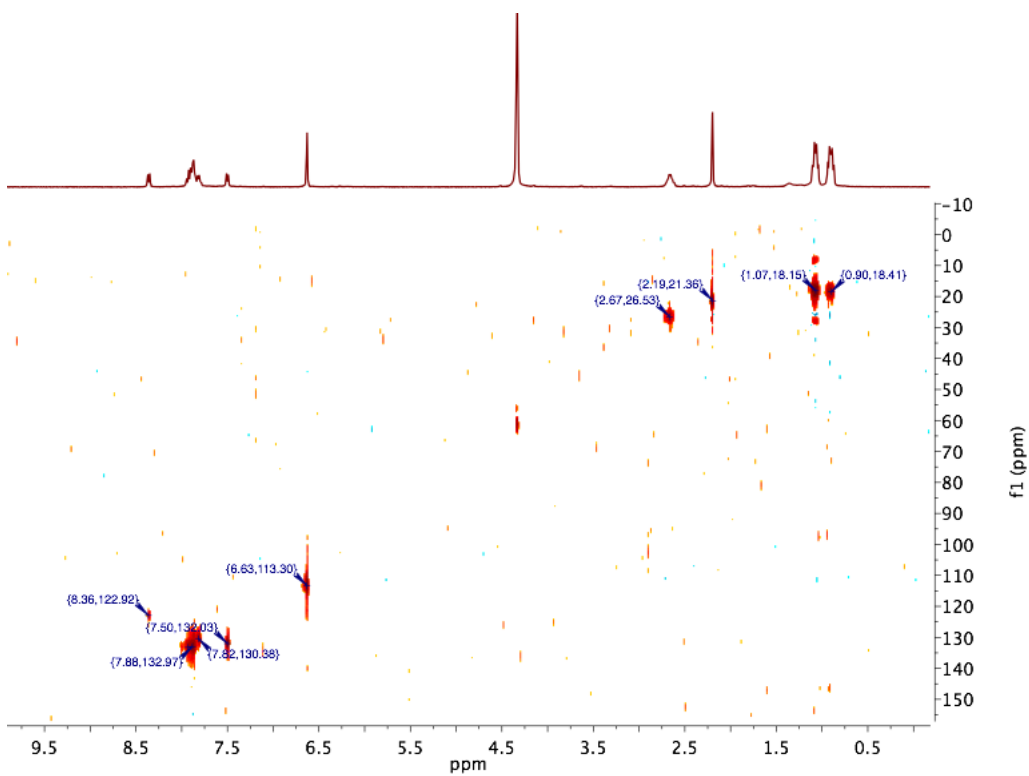


Figure C.108. HSQC spectrum (CD₃NO₂, 400 MHz) for 4,6-dimethyldibenzothiophene adduct **39**.

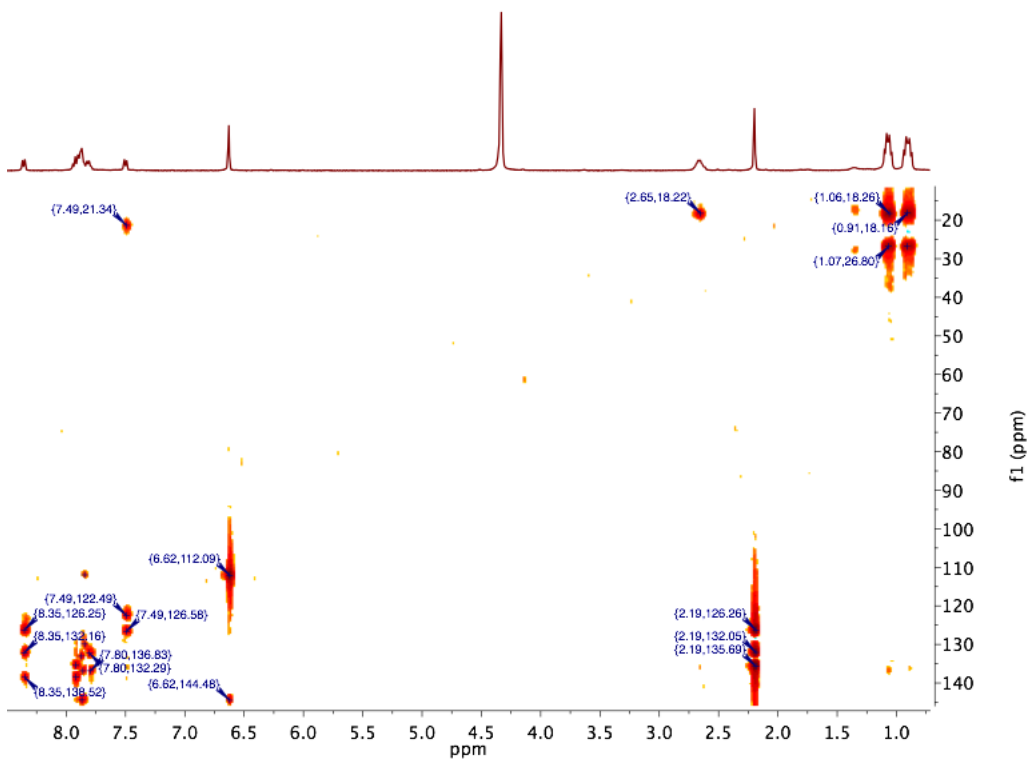


Figure C.109. HMBC spectrum (CD₃NO₂, 400 MHz) for 4,6-dimethyldibenzothiophene adduct **39**.

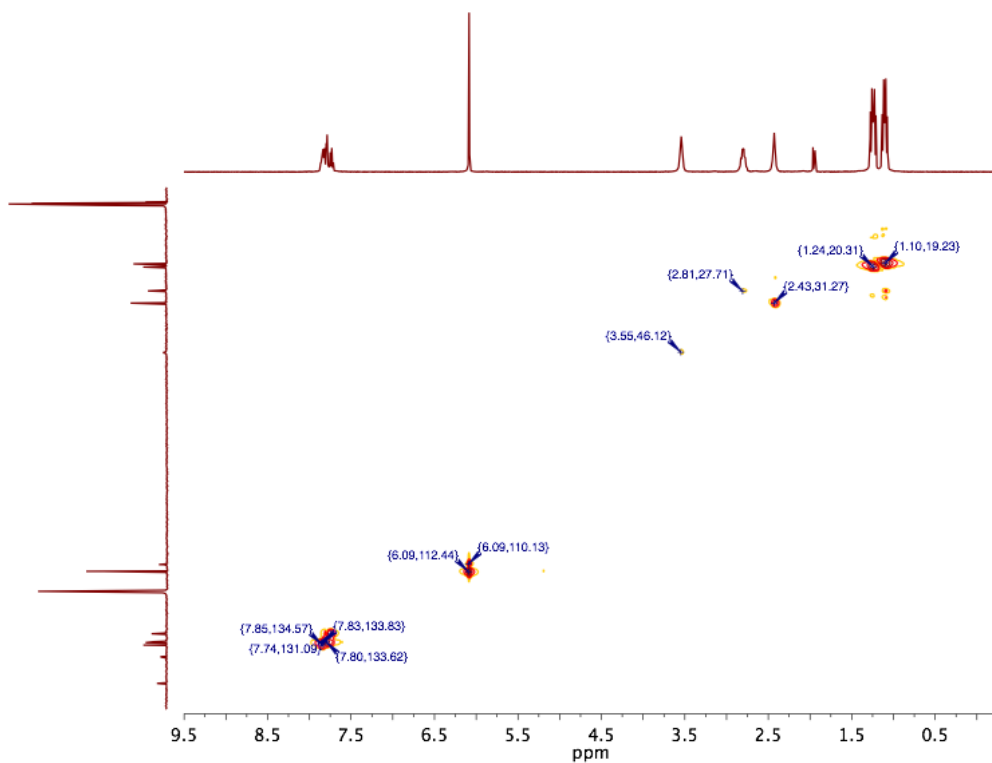


Figure C.110. HSQC spectrum (CD_3CN , 400 MHz) for tetrahydrothiophene adduct **40**.

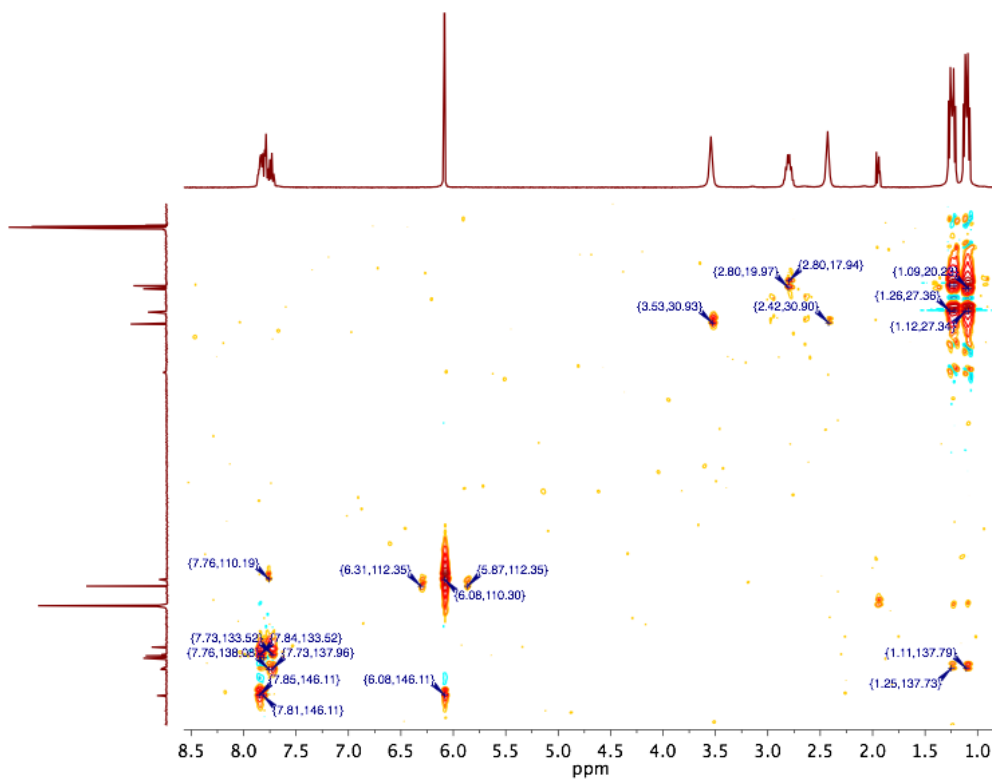


Figure C.111. HMBC spectrum (CD_3CN , 400 MHz) for tetrahydrothiophene adduct **40**.

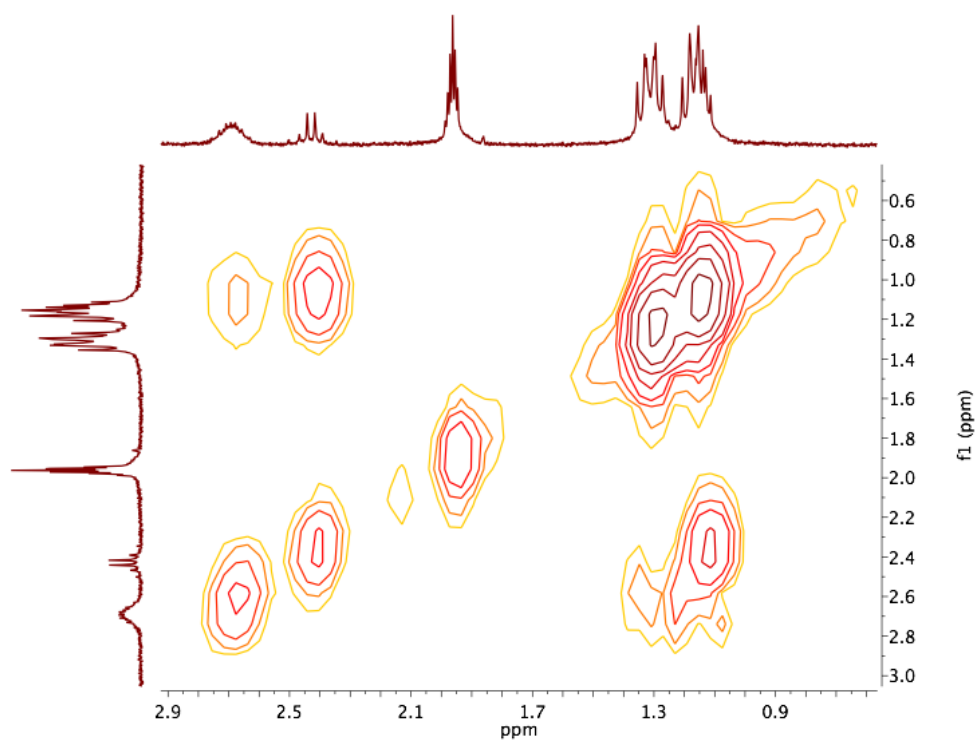


Figure C.112. Aliphatic region of COSY spectrum (CD_3CN , 300 MHz) for propanoate complex **41**.

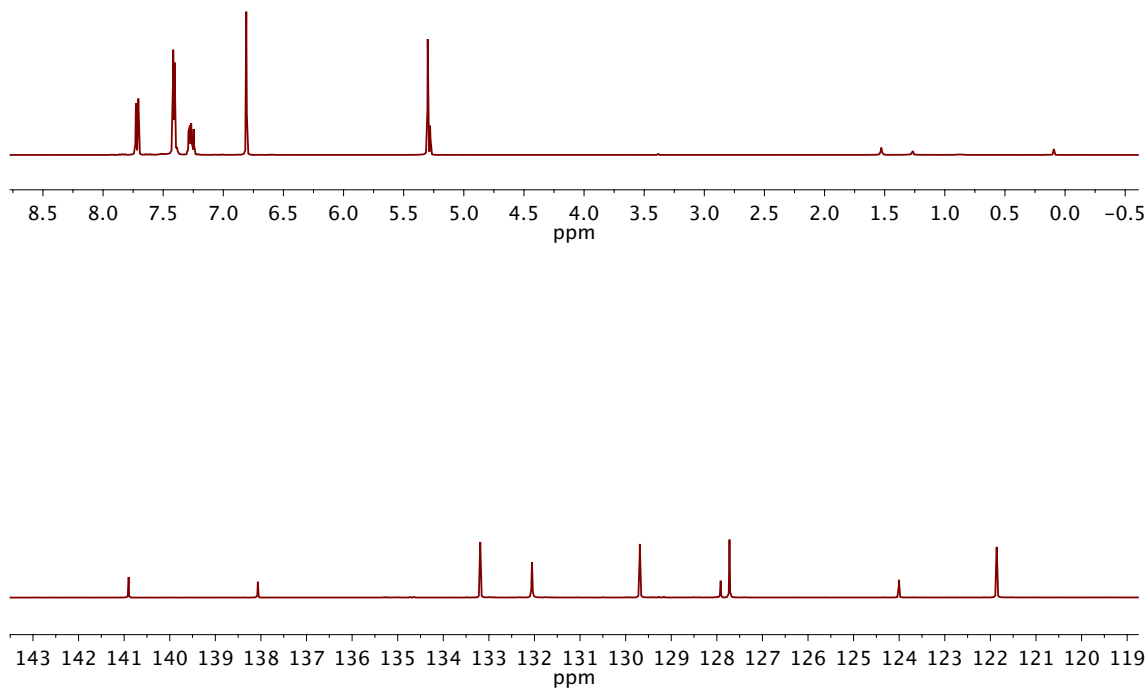


Figure C.113. ^1H (top) and ^{13}C (bottom) NMR spectra of 1,4-bis(2-bromobenzene)-2,3-dihydroxybenzene in CDCl_3 .

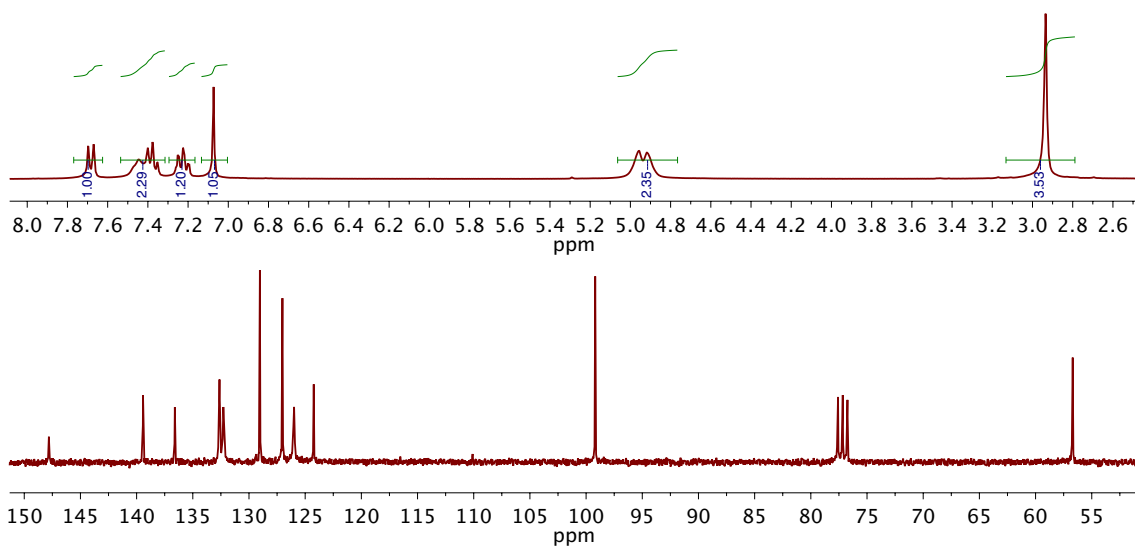


Figure C.114. ^1H (top) and ^{13}C (bottom) NMR spectra of 1,4-bis(2-bromobenzene)-2,3-bis(methoxymethyl)benzene in CDCl_3 .

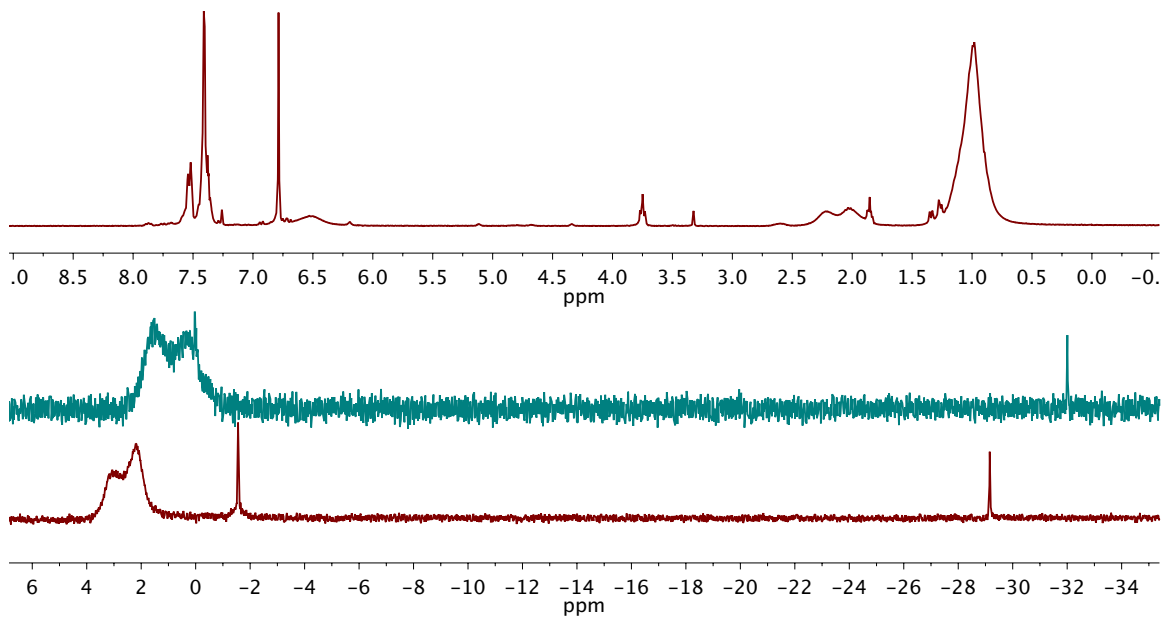


Figure C.115. ^1H (top, CDCl_3) and ^{31}P (bottom) NMR spectra of catechol diphosphine **48**. The top ^{31}P NMR spectrum was recorded with THF as solvent and the bottom spectrum of the same sample was collected with CDCl_3 .

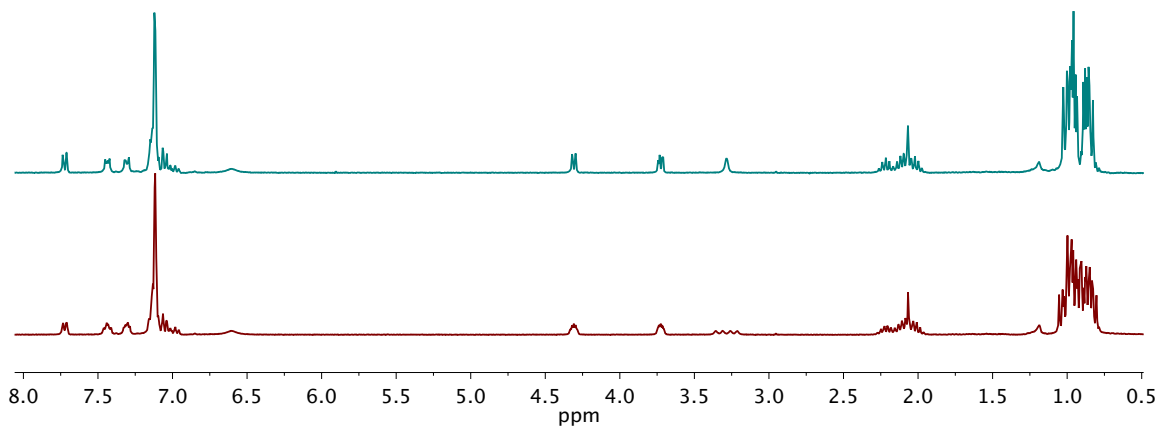


Figure C.116. ^1H NMR spectra (C_6D_6 , 300 MHz) of **49** with (top) and without (bottom) ^{31}P decoupler turned on and centered at 56 ppm.

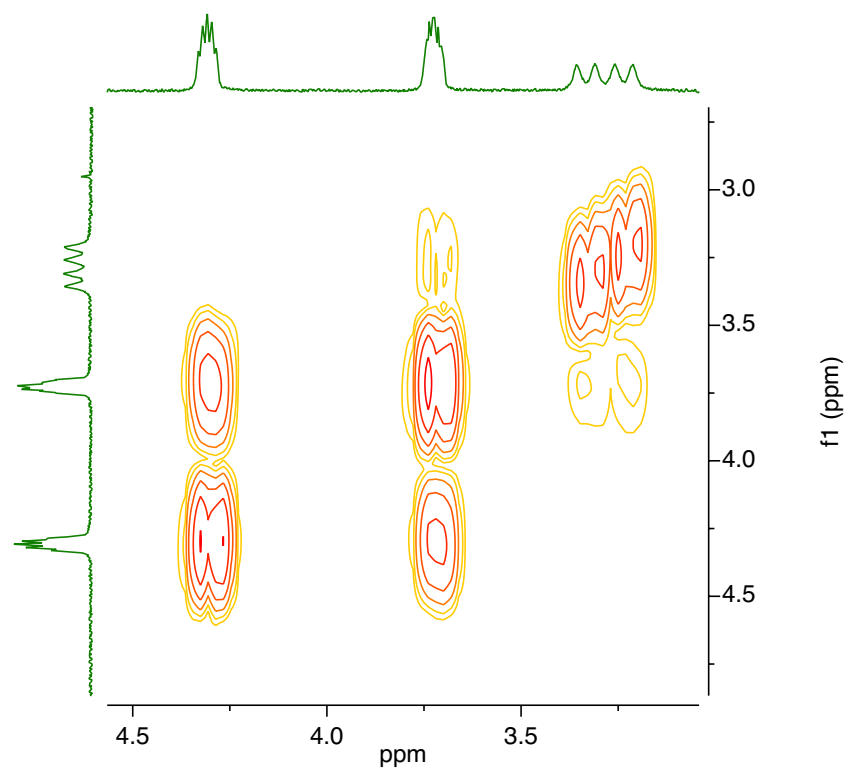


Figure C.117. Excerpt of gCOSY spectrum of **49**.

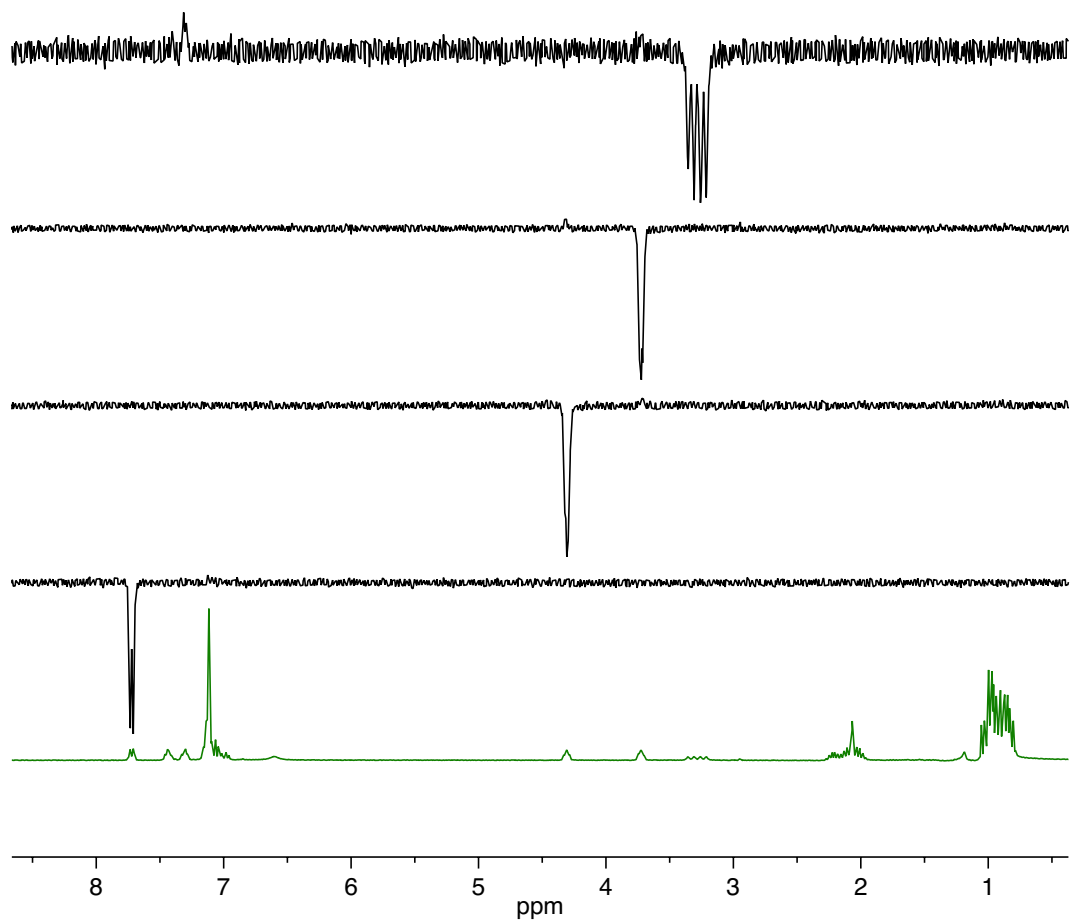


Figure C.118. 1D NOE experiments of **49**.

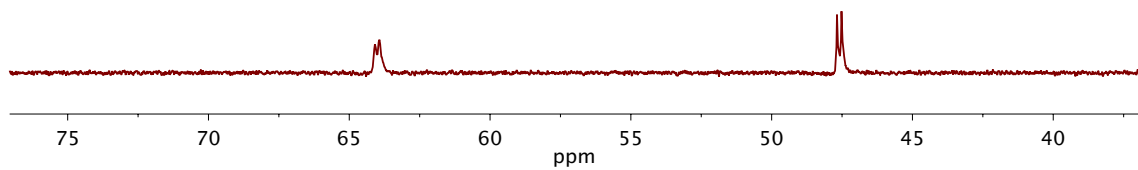


Figure C.119. $^{31}\text{P}\{^1\text{H}\}$ NMR spectrum of **49**.

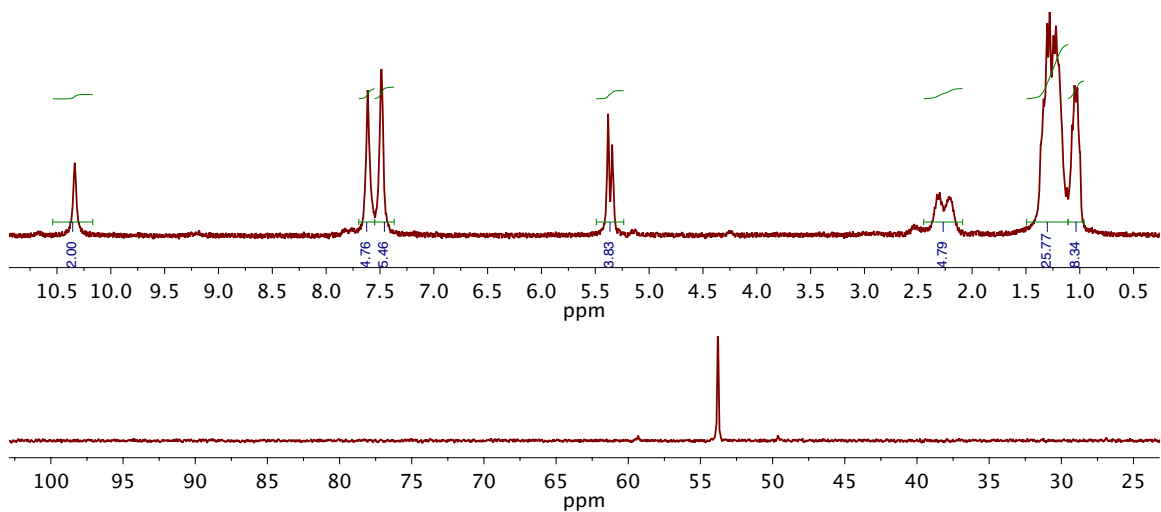


Figure C.120. ^1H (top) and ^{31}P (bottom) NMR spectra of dinickel dichloride **50** (CD_2Cl_2).

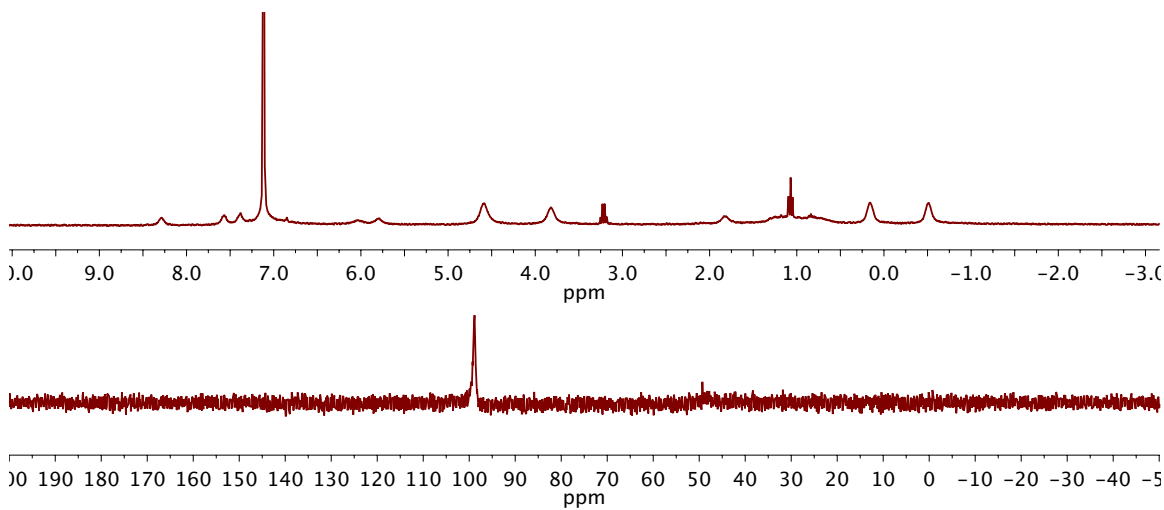


Figure C.121. ^1H (top) and ^{31}P (bottom) NMR spectra of pentanickel dichloride **51** (C_6D_6).

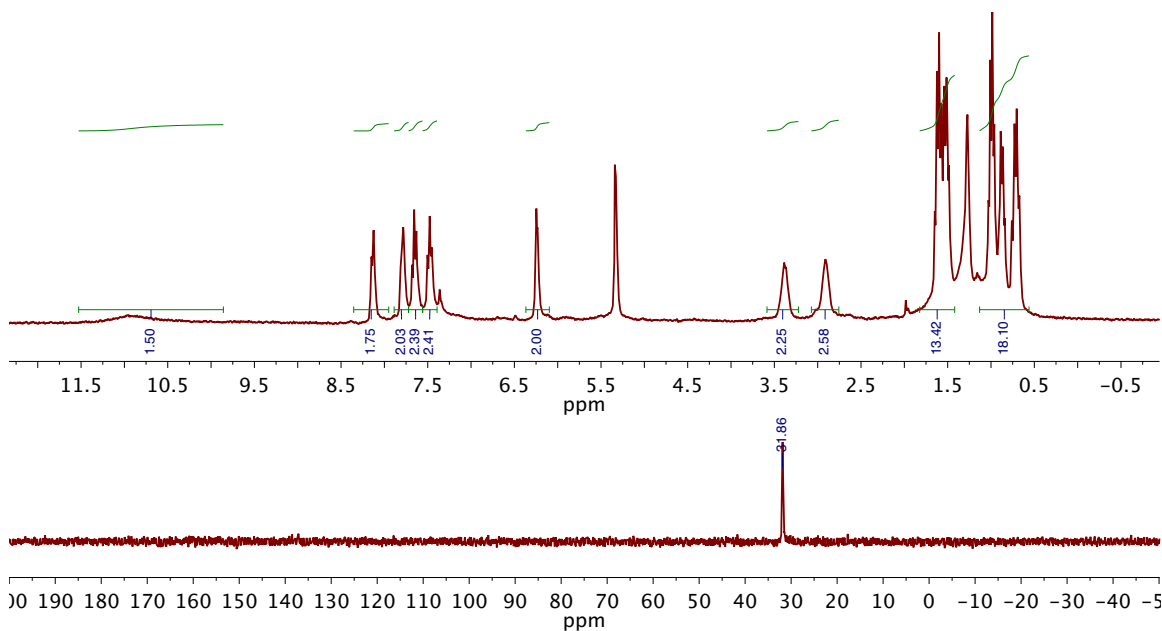


Figure C.122. ^1H (top) and ^{31}P (bottom) NMR spectra of palladium dichloride **52** (CD_2Cl_2).

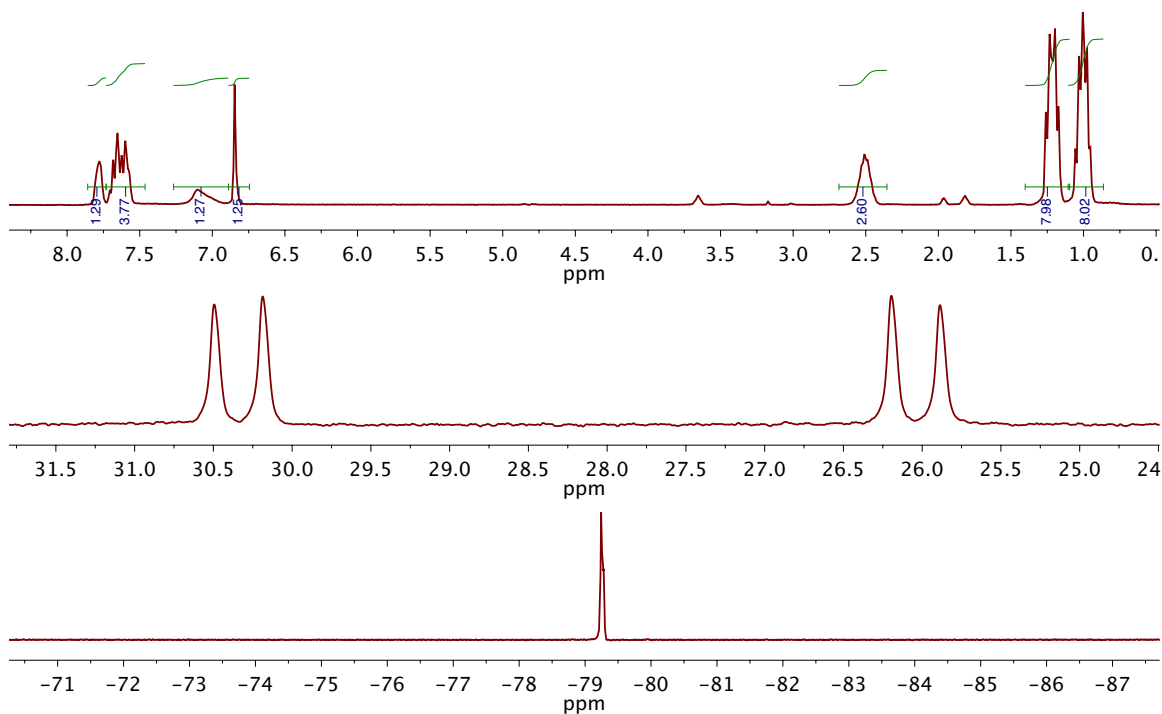


Figure C.123. ^1H (top), ^{19}F (middle), and ^{31}P (bottom) NMR spectra of silver triflate **53** (CD_3CN).

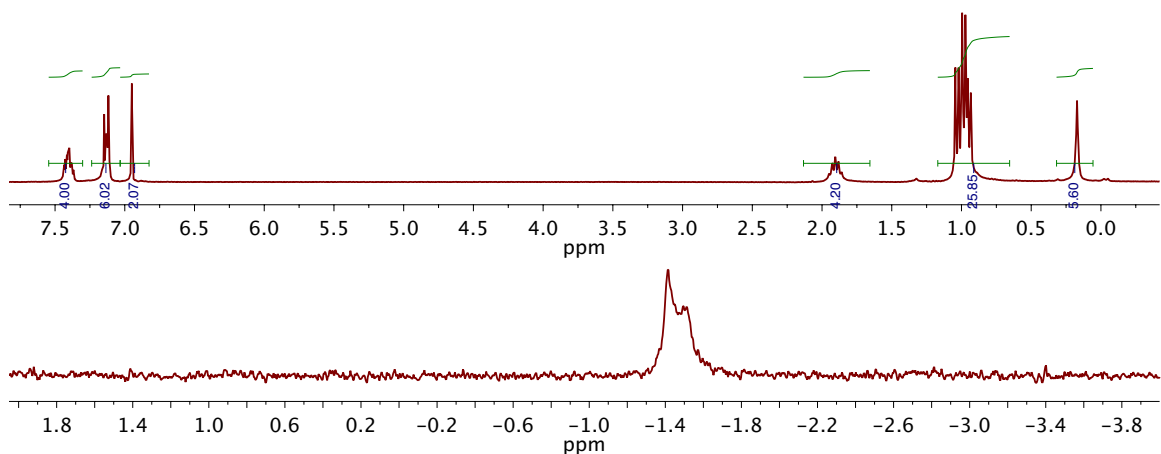


Figure C.124. ^1H (top) and ^{31}P (bottom) NMR spectra of dimethylsilyl protected catechol diphosphine **54** (CD_2Cl_2).

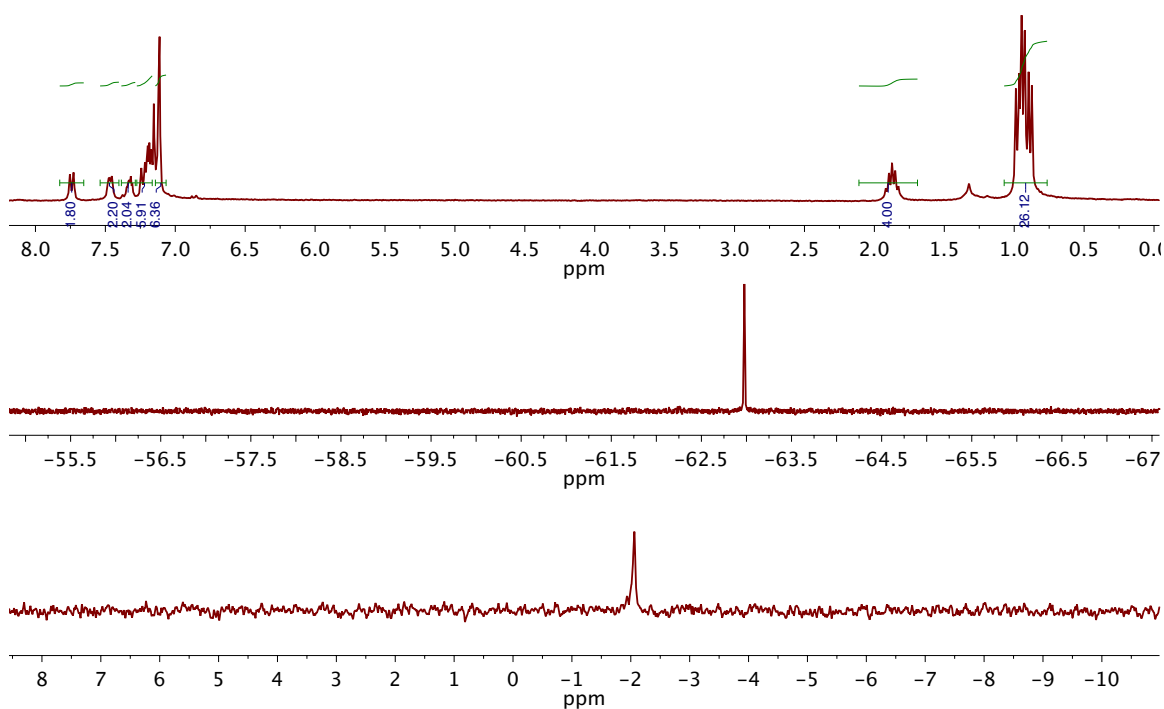


Figure C.125. ^1H (top), ^{19}F (middle), and ^{31}P (bottom) NMR spectra of catechol aryl borane **55** (C_6D_6).

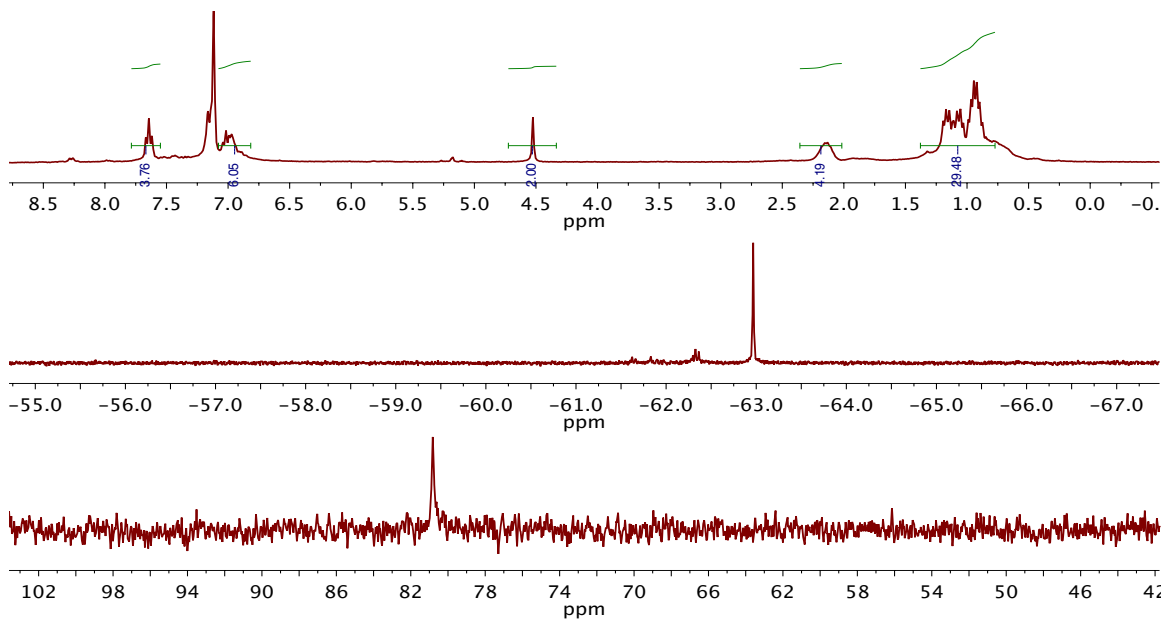


Figure C.126. ^1H (top), ^{19}F (middle), and ^{31}P (bottom) NMR spectra of worked up reaction mixture prior to co-crystallization of dicobalt **56** and pentacobalt **57** (C_6D_6).

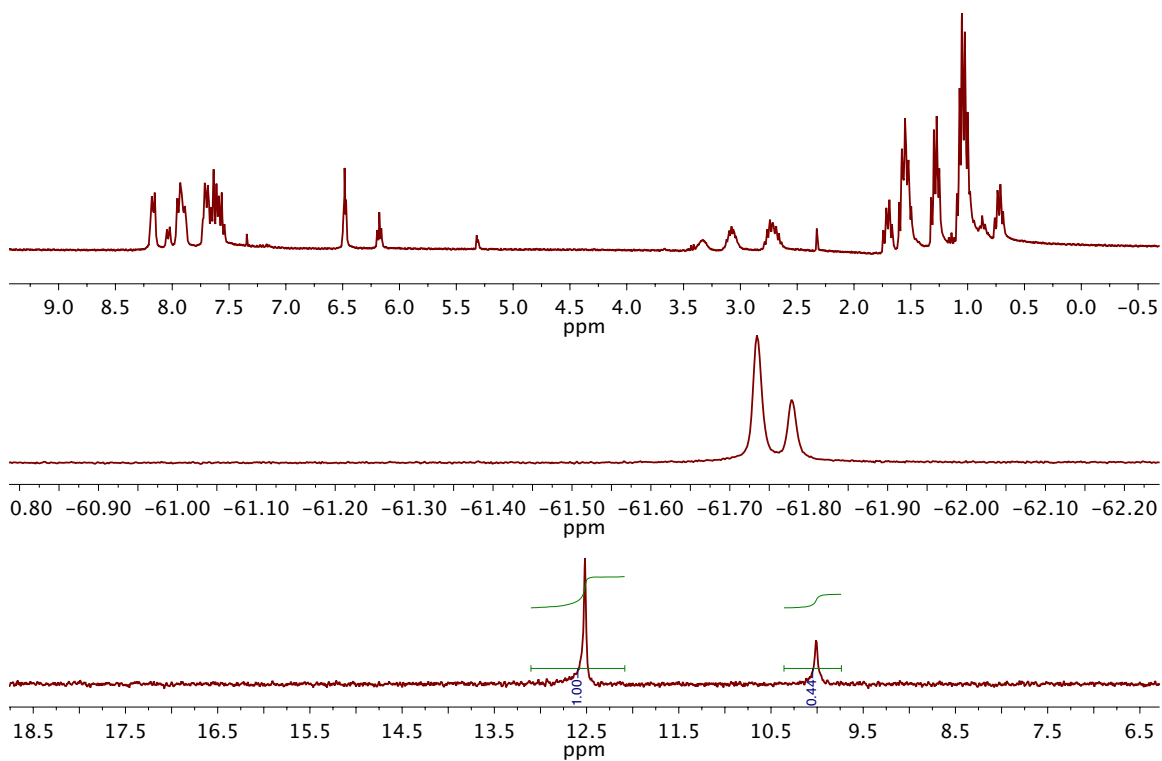


Figure C.127. ^1H (top), ^{19}F (middle), and ^{31}P (bottom) NMR spectra of mixture of two rhenium chloride compounds out of **58-60** $^{\text{CF}_3\text{Ph}}$ (CD_2Cl_2).

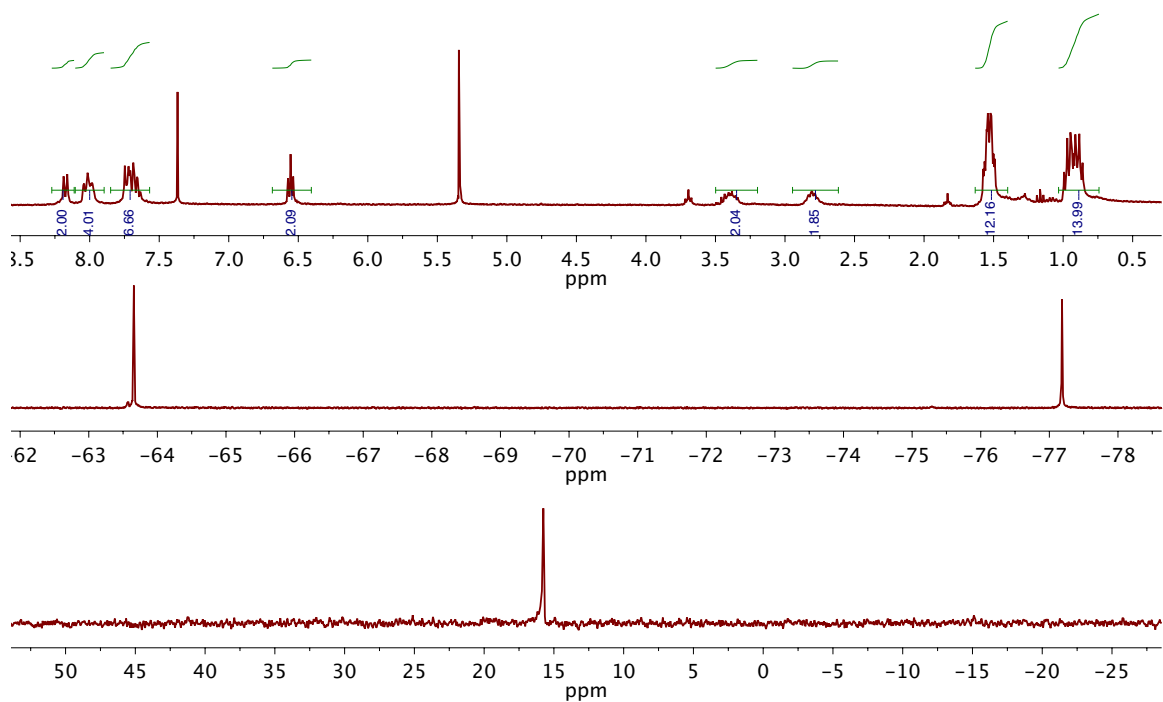


Figure C.128. ^1H (top), ^{19}F (middle), and ^{31}P (bottom) NMR spectra of product of halide abstraction from $58\text{-}60^{\text{CF}_3\text{Ph}}$ (CD_2Cl_2 , not indefinitely stable in solution).

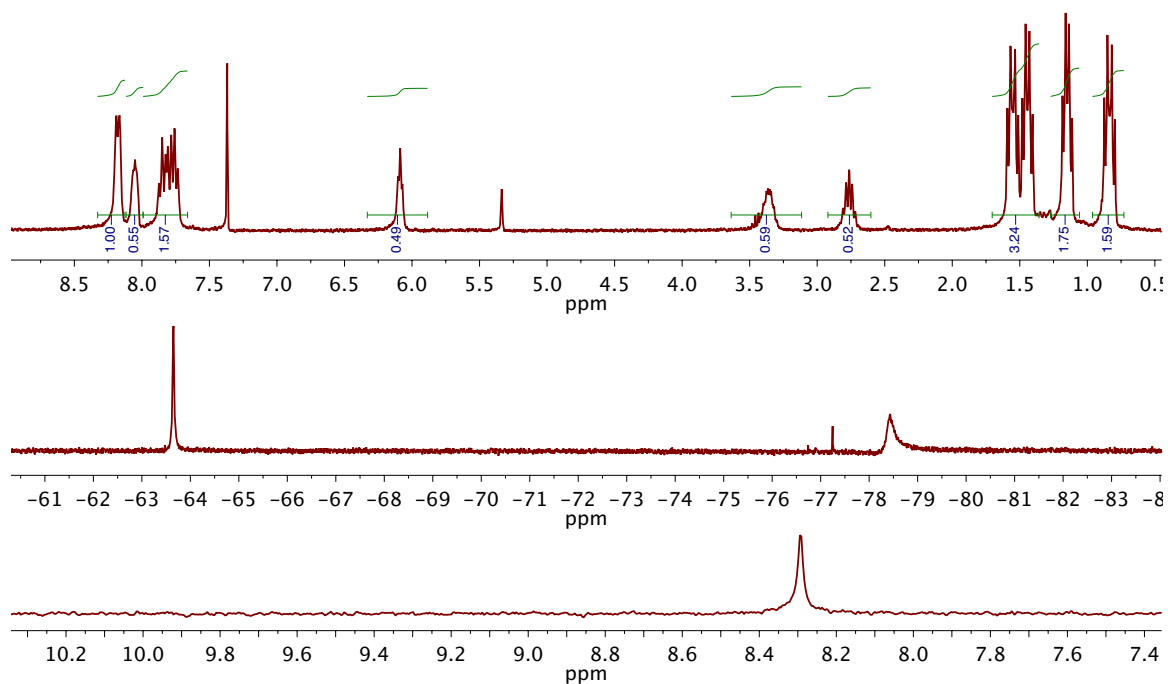


Figure C.129. ^1H (top), ^{19}F (middle), and ^{31}P (bottom) NMR spectra of product of halide abstraction from $58\text{-}60^{\text{CF}_3\text{Ph}}$ under 1 atm CO to yield **61** (CD_2Cl_2 , stable in solution).

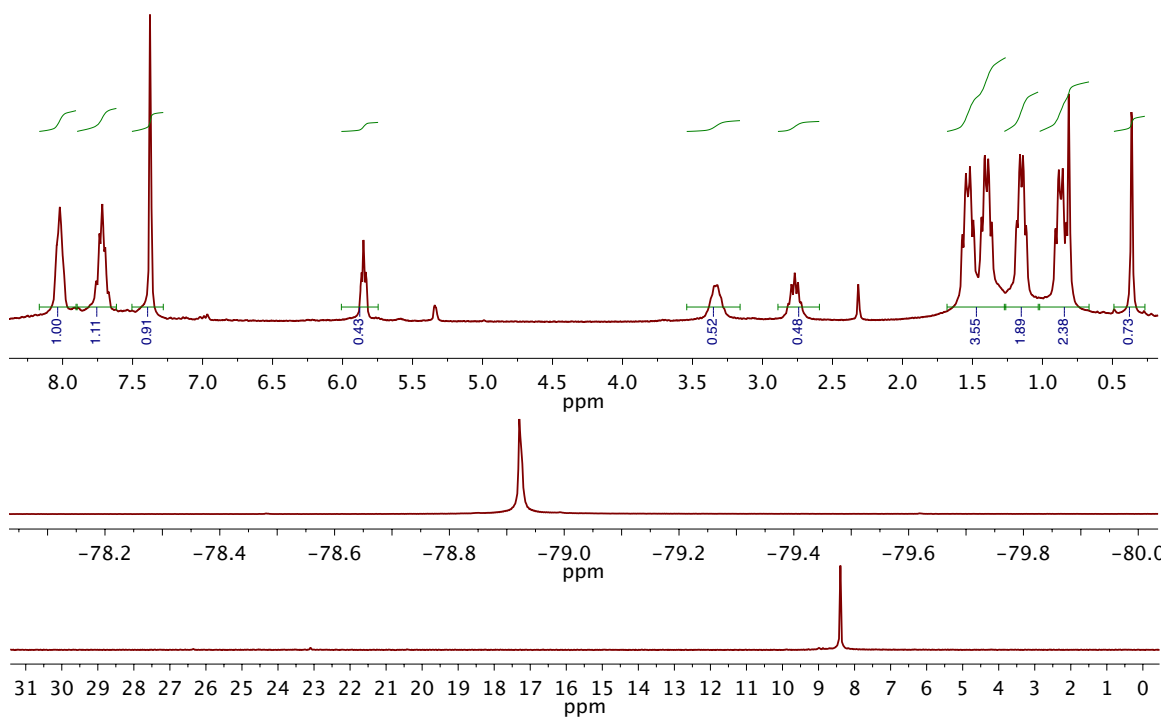


Figure C.130. ^1H (top), ^{19}F (middle), and ^{31}P (bottom) NMR spectra **62** (CD_2Cl_2).

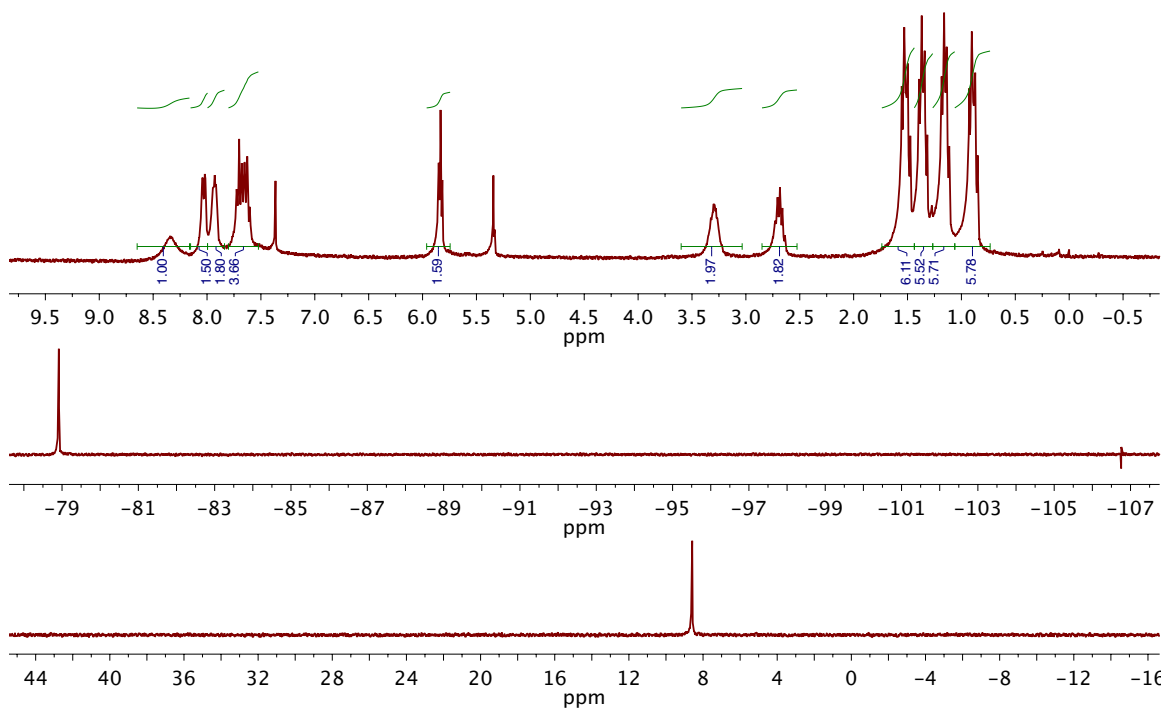


Figure C.131. ^1H (top), ^{19}F (middle), and ^{31}P (bottom) NMR spectra **63** (CD_2Cl_2).

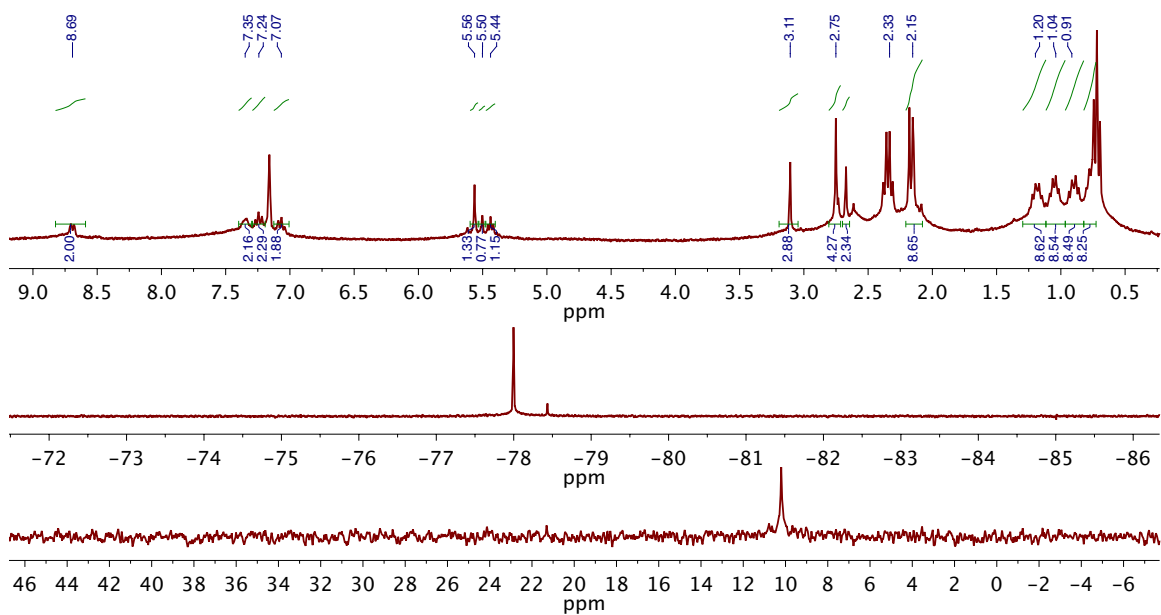


Figure C.132. 1H (top), ^{19}F (middle), and ^{31}P (bottom) NMR spectra **64** (C_6D_6).

